B. K. Jana

M. Majumder

(Eds.)

Impact of Climate Change on Natural Resource Management

Impact of Climate Change
on Natural Resource Management

Bipal K. Jana · Mrinmoy Majumder
Editors

Impact of Climate Change on Natural Resource Management

Springer

Editors
Bipal K. Jana
Jadavpur University,
Kolkata, India
bipalkjana10@rediffmail.com

Mrinmoy Majumder
Jadavpur University,
Kolkata, India
mrinmoy@majumder.info

Printed on acid-free paper

Preface

Climate change is defined as any long-term change in the statistics of weather over periods of time that range from decades to millions of years. Climate change may occur in a specific region, or across the whole world.

The effect of global warming is now predominant in many parts of the world. Twelve warmest years have occurred in the 1900s among which ten have occurred between 1987 and 1998. The energy availability, which was increased due to increase in temperature, had created a ripple effect throughout the Earth system with positive local, regional, and global feedback on each other to amplify and accelerate warming (Stewart and Vemuri 2006).

Abnormality in climatic pattern, induced by the accelerated warming, had started to effect catchment-specific hydrologic cycles. In the last 10 years, floods have caused more damage than in the previous 30 years. Higher temperatures lead to a high rate of evaporation and very dry conditions in some areas of the world. Severe weather events are now more common. The number and strength of hurricanes, tornadoes, and other events had increased over the last 15–20 years. As per IPCC (2007), global climate change is expected to affect the performance of water resource systems according to current indicators and findings.

The biggest casualty of climate change would be the natural resources. A change in the climate could change the resource capacity as well as the pattern by which the resource is used by the adjacent population. The impact on natural resources, if not controlled by mitigating measures, could lead to extreme situations. But still natural resources of many places were managed without any specific plans and according to demands of the users. The ill-managed resources and climate change could lead any place of the world into the verge of extinction.

For example, rivers can cause floods and also supply water for domestic, industrial, and agricultural uses. But if reservoirs and barrages are built to control the river flow, the floods may recede but frequency of floods will increase. As climate change is causing excessive rain in some places and lower than normal in others, a controlled river may behave abnormally and cause more devastating floods than ever. The flood in river Koshi in Bihar, India, is a perfect example of mismanagement of natural resources in face of climate change. River Koshi changed its flow path due to the reservoir built upon the river causing a flood, which in turn destroyed the livelihood of more than 10,000 people.

The book *Impact of Climate Change on Natural Resource Management* tries to highlight and quantify the impact of climate change on natural resources like water and vegetations. The book also tries to show the future status of natural resources in India if the climate change scenarios predicted by various climate models are taken as reality. The mitigation measures of climate change were also explained with simulation of the mitigation measures.

The first part of the book deals with the impact of climate change on water and forest resource.

For example, in Chapter 1, the impact of carbon dioxide emission on GHG levels of a metro city is discussed in great detail.

In Chapter 2, the impact of climate change on the availability of virtual water is estimated with the help of distributed neurogenetic models. The virtual water is defined as the amount of water used by industries to manufacture their products. The impacts on virtual water will help to understand the climate change impacts on industries.

In Chapter 3, the climate change impacts on water availability of a region is discussed. The climate scenarios are simulated by neuro-genetic models which stress the impact of forest cover on basin runoff. So, both the impact of climate change and reduction of forest cover on water availability of the region are analyzed in this chapter.

In Chapter 4, impact of Climatic Uncertainty on water footprint of two river basins is estimated. The water footprint is the water which is used to produce services and products for your benefit. The footprints of water actually delineate the sharing of water within districts, states, or basins. The sharing of water has caused many controversies between countries (India and Bangladesh for sharing of water from River Ganges) and states (Tamil Nadu and Karnataka for sharing of water from River Cauvery).

In Chapter 5, the concept of sequestration of water was proposed and the impact of climatic uncertainty on the parameter is analyzed. The Water Sequestration Capacity of a region could be defined as the amount of water that can be stored within the vegetative zones of the region which could only be used by the vegetations of that region. A clear idea of agricultural output from a watershed could be estimated with the help of this new concept. The chapter tries to predict the impacts of climate change on the agricultural output of basins with the help of water sequestration and neuro-genetic models.

In Chapter 6, the impact of desertification, one of the major impact and also cause of climate change, is simulated to have an idea of desertification impacts on river runoff. A coupled model was used to predict the output.

In Chapter 7, change in quality of rain water due to rapid urbanization of a metro city is compared and the authors have tried to establish a relationship between water quality and urbanization.

In Chapter 8, the concept of Representative Elementary Area has been used to identify the water-stressed regions of a basin. The stressed region for the future is also estimated to analyze the impact of climate change on water availability. The conditions for water stress have been collected from the UNFCC.

Chapters 9–11 is a study which tries to predict the spatial variation of river runoff, water quality, and water pollution within two river basins of Eastern India in face of climate change. The simulations were done by neuro-genetic models and PRECIS climate model.

In Chapter 12, different conditions of a stressed climate is simulated to predict the runoff of a small tributary of West Bengal.

Chapters 13 and 14 deal with the determination of Evapotranspiration where the former tries to predict it from stream flow and the later compares the same parameter for one urban and one metro cities to identify the difference between the two.

The second part of the book tries to analyze the process of mitigating the impacts by forest resources and building control structures.

As for example, in Chapter 15, the process of Carbon stock accumulation by plantation is discussed and in Chapter 16, carbon sequestration and carbon economy are proposed as tools for conservation of the depleting natural resources.

In Chapters 17 and 18, measurement of plant carbon sequestration and soil carbon stock are discussed so that the results could be used as a benchmark for proposing urban plantations as a measure to control temperature within 2°C which is proposed as a measure to counter rising GHG levels of many urban cities.

In Chapters 19 and 20, the utility of the development of reservoirs as a measure to counter hydrologic extremities caused by climate change is analyzed and simulated. The former article tries to estimate the behaviors of reservoir with the help of clusterized neuro-genetic algorithm and to formulate a relationship between various related parameters and reservoir outflow. The latter article deals with the utilization of the stored resource to generate electrical energy so that minimum resource is required for maximum utilization.

A general overview of Hydrologic Models, Artificial Neural Network and Genetic Algorithm, Climate Models and Remote Sensing and GIS are discussed in Chapters 21–24. The current trends of the two basins considered in the chapters about climate change impacts are explained in Chapter 25.

References

IPCC (2007) Climate change 2007: the physical sciences basis, retrieved on http://ipcc-wg1.ucar.edu/wg1/wg1-report.html. on 30th April, 2009

Stewart P, Le CF, Vemuri SR (2006) (Anticipated) Climate change impacts on Australia, Int J Ecol Dev 4:W06

Acknowledgments

Kolkata, West Bengal   Bipal Jana
                                                                   Mrinmoy Majumder

Contents

Part I
Impact of Climate Change: Separating the Causes from the Effects

Chapter 1
Estimation of Carbon Dioxide Emission Contributing GHG Level in Ambient Air of a Metro City: A Case Study for Kolkata

Bipal K. Jana, Soumyajit Biswas, Mrinmoy Majumder, Pankaj Roy, and Asis Mazumdar

Abstract Green house gases (GHGs) such as carbon dioxide (CO_2) emission increase the Earth's ambient temperature with the rapid increase of urbanization and industrialization as well as rapid growth of human population. Kolkata Metro City has an area of 185 km^2 and consists of 4,572,876 populations with a density of 24,718 persons/km^2 in 2001. Main sources of CO_2 emission are vehicular exhaust, emission from small-scale industries, emission from commercial and domestic fuel burning, human respiration, soil respiration, etc. The specific objective of this article is to estimate the CO_2 emission from different sources mainly from the sections of automobile exhaust, small-scale industries, human respiration, and soil respiration.

B.K. Jana (✉)
Senior Research Fellow, School of Water Resources Engineering, Jadavpur University, Kolkata-700032, West Bengal, India
and
Environmental Manager, Consulting Engineering Services, West Bengal, India
e-mail: bipalkjana@gmail.com

S. Biswas
Research Fellow, School of Water Resources Engineering, Jadavpur University, Kolkata-700032, West Bengal, India

M. Majumder
Senior Research Fellow, School of Water Resources Engineering, Jadavpur University, Kolkata-700032, West Bengal, India
and
Geo-information Scientist, Regional Center, National Afforestation and Eco-development Board, Jadavpur University, Kolkata-700032, West Bengal, India

P. Roy
Lecturer, School of Water Resources Engineering, Jadavpur University, Kolkata-700032, West Bengal, India

A. Mazumdar
Coordinator, Regional Center, National Afforestation and Eco-development Board, Jadavpur University, Kolkata-700032, West Bengal, India
and
Director, School of Water Resources Engineering, Jadavpur University, Kolkata-700032, West Bengal, India

Other emission sources have not been discussed here due to nonavailability of existing data. In Kolkata, vehicular exhaust emitted 257.63 t CO_2/day in 2005, small-scale industries emitted 64.65 t CO_2/day, and human respiration emitted 3.16×10^3 t CO_2/day in 2001. Measurement of soil respiration as conducted in two gardens in and around the city was 1.23×10^{-6} t CO_2/m²/day in Botanical Garden and 5.09×10^{-6} t CO_2/m²/day in Banobitan. The vehicular pollution has to be minimized through emission control by the strict regulations in conjunction with increasing environment-friendly technologies. CO_2 emission from small-scale industries in Kolkata has already been reduced by applying process change and alternative fuel use. Human respiration is also contributing to increase the GHG-CO_2 level in the atmosphere with the rapid increase of human population. There is also an urgent need to control human population that will help to conserve and protect natural resources in all respects.

Keywords Carbon dioxide • human respiration • small-scale industries • soil respiration • vehicular exhaust

1.1   Introduction

The aim of Kyoto protocol is to reduce the green house gas (GHG) emission by 5.2% below the 1990 levels by 2012. The first phase of the protocol had begun in 2007 and the second phase has started in 2008. The best known green house gas is carbon dioxide (CO_2). The target of CO_2 reduction could be achieved through two major processes: by reducing anthropogenic emissions of CO_2 and by creating and/or enhancing carbon sink in the biosphere. The outcome of the Kyoto Conference has directed us to think about the effect of global warming and to minimize the emission of the green house gases (GHGs). Population growth and economic development are causing too many serious environmental problems in any corner of the world specifically applicable to our country. These create pressure on land, forests, habitat destruction and loss of biodiversity, rising demand of energy, increase of air pollution, global warming and climate change, and water scarcity and water pollution. Climate change would cause changes in precipitation patterns, marine systems, water availability, and sea-level rise. All these would have significant socioeconomic consequences.

Different control technologies are available for minimizing NO_2 and SO_2 emission; while sequestration devices have been advanced for CO_2 and special scientific control system with low CO_2 emission have been considered in transport system. Apart from industrial CO_2 production through various industrial combustion processes, the CO_2 production in ambient air is largely contributed by the fuel combustion of vehicles. Different types of vehicles emanate CO_2 in different emission rate that depends upon the fuel quality and the upgraded modernized vehicles. The pollution from the vehicles has significant environmental implications, which cannot be ignored. The need to reduce vehicular pollution has led to emission control through regulations in conjunction with increasing environment-friendly technologies. The first emissions norms in India came into force for petrol vehicles in 1991 and for diesel vehicles in 1992. The important steps were taken to reduce the vehicular emission level in India on April

1995 by the mandatory fitment of catalytic converters and the use of unleaded petrol (ULP). The emission reduction achieved from pre-89 levels is over 85% for petrol-driven vehicles and 61% for diesel vehicles from 1991 levels. In 2000, passenger cars and commercial vehicles were in effect for meeting Euro-I equivalent India 2000 norms. Euro-II equivalent Bharat Stage-II norms were in force from 2001 in four metro cities: Delhi, Mumbai, Chennai, and Kolkata (SIMA 2008). Bharat Stage III equivalent to Euro-III norms were in effect from April 2005 for 11 major cities and Bharat Stage IV equivalent to Euro IV norms will be affected from the year 2010. Vehicular emissions depend upon four important factors: vehicular technology, fuel quality, inspection and maintenance of in-use vehicles, and road and traffic management. Among these four factors, vehicular technology and fuel quality have direct environmental implications have to be optimized in order to achieve significant reduction in emission. The Ministry of Environment and Forests had notified fuel specifications in 1996. Maximum limits for critical ingredients like benzene level in petrol have been specified. The high levels of pollution have necessitated eliminating leaded petrol throughout the country. There is a need for a holistic approach so that upgradation in engine technology can be optimized for maximum environmental benefits.

A study on fuel conversion of coal-fired small boilers and ceramic kilns in Kolkata Metropolitan Area (KMA) in a joint venture project by West Bengal Pollution Control Board and India–Canada Environment Facility Project has been carried out in 2006. The change of fuel from coal to other fuels has resulted in reduction of CO_2 emission. Besides different activities like transportation, industries, hotels and shops, domestic fuel burning, etc. due to highly anthropogenic stress, the human respiration is also enhancing GHGs-CO_2 emission in the atmosphere. Soil organic matter (SOM) decomposition involves an enzymatic oxidation that produces mineral compounds (e.g., ammonium) and CO_2, which is then returned to the atmosphere by soil respiration. While part of the carbon is lost as soil respiration the simpler compounds are metabolized by soil microbes (Rodriguez-Iturbe and Porporato 2004). Kolkata city with its large infrastructure and dense population is emanating CO_2 (a major GHG) from vehicular exhaust, small-scale industries, commercial shops and hotels, residential fuel burning, human respiration, soil respiration, and other sources. This article mainly emphasizes on the quantum of CO_2 emission from different sources increasing GHGs level in the atmosphere of Kolkata.

1.2   The Study Area

Overview of urban peoples' environment in West Bengal is mainly the KMA. The KMA has been defined in Town and Country (Planning and Development) Act of 1979. It has an area of 1,785 km^2 with a population of about 14.96 million (Directorate of census operation 2001). The KMA is a part of the lower Bengal Delta. A number of distinguishing features are observed in KMA such as:

- The area is flat.
- The master slope is from north to south.
- The land lies between 1.5 m and 9.0 m above MSL.

Fig. 1.1 Figure showing the location of Kolkata Metro City (picture taken from Google Earth™)

- The river Hooghly divides KMA into two parts and forms the principal drainage line for the both.
- The physiographic characteristics are generated from a combination of alluvial, aeolian, lagoon, and swamp conditions.

Kolkata Metro City is the heart of KMA and Kolkata Municipal Corporation (KMC) is the administrative body of this city (Fig. 1.1). As per the Directorate of Census Operation, West Bengal, 2001, the geographical area of Kolkata is 185 km², which is 0.21% of the total area of West Bengal and 5.56% of the total urban area of West Bengal.

1.3 CO$_2$ Emission from Vehicular Exhaust

Automobile pollution arises due to combustion of fossil fuel with air inside the cylinder of the vehicle. Exhaust waste gases cause pollution when individual exhaust gases exceed their limits.

Fuel + air $\Rightarrow$ unburned hydrocarbons + nitogen oxides + carbon monoxide
+ carbon dioxide + water
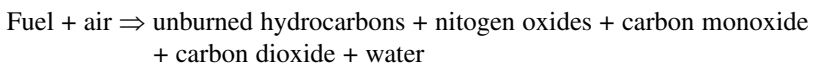
The main automobile exhaust gases are carbon monoxide (CO), CO_2, hydrocarbon (HC), oxides of nitrogen (NO_x), particulate matter (PM), steam (H_2O), etc. Within a certain range, they are acceptable, but when they exceed the limits they are very harmful. In general, pollution increases due to old vehicular technology and the quality of fuel. The study concentrates on CO_2 and CO (equivalent to CO_2) emitted from the vehicular emission in Kolkata. More precisely, it concentrates mainly on the present-day CO_2 emission from different vehicular systems.

Transport undertakings of West Bengal play a pivotal role in the sphere of passenger transportation on road as well as on water transport sector through the state-wide net works. There are five state transport undertakings:

- Calcutta State Transport Corporation (CSTC)
- South Bengal State Transport Corporation (SBSTC)
- North Bengal State Transport Corporation (NBSTC)
- West Bengal Surface Transport Corporation (WBSTC)
- The Calcutta Tramways Company (1978) Ltd. (CTC)

Among these state transport undertakings, the West Bengal Surface Transport Corporation is providing services on water surfaces in addition to its bus services. Besides the state transport undertaking , so many private transport systems (private car, taxi, autorickshaw, private bus, two wheeler, etc.) are also available in Kolkata which are plying on the road in good numbers. The individual and total numbers of motor vehicles on road in Kolkata have been collated from the Statistical Abstract 2005–2006 and Statistical Handbook 1999. There are nine types of individual motor vehicles mentioned in the Statistical Reports such as goods vehicles, motor car/jeeps, motor cycles/scooters, taxi/contract carriage/luxury taxi, mini bus, stage carriage, autorickshaw, tractor/trailors, and others. The total vehicular growth in Kolkata is depicted in Fig. 1.2.

The vehicular population of Kolkata in 1981, 1991, and 2001 was 172,323, 476,745, and 762,924, respectively. The total number of motor vehicles in Kolkata increased from 729,302 in 2000 to 911,921 in 2005. The vehicular number increased by 2.76 times during 1981–1991 and 1.60 times during 1991–2001. Among the total number of vehicles in 2001, percentage of different types of vehicles were 8.49% goods vehicles, 36.78% motor car/jeeps, 44.10% two wheelers, 4.32% taxi, contract
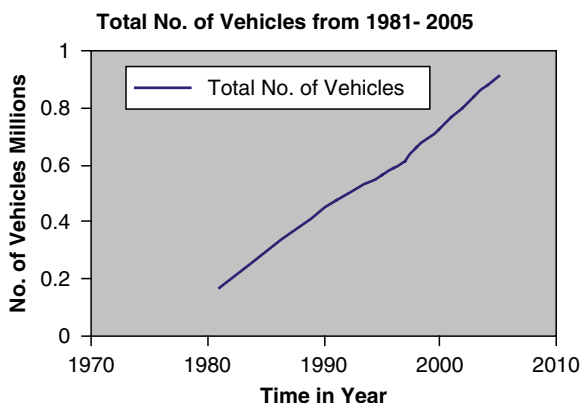
Fig. 1.2 Figure showing growth of vehicles in Kolkata

carriage, luxury taxi, 0.15% minibus, 1.06% stage carriage, 1.72% autorickshaw, 0.62% tractor/trailor, and 2.72% others (Jana et al. 2008). During the period 2000–2005, the percentage of vehicular population increased by 25.04 in Kolkata. The vehicular population of Kolkata contributed 41.90% to the West Bengal vehicle number in 2000, while the vehicular population contributed 34.01% to the state vehicle population in 2005. It should also be noted that different types of vehicle numbers in Kolkata were sometimes in decreasing trend. This may be due to restriction of governmental policies and some other factors, which influence the growth of vehicles.

If the ratio of air and fuel mixture is not adjustable/suitable to the specification, then it increases the chances of pollution that leads to the increasing emission of CO as well as CO_2. It also results in the loss of power and fuel wastage, which in turn means less efficient performance of the engine along with lower fuel economy. To solve these problems, the respective government agencies create clean-air laws, and many laws have been enacted that restrict the amount of pollution that cars can produce. To keep up with these laws, automakers have made many refinements to car engines and fuel systems. To help in reducing the emissions further, they have developed an interesting device called a catalytic converter, which treats the exhaust before it discharges from the car and removes a lot of air pollution (ECMA 2008).

The vehicular emission load of CO_2 can be calculated by multiplying emission coefficient of CO_2 (as derived from equivalent emission coefficient of CO) with distance traveled by each vehicle. The emission coefficient of CO (molecular weight-28) has been used to convert to its equivalent load of CO_2 (molecular weight-44). Therefore, the equivalent load of CO_2 can be calculated from the pollution load of CO. Table 1.1 provides information about these norms vis-à-vis the emission coefficient of CO corresponding to different emission technologies.

This is to be noted that the emission coefficient of CO for different vehicles for the period of 1981–1990 has been considered the same value of PreEuro (1991–1995) emission coefficient, since the values for those period were unavailable and undefined. The average distance traveled by each category of vehicles per day has been derived by the survey of different types of vehicles within Kolkata area. As obtained, the average distance traveled by each category of vehicle multiplied by the emission

Table 1.1 Emission coefficients (kg/km) of CO corresponding to different emission technologies

	Buses	Trucks	PCG	PCD	2W	LCV (tractor, water carrier)
PreEuro (1991–95)						
CO	0.0055	0.006	0.0098	0.0073	0.0065	0.0087
PreEuro (1996–2000)						
CO	0.0045	0.005	0.0039	0.0012	0.004	0.0069
Euro1/India stage 2000						
CO	0.0036	0.0036	0.0024	0.0011	0.0022	0.0051
Euro2/Bharat stage 2 – 2001						
CO	0.0032	0.0032	0.0022	0.001	0.0015	0.00072
Euro3/Bharat stage 3 – 2005						
CO	0.0028	0.0028	0.00139	0.00058	–	0.00064

Transport Fuel Quality (2005)

coefficient of CO_2 (equivalent of CO) gives us the per day emissions of CO_2 per vehicle, which can be converted for obtaining total emissions of CO_2 by further multiplying by the total number of vehicles. The average distance traveled by each category of vehicles per day are surveyed on more than 100 vehicles in Kolkata and the average productivity (km/day) of the individual vehicles are 64.38 km by motor car/jeeps, 42 km by motor cycles/scooter, 185.8 km by taxi, contract carriage/luxury taxi, 162.8 km by mini bus, 198.28 km by stage carriage, 80.12 km by autorickshaw, 270.52 km by goods vehicles, 58.65 km by tractor/trailors, and 34.36 km by other vehicles. It is observed from the survey data that the average distance traveled per day (average productivity) by each category of vehicles is comparatively higher with respect to India's scenario. This may be due to better road condition, the upgradation and construction of new roads, less traffic congestion, operation of more flyovers and bridges, etc. in and around Kolkata. This has been observed from different research works that a passenger car travels on an average 30–35 km/day in India (Mashlekar Committee Report, 2002). The average productivity of a truck is 200 km/day as against 350–400 km that would be possible through reduction of congestion (Pant 2001). The yearwise CO_2 emission load from vehicular exhaust is estimated for Kolkata (based on survey data) and is presented in Table 1.2.

The total CO_2 emission load by vehicular exhaust in Kolkata is pictorially depicted in Fig. 1.3.

Table 1.2 Yearwise CO_2 emission load (t/day) from vehicular exhaust in Kolkata

Year	CO_2 emission (t/day)	Year	CO_2 emission (t/day)
1981	205.53	2000	254.45
1991	476.31	2001	265.87
1995	562.69	2002	275.88
1996	450.68	2003	287.45
1997	466.25	2004	295.84
1998	363.93	2005	257.63
1999	377.94		
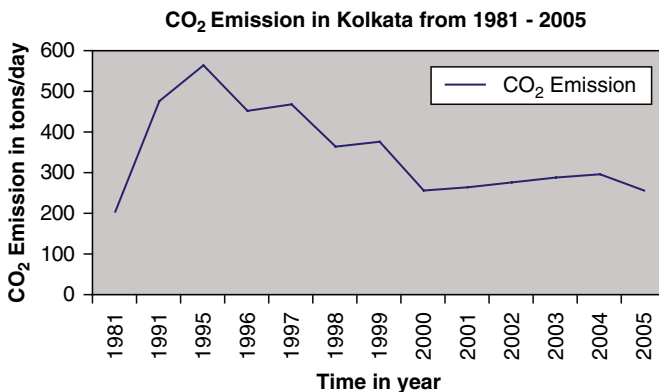
Fig. 1.3 CO_2 emission in Kolkata from 1981 to 2005

It is to be noted that the total CO_2 emission load in Kolkata was 205.53 t/day in 1981, 476.306 t/day in 1991, 265.87 t/day in 2001, and 257.63 t/day in 2005. The CO_2 emission load of Kolkata increased by 131.74% during 1981–1991, then decreased by 44.18% during 1991–2001, and again decreased by 3.09% during 2001–2005. Among the individual type of vehicles, major contributors of CO_2 emission to ambient air are goods vehicles, motor car/jeeps, motorcycles/scooters, and taxi/ contract carriage. CO_2 contribution by goods vehicles was 63.96 t/day in 1981, 124.15 t/day in 1991, 99.14 t/day in 2001, and 94.99 t/day in 2005. CO_2 contribution by motor cars and jeeps was 84.55 t/day in 1981, 180.6 t/day in 1991, 68.13 t/day in 2001, and 83.88 t/day in 2005. While the CO_2 contribution by motor cycle/ scooter and taxi/ contract carriage was 19.08 and 29.48 t/day in 1981, 85.30 and 54.46 t/day in 1991, 48.85 and 23.13 t/day in 2001, and 40.16 and 24.43 t/day in 2005, respectively. CO_2 contribution in air by other types of vehicles is comparatively on the lower side (Jana et al. 2008).

This is also important to note that CO_2 emission load are sometimes in decreasing trend, may be due to stricter emission norms in decreasing emission coefficient, decreasing strength of registered motor vehicles, and wide variation of distance traversed per day by different motor vehicles in Kolkata. This may also be noted that the total number of registered vehicles was not classified in different Euro or Bharat Stages in the record of Transport Department or Motor Vehicles Department. Therefore, the CO_2 emission load has been estimated/evaluated based on single Euro/Bharat stage basis. So, the estimated CO_2 emission load may have a slight deviation to some extent from the actual CO_2 emission load though the trend of CO_2 emission load yearwise will remain similar as obtained. Automobile emission can be reduced by improving the vehicular technologies and the fuel quality. The vehicular technologies and fuel quality are different for different norms (Euro I, II, III, and IV) (Chatterjee et al. 2005).

The improvement and upgradation of the national highways, state highways, and other roads would enhance the speed of the vehicles and avoid traffic congestion on the junction of the road crossings. This leads to further reduction of vehicular emission. Further advancement of vehicular technology and fuel quality in near future will also reduce the vehicular emission in ambient environment.

1.4 CO_2 Emission from Small-Scale Industries in KMA

A study has been carried out on fuel conversion of coal-fired small boilers and ceramic kilns in KMA in a joint venture project by West Bengal Pollution Control Board and India–Canada Environment Facility Project in 2006. The change of fuel from coal to other fuels has resulted in reduction of CO_2 emission. The emission factor used for coal is 1,507 kg of CO_2 per ton of coal used and for oil fuels is taken at 2,680 kg of CO_2/kl. The reduction in the emission per annum from already converted units is estimated to be 28,000 t of CO_2/annum. This is a reduction of 55% over the base of using coal (West Bengal Pollution Control Board – India–Canada Environment Facility Project 2006).

1.5 CO$_2$ Emission from Human Respiration

Rapid human population growth creates tremendous pressure on the Earth. As on 2003, approximately 6.3 billion people inhabit the Earth. Nearly 9,000 people are added each hour, over 200,000 persons/day. The global population increased by approximately 77 million persons in 2001 (131.5 million babies were born and roughly 54.5 million individuals died), a rate of about 1.26%/year. Overpopulation is one of the main issues in environmental science. No longer can population, or overpopulation, be viewed simply as a cause of environmental destruction; rather, it must be viewed as a major symptom of underlying social, economic, and environmental issues. Poverty, high fertility, and environmental degradation go hand in hand, each reinforcing the other. Human population pressure has progressively modified the environment. The growth of human population in Kolkata has been taken into account in this study. Based on population growth, the emission of CO$_2$ has been established.

1.5.1 World Population Changes over Time

After late ancient times, the world's population slowly but steadily had increased, except for a slight decline in the fourteenth century due to plague, until the mid-seventeenth century when it totaled approximately 500 million. Since about 1650, the human population has grown at an ever-increasing rate, reaching 800 million around 1750, 1.2 billion in 1850, slightly over 2.5 billion in 1950, 4.44 billion in 1980, and 6.1 billion in 2000 (Mckinney and Schoch 2003). The world human population growth is presented in Table 1.3. The estimated population growth, which indicates a vertical and unending rise in population, is depicted in Fig. 1.4. Figure 1.5 also depicts the projected population until 2050 and shows the population beginning to level out at below 10 billion in approximately 50 years (using the medium or low variant).

Recent United Nations projections estimated that the world population will reach 6.8 billion in 2010 and 9.3 billion in 2050 (using a medium-fertility projection, generally considered as "most likely" (Fig. 1.4). However, these estimates are based on many uncertain variables, such as how quickly modern birth control methods will spread and fertility rates drop. Even assuming that continued advances are made in decreasing global fertility rates and increasing global use of contraceptives,

Table 1.3 How long has it taken to add an additional one billion people to earth's human population?

World population reached	World population may reach
1 billion in 1800	7 billion in 2013 (14 years later)
2 billion in 1930 (130 years later)	8 billion in 2025 (17 years later)
3 billion in 1960 (30 years later)	9 billion in 2044 (19 years later)
4 billion in 1974 (14 years later)	
5 billion in 1987 (13 years later)	
6 billion in 1999 (12 years later)	
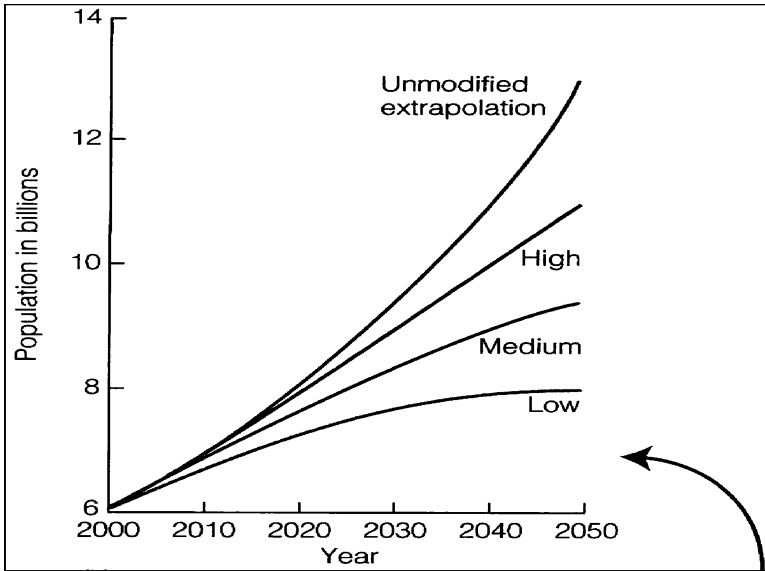
Fig. 1.4 World human population changes over time. Estimated population growth in billions since the Neolithic age
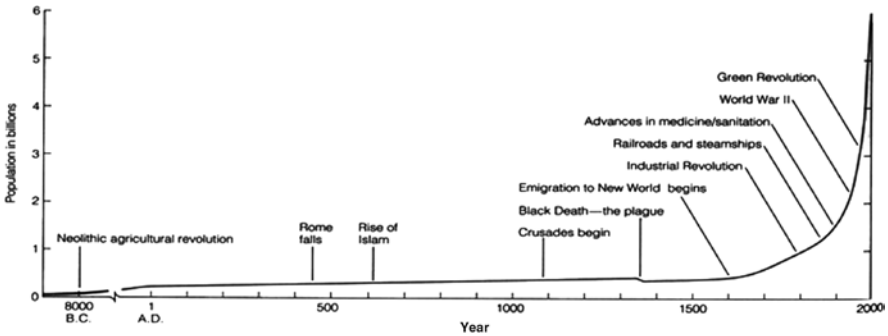
Fig. 1.5 World human population changes over time. World population projections until 2050 (medium, high, and low-fertility variants) in billions. Note: the timescales for the two graphs are different

the global population may not stabilize until it reaches around 10 billion toward the end of the twenty-first century (Mckinney and Schoch 2003).

1.5.2 Regional Population Growth

The rapid human population growth and economic development in India are degrading the environment through uncontrolled growth of urbanization and

industrialization, extensive use of fertilizers and pesticides in agriculture, and rapidly degrading the natural forest. India is the second most populous country in the world after China. Recently, the population of India has crossed the one billion mark. According to the Census of India (2001), the population of India on 1 March 2001 was 1,027 millions (Central Statistical Organization 1999a, b). At the time of independence, the country's population was 342 million. The number has multiplied threefold in around 5 decades. The total population size of India had grown from 361 million in 1951 to around 1027 million in 2001. The population of India increased by three times during the period of 1951–2001. It is estimated that the country's population will increase to 1.107 billion by the year 2010 and 1.26 billion by the year 2016 (Census of India 2001). The projected population indicates that India will be the first most populous country (population of 1.572 billion) in the world and China will be second in 2050 (Population Reference Bureau (PRB) 2001). The increase of population has been trending toward alarming situation. India is having 18% of the world's population on 2.4% of its land area has great deal of pressure on its all natural resources (Central Statistical Organization 1999a, b and Central Statistical Organization 2000).

West Bengal covers the bottleneck of India in the east, stretching from Himalayas in the north to the Bay of Bengal in the south, on the east by Assam and Bangladesh and on the west by states of Orissa and Bihar. The state lies between 27°13′15″ and 21°25′24″ N latitudes and 85°48′20″ and 89°53′04″ E longitudes. The state of West Bengal has an area of 88,752 km^2 (M/O Health and F.W. GoI 2006). The total population of West Bengal as of 1 March 2001 stood at 80,221,171 registering an increase of 17.84% over the population of previous census 1991. In terms of population it holds the fourth position among states and union territories in the country. Among the states in the country, West Bengal is on the top of the heap when it comes to the density of population, which is 904/km^2 (as against the national average of 324) (Census of India 2001). Decadal population density increased from 615 in 1981 to 767 in 1991 and 903 in 2001. The decadal growth rate of the state is 17.77% (against 21.35% for the country) and the population of the state is growing at a slower rate than the national rate.

Kolkata Metro City is the heart of KMA and KMC is the administrative body of this city. As per the Directorate of Census Operation, West Bengal, 2001, the geographical area of West Bengal is 88,752 km^2 of which 96.25% (85,427.26 km^2) is rural and 3.75% (3,324.74 km^2) is urban. The geographical area of Kolkata is 185 km^2, which is 0.21% of the total area of West Bengal and 5.56% of the total urban area of West Bengal. The density of population of Kolkata per square kilometer as per census 1981, 1991, and 2001 are 22,260, 23,783, and 24,718, respectively. The decadal population growth, density of population, and percentage decadal variation of population of Kolkata (Census of India 2001) are presented in Table 1.4.

The population of Kolkata was 933,754 in 1901. The number has multiplied threefold in around 5 decades. The population increased slowly from 2,698,494 in 1951 to 3,305,006 in 1981. During the next decade, 1981–1991, the population of Kolkata increased sharply in the order of about 1,000,000 and reached 4,399,819 in 1991. As per census 2001, the population of Kolkata reached 4,572,876 with the percentage decadal variation of population 3.93 (1991–2001).

Table 1.4 Decadal population, density of population per square kilometers and percentage decadal variation of population in Kolkata

| Year | Decadal growth of population | Population density/km^2 | Percentage decadal variation of population | | |
			1971–1981	1981–1991	1991–2001
1901	933,754	–	10.73	6.61	3.93
1951	2,698,494	–			
1971	3,148,746	–			
1981	3,305,006	22,260			
1991	4,399,819	23,783			
2001	4,572,876	24,718			

1.5.3 CO$_2$ Emission from Human Respiration

Breathing transports oxygen into the body and CO$_2$ out of the body. The process of gas exchange occurs in the alveoli by passive diffusion of gases between the alveolar gas and the blood passing by in the lung capillaries. Human typically breathes between 12 and 20 times/min (Ramey et al. 2001) and also consulted with so many Doctors. The air we inhale is roughly 78% nitrogen, 21% oxygen, 0.96% argon, and 0.04% CO$_2$, He, H$_2$O, and other gases (% by volume). The air we exhale is roughly 78% nitrogen, 18% oxygen, 0.96% argon, and 4% CO$_2$ (% by volume) (Parkes 2006). (Note that the amount of exhaled oxygen varies according to the fitness of that particular person.) Not all of the oxygen breathed in is converted into CO$_2$.

A reference volume of air is defined as the volume one average human needs for breathing during 24 h (better we call one human day breathing). In a normal quiet breathing we exchange about 0.5 l of air per breathing (Lewis 2006). One person takes 13.5 breaths per minute. Therefore, the volume of one human day breathing derived at the rate of inhaled volume of 0.5 l per breath is 9,700 l/human (approximately), considering that a constant volume of air is exchanged during respiration. Again, volume of CO$_2$ inhaled per human in a day is 3.88 l and volume of CO$_2$ exhaled per human in a day is 388 l. So, the net volume of CO$_2$ emitted per human per day is 384.12 l. Assuming the emitted temperature to be 25°C (298 K), we can convert this volume to STP condition using the relation of Ideal Gas Laws (according to the Boyles & Charles Combination Gas Laws) and the volume stands to 351.895 l of CO$_2$ at STP. So, weights of 351.895 l CO$_2$ at STP exchanged with air by one human day respiration is 691.22 g CO$_2$. Therefore, one human day emits 691.22 g CO$_2$ by respiration which would help to calculate the amount of CO$_2$ generated by the population of Kolkata in a day through only respiration (Jana et al. 2007).

The population of Kolkata Metro City contributes 0.00316 Tg of CO$_2$/day as per 2001 census. These values are significantly alarming and slightly a cause of GHG-CO$_2$ increment in the atmosphere.

As the population increases rapidly with the decade, CO$_2$ emission also increases more prominently (Table 1.5).

Table 1.5 CO_2 emission by population of Kolkata

Year	Total CO_2 emission in Tg @ 691.22 g/human day respiration
1901	0.0006454
1951	0.0018652
1971	0.0021764
1981	0.0022844
1991	0.0030412
2001	0.0031608

Kolkata's CO_2 emission through human respiration is increased by threefold during 1901–1951; while this value is increased by fivefold during last century. Kolkata's population contributes 18% of the total CO_2 emission by human respiration of West Bengal in 2001. From the human respirated CO_2 values, as estimated, restriction should be imposed to control the human population in a certain limit to control the CO_2 emission from mass within the threshold limit to safeguard the environment in future (Jana et al. 2007).

1.6 CO_2 Emission from Soil Respiration

Two sites in and around Kolkata have been selected for CO_2 emission from soil respiration. First site was selected in Banobitan and second site was in Botanical Garden. Banobitan is one of the largest man-made urban forest at Salt Lake in Kolkata Metro City under the Forest Department of Government of West Bengal. It is also known as Central Park. The Indian Botanical Garden is situated on the west bank of the River Ganga (Hooghly) in Howrah district of West Bengal. The garden is the living respiratory of more than 12,000 trees, shrubs, and climbers representing over 1,400 species together with a large number of wild and cultivated herbs (BSI, MoEF, GoI). The elevation of the working site, as measured by GPS, is 22°33.423′N Latitude and 88°17.259′E Longitude. Altitude of the area is 12 m above MSL.

1.6.1 Soil Quality

Soil sample of Banobitan was collected in winter season and analyzed in our laboratory. It is observed from the physiochemical analysis result of soil sample that soils in the area was neutral in nature (pH 7.06); electrical conductivity was 0.104 ms/cm; moisture content was 9.74%; water-holding capacity was 0.35 kg/kg; and bulk density was 1.46 g/cc. The soil texture was sandy loam (sand – 71.6%, silt – 19.7%, and clay – 8.7%). Total nitrogen and total phosphorus of the soil were 706 and 39.1 mg/kg, respectively; total potassium present in the soil was 4,490 mg/kg; total calcium level was 5,192 mg/kg and sodium absorption ratio of the soil was

0.25. Total carbon and soil organic carbon present in the soil were 36.5 and 8.3 g/kg, respectively. Carbon and nitrogen ratio (C/N) of the soil was 11.8.

Soil sample of Botanical Garden was also collected during the end of winter season and physiochemical parameters were analyzed. Soils in the area were slightly acidic in nature (pH 5.90); electrical conductivity was 0.107 ms/cm; moisture content was 16.2%; water-holding capacity was 0.684 kg/kg; and bulk density was 1.42 g/cc. The soil texture was clayey (sand – 17.8%, silt – 24.9%, and clay – 57.2%). Total nitrogen and total phosphorus of the soil were 802 and 360 mg/kg; total potassium present in the soil was 6,525 mg/kg; total calcium was 8,501 mg/kg, and sodium absorption ratio of the soil was 1.32. Total carbon and soil organic carbon present in the soil were 58 and 8.3 g/kg, respectively. C/N ratio of the soil was 10.4.

SOM is a complex and varied mixture of organic substances with three main components: plant residues, microorganisms, and biomass and humus. The amount of organic matter in soils varies widely and usually increases with humidity and to a lesser extent with temperature. Bogs and marshes are very important carbon pools in the terrestrial carbon cycle. SOM decomposition involves an enzymatic oxidation that produces mineral compounds (e.g., ammonium) and CO_2, which is then returned to the atmosphere (soil respiration). While part of the carbon is lost by soil respiration the simpler compounds are metabolized by soil microbes (Rodriguez-Iturbe and Porporato 2004).

1.6.2 CO_2 Emission for Soil Respiration

CO_2 emission from soil respiration has been measured at Banobitan during winter season. The specified area of the soil was fully covered (air tight) by transparent plastic. We have started monitoring from 12:54 h at CO_2 concentration of 411.8 ppm within the closed plastic cover. CO_2 level increased to 1,008.9 ppm at 15:00 h and at 18:00 h to 1,473.4 ppm. At 17:30 h CO_2 concentration decreased to 1,536.6 ppm.

CO_2 emission from soil respiration was also measured at Botanic Garden during winter. The specified area of the soil was fully covered (air tight) by transparent plastic. We have started monitoring from 16:15 h at CO_2 concentration of 466.6 ppm within the closed plastic cover. CO_2 level increased to 1,375.6 ppm at 19.15 h and at 22.15 h reached to 1,541.5 ppm. At 1:15 h CO_2 concentration decreased to 1,494.5 ppm. At 4:15 h CO_2 level reached to 1,393.1 ppm and in the morning at 7:15 h, CO_2 decreased to 1,361.6 ppm. At 10:15 h and 13:15 h CO_2 concentrations increased to 1,427.9 and 1,370.5 ppm, respectively.

CO_2 emissions from soil respiration for these sites measured during winter season are presented in Table 1.6.

The results of CO_2 emission from soil respiration reveal that the CO_2 emitted by soil respiration was higher at Banobitan (0.2122 g/m^2/h, i.e., 5.09×10^{-6} t/m^2/day) than at Botanical Garden (0.0512 g/m^2/h, i.e., 1.23×10^{-6} t/m^2/day).

Table 1.6 Results of CO_2 emission from soil respiration

Sl no.	Location of project site	Soil CO_2 respiration rate
1	Banobitan	0.2122 g/m²/h, i.e., 5.09×10^{-6} t/m²/day
2	Botanical Garden	0.0512 g/m²/h, i.e., 1.23×10^{-6} t/m²/day

1.7 Conclusion

The vehicular population increases manyfold in every decade. So there is a need for controlling vehicular emission in a stricter way. It is now time for the auto and oil industry to come together under the guidance of the government in evolving fuel quality standards and vehicular technology to meet air quality limits. The Government of India has made exhaust emission standards for various categories of new vehicles conforming to Euro-II and Euro-III norms and have been made effective from 2000 and 2005. These norms are strictly adhered to their enforcement ensured. Emission standards for new vehicles should be made more stringent conforming to Euro-IV norms, which will be effective in 2010. Therefore, the vehicular pollution should be controlled by an integrated and holistic approach by adopting: (a) the stricter vehicle emission norms (e.g., EURO-IV); (b) improvement in vehicular technology (e.g., mandatory fitment of catalytic converters); (c) improvement of fuel quality (e.g., benzene and aromatics in petrol, avoid unleaded petrol); (d) improvement of transport system; (e) improvement of traffic management system (e.g., traffic control system, timers at intersection, regulation of digging of roads, etc.); and (f) improvement and upgradation of the national highways, state highways, and other roads. This may be concluded that the reduction of vehicular pollution has led to emission control through regulations in conjunction with increasing environment-friendly technologies.

Fuel conversion of coal-fired small boilers and ceramic kilns in urban area by the less CO_2-emitted alternative fuel is necessary for clean environment. The change of fuel from coal to other fuels has resulted in reduction of CO_2 emission. In the natural phenomena soil respirated CO_2 emits in the environment and also CO_2 sequestration by soil occurs simultaneously. Rapid increase of population is producing an impact on GHG emission. This leads to major physical, environmental, and socioeconomic consequences. The global population would be more vulnerable to health problems due to the global warming. Human respiration is also contributing to increase the GHG-CO_2 level in the atmosphere with the rapid increase of human population. So, there is an urgent need to control human population that will help to conserve and protect natural resources in all respects.

emission from vehicular exhaust: A case study on Kolkata' and West Bengal Pollution Control Board—India- Canada Environment Facility Project, Kolkata (2006) 'Assessment of Social and Environmental Impact of Fuel Conversion in Coal Fired Small Boilers and Ceramic Kilns in Kolkata Metropolitan Area---; Pollution prevention and waste minimization of small scale industrial units in Kolkata Metropolis Area."

References

Census of India (2001) Size, growth rate and distribution of population, Provisional Population Totals, Chapter 3, Series 1, Paper 1, India

Central Statistical Organization (1999a) Statistical Abstract of India, Ministry of Statistics and Programme Implementation, Government of India, New Delhi

Central Statistical Organization (1999b, 2000) Compendium of Environment Statistics, Ministry of Statistics and Programme Implementation, Government of India, New Delhi

Chatterjee S, Dhavala K, Murty MN (2005) Estimating cost of air pollution abatement for road transport in India: Case studies of Andhra Pradesh and Himachal Pradesh, MPRA (Munich Personal RePEc Archive). Retrieved from http:// mpra.ub.uni-muenchen.de/ 1691/ MPRA Paper No. 1691 on 24/4/2008

Directorate of Census Operation (2001) WB/Statistical Abstract 2002–2003

ECMA (2008) Emission Controls Manufacturers Association. Retrieved from http://www.ecmaindia. com/indian.html on 14/2/2008

Jana BK, Roy P, Mazumdar A (2007) An observation on GHG emission with special emphasis on human respiration. J Ind Assoc Environ Manage 34(3):188–194

Jana BK, Roy P, Mazumdar A (2008) Advanced vehicular technology and improved fuel quality mitigating CO_2 emission from vehicular exhaust: a case study on Kolkata. Ind J Environ Prot 28(8):676–682

Lewis P (2006) Canadian meteorological centre in Dorval, Quebec, Canada, Earth Day, April 22, Published in CMOS, Bulletin SCMO, vol 34, No. 4

M/O Health & F.W., GoI (March 2006) Retrieved from http://mohfw.nic.in/NRHM/State%20 Files/wb.htm and RHS Bulletin on 24/10/2007

Mashlekar Committee Report (2002)

McKinney ML, Schoch RM (2003) Environmental science system and solutions, 3rd edn. Jones & Bartlett, Boston, MA, pp 30–33

Pant KC (2001) Task force on integrated transport policy

Parkes M (2006) Breath-holding and its breakpoint. Exp Physiol 91(1):1–15

Population Reference Bureau (PRB) (2001) World population data sheet. Washington, DC

Ramey CA, Ramey DN, Hayward JS (2001) Dive response of children in relation to cold water near drowning. J Appl Physiol 001; 62(2):665–668; Diana Hacker (Bedford/St. Martin's, Boston, 2002). Adapted from Victoria E. McMillan, Bedford/St. Martin's, Boston

Rodriguez-Iturbe I, Porporato A (2004) Ecohydrology of water- controlled ecosystems: soil moisture and plant dynamics. Cambridge University Press, Cambridge, MA

SIMA (2008) Society of Indian automobile manufacturers. Retrieved from http://www.siamindia. com/scripts/emission-standards.aspx on 12/1/2008

Statistical Handbook (1999) Bureau of Applied Economics & Statistics, Government of West Bengal

Statistical Abstract (2005–2006) Government of West Bengal

Transport Fuel Quality Report (2005) Central Pollution Control Board, Delhi

West Bengal Pollution Control Board, India–Canada Environment Facility Project, Kolkata (2006) Assessment of social and environmental impact of fuel conversion in coal fired small boilers and ceramic kilns in Kolkata metropolitan area. Pollution prevention and waste minimization of small scale industrial units in Kolkata Metropolis Area

Chapter 2
Impact of Climate Change on the Availability of Virtual Water Estimated with the Help of Distributed Neurogenetic Models

Mrinmoy Majumder, Sabyasachi Pramanik, Rabindra Nath Barman, Pankaj Roy, and Asis Mazumdar

Abstract Impact of climate change on virtual water of a tropical multireservoir system was estimated with the help of models developed by neural network and genetic algorithm. Virtual water or embedded water or embodied water, or hidden water refers to the water used in the production of goods or services. For instance, it takes 1,300 m³ of water on an average to produce 1 t of wheat. The precise volume can be more or less depending on climatic conditions and agricultural practice. The virtual water has major impacts on productive use of water and global trade policy especially in water-scarce regions.

M. Majumder (✉)
Senior Research Fellow, School of Water Resources Engineering, Jadavpur University, Kolkata-700032, West Bengal, India
and
Geo-information Scientist, Regional Center, National Afforestation
and Eco-development Board, Jadavpur University, Kolkata-700032, West Bengal, India
e-mail: mrinmoy@majumder.info

S. Pramanik
Assistant Engineer, Durgapur Projects Limited, Bardhaman, West Bengal, India
and
Former PG Student, School of Water Resources Engineering, Jadavpur University, Kolkata-700032, West Bengal, India

R.N. Barman
Pertime Research Fellow, School of Water Resources Engineering, Jadavpur University, Kolkata-700032, West Bengal, India
and
Assistant Professor, Department of Production, National Institute of Technology, Agartala, Tripura, India

P. Roy
Lecturer, School of Water Resources Engineering, Jadavpur University, Kolkata-700032, West Bengal, India

A. Mazumdar
Coordinator, Regional Center, National Afforestation and Eco-development Board, Jadavpur University, Kolkata-700032, West Bengal, India
and
Director, School of Water Resources Engineering, Jadavpur University, Kolkata-700032, West Bengal, India

The impact of climate change on virtual water could open a path for the efficient use of virtual water in the face of climatic uncertainties, which may directly impact availability of raw water. The present study tried to estimate the future virtual water with the help of neurogenetic models, which estimates stream flow as function of various hydrological, meterological variables, and basin characteristics. The models prepared were distributed in nature and also consider temporal variability. In total, two models were prepared with rainfall, time of concentration, and catchment loss as input and stream flow as output. One model was prepared by classifying the dataset, based on the magnitude of the variable, and the other model was prepared with normal dataset. First, the better performing model was identified and then output from RCM-PRECIS model was applied to the chosen model to estimate the impact of climate change on stream flow. The estimation results were used to calculate the amount of virtual water, and the result was compared with the present-day virtual water to analyze the change in virtual water availability due to climate change. According to the results, model prepared with normal dataset was identified as a better model, and from the estimations it could be concluded that virtual water availability would increase in case of both A2 and B2 scenario of climate change where the change would be more pronounced in case of the latter.

Keywords   Climate change • water availability • virtual water • neurogenetic models

2.1   Introduction

Global warming is defined as a natural or human-induced increase in the average global temperature of the atmosphere near the Earth's surface. The earth as a planet is a complex combination of many elements, which constitute the solid earth, atmosphere, biosphere, cryosphere, and the hydrosphere. These components interact with each other in a nonlinear manner involving the feedbacks of energy, mass, and momentum. The energy is derived from the sun in the form of short-wave solar radiation, which penetrates the Earth surface with little loss of energy in transit. In the process, the heated Earth emits thermal or long-wave radiation outward, which mostly gets absorbed by the atmospheric constituent. Water vapor and several other gases including carbon dioxide, methane, and CFCs warm the Earth's atmosphere because they absorb and remit radiations. They trap some of the heat energy radiations from the Earth's atmospheric system. The trapping or warming is somewhat analogous to a greenhouse, which also traps heat; thus, the process has been called the greenhouse effect. The excessive increase in the concentration of green house gases (GHGs) makes the atmosphere warmer, which in turn induce the climate to change.

2.1.1   Impact of Global Warming

The effect of global warming is now predominant in many parts of the world. Twelve warmest years have occurred in 1900s among which 10 have occurred between 1987

and 1998. The energy availability, which was increased due to increase in temperature, had created a ripple effect throughout the Earth system with local, regional, and global positive feedbacks feeding on each other to amplify and accelerate warming (Stewart et al. 2006). Abnormality in climatic pattern, induced by the accelerated warming, had started to effect catchment-specific hydrologic cycles. In the last 10 years, floods have caused more damage than in the previous 30 years. Higher temperatures lead to a higher rate of evaporation and very dry conditions in some areas of the world. Severe weather events are now more common. The number and strength of hurricanes, tornadoes, and other events had increased over the last 15–20 years. As per IPCC (2007), global climate change is expected to affect the performance of water resource systems according to current indicators and findings.

2.1.2 Climate Models

The uncertainty in the climatic pattern had made the estimation of future climate more complex. Global Climate Model (GCM) were widely used to estimate future climatic parameters, but the complexity of the present climatic pattern had forced many modifications. HadCM2 AOGCM model was developed by Met Office Hadley in 1994 and its successor, HadCM3 AOGCM (Atmosphere-Ocean General Circulation Models), was published in 1998. AOGCM coupled with an atmospheric chemistry model, which can predict the changes in the concentration of other atmospheric constituents in response to climate change and to the changing emissions of various gases was later built on 1999. In HadCM3, thermohaline circulation, ventilation, and vertical mixing of chemical constituents along with decadal variability in the ocean were included.

Local climate change is influenced greatly by local features such as mountains, which are not well represented in global models (GCMs) because of their coarse resolution, and models of higher resolution could not practically be used for global simulation for long periods of time due to spatial variance of the considered parameters. These problems were tried to be mitigated with the help of regional climate models (RCM). The RCM had higher resolution (typically 50 km) were constructed for limited areas and allowed to run for shorter periods (20 years or so). The Met Office Hadley Centre had run RCMs for three regions: Europe, the Indian subcontinent, and southern Africa and had developed an RCM to run on PCs for any region as part of a regional climate modeling system called "Providing REgional Climates for Impacts Studies (PRECIS)."

PRECIS is based on the Hadley Centre's regional climate modeling system. It has been ported to run on a PC (under Linux) with a simple user interface, so that experiments can easily be set up over any region. PRECIS was developed in order to help generate high-resolution climate change information for as many regions of the world as possible. The intention is to make PRECIS freely available to groups of developing countries in order that they may develop climate change scenarios at national centers of excellence, simultaneously building capacity and drawing on local climatological expertise. These scenarios can be used in impact, vulnerability, and adaptation studies, and to aid in the preparation of National Communications, as required under Articles 4.1 and 4.8 of the United Nations Framework Convention on Climate Change. A more detailed description of climate models was given in Chapter 23.

The estimations from these climatic models were applied to hydrologic models to estimate the future impacts of climate change on different hydrologic parameters as explained in the next section.

2.1.3   Coupled Climatic and Hydrologic Models

A dynamic downscaling method, referred as pseudowarming, was used by Fujihara et al. (2008) to connect the output of raw general circulation models (GCMs) into river basin hydrologic models, which was applied to explore the potential impact of climate change on hydrology and water resources of the Seyhan River Basin in Turkey. The results showed that the decreased precipitation as formulated by the climate model would result in a considerably decreased inflow and time of peak. Hotchkiss et al. (2000) predicted the changes in global river flow under the IPCC SRES A1B and A2 scenarios found from HadGEM1-TRIP model and concludes that there will be significant change in the seasonality of river flow, such as earlier peaks in spring runoff, large increases in monthly maximum flow, and decreases in monthly minimum flow. Climatologic data bases (SICLIM and CLICOM) built by the Servicio Meteorológico Nacional (SMN) of Mexico (Mendoza et al. 2008) were fed to a hydrologic model to predict the annual volume of superficial available water. A climate variability indicator (the El Niño-Southern Oscillation, ENSO) was applied by Muluye and Coulibaly (2007) to predict seasonal reservoir inflows. GCM, CGCM2, CSIROMk2, and HadCM3 was applied by Merritt et al. (2006) to estimate future water availability of Okanagan Basin in England. Each of the research work advocates decrease in quantity of water as the common effect of climate change.

2.1.4   Application of Computer Models in Hydrology

The complexity of interrelationship of hydrometeorological parameters enforced hydrologic engineers to employ computer models with conditional variability to estimate future pattern of important hydrological parameters such as reservoir inflow (El-Shafie et al. 2007); Long et al. 2007); Kim et al. 2007), reservoir operation (He et al. 2008), and reservoir optimization (Wei and Hsu 2007; Majumder et al. 2007; Eslami and Mohammadi 2002; Xu and Li 2001; Luo and Weiss 2002). Single-event models such as HECHMS, TR55, MODRAT, etc., were widely employed by many engineers all over the world. A detailed description about hydrologic models is given in Chapter 21.

2.1.4.1   Application of Artificial Neural Network in Hydrology

In recent years, artificial neural networks (ANNs) had been successfully applied in forecasting of time series problems. As ANNs offer a relatively quick and flexible means of modeling, the application of ANN modeling was widely reported in various hydrological

literatures (Zhang and Stanley 1999; Neelakantan and Pundarikanthan 2000; Ray and Klindworth 2000) such as for rainfall–runoff modeling (Hsu et al. 1995; Fernando and Jayawardena 1998; Tokar and Johnson 1999; Elshorbagy et al. 2000; Liong et al. 2001), for stream flow prediction (Clair and Ehrman 1998; Imrie et al. 2000), for reservoir inflow forecasting (Jain et al. 1999; Coulibaly et al. 2000), and for water quality parameters (Maier and Dandy 1999). All the papers reported high degree of satisfaction and advocates for neural network as a promising alternative for improved hydrologic predictions. For a more detail description about neural network and genetic algorithm refer Chapter 22.

2.1.4.2 Virtual Water and Its Impacts

Water-scarce countries like Israel discourage the export of oranges (relatively heavy water guzzlers) precisely to prevent large quantities of water being exported to different parts of the world. In recent years, the concept of virtual water trade has gained weight both in the scientific and in the political debate. The notion of the concept is ambiguous. It changes between an analytical, descriptive concept and a political induced strategy. As an analytical concept, virtual water trade represents an instrument, which allows the identification and assessment of policy options not only in the scientific, but also in the political discourse. The data that underlie the concept of virtual water can readily be used to construct water satellite accounts, and brought into economic models of international trade such as the GTAP Computable General Equilibrium Model (Berrittella 2007). Such a model can be used to study the economic implications of changes in water supply or water policy, as well as the water resource implications of economic development and trade liberalization. In sum, virtual water trade allows a new, amplified perspective on water problems.

In the framework of recent developments from a supply-oriented to a demand-oriented management of water resources it opens up new fields of governance and facilitates a differentiation and balancing of different perspectives, basic conditions, and interests. Analytically, the concept enables to distinguish between global, regional, and local levels, and their linkages. This means that water resource problems have to be solved in problemsheds (Allan 1998) if they cannot be successfully addressed in the local or regional watershed. Virtual water trade can thus overcome the hydro-centricity of a narrow watershed view.

2.1.4.3 Limitations of Virtual Water Concept

The virtual water concept proposed by Allan has some serious shortcomings, which could impact the conclusions found from trend analysis of virtual water. The next section highlights a few of the major limitations:

1. The virtual water concept assumes all sources of water, whether in the form of rainfall or provided through an irrigation system, is of equal value.
2. Implicitly assumes that water that would be released by reducing a high water use activity would necessarily be available for use in a less water-intensive activity.
3. Fails as an indicator of environmental harm.

2.1.5   Objective and Scope

The model in the present study was prepared to estimate stream flow with the help of ANN and input variables like rainfall, time of concentration, and loss coefficient. The output from climatic model, RCM-PRECIS, was then applied to the model to estimate the impact of climate change on stream flow. The soil condition, land use and bed slope, travel length of water, and distance from the catchment centroid was calculated with the help of remote-sensed images of the study area and GIS. The land use and soil conditions were used to calculate loss coefficient of the catchment. The bed slope, length of water travel, and length from the centroid to the river was applied to calculate time of concentration with the help of Bend County method. Groundwater balance was included with hydrological variables along with water level. In climatological variables rainfall of each of the gauge station and distributed rainfall from TYNDAL dataset for ungauged stations were used in the development of the model. In case of reservoirs, reservoir storage along with reservoir level was included in the hydrological variables. The estimated stream flow from the model was used to calculate virtual water, that is, the amount of water used in the industries within the catchments. Basin discharge of a station is added to the same of next station after removing channel loss to get the discharge of the next station. The channel loss was calculated by dividing area of sediments from total area of the channel between two gauge stations and subtracting the result from 1. In case of reservoirs, monthly values of storage coefficient were calculated and multiplied with the basin discharge of the same place to get the actual discharge of the location. The storage coefficient was calculated with the help of storage-discharge routing or modified pulse routing method. The result is normalized to estimate the storage coefficient. In summary, it may be said that the main objective of the study was to estimate the availability of virtual water in face of climatic uncertainties but scopes of the study included estimation of stream flow, loss coefficient, and channel loss with the help of GIS along with estimation of storage coefficient with the help of Modified Pulse Routing.

2.1.6   Study Area

The impact of climatic uncertainties on availability of virtual water was shown on two major river networks of East India, Damodar and Rupnarayan. Both the river networks have many industries within their catchment. A detailed description of the two river networks and its industrial status are given in Chapter 25.

2.2   Methodology

The present study developed two models to predict stream flow of the gauged and ungauged catchments of rivers Damodar and Rupnarayan for 2010–2100, according to A2 and B2 scenario of climate change (Chapter 23). The predicted stream flow

was later applied to the equation of water availability and from the water availability, amount of available virtual water was determined.

Neural network was used to prepare the two models, whereas genetic algorithm was applied to find the most suitable network architecture. The model was trained with three types of training algorithms to identify or learn the encoded pattern within considered input and output variables. The better trained model was identified with the help of three performance validation criteria. The selected model was calibrated by comparing with the observed stream flow data and validated with the output from HECHMS, TR55, and MODRAT model.

2.2.1   Neurogenetic Spatially Distributed Rainfall–Runoff Model (NSRRM)

2.2.1.1   Model Variables of NSRRM

The NSRRM was developed to consider the influence of metereologic and hydrologic variables along with basin characteristics upon basin runoff. Peak average monthly rainfall of 32 years (1970–2002) and 12 months, monthly time of concentration, and monthly variation of loss coefficient of the basins at 42 sampling points were used to predict peak average monthly basin runoff at the same 42 selected sampling points. In Neurogenetic models, inputs are multiplied with a weightage and then summed to estimate the output after going through an activation function. If differences exist between estimated and desired output the operation is repeated again with updated weightage value until and unless the estimated and desired output becomes equal or a desired root mean square error (RMSE) calculated with the help of the two values is achieved. That is why, in the present model, peak rainfall, time of concentration, and loss coefficient were multiplied and used as input. The same value was subtracted from peak discharge and the difference was used as output variable of the present model so that during the iteration procedure, less computational energy and time was required to learn the problem.

Determination of Peak Average Monthly Rainfall and Runoff

The peak average monthly rainfall or runoff was calculated with the help of daily rainfall and runoff dataset for 32 years (1970–2002). As there were 42 sampling points, and if datasets for each of the sampling points were considered, the size of dataset becomes too large (483,840) for the computational facilities available for the present study. Hence, monthly average values were calculated for each month of each year, from which peak average monthly values were taken as the dataset of present study. In this procedure, size of the dataset becomes 505, which was possible for the computational facilities available for the present study and also reduces the amount of time required to develop the models.

Determination of Basin Loss Coefficient

SPOT imageries collected from different years and months of the sampling points and within 15/15 km grid around the channel was processed with a commercial software. The images were classified according to the DN values of different geographical features so that pixel with same DN values gets categorized into a single class. The DN values of different geographical features were identified and used to categorize the images into classes of different geographical features. Common geographical features of the study area includes forest, cropped and noncropped agricultural fields, ponds, industrial areas, mines, roads and pavements, etc. The area of each geographical class was calculated and divided from the total area. A weighted average of the output of each geographical class was determined where a feature with high runoff retention capacity like forest, pond, etc., was given lower weightage and feature with low runoff receptivity was given higher value of weightage. The result is subtracted from 1 to get the loss coefficient. Imageries of different months and years were used to determine loss coefficient of different months and years. The values were then averaged to get the average monthly loss coefficient of sampling points.

Determination of Channel Loss Coefficient

The channel loss was calculated with the help of the concept utilized to determine loss coefficient. Instead of geographical features of a basin, same of the channels were considered. Channels may have sand dunes and/or agricultural fields. Sand dunes are known to have higher infiltration capacity than agricultural fields. The same weighted average method was used to calculate loss coefficient of channels. Imageries of different months and years were collected to determine channel loss of different months and years.

Determination of Loss Coefficient

The channel loss coefficient along with basin loss coefficient was averaged to estimate the loss coefficient at the sampling points.

Calculation of Time of Concentration

Time of concentration was calculated with the help of Fort Bend County (Wanielista et al. 1997) method. The value of the inputs like length of longest flow path, average slope along longest flow path, average basin slope, and percentage impervious area were calculated with the help of GIS. Fort Bend County method was expressed by the following equation:

$$t_c = 48.64 \times \left(\frac{L}{S^{0.5}}\right)^{0.57} \times \mathrm{Log}\left(\frac{S_0}{S_0^{0.11} \times 10^I}\right) \tag{1}$$

where t_c is the time of concentration (h), L is the length of longest flow path (mi), S is the average slope along longest flow path (ft/mi), S_0 is the average basin slope (ft/mi), and I is the percent impervious area.

Fort Bend County method can be used for calculation of time of concentration only if the area of the catchment is within 0.13–400 mi^2, the longest flow path lies between 0.5 and 55 mi, slope along the longest flow path will lie in between 2 and 33 ft/mi, and the average basin slope will lie within 3–80 ft/mi. As all the subwatersheds considered in the present study satisfy the above conditions, Fort Bend County method was utilized for estimation of time of concentration (Wanielista et al., 1997).

2.2.1.2   Model Development

Three 2.1 input–1 output variable neurogenetic models were developed and trained with QP, CGD, and BBP algorithm, which were respectively named as NSRRMQP, NSRRMCGD, and NSRRMBBP.

Table 2.1 showed the input and output variables of NSRRM hydrologic models and Fig. 2.1. depicts the overview of model algorithm.

2.2.2   Categorized Neurogenetic Spatially Distributed Rainfall–Runoff Model (CNSRRM)

The CNSRRM model was developed similar to NSRRM model except the datasets used for training the neural models were categorized into different groups. Neurogenetic models were found as a better learner of a problem when grouped data were used for training the models. Thus, the dataset was grouped and used to develop another kind of neurogenetic model.

2.2.2.1   Model Variable

Input variables for CNSRRM model were selected as grouped dataset of peak average monthly rainfall of 12 months and 32 years, monthly time of concentration,

Table 2.1 Table showing input and output variables used for the NSRRM model

Input	Abbreviation
Output	Abbreviation
Product of peak average monthly rainfall (P), time of concentration (t_c), and loss coefficient (L_c)	$p\{P, t_c, L_c\}$
Difference between peak average monthly basin runoff (Q) and product of average monthly rainfall (P), time of concentration (t_c), and loss coefficient (L_c)	$F[Q - \{P, t_c, L_c\}]$
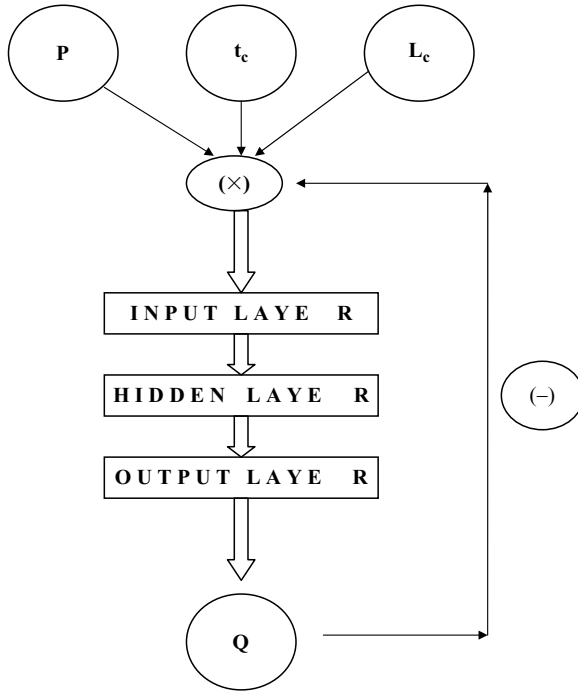
Fig. 2.1 Chart showing algorithms adopted to develop the NSRRM models

and monthly variation of loss coefficient at 42 sampling points. The output variable was selected as peak average monthly basin runoff. The dataset of the output variable was not categorized.

For the CNSRRM model, each variable was encoded into six classes in the following way:

1. The variable dataset was ranked in a descending order according to magnitude.
2. If the rank of a data was less than 5, then the data would cluster into HP class.
3. If the rank of a data was less than 25 and greater than 5, then the data would cluster into P class.
4. If the rank of a data was less than 50 and greater than 25, then the data would cluster into MP class.
5. If the rank of a data was less than 250 and greater than 50, then the data would cluster into MT class.
6. If the rank of a data was less than 500 and greater than 250, then the data would cluster into T class.
7. Remaining dataset was clustered into HT class.

The class/group notation HP, P, and MP separates the peak values from smaller values of the variable, which were again separately denoted by MT, T, and HT.

Table 2.2 shows the input and output variables of CNSRRM Hydrologic models and Fig. 2.2. depicts the overview of model algorithm

Table 2.2 Table showing input and output variables used for the CNSRRM model

Input	Abbreviation
Output	Abbreviation
Peak average monthly rainfall (P), time of concentration (t_c), and loss coefficient (L_c). (Dataset of all the variables were grouped into six classes according to their magnitude.)	P, t_c, L_c
Peak average monthly basin runoff (Q)	Q
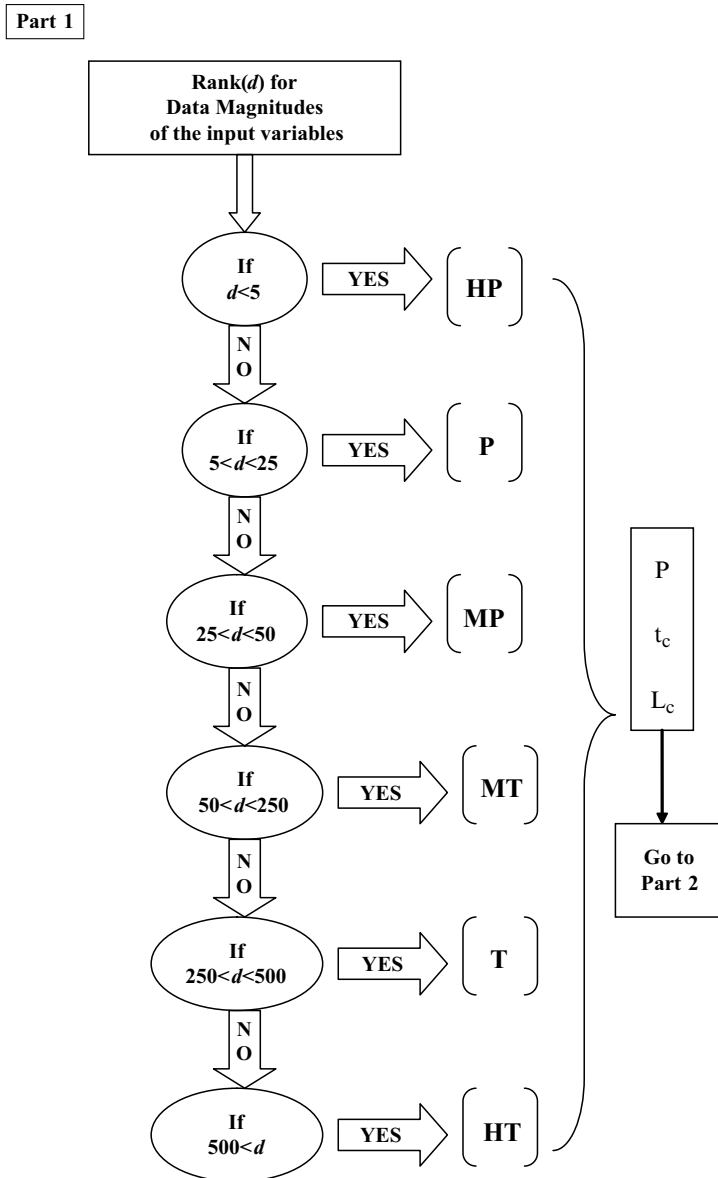
Fig. 2.2 *Part 1*: flowchart showing the conditions used for categorizing the dataset. *Part 2*: flowchart showing the architecture and dataflow of CNSRRM models
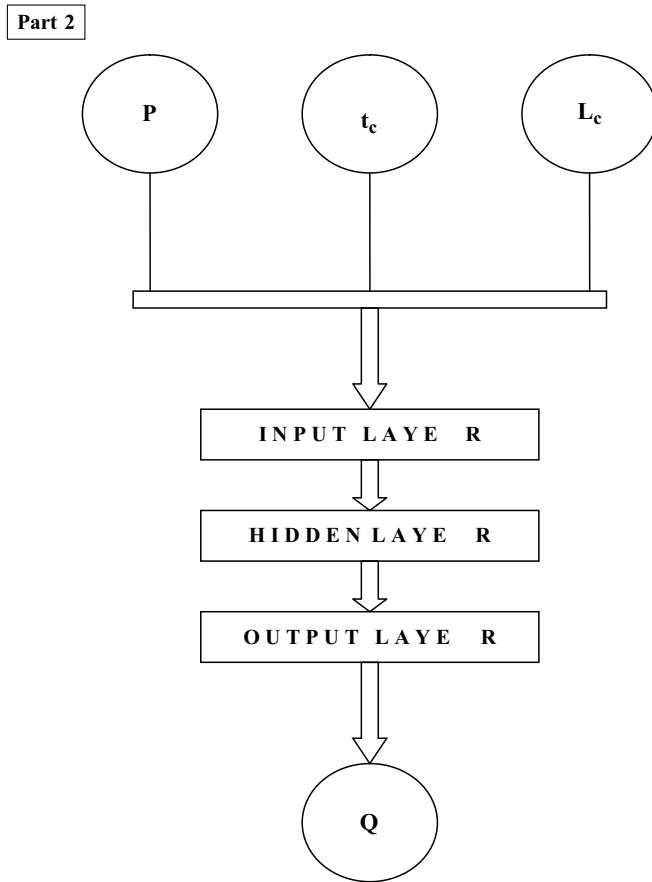
Fig. 2.2 (continued)

2.2.3 Model Validation and Uncertainty Analysis

The discharge from the sampling points was also estimated with the help of HECHMS, TR55, and MODRAT hydrologic model. The output from the three considered conceptual models along with neurogenetic models and observed discharge data were compared to calculate the RMSE (2.2), correlation coefficient (*r*) (2.3), coefficient of efficiency (*E*) (2.4), and first-order uncertainty analysis (*U*) (2.5) of the models. The values would help in selection of the better model among the six models considered in the present study.

$$RMSE = \sqrt{\sum_{n=1}^{n} \frac{(T_p - O_p)^2}{n}} \qquad (2)$$

$$\text{Correlation coefficient} = \sqrt{\frac{\sum (T_p - T_m)(O_p - O_m)}{\sqrt{\sum_1^n (T_p - T_m)^2 \sum_1^n (O_p - O_m)^2}}} \qquad (3)$$

$$\text{Coefficient of efficiency} = 1 - \frac{\sum_{n=1}^n (T_p - O_p)^2}{\sum_{n=1}^n (T_p - T_m)^2} \qquad (4)$$

$$\text{First - order uncertainty}(U) = \left(\frac{Stdev(O_p - O_m)}{n}\right) \qquad (5)$$

where T_p is the target data value for the pth pattern; O_p is the estimated data value for the pth pattern, T_m and O_m are the mean of target and estimated datasets, respectively, and n is the total number of patterns. T_n is the target value of the nth pattern and T_m is the mean value of the targeted dataset.

Correlation coefficient could also be taken as a measure of model reliability whereas coefficient of efficiency was also used as a measure of model sensitivity (Das 1991) toward observed dataset. Hence, both of these validation criteria also help to determine model reliability and sensitivity where high values would represent greater level of reliability and sensitivity of the model.

2.3   Result and Discussion

According to the comparison results given in Table 2.3, RMSE of CNSRRMBBP was found to be 3.00, which was less than any other models. The RMSE of NSRRMQP (3.42), NSRRMBBP (3.44), and NSRRMCGD (4.15) models were found to have the nearest value to RMSE of CNSRRMBBP. But the model reliability or correlation coefficient (0.64) of CNSRRMBBP was found to better than only CNSRRMCGD (0.61). All the other four models had better correlation coefficient than the latter, like, NSRRMQP, NSRRMCGD, and NSRRMBBP had correlation coefficient equal to 0.98, 0.97, and 0.98, respectively. The efficiency of CNSRRMBBP was found to be 0.82, which was less than the other five models considered for the present study where NSRRMQP had better efficiency (0.99) than any other models. NSRRMQP model was found to have only 8.5% uncertainty, whereas the same for CNSRRMBBP was found to be equal to 8.82%. As NSRRM had higher efficiency, second highest correlation coefficient and minimum uncertainty than the considered models of the present study, NSRRMQP was selected as the better model among the neurogenetic models developed for the present study.

If conceptual hydrologic models, like HECHMS, TR55, and MODRAT, were compared with the selected neurogenetic model, NSRRMQP was found to have

Table 2.3 Table showing the comparison of performance validation criteria and model parameters of the neurogenetic models

	NSRRMQP	NSRRMCGD	NSRRMBBP	CNSRRMBBP	CNSRRMQP	CNSRRMCGD
Model variables						
Input	$p\{P, L_c, T_c\}$	$p\{P, L_c, T_c\}$	$p\{P, L_c, T_c\}$	P, L_c, T_c	P, L_c, T_c	P, L_c, T_c
Ouput	$F[Q-\{P, L_c, T_c\}]$	$F[Q-\{P, L_c, T_c\}]$	$F[Q-\{P, L_c, T_c\}]$	Q	Q	Q
Model parameters						
Network topology						
Network type	Feed forward	Feed forward	Feed forward	Feed forward	Feed forward	Feed forward
Network structure	1,8,1	1,17,1	1,15,1	3,2,2,1	2,1,1	2,1,1
Network weight	16	34	30	12	3	3
Training dataset	80	80	80	80	80	80
Testing dataset	10	10	10	10	10	10
Validation dataset	10	10	10	10	10	10
GA parameters						
Population	100	100	100	50	50	50
Generation	150	150	150	100	100	100
Penalty	6	6	6	6	6	6
Crossover rate	0.8	0.8	0.8	0.8	0.8	0.8
Mutation rate	0.2	0.2	0.2	0.2	0.2	0.2
Stop training condition						
MSE	0.05	0.05	0.05	0.05	0.05	0.05
Iteration	200	200	200	200	200	200
Generalization loss	5	5	5	5	5	5
Training algorithm parameters						

Algorithm name	QP	CGD	BBP	BBP	QP	CGD
Activation function	Sigmoid	Sigmoid	Sigmoid	Tanh	Tanh	Tanh
Learning rule	Supervised	Supervised	Supervised	Supervised	Supervised	Supervised
Learning rate	0.8	NR	0.8	0.8	0.8	NR
Momentum	NR	NR	0.8	NR	NR	NR
Propagation coefficient	1.75	NR	NR	1.75	1.75	NR
Training and testing results						
RMSE (training)	5.78	9	8.15	5.78	6.56	6.78
RMSE (testing)	10.51	13.5	16.3	6.05	15.66	12.76
Training stop reason	Generalization loss	Generalization loss	Generalization loss	Generalization loss	Generalization loss	Generalization loss
Model estimation results						
RMSE	3.42	4.11	3.44	3.00	4.15	5.78
Relationship	0.98	0.97	0.98	0.64	0.74	0.61
Efficiency	0.99	0.97	0.98	0.82	0.97	0.98
Uncertainties (%)	8.5	9.79	8.77	8.82	8.89	8.98

Table 2.4 Table showing comparison of performance validation criteria of neurogenetic model with conceptual hydrologic models

Model name	RMSE	r	E	U (%)
NSRRMQP	3.42	0.98	0.99	12
HECHMS	5.45	0.67	0.78	15
TR55	6.78	0.65	0.68	20
MODRAT	10.12	0.71	0.58	45

better RMSE than HECHMS (5.45), TR55 (6.78), and MODRAT (10.12) (Table 2.4) hydrologic models. The efficiency of the neurogenetic model (0.99) was also found to be higher than the any of the considered conceptual models, HECHMS (0.78), TR55 (0.68), and MODRAT (0.58). The coefficient of relationship or reliability (0.98) of NSRRMQP was also found to be higher among the four considered models. The uncertainty analysis of all the four models revealed that NSRRMQP had the minimum uncertainty (12%) than the conceptual models where HECHMS, TR55, and MODRAT had an uncertainty of 15%, 20%, and 45%, respectively.

As NSRRMQP has higher r and E and lower RMSE and U than the three considered hydrologic models. NSRRMQP was selected as the model for the estimation of future basin runoff according to the A2 and B2 baseline climate change scenarios, which were collected from generation of weather scenarios by PRECIS climatic model.

Two types of neural models were prepared. Length of the furthest path from where droplets of water may reach length from the centroid of the catchment and slope were used to calculate time of concentration with the help of Bend County method. The loss coefficient, that is, the variable, which represents the loss of incoming water was also estimated with the help of remote sensing and GIS. The estimated rainfall, calculated time of concentration, and loss coefficient were used as input variables to build the neurogenetic models, which would give stream flow as output.

Virtual water was calculated from the data of industrial demand of the two river basins. The amount of water supplied to the industries as raw water for production of their products is actually the amount of virtual water present in the catchment.

The steel industries were found to be the highest consumer of such water in case of both the river basin according to the data collected from Damodar Valley Corporation followed by chemical and coal industries. Although, coal industries are found only in Damodar catchments. The paper industries developed around Rupnarayan catchment is the third biggest consumer of raw water. The thermal power stations also used water for generation of steam but major part of the water consumed is returned to the river.

Figure 2.3 shows the present variation of virtual water within the selected sampling regions. Figures 2.4–2.9 show the variation of virtual water along the selected sampling regions within the two river basins according to the estimation of NSRRMQP model. Figures 2.10–2.13 and Table 2.5 depict district-wise, state-wise, and basin-wise distribution of virtual water.
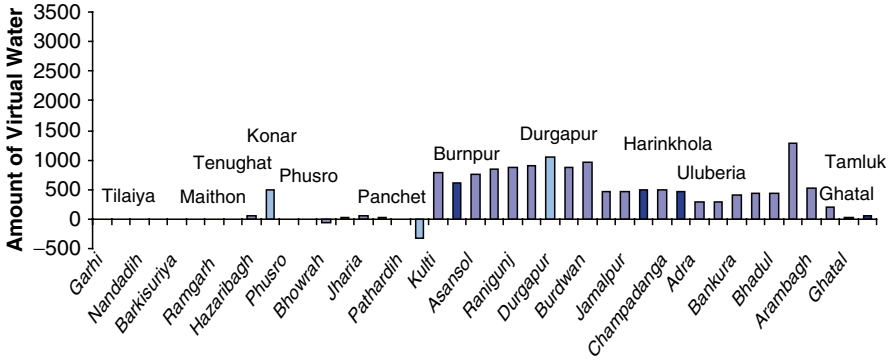
Fig. 2.3 Figure showing observed average available virtual water in different sampling regions considered in the present study (Note: columns with sky blue color represent virtual water of river junctions and columns with blue color represent virtual water at the reservoirs or barrages.)
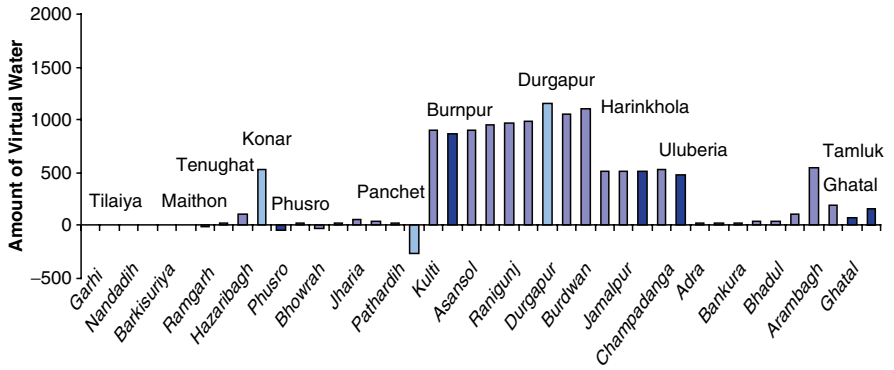
Fig. 2.4 Figure showing estimated available virtual water in different sampling regions considered in the present study from 2010 to 2040 in case of A2 scenario of climate change (Note: columns with sky blue color represent virtual water of river junctions and columns with blue color represent virtual water at the reservoirs or barrages.)
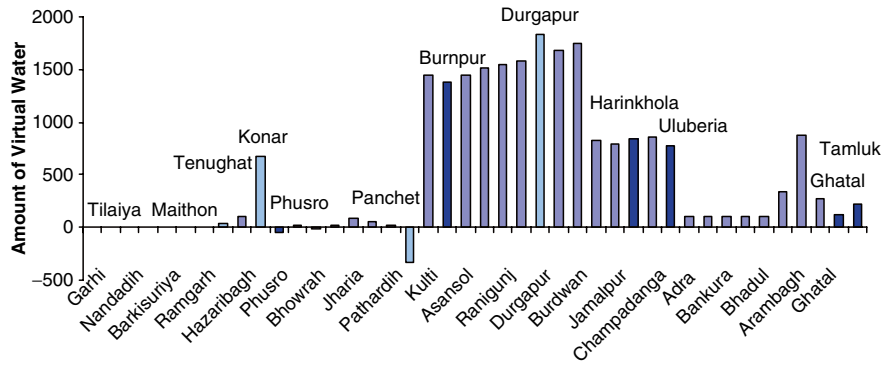
Fig. 2.5 Figure showing estimated available virtual water in different sampling regions considered in the present study from 2041 to 2070 in case of A2 scenario of climate change (Note: columns with sky blue color represent virtual water of river junctions and columns with blue color represent virtual water at the reservoirs or barrages.)

Fig. 2.6 Figure showing estimated available virtual water in different sampling regions considered in the present study from 2071 to 2100 in case of A2 scenario of climate change (Note: columns with sky blue color represent virtual water of river junctions and columns with blue color represent virtual water at the reservoirs or barrages.)
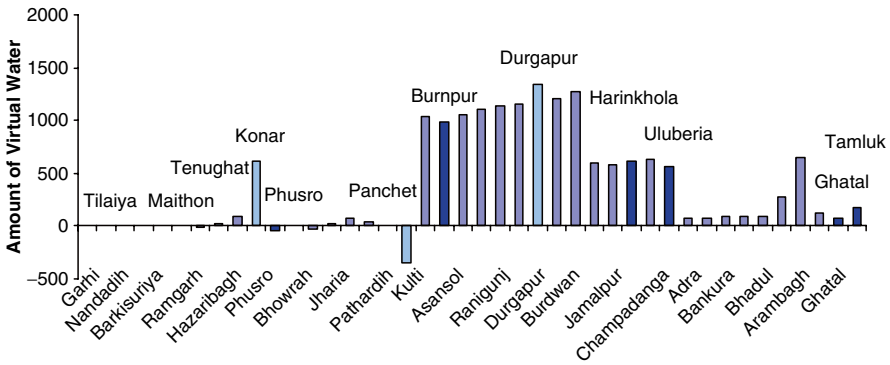
Fig. 2.7 Figure showing estimated available virtual water in different sampling regions considered in the present study from 2010 to 2040 in case of B2 scenario of climate change (Note: columns with sky blue color represent virtual water of river junctions and columns with blue color represent virtual water at the reservoirs or barrages.)

According to Table 2.5, Rupnarayan River Network and the state of Jharkhand would have more available virtual water in B2 scenario of climate change than in A2 scenario of climate change for 2010–2070 but from 2071 to 2100, the trend reverses where A2 scenario would have more available virtual water than B2 scenario. Similar but opposite trend was observed in Damodar River Network and state of West Bengal.

According to observed data of virtual water, West Bengal and Rupnarayan River Networks have more available virtual water than Jharkhand and Damodar River Networks. In the future, West Bengal would have more available virtual water than Jharkhand but when the two river networks were compared the trend would reverse in the future.
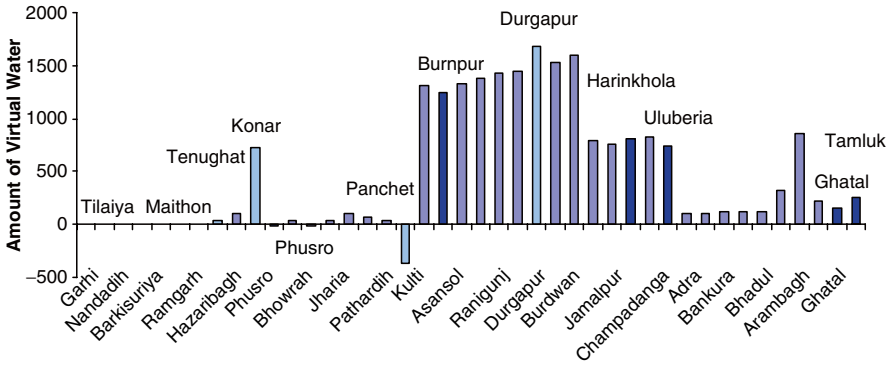
Fig. 2.8 Figure showing estimated available virtual water in different sampling regions considered in the present study from 2041 to 2070 in case of B2 scenario of climate change (Note: columns with sky blue color represent virtual water of river junctions and columns with blue color represent virtual water at the reservoirs or barrages.)
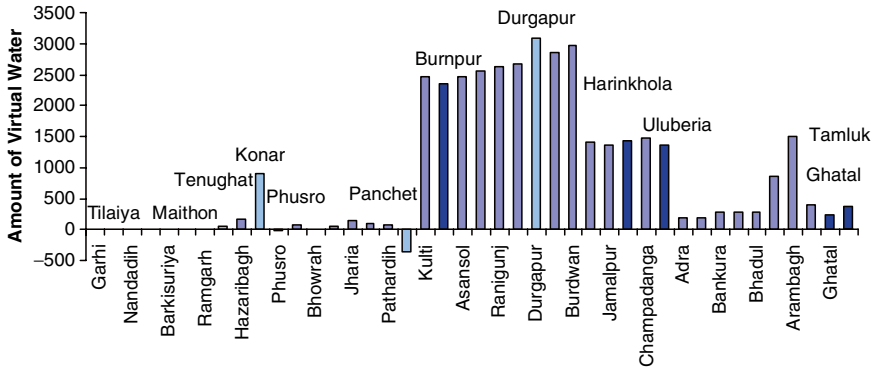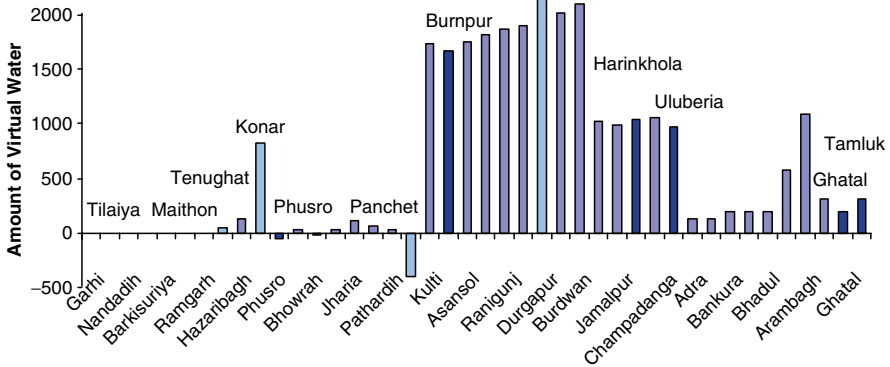

Fig. 2.9 Figure showing estimated available virtual water in different sampling regions considered in the present study from 2071 to 2100 in case of B2 scenario of climate change (Note: columns with sky blue color represent virtual water of river junctions and columns with blue color represent virtual water at the reservoirs or barrages.)

According to observed data of virtual water, Dhanbad, a district of Jharkhand, has a shortage and thus minimum amount of available virtual water and Hooghly, a district of West Bengal, has the maximum amount of available virtual water. The trend remains in the future from 2010 to 2100 for both the scenario of climate change except for 2071–2100 in A2 scenario of climate change when Jamtara becomes the district with minimum amount of available virtual water.

From Fig. 2.3, which represents the variation of virtual water within the sampling regions, it could be concluded that sampling regions of downstream than the same of upstream of both the river networks have more availability of virtual water. The trend remains that way from 2010 to 2100 though the magnitude of virtual water gets increased.
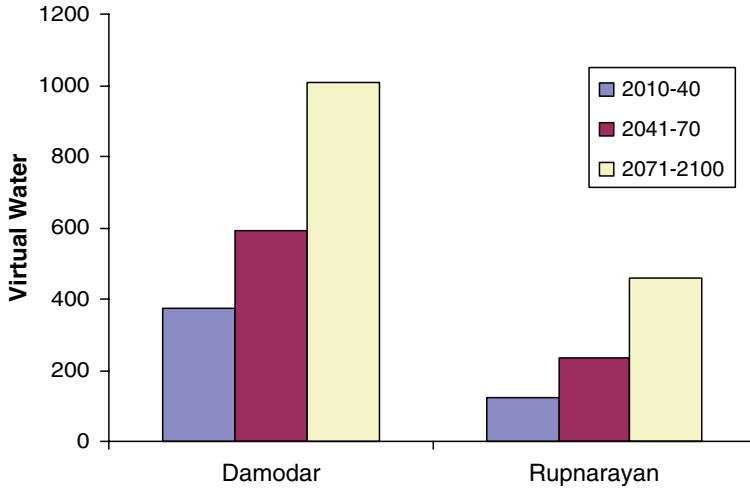
Fig. 2.10 Figure showing comparison of availability of virtual water in between Damodar and Rupnarayan Basins in case of A2 scenario of climate change
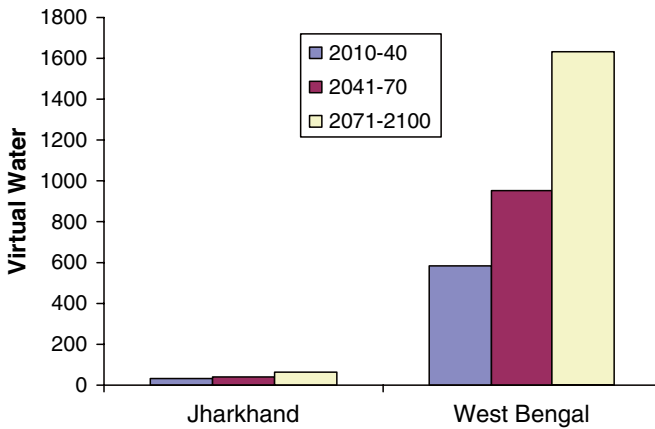
Fig. 2.11 Figure showing comparison of availability of virtual water within Jharkhand and West Bengal in case of A2 scenario of climate change

The above estimation of future availability of virtual water could be explained by the fact that virtual water availability is directly proportional to growth in industry. As industries are the only recipient of virtual water, if there is an increase in industrial consumer, the amount of virtual water will also increase. If the estimations of virtual water showed an increase in magnitude it could be concluded that there is a growth in industrial development and vice versa.
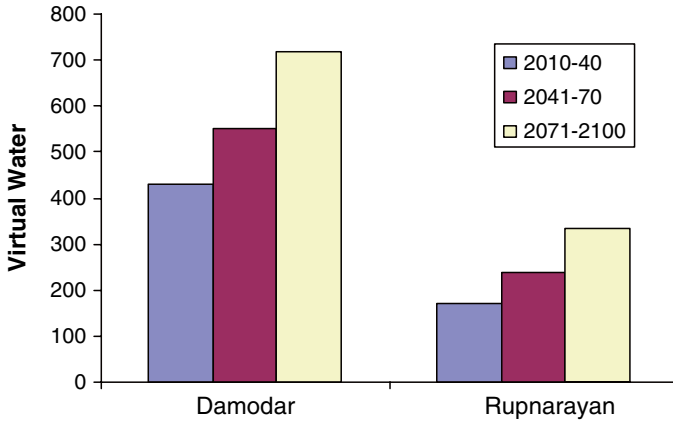
Fig. 2.12 Figure showing comparison of availability of virtual water in between Damodar and Rupnarayan Basins in case of B2 scenario of climate change
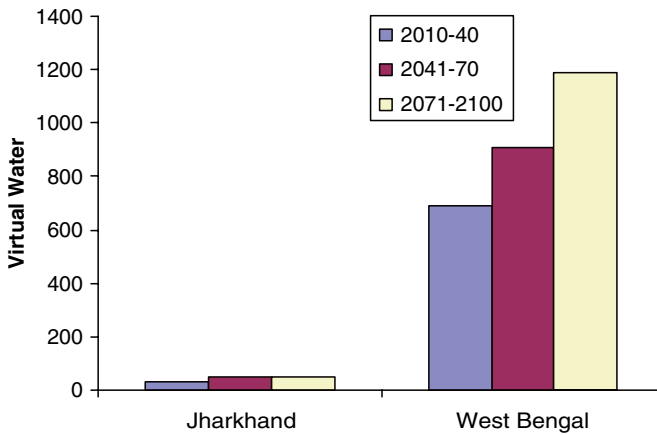
Fig. 2.13 Figure showing comparison of availability of virtual water within Jharkhand and West Bengal in case of B2 scenario of climate change

The districts of Burdwan and Hooghly of West Bengal and Hazaribagh districts of Jharkhand have a high concentration of industries like coal mines, steel, and paper, though industries, which consume maximum amount of water, as for example, steel, have a greater concentration in the former districts than the later. That is why, availability of virtual water is more in the districts of West Bengal (1,524.42 cm^3 in Hooghly) than in the district of Jharkhand (132.36 cm^3 in Hazaribagh).

Table 2.5 Table showing variation of virtual water within districts, states, and river basins due to A2 and B2 scenario of climate change

	A2 scenario			B2 scenario			Observed
Districts	2010–2040	2041–2070	2071–2100	2010–2040	2041–2070	2071–2100	1970–2002
State	2010–2040	2041–2070	2071–2100	2010–2040	2041–2070	2071–2100	1970–2002
Giridih	2.08	3.19	5.15	2.37	2.70	3.20	1.26
Jamtara	−0.79	−1.15	−0.92	−1.27	−1.08	−1.15	−0.51
Bokaro	1.10	1.73	2.78	1.18	1.51	1.73	0.35
Ranchi	11.80	14.60	25.60	12.04	22.00	17.78	4.47
Hazaribagh	196.71	245.76	344.30	218.79	272.23	299.37	132.36
Dhanbad	−18.70	−19.40	14.28	−35.41	−11.12	−22.86	−30.95
Burdwan	997.93	1,590.99	2,701.08	1,154.38	1,455.08	1,914.98	595.21
Hooghly	2,300.18	3,671.02	6,222.82	2,644.62	3,498.74	4,525.34	1,524.42
Howrah	487.23	781.95	1,359.69	571.73	747.64	973.00	327.69
Purulia	31.11	95.81	188.47	72.88	104.15	130.43	193.90
Bankura	46.70	150.96	374.22	121.78	155.34	259.23	392.67
West Midnapur	77.51	122.97	239.74	80.91	154.38	196.90	27.12
East Midnapur	151.89	229.47	365.49	174.93	261.17	310.75	44.43
Jharkhand	32.03	40.79	65.20	32.95	47.71	49.68	17.83
West Bengal	584.65	949.03	1,635.93	688.75	910.93	1,187.23	443.63
Basins	2010–2040	2041–2070	2071–2100	2010–2040	2041–2070	2071–2100	1970–2002
Damodar	373.02	591.11	1,010.30	429.36	552.56	716.54	223.91
Rupnarayan	124.20	235.62	457.03	172.15	237.19	333.67	273.04

2.4 Conclusion

The present study tried to estimate the impact of climate change on availability of virtual water of two subtropical river basins. The model estimation was carried out by the development of two types of neurogenetic models where input was treated as function of rainfall, time of concentration, and basin loss, and output was considered as difference between stream flow and product value of rainfall, time of concentration, and basin loss. The climate change impacts were analyzed with the help of rainfall data collected from A2 and B2 scenario of climate change generated by the PRECIS model and loss coefficient and time of concentration of the future were interpreted from IPCC fourth assessment report (2001). The predictions from the model, which were future stream flow, were used to calculate future availability of virtual water. According to the results, availability of virtual water would get increased in A2 scenario than in B2 scenario of climate change within the basins considered in the study. West Bengal would have more virtual water than Jharkhand, which actually follows the present trend of virtual water availability. The magnitude of virtual water showed increasing trend in both the scenario of climate change where the change is more pronounced in B2 than in A2 scenarios. As A2 baseline scenario was considered to be more economical than B2 and B2 scenario was considered to be more environmental than A2, the model results showed that becoming environmentally stable would actually be beneficial for virtual water, which also shows the industrial growth of a region. Hence, from the predictions, it could also be concluded that the future availability of water could mitigate the growing demand of water from the industries as model predictions of the sampling regions do not show a shortage of virtual water in any scenarios of climate change. As the models were developed with the help of neurogenetic algorithm, the model estimations were entirely based on the empirical relationship between the input and output variables. The models were also not flexible as it could only be used for the present two basins as neural models were data sensitive and would predict erroneously if data of one basin is applied to the other. Even with the above limitations, the selected model, NSRRMQP, had showed a relatively better accuracy of estimations (96.58%) than any other considered conceptual hydrologic models.

References

Allan JA (1998) Moving water to satisfy uneven global needs: 'trading' water as an alternative to engineering it, ICID Journal, 47(2):1–8. ISSN 0971-7412, September 1998

Berrittella M, Hoekstra AY, Rehdanz K, Roson R, Tol RSJ (2007) The economic impact of restricted water supply: A computable general equilibrium analysis, Water Research, 42: 1799–1813

Clair TA, Ehrman JM (1998) Using neural networks to assess the influence of changing seasonal climates in modifying discharge, dissolved organic carbon, and nitrogen export in eastern Canadian rivers. Water Resour Res 34(3):447–455

Coulibaly P, Anctil F, Bobee B (2000) Daily reservoir inflow forecasting using artificial neural networks with stopped training approach. J Hydrol 230(3–4):244–257

Das NG (1991) Statistical methods in commerce. Accountante and economics, M. Das & Co., Kolkata. Part – pp. 1.25–50

El-Shafie A, Taha MR, Noureldin AA (2007) Neuro-fuzzy model for inflow forecasting of the Nile River at Aswan high dam. Water Resource Manage 21(3):533–556

Elshorbagy A, Simonovic SP, Panu US (2000) Performance evaluation of artificial neural networks for runoff prediction. J Hydrol Eng 5(4):424–427

Eslami HR, Mohammadi K (2002) Application of ANN for reservoir inflow forecasting using snowmelt equivalent in the Karaj River watershed. Lowland Technol Int 4(2):17–26

Fernando DA, Jayawardena AW (1998) Runoff forecasting using RBF networks with OLS algorithm. J Hydrol Eng 3(3):203–209

Fujihara Y, Tanaka K, Watanabe T, Nagano T, Kojiri T (2008) Assessing the impacts of climate change on the water resources of the Seyhan river basin in Turkey. J Hydrol 353(1–2):33–48

He W, Chen J, Dai H (2008) Application of decision support system to the Three Gorges Reservoir operation. J Hydroelectric Eng 27(2):11–16

Hotchkiss RH, Jorgensen SF, Stone MC, Fontaine TA (2000) Regulated river modeling for climate change impact assessment: the Missouri River. J Amer Water Resource Assoc 36(2):375–386

Hsu K, Gupta HV, Sorooshian S (1995) Artifical neural network modeling of the rainfall-runoff process. Water Resour Res 31(10):2517–2530

Imrie CE, Durucan S, Korre A (2000) River flow prediction using neural networks: generalization beyond the calibration range. J Hydrol 233(3–4):138–154

IPCC (2007) Climate change 2007: the physical sciences basis, retrieved on http://ipcc-wg1.ucar.edu/wg1/wg1-report.html. on 30th April, 2009

Jain SK, Das A, Srivastava DK (1999) Application of ANN for reservoir inflow prediction and operation. J Water Resource Plan Manage 125(5):263–271

Kisi O (2004) Multilayer perceptrons with Levenberg–Marquardt training algorithm for suspended sediment concentration prediction and estimation. Hydrol Sci J 49(6):1025–1040

Kim Y-O, Eum H-I, Lee E-G, Ko IH (2007) Optimizing operational policies of a Korean multireservoir system using sampling stochastic dynamic programming with ensemble streamflow prediction. J Water Resource Plan Manage 133(1):4–14

Liong SY, Khu ST, Chan WT (2001) Derivation of Pareto front with genetic algorithm and neural network. J Hydrol Eng 6(1):52–61

Long ZQ, Zhang XH, Lin X-D, Chen ZJ (2007) Model for calculating benefit of forecasting intermediate inflow from downstream of reservoirs in water resources dispatch. J Hydraulic Eng 38(3):371–377

Luo W, Weiss E (2002) Evaluation of standard error of forecast of runoff volume using linear regression models. Can J Civil Eng 29(5):635–640

Majumder M, Roy P, Mazumdar A (2007) Optimization of the water use in the river Damodar in West Bengal in India: an integrated multi-reservoir system with the help of artificial neural network. J Eng Comput Architect 1(2) Online Journal: Article No. 1398

Maier HR, Dandy GC (1999) Empirical comparison of various methods for training feed-forward neural networks for salinity forecasting. Water Resour Res 35(8):2591–2596

Merritt WS, Alila Y, Barton M, Taylor B, Cohen S (2006) Hydrologic response to scenarios of climate change in sub watersheds of the Okanagan basin. Br J Hydrol 326:79–108

Mendoza VM, Villanueva EE, Garduño R, Nava Y, Santisteban G, Mendoza AS, Oda B, Adem J (2008) Thermo-hydrological modelling of the climate change effect on water availability in two hydrologic regions of Mexico. Royal Meteorological Society, Reading

Muluye GY, Coulibaly P (2007) Seasonal reservoir inflow forecasting with low-frequency climatic indices: a comparison of data-driven methods. Hydrol Sci J 52(3):508–522

Neelakantan TR, Pundarikanthan NV (2000) Neural network based simulation-optimization model for reservoir operation. J Water Resource Plan Manage 126(2):57–64

Ray C, Klindworth KK (2000) Neural networks for agrichemical vulnerability assessment of rural private wells. J Hydrol Eng 5(2):162–171

Stewart P, Le CF, Vemuri SR (2006) (Anticipated) Climate change impacts on Australia, Int J Ecol Dev 4:W06

Tokar AS, Johnson PA (1999) Rainfall-runoff modeling using artificial neural networks. J Hydrol Eng 4(3):232–239

US Army Corps of Engineers, Hydrologic Engineering Center (HEC). Hydrologic modeling system, HECHMS: technical reference manual. CPD-74B. US Army Corps of Engineers, Hydrologic Engineering Center, Davis, CA, http://www.hec.usace.army.mil/software/hec-hms/documentation/hms_technical.pdf, 2000

Wang QJ (1991) The genetic algorithm and its application to calibrating conceptual rainfall-runoff models. Water Resour Res 27(9):2467–2471

Wardlaw R, Sharif M (1999) Evaluation of genetic algorithms for optimal reservoir system operation. J Water Resour Plan Manage 125(1):25–33

Wang AP, Liao HY, Kou CH, Huang CY (2006) Artificial neural networks on reservoir inflows forecasting during typhoon season – a case in Taiwan. WSEAS Trans Math 5(4):416–422

Wei CC, Hsu NS (2007) Development of a real-time optimization model for flood control of a multipurpose reservoir. J Chinese Institute Civil Hydraulic Eng 19(3):355–365

Xu ZX, Li JY (2001) Short-term inflow forecasting using an artificial neural network model. Hydrological Processes, 16(12):2423–2439

Yitian L, Gu RR (2003) Modeling flow and sediment transport in a river system using an artificial neural network. J Environ Manage 31(1):122–134

Wanielista M, Kersten R, Eaglin R (1997) Hydrology: water quantity and quality control, 2nd edn. Wiley, New York

Zhang Q, Stanley SJ (1999) Real-time treatment process control with artificial neural networks. J Environ Eng 125(2):153–160

Chapter 3
Use of Forest Index or PLANOBAY in Estimation of Water Availability Due to Climate Change

Mrinmoy Majumder, Suchita Dutta, Rabindra Nath Barman, Bipal K. Jana, Pankaj Roy, and Asis Mazumdar

Abstract The present study tried to estimate future water availability with the help of Forest Index or *Plantation-Prioritized Basin Yield Estimation* (PLANOBAY) Hydrologic model, which is a multi-event, discharge prediction model based on variation of discharge with basin area and canopy cover. RCM-PRECIS model was applied to generate

M. Majumder (✉)
Senior Research Fellow, School of Water Resources Engineering, Jadavpur University, Kolkata-700032, West Bengal, India
and
Geo-information Scientist, Regional Center, National Afforestation and Eco-development Board, Jadavpur University, Kolkata-700032, West Bengal, India
e-mail: mrinmoy@majumder.info

S. Dutta
Research Assistant, Regional Center, National Afforestation and Eco-development Board, Jadavpur University, Kolkata-700032, West Bengal, India

R.N. Barman
Pertime Research Fellow, School of Water Resources Engineering, Jadavpur University, Kolkata-700032, West Bengal, India
and
Assistant Professor, Department of Production, National Institute of Technology, Agartala, Tripura, India

B.K. Jana
Senior Research Fellow, School of Water Resources Engineering, Jadavpur University, Kolkata-700032, West Bengal, India
and
Environmental Manager, Consulting Engineering Services, West Bengal, India

P. Roy
Lecturer, School of Water Resources Engineering, Jadavpur University, Kolkata-700032, West Bengal, India

A. Mazumdar
Coordinator, Regional Center, National Afforestation and Eco-development Board, Jadavpur University, Kolkata-700032, West Bengal, India
and
Director, School of Water Resources Engineering, Jadavpur University, Kolkata-700032, West Bengal, India

future weather scenarios. The observed rainfall along with Vegetated Area Index (VAIn) was used as input to estimate basin runoff. Presence of vegetated area (forest, plantations, cropped land) in any basin would impact the quantity of basin runoff as vegetated areas could hold water with greater capacity than any nonvegetated area. Hence the estimation of runoff from vegetated and nonvegetated catchment must differ and for former, models must include or consider the relationship between vegetated area and the amount of basin runoff. In PLANOBAY, VAIn represents the relationship between vegetated area and basin runoff. VAIn represented the variance of basin area and vegetated area with respect to basin runoff. A neurogenetic model was developed to identify the patterns associated with VAIn, rainfall, and basin runoff. Dataset of 3 decades (1970–2002) was employed to train the model. After the successful completion of training, models were compared with three conceptual models, namely, Hydrologic Engineering Centre – Hydrologic Modeling System (HECHMS), Trend Research Manual of 1955 (TR55), and MODified RATional (MODRAT) hydrologic model. The better model among the four was identified with the help of root mean square error (RMSE), correlation coefficient (r), coefficient of efficiency (E), and first-order uncertainty analysis (U). Future water availability was estimated with the help of estimated stream flow from the selected model, estimated rainfall from PRECIS climatic model-generated weather scenarios, and Water Budget equation. According to the results, PLANOBAY model was selected as better model among the four, and according to the estimations from the same model, future water availability of the two river basins would reduce for both A2 and B2 scenario of climate change where the water scarcity would be more pronounced in A2 than in B2.

Keywords Climate change • forest • global warming • neurogenetic models

3.1 Introduction

3.1.1 Forest Hydrology

Forest hydrology combines aspects of two separate disciplines: hydrology and forestry. Hydrology is the science that studies the waters of the Earth. Hydrology seeks to understand where water occurs, how water circulates, how and why water distribution changes over time, the chemical and physical properties of water, and the relation of water to living organisms.

Forestry is the science that seeks to understand the nature of forests and the interactions between the parts comprising a forest. Forest reserves are important as they protect and enhance water supplies, reduce flooding, and secure favorable conditions of water flow within the basin.

3.1.1.1 Forests and the Hydrologic Cycle

After precipitation, water flows over the surface as basin runoff into a stream, lake, or wetland. If a surficial aquifer is present and hydraulically connected to a surface-water

body, the aquifer can sustain surface flow by releasing water to it. During long dry spells, streams with a base flow component will keep flowing, whereas streams relying totally on precipitation will cease flowing.

A natural, expansive forest environment can enhance and sustain relationships in the water cycle because there are less human modifications to interfere with its components. A forested watershed helps moderate storm flows by increasing infiltration and reducing overland runoff. Further, a forest helps sustain runoff by reducing evaporation. Forests can help increase recharge to aquifers by allowing more precipitation to infiltrate into the soil, as opposed to rapidly running off the land to the downstream.

3.1.1.2 Water–Forest Interactions in Riparian Catchments

The riparian zone is broadly defined as the area between a body of water and the upland parts of the landscape that are rarely flooded except under the most extreme conditions. But the term also can refer more specifically to the immediate streamside area.

Riparian areas represent less than 10% of most forest ecosystems, yet these areas often are the most productive portions. Compared to upland regions, riparian areas have more water available, the vegetation is more robust, the soils are deeper, the timber often is of higher quality, and the water bodies have more shade. The riparian zone also may include wetlands bordering streams and lakes. This combination of factors makes riparian areas among the most heavily used portions of a forest. Riparian and wetland areas provide abundant and reliable forage for wildlife, as well as transportation corridors. They may also receive heavy human use for recreation.

3.1.1.3 Aquatic Biodiversity

Forest lands and waters are vitally important in maintaining *biodiversity* and providing *habitat* for fish and wildlife, including threatened or endangered aquatic species. In the USA, over one third of national forest lands are critical for maintaining aquatic biodiversity and protection of listed species.

For aquatic species, watersheds provide the basic unit of any conservation strategy. Many watersheds also contain isolated habitats with unique characteristics producing a high potential for rare species. Some species occur only near a single *spring* or in a single stream within a given watershed. Lands set aside to protect these unique habitats also benefit the entire watershed and its ecosystem.

3.1.1.4 Forest Management and Watershed Quality

Wind, fire, insects, and disease are all part of properly functioning, healthy ecosystems in watersheds. For example, natural fires, although temporarily devastating, periodically restore the balance between vegetation types, and release nutrients from the vegetation and soil. In contrast, widespread clear-cut logging and excessive or improper road building can degrade watersheds, like land uses such as ski runs and housing

projects. Many human activities can increase overland runoff, resulting in more erosion of the land surface and concurrently reducing the amount of water that soaks in the ground to potentially reach nearby streams or recharge underlying aquifers.

Moreover, fire prevention and suppression have created "imbalanced" forests with excessive amounts of undergrowth and dead vegetative matter that serve as fuels when fire does occur. Hence, these forests are at increased risk of high-intensity, destructive fires.

Watershed management and restoration may include controlled thinning, prescribed burning, and other management practices to restore the proper balance of timber, undergrowth, and grassy meadows in the watershed. Restoration also may include planting of appropriate native plants (Brooks et al. 1990; Hewlett 1982; Miller and Tyler 1990; Perry 1994; Spurr and Barnes 1980).

3.1.1.5   Impact of Forest on Basin Runoff

According to Gomi et al. (2008), forest cover of deciduous forests could reduce overall basin runoff better than the Japanese cypress, which has a lesser canopy cover. Ibson agrees that forest cover would reduce runoff by preventing evaporation and inducing precipitation. Again, different types of species could alter runoff in different ways, as explained by Gomi et al with the help of Japanese cypress, Hinoki plantations, and deciduous forest, Lau et al. (1999) with the help of $1 \times CO_2$ and $2 \times CO_2$ type forests, Tiju and Xiaojing (2007) with *Larix gmelini* plantations, and Oliviera (2006) with roadside *Eucalyptus* sp. plantations, when different species had reduced runoff in different amount and manner (Table 3.1).

3.1.2   Hydrologic Models

The hydrologic model tries to imitate the interrelationship among climatological, hydrological, and geomorphological characteristics of watersheds to estimate future values of any hydrological variable. There are different types of hydrologic models used in different purpose of hydrologic problems. Detail descriptions of hydrologic models are given in Chapter 21.

3.1.3   Neurogenetic Models

The application of neurogenetic models in prediction of hydrologic parameters is widely popular within various fields of hydrologic science. A brief overview of artificial neural network and genetic algorithms and their working methodology are given in Chapter 22.

Table 3.1 Table showing some literatures regarding the impact of forestry on basin runoff and other related hydrologic parameters

Authors	Study area	Variables used	Catchment characteristic	Forest area/forest species used	Conclusion
Gomi et al. (2008)	Japan	Input: forest cover, slope, two sizes of plots, rainfall, runoff volume of small plots Output: runoff volume of large plots	Steep hillslope covered with forest	(1) Japanese Cypress (*Chamecyparis obtusa*) with sparse understory vegetation, (2) Hinoki plantations with fern understory vegetation, and (3) deciduous forests	Runoff maximum from Japanese Cypress and minimum from deciduous forest
GWSP digital water atlas (2008)	Worldwide	Input: distributed runoff data from preindustrial and contemporary period Output: runoff per grid	Runoff changes per 3,600 km^2 of grid area	Only grids with forest cover and agricultural land use was considered	Results showed that for every 3% of forest area change water yield changes by 1%
Idson (2009)	No specific study area was selected	Input: physico-geochemical and geological properties of basins, climatological variables like precipitation, evaporation, and forest cover Output: basin runoff	Different basins with different percentage of forest cover were considered. Relief, soil type, water-holding capacity of the basins were also different	Not required	Forest can induce precipitation and prevent water from evaporation
Lau et al. (1999)	Four basins located in Taiwan: Fusan (north region), Lisan (east region), Chichiawan (middle region) and Sandiman (south region)	Input: surface, subsurface, and ground water storage, precipitation, evapotranspiration, infiltration coefficient, interflow, vegetation index, outlet ground water Output: flow duration curve	River basins with very low human activity were selected	$1 \times CO_2$ and $2 \times CO_2$ type forests were considered	Mean flow rate (Q_{50}) on southern region where $2 \times CO_2$ plantation was dominant, which is five times more than that in other regions where $1 \times CO_2$ type plantation exists

Table 3.1 (continued)

Authors	Study area	Variables used	Catchment characteristic	Forest area/forest species used	Conclusion
Tiju and Xiaojing (2007)	Mountains of Xiaoxing, China	Input: runoff and forest resources data of the past 35 years Output: forest runoff	Mountaineous catchment	*Larix gmelini* plantations	The river flow increased in the initial 10 years after forest harvesting, but decreased gradually with the growth and crown closure of the *L. gmelini* plantations
Oliviera (2006)	The Rio Doce Valley, central-east area of the state of Minas Gerais	Input: erosivity index, soil, water, nutrient, and organic carbon loss Output: soil and water loss	Roadside forest catchment	*Eucalyptus* sp.	The results indicate that all the eucalyptus plantations allowed very low values of soil and water loss

3.1.4 Objective and Scope

The present study tried to estimate future water availability due to climatic uncertainties, which were predicted by PRECIS climate models (Chapter 23). The present study also tried to analyze the interrelationship between forest area, basin area, and basin runoff. The model, Plantation-Prioritized Basin Yield Estimation (PLANOBAY) or Forest Index-based hydrologic model incorporates and stresses on the relationship between forest area and basin runoff while estimating the basin runoff as output. With the help of predicted runoff, Water Budget equation and population of the catchment water availability/capita/year was calculated. Future water availability was estimated with the help of estimated stream flow, rainfall, and evapotranspiration estimated and calculated from PRECIS-generated weather scenarios, forest cover change, and basin loss was predicted by IPCC (2007) along with Goldman Sachs-predicted population scenarios. The variation of water availability within the districts, states through which the considered two river basins passed was also calculated with the estimated data, which may help identify the exact locations of vulnerability due to climatic uncertainties.

3.1.5 Study Area

Climatic uncertainties could be understood if basins with diverse climates were used to estimate the impact of climatic uncertainties. Damodar and Rupnarayan River Networks were two such river basins situated in East India's tropical region where diversified climates were observed. Besides climates, there is a very irregular distribution of population within the two basins. A detailed description about the catchment and its climatic and geomorphological pattern are given in Chapter 25.

3.2 Methodology

According to Callahan et al. (2004), Franco et al. (2008), Gomi et al. (2008), GWSP Digital Water Atlas (2008), Idson (2009), Lau et al. (1999), Oliviera (2006), Tiju and Xiaojing (2007), Wemple and Jones (2003), and others and as described in Table 1, vegetated area has a clear impact on basin runoff where increase in vegetated area decreases the basin runoff. The PLANOBAY model tried to estimate basin runoff considering the impact of vegetated area on basin runoff. The simple, neurogenetic model involves a Vegetated Area Index (VAIn) or Forest Index to predict the basin runoff, which categorizes the runoff into vegetated area and basin area variant and invariant classes. According to the A2 scenario of climate change, there would be considerable amount of change in forest area. Most of the hydrologic models (Chapter 21) does not consider forest area separately but clubbed it under basin loss and/or canopy evapotranspiration. As the PLANOBAY model considers the impact of change in area explicitly, the model could give more accurate results in this regard.

3.2.1 Model Variables

The model variables considered for development of the model includes monthly average rainfall and VAIn as input and monthly basin runoff as output.

3.2.1.1 Determination of VAIn

VAIn was developed in the following methodology:

1. The basin area (A), vegetated area (A_v), and basin runoff (Q) of all the sampling regions were sorted from lower value to higher value.
2. The values were then ranked in an ascendant manner according to their magnitude and odd ranked values were subtracted from even ranked values.
3. The resultant value (dA, dA_v, and δQ) from the mathematical operation of all the three variables (A, A_v, and Q) was ranked from higher values to lower values.
4. The ranked values of basin area and vegetated area were divided into four categories each with respect to magnitude of change in basin runoff and basin and vegetated area to identify the variability of basin runoff with basin and vegetated area.
5. The four categories considered for basin area could be explained as

   (a) Area Invariant (AI) The rank of change in runoff variable was large (below rank 400) compared to rank of change in basin area (above rank 10). This implies that a very large change in basin area contributes to very small change in basin runoff, that is, basin runoff was invariant to change in basin area.
   (b) Area Variant 1 (AV1) The rank of change in basin area was large (below rank 400) but rank of change in basin runoff was small (above rank 10). That means, for small change in basin area there was a large change in runoff, which implies the high variability of runoff with basin area.
   (c) Area Variant 2 (AV2) The rank of both change in runoff and change in basin area was large (below rank 400), that is, for small change in basin area, change in runoff was also small. That means AV2 category identifies the basin areas, which could vary the basin runoff but not as much as AV1 category basin areas.
   (d) Area Variant 3 (AV3) The rank of both change in runoff and change in basin area was small (above rank 10), that is, for large change in basin area, change in runoff was also high. That means AV3 category identifies the basin areas, which could vary the basin runoff but not as much as AV1 category basin areas.

6. The four categories considered for vegetated area could be explained as

   (a) Vegetated Area Invariant (A_vI) The rank of change in runoff variable was large (below rank 400) compared to rank of change in vegetated area (above rank 10). This implies that a very large change in vegetated area contributes to very small change in basin runoff, that is, basin runoff is invariant to change in vegetated area.
   (b) Vegetated Area Variant 1 (A_vV1) The rank of change in vegetated area was large (below rank 400) but rank of change in basin runoff was small (above rank

  10). That means, for small change in vegetated area there was a large change in runoff which implies the high variability of runoff with vegetated area.

(c) Vegetated Area Variant 2 (A_vV2) The rank of both change in runoff and change in vegetated area was large (below rank 400), that is, for small change in vegetated area; change in runoff was also small. That means, AV2 category identifies the vegetated areas, which could vary the basin runoff but not as much as AV1 category vegetated areas.

(d) Vegetated Area Variant 3 (A_vV3) The rank of both change in runoff and change in vegetated area was small (above rank 10), that is, for large change in basin area, change in runoff was also high. That means, AV3 category identifies the vegetated areas, which could vary the basin runoff but not as much as AV1 category vegetated areas.

7. The categorized runoff datasets with respect to basin area and vegetated area were merged to form a single variable, which was given a name as VAIn that represents runoff as a function of change in basin as well as vegetated area.

8. For example, if change in basin area was categorized as AI and change in vegetated area was categorized as A_vI, then the variables would be merged as AI-A_vI, which would be collectively called as VAIn of the region.

3.2.2 Data Collection

Daily peak runoff of 30 years (1972–2002) and of each of the sampling points were collected and daily peak rainfall of 30 years were collected. The peak rainfall data of ungauged sampling points were derived from Tyndall Distributed Rainfall database where distributed values of rainfall at a resolution of 20/20 m grid was calculated with the help of relationship between energy flux and land-use pattern. The daily peak runoff as well as rainfall was averaged to find the monthly average runoff and rainfall from which the peak monthly average runoff and rainfall was selected. Basin area and forest cover of the sampling points were deduced from aerial photographs of the sampling points. The satellite images (Chapter 24) of the sampling points were processed through image processing software to identify the locations of vegetation, forests, plantations, and cropped agricultural fields. Then unsupervised classification was applied, which classify the images into different land-use features with same or range of iso-DN values. The DN values of a point in an image denote the Digital Number, which depends upon reflectance from a point within that image. Different land use or geographical features have different reflectance. This property helps to identify the differences between land use or geomorphological features shown in an image. The class representing the DN values of vegetative (including forest area, cropped field, plantations, etc.) regions of the image was identified and the area of the region was calculated as area of vegetation in the region. The basin area of the sampling points were delineated with the help of iso-elevation contours collected from Survey of India (SOI) toposheets and GPS elevation points taken from the various points of the region.

3.2.3 Development of Neurogenetic Models

As described in Chapter 23, neurogenetic models were required to be trained with different algorithms to identify the better algorithm from many. The algorithm which gives the smallest testing root mean square error (RMSE) and if the same is less than training RMSE was selected as the best training algorithm to train the neurogenetic model for the present problems. Accordingly, three neurogenetic models were developed with two inputs and one output employing a feed-forward structure and supervised learning rule with QP, CGD, and BBP as training algorithms (Chapter 22). The network structure was selected with the help of GA. Table 3.2. shows the information regarding the necessary parameters of the neurogenetic models. Figure 3.1 depicts the flowchart of the model development procedure.

Table 3.2 Table showing input and output variables used for the NGHYD model

Input	Abbreviation
Output	Abbreviation
Peak average monthly rainfall (*P*) and VAIn	*P*, VAIn
Peak average monthly basin runoff (*Q*)	*Q*

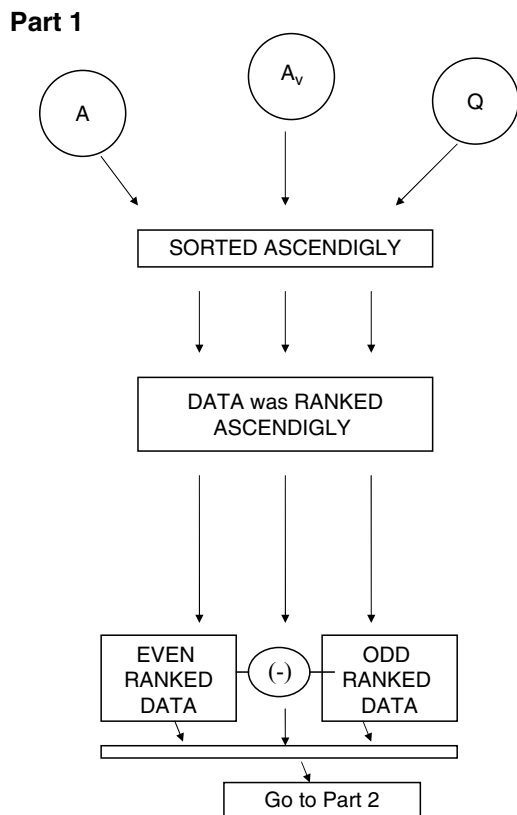**Fig. 3.1** *Part 1*: Chart showing the data preprocessing adopted to develop PLANOBAY model. *Part 2*: Chart showing the algorithm used to categorize basin area based on its variation with basin runoff. *Part 3*: Chart showing the algorithm used to categorize vegetated area based on its variation with basin runoff. *Part 4*: Chart showing the flowchart of the development of VAIn and the neurogenetic models
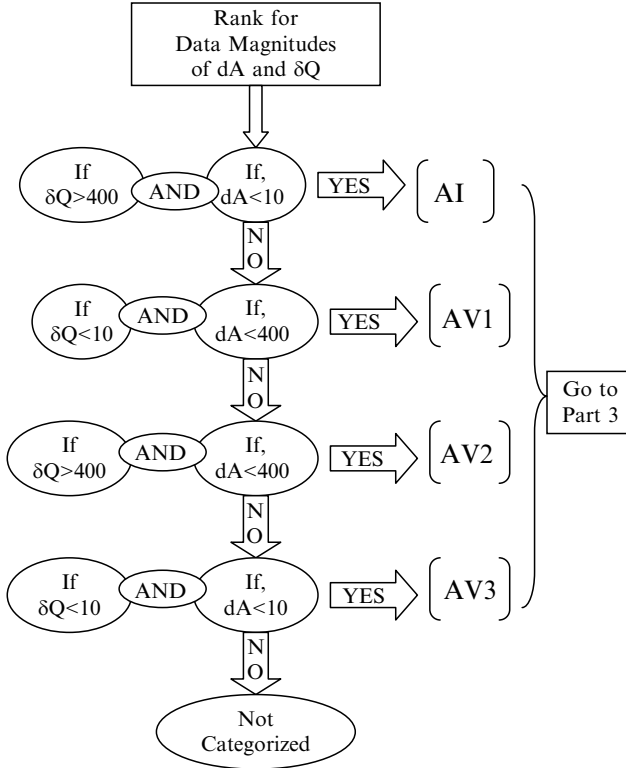
Part 2

Fig. 3.1 (continued)

3.2.4 Model Validation and Uncertainty Analysis

The discharge from the sampling points was also estimated with the help of HECHMS, TR55, and MODRAT hydrologic model. The output from the three considered conceptual models along with neurogenetic models and observed discharge data were compared to calculate the RMSE (1), correlation coefficient (*r*) (2.), coefficient of efficiency (*E*) (3), and first-order uncertainty analysis (*U*) (4) of the models. The values would help in selection of the better model among the six models considered in the present study.

$$\text{RMSE} = \sqrt{\sum_{n=1}^{n} \frac{(T_p - O_p)^2}{n}} \tag{1}$$

$$\text{Correlation coefficient} = \sqrt{\frac{\sum (T_p - T_m)(O_p - O_m)}{\sqrt{\sum_{1}^{n}(T_p - T_m)^2 \sum_{1}^{n}(O_p - O_m)^2}}} \tag{2}$$

Part 3
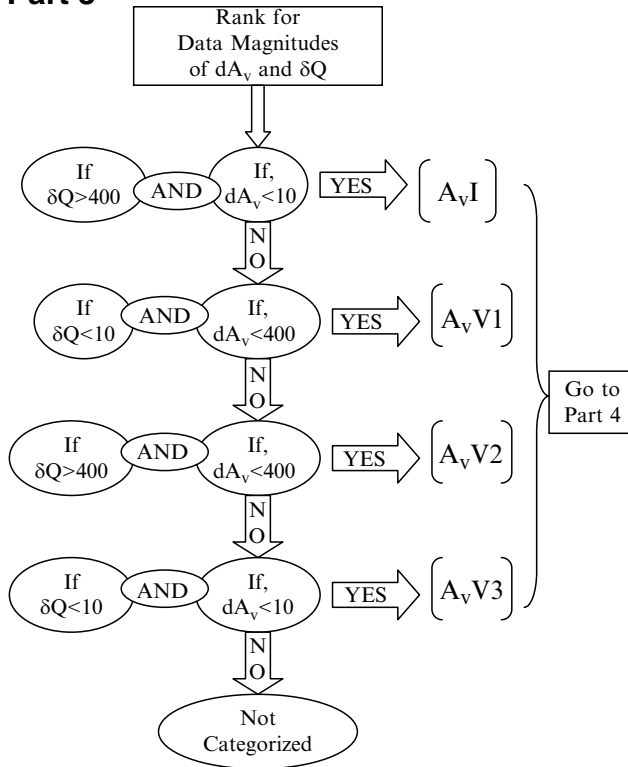
Fig. 3.1 (continued)

$$\text{Coefficient of efficiency} = 1 - \frac{\sum\limits_{n=1}^{n}(T_p - O_p)^2}{\sum\limits_{n=1}^{n}(T_p - T_m)^2} \tag{3}$$

$$\text{First-order uncertainty } (U) = \left(\frac{Stdev(O_p - O_m)}{n}\right) \tag{4}$$

where T_p is the target data value for the p th pattern; O_p is the estimated data value for the p th pattern, T_m and O_m are the mean of target and estimated dataset, respectively, and n is the total number of patterns. T_n is the target value of the nth pattern and T_m is the mean value of the targeted dataset.

Correlation coefficient could also be taken as a measure of model reliability (Statistics Solution 2009) whereas coefficient of efficiency was also used as a measurement of model sensitivity (Das 1991) toward observed dataset. Hence, both of these validation criteria also help to determine model reliability and sensitivity where high values would represent greater level of reliability and sensitivity of the model.

Fig. 3.1 (continued)

3.2.5   *Estimation of Climate Change and Water Availability*

The water availability was calculated as per the UNFCC-recommended water budget equation which states that

Water availability is equal to

$$= \left(\frac{P - (Q + E + G + T)}{p} \right) \tag{5}$$

$$= \left(\frac{P - (Q + \mathrm{ET} + L_c)}{p} \right) \tag{6}$$

Evaporation (*E*) and transpiration (*T*) could be collectively represented as evapotranspiration (ET) and infiltration could be replaced by basin loss coefficient (Section 10.3).

All parameters are represented as volume and unit of water availability is cubic meter/capita/year. Output from PRECIS climatic model (Chapter 23) for the Indian region was fed to the selected model to estimate discharge for 2010–2100. The estimated discharge along with estimated ET (PRECIS also generates temperature data based on the climate change scenario and PET was calculated from the temperature data and Penmann equation) was then used to calculate water availability per capita per region of the river basins.

3.2.5.1 Determination of Basin Loss Coefficient

SPOT imageries collected from different years and months of the sampling points and within 15/15 km grid around the channel was processed with a commercial software. The images were classified according to the DN values of different geographical features so that pixel with same DN values gets categorized into a single class. The DN values of different geographical features were identified and were used to categorize the images into classes of different geographical features. Common geographical features of the study area includes forest, cropped and non-cropped agricultural fields, ponds, industrial areas, mines, roads, and pavements, etc. The area of each geographical class was calculated and divided from the total area. A weighted average of the output of each geographical class was determined where a feature with high runoff retention capacity like forest, pond, etc. was given lower weightage and features with low runoff receptivity was given higher value of weighted. The result is subtracted from 1 to get the loss coefficient. Imageries of different months and years were used to determine loss coefficient of different months and years. The values were then averaged to get the average monthly loss coefficient of sampling points.

3.2.5.2 Determination of Channel Loss Coefficient

The channel loss was calculated with the help of the concept utilized to determine loss coefficient. Instead of geographical features of a basin, same channels were considered. Channels may have sand dunes and/or agricultural fields. Sand dunes are known to have higher infiltration capacity than agricultural fields. The same weighted average method was used to calculate loss coefficient of channels. Imageries of different months and different years were collected to determine channel loss of different months and different years.

3.2.5.3 Determination of Loss Coefficient

The channel loss coefficient along with basin loss coefficient was averaged to estimate the loss coefficient at the sampling points.

3.3 Result and Discussion

3.3.1 Validation of PLANOBAY Model

The predicted values of discharge from all the developed three neurogenetic models (Table 3.3) along with the three conceptual hydrologic models were compared with

Table 3.3 Table showing the model parameters adopted for development of the three neurogenetic models

Model name	PLANOBAYQP	PLANOBAYCGD	PLANOBAYBBP
Model variables			
Input	P, VAIn	P, VAIn	P, VAIn
Ouput	Q	Q	Q
Model parameters			
Network topology			
Network type	Feed forward	Feed forward	Feed forward
Network structure	2,6,4,1	2,1,1	2,1,1
Network weight	40	3	3
Training dataset (%)	80	80	80
Testing dataset (%)	10	10	10
Validation dataset (%)	10	10	10
GA parameters			
Population	50	50	50
Generation	100	100	100
Penalty	6	6	6
Crossover rate	0.8	0.8	0.8
Mutation rate	0.2	0.2	0.2
Stop training condition			
RMSE	0.05	0.05	0.05
Iteration (10^6)	200	200	200
Generalization loss (%)	5	5	5
Training algorithm parameters			
Algorithm name	QP	CGD	BBP
Activation function	Sigmoid	Sigmoid	Sigmoid
Learning rule	Supervised	Supervised	Supervised
Learning rate	0.8	NR	0.8
Momentum	NR	NR	0.8
Propagation coefficient	1.75	NR	NR
Training and testing results			
RMSE (training)	10.98	11.67	11.55
RMSE (testing)	10.05	14.56	18.78
Training stop reason	Generalization loss	Generalization loss	Generalization loss
Model estimation results			
RMSE	3.53	3.95	3.56
Relationship	0.94	0.90	0.98
Efficiency	0.99	0.95	0.97
Uncertainty (%)	7	8.56	8.88

Table 3.4 Table showing comparison of performance validation criteria calculated within selected neurogenetic model and the three conceptual hydrologic models

Model name	RMSE	Relationship (r)	Efficiency (E)	Uncertainty (U)
PLANOBAYQP	3.53	0.94	0.99	7
HECHMS	5.45	0.67	0.78	8.5
TR55	6.78	0.65	0.68	15.67
MODRAT	10.12	0.71	0.58	17.25

the observed basin runoff and RMSE, r^2, E, and U were calculated to validate the models as well as to select the better model out of the six models considered.

According to the comparison results as depicted in Table 3.2, RMSE of PLANOBAYQP was found to be lesser than any other model (3.53) along with model efficiency (0.99) was better than PLANOBAYBBP (3.56 and 0.97) and PLANOBAYCGD (3.95 and 0.95). Uncertainty for PLANOBAYQP was found to be equal to 7% whereas the same for PLANOBAYBBP and PLANOBAYCGD were, respectively, 10% and 25%.

If conceptual hydrologic models were compared with the selected neurogenetic model, the PLANOBAYQP was found to be 35.3%, 47.94%, and 65.12% more accurate than HECHMS (5.45), TR55 (6.78), and MODRAT (10.12) (Table 3.4) hydrologic model.

As, PLANOBAYQP has the lesser RMSE, higher model efficiency, and correlation among the six considered models, it was selected as the model for the estimation of future basin runoff according to the A2 and B2 baseline climate change scenarios, which were generated from PRECIS climate model.

The water availability was calculated with the help of Eq. 6) and from the estimated maximum monthly average runoff, which was found from the PLANOBAYQP. The water availability of sampling regions was averaged as per their state, basins, or district to estimate state-wise, basin-wise, and district-wise variation of water availability. The estimated runoff along with generated rainfall or PET data was converted to volumetric unit. The future population was collected from IPCC 4th (IPCC, 2007).

The estimated water availability per capita per year within selected sampling regions was depicted in Figs. 3.2–3.7. The basin and state-wise distribution of estimated water availability per capita per year for A2 and B2 climate change scenario is shown in Figs. 3.8–3.11. Table 3.5 depicts the estimated average water availability per capita per year according to A2 and B2 climate change scenario, respectively, within the states, basins, and districts that the two river networks had passed.

According to Figs. 3.8–3.11 and Table 3.5., the water available per person living in catchments of river Damodar would face severe water shortage in the future where water availability would be reduced by 46.61%, 72.11%, and 81.75% than the present water availability/capita/year respectively in 2010–2040, 2041–2070, and 2071–2100 in case of A2 scenario of climate change. In case of B2 scenario, water available per person per year of the Damodar basin would be reduced by 33.18%, 63.57%, and 80.36% than the observed water availability respectively in 2010–2040, 2041–2070, and 2071–2100.
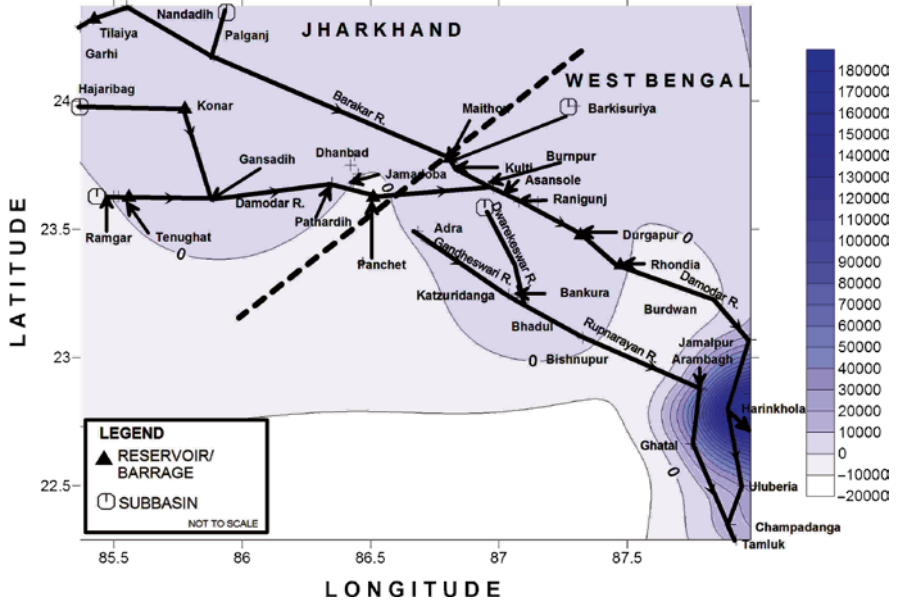
Fig. 3.2 Figure showing spatial variation of water availability/capita/year for A2 scenario of climate change and in 2010–2040
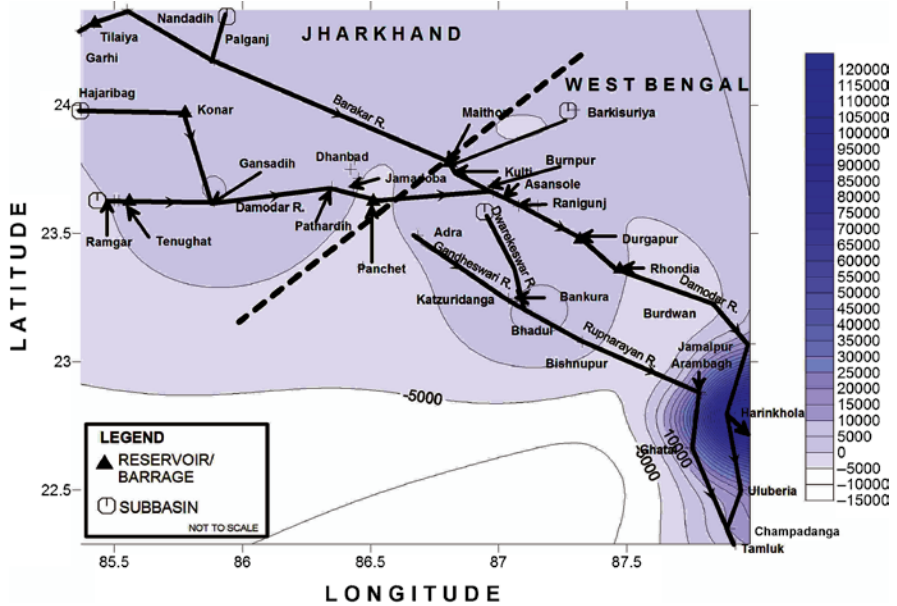

Fig. 3.3 Figure showing spatial variation of water availability/capita/year for A2 scenario of climate change and in 2041–2070

Fig. 3.4 Figure showing spatial variation of water availability/capita/year for A2 scenario of climate change and in 2071–2100

Fig. 3.5 Figure showing spatial variation of water availability/capita/year for B2 scenario of climate change and in 2010–2040

Fig. 3.6 Figure showing spatial variation of water availability/capita/year for B2 scenario of climate change and in 2041–2070
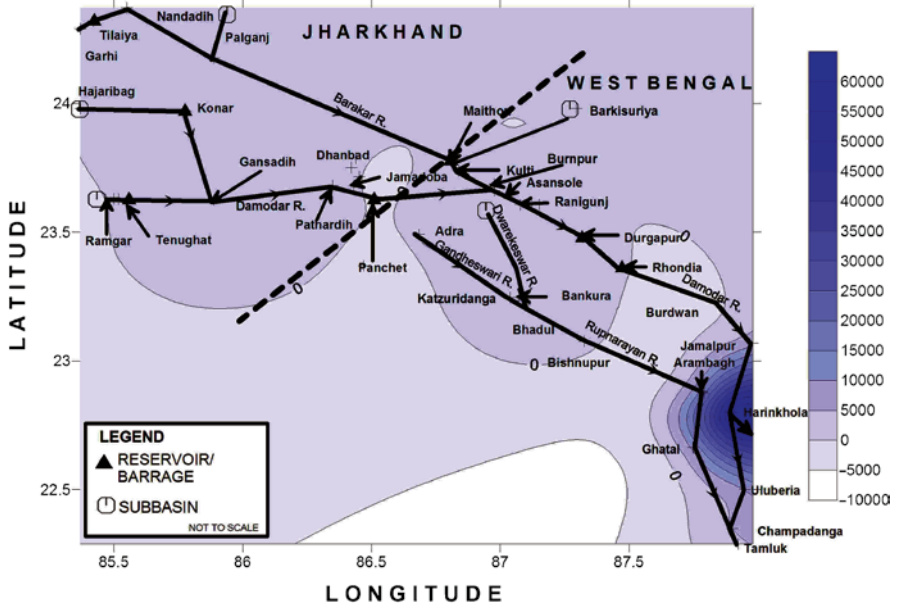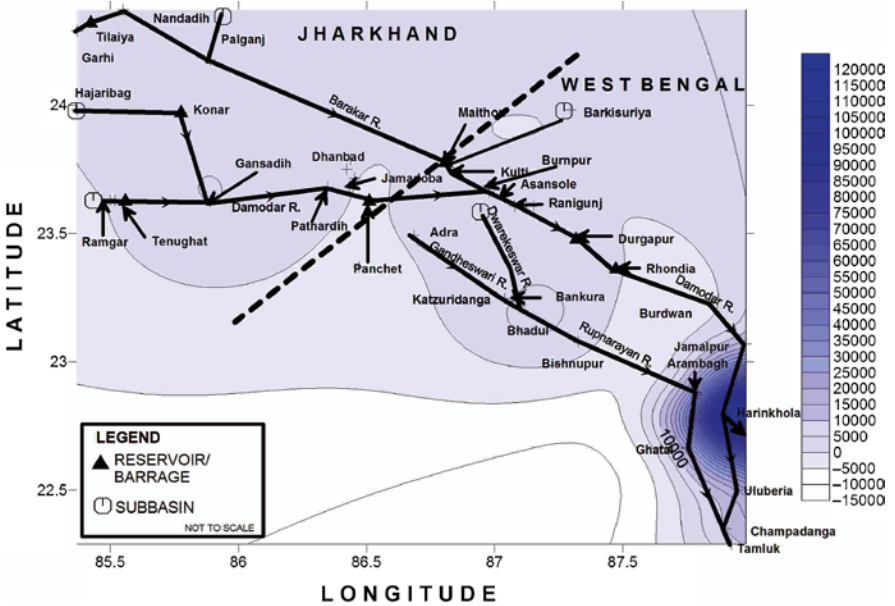

Fig. 3.7 Figure showing spatial variation of water availability/capita/year for B2 scenario of climate change and in 2071–2100
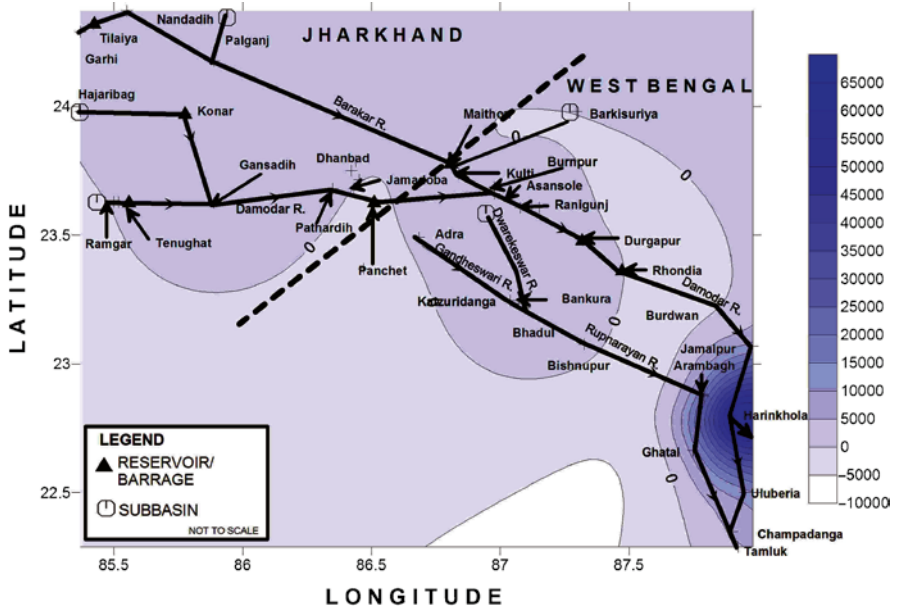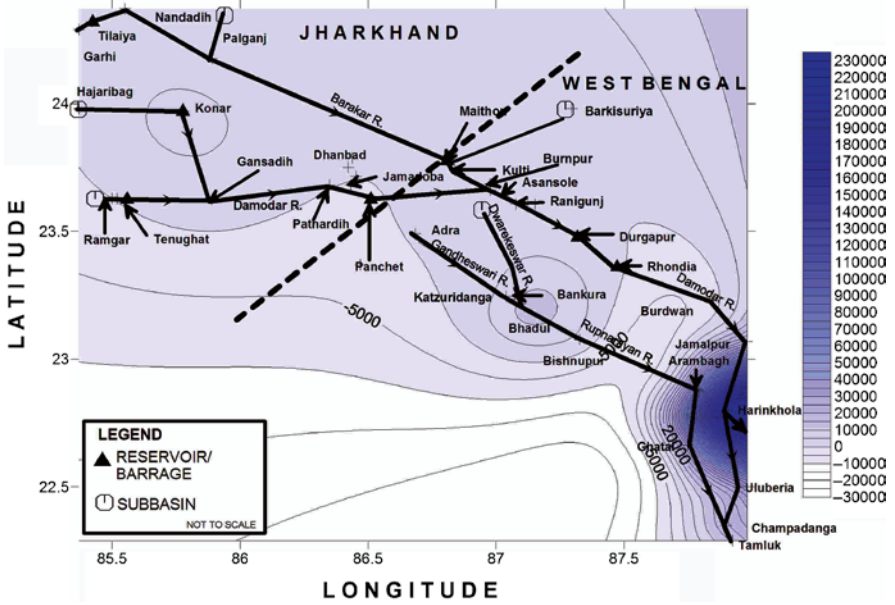
Fig. 3.8 Figure showing comparison of water availability in between Damodar and Rupnarayan basin in case of A2 scenario of climate change

Fig. 3.9 Figure showing comparison of water availability within Jharkhand and West Bengal in case of A2 scenario of climate change

Fig. 3.10 Figure showing comparison of water availability in between Damodar and Rupnarayan basin in case of B2 scenario of climate change

Fig. 3.11 Figure showing comparison of water availability within Jharkhand and West Bengal in case of B2 scenario of climate change

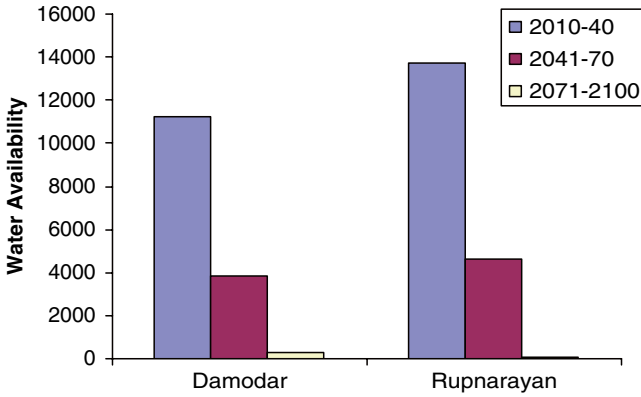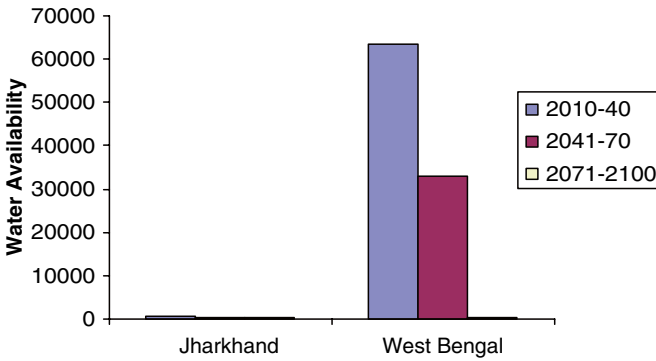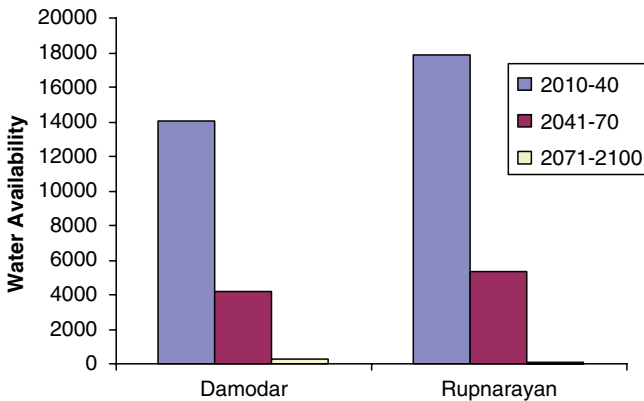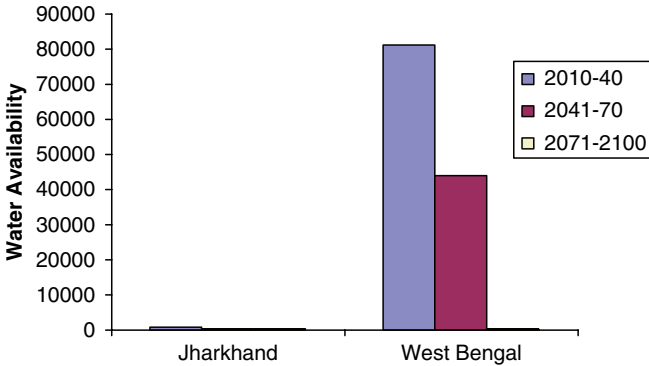The water availability of Rupnarayan basin including rivers Dwarakeswar and Gandheswari would face severe shortage of water where in case of A2 scenario of climate change the available water for each person in the catchments would be reduced by 49.66%, 74.16%, and 82.91%, respectively, in 2010–2040, 2041–2070, and 2071–2100. Again, for B2 scenario, the percentage reduction would be equal to 34.59%, 62.64%, and 80.48%, respectively in 2010–2040, 2041–2070, and 2071–2100.

The severity of water scarcity would be more in case of A2 baseline scenario of climate change and would be highest in 2071–2100. The reduction of water availability would be more in case of Rupnarayan than for Damodar watersheds where the difference in water availability was more pronounced in A2 scenario than in B2 scenario.

As A2 was a scenario where industrial development was given high priority but increase in industry would induce increase in demand of water along with degradations of catchments. Hence, more water would go out of the watershed and more water would be used up by the industries. The concept justifies the prediction results as explained above as Damodar basin falls within a highly industrialized zone whereas industrial concentration is high only in the confluence of the river with river Hoogly (Tamluk).

If water availability was compared within the two states through which the two river basins of the present study had passed, change in availability of water in state of Jharkhand would be more than in the state of West Bengal. The water availability per capita per year for West Bengal would reduce by 48.15%, 73.07%, and 82.63% from the present water availability/capita/year respectively in 2010–2040, 2041–2070, and 2071–2100 in case of A2 scenario and the available water content for B2 scenario will face a reduction of 33.86%, 64.13%, and 80.66% from the present water availability/capita/year respectively in 2010–2040, 2041–2070, and 2071–2100, whereas the same for Jharkhand is 29.3%, 62.22% and 68.74% and 24.9%, 44.42%, and 74.6% respectively in 2010–2040, 2041–2070, and 2071–2100 and in case of

Table 3.5 Table showing district-wise, state-wise, and basin-wise variation of water availability due to A2 and B2 scenario of climate change

Districts	A2 scenario			B2 scenario			Observed	
State	2010–2040	2041–2070	2071–2100	2010–2040	2041–2070	2071–2100	1970–2002	1970–2002
Giridih	732.85	377.84	249.58	954.60	557.63	253.01	1,440.88	
Jamtara	−69.49	−33.69	−11.53	−119.03	−50.30	−22.28	−127.81	
Bokaro	418.44	218.68	151.24	478.21	306.68	145.78	386.27	
Ranchi	34.10	19.68	16.27	45.49	41.56	13.30	44.30	
Hazaribagh	2,571.29	1,301.90	830.30	3,158.51	1,693.51	869.26	4,792.90	
Dhanbad	518.83	363.13	623.52	−49.81	757.26	252.19	−587.84	
Burdwan	875.45	440.12	278.52	1,053.09	543.20	301.66	1,525.41	
Hooghly	86,998.05	45,200.09	29,136.68	554,804.20	300,656.98	162,147.21	838,495.57	
Howrah	206.65	104.57	67.85	251.47	134.53	74.07	394.64	
Purulia	847.19	434.92	287.57	1,102.75	630.34	328.91	1,671.34	
Bankura	7,793.11	3,990.66	2,624.46	10,052.80	5,680.94	2,983.33	15,294.26	
West Midnapur	81.96	45.84	44.26	92.27	80.88	47.71	293.05	
East Midnapur	180.79	96.30	75.96	224.54	154.03	84.76	540.40	
Jharkhand	701.00	374.59	309.90	744.66	551.06	251.88	991.45	
West Bengal	63,567.91	33,016.12	21,294.58	81,083.02	43,982.99	23,709.66	122,602.09	
Basins	2010–2040	2041–2070	2071–2100	2010–2040	2041–2070	2071–2100	1970–2002	1970–2002
Damodar	11,252.37	5,877.06	3,845.73	14,082.64	7,678.67	4,138.89	21,075.63	
Rupnarayan	13,719.72	7,042.55	4,656.89	17,827.57	10,182.78	5,320.78	27,253.81	

A2 and B2 scenarios. If water availability is compared within Jharkhand and West Bengal, Jharkhand would have less amount of water than that of West Bengal.

According to the Table 3.5, changes or reduction of water availability was more pronounced in case of the districts of West Bengal than the districts of Jharkhand where water availability of East Midnapore, a highly industrialized district in the present days, faces the highest reduction of water availability (85.94% within 2071–2100 in case of A2 scenario) whereas an increase of water availability was observed in the district of Bokaro where the available water would get increased by 23.8% within 2010–2040 (in case of B2 scenario of climate change), which could be contributed to the fact that Bokaro is the least populated districts among the other districts considered in the present study and also in B2 scenario of climate change basins were taken as health and environmentally stable so that the water holding capacity would be high in case of B2 than in A2 scenario of climate change where opposite status of watersheds were considered. That is why highest reduction of water availability was observed in A2 scenario of climate change.

Overall, from the predictions of water availability it could be concluded that reduction of water availability would be more in A2 scenario of climate change than in B2 scenario of climate change but if water availability was compared within Damodar basin and Jharkhand and Rupnarayan basin and West Bengal, former would have lesser amount of water available for its people than the later. The amount of vegetated area was also a reason for this estimation. As Jharkhand and Damodar basins has less amount of vegetation than the West Bengal and Rupnarayan, more water was flowed out of Damodar basin than that of Rupnarayan. Hence, water availability was more in West Bengal than in Jharkhand. But as both zone falls in the same level of basin degradation in the *IPCC* report the reduction of available water was more in West Bengal than in Jharkhand.

According to Figs. 3.2–3.7, upstream of both the rivers had moderate water availability but the availability decreases in the downstream except near the confluence point of the three rivers, Damodar, Rupnarayan, and Hooghly. The magnitude of the water availability also decreases from 2010 to 2100 for both the scenarios of climate change. The up moving 0 water availability contour also show the decrease in availability of water as area under the 0 contour increases with time and become maximum, covering even the major part of upstream, including river Damodar, during 2071–2100. The increase in area was more clear in case of A2 scenario, which was represented by Figs. 3.2–3.4 than that of B2 scenario (Figs. 3.5–3.7).

3.4 Conclusion

The present study tried to estimate future water availability according to A2 and B2 scenario of climate change with the help of PLANOBAY or Forest Index hydrologic model. The PLANOBAY model was developed in such a way that it considers the impact of forested or vegetated area on basin runoff. VAIn or Forest Index represented the impact of vegetated area, along with basin area, on the overall basin runoff.

The model has two inputs, rainfall and VAIn and was validated with HECHMS, TR55, and MODRAT conceptual hydrologic models and three neurogenetic models, which were nothing but the PLANOBAY model that differs with respect to the training algorithms used to train the model. Among the six considered models, PLANOBAYQP, that is, PLANOBAY model trained with QP algorithm, was selected due to its high efficiency, correlation, and low RMSE and uncertainty among all other considered models. The basin runoff was estimated with the help of PLANOBAYQP and from the basin runoff and predicted rainfall and temperature by PRECIS climatic model along with future population; the water availability/ capita/year for 2010 to 2100 was estimated. According to the model estimates, water availability would decrease at a steady rate from 2010 to 2100. The decrease in water availability would be more pronounced in case of A2 than in B2 scenario of climate change. A2 scenario represents a future world with uncontrolled population and industrial activities which in turn would make any basins of that time deserted or impervious as growth in industry would imply degradation of forest area. Also the population of that time was predicted to be increased abnormally. Hence, the reduction of A2 scenario was found to be more pronounced than B2 scenario of climate change.

References

Brooks K et al (1990) Hydrology and the management of watersheds. Iowa State University Press, Ames

Callahan TJ, Cook JD, Coleman MD, Amatya DM, Trettin CC (2004) Modeling storm water runoff and soil interflow in a managed forest, upper coastal plain of the southeast US, Proceedings of ASAE annual meeting, American Society of Agricultural and Biological Engineers, Paper number 042254

Das NG (1991) Statistical methods in commerce, accountance and economics, Part – 1. M. Das & Co., Kolkata, pp 25–50

Franco C, Drew AP, Heisler G (2008) Impacts of urban runoff on native woody vegetation at Clark reservation state park, Jamesville, NY, J Urb Habitats. Retrieved from http://www.urbanhabitats.org/v05n01/runoff_full.html on June 2009

Gomi T, Sidle RC, Miyata S, Kosugi K, Onda Y (2008) Dynamic runoff connectivity of overland flow on steep forested hillslopes: scale effects and runoff transfer. Water Resour Res 44:W08411, doi:10.1029/2007WR005894

GWSP Digital Water Atlas (2008) Map 52: change in runoff due to deforestation (V1.0). Available online at http://atlas.gwsp.org

Hewlett JD (1982) Principles of forest hydrology. University of Georgia Press, Athens

Idson PFF (2009) Methods of studying the dependence of river runoff on the forest coverage of its basin. Retrieved from http://www.cig.ensmp.fr/~iahs/redbooks/a048/048032.pdf on June, 2009

IPCC (2007) Climate change 2007: the physical sciences basis, retrieved on http://ipcc-wg1.ucar.edu/wg1/wg1-report.html. on 30th April, 2009

Lau CC, Lee KT, Tung CP, Chang CH (1999) Assessment of climate-change impact on runoff using normalized difference vegetation index. Retrieved from http://www.gisdevelopment.net/aars/acrs/1999/ts2/ts2045.asp on June 2009

Jr M, Tyler G (1990) Living in the environment, 6th edn. Wadsworth Publishing Company, Belmont, CA

Oliviera FP (2006) Hydric erosion in forest areas in the Rio DoceValley, central-east region of the state of Minas Gerais, University Federal de Lavras, Brasil. Retrieved from http://biblioteca. universia.net/html_bura/ficha/params/id/17531366.html on June 2009

Perry DA (1994) Forest ecosystems. The Johns Hopkins University Press, Baltimore, MD

Spurr SH, Barnes BV (1980) Forest ecology. Wiley, New York

Statistics Solution (2009) Retrieved from http://www.statisticssolutions.com/reliability-analysis on July 16, 2009

Tiju C, Xiaojing T (2007) Impact of forest harvesting on river runoff in the Xiaoxing'an Mountains of China. J Frontiers Forest China 2(2):143–147

Wemple BC, Jones JA (2003) Runoff production on forest roads in a steep, mountain catchment. Water Resour Res 39(8):1220, doi:10.1029/2002WR001744

Chapter 4
Application of Parity Classified Neurogenetic Models to Analyze the Impact of Climatic Uncertainty on Water Footprint

Mrinmoy Majumder, Rabindra Nath Barman, Bipal K. Jana, Pankaj Roy, and Asis Mazumdar

Abstract Water footprint of an individual, community, or business is defined as the total volume of freshwater that is used to produce the goods and services consumed by the individual or community, or produced by the business. Neurogenetic models were widely used in the prediction of hydrologic variables, and outcome of such applications were found to be satisfactory. The irregular rainfall and temperature pattern, and degradation of watersheds were causing worldwide reduction of water availability (UNFCC). As water footprint is directly related to water availability and

M. Majumder (✉)
Senior Research Fellow, School of Water Resources Engineering,
Jadavpur University, Kolkata-700032, West Bengal, India
and
Geo-information Scientist, Regional Center, National Afforestation
and Eco-development Board, Jadavpur University, Kolkata-700032, West Bengal, India
e-mail: mrinmoy@majumder.info

R.N. Barman
Pertime Research Fellow, School of Water Resources Engineering,
Jadavpur University, Kolkata-700032, West Bengal, India
and
Assistant Professor, Department of Production, National Institute of Technology,
Agartala, Tripura, India

B.K. Jana
Senior Research Fellow, School of Water Resources Engineering,
Jadavpur University, Kolkata-700032, West Bengal, India
and
Environmental Manager, Consulting Engineering Services, West Bengal, India

P. Roy
Lecturer, School of Water Resources Engineering, Jadavpur University,
Kolkata-700032, West Bengal, India

A. Mazumdar
Coordinator, Regional Center, National Afforestation and Eco-development Board,
Jadavpur University, Kolkata-700032, West Bengal, India
and
Director, School of Water Resources Engineering, Jadavpur University,
Kolkata-700032, West Bengal, India

also shows the demand from industrial consumers, the present study tried to estimate the impact of climate change on water footprint between two river basins of East India with the help of neurogenetic models. The climate change scenarios were generated with the help of PRECIS climate models, and future runoff was estimated by a neurogenetic model trained with orthopareto dataset. The output from the neurogenetic model, named as PARITYCGD, was compared with a neurogenetic model trained with normal dataset (NGHYD) and conceptual hydrologic models. According to the results, the neurogenetic model trained with orthopareto dataset was selected as the better model among the five models, which shows that neural models trained with orthopareto dataset learn a problem better than a neurogenetic model trained with normal dataset. From the prediction of stream flow, water footprint of the sampling regions were calculated and according to the estimations, water footprint would be reduced in both A2 and B2 climate change scenarios where reductions would be more pronounced in A2 than in B2. Although, due to data dependency of neurogenetic models, the PARITYCGD model may not work for other basins but for the present study, it was found to have better accuracy than the conceptual hydrologic model.

4.1 Introduction

4.1.1 Water Footprint

The *water footprint* is an indicator of water use that includes both direct and indirect water use of a consumer or producer. Water use is measured in water volume consumed (evaporated) and/or polluted per unit of time. A water footprint can be calculated for any well-defined group of consumers (e.g., an individual, family, village, city, province, state, or nation) or producers (e.g., a public organization, private enterprise, or economic sector). It is a geographically explicit indicator which not only showing volumes of water use and pollution but also the locations (Hoekstra and Chapagain 2008). However, the water footprint does not provide information on how the embedded water is contributing to water stress or environmental impacts.

"The interest in the water footprint is rooted in the recognition that human impacts on freshwater systems can ultimately be linked to human consumption, and that issues like water shortages and pollution can be better understood and addressed by considering production and supply chains as a whole," says Professor Arjen Y. Hoekstra, creator of the water footprint concept and scientific director of the water footprint network. "Water problems are often closely tied to the structure of the global economy. Many countries have significantly externalised their water footprint, importing water-intensive goods from elsewhere. This puts pressure on the water resources in the exporting regions, where too often mechanisms for wise

water governance and conservation are lacking. Not only governments, but also consumers, businesses and civil society communities can play a role in achieving a better management of water resources."

- The production of 1 kg of beef requires 16,000 l of water.
- To produce one cup of coffee we need 140 l of water.
- The water footprint of China is about 700 m^3/year/capita. Only about 7% of the Chinese water footprint falls outside China.
- Japan with a footprint of 1,150 m^3/year/capita has about 65% of its total water footprint outside the borders of the country.
- The USA water footprint is 2,500 m^3/year/capita.

4.1.2   Climatic Uncertainty

Impact of global warming is one of the major reasons for watershed decay. Global warming has induced climate change which in turn had increased the frequency and extent of hydrologic extremities. High temperature had increased evaporative losses in reservoirs and stream flows. High temperatures with long growing seasons (as a result of high temperatures) had increased water consumption for domestic use, irrigation, and energy production. Periodic increase in winter and early spring time stream flows as well as higher frequency of intense storms produce extreme floods. Early rainfall causes reservoirs to fill early in the year. Consequently, reservoirs were drained to avoid floods, which waste the limited water that can be stored to satisfy human needs.

The effect of global warming is now predominant in many parts of the world. Twelve warmest years have occurred in 1900s among which 10 have occurred between 1987 and 1998. The energy availability, which was increased due to increase in temperature, had created a ripple effect throughout the Earth system with local, regional, and global positive feedbacks feeding on each other to amplify and accelerate warming. Abnormality in climatic pattern, induced by the accelerated warming, had started to effect catchment-specific hydrologic cycles. In the last 10 years, floods have caused more damage than in the previous 30 years. Higher temperatures lead to a high rate of evaporation and very dry conditions in some areas of the world. Severe weather events are now more common. The number and strength of hurricanes, tornadoes, and other events had increased over the last 15–20 years. As per IPCC (2007), global climate change is expected to affect the performance of water resource systems according to current indicators and findings.

In a recent report published in the American Meteorological Society's Journal of Climate, climate change with effects from damming, irrigation, and other water use reduced the runoff and increase the pressure on freshwater resources in much of the world. Rivers with decreased flow had outnumbered those with increased flow by 2.5–1.The impact of climate change is now regarded as one of the major causes of watershed degradation (Majumder, in press).

4.1.3   Climate Change and Climate Models

Climate change is defined as the change in 30 year's weather pattern of a certain region. The changes can be abrupt or periodical. The abrupt changes of climate are often known as climatic uncertainty. Due to global warming climate and uncertainties seem to be eminent, hence many models were developed to estimate future climate. An explanation of various climatic models and justification of their development is given in Chapter 23.

4.1.4   Hydrologic Models

Hydrologic models are simplified, conceptual representations of a part of the hydrologic cycle. They are primarily used for hydrologic prediction and for understanding hydrologic processes. Hydrologic models were now used with climate models to predict the future hydrologic pattern of different river basins. A detailed explanation of hydrologic models and their applications in problem solving is given in Chapter 21.

4.1.5   Neurogenetic Models

Neurogenetic models were widely used to solve various hydrologic problems due to its proficiency in the identification of patterns within a large dataset. A detailed explanation of neurogenetic models and their applications in water resource and hydrologic problems are given in Chapter 2.

4.1.6   Objective and Scope

The present study tried to estimate impact of climate change and its uncertainties on water footprint of various sampling regions within two river networks. Estimation of stream flow due to climate change is now a common objective of many hydrologic researchers. But water footprint, which determines the distribution of water within business and domestic consumers could more efficiently determine the vulnerabilities associated with climatic uncertainties. A reduction of water footprint area would imply reduction of water resources and would represent the vulnerable regions within a catchment. If future vulnerable regions of a watershed could be identified with the help estimated water footprint of the future, managers of watershed could adopt necessary mitigation measures to prevent the estimation from becoming a reality. Another objective of the study was to verify whether neural models work more efficiently if trained with orthopareto dataset.

4.1.7 Study Area

The study area of the present study was selected in the tropical regions of East India. Two river basins with diverse geomorphologic and climatic features and multiple types of water resources were chosen to estimate water footprint of the two basins. A detailed description of the two river networks, rivers Damodar and Rupnarayan, is given in Chapter 25.

4.2 Methodology

4.2.1 Estimation of Stream Flow with the Help of PARITYCGD Model

If a data of different variables are weighted according to their sensitivity toward the dependant variable that dataset is collectively called as orthopareto dataset. In the present study, an orthopareto dataset was used to develop a model based on neurogenetic algorithm. The model was named as PARITY model due to the type of dataset used to develop the model. A neural model generally improves its learning capability when orthopareto dataset is used to train the model. Since such dataset already conveys the interrelationship between the independent variables to the dependant variable a neural model developed with orthopareto dataset can be estimated to give better results from a same type of model using ordinary dataset. The present study tried to verify this by developing two types of neurogenetic models for estimation of basin runoff. The neurogenetic models were compared with conceptual hydrologic models like HECHMS, TR55, and MODRAT, to calibrate as well as validate the neural model and also to select the better model among the nine models considered.

4.2.1.1 Model Variables

PARITY Neurogenetic Hydrologic Model uses Parity Classification Index (*PCI*) multiplied by Basin Runoff Index as input and basin runoff as output (Table 4.1).

Determination of PCI

The input variables include precipitation (P), evapotranspiration (ET), ground water table (GWT), ground water balance (GWB), basin loss coefficient (L_c), time of concentration (T_c), and soil texture (ST) of the sampling regions.

Table 4.1 Table showing input and output variables used for the NGHYD model

Input	Abbreviation
Output	Abbreviation
Product of PCI and Basin Runoff Index (Q/Q_{max})	$p\{PCI, Q/Q_{max}\}$
Peak average monthly basin runoff (Q)	Q

Table 4.2 Table showing sensitivity
of input variables toward basin
runoff

Input variables	Sensitivity toward basin runoff (%)
P	92
ET	90
T_c	88
L_c	86
GWT	84
GWB	80
ST	80

P was found to be most sensitive toward runoff (Q) followed by ET, T_c, L_c, GWT, GWB and ST. The results of the sensitivity analysis could be found in Table 4.2.

Soil texture data of soil samples were collected from sampling regions, soil maps and historical records from 1970 to 2002 were collected from different reports published by Soil and Land Use Survey of India (SLUSI), and the yearly and seasonal soil texture of the sampling regions was estimated from them. Lastly, monthly classes of soil texture were computed with the help of yearly and seasonal soil texture of the region.

The input variables were given weightage (w_n) according to their sensitivity toward basin runoff (S_Q) to prepare a weighted average value, which was normalized to develop an orthopareto dataset called as PCI.

Determination of Basin Runoff Index

The Basin Runoff Index developed in case of CONCONGDHM was also used in case of the present model but in a different manner than the previous model.

The efficiency of neurogenetic models increases if scaled dataset, that is, data which were near to 0 or 1, is used. As first step, development of neurogenetic models requires the dataset to be converted into binary which was known as Scaling; an already scaled dataset would greatly reduce the computation time for development of the model.

The Basin Runoff Index was multiplied by PCI and used as input and basin runoff was selected as output. As variables with high correlated data would also increase efficiency of neurogenetic models and reduce requirement of training for a long time as relationship between highly correlated data was easy to estimate for any models. Hence, runoff index was multiplied with PCI as the result of the calculation will be highly correlated with the output.

Model Development

Three one-input one-output neurogenetic models were developed by the procedures described in Chapter 23. Training algorithm for training the models were selected as CGD for PARITYCGD, QP for PARITYQP, and BBP for PARITYBBP. The performance validation and model reliability and sensitivity analysis was performed to test the developed models and selection of the better model among the nine considered models.
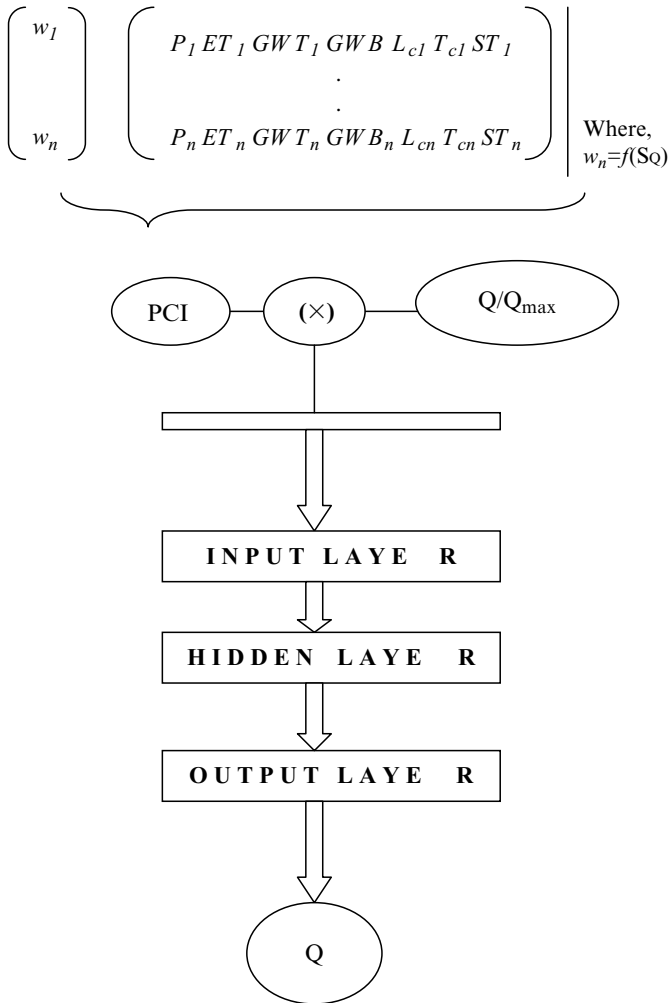
$$\begin{bmatrix} w_1 \\ \\ \\ w_n \end{bmatrix} \begin{pmatrix} P_1\ ET_1\ GW\ T_1\ GW\ B\ L_{c1}\ T_{c1}\ ST_1 \\ . \\ . \\ P_n\ ET_n\ GW\ T_n\ GW\ B_n\ L_{cn}\ T_{cn}\ ST_n \end{pmatrix} \Bigg|$$

Where,
$w_n = f(S_Q)$

Fig. 4.1 Figure showing algorithms adopted to develop the PARITY models

Table 4.2 shows the input and output variables of PARITY hydrologic models and Fig. 4.1 depicts the overview of model algorithm.

4.2.2   Estimation of Stream Flow with the Help of Neurogenetic Model for Estimation of Basin Hydrograph (NGHYD)

In surface water hydrology, a hydrograph is a time record of the discharge of a stream, river, or watershed outlet. Rainfall is typically the main input to a watershed and the stream flow is often considered the output of the watershed;

a hydrograph is a representation of watershed response to rainfall. A watershed's response to rainfall depends on a variety of factors, which affect the shape of a hydrograph:

- Watershed topography and geology (i.e., bedrock permeability)
- The area of a basin receiving rainfall
- Land use
- Drainage density
- Duration of rainfall and precipitation intensity and type
- Evapotranspiration rates
- River geometrics
- The season
- Previous weather
- Vegetation type and cover
- River conditions (e.g., dams)
- Initial conditions (e.g., the degree of saturation of the soil and aquifers)
- Soil permeability and thickness

When, data of rainfall and runoff is unavailable, synthetic hydrograph, i.e., artificial generation of catchment response to rainfall is performed with factors described above. There are many empirical or conceptual models for estimation of synthetic hydrograph all of which try to estimate peak flow and time of peak flow. Then 50% and 70% of peak runoff is found out along with the time required to reach the same amount of runoff .The relationship between runoff and rainfall in the rising limb and impact of basin characteristic on runoff at the recession limb is included in the model to draw the entire hydrograph. It was observed that time to peak is equal to time of concentration of the basin. Yeh et al. (1997), Blazkova et al. (2002), Sui (2005), Lopez et al. (2005), Taskinen and Bruen (2007), Ahmad et al. (2009), and others have investigated the use of hydrograph in the estimation of parameters, design flood, uncertainty analysis, geomorphology, etc. and most of them advocates the use of hydrograph in hydrologic models as it helps to estimate runoff volume and time to peak, which are necessary in case of hydrologic or hydraulic design.

Hydrograph is not essential for impact analysis of climate change but to analyze impacts of climatic variability on duration of peak storm and response time of a catchment due to the storm.

In the present study, a model was developed to estimate hydrograph and corresponding peak basin runoff of the sampling regions with the help of neurogenetic models.

4.2.2.1 Model Variables

Abstraction from rainfall is calculated with the help of rainfall and basin loss (Subramanya 1994). Basin loss is represented by basin characteristic like soil texture, porosity, vegetation or plant cover, depreciations or pondages, etc.

Abstraction from rainfall was divided by time of concentration to find incremental rainfall abstraction (dP) and was used as input whereas basin runoff divided by time

of concentration was used as output (dQ) variable to develop a neurogenetic model for prediction of incremental basin runoff at the different sampling regions.

Data Collection

The peak average monthly rainfall or runoff was calculated with the help of daily rainfall and runoff dataset for 32 years (1970–2002). As there were 42 sampling points and if datasets for each of the sampling points were considered the size of dataset becomes too large (483,840) for the computational facilities available for the present study. Hence, monthly average values were calculated for each month of each year, from which peak average monthly values were taken as the dataset of present study. In this procedure, size of the dataset becomes 505, which were possible for the computational facilities available for the present study and also reduces the amount of time required to develop the models.

   Time of concentration was calculated with the help of Fort Bend County (Wanielista 1987) method. The value of the inputs like length of longest flow path, average slope along longest flow path, average basin slope, and percentage impervious area were calculated with the help of GIS. Fort Bend County method was expressed by the following equation:

$$t_c = 48.64 \times \left(\frac{L}{S^{0.5}} \right)^{0.57} \times \mathrm{Log} \left(\frac{S_0}{S_0^{0.11} \times 10^I} \right) \tag{1}$$

   t_c is the time of concentration (h), L is the length of longest flow path (mi), S is the average slope along longest flow path (ft/mi), $_0$ is the average basin slope (ft/mi), and I is the percentage impervious area

   Fort Bend County method can be used for calculation of time of concentration only if the area of the catchment is within 0.13–400 mi^2, the longest flow path lies between 0.5 and 55 mi, slope along the longest flow path lies between 2 and 33 ft/mi, and the average basin slope lies within 3–80 ft/mi. As all the sub-watersheds considered in the present study satisfy the above conditions Fort Bend County method was utilized for estimation of time of concentration.

Determination of Incremental Rainfall Abstraction

Peak average monthly evapotranspiration was first determined with the help of 32 years of daily evapotranspiration, data which were collected from Indian Metereological Department and Tyndal Distributed Metereological Dataset and in the same way peak average monthly rainfall was calculated. Peak average monthly evapotranspiration was decremented from peak average monthly rainfall of the sampling regions and were multiplied with the basin loss coefficient. The result, which is actually the rainfall abstracted by the basin, was divided by time of concentration to estimate the incremental rainfall abstraction. Basin loss coefficient as described earlier represents the basin characteristics of the sampling regions, which also shows the amount of water abstracted by the basin. Time of concentration

depends upon length of longest flow path and slope of the basin. It also determines the amount of time required for a basin to emit maximum runoff for a given rainfall. So if abstraction for rainfall was divided by time of concentration, the result would give the incremental abstraction of rainfall for a given rainfall event.

Determination of Incremental Basin Runoff

The basin runoff was also divided by the time of concentration to find the incremental basin runoff of the regions.

4.2.2.2 Model Development

Three neurogenetic models were developed with the help of three different training algorithms. The algorithms are already explained in Chapter 22 and procedures of development of neurogenetic models are described in Chapter 23 and are not mentioned here to avoid repetition.

The output of the model was incremental basin runoff from the sampling regions. The hydrograph from the model was drawn with the help of estimated values of the incremental runoff due to the incremental rainfall abstraction. The rainfall abstraction was calculated according to the magnitude of rainfall for the rising limb and according to the basin characteristics for the recession limb. The separation between the two parts of the hydrograph was performed on consideration of basin loss in the recession limb and removal of the same at the rising limb. The peak value of runoff, that is, model output for the peak rainfall was compared with the output from other models for necessary validations.

Table 4.3. shows the input and output variables of NGHYD hydrologic models and Fig. 4.2 depicts the overview of model algorithm.

4.2.3 Calculation of Water Footprint of a Region

Water footprint is calculated from the equation of water availability, which again was derived from Water Budget Equation described by Subramanya (1994).The equations for calculation of water footprint from the equation of water availability is given next.

Table 4.3 Table showing input and output variables used for the NGHYD model

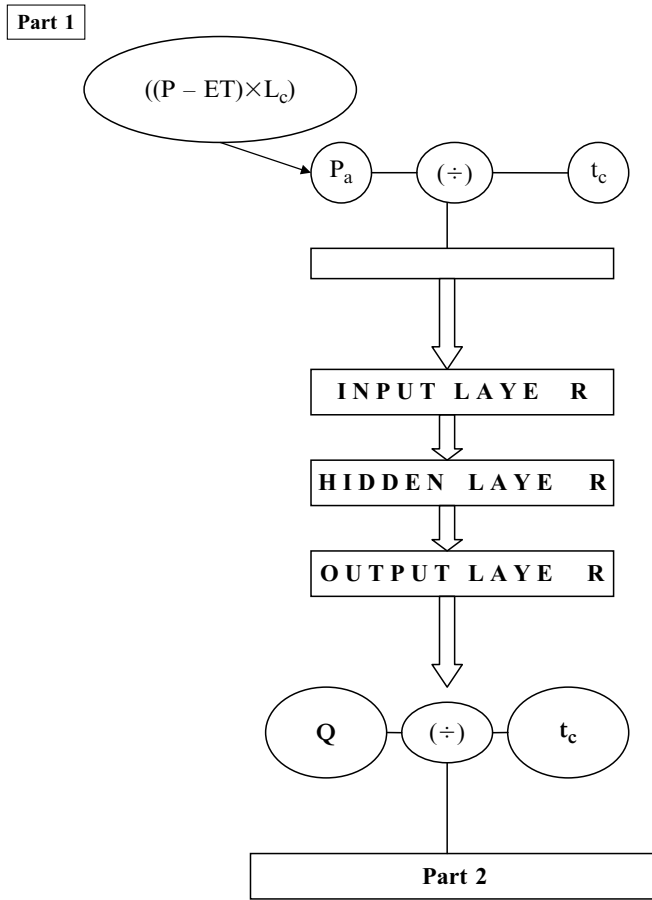| Input	Abbreviation
Output	Abbreviation
Abstraction from rainfall (P_a) divided by time of concentration, i.e., incremental rainfall abstraction (dP)	dP
Basin runoff divided by time of concentration, i.e., incremental basin runoff (dQ)	dQ

Fig. 4.2 *Part 1*: figure showing the flowchart of the methodology adopted to develop the NGHYD models. *Part 2*: figure showing the flowchart of the methodology adopted to draw the synthetic hydrograph

Water availability is equal to

$$= \left(\frac{P - (Q + E + G + T)}{p} \right) \tag{2}$$

$$= \left(\frac{P - (Q + ET + L_c)}{p} \right) \tag{3}$$

Evaporation (E) and transpiration (T) could be collectively represented as evapotranspiration (ET) and infiltration could be replaced by basin loss coefficient (Section 10.3). All parameters are represented as volume and unit of water availability is cubic meter/capita/year.
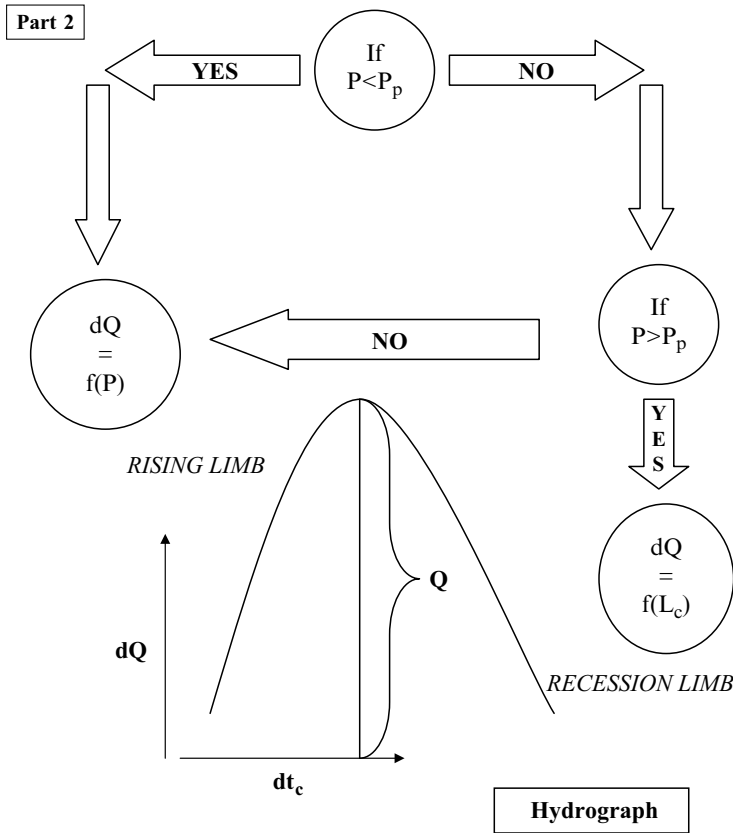
Fig. 4.2 (continued)

Let water availability per capita per year = *WA*.
Then,

$$\text{Availability of fresh water} = \text{WA} \times f \tag{4}$$

where f is the percentage of water supplied as fresh water for domestic use.

Again, fresh water supplied to industry for development of their products or maintaining their service is given by

$$= (\text{WA} \times f) \times f_i \tag{5}$$

where f_i is the percentage of fresh water supplied to industry or businesses for maintaining their service and development of their product.

Equation (4.4) is actually the water footprint of the region.

The estimated stream flow and PRECIS prescribed *P* and *ET* for both A2 and B2 scenario of climate change along with the basin loss coefficient as deduced from IPCC 4th Assessment Report was fed to Eq. (4.4) which estimated the maximum possible water footprint of the sampling regions (Chapter 25). The basin-wise as well as

state-wise and district-wise water footprint was also estimated from the equation and spatial variation of the same was also predicted with the help of surface algorithms.

4.2.4 Model Validation

All the nine models were validated for accuracy with the help of root mean square error (RMSE), coefficient of determination (r), coefficient of efficiency (E), and first-order uncertainty analysis (U) which could be mathematically represented as

$$\text{RMSE} = \sqrt{\sum_{n=1}^{n} \frac{(T_p - O_p)^2}{n}} \tag{6}$$

$$\text{Coefficient of determination} = \sqrt{\frac{\sum (T_p - T_m)(O_p - O_m)}{\sqrt{\sum_{1}^{n} (T_p - T_m)^2 \sum_{1}^{n} (O_p - O_m)^2}}} \tag{7}$$

$$\text{Coefficient of efficiency} = 1 - \frac{\sum\limits_{n=1}^{n} (T_p - O_p)^2}{\sum\limits_{n=1}^{n} (T_p - T_m)^2} \tag{8}$$

$$\text{First- order uncertainty } (U) = \left(\frac{Stdev(O_p - O_m)}{n} \right) \tag{9}$$

where T_p is the target data value for the p th pattern; O_p is the estimated data-value for the p th pattern, T_m and O_m are the mean of target and estimated dataset, respectively, and n is the total number of patterns. T_n is the target value of the nth pattern, and T_m is the mean value of the targeted dataset.

Correlation coefficient could also be taken as a measure of model reliability whereas coefficient of efficiency was also used as a measurement of model sensitivity (Das 1991) toward observed dataset. Hence, both of these validation criteria also help to determine model reliability and sensitivity where high values would represent greater level of reliability and sensitivity of the model.

4.3 Result and Discussion

4.3.1 Model Validation

According to the comparison results as given in Table 4.4, PARITYCGD model was found to have the minimum RMSE (2.58) and U (5.5%) among the six considered neurogenetic models, whereas PARITYQP (3.78% and 5.8%) and PARITYBBP

Table 4.4 Table showing the model parameters and performance validation criteria of PARITY and NGHYD models

Model name	PARITYCGD	PARITYQP	PARITYBBP	NGHYDQP	NGHYDCGD	NGHYDBBP
Model variables						
Input	$p\,(PCI,Q/Q_{max})$	$p\,(PCI,Q/Q_{max})$	$p\,(PCI,Q/Q_{max})$	dP	dP	dP
Ouput	Q	Q	Q	dQ	dQ	dQ
Model parameters						
Network topology						
Network type	Feed forward	Feed forward	Feed forward	Feed forward	Feed forward	Feed forward
Networkstructure	1,2,1	1,1,1	1,1,1	1,1,1	1,1,1	1,1,1
Network weight	4	2	2	2	2	2
Training dataset	80	80	80	80	80	80
Testing dataset	10	10	10	10	10	10
Validation dataset	10	10	10	10	10	10
GA parameters						
Population	50	50	50	50	50	50
Generation	100	100	100	100	100	100
Penalty	6	6	6	6	6	6
Crossover rate	0.8	0.8	0.8	0.8	0.8	0.8
Mutation rate	0.2	0.2	0.2	0.2	0.2	0.2
Stop training condition						
MSE	0.05	0.05	0.05	0.05	0.05	0.05
Iteration	200	200	200	200	200	200
Generalization loss	5	5	5	5	5	5
Training algorithm parameters						
Algorithm name	CGD	QP	BBP	QP	CGD	BBP
Activation function	Sigmoid	Sigmoid	Sigmoid	Sigmoid	Sigmoid	Sigmoid
Learning rule	Supervised	Supervised	Supervised	Supervised	Supervised	Supervised
Learning rate	NR	0.8	0.8	0.8	NR	0.8
Momentum	NR	NR	0.8	NR	NR	0.8
Propagation coefficient	NR	1.75	NR	1.75	NR	NR

Training and testing results	Maximum no. of iteration reached	Maximum no. of iteration reached	Maximum no. of iteration reached	Generalization loss	Generalization loss	Generalization loss
RMSE (training)	1.5	1.6	1.98	5.5	5.8	6.5
RMSE (testing)	0.56	3.34	3.07	4.87	4.56	4.06
Model estimation results						
RMSE (3.5)	2.58	3.78	3.96	4.90	5.55	5.65
Relationship (3.6)	0.96	0.94	0.94	0.59	0.55	0.61
Efficiency (3.7)	0.99	0.99	0.97	0.76	0.72	0.75
Uncertainty (%) (3.8)	5.5	5.8	7.45	11.34	11.87	11.98

(3.76% and 7.45%) models have the second and third better RMSE and U among the considered neurogenetic models. The above results would imply that a neurogenetic model with orthopareto dataset has better model validation than a neurogenetic model trained with ordinary dataset as NGHYD. The neurogenetic model, which was trained with ordinary dataset had the maximum RMSE and U, which was found to be equal to 5.65% and 11.98% (NGHYDBBP). The reliability (0.96) and efficiency (0.99) of PARITYCGD and other PARITY models were also found to be better than the reliability (0.59) and efficiency (0.79) of NGHYDQP and other NGHYD models.

As PARITYCGD had higher efficiency and reliability and lower RMSE and uncertainty than any other six considered neurogenetic models, it was selected as the better model among the neurogenetic models developed for the present study.

The model output of PARITYCGD was also compared with conceptual hydrologic models like HECHMS, TR55, and MODRAT (Sections 21.8–21.10) and RMSE, U, r, and E were calculated from the comparison to find the better model among the four considered models. From the comparison it was observed that PARITYCGD was found to have better RMSE, which was equal to 2.58 than HECHMS (5.45), TR55 (6.78), and MODRAT (10.12) (Table 4.5) hydrologic models. The efficiency of the neurogenetic model (0.99) was also found to be higher than the any of the considered conceptual models, HECHMS (0.78), TR55 (0.68) and MODRAT (0.58). The coefficient of relationship or reliability (0.96) of PARITYCGD was also found to be higher among the four considered models. The uncertainty analysis of all the four models revealed that PARITYCGD had the minimum uncertainty (5.5%) than the conceptual models where HECHMS, TR55 and MODRAT had an uncertainty of 15%, 20%, and 45%, respectively.

As PARITYCGD has higher r and E and lower RMSE and U than the three considered hydrologic models, the later model was selected as the model for the estimation of future basin runoff according to the A2 and B2 baseline climate change scenarios, which were collected from PRECIS climatic model-generated weather scenarios. From the predicted stream flow, water footprint of the sampling regions was calculated with the help of Eq. (4.4).

4.3.2   Impact of Climate Change on Basin Runoff

According to the IPCC Report on Climate Change et al. (2001) and PRECIS model output, in A2 baseline scenario precipitation of the selected basins would increase by 45–50% during post-monsoon and 15–20% in monsoon for the year 2080–2100. The same increasing trend would be observed during 2010–2079. The soil moisture capacity of the basins would also increase by 5% in the upstream areas of river Damodar but decrease by 5% in the downstream of the river Rupnarayan. Catchment condition of the basins would remain unchanged and for some places it would be better than the present time.

Table 4.5 Table showing district-wise, state-wise, and basin-wise variation of water footprint due to A2 and B2 scenario of climate change

Districts	A2 scenario			B2 scenario			Observed
	2010–2040	2041–2070	2071–2100	2010–2040	2041–2070	2071–2100	1970–2002
Giridih	2.93	2.27	2.00	4.77	2.79	1.52	5.76
Jamtara	−0.28	−0.20	−0.09	−0.60	−0.25	−0.13	−0.51
Bokaro	1.67	1.31	1.21	2.39	1.53	0.87	1.55
Ranchi	3.34	2.13	2.25	4.55	4.57	1.73	4.34
Hazaribagh	1,021.81	643.89	491.73	1,562.52	920.18	523.19	1,916.67
Dhanbad	209.54	183.00	377.51	−27.83	419.92	154.70	−242.62
Burdwan	306.41	244.27	236.74	473.89	298.76	196.08	541.52
Hooghly	29,486.46	23,552.42	22,472.43	43,654.50	29,471.94	19,202.59	57,421.32
Howrah	72.33	58.04	57.67	113.16	73.99	48.15	140.10
Purulia	42.36	65.24	73.33	132.33	94.55	59.20	760.46
Bankura	389.66	637.74	939.49	1,403.52	907.84	771.03	9,958.25
West Midnapur	45.08	35.76	39.83	62.74	59.85	38.17	45.42
East Midnapur	99.44	75.11	68.36	152.69	113.98	67.81	83.76
State	2010–2040	2041–2070	2071–2100	2010–2040	2041–2070	2071–2100	1970–2002
Jharkhand	206.50	138.73	145.77	257.63	224.79	113.65	280.87
West Bengal	4,348.82	3,524.08	3,412.55	6,570.40	4,431.56	2,911.86	9,850.12
Basins	2010–2040	2041–2070	2071–2100	2010–2040	2041–2070	2071–2100	1970–2002
Damodar	3,919.86	3,220.69	3,184.79	6,290.15	4,179.47	2,661.05	7,427.83
Rupnarayan	3,131.35	2,338.85	2,149.32	3,294.24	2,671.27	1,922.69	10,883.61

4.3.3   Estimation of Future Water Footprint

The stream flow along with the estimated climatological (for *P* and *ET*), land use (for L_c) data, and population data (as predicted by United Nations) was applied to Eq. (4.4) for the estimation of water footprint for 2010–2100 according to A2 and B2 scenario of climate change, which was generated by PRECIS climate model. Figures 4.2–4.7 show the spatial variation of water footprint within the sampling regions of the considered river networks.

4.3.4   Impact of Climatic Uncertainty

According to Table 6, water footprint was reduced in both A2 and B2 scenario but the reduction is more prominent in case of A2 scenario than in B2 except for 2071–2100 when the trend seems to be reversed. The districts (Dhanbad and Jamtara) with negative water footprint were found to have an increase in their water footprint for both the scenario of climate change. The reason for such outcome might be contributed to the consideration of environmental stability and thus upgradation of river basins during B2 scenario of climate change, which had increased the water holding capacity of the basins.

If footprint of water was compared within the state of West Bengal and Jharkhand, observed footprint of water was found to be more in former (9,850.12) than in the
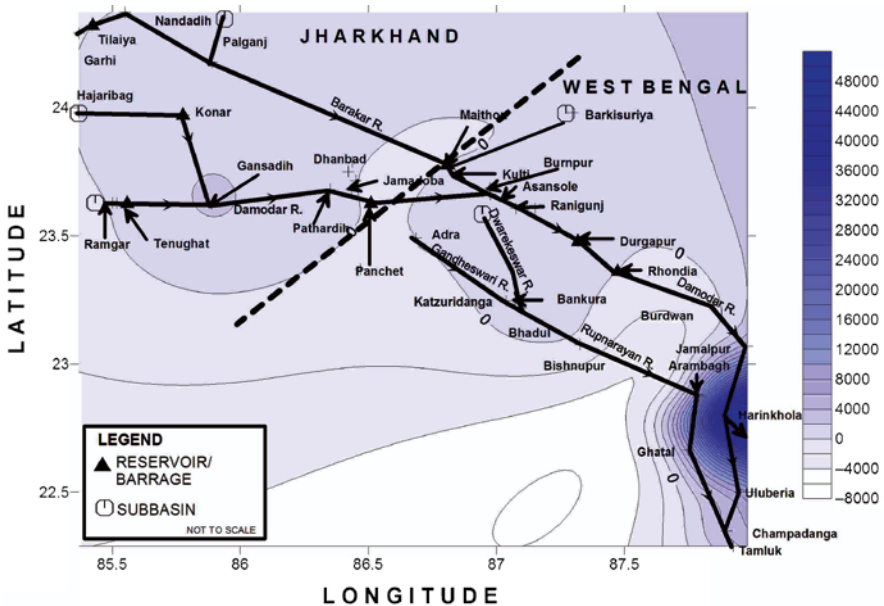
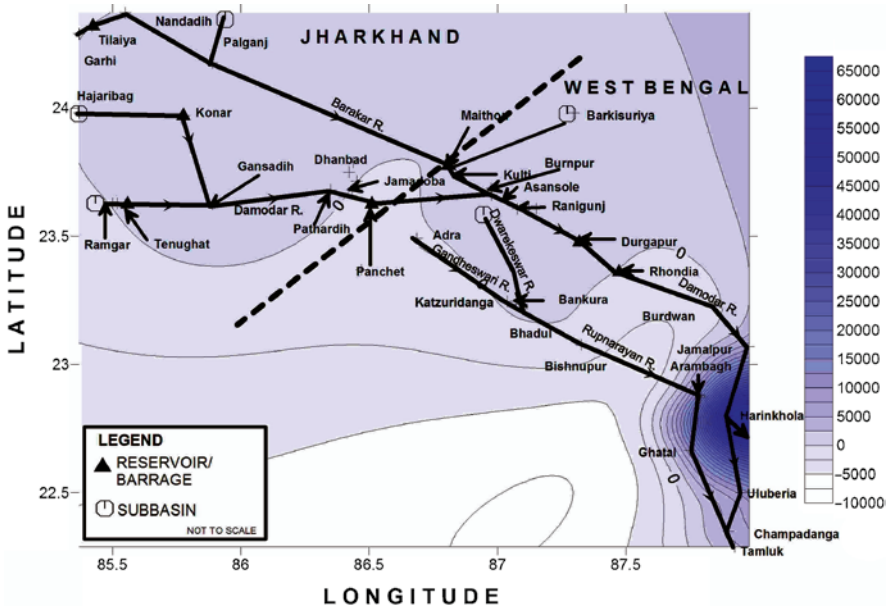**Fig. 4.3** Figure showing spatial variation of water footprint in 2010–2040 due to A2 scenario of climate change

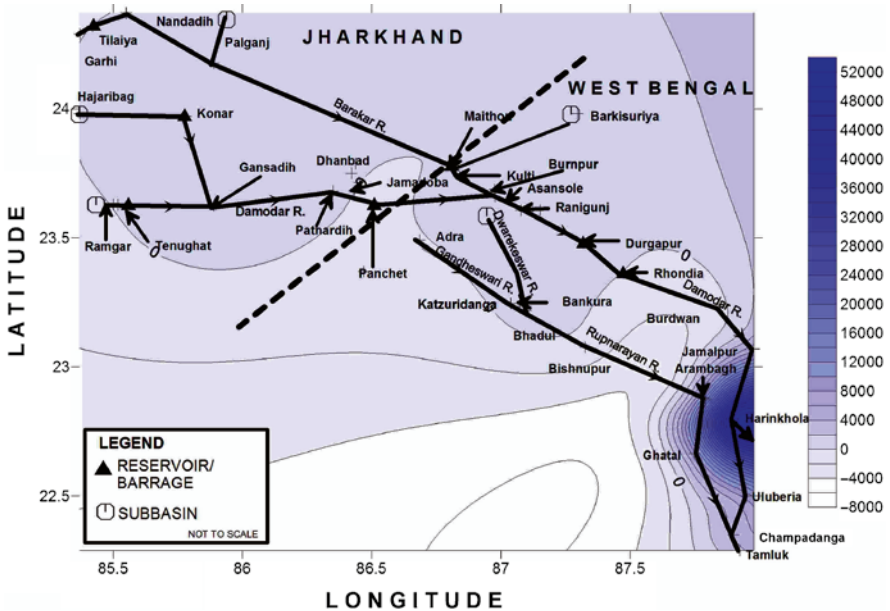**Fig. 4.4** Figure showing spatial variation of water footprint in 2041–2070 due to A2 scenario of climate change

Fig. 4.5 Figure showing spatial variation of water footprint in 2071–2100 due to A2 scenario of climate change
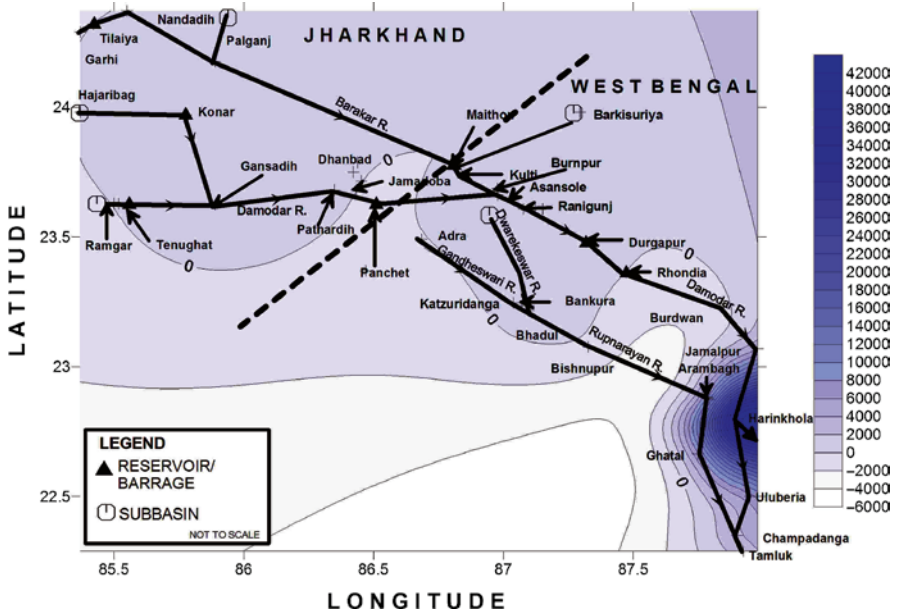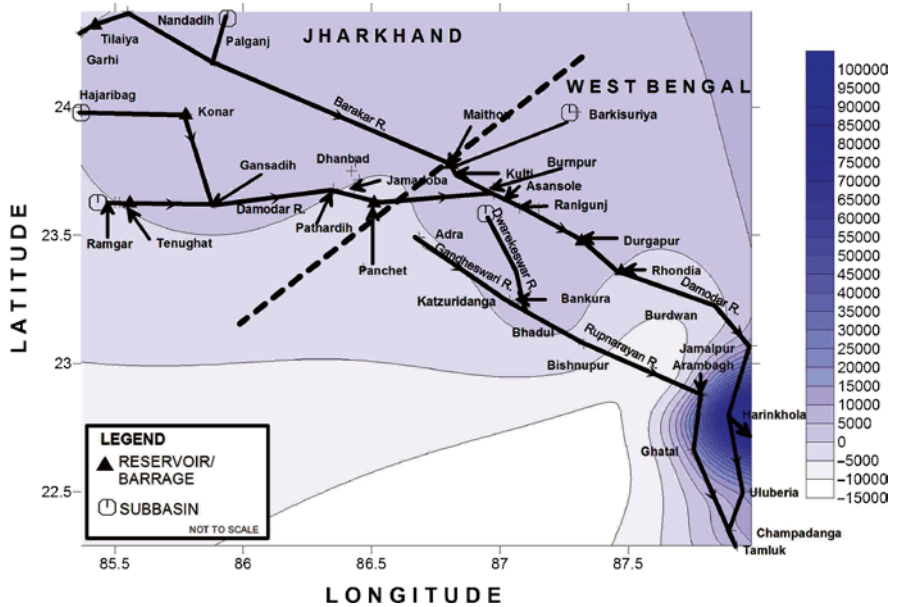
Fig. 4.6 Figure showing spatial variation of water footprint in 2010–2040 due to B2 scenario of climate change

Fig. 4.7 Figure showing spatial variation of water footprint in 2041–2070 due to B2 scenario of climate change

latter (280.87). As found from the predictions the water footprint would get reduced in both the states but the reduction would be more for A2 scenario than for B2 scenario of climate change except for the 2071–2100 time domain when the trend was found to be reversed. When the water footprints of the two basins were compared it was found that during 1970–2002, Rupnarayan has more water than Damodar. The same trend would be followed in the future for both the scenario of climate changes where A2 had more reduction of water footprint than B2 but the trend would be reversed after 2071. This might be contributed to the fact that UN estimations of future population will show a decreasing trend after 2071. As population is inversely proportional to water footprint the reversal of trend would be observed.

If water footprints of districts were compared, then it could be observed that same trend of reduction of water footprint was followed except for the districts with negative footprint of water, where climatic uncertainty may increase the availability of water. That is why water footprints of Dhanbad (–242.62) and Jamtara (–0.51) were found to be increased to 209.54,183 and 377.51, respectively in 2010–2040, 2041–2070, and 2071–2100 for A2 scenario of climate change and –27.83, 419.92, and 154.70 for the same time span but in case of B2 scenario of climate change.

From Figs. 4.2–4.7, it could be concluded that water footprint would be maximum within downstream regions of rivers Damodar and Rupnarayan during the A2 and B2 climatic scenarios but upstream regions of both the rivers would remain in reduced zones of water footprint. This may be justified by the fact that industry as well as population is more in the upstream than in the downstream. This difference of consumption of water may reduce the overall footprint of water in the upstream.

4.4 Conclusion

The present study tried to estimate the impact of climatic uncertainty on water footprint with the help of Parity Classified Neurogenetic Model. The model was developed by encoding the available dataset of input variables into a number of even and odd groups and scoring the variable dataset to an even scale for development of PCI. The PCI was used as input variable and observed discharge was considered as output. The model output was used to calculate the water footprint of districts and states. The same model was applied to analyze the impact of climate change on water footprint for the same districts and states from the output of PRECIS climate models. According to the results, water footprint would get reduced in both A2 and B2 scenario of climate change. The footprint area as depicted in Figs. 4.2–4.7 would also get reduced where reduction would be maximum during 2071–2100 for both A2 and B2 scenario of climate change. As A2 was considered to be an industrially active scenario, reduction of footprint area would be more in A2 than in B2 (Fig. 4.8). The model results also helped to understand that a neurogenetic model could increase its efficiency if it was trained with orthopareto dataset due to which all the performance validation criteria selected PARITYCGD as the better model among the other six models, three of which were neurogenetic model trained with normal dataset (NGHYDQP, NGHYDCGD, and NGHYDBBP)
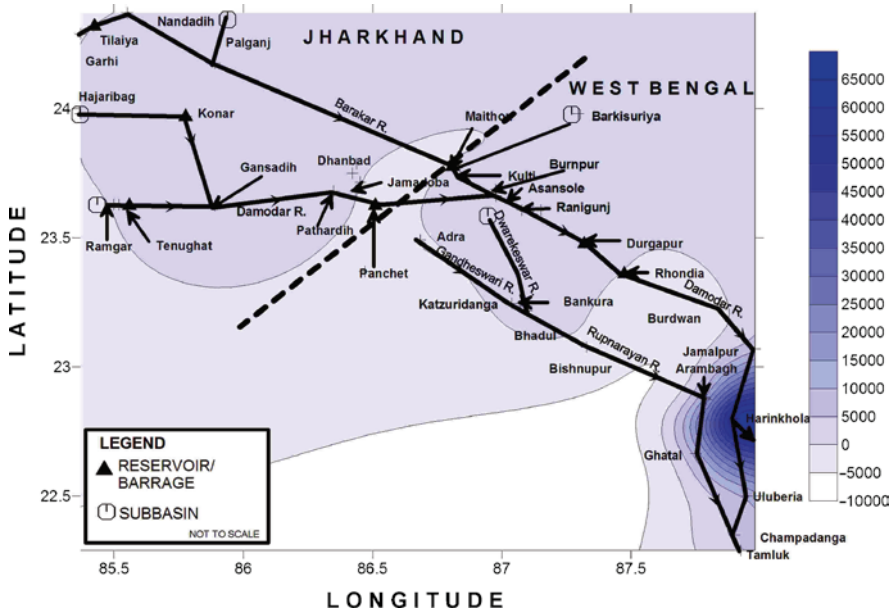
Fig. 4.8 Figure showing spatial variation of water footprint in 2071–2100 due to B2 scenario of climate change

References

Ahmad M, Ghumman A, Ahmad S (2009) Estimation of Clark's instantaneous unit hydrograph parameters and development of direct surface runoff hydrograph. Water Resour Manage 23:2417–2435

Blazkova S, Beven KJ, Kulasova A (2002) On constraining topmodel hydrograph simulations using partial saturated area information. Hydrol Process 16(2):441–458

Das NG (1991) Statistical methods in commerce, accountance and economics, Part – 1. M. Das & Co., Kolkata, pp 25–50

Hoekstra AY, Chapagain AK (2008) Globalization of water: sharing the planet's freshwater resources. Blackwell, Oxford

IPCC (2007) Climate change 2007: the physical sciences basis, retrieved on http://ipcc-wgl.ucar.edu/wg1/wg1-report.html. on 30th April, 2009

Lopez JJ, Gimena FN, Goni M, Agirre U (2005) Analysis of a unit hydrograph model based on watershed geomorphology represented as a cascade of reservoirs. Agric Water Manage 77(1–3):128–143

Majumder M, Roy P, Mazumdar A (2010) Watershed modeling of river Damodar with the help of neural network and genetic algorithm, PhD thesis, school of water resources engineering, Jadavpur University, Kolkata (in press)

Subramanya K (1994) Engineering hydrology, 2nd edn. Tata McGraw Hill, New Delhi, pp 60–90

Sui J (2005) Estimation of design flood hydrograph for an ungauged watershed. Water Resour Manage 19(6):813–830

Taskinen A, Bruen M (2007) Incremental distributed modelling investigation in a small agricultural catchment: 1. Overland flow with comparison with the unit hydrograph model. Hydrol Process 21(1):80–91

Wanielista M, Kersten R, Eaglin R (1987) Hydrology: water quantity and quality control. Wiley, New York, p 208

Yeh K, Yang J, Tung Y (1997) Regionalization of unit hydrograph parameters: 2. Uncertainty analysis. Stochast Hydrol Hydraulic 11(2):173–192

Chapter 5
Impact of Climatic Uncertainty on Water Sequestration of a Subtropical River Basin

Mrinmoy Majumder, Rabindra Nath Barman, Bipal K. Jana, Pankaj Roy, and Asis Mazumdar

Abstract The water sequestration capacity (WSC) of a region could be defined as the amount of water possible to be stored within the vegetative zones of the region, which could only be used by the vegetations of that region. The storage capacity of vegetated areas of a basin could also be called as WSC of that basin. The sequestration value could estimate or give an idea of the amount of vegetation/crop possible from the basin. In the present study, water sequestration is predicted with the help of neurogenetic models in face of climatic uncertainty. Water sequestration is important as it directly impacts the agricultural activity

M. Majumder (✉)
Senior Research Fellow, School of Water Resources Engineering,
Jadavpur University, Kolkata-700032, West Bengal, India
and
Geo-information Scientist, Regional Center, National Afforestation
and Eco-development Board, Jadavpur University, Kolkata-700032, West Bengal, India
e-mail: mrinmoy@majumder.info

R.N. Barman
Pertime Research Fellow, School of Water Resources Engineering,
Jadavpur University, Kolkata-700032, West Bengal, India
and
Assistant Professor, Department of Production, National Institute of Technology,
Agartala, Tripura, India

B.K. Jana
Senior Research Fellow, School of Water Resources Engineering,
Jadavpur University, Kolkata-700032, West Bengal, India
and
Environmental Manager, Consulting Engineering Services, West Bengal, India

P. Roy
Lecturer, School of Water Resources Engineering, Jadavpur University,
Kolkata-700032, West Bengal, India

A. Mazumdar
Coordinator, Regional Center, National Afforestation and Eco-development Board,
Jadavpur University, Kolkata-700032, West Bengal, India
and
Director, School of Water Resources Engineering, Jadavpur University,
Kolkata-700032, West Bengal, India

of a catchment. The study can tell us about the impacts of climate change on agricultural activity as water sequestrated by a catchment can decide the agricultural yield of the same. River Damodar was selected as the study area for the present study. The Damodar catchment is widely known for its high-scale soil erosion and variable water retention capacity. The PARITYCGD, a neurogenetic model trained with orthopareto dataset, was applied to estimate future stream flow and from the estimated stream flow, WSC of a basin was calculated. The estimated WSC of the basin showed the impact of climatic uncertainties on the basin's overall agricultural output. According to the results, WSC of upstream and downstream of river Barakar, river Damodar, and entire river network of Rupnarayan would be less than that of upstream of river Damodar in the future from 2010 to 2100 due to both A2 and B2 scenario of climate change. The magnitude of WSC was found to be greater in case of A2 scenario than B2 scenario of climate change. Although, WSC is a relatively new concept, it needs lot of revisions and rejudgments for considering as a more scientific and reliable parameter for agricultural output of a basin.

5.1 Introduction

5.1.1 *Hydrological Cycle*

The hydrologic cycle begins with the evaporation of water from the surface of the ocean. As moist air is lifted, it cools and water vapor condenses to form clouds. Moisture is transported around the globe until it returns to the surface as precipitation. Once the water reaches the ground, one of two processes may occur:

1. Some of the water may evaporate back into the atmosphere.
2. The water may penetrate the surface and become groundwater.

Groundwater either seeps its way to the oceans, rivers, and streams, or is released back into the atmosphere through transpiration. The balance of water that remains on the Earth's surface is runoff, which empties into lakes, rivers, and streams, and is carried back to the oceans, where the cycle begins again.

5.1.2 *Water Sequestration*

The water unused by plant could be collectively called as water sequestrated by a catchment. If volume of ground water, surface runoff, interflow, and transpired water was removed from the total volume of precipitation and stored water of a basin, the

remaining volume of water would be the water sequestrated by the river basin. The concept is similar to the concept of carbon sequestration of plants where carbon gets converted into biomass. The amount of carbon converted into biomass is known as carbon sequestrated by a plant (see Chapter 1). If a plant is replaced by river basin and carbon by water a similarity can be observed. The only difference would be that water is not converted into any other substance but remains as water only in a different place. Water sequestration could give an idea the condition of a catchment for agricultural productivity. If sequestration of water is low agricultural potential, will be high and vice versa. The factors that influence water sequestration are described next.

5.1.3 Influencing Factors

5.1.3.1 Infiltration Capacity

The infiltration capacity of a catchment would affect the amount of water sequestrated by river basin. The factor would be directly proportional to water sequestration, but plant population and holding capacity of catchment could reduce the amount even if basin had high infiltration capacity. Porosity, soil conductivity, and soil texture were some of the factors, which could influence infiltration capacity of a river basin.

5.1.3.2 Soil Texture

Soil texture of a basin would largely control water sequestration but would have complex relationship with the same. Sandy soils are unproductive for plantation, hence such soils may increase the water sequestration, but such soils are unable to hold water and release the water back to the channel flow as baseflow. Clayey soil in the other hand would hold water but as it is productive for plantation, water would be invested into plants. Plants like wheat and maize would use lesser amount of water, but big trees like bamboo or oak would reduce the amount of water unused in a large amount. Even if soil texture is not suitable for holding water, underneath geological structure may prevent water from flowing out. Similarly, if sandy soil has a low retention capacity, an impermeable layer beneath the soil layer may prevent water from being added to channel flow. So, amount of water unused may also vary depending upon the geological structure that is present under the soil and the amount and type of plantation grown in the basin.

5.1.3.3 Soil Erosion

An eroded soil would reduce the amount of water that could be sequestrated by a river basin. Catchments with eroded soils could not retain water and return it to channel flow. A highly eroded basin is often considered as a degraded basin. Agricultural potential of such catchment is also very low.

5.1.3.4 Plant Population

The amount of plant in a river basin would be inversely proportional to water sequestration as more plant in a basin would require more water. The amount of unused water would be low.

5.1.4 Literature Review

The annual hydrological regime of the Nakambe River shows substantial changes during the period 1955–1998 with a shift occurring around 1970. From 1970 to the mid-1990s, despite a reduction in rainfall and an increase in the number of dams in the basin, average runoff and maximum daily discharges increased. This chapter reviews the hydrological behavior of the Nakambe River from 1955 to 1998 and examines the potential role of land-use change on soil water holding capacity (WHC) in producing the counterintuitive change in runoff observed after 1970. We compare the results of two monthly hydrological models using different rainfall, potential evapotranspiration, and WHC datasets. The extent of natural vegetation declined from 43% to 13% of the total basin area between 1965 and 1995, while the cultivated areas increased from 53% to 76% and the area of bare soil nearly tripled from 4% to 11%. The total reduction in WHC is estimated to range from 33% to 62% depending on the method used, either considering that the WHC values given by the FAO stand for the environmental situation in 1965 or before. There is a marked improvement in river flow simulation using the time-varying values of soil WHC.

A water balance model combined with the Priestley–Taylor method for computing potential evapotranspiration has been developed as an integrated tool for modeling the response of river basins to potential climate change. The system was designed in the EXCEL 5.0 spreadsheet environment making use of the Visual Basic programming language. The model is simple to use and takes advantage of IIASA's mean monthly hydrologic data base (Leemans and Cramer 1991). The model environment and two case studies are described.

Remote sensing (RS) data from the moderate resolution imaging spectrora-diometer (MODIS), a climatic water budget model, and the STATSGO database were used within a GIS environment to determine the influences of hydrologic soil properties on soil moisture and thermal emission in western-central Kansas for a dry year, 2000. Two important variables, WHC and hydrologic soil group (HSG), were controlled in our water budget experiment to evaluate their impacts on soil moisture content (SMC) changes throughout the period. Results showed that HSG affected drought detection and occurrence very little, but WHC variations explained most local variations of SMC. As a strong indicator of relative soil moisture deficit, the Standardized Thermal Index (STI) patterns were also influenced by WHC.

This study uses evidence for the long-term (35 years) pattern of soil redistribution within two agricultural fields in the UK to identify the relative importance of tillage and overland flow erosion. Spatially distributed long-term total soil redistribution

data for the fields (Dalicott Farm and Rufford Forest Farm) were obtained using the caesium-137 (^{137}Cs) technique. These data were compared with predicted patterns of soil redistribution. These results give a clear indication that diffusive processes are dominant in soil redistribution within these fields. Possible diffusive processes include splash erosion, soil creep, and tillage. However, the magnitude of the diffusion coefficients for the optimum predicted pattern (~350–400 kg/m/a) demonstrates that tillage is the only process capable of explaining the very significant soil redistribution, which is indicated by the ^{137}Cs data. Consideration is given to the implications of these results for both soil erosion prediction and landscape interpretation.

5.1.5   Artificial Neural Network and Genetic Algorithm

The neurogenetic models were popular for its ability to identify patterns from dataset of input and output variable. A detailed description of artificial neural network and genetic algorithm is given in Chapter 22.

5.1.6   GIS and Hydrology

Geographical information system (GIS) and RS were now applied in hydrology for delineation of catchment and estimation of runoff with the help of distributed hydrologic models. An explanation of GIS and RS is given in Chapter 24.

5.1.7   Climate Change and Climate Models

Climate change is defined as the change in 30 year's weather pattern of a certain region. The changes can be abrupt or periodical. The abrupt changes of climate are often known as climatic uncertainty. Due to global warming climate and uncertainties seem to be eminent, hence many models were developed to estimate future climate. An explanation of various climatic models and justification of their development is given in Chapter 23.

5.1.8   Objective and Scope

The present study tried to estimate future water sequestration capacity (WSC) with the help of stream flow predicted by PARITYCGD model. WSC is directly proportional to agricultural output of a basin. As climate change is influencing the water availability of basins, it would impact the WSC of the same. Thus, climate change could also impact the basin agricultural productivity. The impact of climatic uncertainty on WSC was found out with the help of PARITYCGD neurogenetic

models, which had found to be successfully estimated water footprint of two river basins situated in Eastern India's tropical region.

5.1.9 Study Area

The study area of the present study was selected in the tropical regions of East India. Two river basins with diverse geomorphologic and climatic features and multiple types of water resource consumers were chosen to estimate water footprint of the two basins. A detailed description of the two river networks, river Damodar and river Rupnarayan, are given in Chapter 25.

5.2 Methodology

Neural models are popular for their ability to identify inherent patterns between variables with the help of available dataset. The models cannot predict the patterns, which are not present in the available dataset with which the model is trained. Climate change can 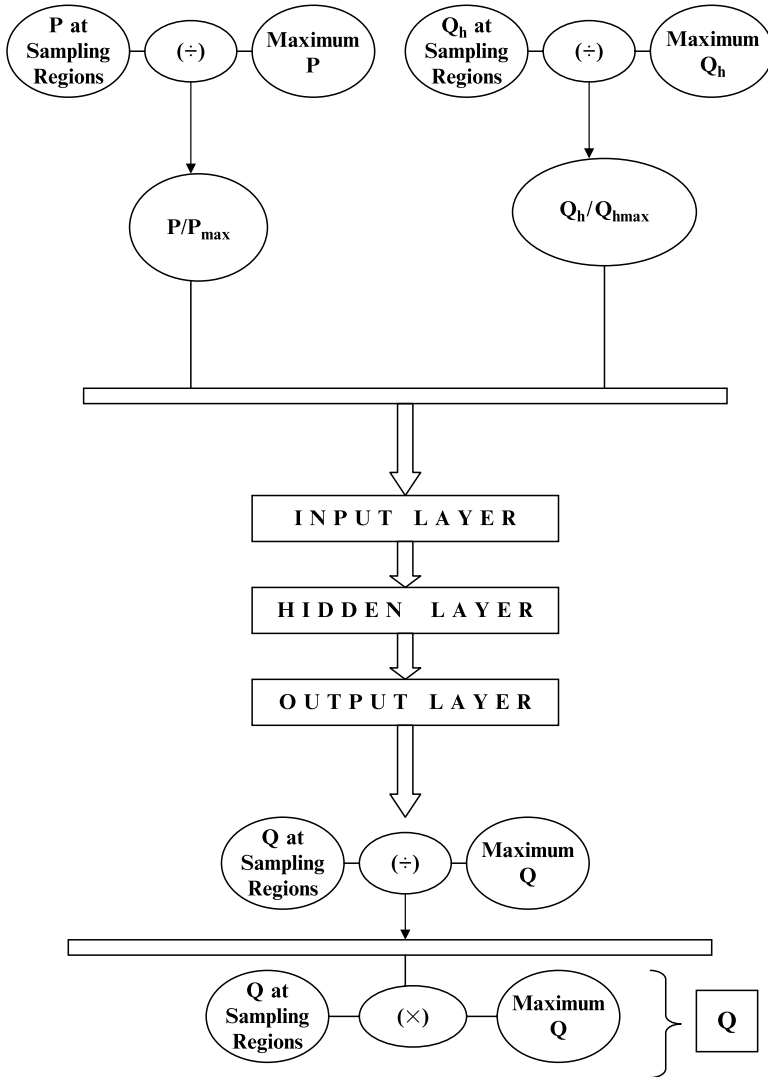induce extreme change in dataset patterns. If the models are trained with available dataset it will be unable to predict impact of climate change on the model output. A solution can be to precede the development of neural models with process-based models like HECHMS, TR55, or Rational modeling system. In the present study, three conceptual hydrologic models were first prepared and discharge was estimated with the help of those models. A sensitivity analysis was performed with the output from three models and observed discharge. This would help to select the better model among the three considered. A neural model was developed from the output of the selected model, which was considered as input variable and observed discharge as output. The advantage of this method was that the future discharge will be predicted first with the help of conceptual model and then with the neural model. As neural models are popular and known to be efficient in identification of patterns they were used to estimate the discharge but as such models can be erroneous for values with which it was not trained, the unknown values were predicted by conceptual model. The relationship between the outputs of conceptual model with observed discharge was used to estimate the future discharge.

5.2.1 Conceptual Coupled Neurogenetic Distributed Hydrologic Model (CONCONGDHM)

Neural models are popular for their ability to identify inherent patterns between variables with the help of available dataset (Fig. 5.1). The models cannot predict the patterns, which are not present in the available dataset with which the model is trained. Climate change can induce extreme changes in dataset patterns. If the models are

Fig. 5.1 Figure showing methodologies adopted to develop the CONCONGDHM models

trained with available dataset it will be unable to predict impact of climate change on the model output. A solution can be to precede the development of neural models with a process based models like HECHMS, TR55, or MODRAT. As neural models were known to be efficient in identification of patterns they were used to estimate the discharge but as such models can be erroneous for values with which it was not trained, the unknown values were predicted by conceptual model. The relationship between the outputs of conceptual model with observed discharge was identified with the help of neurogenetic models and used to estimate the future discharge.

5.2.1.1 Model Variables

In the present study, three conceptual hydrologic models were first prepared and basin runoff was estimated with the help of those models. A sensitivity analysis was performed with the output from three models and observed discharge. The sensitivity analysis helped to identify a variable's influence on other variable. Then, a neurogenetic model was developed where output of the selected model was considered as input variable of the neurogenetic model. The peak average monthly observed discharge was considered as output variable of the neurogenetic model. Peak average monthly rainfall was also included as input variable of the neurogenetic models.

Determination of Estimated Basin Runoff from the Conceptual Models

The first step of the model development methodology was to apply HECHMS, TR55, and MODRAT model to prediction runoff at the sampling points with the observed values of the input variables. The input variables and governing equation of considered conceptual models are given in Chapter 21.

For HECHMS model, Snyder's Unit Hydrograph method was used as basin transfer method, SCS curve number for estimation of catchments loss along with initial and constant method was selected for representation of base flow of the modeled basin.

The estimations from all the three models were compared with observed basin discharge and sensitivity analysis among the output of the conceptual models and the observed basin runoff was performed to select the better model among the three considered models. According to the sensitivity analysis, HECHMS was found to be more sensitive than the other two models and thus, output from the HECHMS model was fed as an input of the neurogenetic models.

5.2.1.2 Development of Neurogenetic Models

A 2 input–1 output neurogenetic model was developed where the output was considered as function of rainfall and estimated basin runoff from the conceptual model. The weight was updated according to the training algorithms applied for enabling the model to learn the inherent relationship between the input variables and the output.

QP, CGD, and BBP were used as training algorithm and a dataset of 505 records of the input and output variables. Seventy percent of which were used for training the models, 15% was used for testing, and the remaining 15% was used for testing the models. After the development of the model, it was trained repetitively until the desired output was estimated or a desired RMSE was achieved. The details of the model are given in Table 5.1. The CONCONGDHM when trained with CGD algorithm was called as CONCONGDHMCGD and when trained with QP and BBP algorithm were called as CONCONGDHMQP and CONCONGDHMBBP, respectively.

Table 5.1 Table showing input and output variables used for the CONCONGDHM model

Input	Abbreviation
Output	Abbreviation
Monthly peak average HECHMS-predicted basin runoff (Q_h) at the sampling regions divided by maximum monthly average HECHMS-predicted basin runoff (Q_{hmax}), Monthly average peak rainfall at the sampling regions divided by maximum peak monthly average rainfall (P_{max})	Q_h/Q_{hmax}, P/P_{max}
Peak average monthly basin runoff at sampling regions divided by maximum peak monthly average basin runoff (Q_{max})	Q/Q_{max}

5.2.1.3   Estimation of Basin Runoff

The estimated runoff index was multiplied with maximum runoff to find the predicted discharge from the model. The model outputs were compared with the help of performance validation criteria to find the better model among the seven models considered in the present study. Table 5.1 shows the input and output variables of CONCONGDHM hydrologic models and Fig. 5.1 depicts the overview of model algorithm.

5.2.2   *PARITYCGD Model*

The PARITYCGD model was developed with the help of neurogenetic model trained with an orthopareto dataset, detailed description of which are given in Table 5.2.

5.2.3   *Model Validation*

All the nine models were validated for accuracy with the help of root mean square error (RMSE), coefficient of determination (r), coefficient of efficiency (E), and first-order uncertainty analysis (U), which could be mathematically represented as

$$\mathrm{RMSE} = \sqrt{\sum_{n=1}^{n} \frac{(T_p - O_p)^2}{n}} \tag{1}$$

$$\text{Coefficient of determination} = \sqrt{\frac{\sum (T_p - T_m)(O_p - O_m)}{\sqrt{\sum_{1}^{n}(T_p - T_m)^2 \sum_{1}^{n}(O_p - O_m)^2}}} \tag{2}$$

Table 5.2 Table showing the model parameters and performance validation criteria of PARITYCGD and CONECOMO models

	PARITYCGD	CONECOMOQP	CONECOMOCGD	CONECOMOBBP
Model variables				
Input	$p(PCI, Q/Q_{max})$	$Q_{hec}/Q_{hecmax}, P/P_{max}$	$Q_{hec}/Q_{hecmax} P/P_{max}$	$Q_{hec}/Q_{hecmax} P/P_{max}$
Ouput	Q	Q/Q_{max}	Q/Q_{max}	Q/Q_{max}
Model parameters				
Network topology				
Network type	Feed forward	Feed forward	Feed forward	Feed forward
Network structure	1,2,1	2,1,1	2,1,1	2,1,1
Network weight	4	3	3	3
Training dataset	80	80	80	80
Testing dataset	10	10	10	10
Validation dataset	10	10	10	10
GA parameters				
Population	50	50	50	50
Generation	100	100	100	100
Penalty	6	6	6	6
Crossover rate	0.8	0.8	0.8	0.8
Mutation rate	0.2	0.2	0.2	0.2
Stop training condition				
MSE	0.05	0.05	0.05	0.05
Iteration	200	200	200	200
Generalization loss	5	5	5	5
Training algorithm parameters				
Algorithm name	CGD	QP	CGD	BBP
Activation function	Sigmoid	Sigmoid	Sigmoid	Sigmoid
Learning rule	Supervised	Supervised	Supervised	Supervised
Learning rate	NR	0.8	NR	0.8
Momentum	NR	NR	NR	0.8
Propagation Coefficient	NR	1.75	NR	NR
Training and testing results				
RMSE (training)	1.5	0.008	0.008	0.007
RMSE (testing)	0.56	0.005	0.004	0.004
	Maximum no. of iteration reached	Required RMSE achieved	Required RMSE achieved	Required RMSE achieved
Model estimation results				
RMSE	2.58	3.38	3.46	3.75
Relationship	0.96	0.68	0.67	0.92
Efficiency	0.99	0.95	0.96	0.97
Uncertainty (%)	5.5	7.5	7.67	7.8

$$\text{Coefficient of efficiency} = 1 - \frac{\sum\limits_{n=1}^{n}(T_p - O_p)^2}{\sum\limits_{n=1}^{n}(T_p - T_m)^2} \tag{3}$$

$$\text{First-order uncertainty } (U) = \left(\frac{\text{Stdev}(O_p - O_m)}{n}\right) \tag{4}$$

where T_p is the target data value for the p th pattern; O_p is the estimated data value for the p th pattern, T_m and O_m are the mean of target and estimated dataset, respectively and n is the total number of patterns. T_n is the target value of the nth pattern and T_m is the mean value of the targeted dataset.

Correlation coefficient could also be taken as a measure of model reliability (Statistics Solution 2009), whereas coefficient of efficiency was also used as a measurement of model sensitivity (Das 1991) toward observed dataset. Hence, both of these validation criteria also help to determine model reliability and sensitivity where high values would represent greater level of reliability and sensitivity of the model.

5.2.4   Calculation of Water Sequestration

The WSC was calculated with the following equation (5.5).

Let area of moisture content that is stored within a region is s (km^2).

Let basin area of the same region be A (km^2) and percentage of vegetated area of that region is a_v, and, water availability of the same region is WA (m^3), then, WSC could be calculated as

$$\text{WSC} = \text{WA} \times \{s / (A \times a_v)\} \text{m}^3 \tag{5}$$

5.3   Result and Discussion

5.3.1   Model Validation

The predicted values of discharge from all the developed seven neurogenetic models along with three hydrologic models were compared with the observed discharge and RMSE, r^2, and E were calculated to validate the models as well as to select the better model out of the seven models considered.

Table 5.3 Table showing comparison of performance validation criteria of neurogenetic model with conceptual hydrologic models

Model name	RMSE	r	E	U (%)
PARITYCGD	2.58	0.96	0.99	7
HECHMS	5.45	0.67	0.78	15
TR55	6.78	0.65	0.68	20
MODRAT	10.12	0.71	0.58	45

According to the comparison results as given in Table 5.3, RMSE of PARITYCGD was found to be 2.58, which was less than any other models. The RMSE of CONECOMOQP (3.38), CONECOMOCGD (3.46), and CONECOMOBBP (3.75) models were found to have the values nearest to RMSE of PARITYCGD model. The model efficiency (0.99) of PARITYCGD was also better than that of CONECOMOQP (0.95), CONECOMOCGD (0.96), and CONECOMOBBP (0.97). The coefficient of relationship (r) or measurement of model reliability of PARITYCGD (0.96) was found to be higher than CONECOMOBBP (0.92), CONECOMOQP (0.68), and CONECOMOCGD (0.67) model. The uncertainty analysis of all the four neurogenetic models reveals that, here also, PARITYCGD had the least U than CONECOMOQP (7.50), CONECOMOCGD (7.67), and CONECOMOBBP (7.80). As both RMSE and U of PARITYCGD were found to be minimum and r and E of the same model were found to be maximum among the considered four neurogenetic models, PARITYCGD was selected as the better model among the considered neurogenetic models.

If conceptual hydrologic models, like HECHMS, TR55, and MODRAT, were compared with the selected neurogenetic model, PARITYCGD was found to be 2.11, 2.63, and 3.92 times more accurate than HECHMS (5.45), TR55 (6.78), and MODRAT (10.12) (Table 5.3). The efficiency of the neurogenetic model (0.99) was also found to be higher than the any of the considered conceptual models; HECHMS (0.78), TR55 (0.68), and MODRAT (0.58). The coefficient of relationship or reliability (0.96) was also found to be higher among the four considered models. The uncertainty analysis of all the four models revealed that PARITYCGD has minimum uncertainty (5.5%) and MODRAT (45%) has the maximum uncertainty among the four hydrologic models.

As PARITYCGD has higher r and E and lower RMSE and U than the three considered hydrologic models, PARITYCGD was selected as the model for the estimation of future basin runoff according to the A2 and B2 baseline climate change scenarios, which were collected from generation of weather scenario by PRECIS climatic model.

The RMSE and uncertainty of PARITYCGD was lower and relationship coefficient and efficiency was found to be higher than the other three models as neural models generally learn their problems with the help of the data with which they are trained. The algorithms try to identify the patterns associated with the dataset and according to patterns of input with output dataset, output data of unknown input data was estimated. In case of PARITYCGD, the datasets were weighted

according to their sensitivity toward the output dataset. That is why the training algorithm of the neurogenetic models could easily identify the inherent encoded patterns of the dataset by which they were trained. But in case of conceptual hydrologic models, the accuracy depends upon the constants used in the model. The relationship between the input variables was equalized by different constants, which changes with change of location, magnitude, and direction of the variables. Also some parameters were ignorable in some places and unavoidable in other places. So, when a model is used with unwanted parameters it tends to use more computational power and often calculate the results of problem erroneously.

5.3.2 Estimation of Future WSC of the Rivers

The output of PARITYCGD was used along with PRECIS-generated weather scenarios to estimate WA as explained in (3.6). The results were fed to Eq. (5) to find WSC of the sampling region. The average WSC of each districts through which the two river basins have passed was calculated along with the WSC for states and river basins by averaging the district and station WSC for respective states and river basins. The results are depicted in Figs. 5.2–5.7 and Table 5.4.
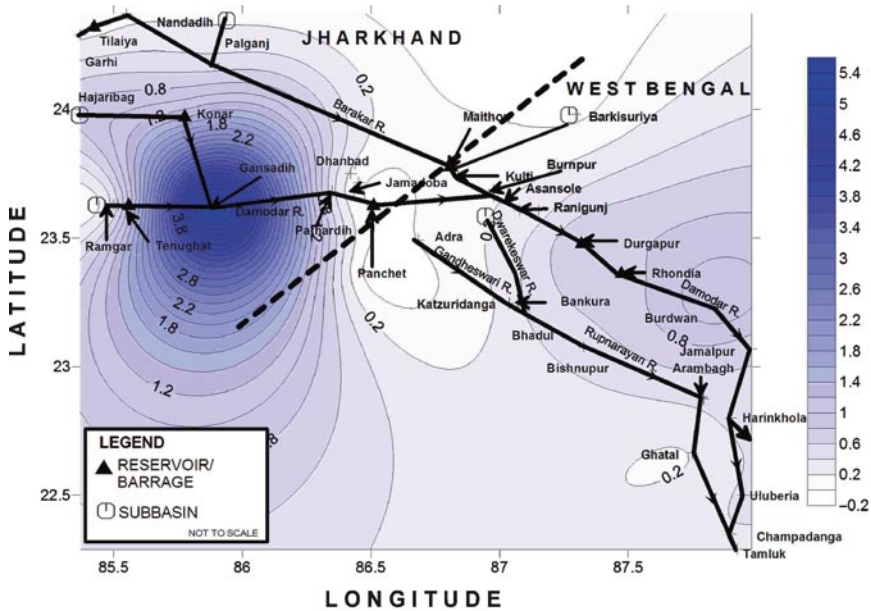
Fig. 5.2 Figure showing spatial variation of WSC in 2010–2040 for A2 scenario of climate change
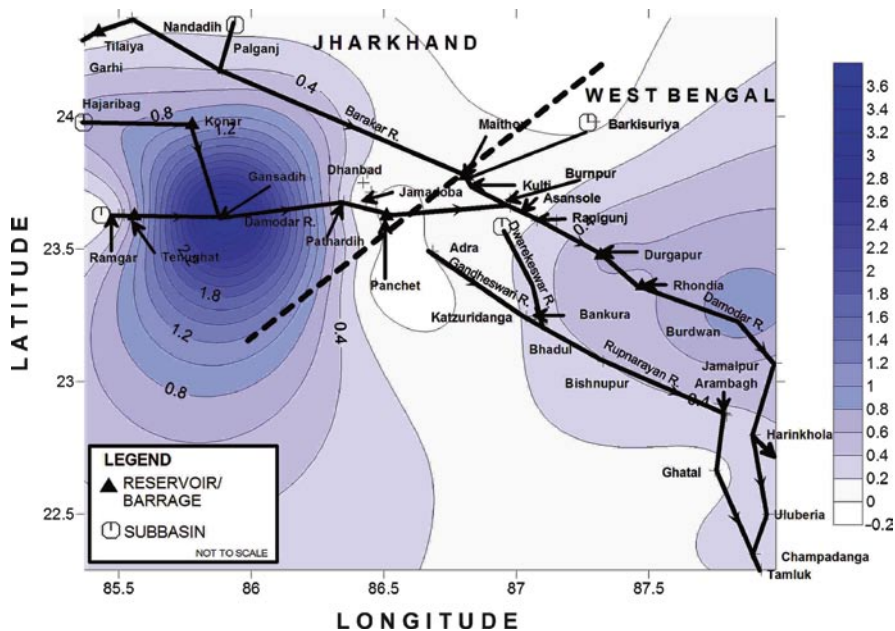
Fig. 5.3 Figure showing spatial variation of WSC in 2041–2070 for A2 scenario of climate change
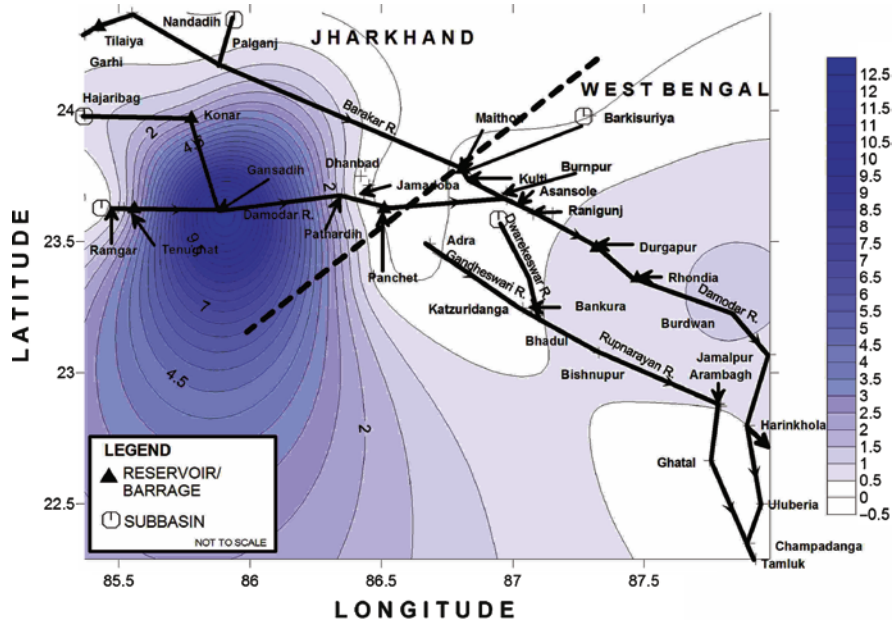
Fig. 5.4 Figure showing spatial variation of WSC in 2071–2100 for A2 scenario of climate change
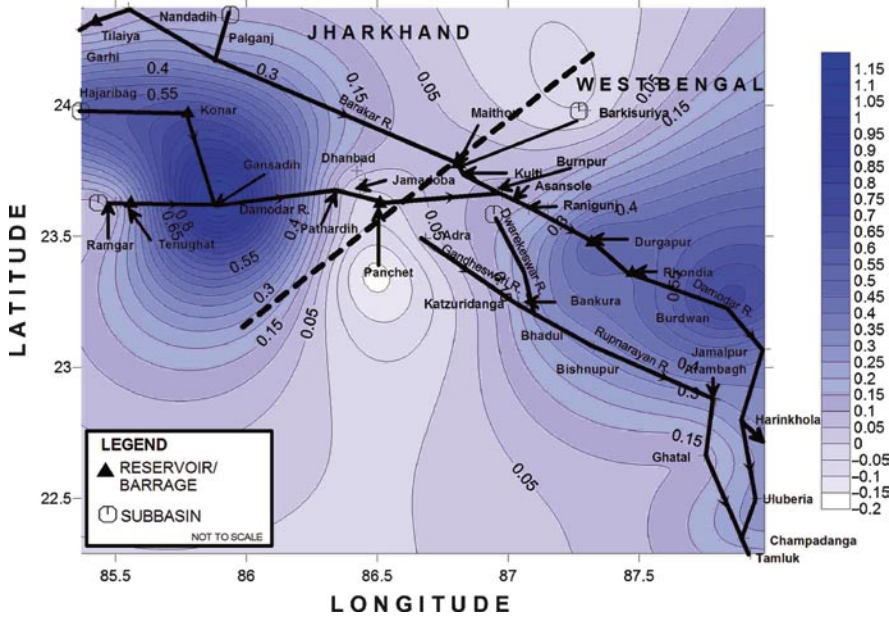
Fig. 5.5 Figure showing spatial variation of WSC in 2010–2040 for B2 scenario of climate change
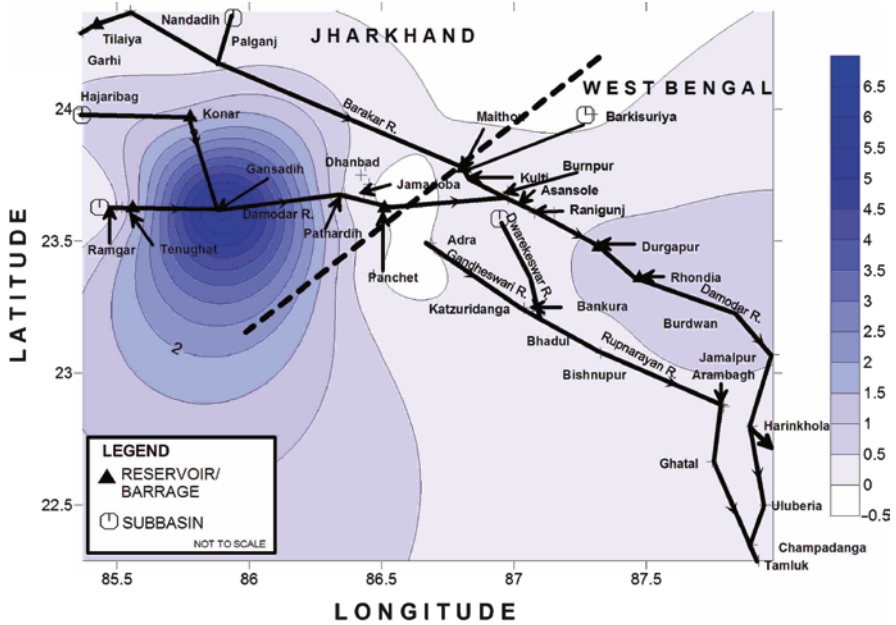
Fig. 5.6 Figure showing spatial variation of WSC in 2041–2070 for B2 scenario of climate change
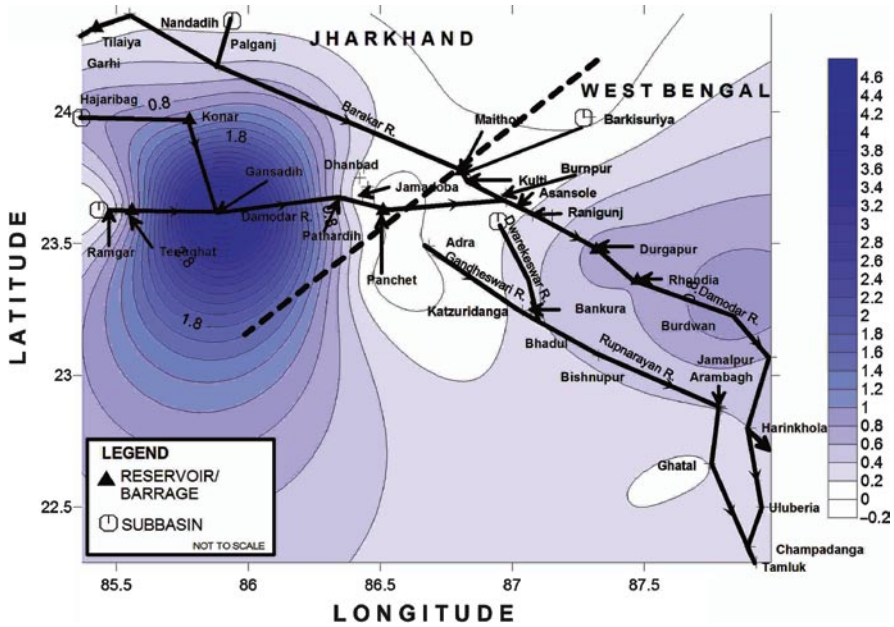
Fig. 5.7 Figure showing spatial variation of WSC in 2071–2100 for B2 scenario of climate change

Table 5.4 Table showing district-wise, state-wise, and basin-wise variation of WSC (m³) due to A2 and B2 scenario of climate change

	A2 scenario			B2 scenario			Observed
Districts	2010–2040	2041–2070	2071–2100	2010–2040	2041–2070	2071–2100	1970–2002
State	2010–2040	2041–2070	2071–2100	2010–2040	2041–2070	2071–2100	1970–2002
Basins	2010–2040	2041–2070	2071–2100	2010–2040	2041–2070	2071–2100	1970–2002
Giridih	0.153	0.195	0.236	0.118	0.159	0.163	0.100
Jamtara	−0.090	−0.109	−0.065	−0.101	−0.102	−0.090	−0.069
Bokaro	0.129	0.168	0.204	0.097	0.147	0.140	0.050
Ranchi	0.039	0.054	0.072	0.034	0.065	0.045	0.016
Hazaribagh	0.588	0.746	0.843	0.467	0.606	0.622	0.405
Dhanbad	0.656	1.026	2.462	0.193	1.199	0.880	0.027
Burdwan	0.408	0.512	0.567	0.321	0.394	0.438	0.293
Hooghly	0.384	0.489	0.550	0.314	0.402	0.435	0.301
Howrah	0.376	0.476	0.540	0.300	0.382	0.421	0.299
Purulia	0.105	0.135	0.156	0.090	0.122	0.128	0.087
Bankura	0.305	0.390	0.447	0.257	0.343	0.362	0.248
West Midnapur	0.046	0.065	0.109	0.034	0.071	0.084	0.069
East Midnapur	0.082	0.110	0.151	0.067	0.110	0.121	0.103
Jharkhand	0.246	0.347	0.625	0.135	0.346	0.293	0.088
West Bengal	0.244	0.311	0.360	0.198	0.261	0.284	0.200
Damodar	0.729	0.729	0.728	0.239	0.513	0.462	0.183
Rupnarayan	0.596	0.596	0.595	0.201	0.271	0.288	0.201

According to Table 5.4, the WSC of West Bengal and Rupnarayan is more than Jharkhand and Damodar. The trend will be followed in the future from 2010 to 2100 during both A2 and B2 scenario of climate change. WSC of Hoogly district was found to be maximum, whereas the same of Jamtara was found to be minimum and negative. In the future though, during both A2 and B2 scenario of climate change, maximum WSC was found from Dhanbad (2010–2100, A2 scenario and 2010–2040 and 2071–2100, B2 scenario) in Hazaribagh (2041–2070, B2 scenario). The minimum WSC was found from Jamtara similar to the present status of water shortage, which would continue in the future and may increase in 2010–2040 and 2071–2100 in A2 scenario of climate change and in 2071–2100 due to B2 scenario of climate change.

According to Figs. 5.2–5.7, WSC of upstream and downstream of river Barakar, river Damodar, and entire river network of Rupnarayan would be less than that of upstream of river Damodar in the future from 2010 to 2100 due to both A2 and B2 scenario of climate change. The magnitude of WSC was found to be greater in case of A2 scenario than in B2 scenario of climate change. Although, magnitude of WSC in 2041–2070 decreases from that in 2010–2040 and then again increases in 2071–2100 during A2 scenario of climate change. In case of B2 scenario, the WSC gets increased in 2041–2070 from that of 2010–2040 and then again decreases in 2071–2100. But if overall magnitude of WSC during A2 scenario is compared with B2 scenario, the WSC is more in former than that in later except for Jamtara districts where B2 would have more WSC than A2 scenario.

The above observations could be justified as Damodar or Jharkhand has less amount of vegetation/cropped field than West Bengal or river Rupnarayan, hence WSC is more where vegetation is more. Also, the basins of Damodar and Barakar are already in degraded stage, where erosion is causing a havoc problem. So, WHC, which greatly influences WSC is already lesser than the healthy catchments of Rupnarayan. The impacts were observed also in the future.

5.4   Conclusion

The present study tried to estimate future sequestration of water of basins with the help of neurogenetic models trained with orthopareto dataset. According to the results, WSC of upstream and downstream of river Barakar, river Damodar, and entire river network of Rupnarayan would be less than that of upstream of river Damodar in the future from 2010 to 2100 due to both A2 and B2 scenario of climate change. The magnitude of WSC was found to be greater in case of A2 scenario than in B2 scenario of climate change. The above observations could be justified as Damodar or Jharkhand has less amount of vegetation/cropped field than West Bengal or river Rupnarayan, hence WSC is more where vegetation is more. Also, the basins of Damodar and Barakar are already in degraded stage, where erosion is causing a havoc problem. So, WHC, which greatly influences WSC is already lesser than the healthy catchments of Rupnarayan.

References

Das NG (1991) Statistical methods in commerce, accountance and economics, Part – 1. M. Das & Co., Kolkata

Leemans R, Cramer W (1991) The IIASA database for mean monthly values of temperature, precipitation and cloudiness of a global terrestrial grid. International Institute for Applied Systems Analysis (IIASA). RR-91–18

Statistics Solution (2009) Retrieved from http://www.statisticssolutions.com/reliability-analysis on July 16, 2009

Chapter 6
Estimating Spatial Variation of River Discharge in Face of Desertification Induced Uncertainty

Arnab Barua, Mrinmoy Majumder, and Rajib Das

Abstract Climate change and global warming along with wide scale forest degradation have induced desertification in different parts of the world including India. The problem of desertification includes excess runoff, soil erosion, etc., which ultimately leads to catchment degradation. A study was performed to analyze the impact of desertification on river discharge. River Ajay, a small tributary of river Bhagirathi in the west of West Bengal was chosen as the study area due to the semideserted condition of the catchment. DIStributed COupled RATional Model (DISCORAT) where Orange County rational method (Rational OC) and MODified RATional (MODRAT) were coupled to estimate river runoff due to desertification-induced uncertainty. The desertification-induced uncertainty was generated by three scenarios where two scenarios represent extreme desertification (Actual-50%) and semi-desertification (Actual-5%). The input variables were modified according to the generated scenarios and applied to DISCORAT model for estimation of stream flow. As the catchment was divided into 16 15/15 grids and contribution of each grid was included in the estimation, the predicted stream flow for the desertification scenarios would give a distributed variation of stream flow and impact of desertification for each grid could be observed from the estimated stream flow at the grids. Cumulatively, a continuous variation of stream flow due to desertification could be generated and analysis could be made about the

A. Barua (✉)
Lecturer, Sylvan Polytechnic College, Bardhaman-713101, West Bengal, India
and
Former PG Student, School of Water Resources Engineering, Jadavpur University, Kolkata-700032, West Bengal, India
e-mail: arnabbarua83@gmail.com

M. Majumder
Senior Research Fellow, School of Water Resources Engineering, Jadavpur University, Kolkata-700032, West Bengal, India
and
Geo-information Scientist, Regional Center, National Afforestation and Eco-development Board, Jadavpur University, Kolkata-700032, West Bengal, India

R. Das
Lecturer, School of Water Resources Engineering, Jadavpur University, Kolkata-700032, West Bengal, India

impact of desertification on stream flow. According to the results, reduction of stream flow was observed due to desertification and the relationship between desertification and reduction of stream flow was found to be inversely proportional, that is, more intense desertification would imply more reduction of stream flow except in the outlet of the river basin where an opposite relationship was observed between desertification and stream flow. A reason for this estimation could be contributed to the reduction of rainfall as considered in the scenarios of desertification. The reversal of relationship at the outlet could be because of runoff-rainfall ration, which was considered to be well above 150% in Actual-50% scenario of desertification.

Keywords Combined modeling • desertification • spatial variation • stream flow

6.1 Introduction

6.1.1 Hydrologic Models

Hydrologic models are simplified, conceptual representations of a part of the hydrologic cycle. They are primarily used for hydrologic prediction and for understanding hydrologic processes. Two major types of hydrologic models can be distinguished:

- Models based on data. These models are black box systems, using mathematical and statistical concepts to link a certain input (e.g., rainfall) to the model output (e.g., runoff). Commonly used techniques are regression, transfer functions, and system identification. The simplest of these models may be linear models but is common to deploy nonlinear components to represent some general aspects of a catchment's response without going deeply into the real physical processes involved. An example of such an aspect is the well-known behavior that a catchment will respond much more quickly and strongly when it is already wet than it is dry.
- Models based on process descriptions. These models try to represent the physical processes observed in the real world. Typically, such models contain representations of surface runoff, subsurface flow, evapotranspiration, and channel flow, but they can be far more complicated. These models are known as deterministic hydrology models. These can be subdivided into single-event models and continuous simulation models.

A detailed description of hydrologic models and their applications in various problems of watershed is given in Chapter 21.

6.1.1.1 Rational OC and MODRAT Hydrologic Model

The Orange County rational method (Rational OC) can be used to determine runoff rates for watersheds with an area less than or equal to 1 mi^2 (640 acres). Infiltration is accounted for in the losses rather than using standard runoff coefficients (based

on percentage of impervious area) as in the rational equation. Complex reach routing could also be included while estimating time of concentration. MODified RATional (MODRAT) hydrologic model is a modified rational method computer program developed by the Los Angeles County Department of Public Works (LACDPW) to compute runoff rates under a variety of conditions common to the area of Los Angeles, California. MODRAT can compute runoff rate and corresponding hydrographs with the help of rational equation if rainfall–runoff mass curve and rainfall intensity duration frequency curve are provided. The rational equation was shown by Eq. (6.1)

$$Q = c \times i \times A \tag{1}$$

where c is the runoff coefficient, i is the rainfall intensity, and A is the basin area.

As a method of urban hydrology, the *rational* method had the following shortcomings:

- The method does not produce a hydrograph.
- The rational method does not account for changing (time-dependent) conditions such as soil condition or rainfall intensity.

Although the MODRAT hydrologic model can produce hydrograph, it represents basin loss due to infiltration with the help of runoff coefficient which is just an empirical constant determined with the help of relationship curves between 5 and 100 years of runoff and rainfall of that basin. Runoff coefficient is often found to be erroneous and often misleading. But Rational OC hydrologic model can represent basin loss in a better way than the MODRAT hydrologic model as the representation of basin loss is estimated with the help of soil groups.

6.1.2   Combined Modeling System

A combined model is defined as a model or combination of models, which simultaneously represents both the models but generally takes the advantage of one model to replace the disadvantage of the other. For example, climate models were often connected to hydrologic models where the output from climate models were used as input of the hydrologic model (Nakatsugawa et al. 1996; Soden and Held 2006; Butts et al. 2008). Some coupled models use GIS with available hydrologic models to develop distributed hydrologic model (Nunes et al. 1998; Pullar and Springer 2000; Vieux 2004; Di Luzio et al. 2004). Again, in another type of coupled models, specialty of one model is merged with specialty of other models to remove the shortcomings of both the models (Dutta et al. 2000). According to recent hydrologic literatures; models for different types of variables were coupled to predict some other related variables (Loheide and Gorelick 2007). Generally, for any other types of coupled or combined models, the output was found to be more accurate than when the models were used separately (Fig. 6.1).
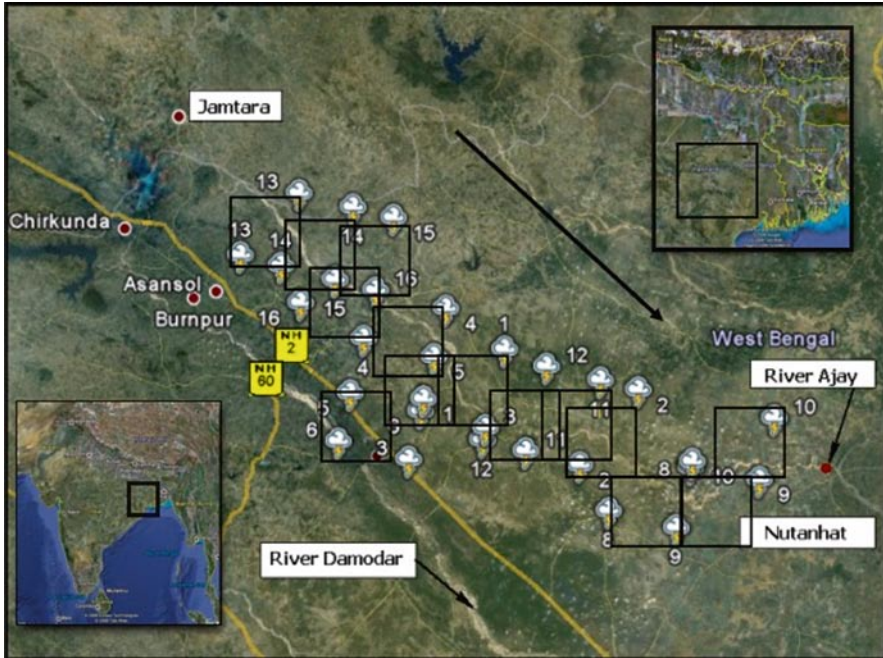
Fig. 6.1 Grid diagram, storm clouds, and corresponding numbers show the position of the grid (Note: Google Earth Image of the river basin along with the considered grids. Deep green areas of the image represent deep vegetation, whereas light green areas represent agricultural land. Area with white or gray color represents the human settlements. Lines with orange color show the National Highway and grayish white irregular lines represent the rivers. The *arrow* parallel to the river basin shows the average basin slope of the river Ajay)

6.1.3   Desertification

Desertification is the degradation of land in arid and dry subhumid areas, resulting primarily from man-made activities and influenced by climatic variations. It is principally caused by overgrazing, overdrafting of groundwater, and diversion of water from rivers for human consumption and industrial use, all of these processes fundamentally driven by overpopulation.

A major impact of desertification is biodiversity loss and loss of productive capacity, for example, by transition from land dominated by shrublands to nonnative grasslands. In the semiarid regions of southern California, many coastal sage scrub and chaparral ecosystems have been replaced by nonnative, invasive grasses due to the shortening of fire return intervals. This can create a monoculture of annual grass that cannot support the wide range of animals once found in the original ecosystem. In Madagascar's central highland plateau, 10% of the entire country has been lost to desertification due to slash and burn agriculture by indigenous peoples. In Africa, if current trends of soil degradation continue, the continent will be able to feed only

25% of its population by 2025, according to UNU's Ghana-based Institute for Natural Resources in Africa (United Nations 2009). Globally, desertification claims a Nebraska-sized area of productive capacity each year (Speth 2009).

Desertification is induced by several factors, primarily anthropogenic causes, which began in the Holocene era and continue at the highest pace today. The primary reasons for desertification are overgrazing, overcultivation, increased fire frequency, water impoundment, deforestation, overdrafting of groundwater, increased soil salinity, and global climate change (Wilson 2001).

6.1.3.1 Causes of Desertification

Deserts may be separated from surrounding, less arid areas by mountains and other contrasting landforms that reflect fundamental structural differences in the terrain. In other areas, desert fringes form a gradual transition from a dry to a more humid environment, making it more subtle to determine the desert border. These transition zones can have fragile, delicately balanced ecosystems. Desert fringes often are a mosaic of microclimates. Small pieces of wood support vegetation that picks up heat from the hot winds and protects the land from the prevailing winds. After rainfall the vegetated areas are distinctly cooler than the surroundings.

In these marginal areas activity centers may stress the ecosystem beyond its tolerance limit, resulting in degradation of the land. By pounding the soil with their hooves, livestock compact the substrate, increase the proportion of fine material, and reduce the percolation rate of the soil, thus encouraging erosion by wind and water. Grazing and collection of firewood reduce or eliminate plants that bind the soil and prevent erosion. All these occur due to the trend toward settling in one area instead of a nomadic culture.

Sand dunes can encroach on human habitats. Sand dunes move through a few different means, all of them assisted by wind. One way that dunes can move is through saltation, where sand particles skip along the ground like a rock thrown across a pond might skip across the water's surface. When these skipping particles land, they may knock into other particles and cause them to skip as well. With slightly stronger winds, particles collide in mid-air, causing sheet flows. In a major dust storm, dunes may move tens of meters through such sheet flows. And like snow, sand avalanches, falling down the steep slopes of the dunes that face away from the winds, also move the dunes forward.

It is a common misconception that droughts by themselves cause desertification. While drought is a contributing factor, the root causes are all related to overexploitation of the environment by human beings (Wilson 2001). Droughts are common in arid and semiarid lands, and well-managed lands can recover from drought when the rains return. Continued land abuse during droughts, however, increases land degradation. Increased population and livestock pressure on marginal lands has accelerated desertification. In some areas, nomads moving to less arid areas disrupt the local ecosystem and increase the rate of erosion of the land. Nomads typically try to escape the desert, but because of their land-use practices, they are bringing the desert with them.

Some arid and semiarid lands can support crops, but additional pressure from greater populations or decreases in rainfall can lead to the disappearance of few plants. The soil becomes exposed to wind, causing soil particles to be deposited elsewhere. The top layer becomes eroded. With the removal of shade, rates of evaporation increase and salts become drawn up to the surface. This increases soil salinity, which inhibits plant growth. The loss of plants causes less moisture to be retained in the area, which may change the climate pattern leading to lower rainfall.

This degradation of formerly productive land is a complex process. It involves multiple causes, and it proceeds at varying rates in different climates. Desertification may intensify a general climatic trend toward greater aridity, or it may initiate a change in local climate. Desertification does not occur in linear, easily mappable patterns. Deserts advance erratically, forming patches on their borders. Areas far from natural deserts can degrade quickly to barren soil, rock, or sand through poor land management. The presence of a nearby desert has no direct relationship to desertification. Unfortunately, an area undergoing desertification is brought to public attention only after the process is well under way. Often little data are available to indicate the previous state of the ecosystem or the rate of degradation.

Desertification is both an environmental and developmental problem. It affects local environments and populations' ways of life. Its effects, however, have more global ramifications concerning biodiversity, climatic change, and water resources. The degradation of terrain is directly linked to human activity and constitutes both the consequences of poor development and a major obstacle to the sustainable development of dryland zones (Cornet 2002). Combating desertification is complex and difficult, usually impossible without alteration of land management practices that led to the desertification. Overexploitation of the land and climate variations can have identical impacts and be connected in feedbacks, which makes it very difficult to choose the right mitigation strategy. Investigating the historic desertification plays a special role since it allows better identification of human and natural factors. In this context, recent research about historic desertification in Jordan questions the dominant role of man. It seems possible that current measures like reforestation projects cannot achieve their goals if global warming continues. Forests may die when it gets drier, and more frequent extreme events as testified in sediments from earlier periods could become a threat for agriculture, water supply, and infrastructure.

6.1.4 Objective and Scope

OC Rational and MODRAT are two widely used models for estimation of discharges. But, Rational OC cannot produce a hydrograph and MODRAT cannot estimate loss as accurately as the former model. Estimation of hydrologic models varies due to their capability of estimating watershed loss and as change in stream flow is highly dependant on change in time, a hydrograph is necessary to be drawn if a proper flow rate is required to be estimated. In the present study, an approach has been made to combine Rational OC and MODRAT to remove the disadvantages of

both the model and to add the advantages of the same, so that the new model could estimate watershed loss more accurately than when the model is used separately. The model was named as DISCORAT model according to **Dis**tributed **Co**upled **Rat**ional Hydrologic Model.

The DISCORAT model was applied to estimate the spatial variation of discharge due to desertification. Desertification of a catchment implies large-scale reduction of canopy cover along with soil erosion. Another objective of the present study was to estimate stream flow in face of basin desertification. The results could conclude the impact of desertification on stream flow of a river basin.

6.1.5 Study Area

The Ajay River emerges from the forest-covered hills of Chakai block in Munger district of Bihar and flows over a length of 132 km in Jharkhand, enters West Bengal near Kalipahari, and flows over a length of 144 km over West Bengal and falls into the Bhagirathi, which is a distributary emerging out of river Ganga, near Katwa. A small number of riverlets like Kedhasa and Darwa join it at the upper reaches. The total basin area of Ajay River is 6,888 km^2. The basin area in Jharkhand is 3,554 km^2, which is 51.6% of the total basin area. In West Bengal, the basin area is 3,334 km^2, which is 48.4% of the total basin area. The basin area in Jharkhand is hilly, whereas that in West Bengal is mostly plain. About 7% of the total area is under forest and 63% is under cultivation. The observed discharge for two gauge stations in Ajay River located at Jamtara, in Jharkhand and Natunhat in Barddhaman district in West Bengal, was collected. The river basin between these two gauge stations represents the study area. The Jamtara station is located at latitude 23°58′18″ and longitude 86°54′25″ and the Natunhat station is located at latitude 23°32′44″ and longitude 87°54′25″. The basin area between these two stations is about 2,906 km^2. Average annual precipitation of the study area is about 120 cm. The elevation of the study area ranges from 232 to 48 m. The major portion of the study area is under agriculture. Soils of the study area are red loamy soil, older alluvium, and younger alluvium.

6.2 Methodology

Both Rational OC and MODRAT require some dimensional parameters like length of longest flow path, length from the basin centroid, slope, etc., along with some variables, which represent basin loss like runoff coefficient, soil groups, infiltration, etc. (Chapter 21). The dimensional parameters were retrieved from Survey of India Toposheets and with the help of GIS. The loss variables were calculated with the help of Soil and Land Use Survey of India (SLUSI) maps (for soil groups) and rainfall–runoff curve of the basin area. The methods of data retrieval are described next.

6.2.1 Data Collection

The following steps were adopted to measure the dimensional parameters of the basin:

1. First of all the toposheets were divided into nine grids, each of 15″/15″ dimension. Then, the grids of the toposheets were scanned and imported and digitized with the help of the "MapWindow GIS" software, details of which can be found from www.mapwindow.org.
2. During digitization, the area and length of the river, the area of the sand dunes, village, pond, forest, the distance between highest and lowest contour, the contour elevation, and the total area of the grid was digitized.
3. Now, with the help of the digitized informations, the required area and length of river, area of sand, pond, village, forest, the distance between highest and lowest contour, and the contour elevation was measured.
4. The slope was calculated with the help of elevation difference between highest and lowest elevation of the grid and distance between the same. The percentage impervious area was calculated by subtracting the area of pond and forest from the total area of the grid.
5. After completion of digitization and retrieval of dimensional data, the next step was to identify soil groups and runoff coefficient of the basin grids.
6. The soil groups were identified with the help of soil maps found from the reports of SLUSI. The runoff coefficient was collected by dividing observed 30 years annual volume of runoff (m^3) with observed 30 years annual volume of rainfall (m^3).
7. The toposheets of Ajay River basin was divided into 16 grids and dimensional values, soil groups, and runoff coefficient were identified for each of the grid. As rainfall for all the grids were unavailable, the distributed rainfall dataset given by Tyndall was used in the estimation work and calculation of runoff coefficient. Basin runoff for ungauged grids were calculated with the help of Central Water Commission prescribed Area Runoff Equation (Subramanya 1994).

6.2.2 Model Development

According to the Rational OC hydrologic model, peak Runoff (Q) is calculated with the help of Eq. (6.2),

$$Q = 0.90(I - F_m)A \tag{2}$$

where Q is the peak flow (ft^3/s), I is the rainfall intensity (in./h), F_m is the maximum loss rate, where $F_m = a_p \times F_p$ (a_p is the area of pervious parts of the basin and F_p is the soil group of the pervious area), and A is the catchment area (acres).

The peak discharge for MODRAT hydrologic model is calculated with the help of Eq. (6.3).

$$Q = C_i A \tag{3}$$

where Q is the flow rate (in./h), c is the runoff coefficient, i is the rainfall intensity, and A is the area of the river basin (mi).

Now from Eq. (6.2),

$$Q/A = 0.90(I - F_m) \tag{4}$$

From Eq. (6.3),

$$Q/A = C_i \tag{5}$$

From Eqs. (6.4) and (6.5),

$$\Rightarrow C = 0.90(I - F_m)/i \tag{6}$$

The runoff coefficient (c) of Eq. (6.4) was substituted by Eq. (6.7) to find the maximum loss rate (F_m) as

$$F_m = (i - Q/A) \tag{7}$$

From Eqs. (6.3), (6.6), and (6.7), peak basin runoff could be represented as,

$$Q = F_m A_i \tag{8}$$

where F_m is calculated with the help of Eq. (6.7) not as calculated in Eq. (6.2).

For Eq. (6.8), data requirement was small, where only rainfall intensity, basin area, and observed runoff were required to estimate peak basin runoff. The introduction of the observed runoff also make the DISCORAT model a catchment-sensitive one as it would definitely estimate runoff based on present data of runoff, which would automatically calibrates the model according to the catchment it was applied. The introduction of rainfall intensity would make it possible for the model to draw hydrographs according to the rainfall and basin characteristic if rainfall intensity is taken as a function of excess rainfall. As explained earlier, Rational OC has a disadvantage that only a single flow rate is possible to be estimated and MODRAT has a disadvantage that the estimation of watershed loss is not accurate as that of Rational OC, in (6.8) the model, DISCORAT, can estimate loss similar to Rational OC and can generate hydrograph similar to MODRAT. So, both the models were combined to include the advantages and to remove the disadvantage, and build a model, which shall be more accurate and efficient than the models with which it was developed. The model output was compared with observed data and output from both MODRAT and Rational OC to calibrate as well as validate and select the better model among the three considered models.

6.2.3   Model Validation

The output and observed discharge data were compared to calculate the root mean square error (RMSE) (6.9), correlation coefficient (*r*) (6.10), coefficient of efficiency (*E*) (6.11), and first-order uncertainty analysis (*U*) (6.12) of the models. The values would help in selection of the better model among the six models considered in the present study.

$$\text{RMSE} = \sqrt{\sum_{n=1}^{n} \frac{(T_p -}{}} \tag{9}$$

$$\text{Correlation coefficient} = \sqrt{\frac{\sum (T_p - T_m)(O_p - O_m)}{\sum_{1}^{n} (T_p - T_m)^2 \sum_{1}^{n} (O_p - O_m)^2}} \tag{10}$$

$$\text{Coefficient of efficiency} = 1 - \frac{\sum_{n=1}^{n} (T_p - O_p)^2}{\sum_{n=1}^{n} (T_p - T_m)^2} \tag{11}$$

$$\text{First-order uncertainty } (U) = \left(\frac{Stdev(O_p - O_m)}{n} \right) \tag{12}$$

6.2.4   Development of Desertification-Induced Model Uncertainty Scenario

Desertification of a basin is an effect, which is generally caused by long duration of less-than-normal rainfall, basin degradation, reduction of canopy cover and soil erosion.

In the present study, three scenarios of rainfall and basin characteristic were generated from the observed dataset and IPCC recommendation for desertification-prone areas. The first scenario, which was named as Actual-5%, annual observed rainfall was decreased by 5% and basin characteristic was degraded, which was represented by increasing the runoff to rainfall ratio more than 1 (generally for a healthy basin the ratio would always be under 1). In case of the second scenario, which was named as Actual-10%, annual observed rainfall was decreased by 10% and runoff to rainfall ratio was considered more than 1.15 and for the third scenario, which was considered as Actual-50%, rainfall was decreased by 50% and runoff to rainfall ratio was increased by 1.5. As one of the conditions of basin desertification is less than normal rainfall, the amount of rainfall was reduced. As runoff to rainfall ratio represents the status of a basin where values of more than 1 represents

degraded catchment and during desertification, basins release more runoff than rainfall as canopy reduction and soil erosion reduce the water-holding capacity. Thus, the three scenarios were configured to represent desertification of basins where the minimum desertification or drought-like scenario was represented by the first scenario and maximum desertification or a wasted catchment scenario was represented by the last scenario. The rainfall values and corresponding change in runoff–rainfall coefficient was made according to and at similarities with the IPCC predictions for future climate and river basin characteristics. Table 6.1 depicts the description of the rainfall and runoff to rainfall ratio for the three considered scenarios. The rainfall intensity was changed as per the increase in rainfall and runoff to rainfall ratio whereas observed peak runoff was used for the Q, which would automatically calibrate the model according to the selected river basin.

6.3 Result and Discussion

6.3.1 Model validation

Peak basin runoff was estimated with the help of observed data of the input variables and all the three models. The model-predicted runoff was compared with observed runoff and RMSE, r, E, and U were calculated to select the better model among the three models considered.

According to Table 6.2, the RMSE value of DISCORAT (3.29) was found to be less than Rational OC (13.46) and MODRAT (11.19) model. The value of uncertainty in case of DISCORAT (16.60%) is also much less than the MODRAT (95.73%) and Rational OC (146.76%). Among the three models (DISCORAT, Rational OC, and MODRAT), the efficiency of DISCORAT was found to be maximum (98.9%) than Rational OC (98%) and MODRAT (83%). The coefficient of relationship was also higher in case of DISCORAT (0.98) than the other hydrologic models, which show the higher reliability of the combined model. According to the performance validation criteria, DISCORAT model was selected as the better

Table 6.1 Table showing parameters used for creation of desertification scenario

Scenario (%)	Increase in annual rainfall (%)	Runoff to rainfall ratio
Actual-5	5	1<
Actual-10	10	1–1.1
Actual-50	50	1.1–1.5

Table 6.2 Table showing performance validation criteria of the three models

Model name	RMSE	Relationship	Efficiency (%)	Uncertainty (%)
DISCORAT	3.29	0.98	98.9	16.60
MODRAT	11.19	0.87	83	95.73
Rational OC	13.46	0.76	98	146.76

model among the three considered conceptual hydrologic models. The increased accuracy of the combined model could be attributed to the autocalibration characteristic of the model, which had automatically make the model appropriate for the basin it was applied to but both MODRAT and Rational OC did not have such characteristic, which was the reason for lesser accuracy of the later models.

6.3.2   Estimation of Desertification Induced Basin Runoff

As the DISCORAT model was selected as a better model among the three considered models, the desertification scenarios were fed to the DISCORAT model for prediction of basin runoff due to desertification of river basins. The estimations of runoff for the available two-gauge stations were shown in Figs. 6.2 and 6.3. The spatial variation of runoff is shown by Figs. 6.4–6.16.
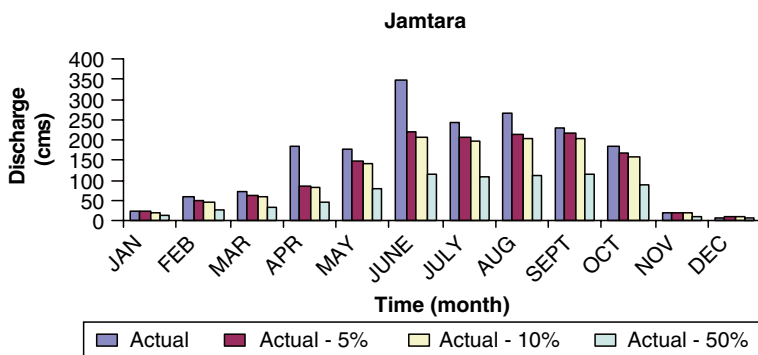
Fig. 6.2 Figure showing monthly variation of basin discharge at Jamtara in face of three desertification scenarios
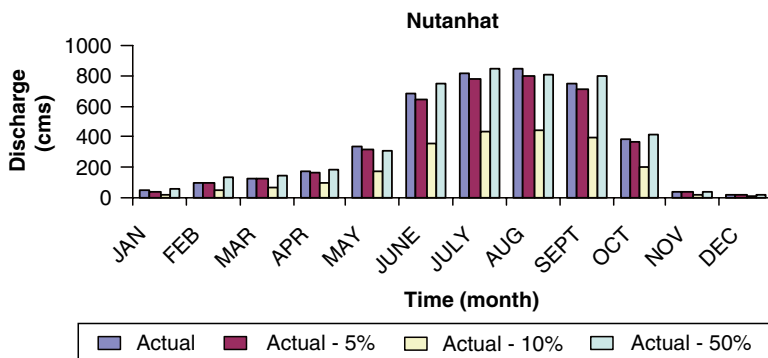
Fig. 6.3 Figure showing monthly variation of basin discharge at Nutanhat in face of three desertification scenarios
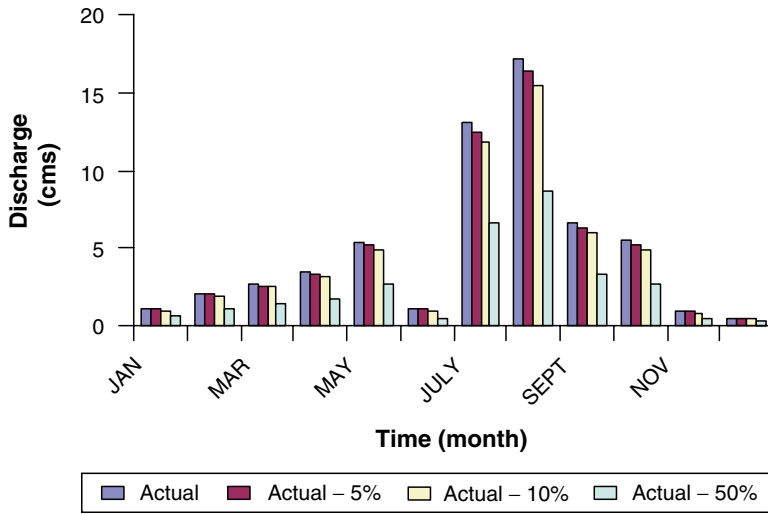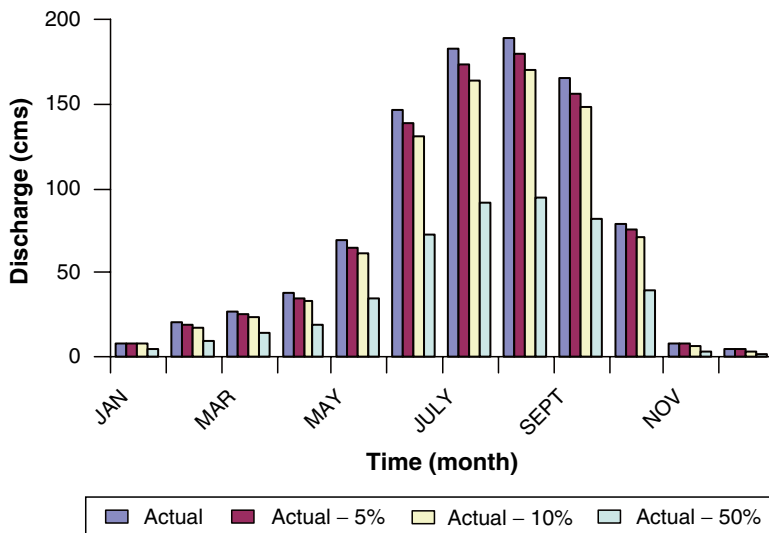
Fig. 6.4 Figure Showing Estimated River Runoff from the Grid 16 as estimated by DISCORAT model
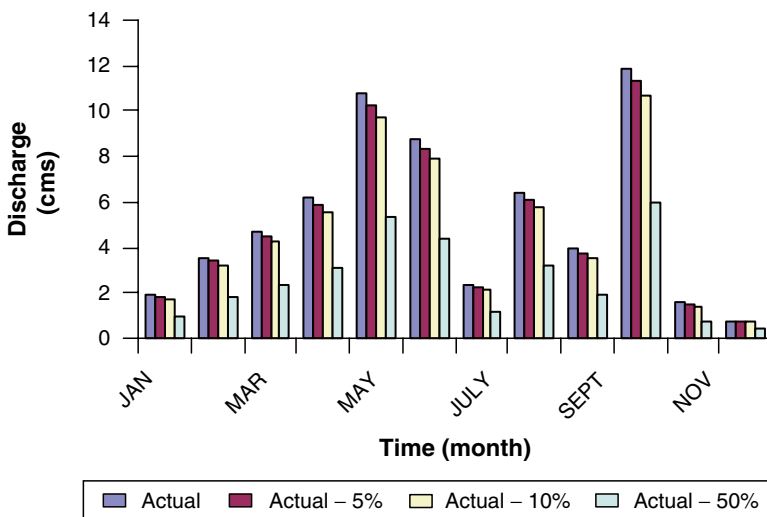
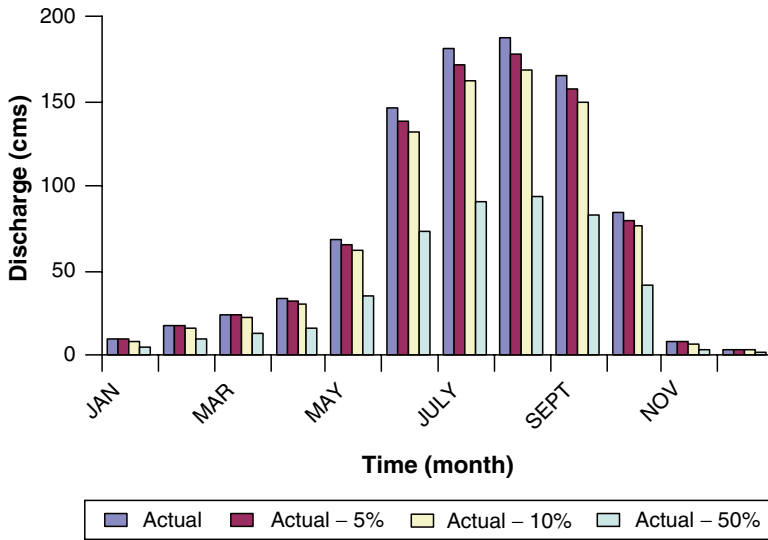**Fig. 6.5** Figure showing estimated river runoff from the grid 15 as estimated by DISCORAT model

According to the Figs. 2 and 3, river runoff would be reduced with reduction in rainfall for both the gauge stations of the river basin except for Nutanhat, where river runoff was predicted as less than that of Actual-50%. The justification of this prediction could be contributed to the fact that along with reduction of rainfall, runoff to rainfall ratio was also increased and in Actual-50% the change was maximum.
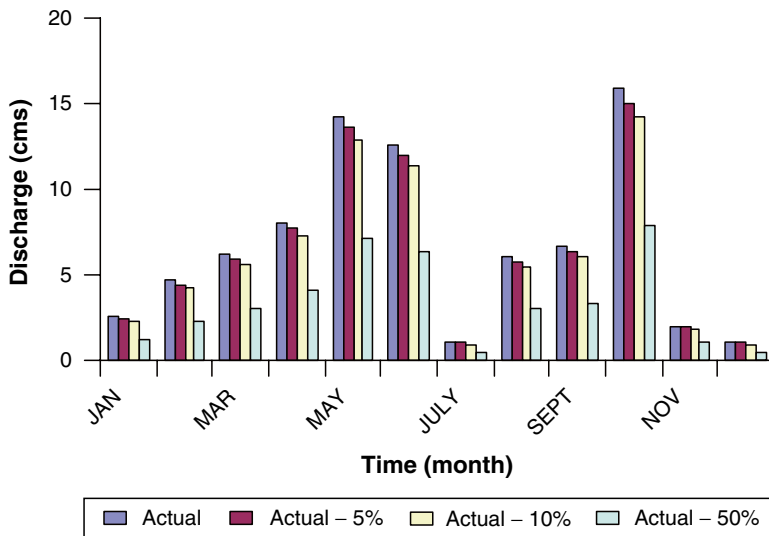
Fig. 6.6 Figure showing estimated river runoff from the grid 14 as estimated by DISCORAT model
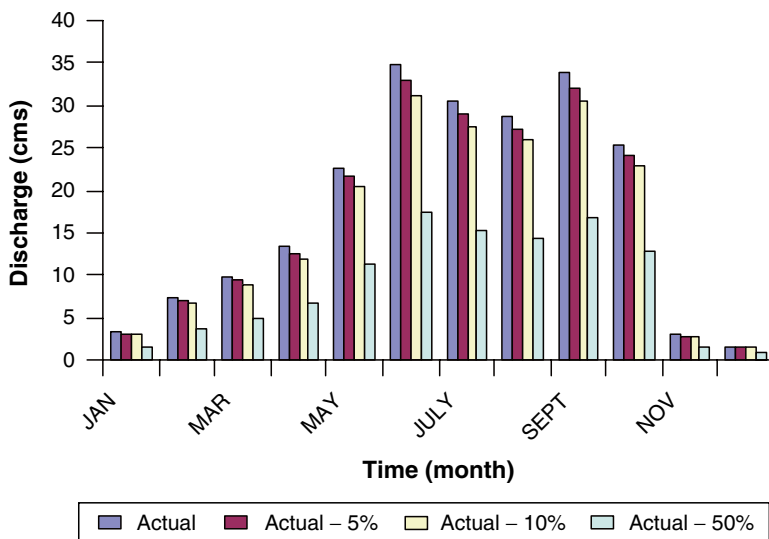
Fig. 6.7 Figure showing estimated river runoff from the grid 13 as estimated by DISCORAT model
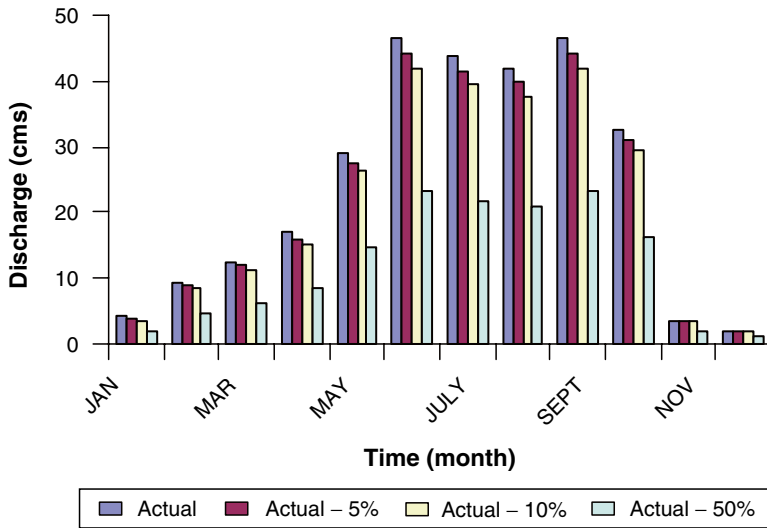
Fig. 6.8 Figure showing estimated river runoff from the grid 12 as estimated by DISCORAT model
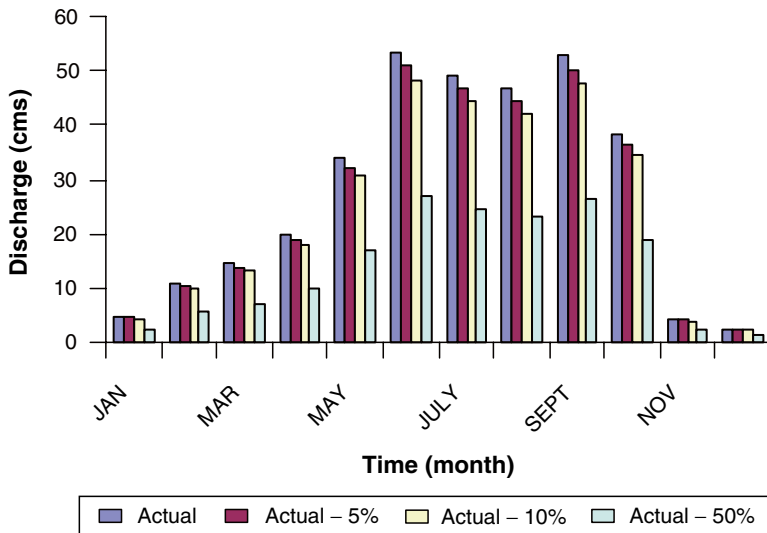
Fig. 6.9 Figure showing estimated river runoff from the grid 11 as estimated by DISCORAT model
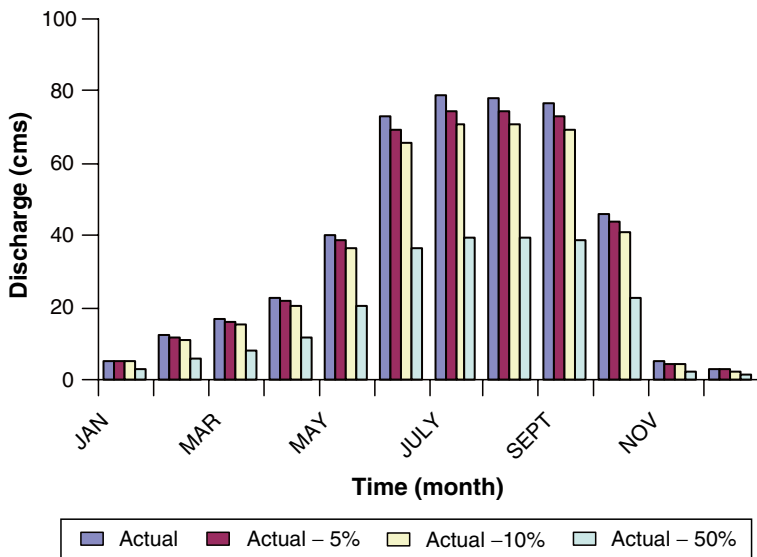
Fig. 6.10 Figure showing estimated river runoff from the grid 10 as estimated by DISCORAT model
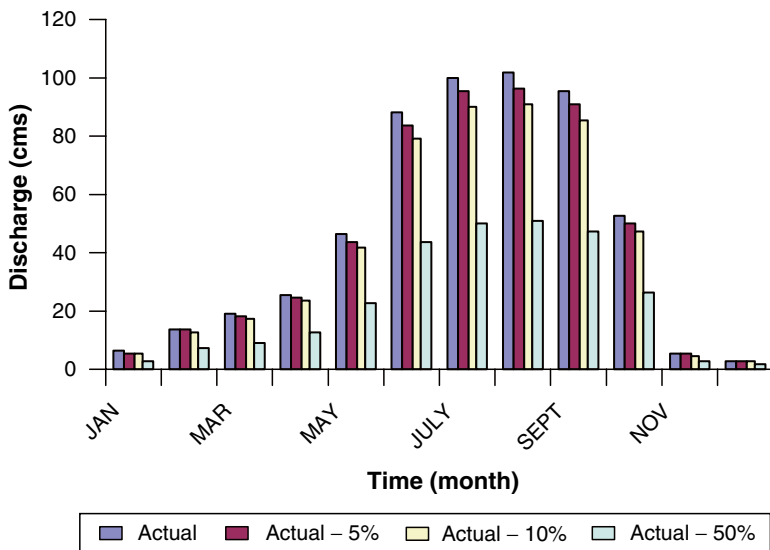
Fig. 6.11 Figure showing estimated river runoff from the grid 9 as estimated by DISCORAT model
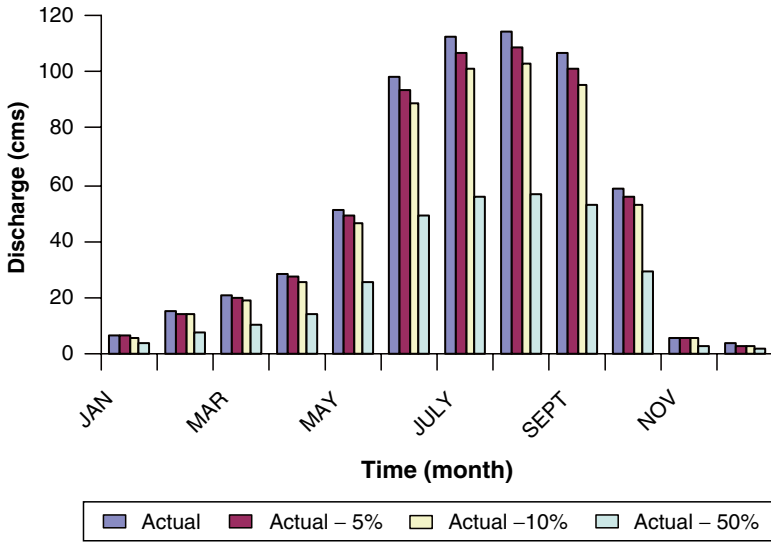
Fig. 6.12 Figure showing estimated river runoff from the grid 8 as estimated by DISCORAT model
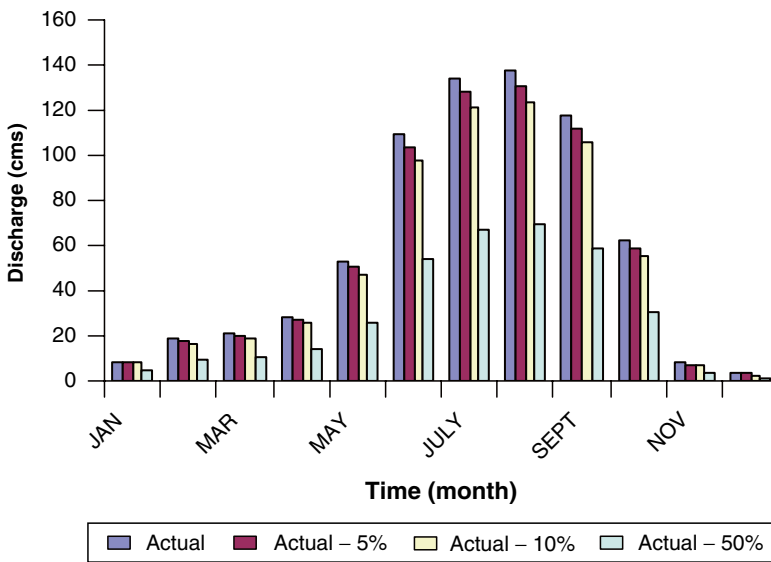
Fig. 6.13 Figure showing estimated river runoff from the grids 4, 5, and 6 as estimated by DISCORAT model
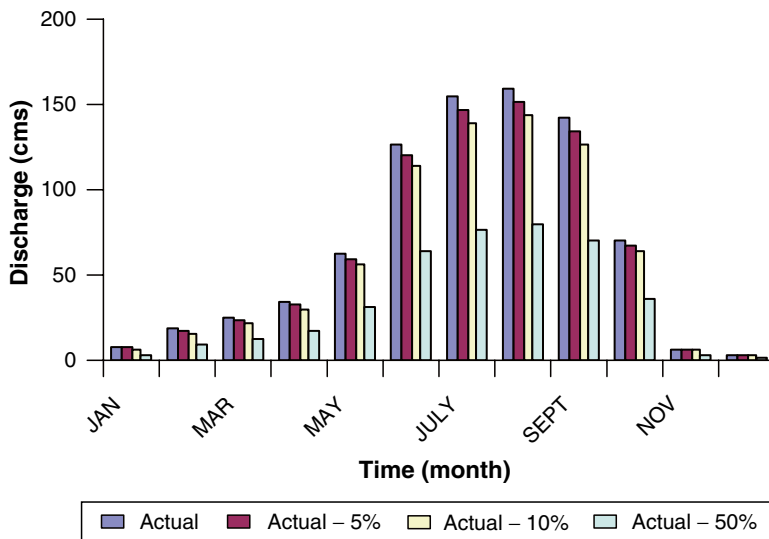
Fig. 6.14 Figure showing estimated river runoff from the grid 3 as estimated by DISCORAT model

Fig. 6.15 Figure showing estimated river runoff from the grid 2 as estimated by DISCORAT model

Fig. 6.16 Figure showing estimated river runoff from the grid 1 as estimated by DISCORAT model

So, the rainfall intensity was adjusted likewise, which influences the predicted basin runoff. But according to Figs. 6.4–6.16, the trend of reduction was followed accordingly to desertification scenarios but influence of increase in runoff to rainfall ratio was not observed within the grids, which may be justified by the fact that basin area of the grids were smaller than the area of the stations.

6.4   Conclusion

In the present study, a combined model, DISCORAT, was developed with the help of basin loss estimation capability of Rational OC and hydrograph generation capacity of MODRAT to remove the drawbacks of Rational OC and MODRAT where the former cannot generate a hydrograph for its peak flow estimation and the later cannot estimate loss including infiltration and with the better model among the three spatial variation of stream flow is estimated in face of desertification-induced uncertainty. Among the three models, DISCORAT was found to estimate discharge more accurately than Rational OC and MODRAT, hence the DISCORAT model was selected to estimate stream flow according to the generated desertification scenarios. According to the results, desertification would have an inversely proportional relationship with stream flow as stream flow was reduced due to desertification except at the outlet where an opposite trend was observed. The reduction in rainfall in the generated scenarios could be the reason for the reduced stream flow. Although the predictions were observed to have less than 95% accuracy as both

MODRAT and Rational OC are linear models, the RMSE was found to be more than 5% even in case of the selected model. Although the estimations may not be very encouragable, the approach to combine the models had actually reduced the RMSE of the models when used separately. The autocalibration characteristic of the DISCORAT model can be taken as another beneficial output from the present study. It would be interesting to note the level of accuracy when the DISCORAT model is applied to a bigger river basin and with more resolution.

References

Butts MB, Overgaard J, Styczen M, Gudbjerg J, Lønborg M, Lørup JK, Graham D, Sinding P (2008) Expanding integrated modelling capabilities using OpenMI. Eos Trans AGU 89(53), Fall Meet Suppl, Abstract H41G-0960

Cornet A (2002) Desertification and its relationship to the environment and development: a problem that affects us all. In: Ministère des Affaires, Johannesburg. World Summit on Sustainable Development, pp 91–125

Das NG (1991) Statistical Methods in Commerce. Accountance and economics, M. Das & Co., Kolkata, Part-1. pp 25–50

Di Luzio M, Srinivasan R, Arnold JG (2004) A gis-coupled hydrological model system for the watershed assessment of agricultural nonpoint and point sources of pollution. Trans GIS 8(1):113–136

Dutta D, Herath S, Musiake K (2000) Flood inundation simulation in a river basin using a physically based distributed hydrologic model. Hydrol Process 14(3):497–519

Loheide SP, Gorelick SM (2007) Riparian hydroecology: a coupled model of the observed interactions between groundwater flow and meadow vegetation patterning. Water Resour Res 43:W07414

Nakatsugawa M, Anderson M, Kavvas ML (1996) A simplified climate model with combined atmospheric-hydrological processes. Hydrol Sci 41(6):915–938

Nunes C, Graca D, Ramos I (1998) Coupling gis with hydrologic and hydraulic flood modelling. Water Resour Manage 12:229–249

Pullar D, Springer D (2000) Towards integrating GIS and catchment models. Environ Model Software 15(5):451–459

Soden BJ, Held IM (2006) An assessment of climate feedbacks in coupled ocean atmosphere models. J Climate 19(14):3354–3360

Speth JG (2009) Environmental failure: a case for a new green politics. Retrieved from http://www.guardian.co.uk/environment/2008/oct/21/network on 22 July 2009

Subramanya K (1994a) Engineering hydrology. Tata McGraw Hill publishing company limited. New Delhi. 2:60–90

United Nations University (2009) Looming desertification could spawn millions of environmental refugees Africa may be able to feed only 25% of its population by 2025. Retrieved from http://news.mongabay.com/2006/1214-unu.html on 22 July 2009

Vieux BE (2004) Distributed hydrologic modeling using GIS (Water Science and Technology Library). Springer, New York

Wilson EO (2001) The future of life. Vintage, New York

Chapter 7
Determination of Urbanization Impact on Rain Water Quality with the Help of Water Quality Index and Urbanization Index

Sanjib Das, Mrinmoy Majumder, Debasri Roy, and Asis Mazumdar

Abstract Rain water quality is a vital factor for deciding whether the water is drinkable or not. But increase in urbanization could degrade the quality of rain water. In the present study, rain water was collected from different sampling locations near and far from urban centers. The influences of urbanization were analyzed with the help of the relationship between water quality index (WQI) of the collected samples and urbanization index (UI) of the sampling location. The WQI was developed with the help of different water quality parameters and their standards. The index was developed as per the standards of drinking water prescribed by All India Public Health Engineering and with the help of "Water Classifier" software developed by Majumder (2008). The urbanization index for the present study was developed as a function of population density, change in population within sampling locations, and density of residential and commercial complexes areas within a radius of 5 km of the sampling locations. According to the results, the relationship between WQI and UI was inversely proportional in sampling locations of both

S. Das
Technical Assistant, School of Water Resources Engineering, Jadavpur University, Kolkata-700032, West Bengal, India
e-mail: das_1977@gmail.com

M. Majumder
Senior Research Fellow, School of Water Resources Engineering,
Jadavpur University, Kolkata-700032, West Bengal, India
and
Geo-information Scientist, Regional Center, National Afforestation
and Eco-development Board, Jadavpur University, Kolkata-700032, West Bengal, India

D. Roy
Reader and Joint Director, School of Water Resources Engineering,
Jadavpur University, Kolkata-700032, West Bengal, India

A. Mazumdar
Coordinator, Regional Center, National Afforestation and Eco-development Board,
Jadavpur University, Kolkata-700032, West Bengal, India
and
Director, School of Water Resources Engineering, Jadavpur University,
Kolkata-700032, West Bengal, India

South and North 24 Parganas, which are located in southern and northern outskirts of Kolkata but the slope of the relationship is more tilted in case of sampling points located in South 24 Parganas, than in case of the samples taken from North 24 Parganas. As most of the polluting commercial complexes (leather, textile) were situated in southern outskirts of Kolkata and huge number of residential complexes were present or in verge of completion in the region, there was a massive migration of population from different parts of Kolkata to South 24 Parganas , The service and IT sectors, the nonpolluting industries of Kolkata were concentrated in the northern outskirts. The justification of the relationship between WQI and UI in southern and northern outskirts of Kolkata can be attributed to the above fact. The present study, thus, concluded that there is an impact of urbanization on quality of rain water in Kolkata. The same study can be made in other metro cities of India to verify the veracity of the relationship. The present study was conducted with very few sampling locations but still the locations were situated in regions of different UI and WQI. The study can be repeated with more sampling locations within the city with samples, which have more diverse WQI and UI.

Keywords Rain water • urban and rural variation • urbanization • water quality index

7.1   Introduction

Rainwater is usually considered as a safe and suitable source of potable water, and it is commonly used as such, especially in urban and rural areas in developing countries of the world. In southern part of India, as well as other parts of the country where surface freshwater sources are scarce and/or where suitable ground water is not easily available (e.g., through hand-dug wells), rainwater is often collected and stored for use over many months of the annual cycle. It is not uncommon for schools in urban and rural areas to use such rainwater sources in place of distilled or deionized water, while food and water vendors use it to produce packaged water (commonly called "pure water") for sale to the public. The desire to investigate the quality of such water sources and how the constructional activities influence rainwater quality in a typical metropolitan town such as Kolkata in eastern India has motivated the present study.

7.1.1   Rain Water Harvesting: Justification and Utility

If one summarizes the reasons for fresh water crisis, following points may emerge out:

- Fresh water sources are being heavily exploited to meet the ever-increasing demand of urban population. Increased awareness of using safe water among the population creates more demand for fresh water.
- Rapid urbanization reduces the open area, thus the open surface for natural recharge of groundwater by rainwater.

- Large-scale extraction results in depletion of ground water table.
- Severe contamination of most surface water sources due to extensive industrial and fertilizer- and pesticide-based agricultural activities.
- Any water manager in the country is deeply concerned with the above points. He or she has to consider that rainwater is the ultimate source of fresh water to overcome the crisis. Potential of rain to meet water demand is tremendous.

  The objectives of rainwater harvesting are as follows:

- To meet the domestic water demand, especially drinking water demand directly.
- To conserve and augment the storage of ground water.
- To reduce water table depletion.
- To improve the quality of ground water.
- To arrest seawater intrusion in coastal areas.
- To avoid flood and water logging in urban areas.
- Rainwater can be stored for direct use or can be recharged into the groundwater aquifer in use.

Broadly, rainwater can be harvested in three ways:

- Collected and stored for ready use in containers
- Collected and stored in surface water sources like lakes and ponds to be supplied to community by providing treatment
- Recharged into the ground for later withdrawal

7.1.2 Water Quality and Pollution

Water pollution is defined as the contamination of water bodies such as lakes, rivers, oceans, and groundwater. It affects organisms and plants that live in these water bodies and in almost all cases the effect is damaging not only individual species and populations, but also the natural biological communities. It occurs when pollutants are discharged directly or indirectly into water bodies without adequate treatment to remove harmful constituents.

About 20% of the world's population lacks access to safe drinking water and about 50% lacks adequate sanitation. In many developing countries, rivers downstream of large cities are little cleaner than open sewers. Levels of suspended solids in Asia's rivers, for example, almost quadrupled since the late 1970s and rivers typically contain four times the world average and 20 times the OECD levels. The fecal coliform count in Asia's rivers is 50 times higher than the WHO guidelines. People using such water for washing, bathing, or drinking are at high risk. In Latin America as a whole, only about 2% of sewage receives any treatment. Worldwide, polluted water is estimated to affect the health of about 1,200 million people and to contribute to the death of about 15 million children under 5 years every year.

A nice little introduction of water pollution, factors and causes and the impact of water pollution on the health of local population are discussed in Chapter 11.

7.1.3   Urbanization

Urbanization is the physical growth of urban areas from rural areas as a result of population immigration to an existing urban area.

The rapid urbanization of the world's population over the twentieth century is described in the 2005 Revision of the UN World Urbanization Prospects report. The global proportion of urban population rose dramatically from 13% (220 million) in 1900, to 29% (732 million) in 1950, and to 49% (3.2 billion) in 2005. The same report projected that the figure is likely to rise to 60% (4.9 billion) by 2030 (UN 2005) However, French economist Philippe Bocquier, writing in *THE FUTURIST* magazine, has calculated that "the proportion of the world population living in cities and towns in the year 2030 would be roughly 50%, substantially less than the 60% forecast by the United Nations (UN), because the messiness of rapid urbanization is unsustainable (Fig.7.1). Both Bocquier and the UN see more people flocking to cities, but Bocquier sees many of them likely to leave upon discovering that there's no work for them and no place to live"(Cetron and Davies 2008).

According to the UN State of the World Population 2007 report, sometime in the middle of 2007, the majority of people worldwide will be living in towns or cities, for the first time in history; this is referred to as the arrival of the "Urban Millennium." In regard to future trends, it is estimated that 93% of urban growth will occur in developing nations, with 80% of urban growth occurring in Asia and Africa.

7.1.4   Urbanization of Kolkata

Kolkata is the main business, commercial, and financial hub of eastern India and the northeastern states. It is home to the Calcutta Stock Exchange – India's second-largest bourse. It is also a major commercial and military port, and the only city in
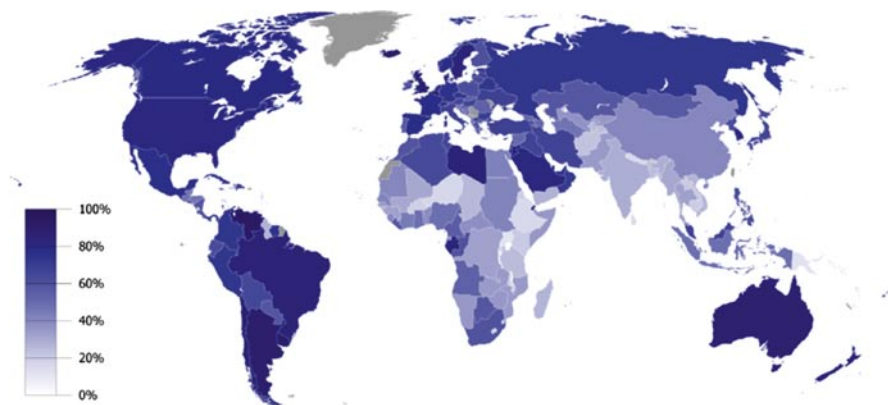
Fig. 7.1 Figure showing urbanization of countries (%) as of 2006 (UNICEF 2008)

the region to have an international airport. Once India's leading city and Capital, Kolkata experienced a steady economic decline in the years following India's independence due to the prevalent unstabilized political condition and rise in trade-unionism. Between the 1960s and the mid-1990s, flight of capital was enormous as many large factories were closed or downsized and businesses relocated. The lack of capital and resources coupled with a worldwide glut in demand in the city's traditional industries (e.g., jute) added to the depressed state of the city's economy. The liberalization of the Indian economy in the 1990s has resulted in the improvement of the city's fortunes. Until recently, flexible production had always been the norm in Kolkata, and the informal sector has comprised more than 40% of the labor force. For example, roadside hawkers generated business worth Rs. 8,772 crore (around US$2 billion) in 2005. State and federal government employees make up a large percentage of the city's workforce. The city has a large unskilled and semi-skilled labor population, along with other blue-collar and knowledge workers. Kolkata's economic revival was led largely by IT services, with the IT sector growing at 70% yearly – twice that of the national average. In recent years there has been a surge of investments in the housing infrastructure sector with several new projects coming up in the city. Kolkata is home to many industrial units operated by large Indian corporations with products ranging from electronics to jute. Some notable companies headquartered in Kolkata include ITC Limited, Bata India, Birla Corporation, Coal India Limited, Damodar Valley Corporation, United Bank of India, UCO Bank, and Allahabad Bank. Recently, various events like adoption of "Look East" policy by the government of India, opening of the Nathu La Pass in Sikkim as a border trade-route with China, and immense interest of the South East Asian countries to enter the Indian market and invest have put Kolkata in an advantageous position.

As of 2001, Kolkata city had a population of 4,580,544, while the urban agglomeration had a population of 13,216,546. Current estimates for 2009 project the city's population to be 5,080,519. The sex ratio is 928 females per 1,000 males – which is lower than the national average, because many working males come from rural areas, where they leave behind their families. Kolkata's literacy rate of 81% exceeds the all-India average of 80%. Kolkata Municipal Corporation area has registered a growth rate of 4.1%, which is the lowest among the million-plus cities in India.

7.1.5 Literature Review

There are many scientific literatures analyzing the impact of urbanization on land use, hydrology, geo-morphology, and agriculture. For example, Lee et al. (2006) explain the impact of urbanization on coastland wetland structures and Liang et al. (2008) examine the change in plant diversity in Beizing due to impacts of rapid urbanization. Vicars-Groening et al. 2007 also highlighted the impact of urbanization on storm hydrographs where a smaller time to peak and lesser time lag was reported for post-urbanized conditions. Bolca et al. (2007) applied GIS in the estimation of change in agricultural land and wetlands due to rapid urbanization of

Balcovas delta. Savard et al. (2000) advocate the application of biodiversity management to mitigate the impacts of land use and cover change. Moglia et al. (2008) explain a participatory approach to solve the problems of fresh water supply in face of rapid urbanization of old cities.

Lin (2009) estimated and established the impact of land use change on regional climate again Salomão et al. (2008) analyzed and concluded that increase in human population could influence CO_2 and O_2 dynamics of the atmosphere. The above paper argues that urbanization change could also impact the climate or chemical compositions of climatic parameters at a regional scale.

From the above literatures importance of urbanization and its impact on local climate can be well justified and can also suggest for a study on the impact of rapid urbanization on quality of rainfall.

7.1.5.1 Objective and Scope

Urbanization changes the population density of an area. Increase in population would imply increase in organic wastes, which would ultimately pollute the local rivers, streams, and lakes. Increase in industry generally attracts large amount of migrants, some of which returns to their home after work but a major portion of these migrants would make their work place to be their home, which would increase the total density of population of that area. So, industrially concentrated regions of a city would have high as well as dynamic density of population. As discussed earlier, the increase in population would ultimately degrade the quality of water of that region. So, there is definitely a relationship which exists between quality of water and urbanization of an area. The present study tried to estimate the impact of urbanization of rain water quality. The relationship between rain water and urbanization is still unknown and it would be interesting to note whether a relationship exists between the two variables. The quality of rainwater is represented by WQI and urbanization is presented by UI.

7.1.5.2 Study Area

The choice of sites for sample collection was made mainly with regard to the accessibility to their locations and adequate security of experimental setup and collecting materials to be deployed. Six sampling stations strategically distributed in the geographical area of Kolkata, West Bengal, India, were set up in order to monitor the influence of constructional activities on rainwater quality in this region, which has an area of 1,880 km² (726 m²) and a population of 15 million. With an elevation of 1.5–9 m, the climate in Kolkata can range from very hot to quite cool. During the summer months of May and June, temperatures vary between 24°C and 42°C (75–108°F). During the winter months of December and January, temperatures range from 8°C to 26°C (47–79°F). It is humid year round in Kolkata, ranging from 85 to 65 in the summer and becoming very humid in winter. During the rainy season, June to September, average rainfall is 158 cm/month.

7.2 Methods and Materials

7.2.1 Sampling Stations and Sample Collection

The description and grid coordinates of six sampling stations (determined using portable global positioning system equipment [GPS]) are given in Table 7.1. Figure 7.2 shows the sampling locations of the present study.

Table 7.1 Sampling station and the grid coordinates of the investigated rain sampling stations at Kolkata

Sl. no.	Sampling station	District	Longitude	Latitude
1	Jadavpur University (JU)	South 24 parganas	88.37	22.49
2	Garia	South 24 parganas	88.3	22.96
3	Baghajatin	South 24 parganas	88.389	22.46
4	Dumdum	Kolkata	88.37	22.48
5	Baguiati	Kolkata	88.43	22.62
6	Sodepur	North 24 parganas	88.38	22.63

Fig. 7.2 Figure showing sampling locations of present study

At each sampling station, bulk samples of free-fall rainwater were collected using plastic buckets with punched holes on the cover so that only a portion of each rain event and dry deposition was actually collected into the bucket. Each bucket was placed on a raised platform about 0.5–1.0 m above ground level to prevent contamination with soil-intercepted rain and adequately supported so that it could not be blown over by strong wind. Sampling started in July 2008 and lasted throughout the rainy season of the year.

After collection, samples were refrigerated and transported to the laboratory in the fastest way possible. Upon reception pH and TDS were measured. Immediately samples were stabilized at 4°C until analysis. Thirty-six single rainwater samples were analyzed for pH, turbidity, TDS, chloride, hardness, calcium, and magnesium. Interesting meteorological parameters such as the quantity of precipitation, temperature, and others were also available for each sampling point.

7.2.2 Laboratory Analysis of Samples

The analytical determinations of the physicochemical parameters of rainwater quality considered were carried out on the samples harvested within the holding time of each parameter, following applicable standard methods. Sample pH was measured using a pH meter with a glass electrode (by Analytical Instruments Consortium, model pH 200). Total dissolved solids was measured with a TDS meter (by EI Instruments Parwanoo [H.P.], model 615E), which gave readings directly in milligram per liter (mg/L) at 25°C, while turbidity was measured with a digital turbidity meter (by EI Instruments Parwanoo [H.P.], model 331E), which also gave readings directly in nephelo-metric turbidity unit (NTU). Total hardness and chloride ion (Cl^-) contents were determined by EDTA titrimetric and argentometric methods, respectively. Calcium (Ca^{2+}) and magnesium (Mg^{2+}) were also determined by EDTA titrimetric method. Quality assurance was controlled by using standard methods (Eaton et al. 2005) of analysis for rainwater samples.

7.2.3 Estimation of Water Quality Index of the Sampling Location

The values of quality parameters were fed to Water Quality Index Calculator software along with the Indian standards of drinking water so that WQI was estimated based on Indian standards. The WQI and ranks of WQI within the sampling locations are given in Table 7.2

7.2.4 Estimation of Urbanization Index

SPOT imagery of the sampling locations at a resolution of 1:10,000 and zoomed into 1:100 were downloaded and processed by image processing software to identify the housing and industrial complexes present at a radius of 5 km around

Table 7.2 Table showing UI and WQI of the sample points

Location	WQI	Rank	UI	Rank
JU	68.05	1	42.00	2
Garia	64.78	4	29.00	5
Baghajatin	63.44	5	37.50	4
Dumdum	65.23	3	52.00	1
Baguihati	59.44	6	38.50	3
Sodepur	67.79	2	27.50	6

the sampling points. Unsupervised classification was applied to retrieve the area of commercial as well as housing complexes of the sampling regions from which the density of housing and commercial complexes were calculated. The population density of the sampling regions were calculated with the help of density of population of Kolkata and density of housing complexes present within the 5 km radius of the sampling points. The change in population within the sampling regions was calculated by subtracting the population of nearest region from the population of the sampling region whose change in population was estimated. The results were fed to the UI equations (7.1–7.3), where each parameter was rated according to the magnitude and maximum values among the sampling locations. After rating, the values of all the variables were summarized where rating received by the variables, population density, change in population, and density of commercial and housing complexes were respectively multiplied by 0.7, 0.2, and 0.1. The summation value was normalized to get a unit less UI (7.4). The UI of different sampling points are given in Table 7.2.

Let population density of a location is p.
Change in population of the same location is dp.
Density of commercial and housing complexes is h.

Then rating given to each variable according to their data value and maximum value within the sampling locations could be represented as

$$p = \left\{ (p_{max} - p)/(p_{max} - p_{min}) \right\} \times m \qquad (1)$$

and similarly

$$dp = \left\{ (dp_{max} - dp)/(dp_{max} - dp_{min}) \right\} \times m \qquad (2)$$

$$h = \left\{ (h_{max} - h)/(h_{max} - h_{min}) \right\} \times m \qquad (3)$$

where $p_{max}, dp_{max}, h_{max}$ are the maximum value of the variables within the sampling points, $p_{min}, dp_{min}, h_{min}$ are the minimum value of the variables within the sampling points, and m is the maximum point of rating say 10 or 100.
Then,

$$UI = (07 \times p + 0.2 \times dp + 0.1 \times h)/(p + dp + h) \qquad (4)$$

7.2.5 Results and Discussion

According to the WQI and UI of the sampling locations, which are given in Table 7.2, WQI of JU was found to be higher and was equal to 68.05, whereas the same of Baguihati was found to be lower and was equal to 59.44 than any other sampling locations. The UI of Dumdum (52) was found to be higher and the same of Sodepur (27.50) was found to be lower than any other sampling locations. The UI of JU and Baguihati was found to be equal to 42 and 38.50, respectively. The WQI of Sodepur and Dumdum was found to be equal to 67.79 and 65.23, respectively. From the above values it could be concluded that when WQI was more UI was less and vice versa. But for the sampling location of South 24 Parganas, the sensitivity of UI toward WQI was lesser than that of the locations in North 24 Parganas. The reason behind the above results could be attributed to the fact that the polluting commercial complexes (leather, textile) were mostly situated in southern outskirts of Kolkata and huge number of residential complexes were present or in verge of completion in the region which was causing a massive migration of population from different parts of kolkata to

Fig. 7.3 (**a**) Bucket used for rainwater collection. (**b**) Collection of rainwater. (**c**) Rainwater stored in a reagent bottle for analysis
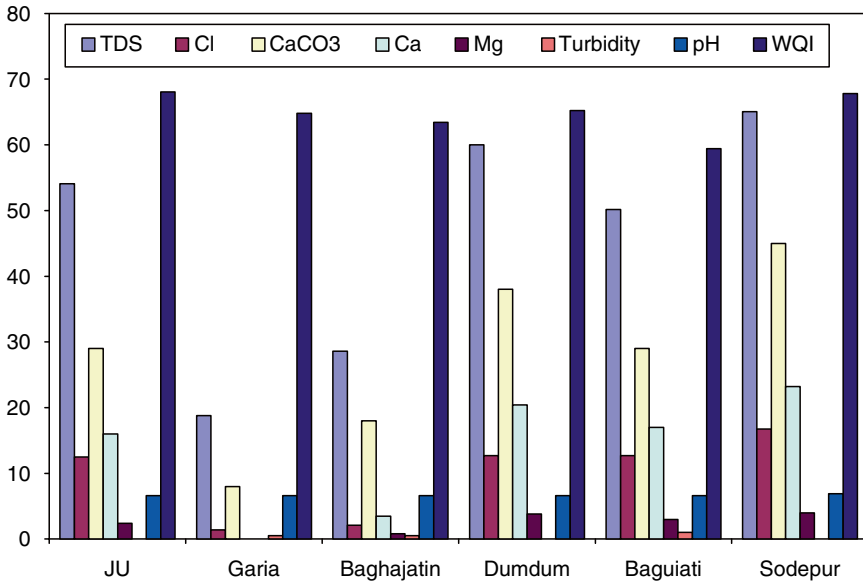
Fig. 7.4 Figure showing variation of water quality with the sampling location

South 24 Parganas, while, service and IT sectors, the nonpolluting industries of Kolkata, were concentrated in the northern outskirts. Figure 7.2 shows the variation of water quality parameters and WQI of the sampling points and Fig. 7.3 shows the relationship curve between WQI and UI (Fig. 7.4).

7.3 Conclusion

The present study tried to assess the impact of urbanization on quality of rain water. Samples were collected from various locations in and around Kolkata metro city. Samples were collected from near industrial, residential, and commercial complexes. The water was laboratory tested and water quality index (WQI) was calculated to find the overall quality of rain water. Urbanization index (UI) was calculated with the help of population density, change in population, and density of industrial and commercial complexes. According to the results and interrelationship between WQI and UI, both were observed to be inversely proportional but the relationship is more prominent in case of samples located at northern outskirts than in the southern outskirts (Fig. 7.5). The reason could be attributed to the concentration of nonpolluted industries in the samples collected from northern outskirts of Kolkata. The present study concluded this relationship based on very few samples but which were diverse in characteristics of urbanization and water quality.
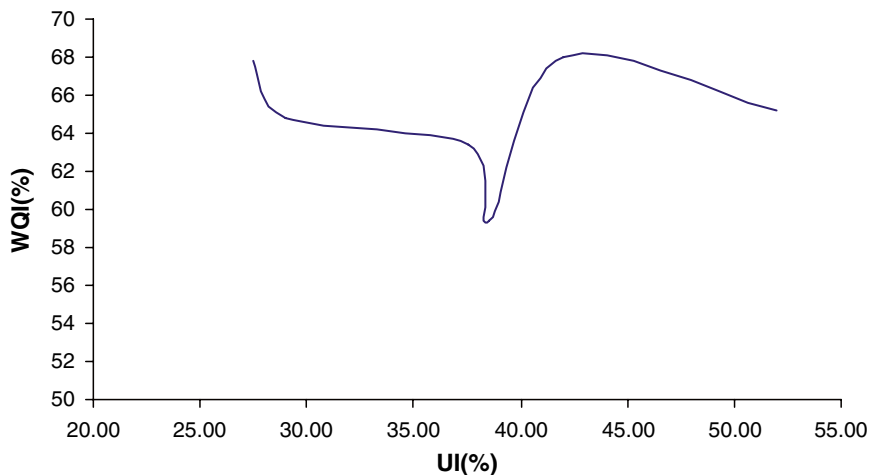
Fig. 7.5 Figure showing the variation of WQI with respect to UI within the considered sampling locations

References

Bolca M, Turkyilmaz B, Kurucu Y, Altinbas U, Esetlili M, Gulgun B (2007) Determination of impact of urbanization on agricultural land and wetland land use in balcovas delta by remote sensing and gis technique. Environ Monitor Assess 131(1–3):409–419

Cetron MJ, Davies O (2008) Trends shaping tomorrow's world, Part one. Futurist 42(2):35–52

Eaton AD, Clesceri LS, Rice EW, Greenberg AE (2005) Standard methods for the examination of water and waste water, 21st edn. APHA, Washington, DC

Lee SY, Dunn RJK, Young RA, Connolly RM, Dale PER, Dehayr R, Lemckert CJ, Mckinnon S, Powell B, Teasdale PR, Welsh DT (2006) Impact of urbanization on coastal wetland structure and function. Austral Ecol 31(2):149–163

Liang Y-Q, Li J-W, Li J, Valimaki S (2008) Impact of urbanization on plant diversity: a case study in built-up areas of Beijing. Forest Stud China 10(3):179–188

Lin W, Zhang L, Du D, Yang L, Lin H, Zhang Y, Li J (2009) Quantification of land use/land cover changes in pearl river delta and its impact on regional climate in summer using numerical modeling. Regional Environ Change 9(2):75

Moglia M, Perez P, Burn S (2008) Urbanization and water development in the pacific islands. Development 51(1):49–55

Salomão M, Cole J, Clemente C, Silva D, de Camargo P, Victoria R, Martinelli L (2008) CO_2 and O_2 dynamics in human-impacted watersheds in the state of são paulo, Brazil. Biogeochemistry 88(3):271–283

Savard J-PL, Clergeau P, Mennechez G (2000) Biodiversity concepts and urban ecosystems. Landscape Urban Plan 48(3–4):131–142

United Nations (2005) World urbanization prospects: the 2005 revision, Pop. Division, Department of Economic and Social Affairs, UN. Retrieved from http://www.un.org/esa/population/publications/WUP2005/2005wup.htm on 31 July 2009

UNICEF (2008) Urbanized population percentage by country as of 2006, The State of the World's Children, UNICEF, p 134

Vicars-Groening J, Harry W (2007) Impact of urbanization on storm response of white rock creek, Dallas, TX. Environ Geol 51(7):1263–1269

Chapter 8
Identification of Water-Stressed Regions of Two Tropical and Subtropical River Basins with the Help of Representative Elementary Area Concept and Neurogenetic Models

Debapriya Basu, Mrinmoy Majumder, and Debasri Roy

Abstract The present study tried to identify water-stressed regions of two river basins of East India. Availability of water was calculated with the help of UNFCC-recommended equation, which use rainfall, evapotranspiration, and basin loss. The result from the calculation was fed to *Falkenmar*- and *Pastor*-prescribed conditions for water stress, which propose that a region with less than 1,000 m^3/capita/year water availability would be under stress for water. One of the major reasons for faulty hydrologic models could be attributed to the area dependency of hydrologic parameter. For example, when river runoff is estimated from a lumped and distributed model the predicted result would be different. When precipitation is converted to runoff, a portion of the rainfall volume is lost due to evaporation, transmission, and infiltration. A lumped model does not consider loss incurred by sub-basins of a river basin, whereas the distributed model predicts runoff from a river basin considering the influence of each of the sub-basin. But even distributed models yield erroneous results when they consider the influence of gauged catchment and ignore the un-gauged one. A continuously distributed hydrologic model considers the influence of both gauged and un-gauged sub-basins of a river and for that model also there would be noticeable amount of error though it would be less than that of the distributed hydrologic models. A distributed or continuously distributed hydrologic model requires a lot of parameters and constants to imitate the hydrologic processes involved in generation of river runoff. Such models

D. Basu
Former PG Student, School of Water Resources Engineering, Jadavpur University, Kolkata-700032, West Bengal, India
e-mail: basu_priya05@yahoo.co.in

M. Majumder
Senior Research Fellow, School of Water Resources Engineering, Jadavpur University, Kolkata-700032, West Bengal, India
and
Geo-information Scientist, Regional Center, National Afforestation and Eco-development Board, Jadavpur University, Kolkata-700032, West Bengal, India

D. Roy
Reader and Joint Director, School of Water Resources Engineering, Jadavpur University, Kolkata-700032, West Bengal, India

are often tedious and time-consuming to develop and also need a lot of computational energy to perform each estimation. Representative elementary area (REA) is an area where change in basin area has no impact on change in basin runoff. If a relationship can be estimated with runoff and area of sub-basins, runoff of entire river basin and REA, a more accurate prediction of river runoff can be made. The present study tried to estimate river runoff with the help of REA where the interrelationship between runoff and area of sub-basin was estimated by neurogenetic models because of their ability to identify patterns more efficiently than the conceptual hydrologic models. The models developed in such a way were compared with a distributed and continuously distributed hydrologic model along with NGHYD (Chapter 4) neurogenetic model. The result of comparison can reveal the validity of the REA concept. The selected model was also used to estimate river runoff from which water-stressed regions of the two river basins considered for the present study was identified. According to the results, REA model was found to be a better model among the five models used in the present study according to the performance validation criteria, like root mean square error, correlation coefficient, coefficient of efficiency, and first-order uncertainty analysis. According to the model estimations, the northeast region of the two river basins would be under water stress in face of the future climatic uncertainty.

8.1   Introduction

Water is an essential and integral part of man's life and environment. It is also the most important natural resource of a country, since no life is possible without water. It has a unique position among other natural resources, such as minerals, fuels, forests, livestock, etc. because a country can survive in the absence of any other resources, except this one. India is primarily an agrarian country. Water is indispensable for agriculture, industry, and for daily use.

As the wheel of civilization progresses, various complexities are arising in the nature due to human interference and progress of urbanization. The main problem is population explosion. Rapid increase in the population demands fresh water for development process of mankind. This means that more agriculture is needed. Also there is urbanization and industrial development. All these created enormous pressure on the water resources all around the globe. Therefore, water in many areas has become a critical factor. In many developing countries, water scarcity is now a fact of life and is rapidly becoming a primary limitation to economic development. Hence, the assessment and management of available water resources in the most economic way to meet the demand placed by the growing population has become the need of the hour.

This problem needs to be tackled through a well-planned and scientific approach. The main aim of any planner is to increase the annual maximum monthly flow of

the existing land utilizing the water resources optimally without endangering the existing ecology and fragile environment. Water resources have to be proportionally utilized to establish a proper balance. The availability of water at different points of different sources needs to be calculated so that planning for meeting of demand can be done optimally.

Exploring the location of maximum availability of water by topographic analysis and some hydrologic analysis is the governing aspect in the present days so that the location can be tapped as an uninterrupted source of water for agriculture, municipal, industrial, and various other uses. So it is very essential to estimate the annual maximum monthly flow at different locations of a stream. The estimation of annual maximum monthly flow is best done by hydrologic simulation model. With the advent of computer, physical model gives way to mathematical computer simulation model, which is very efficient. So, hydrological behavior of any watershed can be predicted through computer modeling

Computer simulation model is traditionally analyzed by means of lumped models. These models assume that excess rainfall and hydrological conditions over a whole watershed is uniform. In practice, the excess rainfall and hydrological conditions over a mid-size or large watershed are spatially nonuniform. Thus, annual maximum monthly flow computed by lumped model may be erroneous. To overcome this deficiency, distributed type model may be used. In distributed type model, a spatial variation of parameters has been incorporated into the model response by dividing the catchment into large number of grids. These grids are known as distributed modeling units. The excess rainfall and hydrological conditions can be approximated to be uniform on each grid and this model is termed as continuous distributed model. As the number of grids division of the watershed is decreased, in other words, the size of the grid is increased, the model becomes less distributed and here after is termed as discrete distributed model.

Recently Wood et al. (1988, 1990) has introduced the representative elementary area (REA) concept in their search of an appropriate spatial scale (the REA) at which a simple description of rainfall-runoff process could be obtained. Once the size of RAE is known, the catchment being studied could presumably be disaggregated into REA sized sub-catchments (the inputs and parameter values need to be specified at the REA scale) and average runoff at the basin outlet can be computed.

In the present study, an attempt has been made to validate the concept, proposed by Woods et al. about REA, with the help of validation results, within the neurogenetic model, one distributed and three continuously distributed conceptual hydrologic models.

8.1.1   Hydrologic Models

A hydrologic model can be divided into lumped and distributed hydrologic models, where the former considers a river basin to be constituted of only one sub-basin, which represents the characteristic of all the sub-basins of the river basin and the

latter considers the influence of each sub-basin of river basin while estimating the total runoff of the entire river basin. If the distributed hydrologic model considers the contribution of both gauged and un-gauged sub-catchments, the model is called as continuously distributed and if only gauged sub-basins are considered, the model is known as discretely distributed hydrologic model. A detailed description of hydrologic models is given in Chapter 21.

8.1.2 Study Area

Two river basins of eastern India are considered as the study area for the present study. A detailed description of both the sub-basin is given in Chapter 25.

8.2 Methodology

In the present study five models were developed for the same purpose of estimating river runoff. The first two models were neurogenetic model, which follows the common model development procedures as described in Section 21.8. The model training algorithms was also compared within quick propagation, batch back propagation, and conjugate gradient descent learning algorithms. The first neurogenetic model used the REA concept and the second one was a neurogenetic model, which can generate hydrographs and estimate peak runoff with the help of the generated hydrograph.

8.2.1 Representative Elementary Area Hydrologic Model

REA is defined as that area where variance of runoff with respect to the area is nil. REA is a concept proposed by Woods et al. where impact of change in area on change in runoff was analyzed. Woods et al. proposed an area where runoff is not a function of area, which makes runoff independent of spatial variation. According to this concept runoff estimated with the help of REA will be the same as that estimated from distributed and lumped hydrologic models.

8.2.1.1 Model Variables

In the present study, incremental change in area with respect to representative elementary area (A') and incremental change in runoff with respect to representative elementary runoff (Q') were considered as input and runoff was taken as output of the developed neurogenetic models.

Representative elementary area and representative elementary runoff were identified in the following procedure.

Determination of Representative Elementary Area and Representative Elementary Runoff

1. At first entire catchment area of river Damodar and river Rupnarayan was divided into 15/15 grid and runoff was calculated with the help of CWC (1973) prescribed empirical formula, which use catchment area and some constants to estimate runoff for un-gauged basins according to average basin slope for the grids.
   The catchment area of each of the grid was calculated with the help of GIS.
2. The catchment area of each of the grid and runoff as calculated from the area equation were sorted and arranged in an ascending manner. The larger catchment area was subtracted from next smaller area to find the change in catchment area. Similarly, change in runoff was also calculated.
3. The change in runoff was divided by change in area and minimum value was identified and the area and runoff which gives the minimum value was identified as representative elementary area and runoff. Hence a dividend is smallest when denominator is very large and numerator is very small. REA, as defined by Woods et al. is an area for which change in runoff is minimum or nil. A division of smallest runoff with largest area would imply that even for a large change in area, change in runoff is minimum. Hence, for this area variation of runoff is minimum at least for the two river basins considered.

8.2.1.2 Model Development

The A′ and R′ were applied as input variables to develop three neurogenetic model for estimation of Q. The procedure for development of neurogenetic model and selection of model parameters, training procedure, and validation is already explained in more detail in Chapter 5.

The model that uses CGD as training algorithm was named as REACGD and model trained with QP and BBP was called as REAQP and REABBP hydrologic model.

Table 8.1 shows the input and output variables of REA hydrologic models and Fig. 8.1 depicts the overview of the model algorithm (Fig. 8.1).

Table 8.1 Table showing input and output variables used for the REA hydrologic model

Input	Abbreviation
Output	Abbreviation
Incremental change in area with respect to representative elementary area (A′) and incremental change in runoff with respect to representative elementary runoff (Q′)	A′, Q′
Peak average monthly basin runoff (Q)	Q

8.2.2   Development of Neurogenetic Model for Estimation of Basin Hydrograph (NGHYD)

In surface water hydrology, a hydrograph is a time record of the discharge of a stream, river, or watershed outlet. Rainfall is typically the main input to a watershed and the stream flow is often considered the output of the watershed; a hydrograph is a representation of watershed response to rainfall. A watershed's response to rainfall depends on a variety of factors, which affect the shape of a hydrograph:

- Watershed topography and geology (i.e., bedrock permeability)
- The area of a basin receiving rainfall
- Land use
- Drainage density
- Duration of rainfall and precipitation intensity and type
- Evapotranspiration rates
- River geometrics
- The season
- Previous weather
- Vegetation type and cover
- River conditions (e.g., dams)
- Initial conditions (e.g., the degree of saturation of the soil and aquifers)
- Soil permeability and thickness

When data of rainfall and runoff is unavailable, synthetic hydrograph, that is, artificial generation of catchment response to rainfall is performed with factors described above. There are many empirical or conceptual models for estimation of synthetic hydrograph, all of which tries to estimate peak flow and time of peak flow. Then 50% and 70% of peak runoff is found out along with the time required to reach the same amount of runoff .The relationship between runoff and rainfall in the rising limb and impact of basin characteristic on runoff at the recession limb is included in the model to draw the entire hydrograph. It was observed that time to peak is equal to time of concentration of the basin. Ahmed et al. (2009), Lopez et al. (2005), Taskinen and Bruen (2007), Yeh et al. (1997), Sui (2005), Blazkova et al., (2002) and others have investigated the use of hydrograph in estimation of parameters, design flood, uncertainty analysis, geomorphology, etc. and most of them advocates the use of hydrograph in hydrologic models as it helps to estimate runoff volume and time to peak, which are necessary in the case of hydrologic or hydraulic design.

Hydrograph is not essential for impact analysis of climate change, but to analyze impacts of climatic variability on duration of peak storm and response time of a catchment due to the storm.

In the present study, a model was developed to estimate hydrograph and corresponding peak basin runoff of the sampling regions with the help of neurogenetic models.
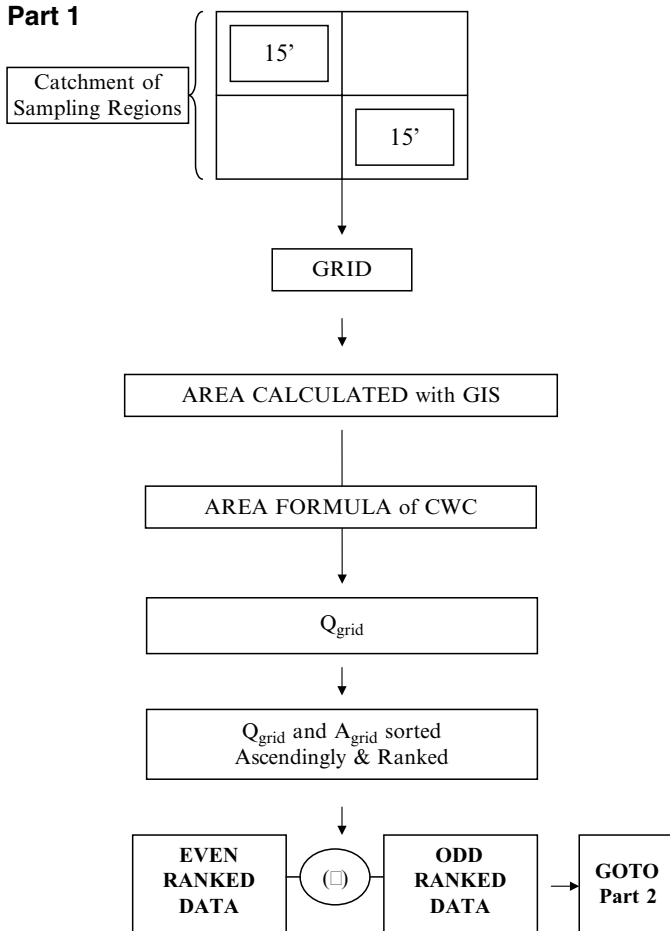
Part 1

Fig. 8.1 Figure showing methodologies adopted to develop the REA hydrologic models where *Part 1* shows the procedures adopted to identify the change in basin area and basin runoff with respect to each grid, *Part 2* shows the procedures to identify elementary area and runoff, and *Part 3* depicts the architecture of the REA neurogenetic model

8.2.2.1 Model Variables

Abstraction from rainfall is calculated with the help of rainfall and basin loss (Subramanya 1994) .Basin loss is represented by basin characteristics like soil texture, porosity, vegetation or plant cover ,depreciations or pondages, etc.

Abstraction from rainfall was divided by time of concentration to find incremental rainfall abstraction (dP) and was used as input, whereas basin runoff divided by time of concentration was used as output (dQ) variable to develop a neurogenetic model for prediction of incremental basin runoff at the different sampling regions.

A detailed description of model methodology is already described in Chapter 4.
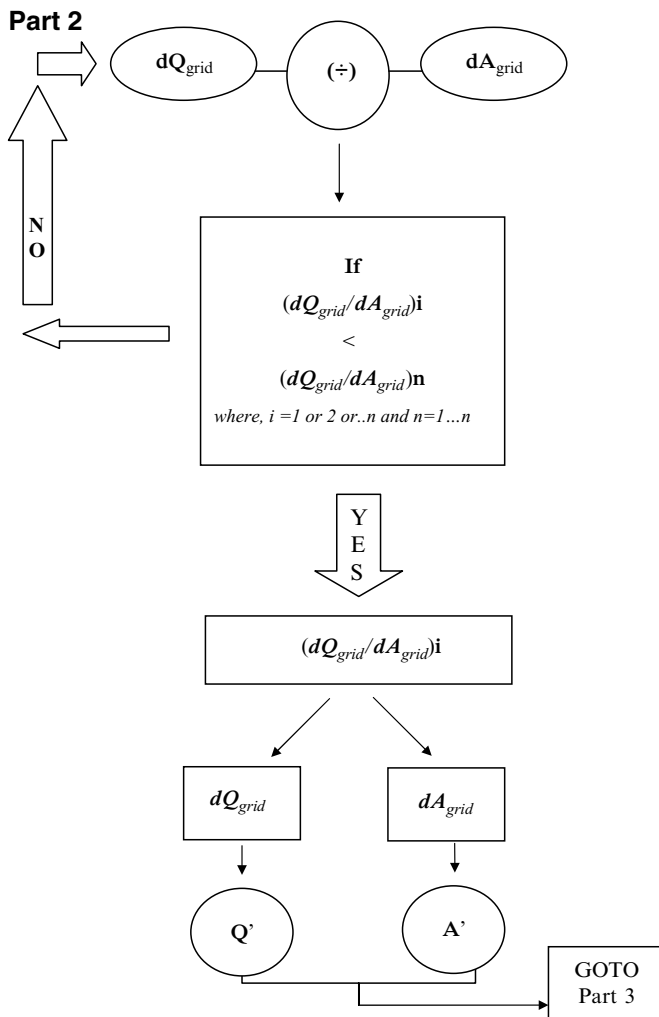
Fig. 8.1 (continued)

8.2.3   Development of the Continuously Distributed Hydrologic Model

The continuously distributed hydrologic model was developed with three types of conceptual hydrologic model: HECHMS, Tr55, and MODRAT, which are described in detail in Section 21.8.

Part 3
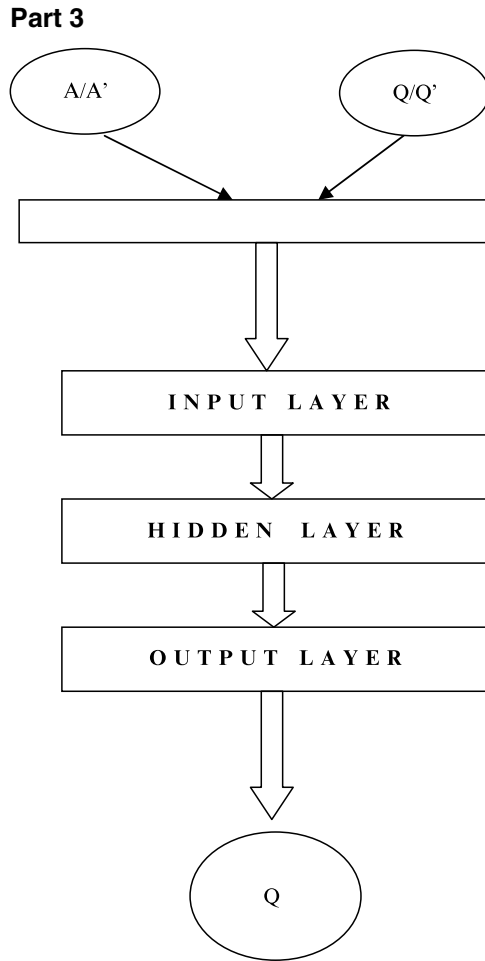
Fig. 8.1 (continued)

8.2.4   Development of the Discretely Distributed Hydrologic Model

The discretely distributed hydrologic model was developed with the help of Tr55 model where only gauged sub-basins of the two rivers were included in the model development.

8.3   Result and Discussion

8.3.1   Model Validation

The predicted values of discharge from all the six developed neurogenetic models along with three continuously distributed and one discretely (TR55(D)) distributed hydrologic models were compared with the observed discharge and RMSE, r^2 and E were calculated to validate the models as well as to select the better model among the considered models.

According to the comparison results given in Table 8.2, RMSE of REANGBBP was found to be 4.21 which was less than that of NGHYDQP (4.90) and other considered neurogenetic models. The correlation coefficient of REANGCGD was found to be equal to 0.95, which was less than REANGCGD (0.97) but better than any other neurogenetic models considered in the study. The E and U of REANGBBP was found to be equal to 0.94% and 7.96%, respectively, which were less than REANGCGD (0.96 and 7.78) but were better than any other considered neurogenetic models. The above results imply that though REANGBBP was accurate than any other neurogenetic models considered in the present study, REANGCGD was more reliable, less uncertain, and more efficient than REANGBBP. That is why REANGCGD was selected as the better model among the six considered neurogenetic hydrologic model (Table 8.3).

If conceptual hydrologic models were compared with the selected neurogenetic model, REANGCGD was found to have RMSE equal to 6.45, which was more than HECHMS (5.45) but less than TR55 (6.78), TR55 (D) (10.34), and MODRAT (10.12). But r or reliability of REANGCGD model was found to be better than HECHMS (0.67), TR55(0.65), TR55 (D) (0.66), and MODRAT (0.71). The efficiency of REANGCGD was found to be equal to 0.96, which was better than HECHMS (0.78), TR55 (0.68), TR55 (D) (0.67), and MODRAT (0.58), whereas U was found to be less for REANGCGD (7.78%) than HECHMS (15), TR55 (20%), TR55 (D) (21%), and MODRAT (45%).

As REANGCGD model has better E and r values among the other conceptual models and is also less uncertain than the conceptual models, it was selected as the better model among all the six conceptual hydrologic models.

The validation result as explained above also favors the REA concept as model developed with REA and was selected as the better model among all the other models. The continuously distributed HECHMS conceptual hydrologic model was found to be the second better model followed by continuously distributed TR55 conceptual hydrologic model. HECHMS model had better RMSE than REANGCGD, but the former was less reliable and more uncertain than the other model. Hence REANGCGD was selected as the better model even if HECHMS had a lesser RMSE than the REANGCGD.

The future river runoff was then estimated with the help of selected hydrologic model, rainfall, and temperature as predicted by PRECIS climate model-generated weather scenarios and basin loss estimated by IPCC 4th Assessment Report (2007).

Table 8.2 Table showing model parameters and performance validation criteria of the six neurogenetic models

Model name	NG-HYDQP	NG-HYDCGD	NG-HYDBBP	REA NGBBP	REA NGCGD	REA NGQP
Model variables						
Input	dP	dP	dP	dA/A_e, dQ/Q_e	dA/A_e, dQ/Q_e	dA/A_e, dQ/Q_e
Output	dQ	dQ	dQ	Q	Q	Q
Model parameters						
Network topology						
Network type	Feedforward	Feedforward	Feedforward	Feedforward	Feedforward	Feedforward
Network structure	1,1,1	1,1,1	1,1,1	2,1,1	2,1,1	2,1,1
Network weight	2	2	2	3	3	3
Training dataset	80	80	80	80	80	80
Testing dataset	10	10	10	10	10	10
Validation dataset	10	10	10	10	10	10
GA parameters						
Population	50	50	50	50	50	50
Generation	100	100	100	100	100	100
Penalty	6	6	6	6	6	6
Crossover rate	0.8	0.8	0.8	0.8	0.8	0.8
Mutation rate	0.2	0.2	0.2	0.2	0.2	0.2
Stop training condition						
MSE	0.05	0.05	0.05	0.05	0.05	0.05
Iteration	200	200	200	200	200	200
Generalization loss	5	5	5	5	5	5
Training algorithm parameters						
Algorithm name	QP	CGD	BBP	BBP	CGD	QP
Activation function	Sigmoid	Sigmoid	Sigmoid	Sigmoid	Sigmoid	Sigmoid
Learning rule	Supervised	Supervised	Supervised	Supervised	Supervised	Supervised

(continued)

Table 8.2 (continued)

Model name	NG-HYDQP	NG-HYDCGD	NG-HYDBBP	REA NGBBP	REA NGCGD	REA NGQP
Learning rate	0.8	NR	0.8	0.8	NR	0.8
Momentum	NR	NR	0.8	0.8	NR	NR
Propagation coefficient	1.75	NR	NR	NR	NR	1.75
Training and testing results						
RMSE (training)	5.5	5.8	6.5	10.98	11.67	11.55
RMSE (testing)	4.87	4.56	4.06	10.05	14.56	18.78
	Required RMSE achieved	Required RMSE achieved	Required RMSE achieved	Generalization loss	Generalization loss	Generalization loss
Model estimation results						
RMSE	4.90	5.55	5.65	4.21	6.45	6.74
Relationship	0.59	0.55	0.61	0.95	0.97	0.57
Efficiency	0.76	0.72	0.75	0.94	0.96	0.95
Uncertainty (%)	11.34	11.87	11.98	7.96	7.78	7.77

Table 8.3 Table showing comparison of performance validation criteria of neurogenetic model with conceptual hydrologic models

Model name	RMSE	r	E	U(%)
REANGCGD	6.45	0.97	0.96	7.78
HECHMS	5.45	0.67	0.78	15
TR55	6.78	0.65	0.68	20
TR55(D)	10.34	0.66	0.67	21
MODRAT	10.12	0.71	0.58	45

The above information were also utilized in calculating water availability and from which the water-stressed region was found out by the water stress index prescribed by *Falkenmar and Pastor*.

8.3.2 Estimation of Future Water Stress

The Water Availability data were fed to UNFCC-recommended conditions for water stress to find the stressful regions within the two basins. Water stress was represented by three classes: class "1" regions has no water stress, class "2" regions has medium scarcity of water, and class "3" regions were totally under water scarcity and facing severe stress for water. This categorization of water availability was proposed by *Falkenmar and Pastor* in 2004. According to the conditions proposed, an area with less than 1,000 m³/capita/year is said to be region under severe water shortage, if within 1,000–1,700 area was said to be under water stress, and other areas with more than 1,700 m³/capita/year is said to have no stress of water.

   As per the present status of water availability, Jharkhand is already under severe shortage of water and falls under class 3, whereas West Bengal falls under class 1. If the two basins were compared, the difference in availability of water could not be shown with the help of water-stress classification as both the basins have more than 1,700 m³/capita/year of water availability, and the selected basins fall under class 1.

   But, if districts of West Bengal and Jharkhand are compared (Table 8.4), Giridih, a district of Jharkhand, and Burdwan, a district of West Bengal are under class 2 according to the observed water availability of the districts, but in 2010–2100 it will fall under class 3 which shows that water stressed but not scarcer district of the basin would ultimately fall under water scarce region. Hazaribagh, a district of Jharkhand would gradually come under water scarce region from water available region from 2010 to 2040 when it falls under class 1, then in 2041–2070 it falls under class 2, and in 2071–2100 it falls under water scarce region.

   According to spatial variation of water stress shown in Figs. 8.2–8.7, the region of water scarcity gets increased in the downstream than in the upstream for both the rivers though, river Rupnarayan was always under class 1 (blue region of Figs. 8.2–8.7) or 2 (sky blue region of the figures), but still in case of 2010–2100, region of class 1 increases downward making region of class 2 and 1 downward and also smaller. The rate of change in area under class 3 (gray region in Figs. 8.2–8.7) was more in A2 scenario of climate change than in B2 scenario.

Table 8.4 Table showing district-wise, state-wise and basin-wise variation of water stress due to A2 and B2 scenario of climate change

	A2 scenario			B2 scenario			Observed
	2010–2040	2041–2070	2071–2100	2010–2040	2041–2070	2071–2100	1970–2002
Districts							
Giridih	3	3	3	3	3	3	2
Jamtara	3	3	3	3	3	3	3
Bokaro	3	3	3	3	3	3	3
Ranchi	3	3	3	3	3	3	3
Hazaribagh	1	2	3	1	2	3	1
Dhanbad	3	3	3	3	3	3	3
Burdwan	3	3	3	2	3	3	2
Hooghly	1	1	1	1	1	1	1
Howrah	3	3	3	3	3	3	3
Purulia	3	3	3	2	1	1	2
Bankura	1	1	1	1	1	1	1
West Midnapur	3	3	3	3	3	3	3
East Midnapur	3	3	3	3	3	3	3
State							
Jharkhand	3	3	3	3	3	3	3
West Bengal	1	1	1	1	1	1	1
Basins							
Damodar	1	1	1	1	1	1	1
Rupnarayan	1	1	1	1	1	1	1

Fig. 8.2 Figure showing spatial variation of water-stressed region for A2 scenario of climate change in 2010–2040

Fig. 8.3 Figure showing spatial variation of water-stressed region for A2 scenario of climate change in 2041–2070
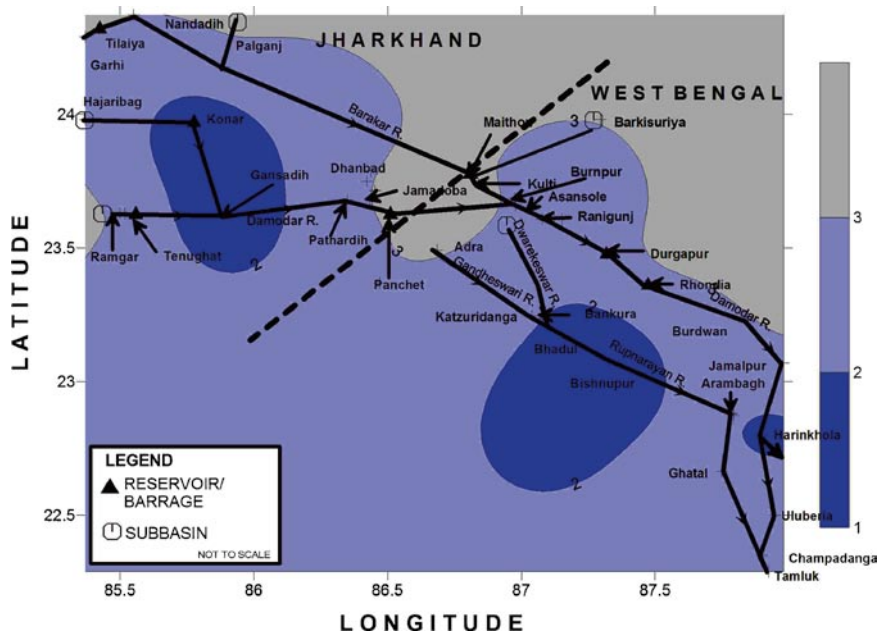
Fig. 8.4 Figure showing spatial variation of water-stressed region for A2 scenario of climate change in 2071–2100
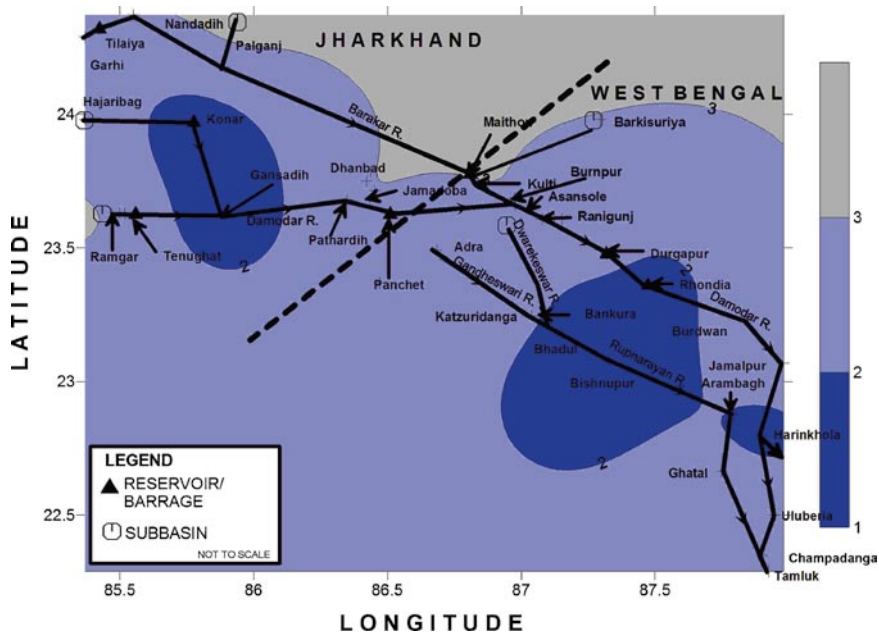
Fig. 8.5 Figure showing spatial variation of water-stressed region for B2 scenario of climate change in 2010–2040
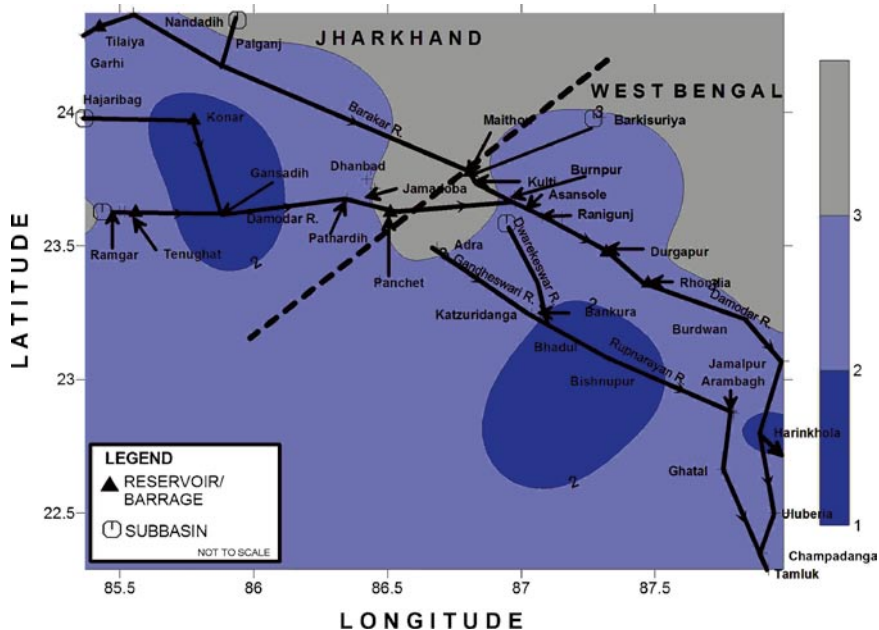
Fig. 8.6 Figure showing spatial variation of water-stressed region for B2 scenario of climate change in 2041–2070
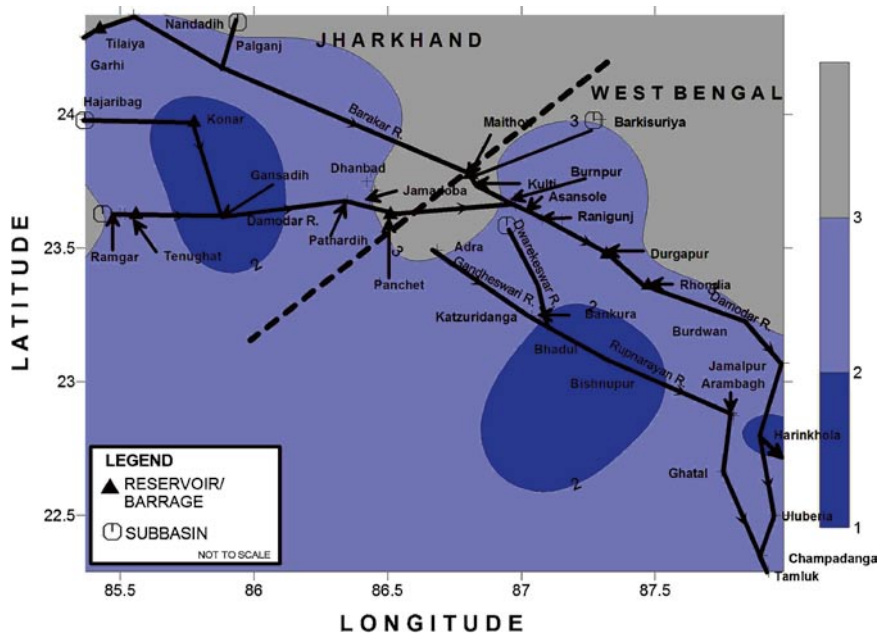
Fig. 8.7 Figure showing spatial variation of water-stressed region for B2 scenario of climate change in 2071–2100

8.4   Conclusion

The present study tried to develop an REA-based hydrologic model where interrelationship among A′, Q′ and A, and Q of each sub-basin or grids was identified by neurogenetic algorithm. The model thus prepared was compared with three types of continuously distributed conceptual hydrologic model and one discretely distributed hydrological model. The model results were compared with observed runoff data to find the RMSE, r, E, and U, which can validate as well as select the better model among the six models. The validation criteria select REANGCGD, the model prepared with the help of REA concept, as the better model even if it had lesser accuracy than REANGBBP and HECHMS due to the better reliability and efficiency and less uncertainty of the former model. The selected model was used to identify water-stressed region of the study area and according to the results, the northeast region was identified as the region under severe water scarcity.

References

Ahmad M, Ghumman A, Ahmad S (2009) Estimation of clark's instantaneous unit hydrograph parameters and development of direct surface runoff hydrograph. Water Resources Management.

Blazkova S, Beven KJ, Kulasova A (2002) On constraining topmodel hydrograph simulations using partial saturated area information. Hydrol Process 16(2):441–458.

Lopez JJ, Gimena FN, Goni M, Agirre U (2005, August) Analysis of a unit hydrograph model based on watershed geomorphology represented as a cascade of reservoirs. Agricultural Water Management 77(1–sss3):128–143.

Subramanya K (1994) Engineering hydrology, 2nd edn. Tata McGraw Hill, New Delhi, pp 60–90

Taskinen A, Bruen M (2007) Incremental distributed modelling investigation in a small agricultural catchment: 1. overland flow with comparison with the unit hydrograph model. Hydrological Processes 21:(1) 80–91.

Wood EF, Sivapalan M, Beven K, Band L (1988) Effects of spatial variability and scale with implications to hydrologic modeling, J Hydrol 102:29–47.

Woods RA, Sivapalan M, Duncan M (1990) Investigating the representative elementary area concept: an approach based on field data, in: Scale Issues in Hydrological Modeling, edited by: Kalma, JD and Sivapalan, M., Advances in Hydrological Processes. Wiley, Sussex, England, 49–70.

Yeh K, Yang J, Tung Y (1997, April) Regionalization of unit hydrograph parameters: 2. uncertainty analysis. Stochastic Hydrology and Hydraulics 11(2):173–192.

Chapter 9
Estimation of the Spatial Variation of Stream Flow by Neural Models and Surface Algorithms

Mrinmoy Majumder, Suchita Dutta, Rabindra Nath Barman, Pankaj Roy, and Asis Mazumdar

Abstract The present study tried to estimate spatial variation of stream flow in face of climatic uncertainty. Seven neurogenetic models with different but related input variables were used to predict stream flow of both gauged and ungauged sub-basins of two river networks of Eastern India's intratropical region. The models were validated and the better model was selected for estimation of stream flow. PARITYCGD was found to be the better model due to its lower RMSE and higher efficiency than any other considered models. The PARITYCGD model was then compared with three conceptual hydrologic models, and here also it was selected as the better model

───────────────

M. Majumder (✉)
Senior Research Fellow, School of Water Resources Engineering, Jadavpur University, Kolkata-700032, West Bengal, India
and
Geo-information Scientist, Regional Center, National Afforestation and Eco-development Board, Jadavpur University, Kolkata-700032, West Bengal, India
e-mail: mrinmoy@majumder.info

S. Dutta
Research Assistant, Regional Center, National Afforestation and Eco-development Board, Jadavpur University, Kolkata-700032, West Bengal, India

R.N. Barman
Pertime Research Fellow, School of Water Resources Engineering, Jadavpur University, Kolkata-700032, West Bengal, India
and
Assistant Professor, Department of Production, National Institute of Technology, Agartala, Tripura, India

P. Roy
Lecturer, School of Water Resources Engineering, Jadavpur University, Kolkata-700032, West Bengal, India

A. Mazumdar
Coordinator, Regional Center, National Afforestation and Eco-development Board, Jadavpur University, Kolkata-700032, West Bengal, India
and
Director, School of Water Resources Engineering, Jadavpur University, Kolkata-700032, West Bengal, India

due to higher efficiency and reliability and lower RMSE and uncertainty than the other considered conceptual models. The radial basis surface interpolation was now used to generate spatial variation of stream flow within the two river networks due to the generated weather scenarios by PRECIS climate models. According to the results, the degradation of catchment, which is generally interpreted from high magnitude of stream flow, was observed in north-west and north-east region within the two river networks as per the surface diagram generated from model predictions due to observed rainfall and land-use data. For the future climatic data, spatial variation of stream flow was found to be concentrated in the same two regions only the areas showed an increasing trend, which was more in A2 scenario than in the case of B2 scenario of climate change. The model output was applied to generate spatial variation of water quality and pollution, which are explained in Chapters 10 and 11.

Keywords Distributed hydrology • neural network • stream flow • surface algorithms

9.1 Introduction

9.1.1 Lumped and Distributed Hydrologic Models

A comparison of lumped and distributed flow reveals a significant improvement in the estimation of stream flow peak and timing of the peak with the later (Meselhe et al. 2004; Smith et al. 2004; Carpenter and Georgakakos 2006).

Carpenter and Georgakakos compared high- and low-resolution models with Kolmogorov–Smirnov uncertainty test and found out that the former model estimate ensemble stream flow at a greater frequency of occurrence within the confidence boundary. Maidment (1993) developed a distributed DEM-driven unit hydrograph for the estimation of stream flow where both peak and time of peak show a significant improvement in accuracy. Olivera and Maidment (1999) proposed a raster-based, spatially distributed, runoff routing technique, where routing from one cell to the other was accomplished using the first-passage-time response function. Saghafian et al. (2002) used time variable isochrone technique to simulate runoff hydrograph where isolines of travel time were drawn and intermediate areas were calculated to find out the unit hydrographs of the basin.

The distributed or semidistributed (Kite 2001) hydrologic models were also applied in the estimation of flood inundation (Dutta et al. 1999), low land stream flow (Hörmann et al. 2007), contaminant transport (Martens and Breshears 2005), runoff change (Shrestha 2003), water budget predictions, etc. All the models show greater level of confidence with distributed models.

9.1.1.1 Deterministic Hydrologic Models

Hydrologic models which try to represent the physical processes observed in the real world are categorized as deterministic or process-based or conceptual hydrologic

models. Typically, such models contain representations of surface runoff, subsurface flow, evapotranspiration, and channel flow, but they can be far more complicated.

Deterministic hydrology models can be subdivided into single-event models (e.g., Rational, MODRAT, Rational OC) and continuous simulation models (e.g., HECHMS, HEC, TR55, SWMM).

The complexity of interrelationship of hydro-metereological parameters had enforced hydrologic engineers to employ computer models with conditional variability to estimate future pattern of important hydrological parameters such as reservoir inflow (El-Shafie et al. 2007; Kim et al. 2007; Long et al. 2007), reservoir operation (He et al. 2008), and reservoir optimization (Xu and Li 2001; Eslami and Mohammadi 2002; Luo and Weiss 2002; Wei and Hsu 2007).

The hydrologic models are plagued by two main difficulties. As hydrologic variables are both space and time dependant, these models are required to embed the inherent relationship between variables with time and space scales. Spatial statistics of watershed are irregular due to the cost involved in acquiring such dataset. Temporal hydrologic data are generally discriminant and often erroneous due to the manner by which the data were acquired or extracted. Artificial neural network (ANN) and application of remote sensing with geographical information systems can help develop more accurate conceptual models.

9.1.1.2 Models Based on Data or Stochastic Hydrologic Models

Hydrologic models, which are developed in black box systems, using mathematical and statistical concepts to link a certain input (for instance, rainfall) to the model output (for instance, runoff) are known as empirical or stochastic or statistical hydrologic models. The commonly used techniques of such models include regression, transfer functions, and system identification. These models are linear models, but nonlinear components are commonly deployed to represent some general aspects of a catchment's response without going deep into the real physical processes involved.

A detailed description of hydrologic model, their types, methodologies, and some examples of the same are given in Chapter 21.

9.1.2 Application of Artificial Neural Network in Hydrology

The research in artificial intelligence has increased dramatically during the 1990s. The ANN was originally developed to mimic basic biological neural systems – the human brain. In general, it is composed of a number of interconnected simple processing elements called neurons or nodes with attractive attribute of information processing characteristics such as nonlinearity, parallelism, noise tolerance, and learning and generalization capability. Contrary to the traditional model-based methods, ANNs are data-driven, self-adaptive methods in which there are few a priori assumptions about the models for problems in the study.

Neural networks learn from examples and capture subtle functional relationships among the data even if the underlying relationships are unknown or difficult to be described. Thus, ANNs are well suited for problems whose solutions require knowledge that is difficult to specify, but for which there are enough data or observations. In this sense, they can be treated as multivariate, nonlinear, nonparametric statistical methods. Due to its highly parallel structure, high-speed self-leaning ability, self-adaptable processing power, arbitrary function mapping capability, powerful pattern classification and pattern recognition character which are conducive for modeling complex nonlinear systems, the application of ANNs to various aspects of hydrologic modeling was widely reported in various hydrological literatures such as for rainfall–runoff modeling (Hsu et al. 1995; Fernando and Jayawardena 1998; Tokar and Johnson 1999; Elshorbagy et al. 2000; Liong et al. 2001), for stream flow prediction (Clair and Ehrman 1998; Imrie et al. 2000), for reservoir inflow forecasting (Jain et al. 1999; Coulibaly et al 2000) and for water quality parameters (Maier and Dandy 1999). All the papers reported high degree of satisfaction and advocate use of neural network as a promising alternative for improved hydrologic estimations. But there are some drawbacks of neural models. Absence of adequate data and ignorance of the embedded concept can induce large errors in estimations. Such models are not recommended for prediction of something that is not included in the available dataset. A detailed description of the procedures and methodology of developing neural models with genetic algorithm is given in Chapter 22.

9.1.3   Climate Models

The uncertainty in the climatic pattern had made the estimation of future climate more complex. Global climate models (GCM) were widely used to estimate future climatic parameters but the complexity of the present climatic pattern had forced many modifications. HadCM2 AOGCM model was developed by Met Office Hadley in 1994 and its successor, HadCM3 AOGCM (Atmosphere-Ocean General Circulation Models), was published in 1998. AOGCM coupled with an atmospheric chemistry model which can predict the changes in concentration of other atmospheric constituents in response to climate change and to the changing emissions of various gases was later built on 1999. In HadCM3, thermohaline circulation, ventilation, and vertical mixing of chemical constituents along with decadal variability in the ocean were included.

Local climate change is influenced greatly by local features such as mountains, which are not well represented in global models (GCMs) because of their coarse resolution, and models of higher resolution could not practically be used for global simulation for long periods of time due to spatial variance of the considered parameters. These problems were tried to be mitigated with the help of regional climate models (RCM). The RCM had higher resolution (typically 50 km), were constructed for limited areas and allowed to run for shorter periods (20 years or so). The Met Office Hadley Centre had run RCMs for three regions, Europe, the Indian subcontinent, and southern Africa and had developed an RCM to run on PCs for any region as part of a regional climate modeling system called PRECIS (Chapter 23).

The estimations from these climatic models were applied to hydrologic models to estimate the future impacts of climate change on different hydrologic parameters.

9.1.4   Surface Algorithms

In engineering applications, data collected from the field are usually discrete and the physical meanings of the data are not always well known. To estimate the outcomes and, eventually, to have a better understanding of the physical phenomenon, a more analytically controllable function that fits the field data is desirable. The process of finding the coefficients for the fitting function is called curve fitting; the process of estimating the outcomes in between sampled data points is called interpolation; whereas the process of estimating the outcomes beyond the range covered by the existing data is called extrapolation. If the sample data points are in 3d, the interpolation or extrapolation is called as surface interpolation and the algorithms, which were used to find the coefficients of the fitting function and so that accurate estimations can be possible from the curve fitting equations are collectively called as Surface Algorithms.

There are various algorithms available for surface interpolation from which polynomial, rational function, cubic spline interpolation are some of the common interpolation algorithms based on Lagrange classical function, Rational function, and Cubic Interval function, respectively. Some algorithms were specifically made for surface interpolations like Kriging, Nearest Neighbor, Radial Basis Function, etc. among which radial basis functions were found to be preferred by many scientists for their surface interpolation requirements (Kojekine et al. 2004). According to Carr et al. (1997, 2001, 2003) radial basis function had performed satisfactorily in surface reconstruction from noisy images, medical imaging, as well as 3d objects. The conclusion was supported by Beatson et al. (1999), Liepa (2003), Nunes et al. (2003), Fasshauer (2007), and others. The present study adopted radial basis function for the estimation of spatial variation of stream flow.

9.1.5   Objective and Scope

The present study tried to estimate spatial variation of stream flow with the help of neurogenetic models and surface algorithms. The study also aimed to analyze the impact of climate change on the spatial variation of stream flow. That is why spatial variation for future stream flow was also estimated. The study area was selected from the tropical and subtropical regions of eastern India.

9.1.6   Study Area

The catchment description, geomorphologic features, and current metereologic and hydrologic trends of the two river networks, river Damodar and river Rupnarayan, and their tributaries and distributaries are explained in detail in Chapter 25.

9.2 Methodology

9.2.1 Conceptual Coupled Neurogenetic Distributed Hydrologic Model (CONCONGDHM)

Neural models are popular for their ability to identify inherent patterns between variables with the help of available dataset. The models cannot predict the patterns, which are not present in the available dataset with which the model is trained. Climate change can induce extreme changes in dataset patterns.

If the models are trained with available dataset it will be unable to predict impact of climate change on the model output. A solution can be to precede the development of neural models with a process-based models like HECHMS, TR55, or MODRAT. As neural models were known to be efficient in identification of patterns it was used to estimate the discharge but as such models can be erroneous for values with which it was not trained, the unknown values was predicted by conceptual model. The relationship between the outputs of conceptual model with observed discharge was identified with the help of neurogenetic models and used to estimate the future discharge. The model variables and methodology adopted to develop CONCONGDHM model was already explained in Section 5.2

9.2.2 Neurogenetic Spatially Distributed Rainfall–Runoff Model

The neurogenetic spatially distributed rainfall–runoff model (NSRRM) was developed to consider the influence of metereologic and hydrologic variables along with basin characteristics upon basin runoff. Peak average monthly rainfall of 32 years (1970–2002) and 12 months, monthly time of concentration and monthly variation of loss coefficient of the basins at 42 sampling points were used to predict peak average monthly basin runoff at the same 42 selected sampling points. In Neurogenetic models, inputs are multiplied with a weightage and then summed to estimate the output after going through an activation function. If differences exist between estimated and desired output the operation is repeated again with updated weightage value until and unless the estimated and desired output becomes equal or a desired RMSE calculated with the help of the two values is achieved. That is why, in the present model, peak rainfall, time of concentration, and loss coefficient were multiplied and used as input. The same value was subtracted from peak discharge and the difference was used as output variable of the present model so that during the iteration procedure, less computational energy and time was required to learn the problem. The methodology and model variables were already discussed in Section 2.2.

9.2.3   *Categorized Neurogenetic Spatially Distributed Rainfall-Runoff Model*

The categorized neurogenetic spatially distributed rainfall-runoff model (CNSRRM) was developed similar to NSRRM except the dataset used for training the neural models were categorized into different groups. Neurogenetic models were found as a better learner of a problem when grouped data were used for training the models. Thus, the dataset was grouped and used to develop another kind of neurogenetic model. The methodology and model variables are already discussed in Section 2.2.2.

9.2.4   *Neurogenetic Model for Estimation of Basin Hydrograph (NGHYD)*

In surface water hydrology, a hydrograph is a time record of the discharge of a stream, river, or watershed outlet. Rainfall is typically the main input to a watershed and the stream flow is often considered the output of the watershed; a hydrograph is a representation of watershed response to rainfall. A watershed response to rainfall depends on a variety of factors, which affect the shape of a hydrograph:

- Watershed topography and geology (i.e., bedrock permeability)
- The area of a basin receiving rainfall
- Land use
- Drainage density
- Duration of rainfall and precipitation intensity and type
- Evapotranspiration rates
- River geometrics
- The season
- Previous weather
- Vegetation type and cover
- River conditions (e.g., dams)
- Initial conditions (e.g., the degree of saturation of the soil and aquifers)
- Soil permeability and thickness

When, data of rainfall and runoff are unavailable, synthetic hydrograph, that is, artificial generation of catchment response to rainfall is performed with factors described above. There are many empirical or conceptual models for the estimation of synthetic hydrograph, all of which try to estimate peak flow and time of peak flow. Then 50% and 70% of peak runoff is found out along with the time required to reach the same amount of runoff. The relationship between runoff and rainfall in the rising limb and the impact of basin characteristic on runoff at the recession limb is included in the model to draw the entire hydrograph. It was observed that time to peak is equal to time of concentration of the basin. Yeh et al. (1997), Blazkova

et al. (2002), Lopez et al. (2005), Sui (2005), Taskinen and Bruen (2007), Ahmad et al. (2009), and others have investigated the use of hydrograph in the estimation of parameters, design flood, uncertainty analysis, geomorphology, etc. and most of them advocates the use of hydrograph in hydrologic models as it helps to estimate runoff volume and time to peak, which are necessary in case of hydrologic or hydraulic design.

Hydrograph is not essential for impact analysis of climate change, but to analyze impacts of climatic variability on duration of peak storm and response time of a catchment due to the storm.

In the present study, a model was developed to estimate hydrograph and corresponding peak basin runoff of the sampling regions with the help of neuro-genetic models. The methodology and model variables are already discussed in Section 3.2.2.

9.2.5 Plantation-Prioritized Basin Yield Estimation Hydrologic Model

According to Lau et al. (1999), Wemple and Jones (2003), Callahan et al. (2004), Oliviera (2006), Tiju and Xiaojing (2007), Franco et al. (2008), Gomi et al. (2008), GWSP Digital Water Atlas (2008), Idson (2009), and others, forest, plantation, or cropped lands (now on collectively called as vegetated area) has a clear impact on basin runoff where increase in vegetated area decreases the basin runoff. The plantation-prioritized basin yield estimation (PLANOBAY) model tries to estimate basin runoff by considering impact of vegetated area on basin runoff. The methodology and model variables are already discussed in Section 3.2.1.

9.2.6 Representative Elementary Area Hydrologic Model

Representative elementary area (REA) is defined as that area where variance of runoff with respect to area is nil. REA is a concept proposed by Woods et al. where the impact of change in area on change in runoff was analyzed. Woods et al. proposed an area where runoff is not a function of area, which makes runoff independent of spatial variation. According to this concept runoff estimated with the help of REA will be the same as runoff estimated from distributed and lumped hydrologic models. In the present study, incremental change in area with respect to representative elementary area (A') and incremental change in runoff with respect to representative elementary runoff (Q') was considered as input and runoff was taken as output of the developed neurogenetic models. A detailed description of the methodology to develop the model and model variables are already explained in Section 8.2.1.

9.2.7   PARITY Neurogenetic Distributed Hydrologic Model

A PARITY model can be defined as a model, which is used to prioritize the possible input variables, perform a sensitivity analysis, and according to the sensitivity of the variable toward output, dataset of each input variable were weighted and used for model development. A weighted dataset, as explained earlier, is called as Ortho-Pareto dataset due to which the model was given a name, PARITY hydrologic model. In the present study, seven hydrological and metereological variables were used and prioritized with respect to sensitivity of each variable toward basin runoff. Any type of neural network prefers weighted dataset for training. A weighted dataset can help the model learn the problem and/or interrelationship/pattern that exist within the dataset more easily than an ordinary dataset as ortho-pareto dataset is already patternized, and interrelationship within variables are already identified. These types of dataset save a lot of computational energy as well as reduce amount of model preparation time. A detailed description of PARITY models are already given in Section 4.2.

9.2.8   Model Validation

All the eight models were validated for accuracy with the help of root mean square error (RMSE), coefficient of determination (r), coefficient of efficiency (E) (Bhatt et al. 2007), and first-order uncertainty analysis (U) which could be mathematically represented as

$$\text{Root mean square error} = \sqrt{\sum_{n=1}^{n} \frac{(T_p - O_p)^2}{n}} \tag{9.1}$$

$$\text{Coefficient of determination} = \sqrt{\frac{\sum (T_p - T_m)(O_p - O_m)}{\sqrt{\sum_{1}^{n} (T_p - T_m)^2 \sum_{1}^{n} (O_p - O_m)^2}}} \tag{9.2}$$

$$\text{Coefficient of efficiency} = 1 - \frac{\sum_{n=1}^{n} (T_p - O_p)^2}{\sum_{n=1}^{n} (T_p - T_m)^2} \tag{9.3}$$

$$\text{First - order uncertainty } (U) = \left(\frac{\text{Stdev}(O_p - O_m)}{n} \right) \tag{9.4}$$

where T_p is the target data value for the pth pattern; O_p is the estimated data value for the pth pattern, T_m and O_m are the mean of target and estimated dataset, respectively,

and n is the total number of patterns. T_n is the target value of the nth pattern and T_m is the mean value of the targeted dataset.

Coefficient of determination could also be taken as a measure of model reliability (Statistics Solution 2009) whereas coefficient of efficiency was also used for measurement of model sensitivity toward observed dataset. Hence, both of these validation criteria also help to determine model reliability and sensitivity where high values would represent greater level of reliability and sensitivity of the model.

9.2.9 Estimation of Spatial Variability

The selected model would be used to predict runoff for other regions, which were not considered in the present study. The predicted runoff along with observed runoff would help to draw a surface diagram of stream flow which in turn would show the spatial variation of basin runoff within the river Basin.

9.3 Result and Discussion

9.3.1 Model Validation

The predicted values of discharge from all the developed three neurogenetic models along with three conceptual hydrologic models were compared with the observed basin runoff and RMSE, r^2, E, and U was calculated to validate the models as well as to select the better model out of the six models considered.

According to the comparison result as given in Table 9.1, RMSE of PARITYCGD was found to be equal to 2.58, which was less than CONECOMOQP (3.38), CONECOMOCGD (3.46), CONECOMOBBP (3.75), PARITYQP (3.78), and any other considered neurogenetic models of the present study. PARITYCGD had an efficiency and correlation or reliability equal to 0.99 and 0.96, respectively, which was lesser than the correlation of NSRRMQP (0.98) and equal to the efficiency of PARITYQP, NSRRMQP, PLANOBAYQP, and more than any other neurogenetic models developed for the present study. The U of PARITYCGD was found to be equal to 5.5%, which was less than PARITYQP (5.8%), REANGQP (7%), and the other neurogenetic models of the present study. As RMSE and U of PARITYCGD was lower than the other considered neurogenetic models and as the model had higher efficiency than any other neurogenetic models, PARITYCGD was selected as the better model among all the neurogenetic models considered in the present study, even if, NSRRMQP had a better correlation coefficient than the selected model.

If conceptual hydrologic models were compared with the selected neurogenetic model, PARITYCGD was found to be 2.11, 2.63, and 3.92 times more accurate than HECHMS (5.45), TR55 (6.78), and MODRAT (10.12) (Table 9.2).

As PARITYCGD has the lesser RMSE and higher model efficiency among the 21(7 × 3 types of training algorithms) considered neurogenetic models and also among the three conceptual hydrologic models, it was selected as the model for the estimation of stream flow.

In the present study, stream flows for 124 ungauged and unknown basins were predicted with the help of PARITYCGD model. This model was capable of predicting runoff as a function of P, ET, T_c, L_c, GWT, GWB, and ST, all weighted according to its sensitivity toward the output variable and as all the above variables change with change in location. For a small change in location, generally only the T_c and L_c may change along with GWT and GWB. A large change would induce above-mentioned changes along with change in P and ET. The distributed nature of the selected model was used to estimate Q for those regions, which were not considered in the study.

The values of stream flow for 124 regions would easily draw a spatial variation of stream flow with the help of Radial Basis (Chapter 22) surface algorithm and the output diagram is depicted by Fig. 9.1.

The spatial variation of stream flow was also predicted for the future and according to A2 and B2 scenario of climate change as generated by PRECIS climate models. The future values of all the input variables were collected from generated weather scenarios like A2 and B2 and prediction of stream flow was made for 2010–2100. Figures 9.2–9.7 shows the future variation of stream flow within the same two river networks.

9.3.2   Estimation of Future Stream flow

According to Figs. 9.2–9.7 and Table 9.3, for A2 scenario of climate change, maximum monthly runoff showed an increasing trend starting from 2010 when change in runoff was 4.46% less than the observed runoff and up to 2100 when the same change in runoff would be equal to 2.83% less than the observed runoff. From the estimated runoff for B2 scenario, it could be concluded that the same increasing trend would be observed where runoff was reduced by 5.8% in 2010, 1.03% in 2070, and 3.94% in 2100.

If tributaries and distributaries of rivers Damodar and Rupnarayan were compared (Table 9.3), Damodar basin would have more runoff than the later but both of the basins would show an increasing trend in basin runoff in case of both A2 and B2 scenario of climate change. Maximum change of runoff in Damodar basin would be observed in same time domain 2010–2040 for both A2 scenario (13.58% less than observed runoff) and B2 scenario (12.46% more than observed runoff). The change of runoff for Rupnarayan basin would be maximum in 2071–2100 for A2 scenario of climate change (144.64% than observed runoff) and in 2041–2100 (147.24% than the observed runoff) for B2 scenario of climate change.

If the states of Jharkhand and West Bengal were compared (Table 9.3), then Jharkhand would have more runoff than West Bengal and an increasing trend would

Table 9.1 Table showing model parameters and performance validation criteria of the considered

	PARITYCGD	PARITYQP	PARITYBBP	NSRRMQP	NSRRMCGD	NSRRMBBP	CNSRRMBBP	CNSRRMQP	CNSRRMCGD	CONECOMOQP
Model variables										
Input	p(PCI,Q/ Qmax)	p(PCI,Q/ Qmax)	p(PCI,Q/ Qmax)	p{P,L$_c$,T$_c$}	p{P,L$_c$,T$_c$}	p{P,L$_c$,T$_c$}	P,L$_c$T$_c$	P,L$_c$T$_c$	P,L$_c$T$_c$	Q$_{hc}$/Q$_{hecmax}$, P/P$_{max}$
Ouput	Q	Q	Q	F[Q-{P,Lc, Tc}]	F[Q-{P,Lc, Tc}]	F[Q-P,Lc, Tc}]	Q	Q	Q	Q/Q$_{max}$
Model parameters										
Network topology										
Network type	Feed-forward	Feed-forward	Feed-forward	Feed-forward	Feed-forward	Feed-forward	Feed-forward	Feed-forward	Feed-forward	Feed-forward
Network structure	1,2,1	1,1,1	1,1,1	1,8,1	1,17,1	1,15,1	3,2,2,1	2,1,1	2,1,1	2,1,1
Network weight	4	2	2	16	34	30	12	3	3	3
Training dataset	80	80	80	80	80	80	80	80	80	80
Testing dataset	10	10	10	10	10	10	10	10	10	10
Validation dataset	10	10	10	10	10	10	10	10	10	10
GA parameters										
Population	50	50	50	100	100	100	50	50	50	50
Generation	100	100	100	150	150	150	100	100	100	100
Penalty	6	6	6	6	6	6	6	6	6	6
Crossover rate	0.8	0.8	0.8	0.8	0.8	0.8	0.8	0.8	0.8	0.8
Mutation rate	0.2	0.2	0.2	0.2	0.2	0.2	0.2	0.2	0.2	0.2
Stop training condition										
MSE	0.05	0.05	0.05	0.05	0.05	0.05	0.05	0.05	0.05	0.05
Iteration	200	200	200	200	200	200	200	200	200	200
Generalization loss	5	5	5	5	5	5	5	5	5	5
Training algorithm parameters										
Algorithm name	CGD	QP	BBP	QP	CGD	BBP	BBP	QP	CGD	QP
Activation function	Sigmoid	Sigmoid	Sigmoid	Sigmoid	Sigmoid	Sigmoid	Tanh	Tanh	Tanh	Sigmoid
Learning rule	Super-vised	Super-vised	Super-vised	Super-vised	Super-vised	Super-vised	Super-vised	Super-vised	Super-vised	Super-vised
Learning rate	NR	0.8	0.8	0.8	NR	0.8	0.8	0.8	NR	0.8
Momentum	NR	NR	0.8	NR	NR	0.8	NR	NR	NR	NR
Propagation coefficient	NR	1.75	NR	1.75	NR	NR	1.75	1.75	NR	1.75
Training and testing results										
RMSE (Training)	1.5	1.6	1.98	5.78	9	8.15	5.78	6.56	6.78	0.008
RMSE (Testing)	0.56	3.34	3.07	10.51	13.5	16.3	6.05	15.66	12.76	0.005
	Maximum no. of iteration reached	Maximum no. of iteration reached	Maximum no. of iteration reached	Generali-zation loss	Generali-zation loss	Generali-zation loss	Generali-zation loss	Generali-zation loss	Generali-zation loss	Required RMSE achieved
Model estimation Results										
RMSE	2.58	3.78	3.96	7.42	9.11	8.44	7.00	6.15	5.78	3.38
Relationship	0.96	0.94	0.94	0.98	0.97	0.98	0.64	0.74	0.61	0.68
Efficiency	0.99	0.99	0.97	0.99	0.97	0.98	0.82	0.97	0.98	0.95
Uncertainty (%)	5.5	5.8	7.45	8.5	9.79	8.77	8.82	8.89	8.98	7.5

neurogenetic models

CONECOMOCGD	CONECOMOBBP	REANGBBP	REANGCGD	REANGQP	PLANOBAYQP	PLANOBAYCGD	PLANOBAYBBP	NG-HYDQP	NG-HYDCCGD	NG-HYDBBP
Q_{hec}/Q_{hecmax}	Q_{hec}/Q_{hecmax}	dA/A_e, dQ/Q_e	dA/A_e, dQ/Q_e	dA/A_e, dQ/Q_e	P,VAIn	P,VAIn	P,VAIn	dP	dP	dP
Q/Q_{max}	Q/Q_{max}	Q	Q	Q	Q	Q	Q	dQ	dQ	dQ
Feed-forward	Feed-forward	Feed-forward	Feed-forward	Feed-forward	Feed-forward	Feed-forward	Feed-forward	Feed-forward	Feed-forward	Feed-forward
2,1,1	2,1,1	2,1,1	2,1,1	2,1,1	2,6,4,1	2,1,1	2,1,1	1,1,1	1,1,1	1,1,1
3	3	3	3	3	40	3	3	2	2	2
80	80	80	80	80	80	80	80	80	80	80
10	10	10	10	10	10	10	10	10	10	10
10	10	10	10	10	10	10	10	10	10	10
50	50	50	50	50	50	50	50	50	50	50
100	100	100	100	100	100	100	100	100	100	100
6	6	6	6	6	6	6	6	6	6	6
0.8	0.8	0.8	0.8	0.8	0.8	0.8	0.8	0.8	0.8	0.8
0.2	0.2	0.2	0.2	0.2	0.2	0.2	0.2	0.2	0.2	0.2
0.05	0.05	0.05	0.05	0.05	0.05	0.05	0.05	0.05	0.05	0.05
200	200	200	200	200	200	200	200	200	200	200
5	5	5	5	5	5	5	5	5	5	5
CGD	BBP	BBP	CGD	QP	QP	CGD	BBP	QP	CGD	BBP
Sigmoid	Sigmoid	Sigmoid	Sigmoid	Sigmoid	Sigmoid	Sigmoid	Sigmoid	Sigmoid	Sigmoid	Sigmoid
Super-vised	Super-vised	Super-vised	Super-vised	Super-vised	Super-vised	Super-vised	Super-vised	Super-vised	Super-vised	Super-vised
NR	0.8	0.8	NR	0.8	0.8	NR	0.8	0.8	NR	0.8
NR	0.8	0.8	NR	NR	NR	NR	0.8	NR	NR	0.8
NR	NR	NR	NR	1.75	1.75	NR	NR	1.75	NR	NR
0.008	0.007	10.98	11.67	11.55	10.98	11.67	11.55	5.5	5.8	6.5
0.004	0.004	10.05	14.56	18.78	10.05	14.56	18.78	4.87	4.56	4.06
Required RMSE achieved	Required RMSE achieved	Generali-zation loss	Generali-zation loss	Generali-zation loss	Generali-zation loss	Generali-zation loss	Generali-zation loss	Generali-zation loss	Generali-zation loss	Generali-zation loss
3.46	3.75	4.21	6.45	6.74	12.53	12.95	12.56	4.90	5.55	5.65
0.67	0.92	0.95	0.97	0.57	0.74	0.70	0.68	0.59	0.55	0.61
0.96	0.97	0.94	0.96	0.95	0.99	0.95	0.97	0.76	0.72	0.75
7.67	7.8	7.96	7.78	7.77	7	8.56	8.88	11.34	11.87	11.98

Table 9.2 Table showing comparison of performance validation criteria calculated within selected neurogenetic model and the three conceptual hydrologic models

Model name	RMSE	Relationship (r)	Efficiency (E)	Uncertainty (U)
PARITYCGD	2.58	0.96	0.99	5.5
HECHMS	5.45	0.67	0.78	8.5
TR55	6.78	0.65	0.68	15.67
MODRAT	10.12	0.71	0.58	17.25
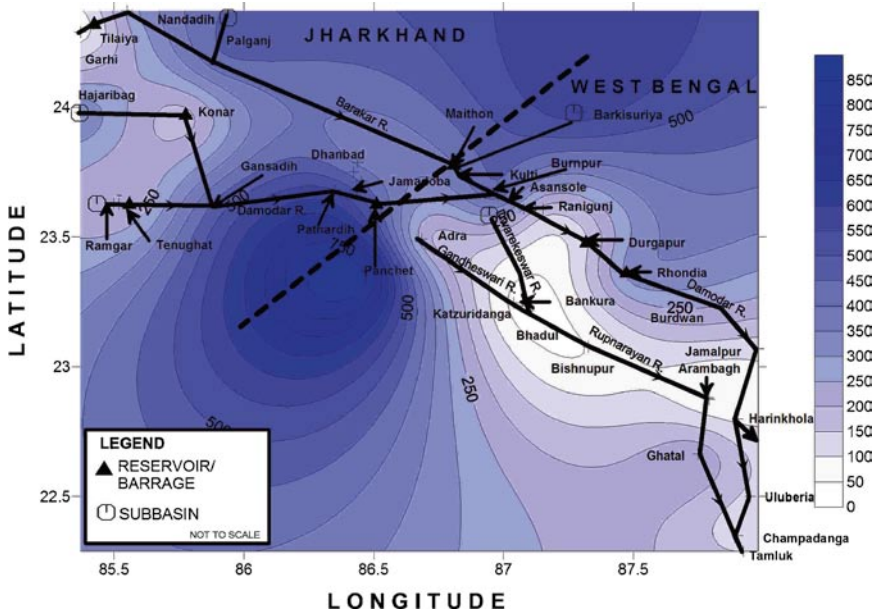
Fig. 9.1 Figure showing the spatial variation of stream flow within the two river networks considered in the present study

be observed in case of A2 (0.45%,1.36%, and 4.44% more runoff would be observed respectively in 2010–2040, 2041–2070, and 2071–2100 within Jharkhand and 102.10%, 111.55%, and 113.95%, respectively in 2010–2040, 2041–2070, and 2071–2100 within West Bengal) and B2 (102.07%, 106.23%, and 101.55%, respectively in 2010–2040, 2041–2070, and 2071–2100 within Jharkhand and 104.14%, 107.37%, and 105.92%, respectively, in 2010–2040, 2041–2070, and 2071–2100 within West Bengal) scenario of climate change.

If estimated runoff from districts were compared (Table 9.3), in case of A2 scenario of climate change, Hooghly districts of West Bengal was found to have the maximum decrease in runoff where observed runoff would decrease by 61.63% in 2010–2040 and maximum increase was observed in Purulia districts of West Bengal where observed runoff would increase by 177.15% in 2071–2100, whereas in case of B2 scenario of climate change, the same two districts were found to have
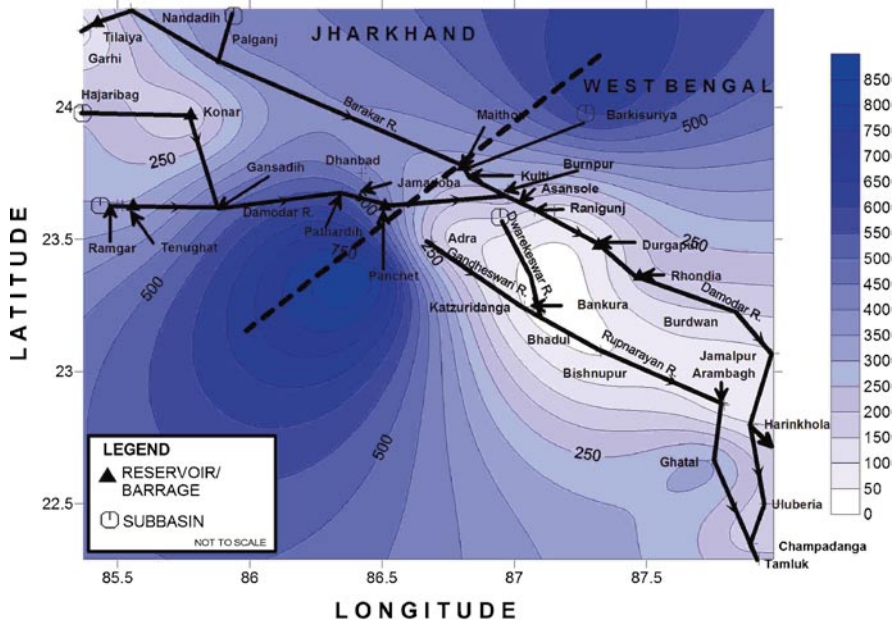
Fig. 9.2 Figure showing spatial variation of river runoff as predicted by PARITYCGD for A2 scenario of climate change in 2010–2040
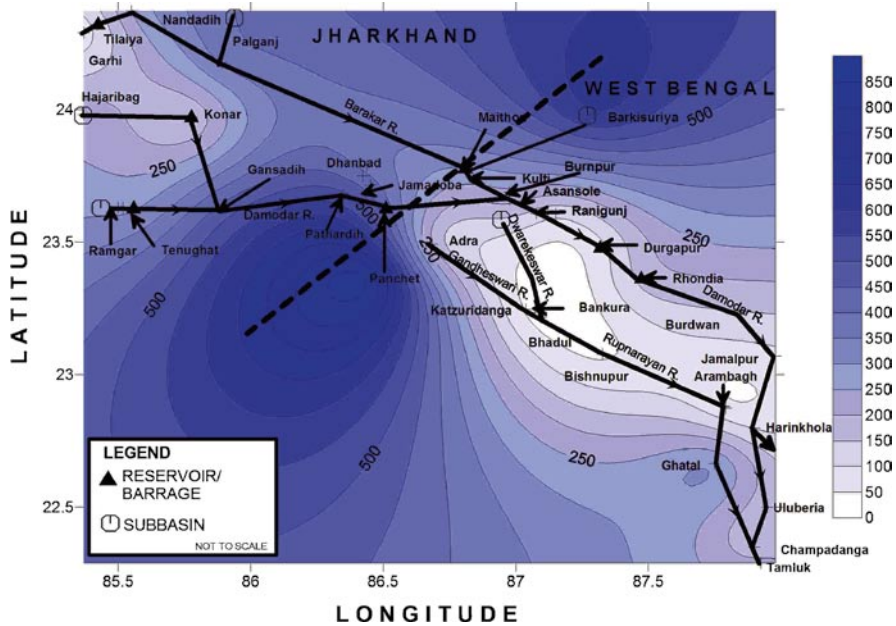
Fig. 9.3 Figure showing spatial variation of river runoff as predicted by PARITYCGD for A2 scenario of climate change in 2041–2070
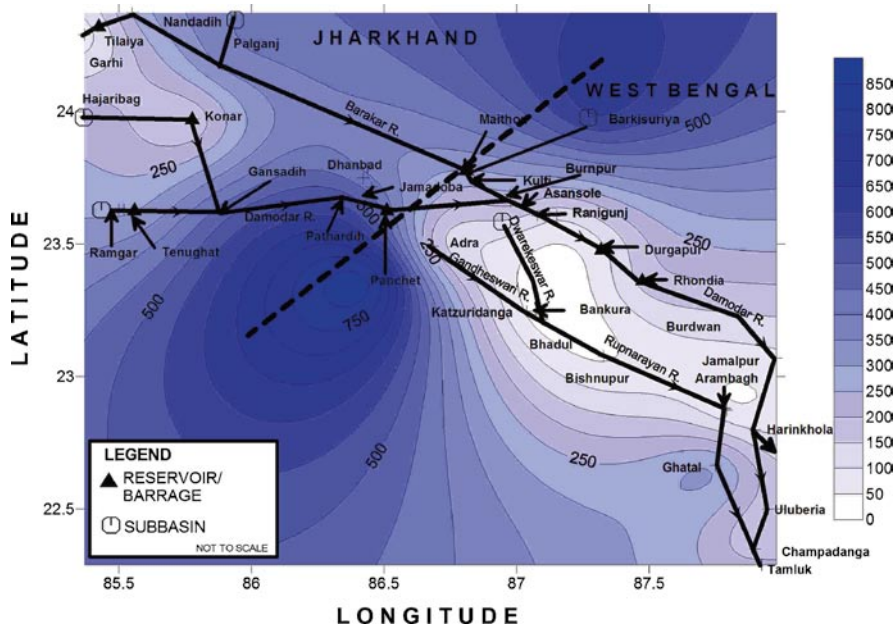
Fig. 9.4 Figure showing spatial variation of river runoff as predicted by PARITYCGD for A2 scenario of climate change in 2071–2100
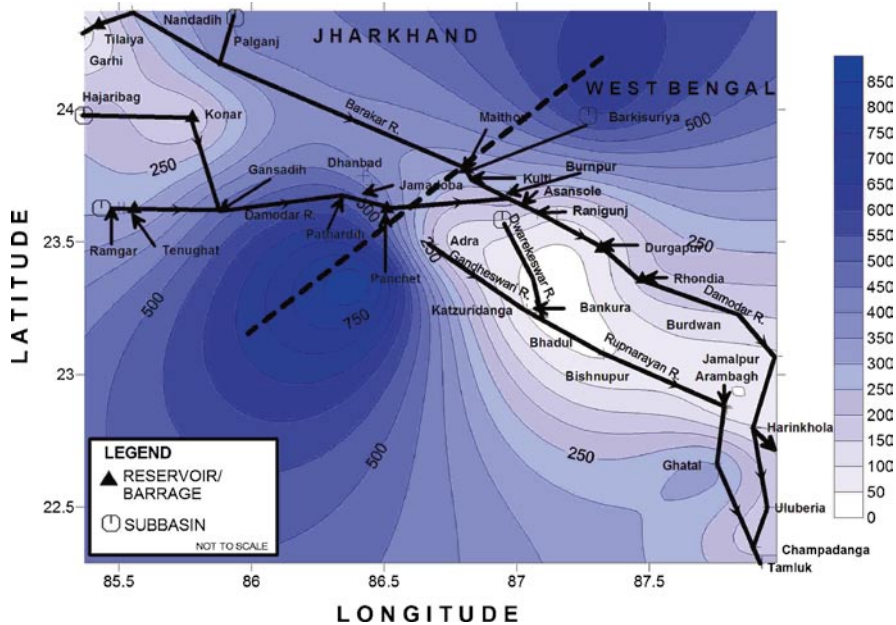
Fig. 9.5 Figure showing spatial variation of river runoff as predicted by PARITYCGD for B2 scenario of climate change in 2010–2040
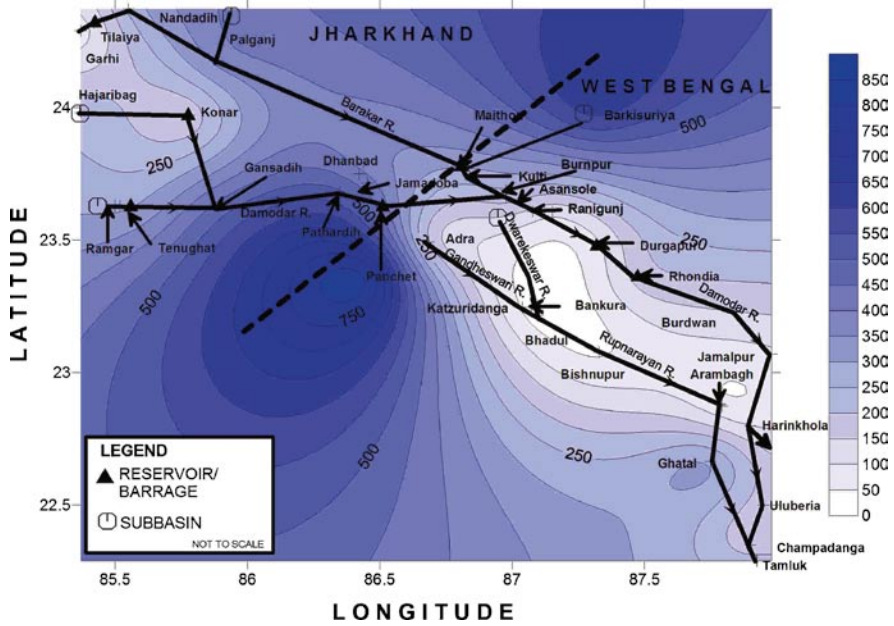
Fig. 9.6 Figure showing spatial variation of river runoff as predicted by PARITYCGD for B2 scenario of climate change in 2041–2070
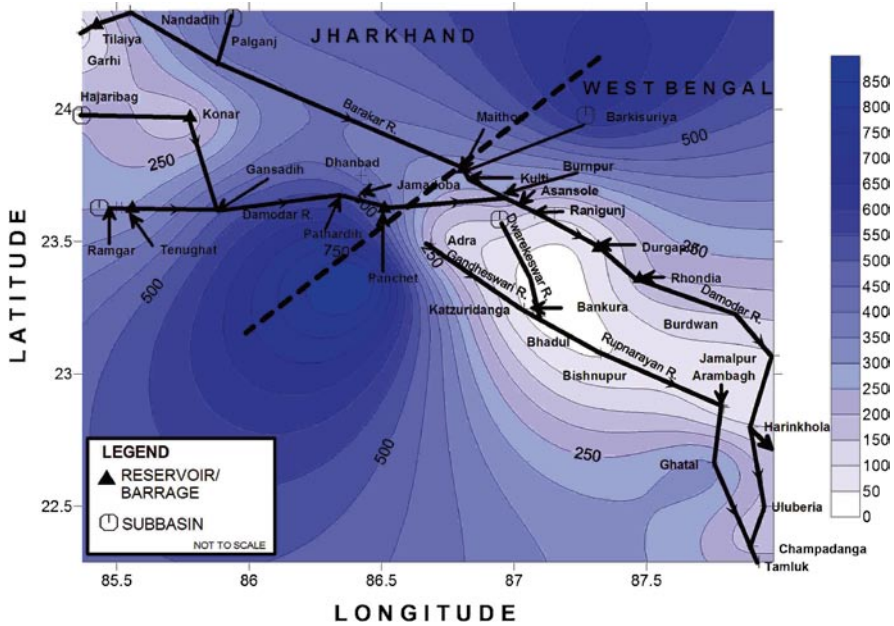
Fig. 9.7 Figure showing spatial variation of river runoff as predicted by PARITYCGD for B2 scenario of climate change in 2071–2100

Table 9.3 Table showing district-wise, state-wise, and basin-wise variation of basin runoff due to A2 and B2 scenario of climate change as predicted by spatially varied PARITYCGD model

	A2 scenario			B2 scenario			Observed
Districts	2010–2040	2041–2070	2071–2100	2010–2040	2041–2070	2071–2100	1970–2002
State	2010–2040	2041–2070	2071–2100	2010–2040	2041–2070	2071–2100	1970–2002
Basins	2010–2040	2041–2070	2071–2100	2010–2040	2041–2070	2071–2100	1970–2002
Giridih	205.48	207.34	210.89	210.43	219.38	207.74	222.33
Jamtara	658.96	666.41	675.63	679.76	713.03	666.84	610.50
Bokaro	328.94	331.89	352.54	337.79	351.96	333.40	411.90
Ranchi	275.3	277.14	291.00	276.27	284.49	277.66	166.60
Hazaribagh	259.09	260.77	269.34	259.32	267.37	261.70	281.42
Dhanbad	521.73	526.35	539.53	522.21	542.71	526.81	546.67
Burdwan	156.64	157.55	165.05	160.52	165.42	162.24	293.77
Hooghly	47.26	144.57	149.21	49.29	52.36	50.78	123.19
Howrah	158.2	160.23	164.23	165.07	174.53	169.23	133.55
Purulia	17.79	17.96	18.66	17.70	18.43	18.68	10.54
Bankura	21.99	22.20	22.85	22.26	23.22	23.13	13.19
West Midnapur	411.93	414.32	420.04	417.64	428.01	424.43	322.87
East Midnapur	315.38	316.85	320.13	319.27	325.44	322.97	208.81
Jharkhand	374.92	378.32	389.82	380.97	396.49	379.02	373.24
West Bengal	161.31	176.24	180.03	164.54	169.63	167.35	157.99
Damodar	272.11	274.42	283.41	275.66	286.44	277.06	314.89
Rupnarayan	89.21	89.75	91.13	90.39	92.78	92.07	63.01

the maximum decrease (59.98% decrease was observed in Hooghly) and increase (177.34% increase was observed in Purulia) in runoff at the same time domain.

According to Figs. 9.2–9.7, the magnitude of stream flow was found to be more in upstream of river Damodar than in river Barakar and downstream of rive Damodar and in entire Rupnarayan River network. The concentration of high-magnitude stream flow was found to increase in the A2 and B2 scenario of climate change and within 2010–2100. The dark blue circles of higher stream flow were found to have increased their area and frequency in the future in case of both A2 and B2 scenario of climate change. The only difference between the two scenarios exists in the magnitude of the stream flows, which would be more in A2 than in B2 scenario of climate change.

The increase of discharge actually shows the decaying conditions of watershed where large discharge would represent a decaying watershed and opposite would show a healthy watershed. Excessive runoff would decrease availability of water and decrease in runoff would increase the water availability of a basin. Accordingly, it could be concluded from the above results that watersheds in West Bengal would be healthier than the watersheds of Jharkhand in case of both A2 and B2 scenario of climate change. Again, watersheds of river Rupnarayan were found to be less healthy than river Damodar in case of both of the baseline scenarios.

9.4 Conclusion

The present study tried to estimate spatial variation of stream flow within two river networks of tropical and subtropical regions of East India. Seven different types of neurogenetic models were developed for the purpose of the present study. Performance validation criteria like RMSE, r, E, and U were used to validate the models and select the better model among seven considered models of the present study. After a model was selected, random points with their stream flow was estimated and applied to a spatial algorithm to generate a spatial variation of stream flow where deep-colored circles represent high stream flow and light-colored circles depict low stream flow. As, catchment condition is inversely proportional to magnitude of stream flow, deep-colored circles of the spatial diagram represent degraded catchment and light-colored region represents healthy catchment. According to the performance validation criteria, PARITYCGD was selected as the better model among all the other seven (actually 21 if same models trained with different training algorithms were taken as separate models) due to the model's higher efficiency and lower RMSE and uncertainty than any other considered models. The neurogenetic model was also compared with conceptual hydrologic model and the comparison also selected PARITYCGD as the better model than the three conceptual models considered in the study. The spatial diagram of stream flow reveals that river Rupnarayan and downstream of river Damodar were not as degraded as upstream of the later river. In the future also, which was predicted from PRECIS model-generated A2 and B2 climate change scenarios, the same trend remains, only

the decay of watershed becomes more pronounced and frequent within the selected river basins. The present study generated the surface diagram with the help of RBF surface algorithm, which also follows neural network and algorithms to estimate the value of stream flow at interpolation. Due to the data dependency of neural networks, this PARITYCGD model could be applied in case of the selected two watersheds, but the model development methodology can be imitated for other basins if data of those basins were used to train the model.

References

Ahmad M, Ghumman A, Ahmad S (2009) Estimation of clark's instantaneous unit hydrograph parameters and development of direct surface runoff hydrograph. Water Resour Manage 23:2417–2435

Beatson RK, Cherrie JB, Mouat CT (1999) Fast fitting of radial basis functions: methods based on preconditioned GMRES iteration. Adv Comput Math 11(2–3):253–270

Bhatt VK, Bhattacharya P, Tiwari AK (2007) Application of artificial neural network in estimation of rainfall erosivity. Hydrol J 1–2(March–June):30–39

Blazkova S, Beven KJ, Kulasova A (2002) On constraining topmodel hydrograph simulations using partial saturated area information. Hydrol Process 16(2):441–458

Brikowski RT (2007) GEOS, 5313, Lecture notes, Spring, UTD, MODRAT, http://www.ladpw.com/wrd/publication/

Callahan TJ, Cook JD, Coleman MD, Amatya DM, Trettin CC (2004) Modeling storm water runoff and soil interflow in a managed forest, Upper coastal plain of the southeast US, Proceedings of ASAE annual meeting, American Society of Agricultural and Biological Engineers, Paper number 042254

Carpenter TM, Georgakakos KP (2006) Intercomparison of lumped versus distributed hydrologic model ensemble simulations on operational forecast scales. J Hydrol 329(1–2):174–185

Carr JC, Beatson RK, McCallum BC, Fright WR, McLennan TJ, Mitchell TJ (2003) ACM graphite 2003, Melbourne, Australia, pp 119–126

Carr JC, Beatson RK, Cherrie JB, Mitchell TJ, Fright WR, McCallum BC, Evans TR (2001) ACM siggraph 2001, Los Angeles, CA, pp 67–76

Carr JC, Fright WR, Beatson RK (1997) Surface interpolation with radial basis functions for medical imaging. IEEE Trans Med Imag 16(1):96–107

Clair TA, Ehrman JM (1998) Using neural networks to assess the influence of changing seasonal climates in modifying discharge, dissolved organic carbon, and nitrogen export in eastern Canadian rivers. Water Resour Res 34(3):447–455

Coulibaly P, Anctil F, Bobee B (2000) Daily reservoir inflow forecasting using artificial neural networks with stopped training approach. J Hydrol 230(3–4):244–257

Draper N, Smith H (1981) Applied regression analysis, 2nd edn. Wiley-Interscience, New York, p 709

Dutta D, Herath S, Musiake K (1999) Distributed hydrologic model for flood inundation simulation, Proceedings of hydraulic engineering, JSCE, vol 43. Tokyo, Japan, pp 25–30

El-Shafie A, Taha MR, Noureldin AA (2007) Neuro-fuzzy model for inflow forecasting of the Nile river at Aswan high dam. Water Resour Manage 21(3):533–556

Elshorbagy A, Simonovic SP, Panu US (2000) Performance evaluation of artificial neural networks for runoff prediction. J Hydrol Eng 5(4):424–427

Eslami HR, Mohammadi K (2002) Application of ANN for reservoir inflow forecasting using snowmelt equivalent in the Karaj river watershed. Lowland Technol Int 4(2):17–26

Fasshauer GE (2007) Meshfree approximation methods with MATLAB. World Scientific, Singapore

Fernando DA, Jayawardena AW (1998) Runoff forecasting using RBF networks with OLS algorithm. J Hydrol Eng 3(3):203–209

Franco C, Drew AP, Heisler G (2008) Impacts of urban runoff on native woody vegetation at Clark reservation state park, Jamesville, NY, J Urb Habit. Retrieved from http://www.urbanhabitats.org/v05n01/runoff_full.html on June 2009

Gomi T, Sidle RC, Miyata S, Kosugi K, Onda Y (2008) Dynamic runoff connectivity of overland flow on steep forested hillslopes: Scale effects and runoff transfer. Water Resour Res 44:W08411. doi:10.1029/2007WR005894

GWSP Digital Water Atlas (2008) Map 52: change in runoff due to deforestation (V1.0). Available online at http://atlas.gwsp.org

He W, Chen J, Dai H (2008) Application of decision support system to the Three Gorges Reservoir operation. J Hydroelectric Eng 27(2):11–16

Hörmann G, Zhang X, Fohrer N (2007) Comparison of a simple and a spatially distributed hydrologic model for the simulation of a lowland catchment in Northern Germany, 209-1, pp 21–28

Hsu K, Gupta HV, Sorooshian S (1995) Artifical neural network modeling of the rainfall-runoff process. Water Resour Res 31(10):2517–253

Idson PFF (2009) Methods of studying the dependence of river runoff on the forest coverage of its basin. Retrieved from http://www.cig.ensmp.fr/~iahs/redbooks/a048/048032.pdf on June 2009

Imrie CE, Durucan S, Korre A (2000) River flow prediction using neural networks: generalization beyond the calibration range. J Hydrol 233(3–4):138–154

Jain SK, Das A, Srivastava DK (1999) Application of ANN for reservoir inflow prediction and operation. J Water Resour Plan Manage 125(5):263–271

Kim Y-O, Eum H-I, Lee E-G, Ko IH (2007) Optimizing operational policies of a Korean multi-reservoir system using sampling stochastic dynamic programming with ensemble streamflow prediction. J Water Resour Plan Manage 133(1):4–14

Kisi O (2004) Multilayer perceptrons with Levenberg–Marquardt training algorithm for suspended sediment concentration prediction and estimation. Hydrol Sci J 1025–1040

Kite G (2001) SLURP 12.7 hydrologic model. Water Resource Publications, http://www.wrpllc.com/books/slurp.html (Accessed on 7 February 2009)

Kojekine N, SavchenkoV, Ichiro H (2004) Geometric modeling: techniques, applications, systems and tools, http://portal.acm.org/citation.cfm?id=985834, 218–231

Lau CC, Lee KT, Tung CP, Chang CH (1999) Assessment of climate-change impact on runoff using normalized difference vegetation index. Retrieved from http://www.gisdevelopment.net/aars/acrs/1999/ts2/ts2045.asp on June 2009

Liong SY, Khu ST, Chan WT (2001) Derivation of Pareto front with genetic algorithm and neural network. J Hydrol Eng 6(1):52–61

Liepa P (2003) Filling holes in meshes. Proceedings of the 2003 eurographics/ACM. Retrieved from portal.acm.org, pp 200–205

Long ZQ, Zhang XH, Lin X-D, Chen ZJ (2007) Model for calculating benefit of forecasting intermediate inflow from downstream of reservoirs in water resources dispatch. J Hydraulic Eng 38(3):371–377

Lopez JJ, Gimena FN, Goni M, Agirre U (2005) Analysis of a unit hydrograph model based on watershed geomorphology represented as a cascade of reservoirs. Agric Water Manage 77(1–3):128–143

Luo W, Weiss E (2002) Evaluation of standard error of forecast of runoff volume using linear regression models. Can J Civil Eng 29(5):635–640

Maidment DR (1993) Developing a spatially distributed unit hydrograph by using GIS. Proceedings of HydroGIS'93. IAHS Publ. no. 211

Maier HR, Dandy GC (1999) Empirical comparison of various methods for training feed-forward neural networks for salinity forecasting. Water Resour Res 35(8):2591–2596

Martens SN, Breshears DD (2005) Assessing contaminant transport vulnerability in complex topography using a distributed hydrologic model. Vadose Zone 4:811–818

Meselhe EA, Habib E, Oche OC, Gautam S (2004) World Water Congress 2004. Part of critical transitions in water and environmental resources management world water and environmental resources congress

Nunes JC, Bouaoune Y, Delechelle E, Niang O, Bunel PH (2003) Image analysis by bidimensional empirical mode decomposition. Image Vision Comput 21(12):1019–1026

Oliviera FP (2006) Hydric erosion in forest areas in the Rio DoceValley, Central-East Region of the state of Minas Gerais, University Federal de Lavras, Brazil. Retrieved from http://biblio-teca.universia.net/html_bura/ficha/params/id/17531366.html on June, 2009

Olivera F, Maidment D (1999) Geographic information systems (GIS)-based spatially distributed model for runoff routing. Water Resour Res 35(4):1135–1164

Saghafian B, Pierre JY, RAJAIE H (2002) Runoff hydrograph simulation based on time variable isochrone technique. J Hydrol 261(1–4):193–203

Shrestha MN (2003) MapAsia. Retrieved from http://www.gisdevelopment.net/application/nrm/overview/ma03041abs.htm on 7 February 2009

Smith MB, Koren V, Reed SM, Zhang Z, Moreda F, Cui Z, Lei F, Cong SS (2004) The distributed hydrologic model intercomparison project phase 2 (DMIP 2): overview and initial NWS results, http://www.nws.noaa.gov/oh/hrl/dmip/2/index.html

Statistics Solution (2009) Retrieved from http://www.statisticssolutions.com/reliability-analysis on 16 July 2009

Sui J (2005) Estimation of design flood hydrograph for an ungauged watershed. Water Resour Manage 19(6):813–830

Taskinen A, Bruen M (2007) Incremental distributed modelling investigation in a small agricultural catchment: 1. Overland flow with comparison with the unit hydrograph model. Hydrol Process 21(1):80–91

Tiju C, Xiaojing T (2007) Impact of forest harvesting on river runoff in the Xiaoxing'an Mountains of China. J Frontiers Forest China 2(2):143–147

Tokar AS, Johnson PA (1999) Rainfall-runoff modeling using artificial neural networks. J Hydrologic Eng 4(3):232–239

Wei CC, Hsu NS (2007) Development of a real-time optimization model for flood control of a multipurpose reservoir. J Chinese Inst Civil Hydraulic Eng 19(3):355–365

Wemple BC, Jones JA (2003) Runoff production on forest roads in a steep, mountain catchment. Water Resour Res 39(8):1220. doi:10.1029/2002WR001744

Xu ZX, Li JY (2001) Short-term inflow forecasting using an artificial neural network model. Wiley, West Sussex

Yeh K, Yang J, Tung Y (1997) Regionalization of unit hydrograph parameters: 2. Uncertainty analysis. Stochast Hydrol Hydr 11(2):173–192

Chapter 10
Estimation of the Spatial Variation of Water Quality by Neural Models and Surface Algorithms

Mrinmoy Majumder, Suchita Dutta, Bipal K. Jana, Rabindra Nath Barman, Pankaj Roy, and Asis Mazumdar

Abstract The present study was a continuation of the scientific investigation described in Chapter 9. The present research tried to estimate spatial variation of water quality, expressed by Weighted Average Water Quality (WAWQ), from the estimated spatial variation of stream flow as explained in Chapter 9. The relationship between

M. Majumder (✉)
Senior Research Fellow, School of Water Resources Engineering, Jadavpur University, Kolkata-700032, West Bengal, India
and
Geo-information Scientist, Regional Center, National Afforestation
and Eco-development Board, Jadavpur University, Kolkata-700032, West Bengal, India
e-mail: mrinmoy@majumder.info

S. Dutta
Research Assistant, Regional Center, National Afforestation
and Eco-development Board, Jadavpur University, Kolkata-700032, West Bengal, India

B.K. Jana
Senior Research Fellow, School of Water Resources Engineering, Jadavpur University, Kolkata-700032, West Bengal, India
and
Environmental Manager, Consulting Engineering Services, West Bengal, India

R.N. Barman
Pertime Research Fellow, School of Water Resources Engineering, Jadavpur University, Kolkata-700032, West Bengal, India
and
Assistant Professor, Department of Production, National Institute of Technology, Agartala, Tripura, India

P. Roy
Lecturer, School of Water Resources Engineering, Jadavpur University, Kolkata-700032, West Bengal, India

A. Mazumdar
Coordinator, Regional Center, National Afforestation and Eco-development Board, Jadavpur University, Kolkata-700032, West Bengal, India
and
Director, School of Water Resources Engineering, Jadavpur University, Kolkata-700032, West Bengal, India

WAWQ and stream flow was estimated with the help of neurogenetic models, and the spatial variation was predicted by radial basis surface algorithm. According to the results, upstream of Damodar River was found to have low quality of water than the upstream of river Barakar, downstream of river Damodar, and the entire river networks of Rupnarayan. But in the future, quality of river water will be estimated to degrade with time for both the scenarios of climate change, which was depicted by the surface diagrams of the future, where area of low WAWQ circles were seemed to be increased with time from 2010 to 2100. The change was more or less similar for both A2 and B2 scenario of climate change.

10.1   Introduction

Water quality is the physical, chemical, and biological characteristics of water. It is most frequently used by reference to a set of standards against which compliance can be assessed. The most common standards used to assess water quality relate to drinking water, safety of human contact, and for health of ecosystems. Natural water contains microorganism as well as solutes. There is a distinction between "pure" water, which means water that is fit to drink and pure water that is a single substance.

A water pollutant is a substance that prevents the use of water for a specified purpose. The signs of polluted water are obvious. Poor drinking water tastes and smells bad. Many types of substances, which are classified as pollutants are listed below.

1. Pathogens, bacteria, and viruses
2. Dissolved organic compounds and inorganic compounds
3. Wastes that have a biochemical oxygen demand (BOD)
4. Nutrients that cause excessive growth of plants
5. Thermal pollution

10.1.1   Important Water Quality Parameters

10.1.1.1   Biochemical Oxygen Demand

Oxygen is used for the respiration of animals. Fish require the highest concentration of oxygen. If the dissolved oxygen (DO) falls below 5 ppm (part per million), fish are the first to suffer and tend to die out. Then, the population of bacteria rises to abnormal levels. The imbalance between species is a sign of water pollution. Substances which use dissolved oxygen and add to the biochemical oxygen demand are pollutants. Such substances come from the human wastes. The amount of dissolved oxygen used up during oxidation by bacteria of the organic matter in a sample of water is called biochemical oxygen demand (BOD). Water is rated as pure if BOD is 1 ppm or less, fairly pure with a BOD of 3 ppm, and suspect when the BOD reaches 5 ppm.

10.1.1.2   Dissolved Oxygen

Dissolved oxygen (DO) means oxygen that is dissolved in water by diffusion from the surrounding air or aeration of water. Fish and aquatic animals cannot split oxygen from water (H_2O) or other oxygen-containing compounds. Only green plants and some bacteria can do that through photosynthesis and similar processes. Virtually, all the oxygen we breathe is manufactured by green plants. A total of three fourths of the Earth's oxygen supply is produced by phytoplankton in the oceans. If water is too warm, there may not be enough oxygen in it. When there are too many bacteria or aquatic animals in the area, they may overpopulate, using DO in great amounts. Oxygen levels also can be reduced through overfertilization of water plants by runoff from farm fields containing phosphates and nitrates (the ingredients in fertilizers). Under these conditions, the numbers and size of water plants increase a great deal. Then, if the weather becomes cloudy for several days, respiring plants will use much of the available DO. When these plants die, they become food for bacteria, which in turn multiply and use large amounts of oxygen.

Numerous scientific studies suggest that 4–5 parts per million (ppm) of DO is the minimum amount that will support a large, diverse fish population. The DO level in good fishing waters generally averages about 9.0 ppm. When DO levels drop below about 3.0 ppm, even the rough fish die.

10.1.1.3   pH

The balance of positive hydrogen ions (H^+) and negative hydroxide ions (OH^-) in water determines how acidic or basic the water is. The pH scale ranges from 0 (high concentration of positive hydrogen ions, strongly acidic) to 14 (high concentration of negative hydroxide ions, strongly basic). In pure water, the concentration of positive hydrogen ions is in equilibrium with the concentration of negative hydroxide ions, and the pH measures exactly 7.

In a lake or pond, the pH of wateris affected by its age and the chemicals discharged by communities and industries. Most lakes are basic (alkaline) when they are first formed and become more acidic with time due to the buildup of organic materials. As organic substances decay, carbon dioxide (CO_2) forms and combines with water to produce a weak acid, called "carbonic" acid – the same stuff that is in carbonated soft drinks. Large amounts of carbonic acid lower the pH of water.

Most fish can tolerate pH values of about 5.0–9.0, but serious anglers look for waters between pH 6.5 and 8.2. The vast majority of American rivers, lakes, and streams fall within this range, though acid rain has compromised many bodies of water in our environment.

10.1.1.4   Turbidity

The American Public Health Association (APHA) defines turbidity as "the optical property of a water sample that causes light to be scattered and absorbed rather than

transmitted in straight lines through the sample." In simple terms, turbidity answers the question, "How cloudy is the water?"

Light's ability to pass through water depends on how much suspended material is present. Turbidity may be caused when light is blocked by large amounts of silt, microorganisms, plant fibers, sawdust, wood ashes, chemicals, and coal dust. Any substance that makes water cloudy will cause turbidity. The most frequent causes of turbidity in lakes and rivers are plankton and soil erosion from logging, mining, and dredging operations.

The APHA specifies that drinking water turbidity shall not exceed 0.5 NTUs. However, some scientists think that this standard is too generous. They want to see the value reduced to 0.1 NTUs.

Water plants need light for photosynthesis. If suspended particles block out light, photosynthesis – and the production of oxygen for fish and aquatic life – will be reduced. If light levels get too low, photosynthesis may stop altogether and algae will die. It is important to realize that the conditions that reduce photosynthesis in plant result in lower oxygen and larger carbon dioxide concentrations. Respiration is the opposite of photosynthesis. Large amounts of suspended matter may clog the gills of fish and shellfish and kill them directly. Suspended particles may provide a place for harmful microorganisms to lodge. Some suspended particles may provide a breeding ground for bacteria. Fish cannot see very well in turbid water and so may have difficulty in finding food. On the other hand, turbid water may make it easier for fish to hide from predators.

10.1.1.5 Total Dissolved Solids

Total dissolved solids (TDS) are the total amount of mobile charged ions, including minerals, salts, or metals dissolved in a given volume of water, expressed in units of milligrams per unit volume of water (mg/l), also referred to as parts per million (ppm). TDS is directly related to the purity of water and the quality of water purification systems and affects everything that consumes, lives in, or uses water, whether organic or inorganic, whether for better or for worse.

10.1.1.6 Total and Fecal Coliform

Coliform bacteria are the commonly used bacterial indicator of sanitary quality of food and water. They are defined as rod-shaped gram-negative nonspore-forming organisms. Some enteron forms can ferment lactose with the production of acid and gas when incubated at 35–37°C. Coliforms are abundant in the feces of warm-blooded animals, but can also be found in the aquatic environment, in soil, and on vegetation. In most instances, coliforms themselves are not the cause of sickness, but they are easy to culture and their presence is used to indicate that other pathogenic organisms of fecal origin may be present. Fecal pathogens include bacteria, viruses, or protozoa, and many multicellular parasites.

Fecal coliform are facultatively anaerobic, rod-shaped, gram-negative, nonsporulating bacteria. They are capable of growing in the presence of bile salts or similar surface agents, oxidase negative, and produce acid and gas from lactose within 48 h at 44 ± 0.5°C (Doyle and Erickson 2006).

Fecal coliforms include the genera that originate in feces, that is, *Escherichia*, as well as the genera that are not of fecal origin, that is, *Enterobacter*, *Klebsiella*, and *Citrobacter*. The assay is intended to be an indicator of fecal contamination, or more specifically *Escherichia Coli*, which is an indicator microorganism for other pathogens that may be present in the feces. As recently as April 2006, many official websites including that of the Environmental Protection Agency failed to address the fact that presence of fecal coliforms does not necessarily indicate the presence of feces (Doyle and Erickson 2006), as well as not being directly harmful.

10.1.1.7   Hardness

Carbon dioxide reacts with water to form carbonic acid (1) which at ordinary environmental pH exists mostly as bicarbonate ion (2). Microscopic marine organisms take this up as carbonate (3) to form calcite skeletons which, over millions of years, have built up extensive limestone deposits. Groundwaters, made slightly acidic by CO_2 (both that absorbed from the air and from the respiration of soil bacteria) dissolve the limestone (4), thereby acquiring calcium and bicarbonate ions and becoming "hard". If the HCO_3^- concentration is sufficiently great, the combination of processes (2) and (3) causes calcium carbonate ("lime scale") to precipitate out on surfaces such as the insides of pipes (Calcium bicarbonate itself does not form a solid, but always precipitates as $CaCO_3$.) (Lower 2009).

10.1.1.8   Dissolved Organic Compounds

Natural organic compounds have been present in the environment for millions of years. Many synthetic chemicals are harmless to living things, but some interfere with biochemical processes. Some of these synthetic chemicals are purposely introduced into the environment to kill insects. Some organic compounds pollute waterways. They are especially dangerous if they are not biodegradable. Some, like DDT, are concentrated by passage through a food chain.

10.1.1.9   Temperature

The rise in temperature of the water is called thermal pollution. Water is taken from waterways, used for cooling, and return to waterways. It decreases the solubility of oxygen, and increases the metabolic rate of organism. If the temperature rises sufficiently, fish may die (Hach Company 2006).

10.1.2 *Different Types of Water*

In general, water for drinking and cooking should be wholesome. It should be both potable and palatable. It must be bacteriologically and chemically safe for drinking and have a good taste. It should be clear, colorless, and have no unpleasant taste or odor.

In our present-day world, we need at least three basic types of water of somewhat different quality, depending on the requirements of each use.

10.1.2.1 Utility Water

Water, which is suitable for use in sanitation and lawn sprinkling; adequate in quantity, bacteriologically safe, but not necessarily treated to the highest quality.

10.1.2.2 Softened Water

Water, which is optimum for bathing, shampooing, personal grooming, laundering, and dishwashing. Since many of these uses demand hot water, fully softened water produces better results with minimum soap and detergent usage, and, in addition, provides conservation of energy required for water heating.

10.1.2.3 Drinking Water

Water to be used for drinking and cooking must be of high quality. It must meet or exceed the bacteriological and chemical requirements of both the EPA Interim Primary and Secondary Drinking Water Regulations. Since, water used for drinking and cooking amounts to only about 1/2 of 1% of the total water supplied by a community, this amounts to 0.875 gallons/person/day of the 175 gallons/person/day furnished by the community. The remaining amount (over 174 gallons/person/day) is used for a variety of purposes such as sprinkling lawns and irrigation, flushing toilets, fighting fires, cleaning streets, as well as utility commercial and industrial uses within the community.

10.1.2.4 Steam Condensate

Water condensed from industrial steam is called steam condensate. It approaches distilled water in purity, except for contamination (as by DO or carbon dioxide) and the effect of deliberate additives (e.g., neutralizing or filming amines).

10.1.2.5 Waste Water

By definition, waste water is any water that is discarded after use. Sanitary waste from private or industrial applications is contaminated with fecal matter, soaps, detergents, etc., but is quite readily handled from a corrosion standpoint. Industrial

wastes from chemical or petrochemical sources can contain strange and specific contaminants, which greatly complicate materials selection, especially in the uses of plastics and elastomers.

10.1.3 Water Quality Standards

The type of water being tested determines what *parameters*, or *analytes*, the analyst looks for. For example, chlorine is an important parameter in finished drinking water, but is not usually a factor in natural water. That is why there are different standards prescribed for different types of water, which were regulated by different monitoring authorities.

In the setting of standards, agencies make political and technical/scientific decisions about how the water will be used (United States Environmental Protection Agency (EPA) 2006). In the case of natural water bodies, they also make some reasonable estimate of pristine conditions. Different uses raise different concerns and therefore different standards are considered. Natural water bodies will vary in response to environmental conditions. Environmental scientists work to understand how these systems function which in turn helps to identify the sources and fates of contaminants. Environmental lawyers and policy makers work to define legislation, which ensures that water is maintained at an appropriate quality for its identified use.

The vast majority of surface water on the planet is neither potable nor toxic. This remains true even if seawater in the oceans (which is too salty to drink) is not counted. Another general perception of water quality is that of a simple property that tells whether water is polluted or not. In fact, water quality is a very complex subject, in part because water is a complex medium intrinsically tied to the ecology of the Earth. Industrial pollution is a major cause of water pollution, as well as runoff from agricultural areas, urban storm water runoff, and discharge of treated and untreated sewage (especially in developing countries).

The parameters for water quality are determined by the intended use. Work in the area of water quality tends to be focused on water that is treated for human consumption or in the environment.

10.1.4 Water Quality/Pollutant Estimation Models

10.1.4.1 Biofilm Model

This study developed a new sewer biofilm model to simulate the pollutant transformation and biofilm variation in sewers under aerobic, anoxic, and anaerobic conditions. The biofilm model can describe the activities of heterotrophic, autotrophic, and sulfate-reducing bacteria (SRB) in the biofilm, as well as the variations in biofilm thickness, the spatial profiles of SRB population, and biofilm density. The model can describe dynamic biofilm growth, multiple biomass evolution, and competitions among organic oxidation, denitrification, nitrification, sulfate reduction, and sulfide oxidation in a

heterogeneous biofilm growing in a sewer. The model has been extensively verified by three different approaches, including direct verification by measurement of the spatial concentration profiles of dissolved oxygen, nitrate, ammonia, and hydrogen sulfide in sewer biofilm. The spatial distribution profile of SRB in sewer biofilm was determined from the fluorescent in situ hybridization (FISH) images taken by a confocal laser scanning microscope (CLSM) and was predicted well by the model (Jiang et al. 2009).

10.1.4.2 Large-Eddy Simulation with a One-Equation Subgrid-Scale

A large-eddy simulation (LES) with a one-equation subgrid-scale (SGS) model was developed to investigate the flow field and pollutant dispersion inside street canyons of high-aspect ratio (AR). A 1/7th power-law wall model was implemented near rigid walls to mitigate the demanding near-wall resolution requirements in LES. This LES model had been extensively validated against experimental results for street canyons of AR = 1 and 2 before it was applied to the cases of AR = 3 and 5. A ground-level passive pollutant line source, located in the middle of the street, was used to simulate vehicular emissions. Three and five vertically aligned primary recirculations were developed in the street canyons of AR 3 and 5, respectively. The ground-level mean wind speed was less than 0.5% of the free stream value, which makes it difficult for the pollutant to be transported upward for removal. High pollutant concentration and variance were found near the buildings where the air flow is upward. It was found that the velocity fluctuation, pollutant concentration and variance were all closely related to the interactions between the primary recirculations and/or the free surface layer. Several quantities, which are nonlinear functions of AR, were introduced to quantify the air quality in street canyons of different configurations (Li et al. 2008).

10.1.4.3 QUAL2K Model

QUAL2EU is a US EPA steady-state model for conventional pollutants in branching streams and well mixed lakes. The model can be operated as either a steady-state or a dynamic model. It is intended for use as a water-quality planning tool. The model can be used to study the impact of waste loads on instream water quality. It also can be used to identify the magnitude and quality characteristics of nonpoint waste loads as part of a field sampling program (Fang et al. 2008).

10.1.4.4 WaterGEMS

WaterGEMS is a comprehensive and easy-to-use water distribution modeling solution featuring interoperability across stand-alone, ArcGIS, AutoCAD, and MicroStation environments. From fire flow and water quality simulations, to criticality and energy cost analysis, to advanced Genetic Algorithm optimization, WaterGEMS comes equipped with everything you need in a flexible multiplatform environment.

10.1.4.5   Hydrological Simulation Program–Fortran

Hydrological Simulation Program–Fortran (HSPF) simulates for extended periods of time the hydrologic, and associated water quality, processes on pervious and impervious land surfaces, and in streams and well-mixed impoundments. HSPF uses continuous rainfall and other meteorologic records to compute stream flow hydrographs and polluto-graphs. It simulates interception soil moisture, surface runoff, interflow, base flow, snowpack depth and water content, snowmelt, evapotranspiration, groundwater recharge, dissolved oxygen, biochemical oxygen demand (BOD), temperature, pesticides, conservatives, fecal coliforms, sediment detachment and transport, sediment routing by particle size, channel routing, reservoir routing, constituent routing, pH, ammonia, nitrite-nitrate, organic nitrogen, orthophosphate, organic phosphorus, phytoplankton, and zooplankton.

10.1.4.6   AQUASEA Finite Element Model

AQUASEA finite element model is used to solve flow in rivers, tidal flow, easturaies, coastal areas, lake circulation and problems involving transport of mass heat and suspended sediments.

10.1.4.7   XPSWMM or XP-SWMM Flood Hydrology and Hydraulic Modeling Software

XPSWMM or XP-SWMM flood Hydrology and Hydraulic Modeling Software uses EPA SWMM engine with enhancements, TUFLOW 2D modeling engine for stormwater management, sanitary sewer modeling, pipe network design, or analysis (Water and Environmental Modeling 2009).

10.2   Methodology

River water was collected from different sampling locations within selected sampling region (Chapter 25) and was analyzed for BOD, DO, pH, TDS, turbidity, hardness, and total and fecal coliform. The results found from the laboratory tests was averaged to find average values of above quality parameters of the sampling regions. A Weighted Average Water Quality (WAWQ) value was calculated by prioritizing the parameters according to their influence on overall quality of water. Basin runoff along with land use of the adjacent catchments was applied to develop neurogenetic models for estimation of WAWQ of a region as a function of basin runoff. The models were validated and better model was selected from the three models. The selected model was used to estimate WAWQ with the help of PARITYCGD predicted river runoff. The future river runoff was again estimated from future climatological data for

A2 and B2 scenario of climate change as generated by PRECIS climate model (Chapter 23) and future land-use data as conceptualized by IPCC report (2007).

10.2.1   Calculation of Weighted Average of Water Quality

The water quality was represented by a Weighted Average of Water Quality (WAWQ), which gives an average dimension-less value representing the status of water quality of the sampling regions. The term weighted was used as influential parameters to quality of water were separated from the not-so-influential parameters by increasing the weights. Similarly, an increment of BOD value could largely alters overall water quality of a sample (ELAW 2009). Thus, BOD was given the highest weightage followed by DO, TDS, total and fecal coliform, Turbidity, and pH. Hardness was not known to influence overall quality of water, so, least weightage was given to that parameter. As water quality is inversely proportional to BOD, TDS, turbidity, and hardness, and WAWQ needs to be proportional to better quality of water, negative values of those parameters were used in the calculation of WAWQ so that water quality would ultimately be represented as directly proportional to the value of WAWQ. The Indian water quality standard for different types of water could be verified for a clear overview of importance of quality parameters on overall quality of water.

10.2.2   Development of the Neurogenetic Models

The neurogenetic models were developed with the help of the procedures adopted in development of the hydrologic models (Chapter 9). The training algorithms for the three models were selected as CGD for WAWQCGD model, QP for WAWQQP model, and BBP for WAWQBBP model. The dataset had 505 records from which 70% was used for training, 15% was used as cross validation, and remaining 15% was used for testing the developed model. As explained in Section 9.2.8, the neurogenetic models considered in the present study was also compared with the WAWQ of observed values of water parameters and RMSE, correlation coefficient, coefficient of efficiency, and first-order uncertainty analysis was calculated with the help of Eqs. (9.1)–(9.4) respectively to validate and select the better model out of the above three neurogenetic models.

10.2.3   Estimation of Spatial Variability

The selected model would be used to predict runoff for other regions, which were not considered in the present study. The predicted runoff along with observed runoff would help to draw a surface diagram of stream flow, which in turn would show the spatial variation of basin runoff within the river Basin. Surface interpolation was performed by radial basin function theorem.

10.3   Result and Discussion

10.3.1   Model Validation

The RMSE achieved by the models when compared with of WAWQ, calculated from observed values of water quality parameters, were found to be equal to 1.33, 3.08, and 11.31, respectively for WAWQCGD, WAWQQP, and WAWQBBP. The efficiencies obtained from the models were 99%, 97%, and 82%, respectively for WAWQCGD, WAWQQP, and WAWQBBP. According to RMSE and E, WAWQCGD was selected as better model than the other two considered models and estimation works were carried out with the help of the selected neurogenetic model.

10.3.2   Estimation of Future Quality of River Runoff

The selected model was used to estimate WAWQ for projected runoff estimated by PARITYCGD model and future land use of the region as conceptualized by IPCC report (2007).

Figures 10.1–10.6 show the variation of water quality within the sampling locations according to A2 and B2 scenario of climate change (Table 10.1). The state-wise and
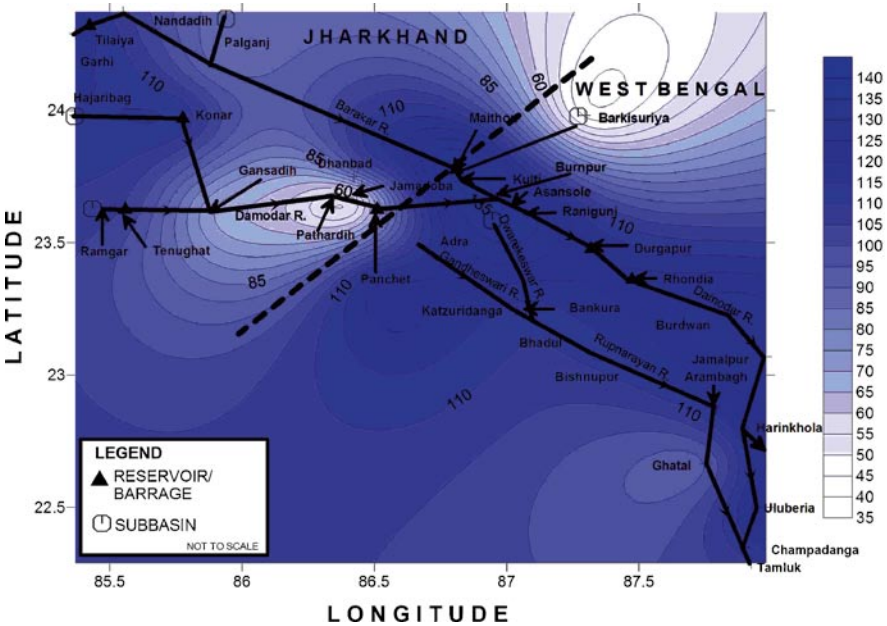
Fig. 10.1 Figure showing spatial variation of weighted average water quality due to A2 scenario of climate change in 2010–2040
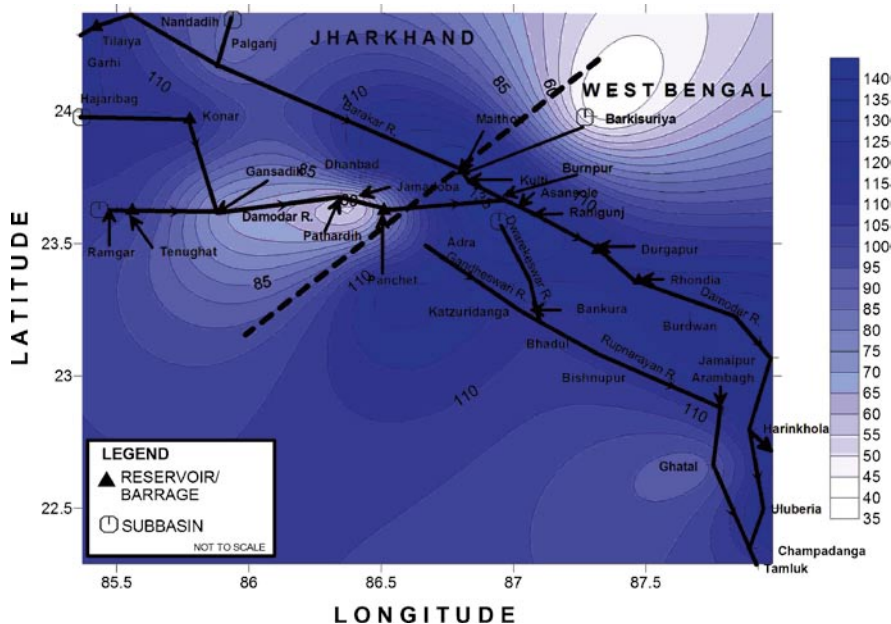
Fig. 10.2 Figure showing spatial variation of weighted average water quality due to A2 scenario of climate change in 2041–2070
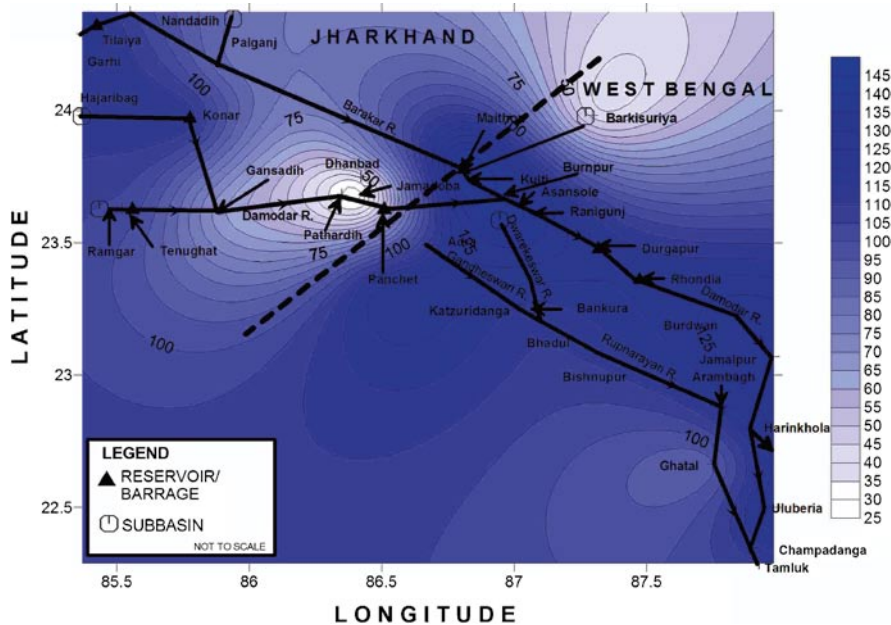
Fig. 10.3 Figure showing spatial variation of weighted average water quality due to A2 scenario of climate change in 2071–2100
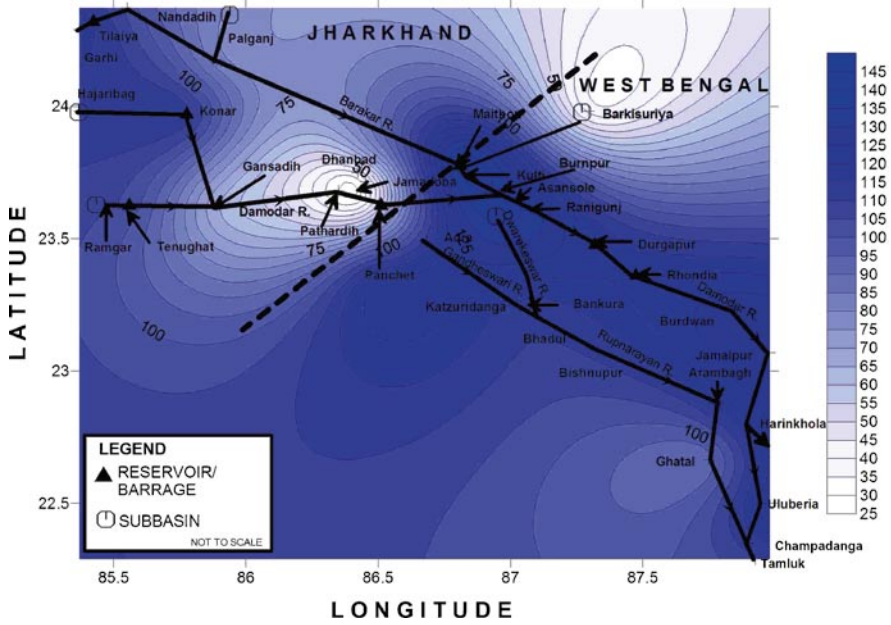
Fig. 10.4 Figure showing spatial variation of weighted average water quality due to B2 scenario of climate change in 2010–2040
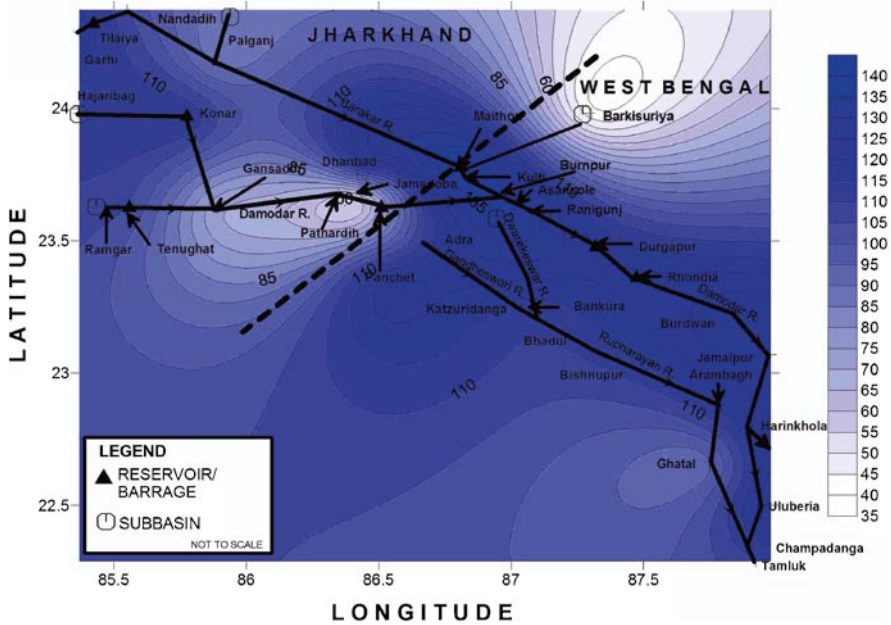
Fig. 10.5 Figure showing spatial variation of weighted average water quality due to B2 scenario of climate change in 2041–2070
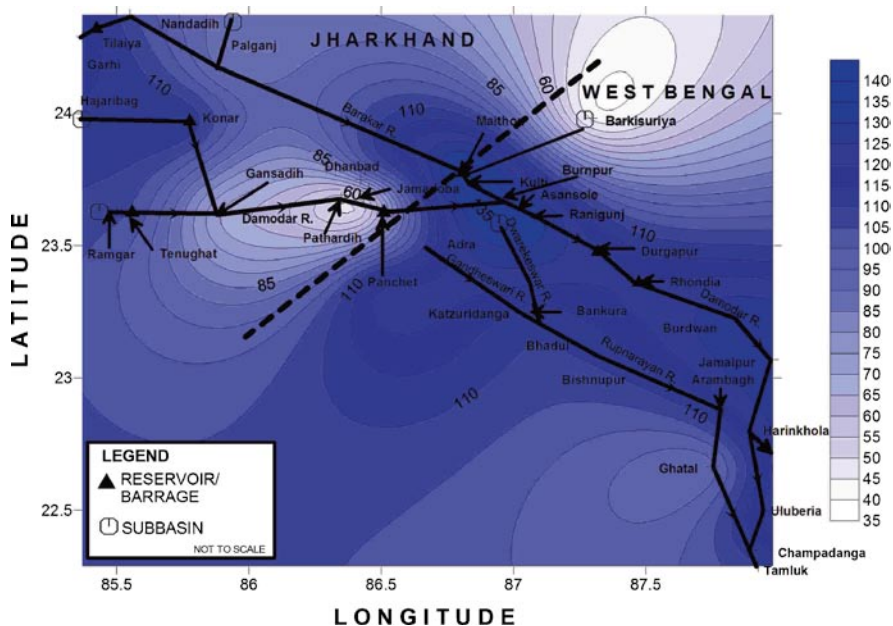
Fig. 10.6 Figure showing spatial variation of weighted average water quality due to B2 scenario of climate change in 2071–2100

Table 10.1 Table showing configuration and performance validation criteria of neurogenetic models used for estimation of WAWQ

Model name	Network architecture (I-H-O)	Parameters for GA (P-G-P'-C-M)	Training RMSE	Testing RMSE	Estimation RMSE	Model efficiency
WAWQCGD	2-5-3-1	50-100-6-0.8-0.2	13.11	25.95	1.33	0.99
WAWQQP	2-5-3-1	50-100-6-0.8-0.2	19.51	18.32	3.08	0.97
WAWQBBP	2-8-2-1	50-100-6-0.8-0.2	49.39	31.27	11.31	0.82

I, input; H, hidden; O, output layer of neurogenetic models; P, population; G, generation reproduced; P', penalty induced; C, crossover rate; M, mutation rate enforced

basin-wise variations of WAWQ in 2010–2040, 2041–2070, and 2071–2100 were depicted by Figs. 10.7 and 10.8 as per A2 scenario of climate change and Figs. 10.9 and 10.10 as per B2 scenario of climate change. Table 10.2 depicts the district-wise variation of WAWQ in case of A2 and B2 scenario of climate change.

According to the surface diagrams depicted in Figs. 10.1–10.6, the quality of river water seems to be better in the downstream of river Damodar and entire river Rupnarayan. The area of blue circles, which represents better quality of water (WWAQ > 100) seems to be shrinking with time from 2010 to 2100. If the blue circles of Figs. 10.1–10.3 were compared, the area of the blue circle was found to be shrinking toward downstream of Damodar, near Durgapur, from Figs. 10.1–10.3, which represents spatial variation of WWAQ in 2010–2040 to 2071–2100 for A2 scenario
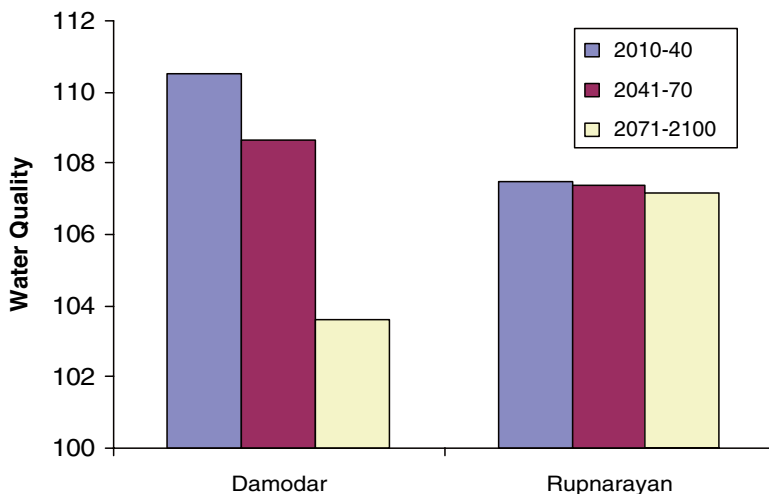
Fig. 10.7 Figure showing variation of estimated weighted average of water quality in between Damodar and Rupnarayan River basins according to A2 scenario of climate change
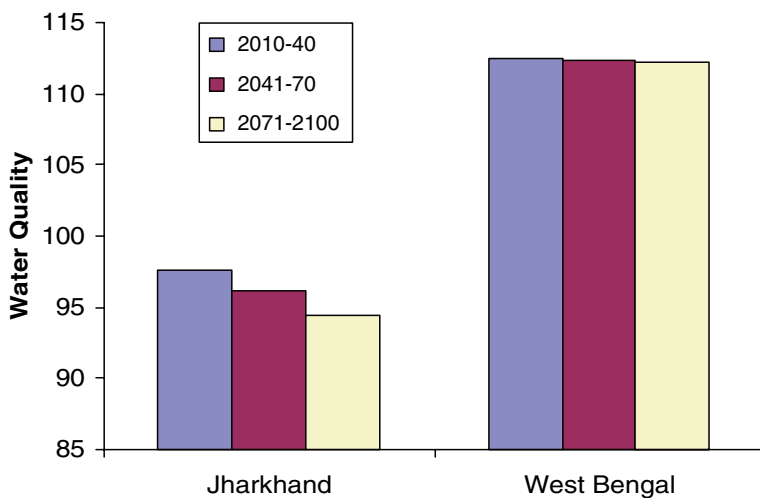
Fig. 10.8 Figure showing variation of estimated weighted average of water quality within Jharkhand and West Bengal according to A2 scenario of climate change

of climate change. The same trend was observed in the estimations of B2 scenario of climate change (Figs. 10.4–10.6). The change in the area of A2 was also very similar to that of B2 where increase was slightly bigger in the later scenario of climate change.

According to the prediction of water quality from neurogenetic model and in case of B2 scenario, water quality of West Bengal would be better than Jharkhand, if the WWAQ of the sampling locations of the two states were compared and the
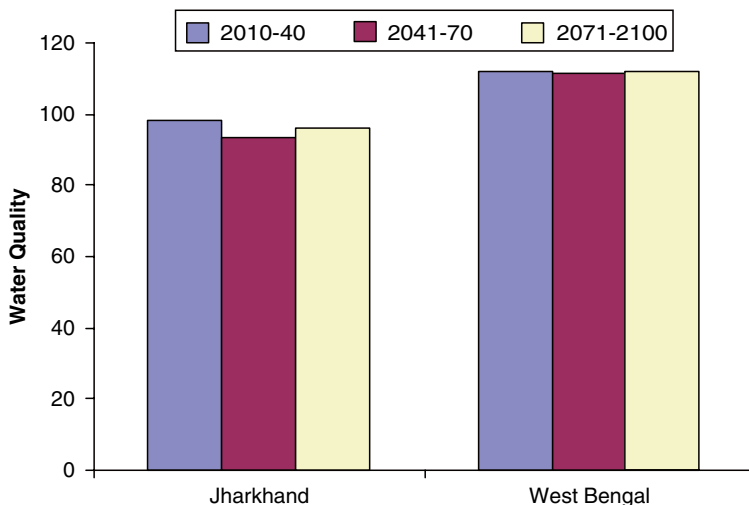
Fig. 10.9 Figure showing variation of estimated weighted average of water quality within Jharkhand and West Bengal according to B2 scenario of climate change
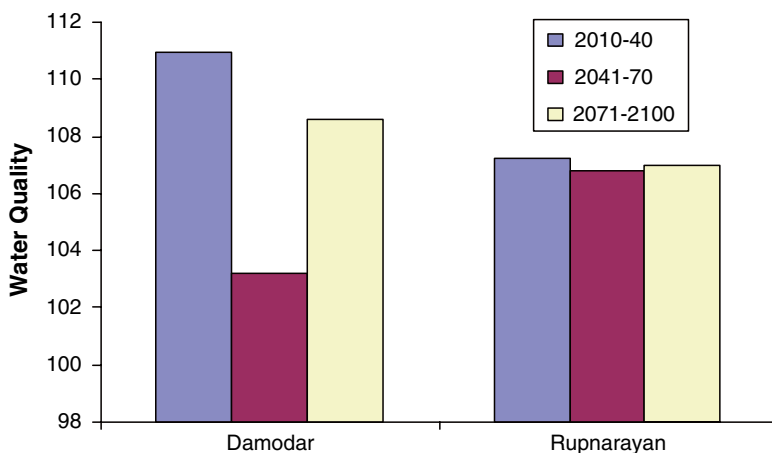
Fig. 10.10 Figure showing variation of estimated weighted average of industrial pollution in between Damodar and Rupnarayan River basins according to B2 scenario of climate change

water quality of Damodar basin would be qualitatively better than the waters of Rupnarayan River system for the same scenario of climate change but the trend would be observed only in 2010–2040 and 2071–2100, not in 2041–2070 when the trend would be reversed if the WWAQ of the sampling locations of the two basins were compared . In case of A2 scenario of climate change, a similar but more prominent trend would be observed if WWAQ of the sampling locations of the two

Table 10.2 Table showing district-wise, state-wise, and basin-wise variation of weighted average water quality due to A2 and B2 scenario of climate change

	A2 scenario			B2 scenario			Observed
Districts	2010–2040	2041–2070	2071–2100	2010–2040	2041–2070	2071–2100	1970–2002
State	2010–2040	2041–2070	2071–2100	2010–2040	2041–2070	2071–2100	1970–2002
Basins	2010–2040	2041–2070	2071–2100	2010–2040	2041–2070	2071–2100	1970–2002
Giridih	105.77	105.39	105.16	104.48	102.64	105.32	131.46
Jamtara	27.42	26.24	24.83	24.21	19.51	26.18	156.46
Bokaro	153.25	155.67	177.36	161.13	176.69	156.99	166.46
Ranchi	108.34	108.00	105.31	108.16	106.59	107.91	104.39
Hazaribagh	105.01	104.77	102.97	105.46	104.26	104.59	88.45
Dhanbad	85.52	77.00	51.20	86.60	50.76	75.93	63.18
Burdwan	130.20	130.26	130.90	130.51	130.99	130.63	142.45
Hooghly	118.09	118.20	119.20	118.51	119.10	118.79	149.76
Howrah	131.93	131.79	131.47	131.40	130.51	131.03	160.00
Purulia	111.15	111.11	110.96	111.17	111.00	110.96	165.59
Bankura	111.39	111.39	111.41	111.37	111.38	111.40	167.20
West Midnapur	80.60	80.01	78.58	79.18	76.60	77.49	149.44
East Midnapur	104.30	103.95	103.18	103.38	101.92	102.51	124.48
Jharkhand	97.55	96.18	94.47	98.34	93.41	96.15	118.40
West Bengal	112.52	112.39	112.24	112.22	111.64	111.83	151.27
Damodar	110.52	108.64	103.62	110.93	103.22	108.62	120.76
Rupnarayan	107.50	107.39	107.15	107.24	106.80	106.96	157.29

states and quality of water of the same in B2 scenario were compared. The quality of water would be better in Damodar than Rupnarayan but similar to B2 scenario of climate change the trend would be reversed from 2071 to 2100 instead of 2041–2070 as was observed in case of B2 scenario. WWAQ was found to be equal to 98.34, 93.41, and 96.15 in Jharkhand and 112.22, 111.64, and 111.83 in West Bengal, respectively, in 2010–2040, 2041–2070, and 2071–2100 in case of B2 scenario, whereas the same was found to be equal to 97.55, 96.18, and 94.47 in Jharkhand and 112.52, 112.39, and 112.24 in West Bengal, respectively, in 2010–2040, 2041–2070, and 2071–2100 in case of A2 scenario. The WWAQ for river Damodar and Rupnarayan for A2 scenario was found to be equal to 110.52 in 2010–2040, 108.64 in 2041–2070, and 103.62 in 2071–2100 and 107.50 in 2010–2040, 107.39 in 2041–2070, and 107.15 in 2071–2100, respectively. In case of B2 scenario, the WWAQ of Damodar watershed was 110.93, 103.22, and 108.62, respectively, in 2010–2040, 2041–2070, and 2071–2100 and of Rupnarayan watershed was 107.24, 106.8, and 106.96, respectively, in 2010–2040, 2041–2070, and 2071–2100. Damodar River was famous for its coal mines, which were mainly concentrated in Jharkhand part of the river and as the water quality model considers land use of the adjacent catchment, quality of water was estimated as worse in Jharkhand than in West Bengal. The quality of water of the two rivers were found to be within 125, which shows that overall quality of water in the two rivers were below standard.

According to Figs. 10.7–10.10, WWAQ was higher in West Bengal (153.01) than in Jharkhand (98.06), but if compared with respect to river basins, Damodar (157.29) was less polluted than Rupnarayan (120.76) though both the rivers had a WWAQ above 100. If the estimated and observed values were compared, water quality was found to be degraded by 4.7% and 1.9%, respectively in 2041–2070 and 2071–2100 for Jharkhand and 26.65%, 27.03%, and 26.91% for West Bengal in case of B2 scenario, whereas for A2 scenario quality of water in Jharkhand is found to be degraded by 0.5%, 1.92%, and 3.66% and in West Bengal the degradation was equal to 26.46%, 26.55%, and 26.64%, respectively in 2010–2040, 2041–2070, and 2071–2100. The quality of water for Jharkhand in case of B2 scenario was found to be upgraded by 0.3% in 2010–2040. Overall, degradation of water quality was more in West Bengal than in Jharkhand.

10.4   Conclusion

The present study tried to estimate spatial variation of water quality for two tropical and subtropical river basins of East India in case of climatic uncertainty. Neurogenetic models were used where the output of PARITYCGD model, which was used to estimate stream flow from a weighted dataset of related parameters, like rainfall, evapotranspiration, groundwater balance, basin loss, etc. is considered as input along with land-use patterns of the adjacent catchment and WAWQ, a average of water quality parameters, which is directly proportional to quality of river

water, was taken as output. The PARITYCGD model was also used to generate a surface diagram of stream flow within the two river networks (Chapter 9). A surface diagram for future WAWQ in face of A2 and B2 scenario of climate change was also generated with the help of radial basis surface interpolation algorithm (9). The surface diagram helped to identify the area of better quality of river water and the change in that area in the future. According to the results, Rupnarayan River network and downstream of river Damodar were found to have and would have better quality of water in the future (2010–2100) for both A2 and B2 scenario of climate change, but the area of the circle representing better quality of river water would decrease with time and ultimately would shrink toward the central region of the river Damodar. The reason for this observation may be attributed to the growing industrial developments considered along the banks of Rupnarayan, which might have forced the model to predict a lower quality of water for these regions in face of climate change.

References

Doyle MP, Erickson MC (2006) Closing the door on the fecal coliform assay. Microbe 1:162–163

ELAW (2009) India – water quality standards, Tables 1.1–1.5 of Environment (Protection) Rules. Retrieved from http://www.elaw.org/system/files/IndiaWQS.doc on 30 July 2009

Fang X, Zhang J, Chen Y, Xu X (2008) Qual2k model used in the water quality assessment of qiantang river, china. Water Environ Res 80(11):2125–2133

Hach Company (2006) Important water quality factors, http://www.h2ou.com/h2wtrqual.htm

IPCC (2007) Climate change 2007: the physical sciences basis, retrieved on http://ipcc-wgl.ucar.edu/wg/wg-report. html. on 30th April, 2009

Jiang F, Leung DH, Li S, Chen G-H, Okabe S, van Loosdrecht MC (2009) A biofilm model for prediction of pollutant transformation in sewers. Water Res 43(13):3187–3198

Li X-X, Liu C-H, Leung D (2008) Large-eddy simulation of flow and pollutant dispersion in high-aspect-ratio urban street canyons with wall model. Boundary-Layer Meteorol 129(2):249–268

Lower S (2009) Hard water and water softening. Retrieved from http://www.chem1.com/CQ/hardwater.html on 30 July 2009

United States Environmental Protection Agency (EPA) (2006) Washington, DC. "Water quality standards review and revision"

Water and Environmental Modeling (2009) A discussion about the present day hydrologic models, advances in hydrology. Wordclay, New York, pp 37–39

Chapter 11
Estimation of the Spatial Variation of Pollution Load by Neural Models and Surface Algorithms

Mrinmoy Majumder, Pankaj Roy, Rabindra Nath Barman, and Asis Mazumdar

Abstract The present study tried to predict spatial variation of water pollutants with the help of two pollution factors: spatial variation of stream flow and spatial variation of water quality and neurogenetic algorithms. The two pollution factors were, respectively, industrial pollution (IP) factor, which identifies the intensity and presence of industrial pollutants from common water quality parameters that got influenced due to the release of industrial effluents in a river and organic pollution (OP) factor, which tries to estimate the intensity of organic pollutants from common quality parameters that get affected due to anthropogenic presence in the adjacent catchments. A neurogenetic model was prepared to estimate industrial pollution (IP) and organic pollution (OP) factors where observed stream flow data from 42 gauged and ungauged sampling points within two river networks in the Eastern India and land use of adjacent

M. Majumder (✉)
Senior Research Fellow, School of Water Resources Engineering, Jadavpur University, Kolkata-700032, West Bengal, India
and
Geo-information Scientist, Regional Center, National Afforestation
and Eco-development Board, Jadavpur University, Kolkata-700032, West Bengal, India
e-mail: mrinmoy@majumder.info

P. Roy
Lecturer, School of Water Resources Engineering, Jadavpur University, Kolkata-700032, West Bengal, India

R.N. Barman
Pertime Research Fellow, School of Water Resources Engineering, Jadavpur University, Kolkata-700032, West Bengal, India
and
Assistant Professor, Department of Production, National Institute of Technology, Agartala, Tripura, India

A. Mazumdar
Coordinator, Regional Center, National Afforestation and Eco-development Board, Jadavpur University, Kolkata-700032, West Bengal, India
and
Director, School of Water Resources Engineering, Jadavpur University, Kolkata-700032, West Bengal, India

catchments of the sampling points were taken as input. The IP and OP factors are prepared to be directly proportional to water pollution, that is, if the factors are more than 0.7, water is polluted and if the same are less than 0.5, water is not polluted at all. The pattern identification capability of neurogenetic models enforces the authors for selection of neurogenetic models for the prediction of the above two factors. After the model was validated with the help of common validation equations, the selected model was applied to predict future IP and OP of the same region due to changed climate scenario generated by PRECIS climate model. The output of PRECIS was fed to PARITYCGD model (9), which estimated the stream flow due to the changed climatic scenario that was again used to predict IP and OP of the sampling points. The estimated values were fed to a surface algorithm to show the spatial variation of the two factors within the river basins. According to the results, area under water pollution from industries were more than the area that was not under pollution during the A2 scenario of climate change, but in B2 the trend reverses and more area without industrial pollution would emerge. But in case of water polluted by organic wastes, more area was predicted to be without pollution than area under pollution in case of A2 scenario and for B2 scenario of climate change the area without pollution will get increased in a fast rate from 2010 to 2100 and in 2071–2100 the increase would be maximum. As A2 scenario was predicted to be economic but without any restrictions on CO_2 emission, the future land use was generated as industrially active but still area under pollution was more in A2 than in B2, which was imagined to be environmentally stable and with severe restrictions on CO_2 emission.

11.1   Introduction

Water pollution is the contamination of water bodies such as lakes, rivers, oceans, and groundwater. This affects organisms and plants that live in these water bodies, and in almost all cases the effect is damaging either to individual species and populations or to the natural biological communities. It occurs when pollutants are discharged directly or indirectly into water bodies without adequate treatment to remove harmful constituents.

Water pollution is a major problem in the global context. It has been suggested that it is the leading worldwide cause of deaths and diseases (Pink 2006; West 2006) and that it accounts for the deaths of more than 14,000 people daily (West 2006). In addition to the acute problems of water pollution in developing countries, industrialized countries continue to struggle with pollution problems as well. In the most recent national report on water quality in the USA, 45% of assessed stream miles, 47% of assessed lake acres, and 32% of assessed bay and estuarine square miles were classified as polluted (EPA 2007).

Water is typically referred to as polluted when it is impaired by anthropogenic contaminants and does not support a human use, like serving as drinking water,

and/or undergoes a marked shift in its ability to support its constituent biotic communities, such as fish. Natural phenomena such as volcanoes, algae blooms, storms, and earthquakes also cause major changes in water quality and the ecological status of water. Water pollution has many causes and characteristics.

About 20% of the world's population lacks access to safe drinking water and about 50% lacks adequate sanitation. In many developing countries, rivers downstream of large cities are little cleaner than open sewers. Levels of suspended solids in Asia's rivers, for example, almost quadrupled since the late 1970s and rivers typically contain four times the world average and 20 times the OECD levels. The fecal coliform count in Asia's rivers is 50 times higher than the WHO guidelines. People using such water for washing, bathing, or drinking are at high risk. In Latin America as a whole, only about 2% of sewage receives any treatment. Worldwide, polluted water is estimated to affect the health of about 1,200 million people and to contribute to the death of about 15 million children under the age of 5 every year.

Factors that cause increased nutrient concentrations can potentially lead to eutrophication. This kind of pollution is a result of nutrient pollution such as the release of sewage effluent and runoff from lawn fertilizers into natural waters, although it may also occur naturally in situations where nutrients accumulate or where they flow into systems on an ephemeral basis. Eutrophication generally promotes excessive plant growth and decay and is likely to cause severe reductions in water quality. Eutrophication causes decreased biodiversity, changes in species composition, dominance (algal boom), and toxicity effects. Any factor that causes increased nutrient concentrations can potentially lead to eutrophication.

Asian rivers are the most polluted in the world. They have three times as many bacteria from human waste as the global average and 20 times more lead than rivers in industrialized countries. Thirty percent of Ireland's rivers are polluted with sewage or fertilizer. The King River, Australia's most polluted river, is suffering from a severe acidic condition related to mining operations. As many as 100,000 marine mammals, one million sea birds, and other aquatic lives are killed due to plastic waste in water and coastal area. Bangladesh has some of the most polluted groundwater in the world. In this case, the contaminant is arsenic, which occurs naturally in the sediments. Around 85% of the total area of the country has contaminated groundwater, with at least 1.2 million Bangladeshis exposed to arsenic poisoning and with millions more at risk. Pollution of freshwater (drinking water) is a problem for about half of the world's population. Each year there are about 250 million cases of water-related diseases, with roughly 5–10 million deaths.

With over 70% of the planet covered by oceans, people have long acted as if these very bodies of water could serve as a limitless dumping ground for wastes. Raw sewage, garbage, and oil spills have begun to overwhelm the diluting capabilities of the oceans, and most coastal waters are now polluted. Beaches around the world are closed regularly, often because of high amounts of bacteria from sewage disposal, and marine wildlife is beginning to suffer. Water! From drinking a glass of cold water to power generation, water has so much utilitarian value that perhaps it would not be an understatement to say that when God thought about life probably he thought of water first. If we do not pay attention to these facts about water pollution, time is not far when from "blue planet" our earth will become "dirty blue planet" (Shandilya 2007).

11.1.2   Types of Water Pollution

Surface water and groundwater are often been studied and managed as separate resources, although they are interrelated (United States Geological Survey (USGS) 1998). Sources of surface water pollution are generally grouped into two categories based on their origin.

11.1.2.1   Point Source Pollution

Point source pollution refers to contaminants that enter a waterway through a discrete conveyance, such as a pipe or ditch. Examples of sources in this category include discharges from a sewage treatment plant, a factory, or a city storm drain. The US Clean Water Act (CWA) defines point source for regulatory enforcement purposes.

11.1.2.2   Nonpoint Source Pollution

Nonpoint source (NPS) pollution refers to diffuse contamination that does not originate from a single discrete source. NPS pollution is often an accumulative effect of small amounts of contaminants gathered from a large area. Nutrient runoff in stormwater from "sheet flow" over an agricultural field or a forest is sometimes cited as examples of NPS pollution.

Contaminated stormwater washed off of parking lots, roads, and highways, called urban runoff, is sometimes included under the category of NPS pollution. However, this runoff is typically channeled into storm drain systems and discharged through pipes to local surface waters, and is a point source. The CWA definition of point source was amended in 1987 to include municipal storm sewer systems, as well as industrial stormwater, such as from construction sites.

11.1.2.3   Groundwater Pollution

Interactions between groundwater and surface water are complex. Consequently, groundwater pollution, sometimes referred to as groundwater contamination, is not as easily classified as surface water pollution (United States Geological Survey (USGS) 1998). By its very nature, groundwater aquifers are susceptible to contamination from sources that may not directly affect surface water bodies, and the distinction of point versus nonpoint source may be irrelevant. A spill of a chemical contaminant on soil, located away from a surface water body, may not necessarily create point source or nonpoint source pollution, but nonetheless may contaminate the aquifer below. Analysis of groundwater contamination may focus on soil characteristics and hydrology, as well as the nature of the contaminant itself.

The specific contaminants leading to pollution in water include a wide spectrum of chemicals, pathogens, and physical or sensory changes such as elevated temperature and discoloration. While many of the chemicals and substances that are regulated may

be naturally occurring (calcium, sodium, iron, manganese, etc.) the concentration is often the key factor in determining what is a natural component of water, and what is a contaminant.

Oxygen-depleting substances may be natural materials, such as plant matter (e.g., leaves and grass) as well as man-made chemicals. Other natural and anthropogenic substances may cause turbidity (cloudiness), which blocks light and disrupts plant growth, and clogs the gills of some fish species (EPA 2005).

Many of the chemical substances are toxic. Pathogens can produce waterborne diseases in either human or animal hosts. Alteration of water's physical chemistry includes acidity (change in pH), electrical conductivity, temperature, and eutrophication. Eutrophication is the fertilization of surface water by nutrients that were previously scarce.

11.1.3   Control of Water Pollution

In urban areas, domestic sewage is typically treated by centralized sewage treatment plants. In the USA, most of these plants are operated by local government agencies. Municipal treatment plants are designed to control conventional pollutants: BOD and suspended solids. Well-designed and operated systems (i.e., secondary treatment or better) can remove 90% or more of these pollutants. Some plants have additional subsystems to treat nutrients and pathogens. Most municipal plants are not designed to treat toxic pollutants found in industrial wastewater (EPA 2008).

Cities with sanitary sewer overflows or combined sewer overflows employ one or more engineering approaches to reduce discharges of untreated sewage, including:

- Utilizing a green infrastructure approach to improve stormwater management capacity throughout the system
- Repair and replacement of leaking and malfunctioning equipment
- Increasing overall hydraulic capacity of the sewage collection system (often a very expensive option)

A household or business not served by a municipal treatment plant may have an individual septic tank, which treats the wastewater on site and discharges into the soil. Alternatively, domestic wastewater may be sent to a nearby privately owned treatment system (e.g., in a rural community).

11.1.3.1   Industrial Waste Water

Some industrial facilities generate ordinary domestic sewage that can be treated by municipal facilities. Industries that generate wastewater with high concentrations of conventional pollutants (e.g., oil and grease), toxic pollutants (e.g., heavy metals, volatile organic compounds), or other nonconventional pollutants such as ammonia, need specialized treatment systems. Some of these facilities can

install a pretreatment system to remove the toxic components, and then send the partially treated wastewater to the municipal system. Industries generating large volumes of wastewater typically operate their own complete on-site treatment systems.

Sediment (loose soil) washed off fields is the largest source of agricultural pollution in the USA (EPA 2005). Farmers may utilize erosion controls to reduce runoff flows and retain soil on their fields. Common techniques include contour plowing, crop mulching, crop rotation, planting perennial crops, and installing riparian buffers (EPA 2003; US Natural Resources Conservation Service (NRCS) 2009).

Nutrients (nitrogen and phosphorus) are typically applied to farmland as commercial fertilizer, animal manure, or spraying of municipal or industrial wastewater (effluent) or sludge. Nutrients may also enter runoff from crop residues, irrigation water, wildlife, and atmospheric deposition (EPA 2003). Farmers can develop and implement nutrient management plans to reduce excess application of nutrients (EPA 2003; US Natural Resources Conservation Service (NRCS) 2009).

To minimize pesticide impacts, farmers may use integrated pest management (IPM) techniques (which can include biological pest control) to maintain control over pests, reduce reliance on chemical pesticides, and protect water quality (EPA 2008).

11.1.4 Water Pollution in India

Out of India's 3,119 towns and cities, just 209 have partial treatment facilities, and only eight have full wastewater treatment facilities (WHO 1992) (Hopfenberg and Pimentel 2008). As many as 114 cities dump untreated sewage and partially cremated bodies directly into the Ganges River. Downstream, the untreated water is used for drinking, bathing, and washing. This situation is typical of many rivers in India as well as other developing countries.

Open defecation is widespread even in urban areas of India (National Geographic Society 1995; Gupta 2006). Water resources have not therefore been linked to either domestic or international violent conflict as was previously anticipated by some observers. Possible exceptions include some communal violence related to distribution of water from the Kaveri River and political tensions surrounding actual and potential population displacements by dam projects, particularly on the Narmada River. (Country Profile: India 2004)

More than 400 million people live along the Ganges River. An estimated 2,000,000 persons ritually bathe daily in the river, which is considered holy by Indians. In the Hindu religion it is said to flow from the lotus feet of Vishnu (for Vaisnava devotees) or the hair of Shiva (for Saivites). The spiritual and religious significance could be compared to what the Nile River meant to the ancient Egyptians. While the Ganges may be considered holy, there are some problems associated with the ecology. It is filled with chemical wastes, sewage, and even the remains of human and animal

corpses, which carry major health risks by either direct bathing in the water (e.g., Bilharziasis infection), or by drinking (the fecal-oral route).

11.2 Models for Water Pollutions

11.2.1 Methodology

Industrial pollution is caused by industries that exist around the river. In the present study neurogenetic models were also developed for the estimation of industrial pollution (IP) from basin runoff and land use of the adjacent catchments. In surface water quality parameters, pH and TDS can be taken as indicators of pollution. Acidic water is a clear sign of pollution caused by adjacent industries. Also, dissolved solids found from industrial effluents can also increase the TDS of river water. IP, like WAWQ, is a dimensionless parameter, which indicates industrial pollution in the river water. It was calculated by weighted average method where pH and TDS were given the highest priority followed by hardness, turbidity, BOD, and DO.

Like WAWQ (10) models, three neurogenetic models namely, IPCGD, IPQP, and IPBBP were prepared and trained with the help of the same algorithms by which WAWQCGD, WAWQQP, and WAWQBBP were trained.

The organic pollution (OP) is the pollution caused from biological wastes and excretes (Table 11.1). The amount of OP in river water can show anthropogenic impacts on a river. OP is indicated by lower values of DO and very high values of BOD, TC, and FC. Like, WAWQ and IP, OP was estimated as a dimension-less parameter, which is just a weighted average of water quality parameters where higher weightage was given to BOD followed by TC, FC, and DO. OP was made directly proportional to organic pollution of a river and so, high OP means higher level of organic pollution, which can easily be contributed to anthropogenic activities adjacent to the sampling regions. Similar to WAWQ and IP, neurogenetic models were also built for OP to predict OP from basin runoff and land use. Table 11.2 depicts the model parameters and performance validation criteria of the model. According to the table as OPQP had lesser RMSE

Table 11.1 Table showing configuration and performance validation criteria of neurogenetic models used for estimation of IP

Model name	Network architecture (I-H-O)	Parameters for GA (P-G-P′-C-M)	Training RMSE	Testing RMSE	Estimation RMSE	Model efficiency
IPCGD	2-1-1	50-100-6-0.8-0.2	0.27	0.45	0.08	0.65
IPQP	2-2-1-1	50-100-6-0.8-0.2	0.23	0.43	0.06	0.90
IPBBP	2-1-1	50-100-6-0.8-0.2	0.26	0.42	0.07	0.76

Table 11.2 Table showing configuration and performance validation criteria of neurogenetic models used for estimation of OP

Model name	Network architecture (I-H-O)	Parameters for GA (P-G-P′-C-M)	Training RMSE	Testing RMSE	Estimation RMSE	Model efficiency
OPCGD	2-1-1-1	50-100-6-0.8-0.2	0.14	0.13	0.03	0.83
OPQP	2-2-1	50-100-6-0.8-0.2	0.13	0.09	0.02	0.92
OPBBP	2-2-1	50-100-6-0.8-0.2	0.14	0.1	0.04	0.79

and higher E than the other two models, it was selected as the better model and estimations of OP from estimated runoff by PARITYCGD was carried out by the selected model.

11.3 Result and Discussion

11.3.1 Model Validation

The RMSE, E, and model parameters are shown in Table 10.2. As RMSE and E of IPQP was found to be equal to 0.06 and 90% whereas same of IPBBP and IPCGD were found to be equal to 0.07 and 76% and 0.08 and 65%, respectively, IPQP was selected as better model among the three considered neurogenetic models.

11.3.2 Estimation of Future Industrial Pollution of River Runoff

The estimated runoff for A2 and B2 scenario along with future land use as recommended by IPCC 4th Assessment Report (2007) was applied to the IPQP model for the estimation of future IP. According to the estimations, IP will be higher (0.6 and above) in case of A2 scenario than B2 scenario (within 0.4), which was normal as in A2 scenario a rapid industrial development was considered but for B2 scenario a reverse trend and a more environmentally conducive Earth was selected while estimating future climatic status.

Figure 11.1 shows present IP of the sampling locations, whereas Figs. 11.2–4 depict the spatial variation of future IP within the sampling locations according to A2 scenario of climate change. Figures 11.5–11.7 shows the variation of IP within the selected sampling locations for future runoff as per the B2 scenario of climate change. Figures 15–18 show basin-wise and state-wise variations of IP according to A2 and B2 scenario of climate change, respectively. Table 11.3 depicts the district-wise variation of IP according to A2 and B2 scenarios.
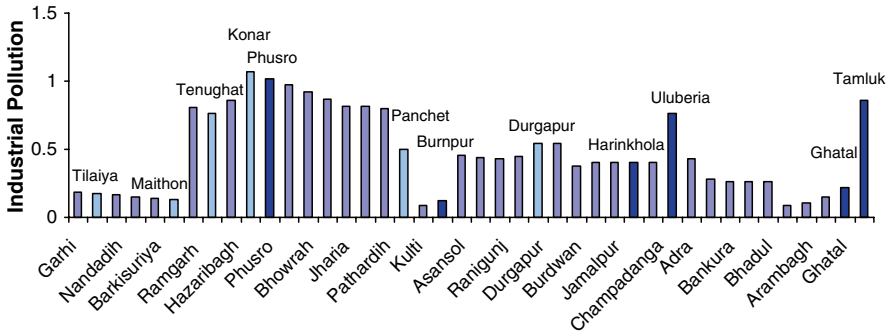
Fig. 11.1 Figure showing variation of industrial pollution (IP) factor according to the observed water quality parameters (Note: Deep and sky blue colored columns represent IP at reservoirs and junction points of river basins.)
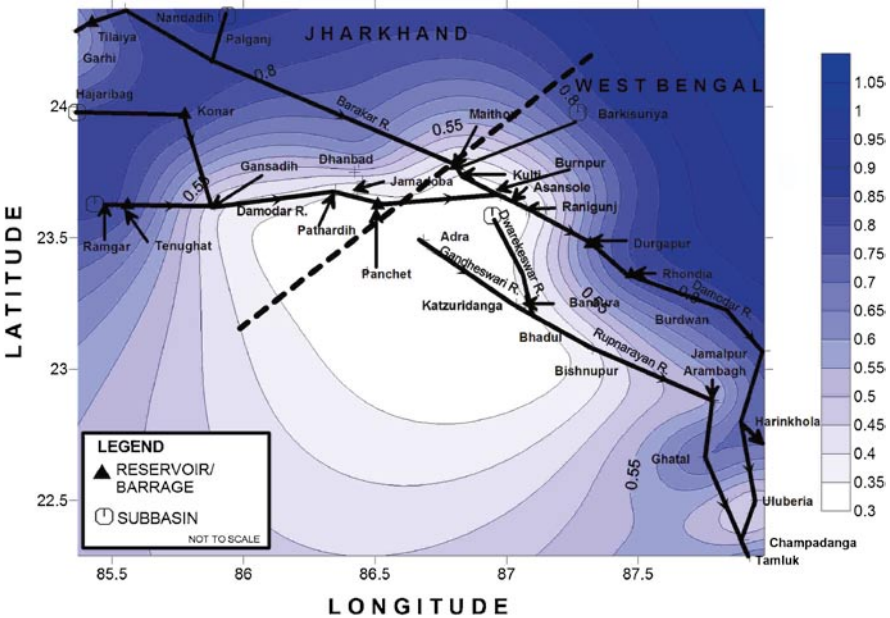
Fig. 11.2 Figure showing spatial variation of industrial pollution due to A2 scenario of climate change in 2010–2040

According to the figures, Rupnarayan will be less polluted than Damodar River in case of A2 scenario; a reverse situation is predicted in case of B2 scenario. The observation is justified as Damodar is one of the most populated industrial zones of the country. Steel, coal, and chemical industries can be seen in plenty along the banks of river Damodar. Whereas in Rupnarayan few paper mills and mainly cottage industries are concentrated along the banks of the river. Cottage
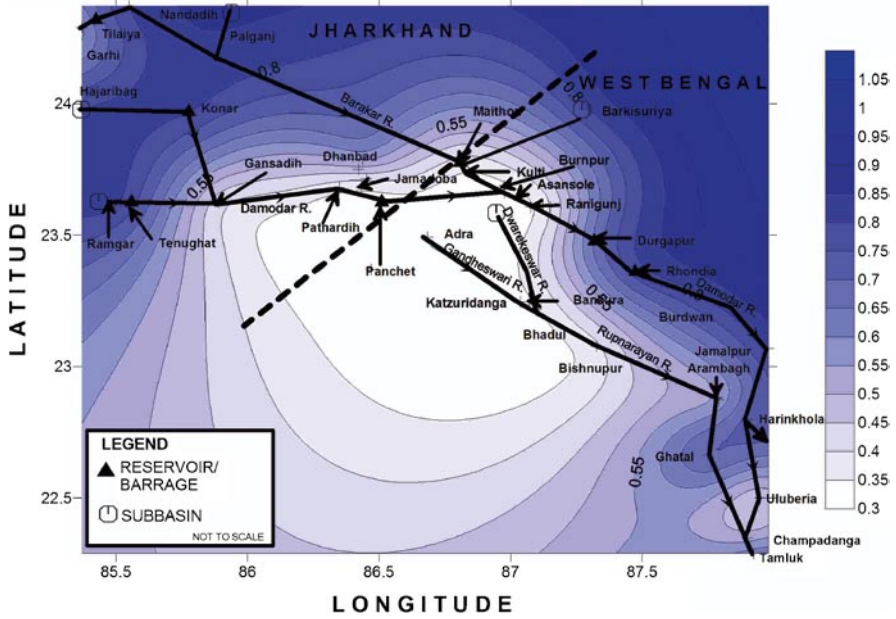
Fig. 11.3 Figure showing spatial variation of industrial pollution due to A2 scenario of climate change in 2041–2070
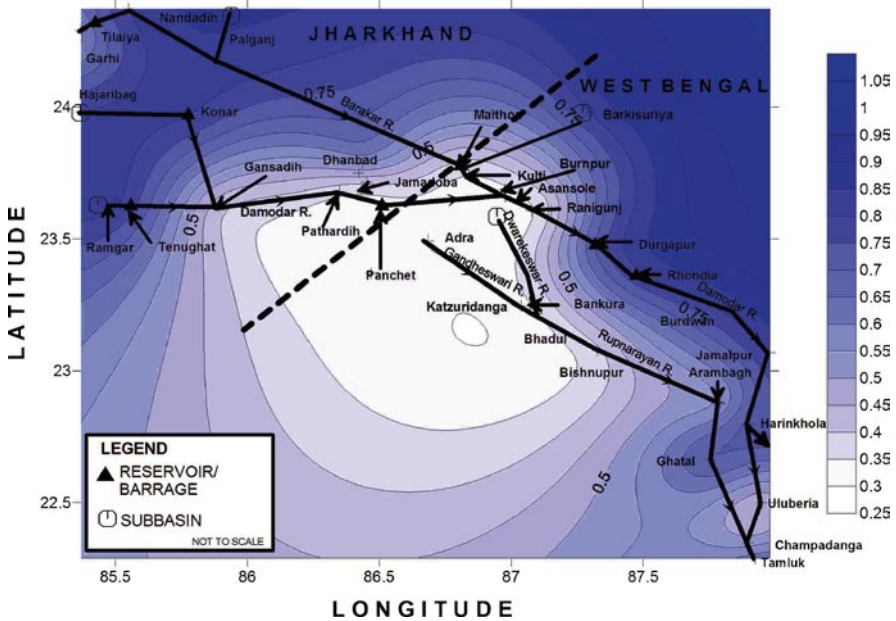
Fig. 11.4 Figure showing spatial variation of industrial pollution due to A2 scenario of climate change in 2071–2100
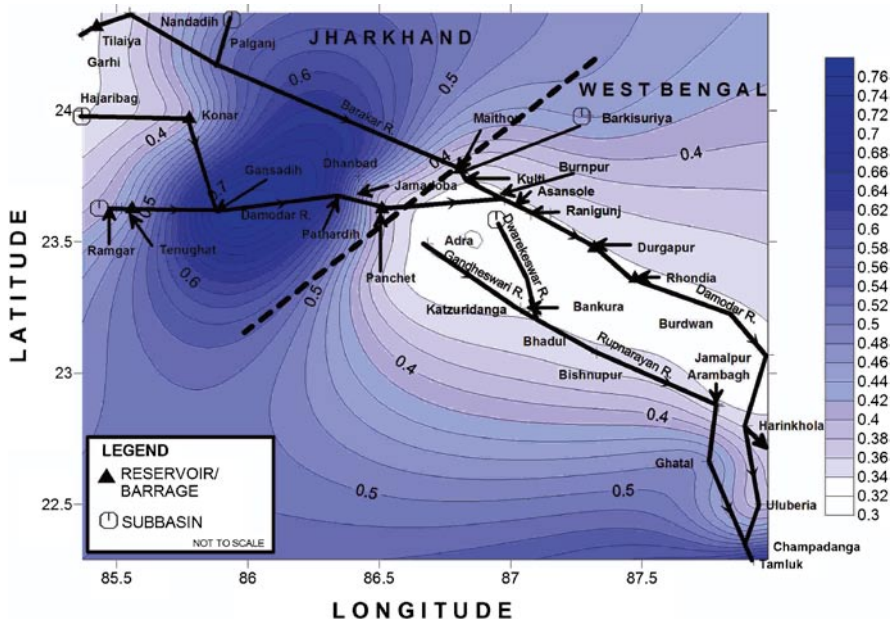
Fig. 11.5 Figure showing spatial variation of industrial pollution due to B2 scenario of climate change in 2010–2040
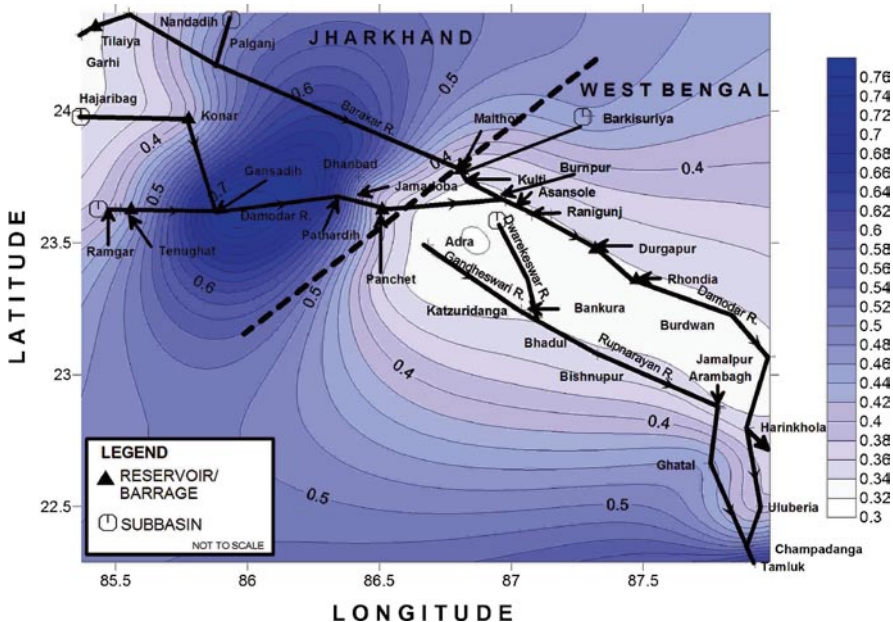
Fig. 11.6 Figure showing spatial variation of industrial pollution due to B2 scenario of climate change in 2041–2070
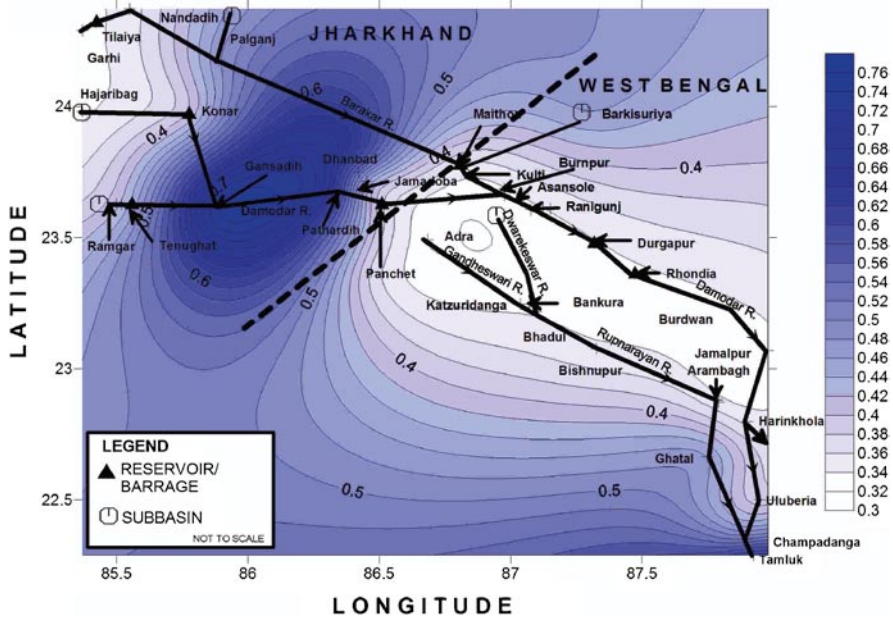
Fig. 11.7 Figure showing spatial variation of industrial pollution due to B2 scenario of climate change in 2071–2100

industry is pollution-free and the severity of pollutants found in paper mill effluents are lesser than the pollutants found in the effluents of steel or chemical industries. As most of the industries are concentrated in Jharkhand, the IP is more in the state than in West Bengal in case of A2 baseline scenarios, whereas the trend simply reverses in case of B2 baseline scenario.

If IP of the two rivers are compared district-wise, the average IP is more or less similar where worst pollution (0.84) will be observed in Jamtara and Ranchi districts of Jharkhand and East and West Midnapur districts of West Bengal and minimum pollution (0.34) will be observed in Howrah, Purulia, and Bankura districts of West Bengal from 2010 to 2100 in case of A2 scenario of climate change.

In case of B2 scenario of climate change, Dhanbad district of Jharkhand will have maximum IP (0.55) and Bokaro districts of Jharkhand along with Burdwan, Hooghly, Howrah, Purulia, and Bankura districts of West Bengal will have minimum IP of 0.34. Although, average IP, as per the samples collected from different sampling regions of West Bengal, is 0.36, which is less than the estimated IP (0.43 and 0.53 in case of A2 and B2 scenario, respectively) and for Jharkhand, observed IP (0.62) is smaller than the estimated IP (0.63) in case of A2 scenario but bigger than the estimated IP (0.42) in case of B2 scenario. According to the above observation, industrial pollution can create a hazard for the two river basins though in case of B2 scenario, which shows a less pollution than the present status, environmental upgradation has reduced the pollution.

Table 11.3 Table showing district-wise, state-wise, and basin-wise variations of industrial pollution due to A2 and B2 scenario of climate change

	A2 scenario			B2 scenario			Observed
Districts	2010–2040	2041–2070	2071–2100	2010–2040	2041–2070	2071–2100	1970–2002
State	2010–2040	2041–2070	2071–2100	2010–2040	2041–2070	2071–2100	1970–2002
Basins	2010–2040	2041–2070	2071–2100	2010–2040	2041–2070	2071–2100	1970–2002
Giridih	0.711	0.711	0.711	0.384	0.394	0.379	0.168
Jamtara	0.836	0.836	0.836	0.470	0.455	0.477	0.143
Bokaro	0.338	0.338	0.338	0.338	0.338	0.338	0.133
Ranchi	0.836	0.836	0.836	0.395	0.412	0.398	0.785
Hazaribagh	0.670	0.670	0.670	0.400	0.408	0.407	0.983
Dhanbad	0.409	0.409	0.409	0.551	0.551	0.551	0.814
Burdwan	0.511	0.513	0.521	0.338	0.338	0.338	0.385
Hooghly	0.537	0.537	0.537	0.338	0.338	0.338	0.760
Howrah	0.338	0.338	0.338	0.338	0.338	0.338	0.430
Purulia	0.338	0.338	0.338	0.338	0.338	0.338	0.233
Bankura	0.338	0.338	0.338	0.338	0.338	0.338	0.292
West Midnapur	0.836	0.836	0.836	0.512	0.536	0.528	0.218
East Midnapur	0.836	0.836	0.836	0.836	0.836	0.836	0.858
Jharkhand	0.633	0.633	0.633	0.423	0.426	0.425	0.504
West Bengal	0.533	0.534	0.535	0.434	0.437	0.436	0.454
Damodar	0.568	0.568	0.570	0.404	0.406	0.404	0.531
Rupnarayan	0.437	0.437	0.437	0.405	0.407	0.407	0.293

11.3.3 Estimation of Future Organic Pollution of River Runoff

Figure 11.8 depicts the observed values of OP within the sampling locations of the two river basins. Figures 11.9–11.14 depict variation of OP within sampling regions according to A2 and B2 scenario, respectively (Figs. 15–18) and Figs. 11.19–11.22 represent the state-wise and basin-wise variations of OP according to the two respective climate change scenarios. Table 11.4 shows the district-wise OP of the river basins.
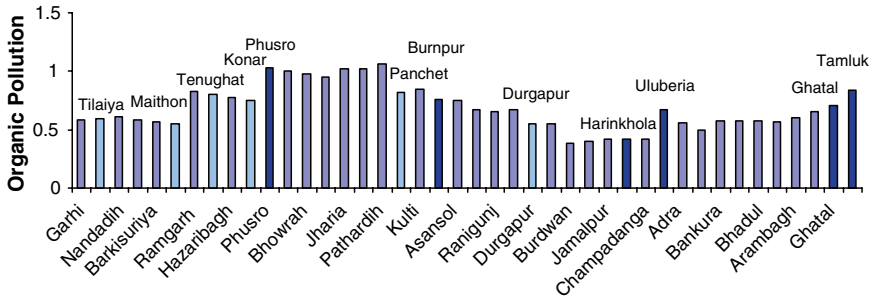
Fig. 11.8 Figure showing variation of organic pollution (OP) factor according to the observed water quality parameters (Note: Deep and sky blue colored columtns represent IP at reservoirs and junction points of river basins.)
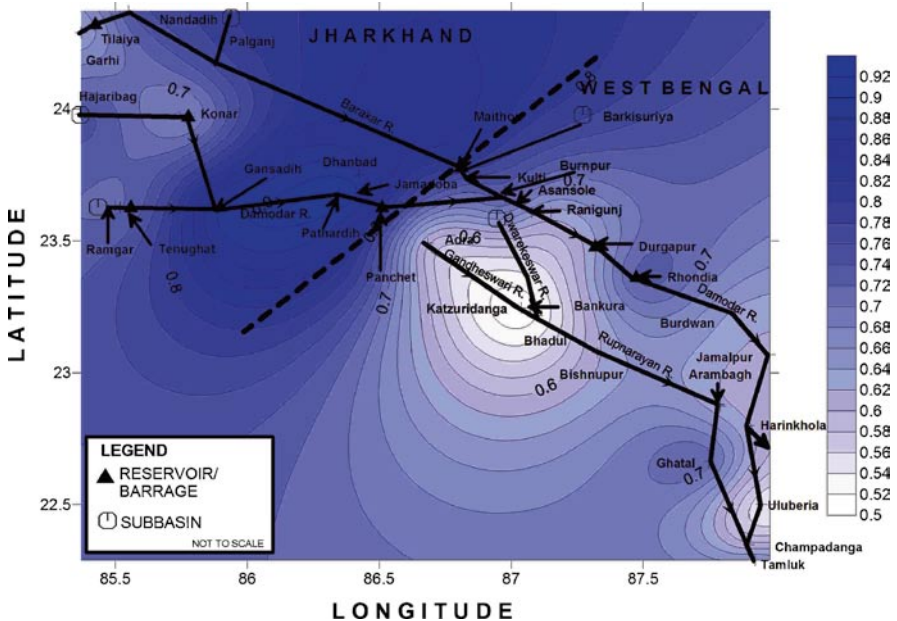
Fig. 11.9 Figure showing spatial variation of organic pollution due to A2 scenario of climate change in 2010–2040
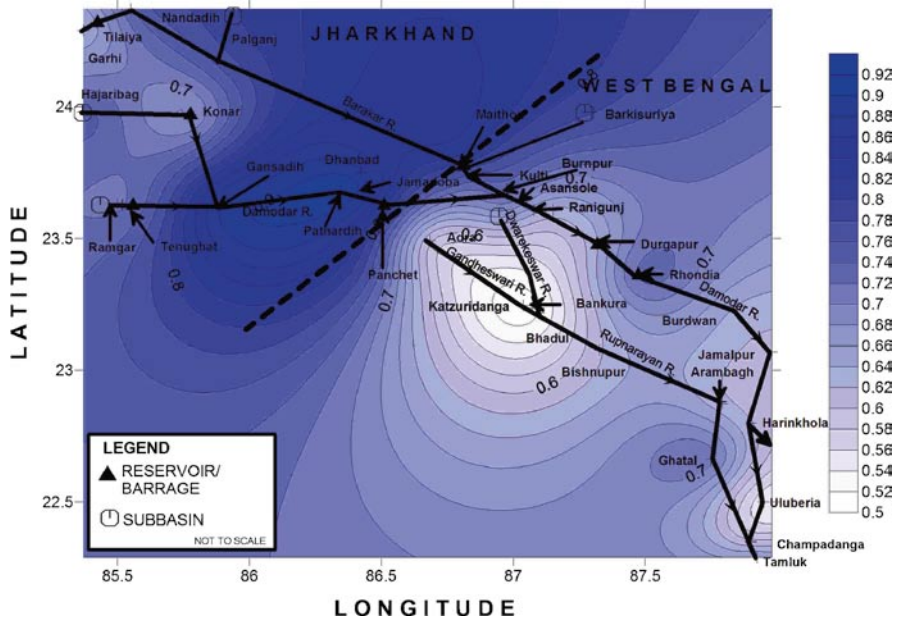
Fig. 11.10 Figure showing spatial variation of organic pollution due to A2 scenario of climate change in 2041–2070
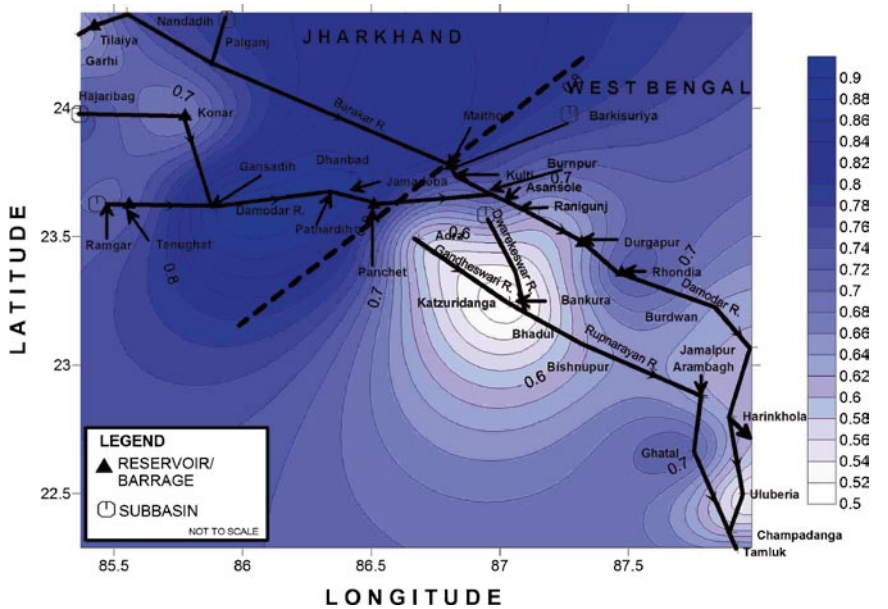
Fig. 11.11 Figure showing spatial variation of organic pollution due to A2 scenario of climate change in 2071–2100
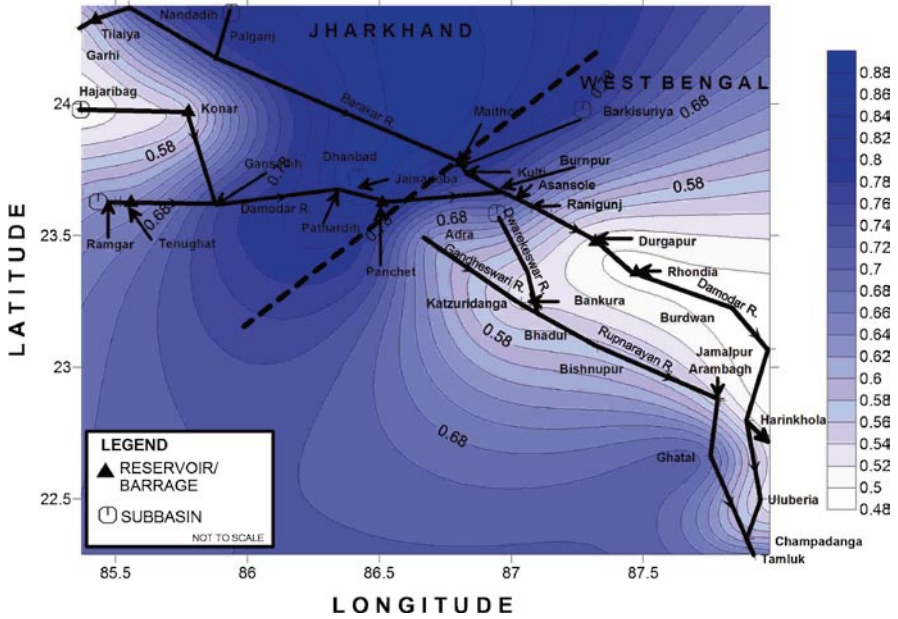
Fig. 11.12 Figure showing spatial variation of organic pollution due to B2 scenario of climate change in 2010–2040
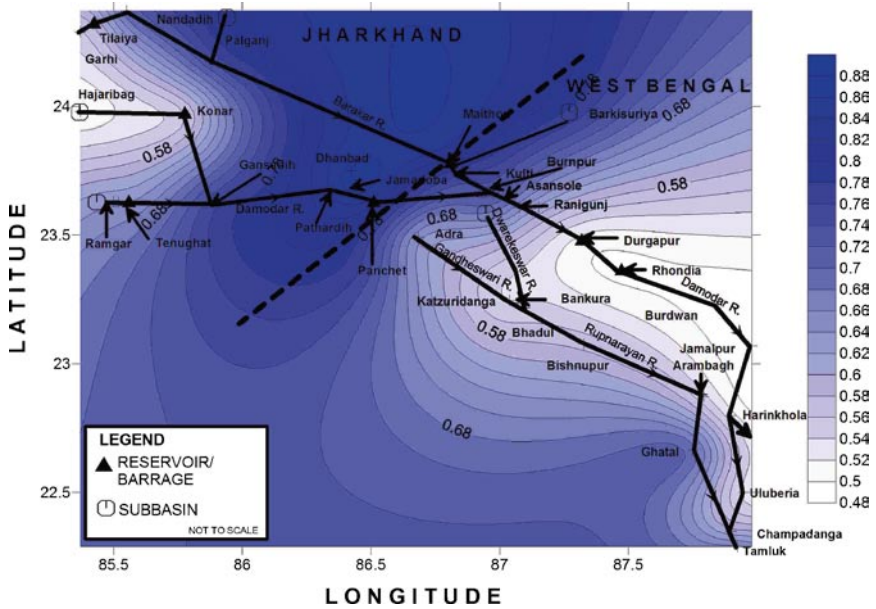
Fig. 11.13 Figure showing spatial variation of organic pollution due to B2 scenario of climate change in 2041–2070
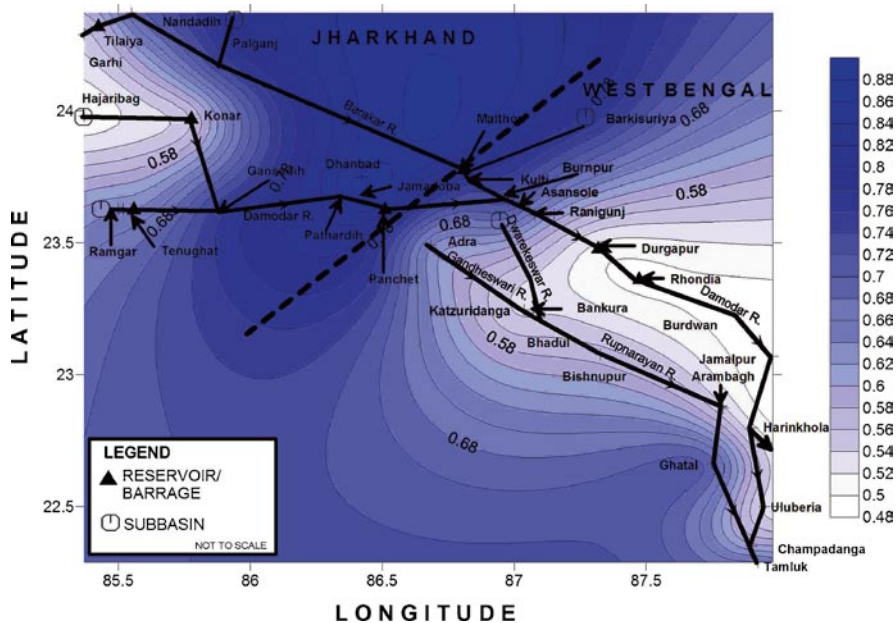
Fig. 11.14 Figure showing spatial variation of organic pollution due to B2 scenario of climate change in 2071–2100
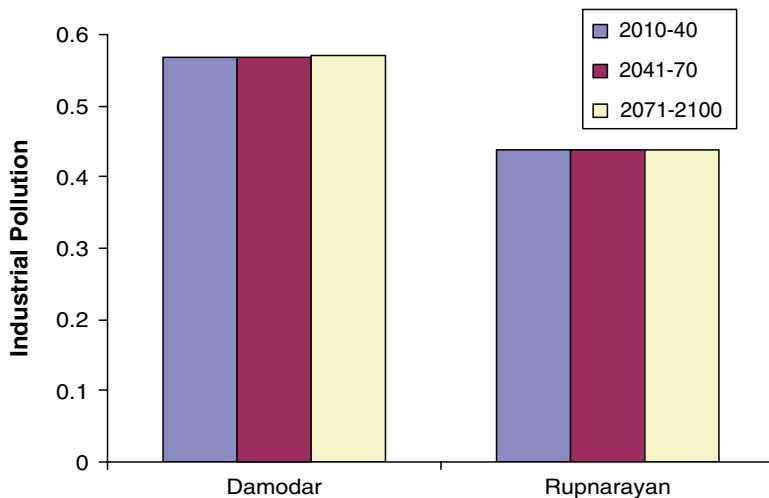
Fig. 11.15 Figure showing variation of estimated weighted average of industrial pollution in between Damodar and Rupnarayan River basins according to A2 scenario of climate change
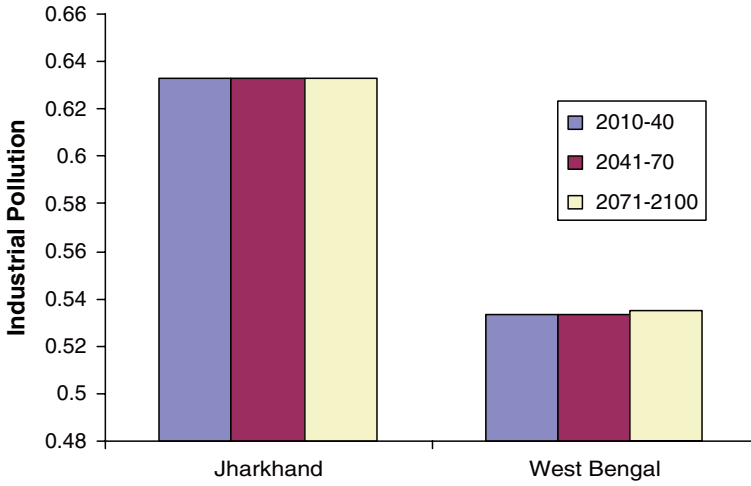
Fig. 11.16 Figure showing variation of estimated weighted average of industrial pollution within Jharkhand and West Bengal according to A2 scenario of climate change
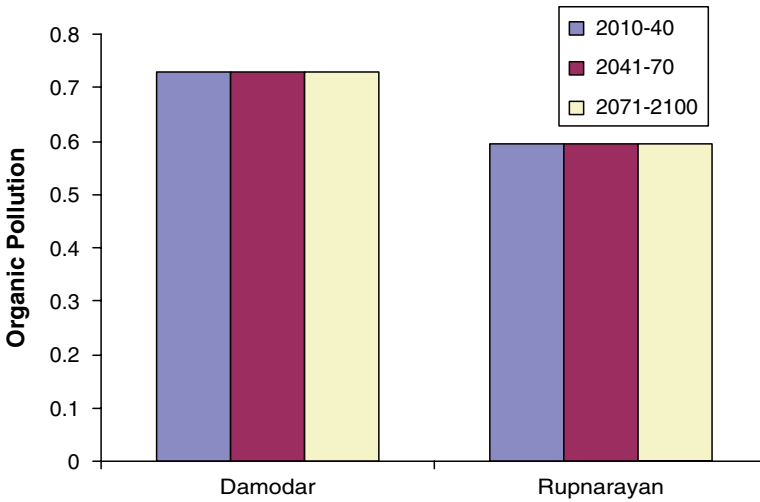
Fig. 11.17 Figure showing variation of estimated weighted average of organic pollution in between Damodar and Rupnarayan River basins according to A2 scenario of climate change
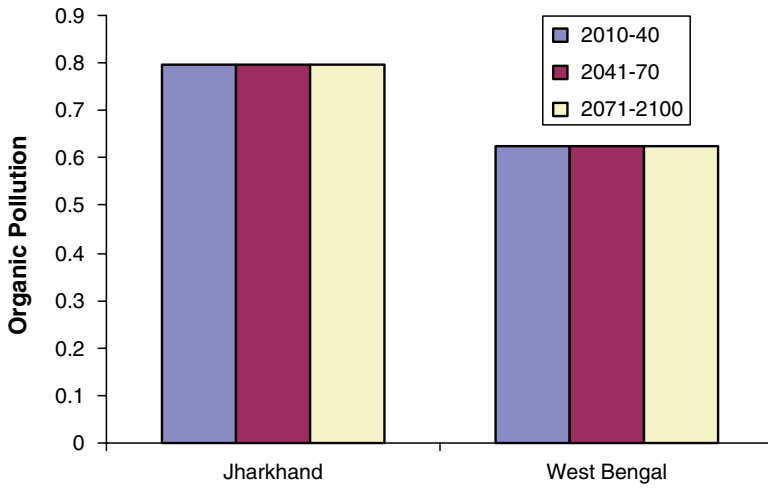
Fig. 11.18 Figure showing variation of estimated weighted average of organic pollution within Jharkhand and West Bengal according to A2 scenario of climate change
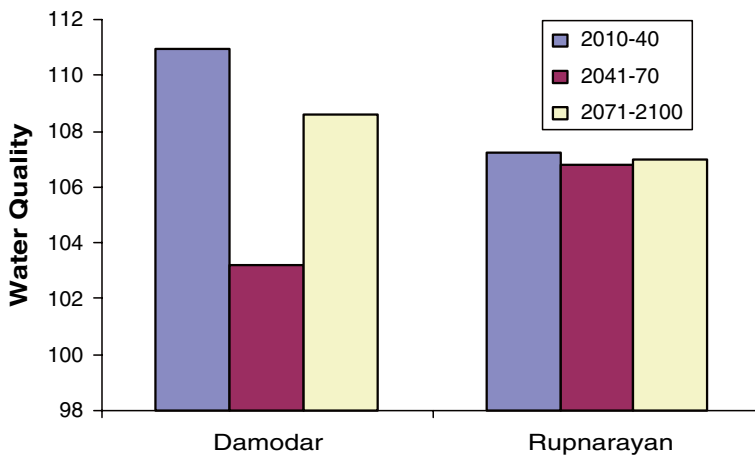
Fig. 11.19 Figure showing variation of estimated weighted average of water quality in between Damodar and Rupnarayan River basins according to B2 scenario of climate change
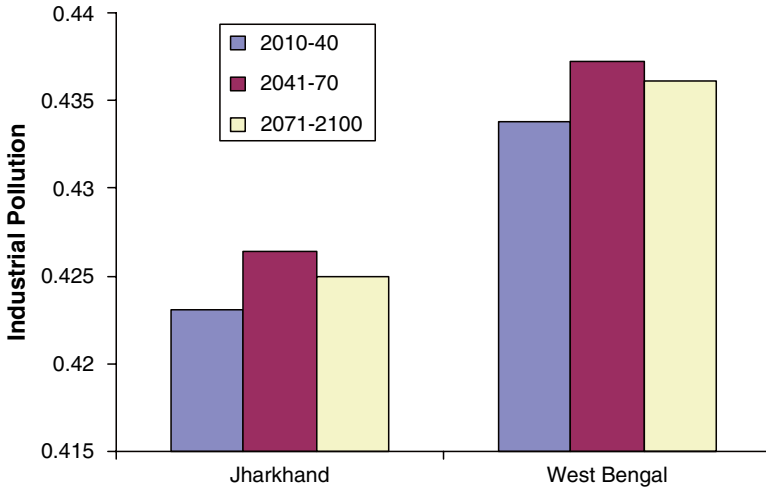
Fig. 11.20 Figure showing variation of estimated weighted average of industrial pollution within Jharkhand and West Bengal according to B2 scenario of climate change
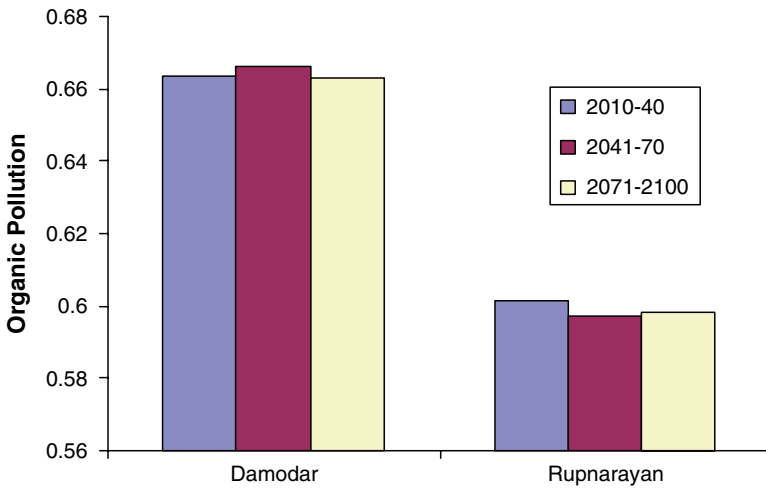
Fig. 11.21 Figure showing variation of estimated weighted average of organic pollution in between Damodar and Rupnarayan River basins according to B2 scenario of climate change
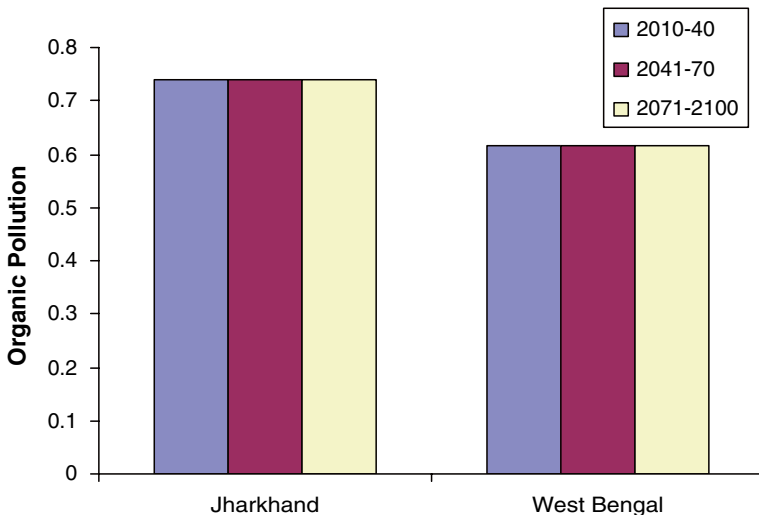
Fig. 11.22 Figure showing variation of estimated weighted average of organic pollution within Jharkhand and West Bengal river basins according to B2 scenario of climate change

According to the figures, OP of Damodar River will be more than that of Rupnarayan and the same of Jharkhand will be more than that of West Bengal in case of both the A2 and B2 baseline scenario of climate change from 2010 to 2100. The range of OP will be 0.66–0.67 for Damodar River whereas the same of Rupnarayan will be 0.59–0.61 in case of B2 baseline scenario. The range of OP in case of A2 baseline scenario will be 0.70–0.71 for river Damodar and the same for river Rupnarayan will be 0.60–0.61. So, the OP will be more in case of A2 baseline scenario than that of B2 baseline scenario, which is justified as industrial concentration is more in Jharkhand and in places like Kulti, Burnpur, Durgapur, etc. and increase in industry means increase in migrant labors. The labors make their house along the banks of the river for ready supply of water, which they use for washing and drinking purposes. But such anthropogenic concentration will increase the value of OP due to the increased amount of human-caused wastes.

If OP is compared for the Jharkhand and West Bengal, for the same reason explained above, West Bengal will have less amount of OP than Jharkhand in case of both the baseline scenarios.

The observed OP of Jharkhand and West Bengal is 0.81 and 0.59, respectively. The estimations of OP shows an increase in the value of OP, which implies

Table 11.4 Table showing district-wise, state-wise, and basin-wise variations of organic pollution due to A2 and B2 scenario of climate change

	A2 scenario			B2 scenario			Observed
Districts	2010–2040	2041–2070	2071–2100	2010–2040	2041–2070	2071–2100	1970–2002
Giridih	0.703	0.703	0.703	0.657	0.662	0.648	0.594
Jamtara	0.787	0.787	0.787	0.787	0.787	0.787	0.566
Bokaro	0.925	0.925	0.925	0.925	0.925	0.925	0.546
Ranchi	0.703	0.703	0.704	0.638	0.638	0.638	0.813
Hazaribagh	0.777	0.777	0.777	0.588	0.588	0.588	0.850
Dhanbad	0.886	0.886	0.879	0.846	0.846	0.846	0.978
Burdwan	0.678	0.678	0.679	0.608	0.609	0.608	0.623
Hooghly	0.592	0.592	0.592	0.520	0.517	0.518	0.670
Howrah	0.488	0.488	0.488	0.488	0.488	0.488	0.560
Purulia	0.514	0.513	0.510	0.577	0.571	0.569	0.558
Bankura	0.528	0.527	0.526	0.546	0.542	0.543	0.497
West Midnapur	0.787	0.787	0.787	0.787	0.787	0.787	0.708
East Midnapur	0.787	0.787	0.787	0.787	0.787	0.787	0.837
State							
Jharkhand	0.797	0.797	0.796	0.740	0.741	0.739	0.725
West Bengal	0.625	0.625	0.624	0.616	0.614	0.614	0.636
Basins							
Damodar	0.729	0.729	0.728	0.664	0.666	0.663	0.708
Rupnarayan	0.596	0.596	0.595	0.602	0.597	0.598	0.614

that OP will get slightly increased in case of A2 baseline scenario but will reduce in case of B2 baseline scenario. As B2 scenario considers a more environmentally integrated world the impact of environmentally stable can be shown with such estimations.

If OP is compared with respect to districts, Bokaro districts of Jharkhand will have maximum OP (0.92) and Howrah districts of West Bengal will have least OP (0.48) among the districts of the two states, which are located in the banks of the two rivers, Damodar and Rupnarayan, in case of both the climate change scenarios.

11.4   Conclusion

The present study tried to estimate spatial variation of water pollution with the help of neurogenetic models and PARITYCGD-predicted stream flow. The future variation of water pollution within the study area was also predicted. According to the predictions, the polluted regions in the basin would reduce in the future where in case of A2 scenario the reduction would be less than that of B2 scenario. The pollutant concentration was collectively represented by two factors: industrial pollutant and organic pollutant. The former represents the water pollutions due to industrial effluents and the later represents the pollution of organic wastes.

References

Country Profile: India. Library of Congress Country Studies (2004) Retrieved from http://lcweb2.loc.gov/frd/cs/profiles on May 18, 2008

EPA (2003) National Management Measures to Control Nonpoint Source Pollution from Agriculture Document No. EPA-841-B-03-004

EPA (2008) Integrated Pest Management Principles (IPM) principles. Retrieved from: http://www.epa.gov/opp00001/factsheets/ipm.htm on 22nd July, 2009

Gupta T (2006) The politics of toilets. Retrieved from http://www.boloji.com/wfs5/wfs739.htm

Hopfenberg R, Pimentel D (2008) Human population numbers as a function of food supply oilcrash.com. Retrieved on February 2008

National Geographic Society (1995) Water: a story of hope. National Geographic Society, Washington, DC

National Geographic (2007) Mumbai slum: Dharavi, National Geographic, May 2007

Pink DH (2006) Investing in tomorrow's liquid gold. Yahoo. Retrieved from http://finance.yahoo.com/columnist/article/trenddesk/3748 on 30 July 2009

Shandilya R (2007) Facts about water pollution. Retrieved from http://www.buzzle.com/articles/facts-about-water-pollution.html on 30 July 2009

United States Geological Survey (USGS) (1998) Denver, CO. Ground water and surface water: a single resource. USGS Circular 1139

U.S. EPA (2005) Protecting water quality from agricultural runoff. Fact Sheet No. EPA-841-F-05-001

U.S. EPA (2004) Report to congress: impacts and control of CSOs and SSOs. Document No. EPA-833-R-04-001

U.S. EPA (2004) Primer for municipal wastewater treatment systems. Document No. EPA 832-R-04-001

US EPA (2008) Green infrastructure case studies: Philadelphia, 9 December 2008

US Natural Resources Conservation Service (NRCS), Washington, DC. National Conservation Practice Standards. National Handbook of Conservation Practices. Accessed on 2009-03-28

West L (2006) World water day: a billion people worldwide lack safe drinking water. Retrieved from http://environment.about.com/od/environmentalevents/a/waterdayqa.htm on 30 July 2009

World Health Organization (WHO) (1992) Environmental health criteria 134 – cadmium international programme on chemical safety (IPCS) monograph

Chapter 12
Impact of Stressed Climatic Condition on a Small Tropical Tributary

Rabindra Nath Barman, Mrinmoy Majumder, Pankaj Roy, and Asis Mazumdar

Abstract The present study tried to analyze the impact of stressed climatic condition on a small tropical tributary of river Hooghly with the help of neural network and genetic algorithm. The stressed conditions of a basin were represented by six categories. According to the results, the retentivity of the catchment is poor that is why even in positively overstressed climatic condition the catchment responded with low discharges. The impacts of change on ground cover, water demand, and land use were ignored or taken to be the same for the different conditions that were applied to evaluate the basin response.

R.N. Barman
Pertime Research Fellow, School of Water Resources Engineering, Jadavpur University, Kolkata-700032, West Bengal, India
and
Assistant Professor, Department of Production, National Institute of Technology, Agartala, Tripura, India
e-mail: rahul.barman@gmail.com

M. Majumder
Senior Research Fellow, School of Water Resources Engineering, Jadavpur University, Kolkata-700032, West Bengal, India
and
Geo-information Scientist, Regional Center, National Afforestation
and Eco-development Board, Jadavpur University, Kolkata-700032, West Bengal, India

P. Roy
Lecturer, School of Water Resources Engineering, Jadavpur University, Kolkata-700032, West Bengal, India

A. Mazumdar
Coordinator, Regional Center, National Afforestation and Eco-development Board, Jadavpur University, Kolkata-700032, West Bengal, India
and
Director, School of Water Resources Engineering, Jadavpur University, Kolkata-700032, West Bengal, India

12.1 Introduction

During the last few decades, the Earth's surface witnessed the increase in the mean temperature due to global warming. Global warming is defined as a natural or human-induced increase in the average global temperature of the atmosphere near the Earth's surface. Anthropogenic activities such as industrialization, thermal power plants, transportation, intensive agriculture, deforestation, etc., are causing substantial increase in the concentration of greenhouse gases, that is, carbon dioxide, methane, ozone, nitrous oxide, and chlorofluorocarbon in the atmosphere. Global circulation models predict that these increased concentrations of greenhouse gases will increase average thermal regime of global atmosphere. An increase in the concentration of greenhouse gases in the atmosphere is thought to have been responsible for increasing the air temperature. There is no doubt that climate is changing. The main reason of climate change is the increase in the concentration of greenhouse gases in the atmosphere due to several natural and anthropogenic activities. The level of greenhouse gases in the atmosphere has already increased considerably over the time particularly after the industrial era. Global warming and climate change have emerged an important global concern, cutting across the geographical and national boundaries.

The Kaliaghai River of West Bengal in India originates from Dudhkundi in Police Station Jhargram, District Midnapur in the western part from high land. The Kaliaghai River is flowing mainly toward east and meets the river New Cossye near Dhewbhanga and is renamed as the river Haldi out-falling into the river Hooghly near Haldia port. Some important tributaries such as Baghai, Kapaleswari, and other streams feed the river Kaliaghai. The main river measures 106 km in length. The river and its tributaries create immense problems either due to flood or inundation in low-lying areas for months together. The people of these areas being mainly dependent on agricultural practices are put to sufferings due to such calamities. The lower reach of the Kaliaghai has tidal influence of the river Hooghly.

After the 1990 flood, the major part of the Kaliaghai basin remained inundated for months together creating immense sufferings to the people.

12.1.1 Location

The Kaliaghye River system and related basin are located in the Haldi subbasin (Rupnarayan–Haldi–Rasulpur River system as identified by GFCC) of Ganga Basin. The entire Kaliaghye River system lies in the south-western part of the District of Midnapur. The sun-basin lies geodetically between latitudes 87°E and 87°50′E and longitudes 21°55′ N and 22°30′N. The location of Kaliaghye River Basin is shown in key map plate number 1 with reference to entire Ganga Basin.

12.1.1.1   River System

The river Kaliaghye originates near Dudhkundi in Police Station Jhargram and 20 km west of Kharagpur. Then, it is joined by the tributaries in the following pattern along with other tributaries attributed to the system. It may be noted here that all distances are shown from Poktapole Railways Bridge, which is 63 km upstream of Dhewbhangga outfall and 46 km downstream of Dudhkundi Mouza. The Kaliaghye catchment is of 2,145 km^2. Index map showing the catchment is attached. The catchment has some special features, which are stated below:

(a) Upper reaches from Dudhkundi mouza to Bakhrabad mouza measuring 568.75 km^2 is of steep slope (1.4 m/km) witnessing hardly any flood problem except the intercept between Railway line at Poktapole and Orrisa Trunk Road at Bakhrabad.
(b) The reach below Poktapole (Bakhrabad to Amgachia measuring 35.5 km) is nontidal, out of which first 20 km upto Dahati mouza is of medium slope (0.5 m/km) and the rest upto Langalkata is almost flat (0.3 m/km) and comprises of major flood-prone areas.
(c) The reach running from Amgachia to Dhewbhangga (43 km) is tidal and becomes the worst affected with the synchronization of flood in the new Cossye and high tide condition. The ground slope is around 0.20 m/km.

The discharge and climatic data from the Amgachia gauge station were collected to prepare the neural model, and response for this part of the basin to extreme climatic conditions was estimated in the present study.

12.2   Data Description

The input parameters considered for the present simulation model were temperature, humidity, rainfall, and cloud cover. The output parameter was taken as discharge from the catchment, which was also considered as the "catchment response." Monsoon data from 1971 to 2001 were collected to train, test, and validate the neural model. The unavailable dataset and 3.5% or more data outliers were replaced by interpolation (Fig. 12.1).

Figures 12.2–12.5 show the maximum possible climatic conditions that were experienced in between 1971 and 2001.

12.3   Methodology

12.3.1   Artificial Neural Network

An artificial neural network (ANN) is a flexible mathematical structure that is capable of identifying complex nonlinear relationships between input and output data sets. The ANN model of a physical system can be considered with *n* input
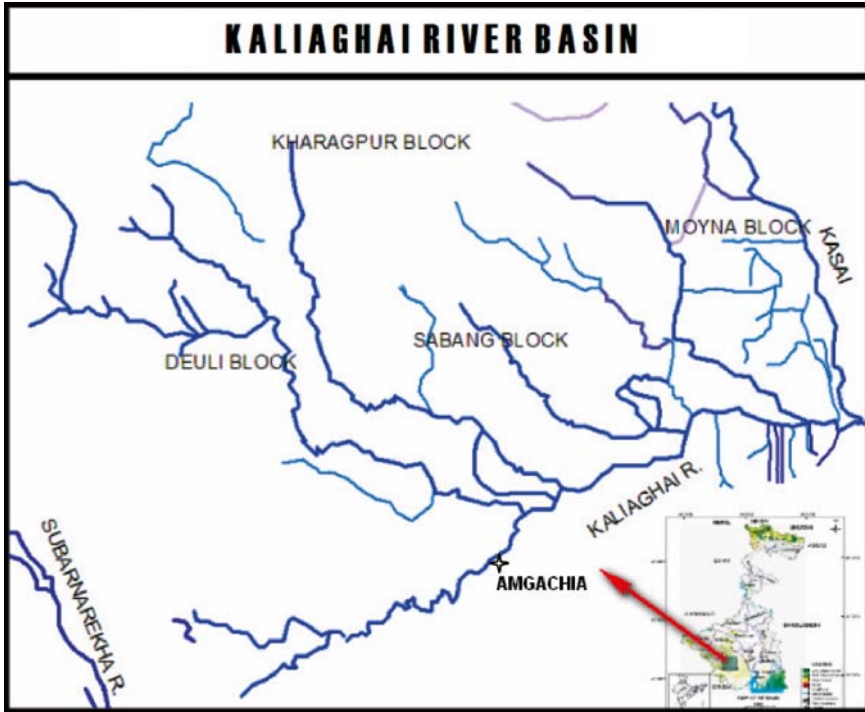
Fig. 12.1 Figure showing a schematic diagram of the Kaliaghayee River and the location of Amgachia station
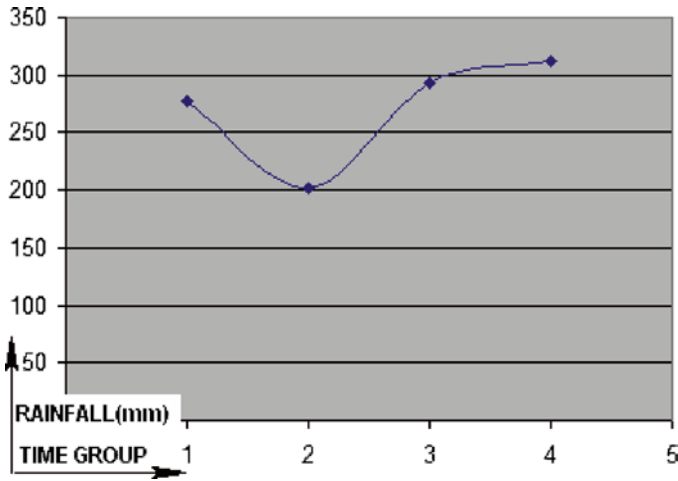
Fig. 12.2 Figure showing maximum rainfall during monsoon in Amgachia
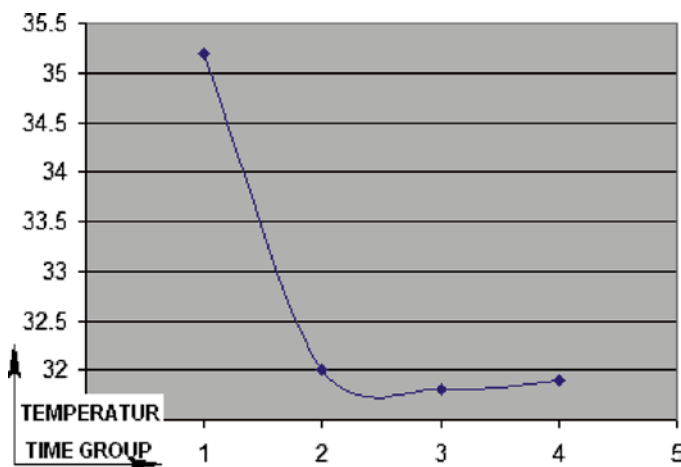
Fig. 12.3 Figure showing maximum temperature during monsoon in Amgachia
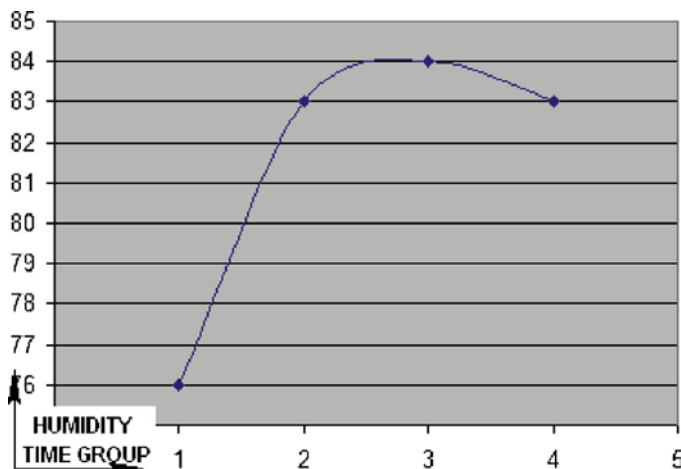
Fig. 12.4 Figure showing maximum humidity during monsoon in Amgachia

neurons $(x_1, x_2, ..., x_n)$, h hidden neurons (z_1, z_2, z_n), and m output neurons $(y_1, y_2, ..., y_n)$. Let t_j be the bias for neuron z_j and f_k for neuron y_k. Let w_{ij} be the weight of the connection from neuron x_i to z_j and beta is the weight of the connection z_j to y_k. The function that ANN calculates is:

$$y_k = g_A \left(\sum z_j b_{jk} + f_k \right)...\left(j = 1 - h \right) \qquad (12.1)$$

In which,

$$z_j = f_A \left(\sum x_i w_{ij} + t_j \right)...\left(i = 1 - n \right) \qquad (12.2)$$
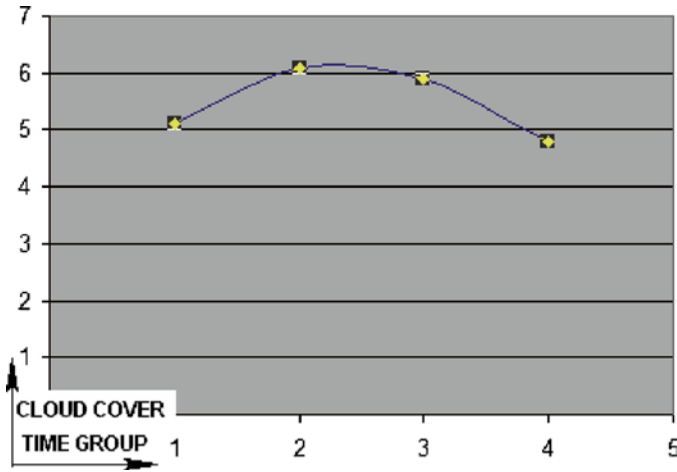
Fig. 12.5 Figure showing maximum cloud cover during monsoon in Amgachia

where g_A and f_A are the activation functions (Sudheer 2005).

The development of an artificial neural network, as prescribed by ASCE (2000), follows the basic rules that are given below:

1. Information must be processed at many single elements called nodes.
2. Signals are passed between nodes through connection links and each link has an associated weight that represents its connection strength.
3. Each of the nodes applies a nonlinear transformation called activation function to its net input to determine its output signal.

The numbers of neurons contained in the input and output layers are determined by the number of input and output variables of a given system. The size or number of neurons of a hidden layer is an important consideration when solving problems using multilayer feed-forward networks. If there are fewer neurons within a hidden layer, there may not be enough opportunity for the neural network to capture the intricate relationships between indicator parameters and the computed output parameters. Too many hidden-layer neurons not only require a large computational time for accurate training, but may also result in overtraining. A neural network is said to be "overtrained" when the network focuses on the characteristics of individual data points rather than just capturing the general patterns present in the entire training set. The network building procedure is divided into three phases, which are described next in a broad way.

12.3.1.1 Network Building Procedure

Selection of Network Topology

Neural network can be of different types, such as feed forward, radial basis function, time lag delay, etc. The type of the network is selected with respect to the knowledge of input

and output parameters and their relationship. Once the type of network is selected, selection of network topology is the next concern. Trial and error method is generally used for this purpose, but many studies now prefer the application of genetic algorithm (Ahmed and Sarma 2005). Genetic algorithms are search algorithms based on the mechanics of natural genetic and natural selection. The basic elements of natural genetics – reproduction, crossover, and mutation – are used in the genetic search procedure. A GA can be considered, and it consists of the following steps (Burn and Yulianti 2001):

1. Select an initial population of strings
2. Evaluate the fitness of each string
3. Select strings from the current population to mate
4. Perform crossover (mating) for the selected strings
5. Perform mutation for selected string elements
6. Repeat steps 2–5 for the required number of generations

Genetic algorithm is a robust method of searching the optimum solution to complex problems like the selection of an optimal network topology where it is difficult or impossible to test for optimality. The basics of GA have already been discussed by many authors like Ahmed and Sarma (2005), Wang (1991), and Wardlaw and Sharif (1999). Hence, the details of the basic procedures of GA are not focused in the present literature.

Training Phase

To encapsulate the desired input–output relationship, weights are adjusted and applied to the network until the desired error is achieved. This is called "training the network." There are innumerable "training the network" algorithms, among which, back propagation (ASCE (2000)) is mostly preferred. In the present study, batch back propagation (BBP), incremental back propagation (IBP), and Levenberg–Marquardt (LM), each of them derived from basic back-propagation algorithms, are used as the training algorithms.

   BBP is an advanced variant of back propagation where network weights update takes place once per iteration.

   IBP is a variation of the back propagation where the network weights are updated after presenting each case from the training subset, rather than once per iteration. This is originally invented as a variant of back propagation and sometimes referred to as standard back propagation.

   LM (Kisi 2004) is an advanced nonlinear optimization algorithm. It is the fastest algorithm available for multilayer perceptrons. However, it has the following restrictions:

• It can only be used on networks with a single output unit.
• It can only be used with small networks (a few hundred weights) because its memory requirements are proportional to the square of the number of weights in the network.

Testing Phase

After training is completed, some portion of the available historical dataset is fed to the trained network and known output is estimated out of them. The estimated

values are compared with the target output to find MSE. If the value of MSE is less than 1%, the networks are said to be sufficiently trained and ready for estimation. Few part of the dataset is also used for cross-validation to prevent overtraining during the training phase (Sudheer 2005).

In the present study, all the above three training algorithms are used to train the model. The best-trained model is selected with the help of training and testing correct classification rate (CCR) and the required connection weight for each of the algorithm (as selected by GA).

12.3.2   Evaluation of the Network

The accuracy of results obtained from the network is assessed by comparing its response with the validation set. The commonly used evaluation criteria include correct classification rate (CCR), correlation coefficient (r), coefficient of efficiency (CE), and standard deviation (STDEV) (Bhatt 2007).

$$\text{MSE} = \left((T_p - O_p)/n \right) \tag{12.3}$$

$$r = \left[\sum \left((T_p - T_m)(O_p - O_m) \right) \left(\sum_1^n (T_p - T_m)^2 \sum_1^n (O_p - O_m)^2 \right)^{12} \right] \tag{12.4}$$

$$\text{CE} = 1 - \left(\sum_1^n (T_p - O_p)^2 / \sum_1^n (T_p - T_m)^2 \right) \tag{12.5}$$

$$\text{STDDEV} = \frac{\sum_1^n (T_n - \bar{T}_n)^2}{n} \tag{12.6}$$

T_p is the target group for the P th pattern; O_p is the estimated group for the Pth pattern, T_m and O_m are the mean target and estimated groups, respectively, and n is the total number of patterns. T_n is the target value of the nth pattern and $\bar{T}_n$ is the mean value of the same.

MSE is used to measure the difference between actual and estimated value. r is the degree of correlation between two variables. CE criterion has the basis of standardization of the residual variance with initial variance (Nash and Sutcliffe 1970). In this criterion, a perfect agreement between the observed and estimated output yields an efficiency of 1. A negative efficiency represents lack of agreement, and zero agreement means all the estimated values are equal to the observed mean. STDDEV is the measure of deviation of the estimated value from the target output. A perfect match between observed data and model simulations is obtained when STDDEV approaches 0.0(Yitian and Gu 2003)

12.4   Result and Discussion

12.4.1   Model Development

From the available data set of 40 years discharge, rainfall, temperature, humidity, and cloud cover, monsoonal data series of 4 years, one each from the last 4 decades, were chosen and ranked in an ascending order with respect to magnitude. Three neural models were developed with the help of these datasets, among which the model with least MSE, highest *r*, maximum CE, and minimum STDDEV was selected for the simulation work.

The input and output parameters are selected as given below:

Temperature id & Rank, Humidity id & Rank, Rainfall id & Rank, Cloud cover id & Rank, Discharge id as input parameters and discharge rank as output parameter. The id in the input parameter represents the time scale or the time sequence. The authors here tried to track the pattern sequence of the parameters with the help of the id parameter. The monsoon season is divided into six groups, which are represented by the "id" parameter.

A total of 68.18% of the dataset was applied for training, and 15.91% of dataset was used as cross-validation and testing purpose. Input and output parameters were scaled by 0.00672 and 0.02424 factors, respectively.

Table 12.1 shows the training, testing, and cross-validation MSE and average error and topology of the networks.

The genetic algorithm was used for the selection of the network topology, and IBP, BP, and LM algorithms were applied to train the network for finding the optimum result. The average MSE after training for LM network was 0.09% which is, respectively, 16% and 131.55% lesser than that for IBP and BP networks. The average MSE after testing for LM was 0.18, which is 399.33% and 170.88% less than the other two networks that forced the authors to select the network trained with LM algorithm.

The predicted results from LM were found to be 11.5% more accurate than BP and 37.5% more than IBP. IBP and BP were found to be 22.9% and 5.28 times more deviated than LM. LM model is also 0.99 times more efficient than BP and 99.69% more efficient than IBP. According to the performance validation criteria, LM is selected as the best model out of the three.

The selected model was applied to estimate the discharge rank for overstressed and stressed conditions, which were created artificially in the following way:

12.4.2   Overstressed Conditions

For positively overstressed condition:

1. Rainfall rank will vary in between 1 and 6
2. Temperature rank will vary in between 65 and 60

Table 12.1 Summary table showing optimum ANN model's architecture and ANN internal parameters

Network name	IBP	BP	LM
Network topology			
Network type	Feed-forward fully connected network	Feed-forward fully connected network	Feed-forward fully connected network
Number of inputs	9	9	9
Number of hidden layers	1	1	1
Hidden units in the 1st hidden layer	1	7	1
Hidden units in the 2nd hidden layer	0	0	0
Number of outputs	1	1	1
Connection weight	10	142	10
All the topologies were created using genetic algorithms with following parameters			
Population size	60	60	50
Number of generations	50	50	50
Network size penalty	6	6	5
Crossover rate	0.8	0.8	0.9
Mutation rate	0.2	0.2	0.2
Training algorithm and parameters			
Training algorithm	Incremental back propagation	Batch back propagation	Levenberg–Marquardt
Training iteration	50	50	50
Stop training conditions			
MSE on training subset must drop below	0.01	0.01	0.01
Maximum allowed number of iterations	100,000	100,000	100,000
Training stop reason	Generalization loss became too high	Generalization loss became too high	Error reduction became too low
Training and testing results			
Average MSE (training)	1.44	11.84	0.09
Average MSE (testing)	35.94	15.38	0.18
Estimated results			
MSE	0.08	0.26	0.03
r	0.988	0.98	0.99
CE	0.987	0.988	0.99
STDEV	0.916	1.11	0.21

3. Humidity rank will vary in between 65 and 60
4. Cloud cover rank will vary in between 65 and 60

For negatively overstressed condition:

1. Rainfall rank will vary in between 65 and 60
2. Temperature rank will vary in between 1 and 6
3. Humidity rank will vary in between 1 and 6
4. Cloud cover rank will vary in between 1 and 6

12.4.3   1Stressed Condition

For positively stressed condition:

1. Rainfall rank will vary in between 7 and 25
2. Temperature rank will vary in between 59 and 41
3. Humidity rank will vary in between 59 and 41
4. Cloud cover rank will vary in between 59 and 41

   For negatively stressed condition:

1. Rainfall rank will vary in between 59 and 41
2. Temperature rank will vary in between 7 and 25
3. Humidity rank will vary in between 7 and 25
4. Cloud cover rank will vary in between 7 and 25

The results showed the response of the catchment for the above-mentioned stressed and overstressed conditions, in terms of discharge. The results are explained in terms of rainfall and discharge in the next section.

12.4.4   Response for Overstressed Condition

In case of overstressed conditions maximum discharge was observed mostly on the fourth time group, that is, in the middle of the monsoon season. Although for the year 1994, maximum discharge was observed in the last two time groups and in the year 2000, peak discharge was achieved in the second time group for negatively overstressed condition. The relationship between rainfall and discharge was for each of the selected 4 years except in the year 2000 where opposite pattern was observed for the overstressed negative condition (Figs. 12.6–12.13). The blue column in Figs. 12.6–12.13 represents the rank of discharge and white columns show the rank of rainfall.

12.4.5   Response for Stressed Condition

For the stressed conditions maximum discharge was observed mostly on the sixth time group with inverse relationship between rainfall and discharge. Although, year 1982 observed maximum discharge in the fifth time group for positively stressed condition, a constant peak discharge was observed for every time group for the negatively stressed condition. In the year 1994, peak discharge was achieved in the fifth and sixth time groups and in the year 2000, maximum discharge was observed in the fourth time group for positively stressed condition. The rainfall and runoff relationship shows a positive proportionality for each of the selected years except for 1972 and 1982. The positively stressed condition shows a negative proportionality between rainfall and runoff (Figs. 12.14–12.21).
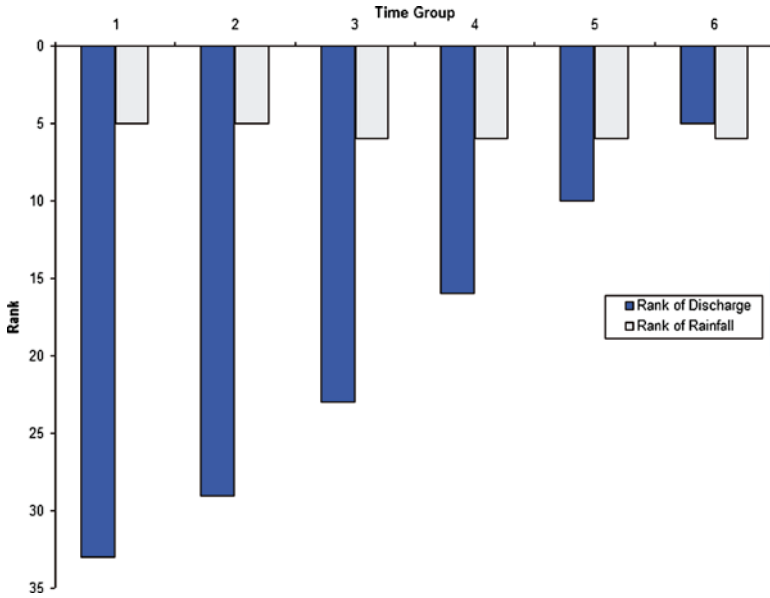
Fig. 12.6 Figure showing discharge response for positively overstressed rainfall condition in monsoon of year 1974
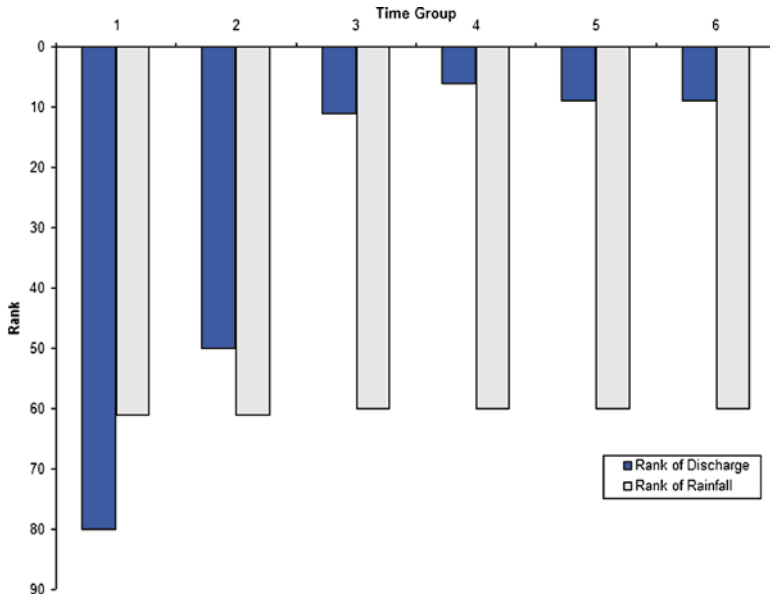
Fig. 12.7 Figure showing discharge response for negatively overstressed rainfall condition in monsoon of year 1974
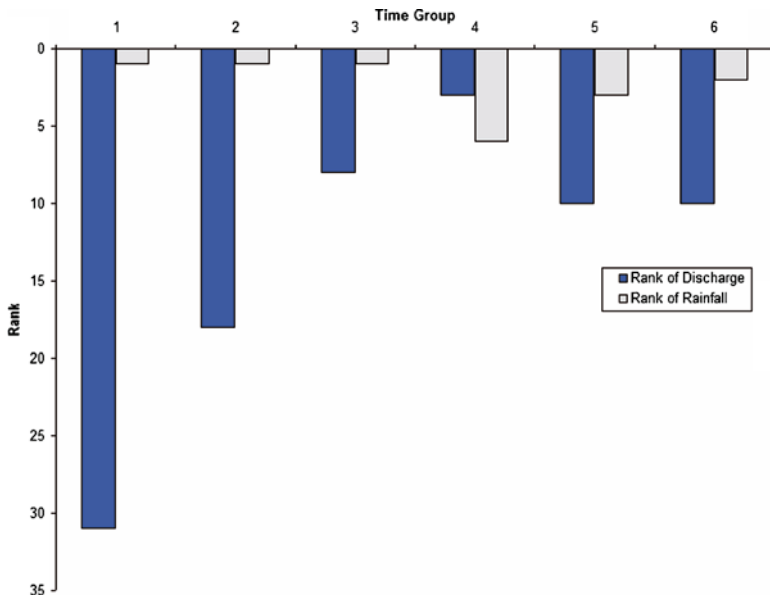
Fig. 12.8 Figure showing discharge response for positively overstressed rainfall condition in monsoon of year 1981
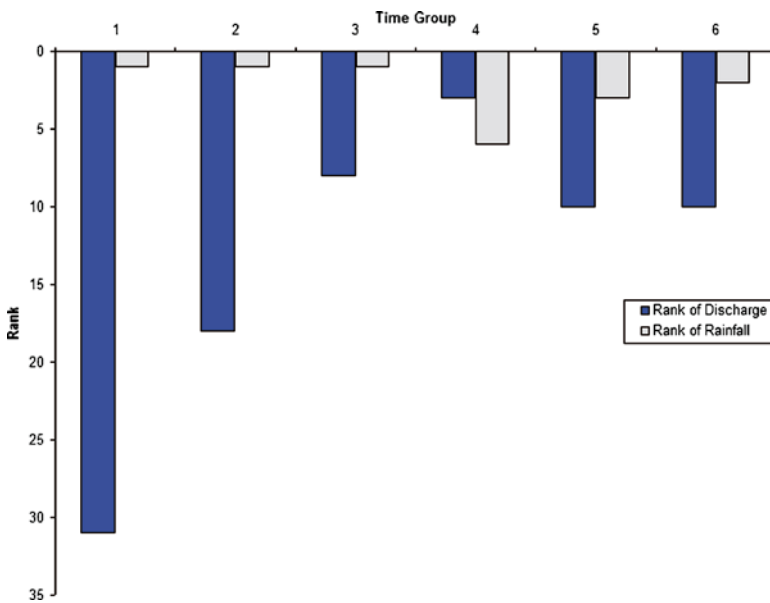
Fig. 12.9 Figure showing discharge response for negatively overstressed rainfall condition in monsoon of year 1981
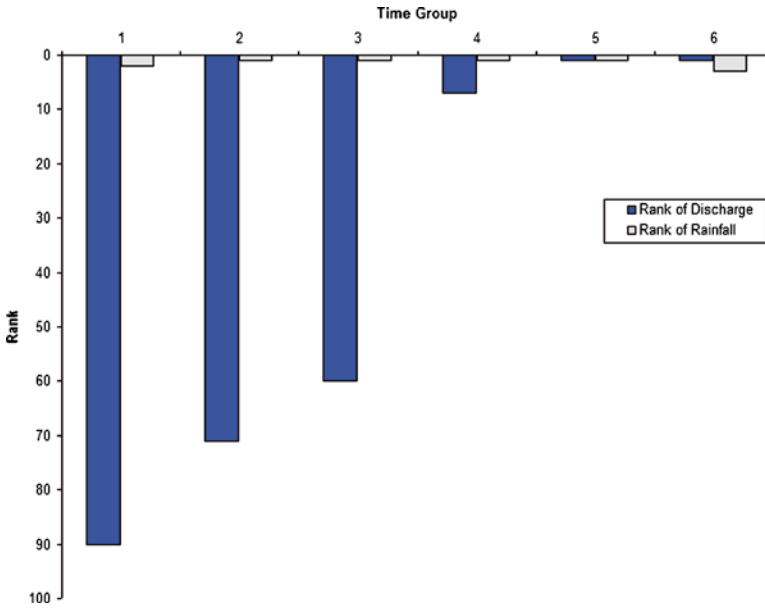
Fig. 12.10 Figure showing discharge response for positively overstressed rainfall condition in monsoon of year 1994
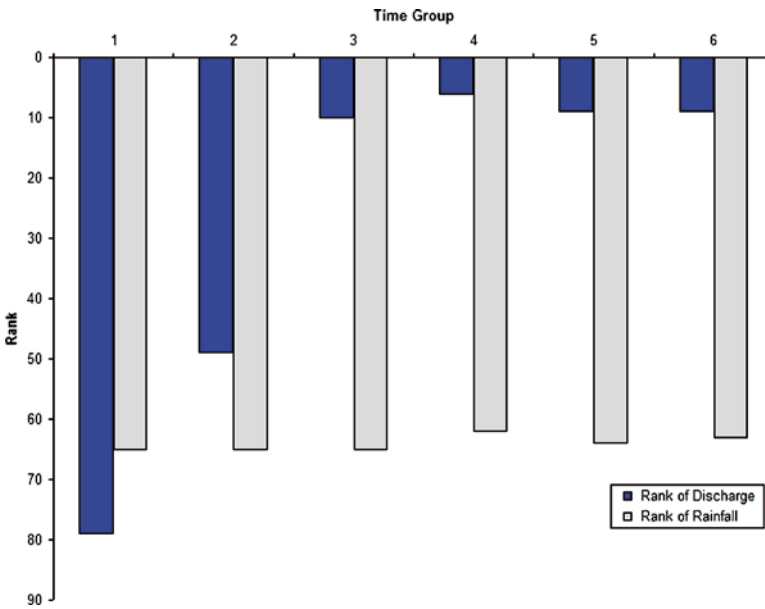
Fig. 12.11 Figure showing discharge response for negatively overstressed rainfall condition in monsoon of year 1994
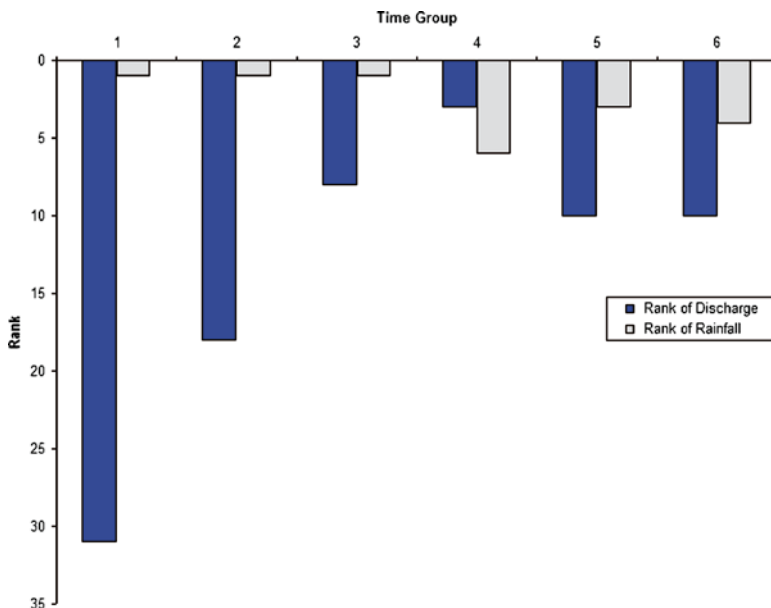
Fig. 12.12 Figure showing discharge response for positively overstressed rainfall condition in monsoon of year 2000
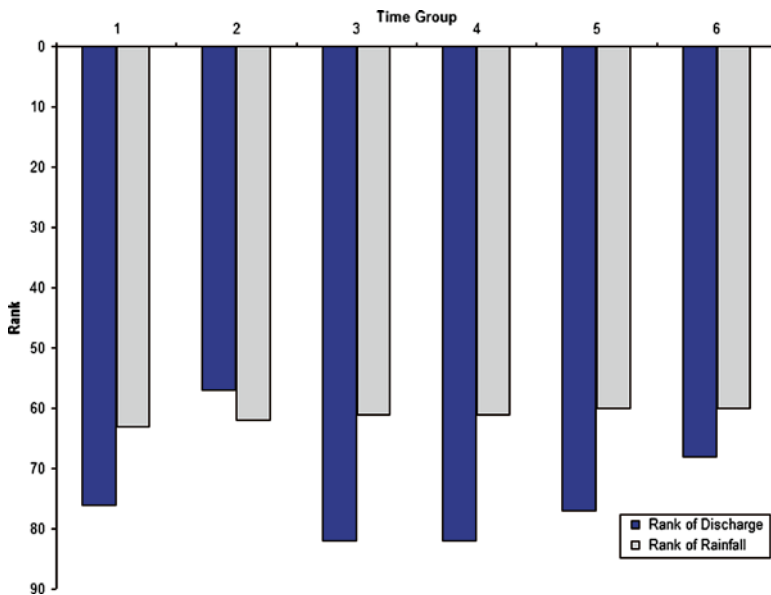
Fig. 12.13 Figure showing discharge response for negatively overstressed rainfall condition in monsoon of year 2000
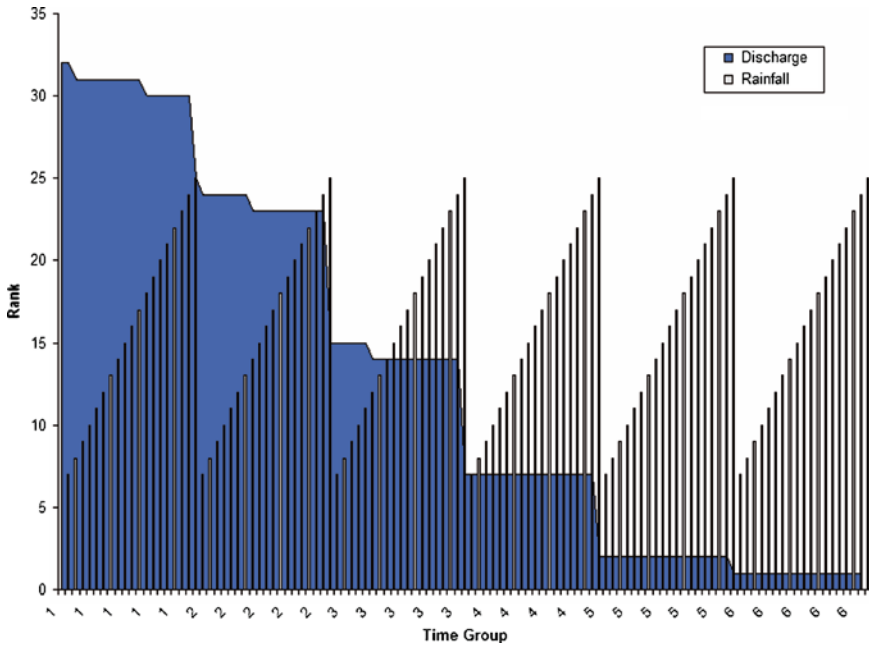
Fig. 12.14 Figure showing discharge response for positively stressed rainfall condition in monsoon of year 1972
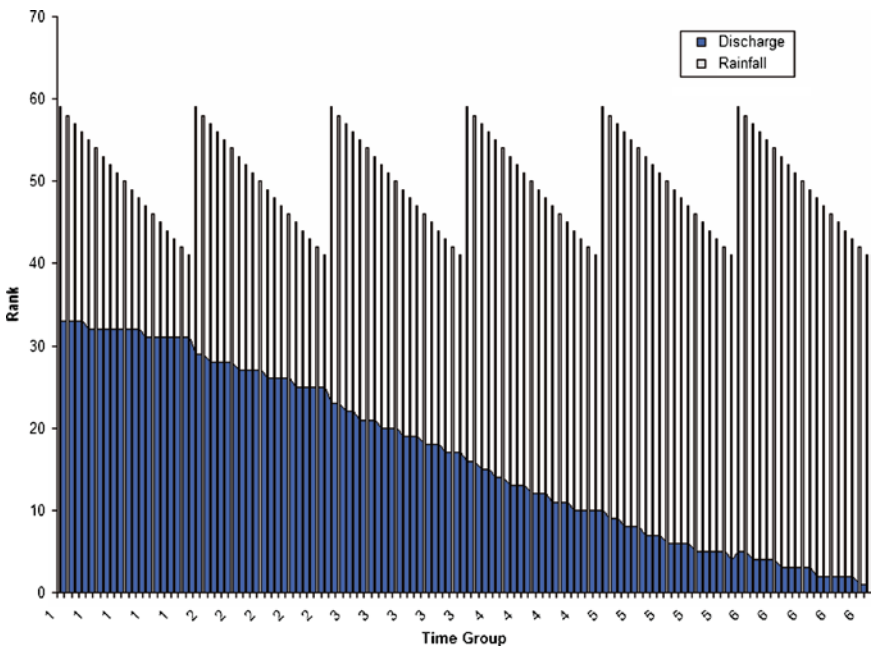
Fig. 12.15 Figure showing discharge response for negatively stressed rainfall condition in monsoon of year 1972
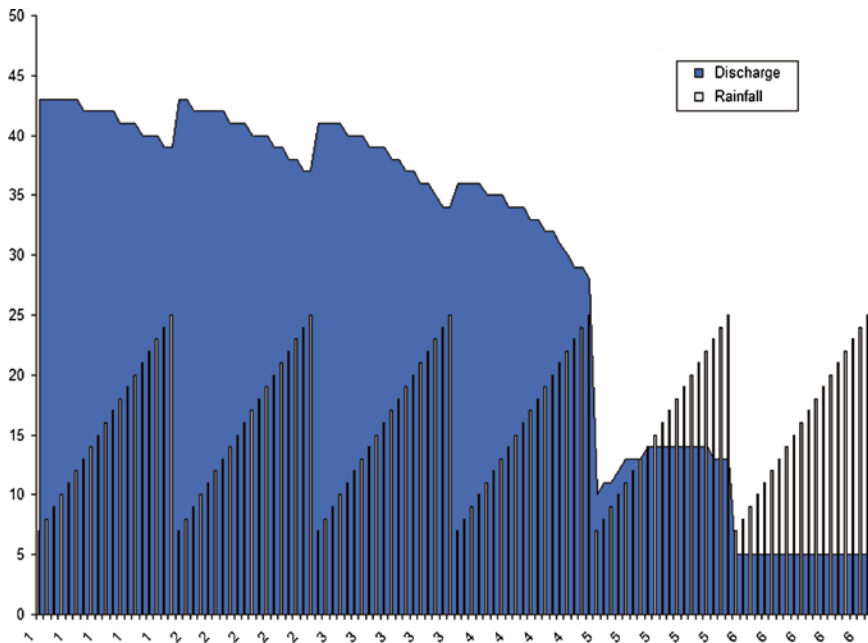
Fig. 12.16 Figure showing discharge response for positively stressed rainfall condition in monsoon of year 1982
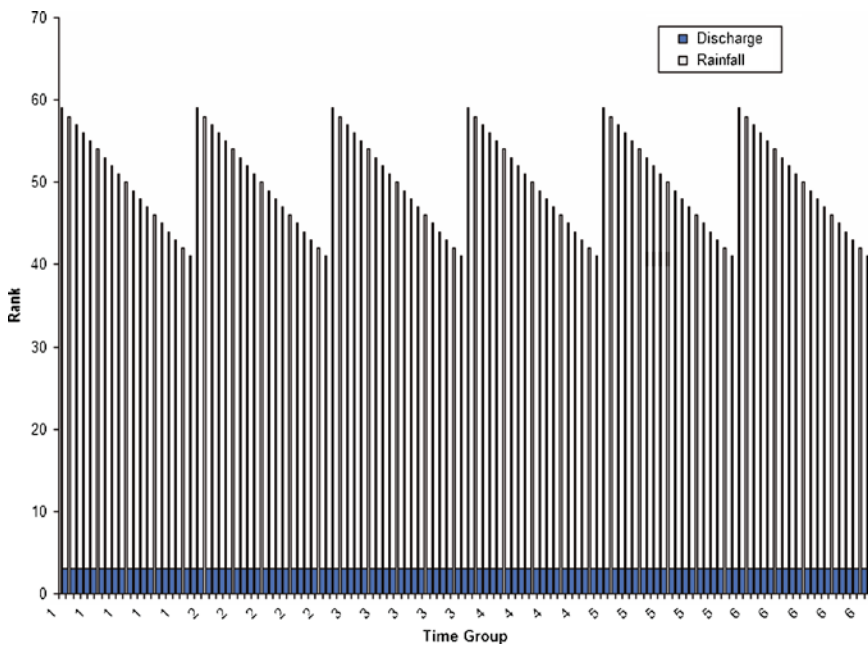
Fig. 12.17 Figure showing discharge response for negatively stressed rainfall condition in monsoon of year 1982
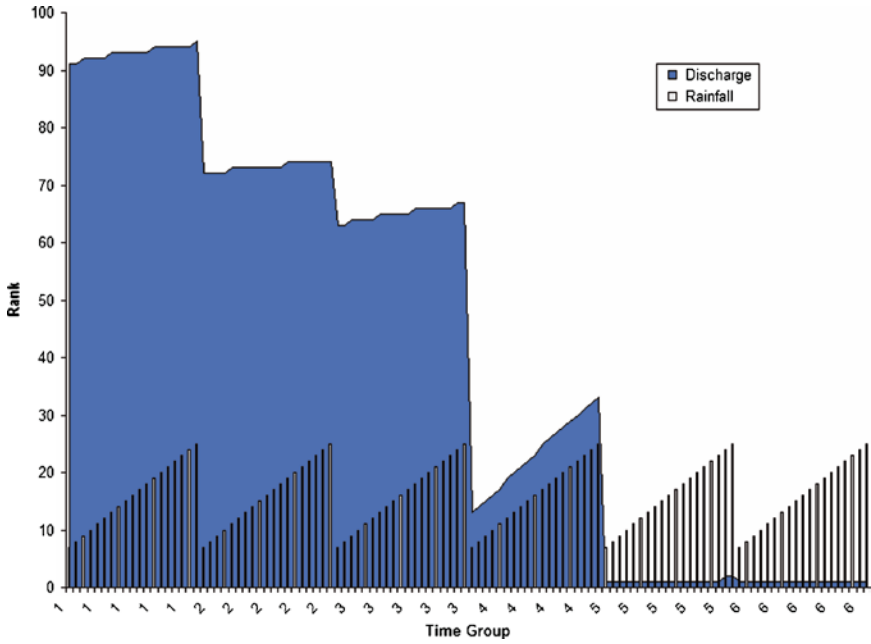
Fig. 12.18 Figure showing discharge response for positively stressed rainfall condition in monsoon of year 1994
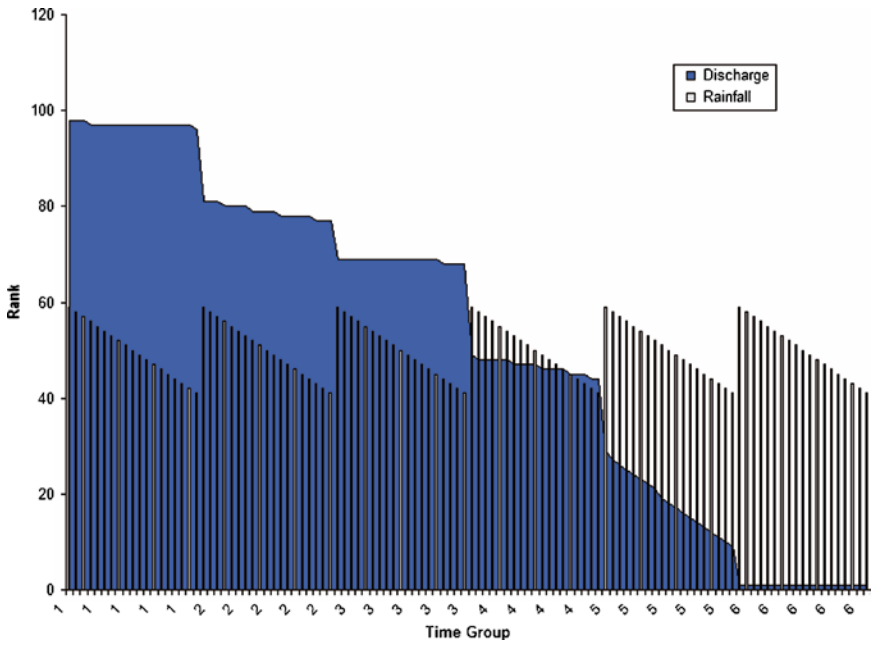
Fig. 12.19 Figure showing discharge response for negatively stressed rainfall condition in monsoon of year 1994
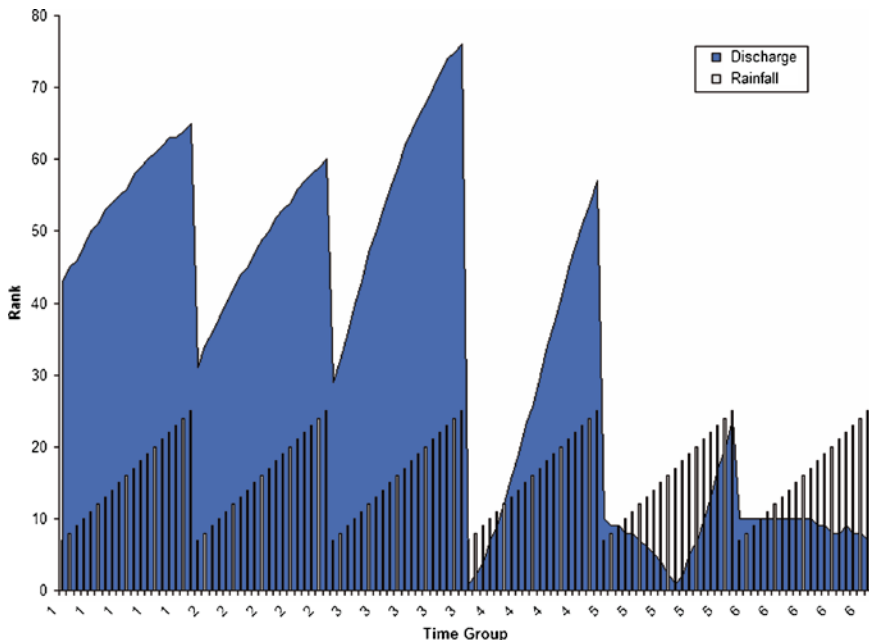
Fig. 12.20 Figure showing discharge response for positively stressed rainfall condition in monsoon of year 2000
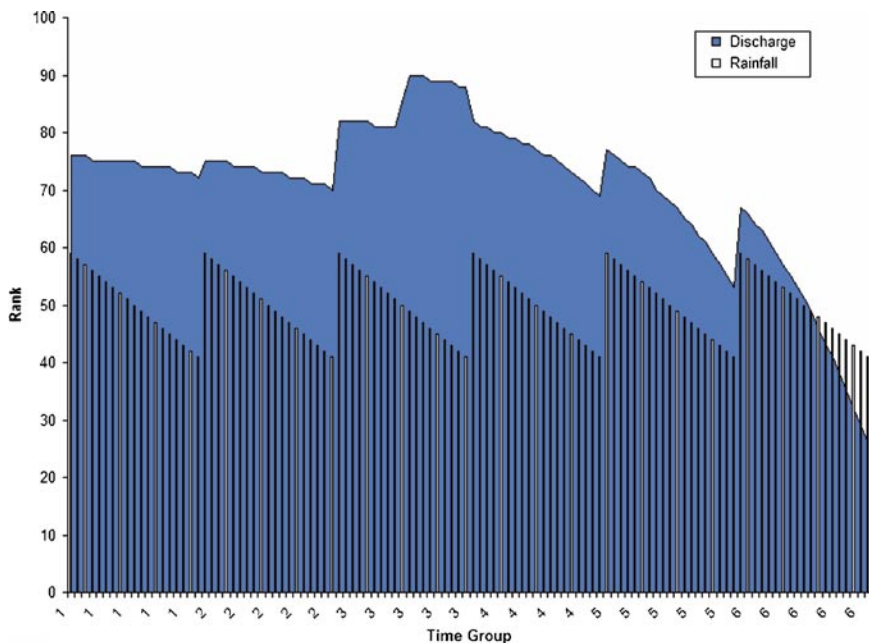
Fig. 12.21 Figure showing discharge response for negatively stressed rainfall condition in monsoon of year 2000

The blue area curve in Figs. 12.14–12.21 shows the rank of discharge as estimated by the model and the columns represent the rank of rainfall applied.

12.5   Conclusion

The present study tried to determine the catchment response to overstressed and stressed climatic conditions with the help of neural network and genetic algorithm. According to the results the retentivity of the catchment is poor, that is why even in positively overstressed climatic condition the catchment responded with low discharges. The method followed in the present study assumed that ground cover, water demand, and land use remains unrelated throughout the different conditions that were applied. The estimated discharge though showed a pattern generally observed in catchments with high ground and porous soil cover in cases of both overstressed and stressed climatic conditions. The study was carried out with only one gauge station. River Kalighayee has many other subbasins. The entire network of basins could be included and simulated in the way prescribed in the present study. The estimated results for the later study could give a more realistic response.

References

Ahmed JA, Sarma AK (2005) Genetic algorithm for optimal operating policy of a multipurpose reservoir. J Water Resour Manage 19:145–161

Bhatt VK, Bhattacharya P, Tiwari AK (2007) Application of artificial neural network in estimation of rainfall erosivity. Hydrology Journal. 1–2 (March–June) 30–39

Burn DH, Yulianti JS (2001) Waste-load allocation using genetic algorithms. J Water Resour Plan Manage ASCE 127(2):121–129

Kisi O (2004) Multilayer perceptrons with Levenberg–Marquardt training algorithm for suspended sediment concentration prediction and estimation. Hydrol Sci J 49(6):1025–1040

Nash JE, Sutcliffe JV (1970) River flow forecasting through conceptual models. J Hydrol 10:282–290

Sudheer KP (2005) Knowledge extraction from trained neural network river flow models. J Hydrol Eng 10(4):264–269

Wang QJ (1991) The genetic algorithm and its application to calibrating conceptual rainfall-runoff models. Water Resour Res 27(9):2467–2471

Wardlaw R, Sharif M (1999) Evaluation of genetic algorithms for optimal reservoir system operation. J Water Resour Plan Manage 125(1):25–33

Yitian L, Gu RR (2003) Modeling flow and sediment transport in a river system using an artificial neural network. J Environ Manage 31(1):122–134

Chapter 13
Determination of Evapotranspiration from Stream Flow with the Help of Classified Neurogenetic Model

Mrinmoy Majumder, Pankaj Roy, and Asis Mazumdar

Abstract The efficiency of an adaptive neuro-fuzzy computing technique in estimation of reference evapotranspiration (ET_0) from limited stream flow is investigated in this chapter. Forty years of stream flow data are clustered into nine groups, with the help of 11 basic rules where a ranking mechanism is used to sort the stream flows, and from these sorted data, top 10 stream flows and the same for that year are applied to the model as input. Corresponding ET_0, derived from Penman equation, is also classified into nine groups with the help of the same 11 basic rules and applied as output of the model. The stream flow dataset predicted by an HECHMS model is also clustered and applied into the same model to verify model flexibility and efficiency. Correct classification rate, coefficient of relationship, standard deviation, and coefficient of efficiency are used as the measure of the applicability of neural model in predicting ET_0 from stream flow. These are compared with the ET_0 derived from the Penman model. The comparison results reveal that the neuro-fuzzy models could be employed successfully in modeling ET_0 from stream flow, if the datasets of both ET_0 and stream flow are clustered according to the basic rules developed as per the stability of the catchment.

M. Majumder (✉)
Senior Research Fellow, School of Water Resources Engineering, Jadavpur University, Kolkata-700032, West Bengal, India
and
Geo-information Scientist, Regional Center, National Afforestation
and Eco-development Board, Jadavpur University, Kolkata-700032, West Bengal, India
e-mail: mrinmoy@majumder.info

P. Roy
Lecturer, School of Water Resources Engineering, Jadavpur University, Kolkata-700032, West Bengal, India

A. Mazumdar
Coordinator, Regional Center, National Afforestation and Eco-development Board, Jadavpur University, Kolkata-700032, West Bengal, India
and
Director, School of Water Resources Engineering, Jadavpur University, Kolkata-700032, West Bengal, India

13.1 Introduction

Evapotranspiration (ET_0) is one of the most influential parameter to estimate water balance, crop pattern, water requirements, etc. Evaporation is the process whereby water is converted to vapor and removed from the water surface. Transpiration consists of the vaporization of water contained in plant tissues and its removal to the atmosphere (Kişi 2007). The combination of these two separate processes whereby water is lost on the one hand from the soil surface by evaporation and on the other hand from the crop by transpiration is referred to as ET_0 (Allen et al. 1998). Knowledge of crop ET_0 is very important, because it allows the optimization of the irrigation water use in arid and semiarid regions where water shortage is a problem. ET_0 is the deciding factor for hydrological, agricultural, and fire hazard forecasts, for detecting the development of errors in hydrometeorological records, and also for detecting and monitoring the effects of land-use changes (Morton 1983). Numerous methods have been proposed for modeling of evapotranspiration as described by Brutsaert (1982) and evaporation into the atmosphere by Jensen et al. (1990). Tracy et al. (1992) showed the unreliability of forecasts obtained by the simple yearly differencing or monthly average (MAV) models.

Priestley and Taylor (1972) equation, a simplification of Penman (1948) equation, is applied to allow calculations of ET_0 under conditions where soil water supply limits ET_0. The use of the equation is appropriate when detailed meteorological measurements are not available (Flint and Childs 1991).

A modified two-source clumped model can significantly improve the predicted surface ET_0 rates (Domingo et al. 1998). The bowen ratio energy balance (BREB) (Malek and Bingham 1993) method is used to calibrate the wind function constants in the aerodynamic term of the Penman equation for the computation of the hourly and 24-h interval ET_0 at an irrigated semiarid valley (Malek 2003).

The Food and Agricultural Organization of the United Nations (FAO) assumed the ET_0 definition from Smith et al. (1997) and adopted the FAO Penman–Monteith (PM) (Montieth 1965) as the standard equation for the estimation of ET_0 (Allen et al. 1998; Naoum and Tsanis 2003).

Neural networks approaches have been successfully applied in a number of diverse fields, including water resources. In the hydrological context, recent experiments have reported that artificial neural networks (ANNs) may offer a promising alternative for modeling hydrological variables, for example, rainfall–runoff, stream flow, suspended sediment, etc. However, the application of ANN to evapotranspiration modeling is limited in the literature. Kumar et al. (2002) used a multilayer perceptron (MLP) with back-propagation training algorithm for the estimation of ET_0. They used various architectures and found that the ANN gave accurate ET_0 estimates. Sudheer et al. (2003b) used radial basis ANN in modeling ET_0 using limited climatic data. Trajkovic et al. (2003) developed a radial basis ANN for forecasting ET_0.

Trajkovic (2005) used temperature-based radial basis ANN for modeling FAO-56 PM ET_0. He compared the ANN results with those of the Hargreaves, Thornthwaite, and reduced PM methods and concluded that the radial basis ANN generally performs better than the others in modeling the ET_0 process. Kisi (2006) investigated the estimation of ET_0 using multilayer perceptron (MLP) method and he compared ANN test results with those of the Hargreaves and Samani (1985) empirical models. He found that the MLP model gave much better results than the empirical models.

In this context, the present study tries to investigate the capability of ANN in modeling ET_0 from limited stream-flow dataset. The ET_0 values are obtained using the standard Penman equation and used as the desired output. Two types of stream-flow datasets are used as input. First set of data is collected from Damodar Valley Corporation (DVC), managing authority of the study area, and the second set of data is derived from rainfall with the help of HECHMS model as done by Roy et al. (2004). First set is used to develop the neural model and the second set is used to verify the model performance. As ANN is a universal classifier (Hassoun 1995) and as the learning process gets improved if both input and output datasets are clustered (Parasuraman and Elshorbagy 2007), stream flow and ET_0 are classified into nine groups with the help of 11 rules developed specifically for this study.

13.2 Study Area

13.2.1 Description of the River Basin

Damodar River basin (Fig. 13.1) is perhaps the most important subbasin of the Ganga–Brahmaputra–Meghna (GBM) basin as it is India's first river development project and second large-scale river project of the last century after the Tennessee Valley Authority (TVA) in the USA. The Damodar River, which lies between the latitudes 23°30′N and 24°19′N and longitudes 85°31′E and 87°21′E, originates from the Palamu Hills of Chota Nagpur at an elevation of about 610 m above mean sea level. It flows in a southeasterly direction, entering the deltaic plains below Raniganj in Burdwan district of West Bengal, India. Near Burdwan the river abruptly changes its course to southerly direction and joins the Hoogli River about 48 km below Kolkata. The slope of the river bed during the first 241 km is about 1.89 m/km. During the next 161 km is about 0.57 m/km, while the same is about 0.19 m/km in subsequent 145 km. The river is fed by six streams of which the principal tributary, Barakar joins it where river Damodar emerges from the Palamu Hills. The four main multipurpose reservoirs are located at Tilaiya, Konar, Maithon, and Panchet, and a Barrage at Durgapur was commissioned during 1953–1959. Another tributary Khudia, whose catchment is neither intercepted by Maithon nor Panchet reservoirs, joins Damodar near its confluence with Barakar. In the plains river splits into several channels and ultimately joins the rivers Roopnarayan and Hoogli. The total length of the river is about 541 km. The total catchment area of the river is 28,015 km^2 of which 10,985 km^2 lies under Panchet (Konar – 997 km^2; Tenughat – 4,500 km^2; and Panchet 5,488 km^2) and 6,293 km^2 under Maithon (Tilaiya – 984 km^2 and Maithon – 5,309 km^2).

Fig. 13.1 The study area showing the modeled watershed

13.2.2 Climate of the River Basin

Moderate winters and hot and humid summers characterize the climate of the area. The mean annual rainfall in different catchments of the Damodar valley is 126 cm in Barakar, 127.2 cm in Damodar, and 132.9 cm in lower valley. As high as 82% of the mean annual rainfall occurs during the four monsoon months from June to September. The mean daily temperature varies from 40°C to below 20°C in winters. The rainfall in this area during the monsoon season is mainly due to the passage of depressions and low pressure over and near the area and the active monsoon conditions due to accentuation of the seasonal trough.

13.2.3 Geomorphology

The upper portion of the catchment consists of rough, hilly regions, whereas the lower portion consists of the nature of flat deltaic plane.

13.2.4 Control Structures

DVC has a network of four dams: Tilaiya and Maithon on river Barakar, Panchet on river Damodar, and Konar on river Konar. Besides, Durgapur barrage and canal network, handed over to Government of West Bengal in 1964, remained a part of total
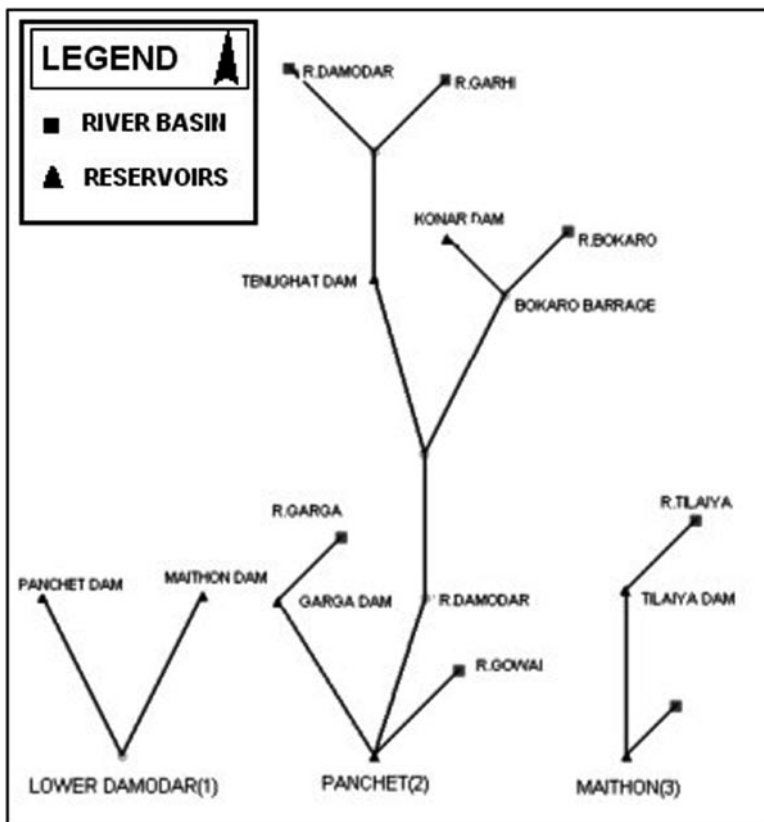
Fig. 13.2 The sectional hydrologic modeling tree of the river basin

system of water management. Four multipurpose dams were constructed during the period 1948–1959, namely, Maithon, Panchet, Tilaiya, and Konar reservoir. Among these four reservoirs, first three are used for hydropower generation. Konar is used for agricultural purpose in the adjacent area. Figure 13.2 shows the network diagram of the river Damodar catchment in three parts. First part shows the connectivity between the Panchet and Maithon subcatchment with Durgapur Barrage. Second and third parts show the hydrologic modeling tree of the two (Panchet and Maithon) subcatchment.

13.3   Data Description

The data sample consist daily records of 40 years (1959–2003) of solar radiation, air temperature, relative humidity, wind speed, and discharge. For stream flow data, only 10 among the selected 40 years are considered, as during these years, stream flow was at the highest value. Peak discharge of those years and corresponding ET_0 is given in Table 13.1. According to the dataset, highest and lowest discharges are observed in 1991 and 1994, respectively.

The ET_0 of the selected years are calculated with the help of Penman equation using solar radiation, air temperature, relative humidity, and wind speed data (Fig. 13.3). The results are given in Table 13.1. According to the results, minimum and maximum ET_0 vary between 0.21 and 3.28 cm. Annual average ET_0 remains within 1.34 and 0.35 cm. Highest and lowest average annual ET_0 are observed in 1995 (1.34 cm) and 1973 (0.35 cm), respectively. The statistical information of the discharge and ET_0 dataset is given in Table 13.2. From Table 13.2, it is observed
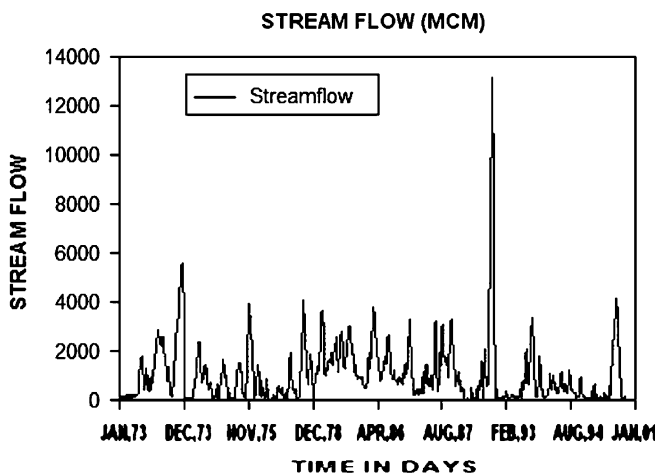
Fig. 13.3 Daily stream flow of the Durgapur catchment for the selected years (1973, 1975, 1978, 1984, 1986, 1987, 1991, 1993, 1994, and 2000) as recorded by DVC

Table 13.1 Peak discharge and corresponding average ET_0 for the selected years

Year	Peak discharge (mcm)	Peak ET_0 (cm)
1973	5,591	0.459
1975	3,954	0.667
1978	4,105	0.529
1984	3,634	0.512
1986	3,785	0.502
1987	3,314	0.537
1991	13,060	1.056
1993	3,386	0.771
1994	1,197	1.056
2000	4,107	0.975

Table 13.2 Statistical information of the discharge and ET_0 dataset

	Discharge	ET_0
Variance	2.75	5.81
Skew	−0.31	−0.76
Mean	1,048.92	0.65
Kurtosis	−0.43	−0.47
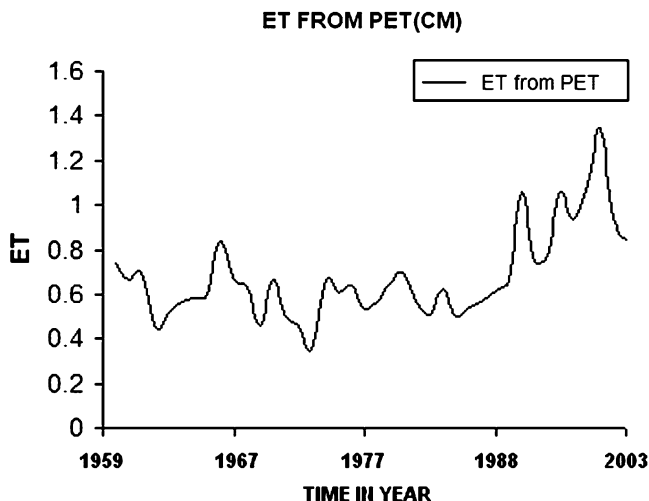
Fig. 13.4 Annual average ET_0 as calculated by the Penman equation (PET) (1959–2003)

that the dataset of ET_0 is 2.11 times varied, 1.66 times negatively skewed, and 1.09 times leptokurtotic than the stream flow dataset.

Figures 13.3 and 13.4 show the daily stream flow of the Durgapur catchment for the peak years (1973, 1975, 1978, 1984, 1986, 1987, 1991, 1993, 1994, and 2000) as recorded by DVC and average ET_0 as calculated from the Penman equation (PET) (1959–2003)

13.4 Methodology

13.4.1 Artificial Neural Network

An ANN is a flexible mathematical structure that is capable of identifying complex nonlinear relationships between input and output datasets. The ANN model of a physical system can be considered with n input neurons ($x_1, x_2, ..., x_n$), h hidden neurons ($z_1, z_2, ..., z_n$), and m output neurons ($y_1, y_2, ..., y_n$). Let t_j be the bias for neuron z_j and f_k for neuron y_k. Let w_{ij} be the weight of the connection from neuron x_i to z_j and beta is the weight of the connection z_j to y_k. The function that ANN calculates is:

$$y_k = g_A \left(\sum z_j b_{jk} + f_k \right) ... \left(j = 1 - h \right) \tag{13.1}$$

in which,

$$z_j = f_A \left(\sum x_i w_{ij} + t_j \right) ... \left(i = 1 - n \right) \tag{13.2}$$

where g_A and f_A are the activation functions (Sudheer 2005).

The development of an artificial neural network, as prescribed by ASCE Task Committee (2000a) follows the basic rules given below:

1. Information must be processed at many single elements called nodes.
2. Signals are passed between nodes through connection links and each link has an associated weight that represents its connection strength.
3. Each of the nodes applies a nonlinear transformation called activation function to its net input to determine its output signal.

The numbers of neurons contained in the input and output layers are determined by the number of input and output variables of a given system. The size or number of neurons of a hidden layer is an important consideration when solving problems using multilayer feed-forward networks. If there are fewer neurons within a hidden layer, there may not be enough opportunity for the neural network to capture the intricate relationships between indicator parameters and the computed output parameters. Too many hidden-layer neurons not only require a large computational time for accurate training, but may also result in overtraining. A neural network is said to be "overtrained" when the network focuses on the characteristics of individual data points rather than just capturing the general patterns present in the entire training set. The network building procedure is divided into three phases, which are described next in a broad way.

13.4.1.1 Network Building Procedure

Selection of Network Topology

Neural network can be of different types, like feed forward, radial basis function, time lag delay, etc. The type of the network is selected with respect to the knowledge of input and output parameters and their relationship. Once the type of network is selected, selection of network topology is the next concern. Trial and error method is generally used for this purpose, but many studies now prefer the application of genetic algorithm (Ahmed and Sarma 2005). Genetic algorithms are search algorithms based on the mechanics of natural genetic and natural selection. The basic elements of natural genetics – reproduction, crossover, and mutation – are used in the genetic search procedure. A GA can be considered, and it consists of the following steps (Burn and Yulianti 2001):

1. Select an initial population of strings
2. Evaluate the fitness of each string
3. Select strings from the current population to mate
4. Perform crossover (mating) for the selected strings
5. Perform mutation for selected string elements
6. Repeat steps 2–5 for the required number of generations

Genetic algorithm is a robust method of searching the optimum solution to complex problems like the selection of an optimal network topology where it is difficult or

impossible to test for optimality. The basics of GA have already been discussed by many authors like Ahmed and Sarma (2005), Wang (1991), and Wardlaw and Sharif (1999). Hence, the details of the basic procedures of GA are not focused in the present literature.

Training Phase

To encapsulate the desired input–output relationship, weights are adjusted and applied to the network until the desired error is achieved. This is called "training the network." There are innumerable "training the network" algorithms, among which, back propagation (ASCE Task Committee 2000b) is mostly preferred. In the present study, quick propagation (QP), conjugate gradient descent (CGD), and Levenberg–Marquardt (LM), each of them derived from basic back-propagation algorithms, are used as the training algorithm.

QP is a heuristic modification of the back propagation algorithm invented by Fahlam (1988). This training algorithm treats the weights as if they are quasi-independent and attempts to use a simple quadratic model to approximate the error surface. In spite of the fact that the algorithm has no theoretical foundation, it is proved to be much faster than standard back propagation for many problems. Although, sometimes the quick propagation algorithm may be instable and inclined to stuck in local minima.

CGD (Kişi 2007) is an advanced method for training multilayer neural networks. It is based on the linear search usage in the line of an optimal network weights' change. The correction of weights is conducted once per iteration. In most cases, this method works faster than back propagation and provides more precise forecasting results.

LM (Kişi 2004) is an advanced nonlinear optimization algorithm. It is the fastest algorithm available for multilayer perceptrons. However, it has the following restrictions:

- It can only be used on networks with a single output unit.
- It can only be used with small networks (a few hundred weights) because its memory requirements are proportional to the square of the number of weights in the network.

Testing Phase

After training is completed, some portion of the available historical dataset is fed to the trained network and known output is estimated out of them. The estimated values are compared with the target output to find MSE. If the value of MSE is less than 1%, the networks are said to be sufficiently trained and ready for estimation. Few part of the dataset is also used for cross-validation to prevent overtraining during the training phase (Sudheer 2005).

In the present study, all the above three training algorithms are used to train the model. The best-trained model is selected with the help of training and testing correct classification rate (CCR) and the required connection weight for each of the algorithm (as selected by GA).

13.4.2   HEC-HMS

A hydrologic modeling system (HEC-HMS) program was developed by a team of engineers from the Hydrologic Engineering Center 2000, US Army Corps of Engineers, led by the Director, Darryl Davis (Hydrologic Engineering Center 2000). The HEC-HMS is designed to simulate the rainfall–runoff processes of watershed systems. It is designed to be applicable in a wide range of geographic areas for solving the widest possible range of problems. It utilizes a graphical user interface to build a watershed model and to set up the rainfall and control variables for simulation. The program features a completely integrated work environment including a database, data entry utilities, computation engine, and results reporting tools. The application of the HEC-HMS model involves two steps. First, the model is calibrated using previous datasets to determine the best parameters. Second, the model is verified by using new sets of data. HEC-HMS is run with the previous hourly rainfall–runoff data in order to predict runoff entering selected catchments. For the present study, the model uses initial-constant infiltration/loss parametrization, the Clark hydrograph transformation routine, and a recession base flow component. The initial loss and initial flow are treated as initial conditions and vary from simulation to simulation. The hydrographs of the catchments are determined by using a trial and error method to get the best-suite parameters that can produce the best results. In the present study, the output from the HECHMS model developed by Roy et al. (2004) is applied into the neural model to verify its flexibility and accuracy with the new but similar dataset.

13.4.3   Evaluation of the Networks

The accuracy of results obtained from the network is assessed by comparing its response with the validation set. The commonly used evaluation criteria include correct classification rate (CCR), correlation coefficient (r), coefficient of efficiency (CE), and standard deviation (STDEV) (Bhatt et al. 2007).

$$\text{CCR} = \left((T_{\text{pc}} - O_{\text{pc}}) / T_{\text{pc}} \right) \times 100 \tag{13.3}$$

$$r = \left[\sum \left((T_{\text{p}} - T_{\text{m}})(O_{\text{p}} - O_{\text{m}}) \right) / \left(\sum_{1}^{n} (T_{\text{p}} - T_{\text{m}})^2 \sum_{1}^{n} (O_{\text{p}} - O_{\text{m}})^2 \right)^{1/2} \right] \tag{13.4}$$

$$CE = 1 - (\sum_{1}^{n}(T_p - O_p)^2 / \sum_{1}^{n}(T_p - T_m)^2) \qquad (13.5)$$

$$STDEV = \frac{\sum_{1}^{n}(T_n - \overline{T}_n)^2}{n} \qquad (13.6)$$

where T_{pc} is the group of the actual dataset; O_{pc} is the estimated group; T_p is the target group for the p th pattern; O_p is the estimated group for the P th pattern, T_m and O_m are the mean target and estimated groups, respectively, and n is the total number of patterns.

CCR is used in classification tasks as a qualitative characteristic. This rate is calculated by dividing the number of correctly recognized records by the total number of records. CCR is measured in relative units or in percents. r is the degree of correlation between two variables. CE criterion has the basis of standardization of the residual variance with initial variance (Nash and Sutcliffe 1970). In this criterion, a perfect agreement between the observed and estimated output yields an efficiency of 1. A negative efficiency represents lack of agreement and zero agreement means all the estimated values are equal to the observed mean. STDDEV is the measure of deviation of the estimated value from the target output. A perfect match between observed data and model simulations is obtained when STDDEV approaches 0.0 (Majumder et al. 2009)

13.5 Result and Discussion

13.5.1 Model Development

The purpose of this study is not to find the parameter, which has highest contribution on ET_0 but to derive ET_0 from limited stream flow dataset. Neural network is a universal classifier (Hassoun 1995). It can estimate clustered dataset with more efficiency than any other model. As every neural model follows a binary system of encoding, accuracy of neural model increases if clustered dataset is used. Unstable dataset is defined as those dataset, which separates maximum or minimum from others. These datasets help to determine the threshold of the entire dataset. To be more precise, every peak and every trough borders the stability of a dataset. In the clusterization process, rules are prepared based on the above conditions.

13.5.1.1 Data Classification

Accordingly, the entire datasets of both stream-flow and ET_0 are divided into nine classes.

For the discharge dataset:

1. Total dataset is rearranged in descending order where maximum discharge is placed on the top and minimum discharge is placed on the bottom.
2. Each of the data are given a rank according to the order of placement after the rearrangement.
3. If the rank of the data is lesser than 5, then the data will be clustered into group PD1.
4. If the rank of the data is lesser than 10 but greater than 5, then the data will be clustered into group PD2.
5. If the rank of the data is lesser than 50 but greater than 10, then the data will be clustered into group PD3.
6. If the rank of the data is lesser than 100 but greater than 50, then the data will be clustered into group HD1.
7. If the rank of the data is lesser than 250 but greater than 100, then the data will be clustered into group HD2.
8. If the rank of the data is lesser than 500 but greater than 250, then the data will clustered into group HD3.
9. If the rank of the data is lesser than 650 but greater than 500, then the data will be clustered into group MD1.
10. If the rank of the data is lesser than 750 but greater than 650, then the data will be clustered into group MD2.
11. If the rank of the data is greater than 750, then the data will be clustered into group MD3.

For the ET_0 dataset:

Similarly, values of ET_0 derived from PET are ranked and clustered with the same rules except the name of the groups, which are changed from PD1, PD2, PD3, HD1, HD2·HD3, MD1, MD2, and MD3 to PE1, PE2, PE3, HE1, HE2·HE3, ME1, ME2, and ME3. So the groups of the two different data types can be identified separately.

Both of the datasets are now converted into nine groups with the help of the above 11 rules. Groups of stream flow are selected as input and groups of the ET_0 datasets are taken as output. Figures 13.5 and 13.6 show the actual stream flow and ET_0 converted into the nine groups or clusters.

Three feed-forward neural models with this clustered input and output are created, where 70% of the dataset is used to train the models, 15% is used for cross-validation, and the rest is used to test the models for their ability to learn the present problem. These three neural models are named as QP, CGD, and LM according to the type of training algorithm used to train them. Genetic algorithm is applied to select the topology of all the three networks. The population pattern is taken as 40.60 generation is forced from these patterns, which are enforced to a 90% crossover rate and 20% mutation capability. The training is stopped whenever CCR on training subset rise above 98%. Networks are trained for 20 times with 100,000 iterations per training. After the training, CCR achieved from the three networks QP, CGD, and LM are 100%, 99.44%, and 99.44%, respectively. The networks are tested with 126 patterns and the testing CCR for the three networks are found out to be 100%, 99.21%, and 99.21%, respectively.
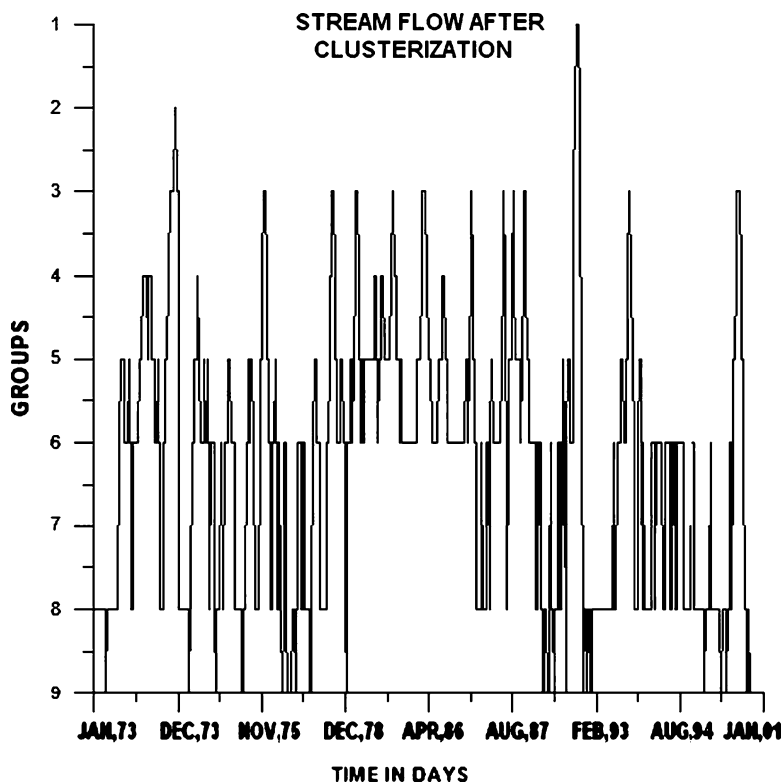
Fig. 13.5 Graph showing actual stream flow after clusterization. Note: 1, 2, 3, 4, 5, 6, 7, 8, and 9 depict the stream flow group PD1, PD2, PD3, HD1, HD2·HD3, MD1, MD2, and MD3

The details of the networks are given in Table 13.3. Among these three neural models, only one model is selected to predict ET_0.

13.5.1.2 Model Selection

Selection of the best performing network from the above three networks are found out to be tricky. QP has the highest CCR among the three networks and has a small connection weight (35) and hence required amount of training dataset is also small (Jain and Prasad Indurthy 2003). Training and testing CCR of CGD and LM are same, but the connection weight of CGD is largest whereas that of LM is equal to the connection weight of QP (35). QP has the best CCR among the three networks but while training this network, it shows signs of overtraining, that is, cross-validation CCR exceeds training CCR. Other two networks have no such problem but both of them have the same training and testing CCR. CGD has heaviest connection weight among the three networks and hence the required amount of training dataset is also highest. Among the three networks, LM had no problem of overtraining (which is present in case of QP), has the best CCR
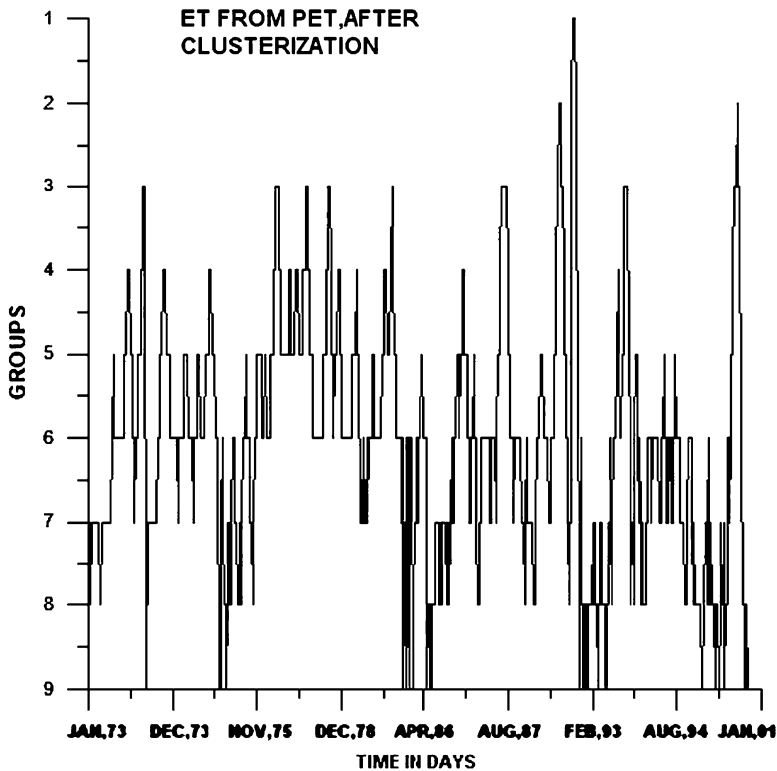
Fig. 13.6 Graph showing ET_0 from PET, after clusterization. Note: 1, 2, 3, 4, 5, 6, 7, 8, and 9 depict the ET_0 group PE1, PE2, PE3, HE1, HE2·HE3, ME1, ME2, and ME3

Table 13.3 Summary table for all model's inputs and outputs

	Input	Output
LM	Stream flow collected from DVC clustered into nine groups	ET_0 as calculated by PET clustered into nine groups
HHR	Stream flow estimated by HECHMS and clustered into nine groups	ET_0 as calculated by PET clustered into nine groups

(similar to QP), and a small connection weight (which is largest in case of CGD network), that is, required amount of training data is smaller than the CGD network. Hence, LM is selected for estimating ET_0 from stream flow dataset. Figure 13.8 shows the grouped ET_0 as predicted by the LM model.

The stream flow predicted by HECHMS model, developed by Roy et al. (2004), is clustered in the same way as the actual stream flow. This clustered dataset is fed to the LM model to predict ET_0 (Table 13.3). This new model is named as HHR. The ET_0 found from Penman equation is compared with the ET_0 predicted by LM and HHR. Figure 13.7 shows the stream flow predicted by HECHMS model. Figures 13.8 and 13.9 depict the estimated ET_0 values respectively from LM
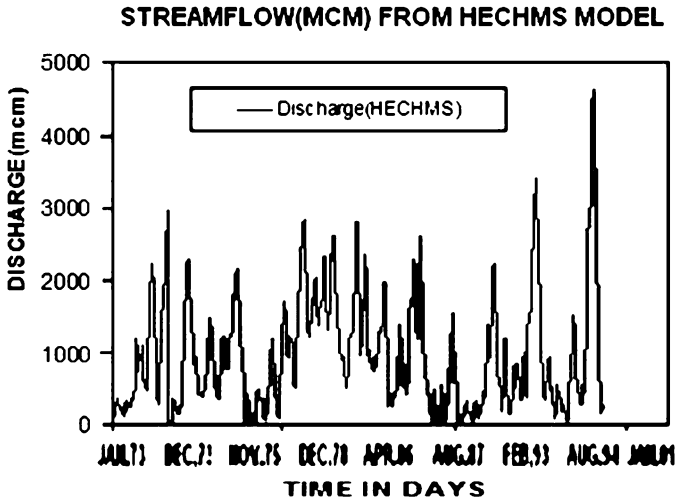
Fig. 13.7 Graph showing the stream flow from the Durgapur catchment as estimated by HHR
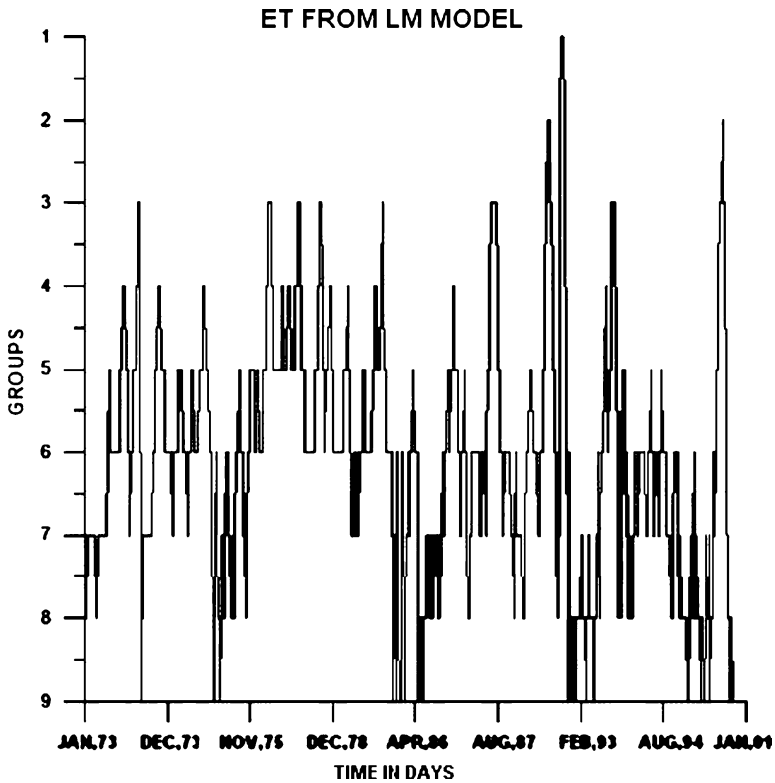
Fig. 13.8 Graph showing ET_0 from LM model
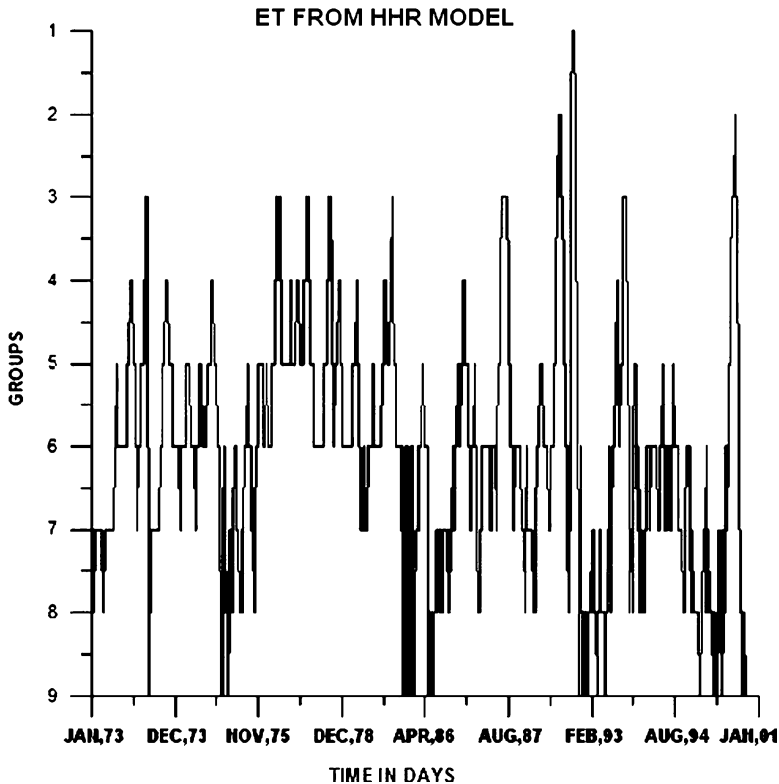
Fig. 13.9 Graph showing ET_0 from HHR model

and HHR model. Table 13.3 shows a summary of the input and output of the LM and HHR model. Model performance is found by comparing estimated ET_0 from the models (LM and HHR) with the ET_0 derived from PET.

The performance of the selected network is compared with the help of CCR, *r*, CE, and STDDEV calculated between computed ET_0 from LM and HHR with the actual ET_0 given by PET. These values helped to select the best performing network (Nash and Sutcliffe 1970). The CCR values obtained are 99.5% and 80.18%, respectively for LM and HHR models. Values from LM and HHR gave high model efficiency equal to 99.3% and 98.7%, respectively. The STDDEV for HHR and LM is found to be 0.13 and 0.16, respectively, nearer to the zero value. Observed value from the LM is found to be 99.3% related with the target values, whereas that of the HHR model is found to be 98.7%. According to the performance validating criterion, predictions from both LM and HHR show a high degree of accuracy when compared with the ET_0 values derived from the PET model. Both LM and HHR values are derived with the help of neural model and both show satisfactory performance and found to be coherent to the values from PET. Figures 13.8 and 13.9 show the estimated ET_0 respectively from LM and HHR.

13.6 Concluding Remarks

The capability of an adaptive neural technique in the estimation of ET_0 using stream flow is presented in this study. The study indicated that modeling of daily ET_0 is possible through the use of neural network. The LM model, whose inputs are clustered stream flow, is found to perform in accordance with the PET model both with the actual dataset and with a predicted dataset. ANN model, containing only one input, stream flow, is developed and tested with two kinds of datasets (Table 13.4); historical stream-flow data and the same predicted from an HECHMS model. Both are first clustered into nine groups with the help of 11 predefined rules and then applied to the LM model. The results are compared with the ET_0 derived from PET. The result reveals that the estimation of ET_0 can be done with the LM model if the

Table 13.4 Summary table showing optimum ANN model's architecture and ANN internal parameters

Network name	QP	CGD	LM
Network topology			
Network type	Feed-forward fully connected network	Feed-forward fully connected network	Feed-forward fully connected network
Number of inputs	1	1	1
Number of hidden layers	2	2	2
Hidden units in the 1st hidden layer	3	11	3
Hidden units in the 2nd hidden layer	8	8	8
Number of outputs	1	1	1
Connection weight	35	107	35
All the topologies were created using genetic algorithms with following parameters			
Population size	50	40	50
Number of generations	50	50	50
Network size penalty	5	5	5
Crossover rate	0.9	0.9	0.9
Mutation rate	0.2	0.2	0.2
Training algorithm and parameters			
Training algorithm	Quick propagation	Conjugate gradient descent	Levenberg–Marquardt
Training iteration	20	20	20
Stop training conditions			
CCR on training subset must drop below	98	98	98
Maximum allowed number of iterations	100,000	100,000	100,000
Training stop reason	Desired error level was achieved	Desired error level was achieved	Error reduction became too low
Training and testing results			
Average CCR (training)	100	99.44	99.44
Average CCR (testing)	100	99.21	99.21

Table 13.5 Statistical measures of model's performance

	CCR (%)	r	CE	STDDEV
LM	99.5	0.94	0.993	0.13
HHR	80.18	0.92	0.987	0.16

clustered dataset of stream flow is used as input. The HHR model developed from estimated discharge by HECHMS can also predict ET_0 with high accuracy. Both the conclusions were supported by r, CE, and STDDEV between the estimated and target ET_0 (Table 13.5). Any estimation must be done to estimate the zone that will be in influence if time or space scale is varied. This clustered approach to predict ET_0 from stream flow as shown in the present study is successful in that context. But it cannot predict the exact value of ET_0 for a specific value of stream flow. The results can be declustered and some approximation can be applied but this can result in a lot of assumptions. The LM model could be used in design of reservoirs and various other hydrological analyses. Also, this approach can easily help a hydrologist to take adequate measures in a specific zone of time when the stream flow will be unstable. The first and last groups are the unstable groups where the peak and lean discharges are included. If the state of ET_0 is known for that time, hydrologists can suggest farmers for adequate protective measurements. The concepts presented in this study can easily be extrapolated to other similar watersheds permitting flow and water quality predictions in response to climatic change scenarios. It can also offer a hydrologic link to the development of forest management plans.

References

Ahmed JA, Sarma AK (2005) Genetic algorithm for optimal operating policy of a multipurpose reservoir. J Water Resour Manage 19:145–161

Allen RG, Pereira LS, Raes D, Smith M (1998) Crop evapo-transpiration guidelines for computing crop water requirements. Proceedings of FAO irrigation and drainage, Paper No. 56, Food and Agriculture Organization of the United Nations, Rome, 1998

ASCE Task Committee (2000a) Application of artificial neural networks in hydrology. Artificial neural networks in hydrology I: preliminary concepts. J Hydrol Eng 5(2):115–123

ASCE Task Committee (2000b) Artificial neural networks in hydrology II. J Hydrol Engg 5(2):124–132

Bhatt VK, Bhattacharya P, Tiwari AK (2007) Application of artificial neural network in estimation of rainfall erosivity. Hydrol J 1–2(March–June):30–39

Brutsaert WH (1982) Evaporation into the atmosphere: theory, history and applications. Springer, Boston, p 299

Burn DH, Yulianti JS (2001) Waste-load allocation using genetic algorithms. J Water Resour Plan Manage ASCE 127(2):121–129

Domingo F, Sanchez G, Moro MJ, Brenner AJ, Puigdefabregas J (1998): Measurement and model-
    ling of rainfall interception by three semi-arid canopies. Agric For Meteor 91:275–292
Fahlam SE (1988) An empirical study of learning speed in back-propagation networks. Technical
    Report cwU-CS-88-w, June 1988
Flint AL, Childs SW (1991) Use of the Priestleye Taylor evaporation equation for soil water
    limited conditions in a small forest clearcut. Agric Forest Meteorol 56:247–260
Hargreaves GH, Samani ZA (1985) Reference crop evapo-transpiration from temperature. Appl
    Eng Agric 1(2):96–99
Hassoun MH (1995) Fundamentals of artificial neural networks. MIT Press, Cambridge, MA
Jain A, Prasad Indurthy SKV (2003) Comparative analysis of event-based rainfall-runoff modeling
    techniques – deterministic, statistical, and artificial neural networks, March/April. J Hydrol
    Eng 8:93–98
Jensen ME, Burman RD, Allen RG (1990) Evapotranspiration and irrigation water requirements.
    ASCE manuals and reports on engineering practices no. 70, New York
Kisi O (2004) Multilayer perceptrons with Levenberg–Marquardt training algorithm for suspended
    sediment concentration prediction and estimation. Hydrol Sci J 49(6):1025–1040
Kisi O (2006) Evapotranspiration estimation using feed-forward neural networks. Nord Hydrol
    37(3):247–260
Kişi Ö (2007) Streamflow forecasting using different artificial neural network algorithms. J Hydrol
    Eng 12(5):532–539
Kumar M, Raghuwanshi NS, Singh R, Wallender WW, Pruitt WO (2002) Estimating evapotrans-
    piration using artificial neural network. J Irrig Drain Eng 128(4):224–233
Majumder M, Barman RN, Roy P, Jana BK, Mazumdar A (2009) Application of neuro-genetic
    algorithm to determine reservoir response in different hydrologic adversaries. J Soil Water
    Resour 4(1):17–27
Malek E, Bingham GE (1993) Comparison of the Bowen ratio-energy balance and the
    water balance methods for the measurement of evapo-transpiration. J Hydrol (Amsterdam)
    146(1–4):209–220
Malek E (2003) Microclimate of a desert playa: evaluation of annual radiation, energy, and water
    budgets components. Int J Climatol 23:333–345
Montieth JL (1965) Evaporation and environment. Symp Soc Exp Biol 19:205–234
Morton FI (1983) Operational estimates of areal evapo-transpiration and their significance to the
    science and practice of hydrology. J Hydrol 66(1–4):1–76
Naoum S, Tsanis IK (2003) Hydroinformatics in evapotranspiration estimation. Environ Modell
    Software 18:261–271
Nash JE, Sutcliffe JV (1970) River flow forecasting through conceptual models. J Hydrol 10:282–290
Parasuraman K, Elshorbagy A (2007) Cluster-based hydrologic prediction using genetic
    algorithm-trained neural networks. J Hydrol Eng 12:52–64
Penman HL (1948) Natural evaporation from open water bare soil and grass, proceedings of the
    Royal Society of London, Series A. Math Phys Sci 193:120–146
Priestley CHB, Taylor RJ (1972) On the assessment of surface heat flux and evaporation using
    large scale parameters. Mon Wea Rev 100:81–92
Roy P, Roy D, Mazumdar A (2004) An impact assessment of climate change and water resources
    availability of Damodar river basin. Hydrol J 27(3–4):53–70
Smith M, Allen R, Pereira L (1997) Revised FAO methodology for crop water requirements. Land
    and Water Development Division, FAO, Rome
Sudheer KP, Gosain AK, Ramasastri KS (2003) Estimating actual evapo-transpiration from limited
    climatic data using neural computing technique. J Irrig Drain Eng 129(3):214–218
Sudheer KP (2005) Knowledge extraction from trained neural network river flow models. J Hydrol
    Eng 10(4):264–269
Tracy JC, Marinõ MA, Taghavi SA (1992) Predicting water demand in agricultural regions using
    time series forecasts of reference crop evapo-transpiration. In: Karamouz M (ed) Water
    resources planning and management: saving a threatened resource-In search of solutions.
    ASCE, New York, pp 50–55

Trajkovic S, Todorovic B, Stankovic M (2003) Forecasting reference evapotranspiration by artificial neural networks. J Irrig Drain Eng 129(6):454–457

Trajkovic S (2005) Temperature-based approaches for estimating reference evapotranspiration. J Irrig Drain Eng 131(4):316–323

US Army Corps of Engineers, Hydrologic Engineering Center (HEC) (2000) Hydrologic Modeling System, HECHMS: Technical Reference Manual. CPD-74B. US Army Corps of Engineers, Hydrologic Engineering Center, Davis, CA, http://www.hec.usace.army.mil/software/hec-hms/documentation/hms_technical.pdf, 2000

Wang QJ (1991) The genetic algorithm and its application to calibrating conceptual rainfall-runoff models. Water Resour Res 27(9):2467–2471

Wardlaw R, Sharif M (1999) Evaluation of genetic algorithms for optimal reservoir system operation. J Water Resour Plann Manage 125(1):25–33

Chapter 14
Determination of Urban and Rural Monsoonal Evapotranspiration by Neurogenetic Models

Chinmoy Boral, Mrinmoy Majumder, and Debasri Roy

Abstract Evaporation measurement is widely used to estimate free water surface evaporation and is of crucial consideration in water resource development project. Evaporation is influenced by air temperature, relative humidity, wind speed, sunshine, etc. In this chapter, an attempt has been made to study the effect of the above-noted factors on reference evapotranspiration. In the present study, a Clusterized Artificial Neural Network (CANN) model was developed to estimate daily mean evapotranspiration from measured meteorological data of a tropical metro city and a rural area. The CANN model was compared with Time Series Model (TSM), Least Square Estimation Model (LSEM), and Mayer's Method (MM) to validate the estimation. Evapotranspiration estimated by CANN model was found to yield values closest to observe ones and according to the estimation, for extreme values of the input parameters there is a difference between the outputs received for the considered two cities where the main cause for the difference was identified as rainfall.

C. Boral
Pertime Researcher, School of Water Resources Engineering, Jadavpur University, Kolkata-700032, West Bengal, India
e-mail: chinmoy_boral1@yahoo.co.in

M. Majumder
Senior Research Fellow, School of Water Resources Engineering, Jadavpur University, Kolkata-700032, West Bengal, India
and
Geo-information Scientist, Regional Center, National Afforestation
and Eco-development Board, Jadavpur University, Kolkata-700032, West Bengal, India

D. Roy
Reader and Joint Director, School of Water Resources Engineering, Jadavpur University, Kolkata-700032, West Bengal, India

14.1   Introduction

Evaporation is an important meteorological parameter that affects both plant and animal life. The process of evaporation is influenced by a large number of meteorological factors such as air temperature, relative humidity, wind speed, bright sunshine duration, atmospheric pressure, etc. These parameters in turn depend upon other factors such as geographical location, season, time of day, etc. (Subramanya 2005).

The influence of meteorological parameters on evaporation was studied by several investigators (Stephens and Stewart 1963; Linarce 1967; Burman 1976; Khan 1992; Aishakh, 1998; Khanikar and Nath 1998; Xu and Singh 1998; Hordofa et al. 2003) in different parts of the world. Most of these estimations (e.g., Stephens and Stewart 1963) tried to fit a linear relationship between the variables. However, the process of evaporation is highly nonlinear in nature, as has been observed by Mahar and Dutta (2000) and should be addressed through better models that will address the inherent nonlinearity in the process.

14.1.1   Artificial Neural Network

Neural networks approaches have been successfully applied in a number of diverse fields, including water resources for estimation of various nonlinear functions. As neural network learns from the available data series, the accuracy of the estimation becomes impressive.

In hydrological context, recent experiments have reported that artificial neural networks (ANN) may offer a promising alternative for modeling hydrological variables, e.g., rainfall-runoff, stream flow, suspended sediment, etc (e.g., Ahmed and Sarma (2005); Allen et al. (1998); Allison (1992); ASCE Task Committee (2000a–c); Brutsaert (1982); Burn and Yulianti (2001); Clayton (1989); Domingo et al. (1999); Fahlam (1988); Flint and Childs (1991); Grubert (1994); Hassoun (1995); Jain and Prasad Indurthy (2003); Jensen et al. (1990); Keshari and Yadav (2005); Kisi (2004); Kişi (2007); Kişi and Öztürk (2007); Kisi and Yildirim (2005a, b); Malek and Bingham (1993); Malek (2003); Montieth (1965); Morton (1983); Morton (1969); Naoum (2003); Nash and Sutcliffe (1970); Parasuraman and Elshorbagy (2007); Penman (1948); Priestley and Taylor (1972); Roy et al. (2004); Smith et al. (1997); Sudheer et al. (2002); Todorovic and Stankovic (2005); and Tracy et al. (1992)). However, the application of ANN to evapotranspiration modeling is limited in the literature. Kumar et al. (2002) used a multilayer perceptron (MLP) with back-propagation training algorithm for the estimation of ET_0. They used various architectures and found that the ANN gave accurate ET_0 estimates. Sudheer et al. (2003) used radial basis ANN in modeling ET_0 using limited climatic data. Trajkovic et al. (2003) developed a radial basis ANN for forecasting ET_0.

Trajkovic (2005) used temperature-based radial basis ANN for modeling FAO-56 PM ET_0. He compared the ANN results with those of the Hargreaves and Samani (1985), Thornthwaite, and reduced PM methods and concluded that the

radial basis ANN generally performs better than the others in modeling the ET_0 process. Kisi (2006) investigated the estimation of ET_0 using multilayer perceptron (MLP) method and he compared ANN test results with those of the Penman and Hargreaves empirical models. He found that the MLP model gave much better results than the empirical models.

The ANN model of a physical system can be considered with n input neurons $(x_1, x_2, ..., x_n)$, h hidden neurons $(z_1, z_2, ..., z_n)$, and m output neurons $(y_1, y_2, ..., y_n)$. Let t_j be the bias for neuron z_j and f_k for neuron y_k. Let w_{ij} be the weight of the connection from neuron x_i to z_j and beta is the weight of the connection z_j to y_k. The function that ANN calculates is

$$y_k = g_A \left(\sum z_j b_{jk} + f_k \right)...\left(j = 1 - h \right) \tag{14.1}$$

in which,

$$z_j = f_A \left(\sum x_i w_{ij} + t_j \right)...\left(i = 1 - n \right) \tag{14.2}$$

where g_A and f_A are the activation functions (Sudheer 2005).

A neural network will have a structure, activation function, and learning rules, which will enable the network to learn the problem and estimate at a desired accuracy. There are numerous types of network structures available among which Recurrent Network, Radial Basis Function, Multi-layer Perceptron, Feed Forward, Associative, and Self-Organized networks are widely used. Some overviews of the mentioned networks are given next.

A detail description of artificial neural network is given in Chapter 22.

The network building procedure includes selection of network topology, which is selected by either trial and error method or by application of genetic algorithm (GA). In the present study, GA was used to find an optimum network topology. The next step is to train the network where the training dataset, which is generally a major portion of the available observed data was fed to the selected network for learning the pattern inherent in the data. In the present study, Quick Propagation (QP), Common Gradient Descent (CGD), and Levenberg–Marquardt (LM) were used to train the network. In the last step, a set of data, which was not used in the training were fed to the network for estimation. The error will show the amount of generalization loss that had incurred in the network. The testing procedure will also help to analyze the performance of the selected network.

14.1.2   Least Square Method

In least square method estimation if $y = a + bx$ be an equation of straight line to be fitted to a given set of a pairs of observations (x_1, y_1), (x_2, y_2), (x_3, y_3), …, (x_n, y_n). The values of a and b are so determined as to minimize $\sum (y_i - a - bx_i)^2$. This leads to the normal equations:

$$\sum y = a_n + b \sum x \tag{14.3}$$

$$\sum xy = a\sum x + b\sum x^2 \tag{14.4}$$

Here, the values of n, $\sum x$, $\sum y$, $\sum x$, and $\sum xy$ are substituted on the basis of given data. Then two equations involving a and b, solving the values of a and b are obtained (Das 1973).

14..1.3 Time Series Method

A series of observations recorded in accordance with the time occurrence is called Time Series where the values of a variable are observed chronologically by days, weeks, months, and years. Symbolically, the value of the variable related to time is denoted by y_i (Das 1973).

14.1.4 Mayer's Formula

Mayer's formula can be defined as

$$E_L = K_M \left(e_w - e_a\right)\left(1 + u_9 / u_9 1616\right) \tag{14.5}$$

where E_L = lake evaporation in mm/day, e_w = saturated vapor pressure at the water-surface temperature in mmHg, e_a = actual vapor pressure of overlying air at a specified height in mmHg, u_9 = monthly mean wind velocity in km/h at about 9 m above ground and KM = coefficient accounting for various other factors with a value of 0.36 for large, deep waters and 0.50 for small, shallow water (Subramanya 2005).

In the present study, effect of various meteorological parameters, namely daily mean air temperature (T_m), daily mean relative humidity (R_m), daily mean wind speed (U_m), daily mean dry bulb temperature (D_m), daily mean wet bulb temperature (W_m), daily mean cloud cover (C_m), daily mean pressure (P_m), daily mean rainfall (R_m), etc. on ET have been studied for the Alipore Station in the District of Kolkata in the State of West Bengal, India.

14.1.5 Model Validation

The accuracy of results obtained from the network is assessed by comparing its response with the validation set. The commonly used evaluation criteria include correct classification rate (CCR) (14.6), correlation coefficient (r) (14.7), and Standard Deviation (STDDEV) (14.8) (Bhatt et al. 2007).

$$CCR = \sum \left(T_c - O_c\right) / \sum \left(T_c - O_c\right) nn \tag{14.6}$$

$$r^2 = \begin{bmatrix} \left((T_p - T_m)(O_p - O_m)\right) / \left((T_p - T_m)(O_p - O_m)\right) \\ \sum \left(\sum_1^n (T_p - T_m)^2 \sum_1^n (O_p - O_m)^2 \right)^{1/122} \\ \left(\sum_1^n (T_p - T_m)^2 \sum_1^n (O_p - O_m)^2 \right)^{1/122} \end{bmatrix}$$ (14.7)

$$\text{STDDEV} = \frac{\sum_1^n (T_n - \bar{T}_n)^2}{n}$$ (14.8)

where, T_c are the clusterized target values; O_c is the clusterized estimated values, T_m and O_m are the mean target and estimated groups, respectively and n is the total number of patterns. T_p, O_p, T_n, and O_n are the target and observed values of the pth and nth pattern, respectively.

14.1.6 Study Area

In the present study, Kolkata, a metro city of West Bengal, India, and Burdwan, a district centre in central West Bengal was selected to estimate evapotranspiration with the help of CANN model. Kolkata is located in eastern India at 22.55°, 88.33° in the Ganges Delta at an elevation ranging between 1.5 m (5 ft) and 9 m (30 ft). The city area spread linearly along the banks of the River Hooghly in a north–south direction. Much of the city was originally a vast wetland, reclaimed over the decades to accommodate the city's burgeoning population. The remaining wetland, known as East Calcutta Wetlands has been designated a "wetland of international importance" under the Ramsar Convention.

According to the Bureau of Indian Standards, the town falls under seismic zone-III, in a scale of I–V (in order of increasing proneness to earthquakes) while the wind and cyclone zoning is "very high damage risk," according to UNDP report. Kolkata has a tropical wet-and-dry climate (Koppen climate classification Aw). The annual mean temperature is 26.8°C; monthly mean temperatures range from 19°C to 30°C. Summers are hot and humid with temperatures in the low 30°C and during dry spells the maximum temperatures often exceed 40°C during May and June. Winter tends to last for only about 2½ months, with seasonal lows dipping to 9–11°C between December and January. The highest recorded temperature is 43.9°C and the lowest is 5°C. On an average, May is the hottest month with daily temperatures ranging from a minimum of 27°C to a maximum of 37°C, while January, the coldest month, has temperatures varying from a minimum of 12°C to a maximum of 23°C. Rains brought by the Bay of Bengal branch of southwest monsoon enters the city between June and September and supplies the city with most of its annual rainfall of 1,582 mm. The highest rainfall occurs during the monsoon in August – 306 mm. The city receives 2,528 h of sunshine per annum, with the maximum sunlight occurring in March.

14.2   Methodology

Daily maximum and minimum air temperatures, relative humidity, wind speed, dry bulb temperature, wet bulb temperature, cloud cover, air pressure, and rainfall data were collected for Alipore Station for the period spanning over 1970–2003. The daily meteorological data like T_m, R_m, U_m, D_m, W_m, C_m, P_m, R_m were considered as Input whereas daily mean evapotranspiration was taken as Output. The TSM, LSEM, MM, and CANN were used to estimate evaporation.

14.2.1   Development of CANN Model

All the daily mean meteorological data along with ET were ranked where highest value receives the smallest rank (i.e., 1) and lowest value receives the largest rank. The entire dataset was then grouped into six groups, namely,

"P1" – data ranked within 1–5 was grouped under P1
"P2" – data ranked within 6–50 was grouped under P2
"P3" – data ranked within 51–180 was grouped under P3
"t3" – data ranked within 181–280 was grouped under t3
"t2" – data ranked within 281–387 was grouped under t2
"t1" – data ranked within 387 to end was grouped under t1

This grouped data were fed to the models for estimation of ET. The normal procedures to develop neural network were followed and after getting satisfactory results extreme values of ET were estimated for extreme values of metereologic parameters considered in the study.

14.2.2   Model Validation

Similarly, TSM, LSM, and MM were also used to estimate ET. The results were compared with observed values of ET and according to model validation criteria the better model was selected. The estimated ET for normal and extreme conditions of both Kolkata and Burdwan was now compared to analyze the impact of other metereological parameters and change of geographic location on ET.

14.2.3   Estimation of ET for Extreme Values

The selected model was used to predict ET for extreme values of the input parameters. Climatic uncertainty will cause either large or least amount of rainfall. The value of ET for extreme conditions of rainfall could estimate the impact of climatic uncertainty on

availability of water as water availability is inversely proportional to ET. The ET for extreme values of climatic parameters was predicted for both Kolkata and Burdwan.

14.3   Result and Discussion

The relationships between evapotranspiration and meteorological parameters for the Alipore Station along with corresponding correlation coefficient have been shown in Table 14.1.

From the comparison of observed and estimated dataset, r^2 values from QP_K model were found to be highest (0.99) and for Mayer's Model it was lowest (0.95). Although, corresponding values of r^2 for all of the neural network models were found to be equal to 0.99.

The comparison of observed and estimated Correct Classification Rate (CCR) values of the considered models was found to be highest (71.31) for CGD_B model and lowest for Time series (0.55) model. Within the CANN models of Kolkata the highest CCR was observed for QP_K (0.49) and the same for Burdwan was found from CGD_B (0.63).

The STDDEV values calculated from the observed and estimated dataset were found to be highest for the QP model (71.01) and lowest for Time series model. Within the neural network models of Kolkata and Bardhaman QP_K and CGD_B were found to have the higher STDDEV values, respectively (Fig. 14. 1).

Table 14.1 Table showing comparison of the performance validation criteria within the developed models

	CCR	r^2	STDDEV
QP_K	0.49	0.99	0.71
CGD_K	0.42	0.99	0.66
BBP_K	0.41	0.99	0.67
QP_B	0.59	0.99	0.67
CGD_B	0.63	0.99	0.75
BBP_B	0.44	0.99	0.65
LSM	0.62	0.96	0.55
TSM	0.55	0.96	0.49
MM	0.6	0.95	0.56

Note 1: QP_K, CGD_K, and BBP_K are the CANN models trained with, respectively, QP, CGD, and BBP algorithm with the dataset of Kolkata and QP_B, CGD_B, and BBP_B are the CANN model trained with, respectively, QP, CGD, and BBP algorithm with the dataset of Burdwan

Note 2: STDDEV and r^2 were calculated by comparing the numerical values of the observed and estimated groups of the dataset
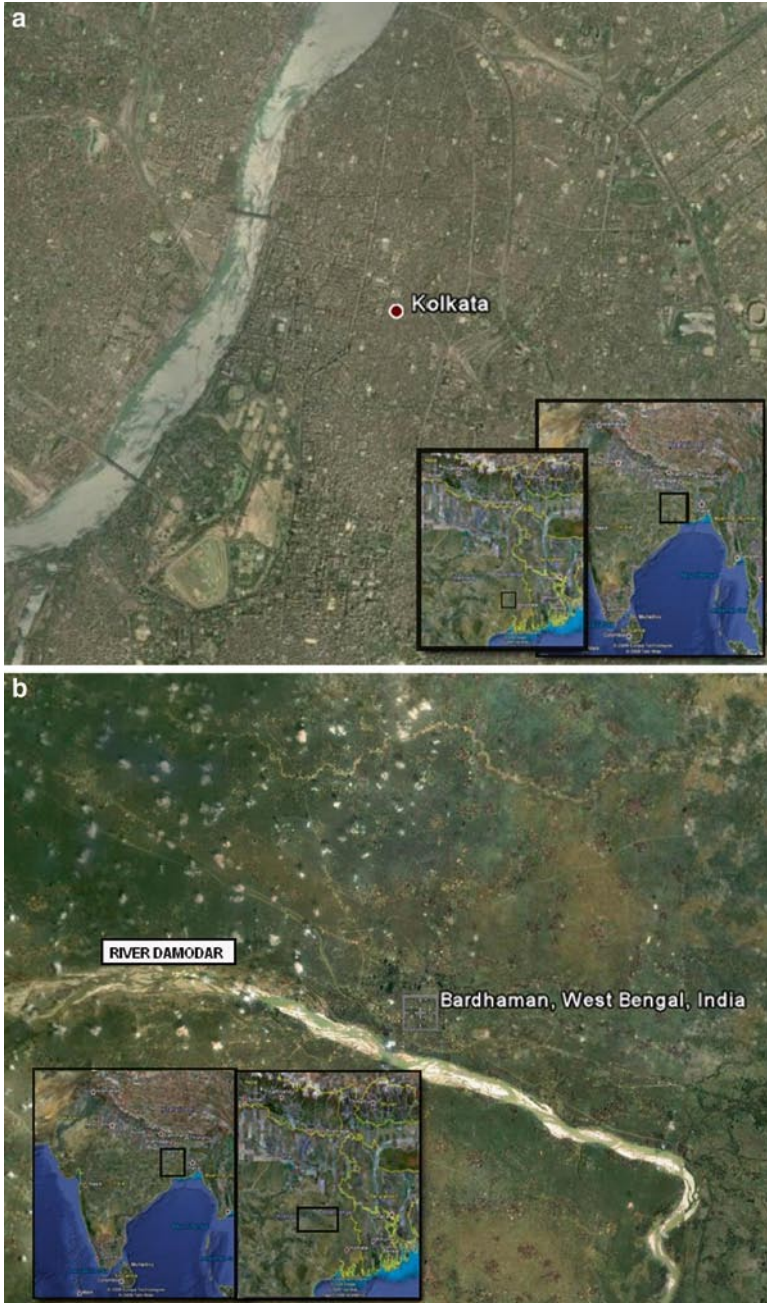
Fig. 14.1 Figure showing the location of (**a**) Kolkata metro city and (**b**) Bardhaman rural areas

According to the applied performance validation criteria, efficiency of CANN model trained with QP, CGD, and BBP was found to be greater than TSM, LSM, and MM models. Among the training algorithms, QP and CGD were found to be the best performing algorithms, respectively for CANN model developed for Kolkata and Burdwan. The QP_K and CGD_B models were used to estimate ET for extreme values of rainfall.

According to the estimation, for peak values of rainfall, temperature, and cloud cover the ET value of Kolkata and Burdwan will be P3 and P2, respectively. Both P3 and P2 groups denote values of higher order, which could derive a conclusion that for peak values of rainfall and other related parameters ET will not be high as the inputs, but will lie at a higher range. If ET of Kolkata and Burdwan is compared, Kolkata would have lower ET than Burdwan.

For low values of rainfall, temperature, and other parameters, ET was found to be in the t3 and t2 group, respectively for Kolkata and Burdwan. t3 and t2 groups had low values of ET, but not as low as the groups of input parameters considered for the estimation. This result implies that even if rainfall and other metereological parameters had low magnitude ET will lie in the midvalues observed in the last 3 decades; when ET of Kolkata and Burdwan was compared, higher values of ET were estimated for Kolkata than that of Burdwan.

The results as discussed in the above parameters clearly indicate that ET is influenced by geographic as well as metereological differences though variation of rainfall of the two places seems to be a major reason for this difference.

14.4   Conclusions

The present study tried to estimate evapotranspiration from various meteorological dataset of Kolkata and Burdwan, two cities of West Bengal, India, with the help of CANN model to observe the difference, if any, within the values of ET of the two cities. The two cities were located in different climatological zones but within the tropic of cancer. The main objective of the study was to identify the cause of the difference, if any, observed in the values of ET of the two cities. The dataset of 32 years (1970–2002), grouped into six groups according to the magnitude of the parameters, was used to develop a neural network model, CANN. Similar models were made with the help of least square, time series, and Mayer's method. r^2, STDDEV, and CCR was calculated from the observed and estimated dataset to select the better model among the four models considered. The selected models were applied to predict ET for extreme values of rainfall and other metereological parameters. According to the results, CANN model was found to be the better model among the models developed for both Kolkata and Burdwan. The estimation of ET for extreme values of the input parameters

showed that there is a difference between the responses received from the models of the two cities where the main cause of the difference was identified as rainfall. The neural network models had a major drawback that these models were not problem sensitive. Different models were required to be developed for similar problems of different area. The CANN model attempts to solve the problem by using classified groups instead of data values for training the model. When the same model is applied for a different study area, if the model is trained with the grouped dataset the same CANN model could be applied for that study area also. But the present neural network model has a disadvantage as the model is unusable when numerical values of ET are required. The CANN models could be improved if catchment-specific variables like soil, elevation, amount of water body, etc. were included as input parameters.

References

Ahmed JA, Sarma AK (2005) Genetic algorithm for optimal operating policy of a multipurpose reservoir. J Water Resour Manage 19:145–161

Aishakh A (1998) Analysis of evaporation data as climate factors in arid regions. Water and land resources development and management for sustainable use. The tenth ICID Afro-Asian regional conference on irrigation and drainage. Denpasar, July 19–26, 1998, Bali, Indonesia

Allen RG, Pereira LS, Raes D, Smith M (1998) Crop evapo-transpiration guidelines for computing crop water requirements. Proceedings of FAO irrigation and drainage, Paper no. 56, Food and Agriculture Organization of the United Nations, Rome

Allison C (1992) Neural network. Sigma press, Wilmslow

ASCE Task Committee (2000a) Artificial neural networks in hydrology. II: hydrological applications. J Hydrol Eng ASCE 5(2):124–137

ASCE Task Committee (2000b) Application of artificial neural networks in hydrology. Artificial neural networks in Hydrology I: preliminary concepts. J Hydrol Eng 5(2):115–123

ASCE Task Committee (2000c) Artificial neural networks in hydrology II. J. Hydrol Eng 5(2):124–132

Bhatt VK, Bhattacharya P, Tiwari AK (2007) Application of artificial neural network in estimation of rainfall erosivity. Hydrol J 1–2(March–June):30–39

Brutsaert WH (1982) Evaporation into the atmosphere. Reidel, Dordrecht, Holland

Burman RD (1976) Intercontinental comparison of evaporation estimates. ASCE J Irrig Drain Eng 102:109–118

Burn DH, Yulianti JS (2001) Waste-load allocation using genetic algorithms. J Water Resour Plan Manage ASCE 127(2):121–129

Clayton LH (1989) Prediction of class A pan evaporation in south Idaho. ASCE J Irrig Drain Eng 115(2):166–171

Das NG (1973) Staiistical method. Published by M. Das, 238, Manicktala Main Road (Suite no. 15) Kolkata – 54, pp 320, 483

Domingo F, Villagarcía L, Brenner AJ, Puigdefábregas J (1999) Evapotranspiration model for semi-arid shrub-lands tested against data from SE Spain. J Agric Forest Meteorol 95(2):67–84

Fahlam SE (1988) An empirical study of learning speed in back-propagation networks. Technical report cwU-CS-88- w, June

Flint AL, Childs SW (1991) Use of the Priestleye Taylor evaporation equation for soil water limited conditions in a small forest clearcut. Agric Forest Meteorol 56:247–260

Grubert JP (1994) "Prediction of interfacial instabilities in estuaries using neural networks". MSc dissertation in computer studies, University of Glamorgan, UK

Hargreaves GH, Samani ZA (1985) Reference crop evapotranspiration from temperature. Appl Eng Agric 1(2):96–99

Hassoun MH (1995) Fundamentals of artificial neural networks. MIT Press, Cambridge, MA

Hordofa T, Sharma A, Singh R, Dashora PK (2003) Dependence of evaporation on meteorological parameters under arid and semi-arid climatic conditions of Ethiopia. Ethiopian Agricultural Research Organization, Box 2003, Addis Ababa, Ethiopia

Jain A, Prasad Indurthy SKV (2003) Comparative analysis of event-based rainfall-runoff modeling techniques – deterministic, statistical, and artificial neural networks. J Hydrol Eng 8:93–98

Jensen ME, Burman RD, Allen RG (1990) Evapotranspiration and irrigation water requirements. ASCE manuals and reports on engineering practices no. 70, New York

Keshari AK, Yadav BK (2005 (Sept–Dec)) Inflow forecasting for flat bay, Andaman and Nicobar Island using artificial neural network. Hydrol J 28(3–4):1–15

Khan SRA (1992) Agricultural development potential of cholistan desert. N.L.C.C.H., Lahore: 127pp

Khanikar PG, Nath KK (1998) Relationship of open pan evaporation rate with some important meteorological parameters. J Agri Sci Soc Northeast India 11(1):46–50

Kisi O (2004) Multilayer perceptrons with Levenberg–Marquardt training algorithm for suspended sediment concentration prediction and estimation. Hydrol Sci J 49(6):1025–1040

Kisi O (2006) Evapotranspiration estimation using feed-forward neural networks. Nord Hydrol 37(3):247–260

Kişi Ö (2007) Streamflow forecasting using different artificial neural network algorithms. J Hydrol Eng 12(5):532–539

Kişi Ö, Öztürk Ö (2007) Adaptive neurofuzzy computing technique for evapotranspiration estimation. J Irrig Drain Eng 133(4):368–379

Kisi O, Yildirim G (2005a) Discussion of "estimating actual evapotranspiration from limited climatic data using neural computing technique" by Sudheer KP, Gosain AK, and Ramasastri KS. ASCE J Irrig Drain Eng 131(2):219–220

Kisi O, Yildirim G (2005b) Discussion of "forecasting of reference evapotranspiration by artificial neural networks" by Trajkovic S, Todorovic B, Stankovic M. ASCE J Irrig Drain Eng 131(4): 390–391

Kumar M, Raghuwanshi NS, Singh R, Wallender WW, Pruitt WO (2002) Estimating evapotranspiration using artificial neural network. J Irrig Drain Eng 128(4):224–233

Linacre ET (1967) Further studies of the heat transfer from a leaf. Plant Physiology 42:651–658

Mahar PS, Bithin Datta (2000) Identification of pollution sources in transient groundwater systems. Water Resources Management 14(3):209–227

Malek E, Bingham GE (1993) Comparison of the Bowen ratio-energy balance and the water balance methods for the measurement of evapo-transpiration. J Hydrol (Amsterdam) 146(1–4):209–220

Malek E (2003) Microclimate of a desert playa: evaluation of annual radiation, energy, and water budgets components. Int J Climatol 23:333–345

Montieth JL (1965) Evaporation and environment. Symp Soc Exp Biol 19:205–234

Morton FI (1983) Operational estimates of areal evapo-transpiration and their significance to the science and practice of hydrology. J Hydrol 66(1–4):1–76

Morton FI (1969) Potential evaporation as a manifestation of regional evaporation. Water Resour Res 5(6):1244–1255

Naoum S, Tsanis IK (2003) Hydroinformatics in evapotranspiration estimation. Environ Modell Software 18:261–271

Nash JE, Sutcliffe JV (1970) River flow forecasting through conceptual models. J Hydrol 10:282–290

Parasuraman K, Elshorbagy A (2007) Cluster-based hydrologic prediction using genetic algorithm-trained neural networks. J Hydrol Eng 12(ASCE):52–62

Penman HL (1948) Natural evaporation from open water, bare soil and grass. Proc Roy Soc Lond Ser A Math Phys Sci 193:120–146

Priestley CHB, Taylor RJ (1972) On the assessment of surface heat flux and evaporation using large scale parameters. Mon Wea Rev 100:81–92

Roy P, Roy D, Mazumdar A (2004) An impact assessment of climate change and water resources availability of Damodar River basin. Hydrol J 27(3–4):53–70

Smith M, Allen R, Pereira L (1997) Revised FAO methodology for crop water requirements. Land and Water Development Division, FAO, Rome

Stephens JC, Stewart EH (1963) A comparison of procedures for computing evaporation and evapo-transpiration, general assembly of Berkeley, 123–133, IAHS Publ No. 62

Subramanya K (2005) Engineering hydrology. Tata McGraw-Hill, New Delhi, pp 58–64

Sudheer KP, Gosain AK, Rangan DM, Saheb SM (2002) Modelling evaporation using an artificial neural network algorithm. Hydrol Process 16:3189–3202

Sudheer KP, Gosain AK, Ramasastri KS (2003) Estimating actual evapotranspiration from limited climatic data using neural computing technique. J Irrig Drain Eng 129(3):214–218

Sudheer KP (2005) Knowledge extraction from trained neural network river flow models. J Hydrol Eng 10(4):264–269

Todorovic S, Stankovic M (2005) ASCE J Irrig Drain Eng 131(4):390–391

Tracy JC, Marin˜o MA, Taghavi SA (1992) Predicting water demand in agricultural regions using time series forecasts of reference crop evapo-transpiration. In: Karamouz M (ed) Water resources planning and management: saving a threatened resource – in search of solutions. ASCE, New York, pp 50–55

Trajkovic S, Todorovic B, Stankovic M (2003) Forecasting reference evapotranspiration by artificial neural networks. J Irrig Drain Eng 129(6):454–457

Trajkovic S (2005) Temperature-based approaches for estimating reference evapotranspiration. J Irrig Drain Eng 131(4):316–323

Xu C-Y*, Singh VP (1998) A review on monthly water balance models for water resources investigation and climatic impact assessment. Water Resources Management 12:31–50

Part II
Natural Resource Management: Mitigating the Impact

Chapter 15
Accumulation of Carbon Stock Through Plantation in Urban Area

Bipal K. Jana, Soumyajit Biswas, Mrinmoy Majumder, Pankaj Roy, and Asis Mazumdar

Abstract Emission of carbon dioxide (CO_2) in urban area is higher compared to the rural area due to the presence of different emission sources within a small area. Carbon is sequestered by the plant photosynthesis and stored as biomass in different parts of the tree. Carbon sequestration rate (CSR) has been measured for young species (6 years age) of *Albizzia lebbek* in Indian Botanic Garden in Howrah district and *Artocarpus integrifolia* at Banobitan within Kolkata in the lower Gangetic plain of West Bengal in India by Automated Vaisala Made Instrument, GMP343 and aboveground biomass carbon has been analyzed by CHN analyzer. The specific objective of this article is to measure carbon sequestration rate and

B.K. Jana (✉)
Senior Research Fellow, School of Water Resources Engineering, Jadavpur University, Kolkata-700032, West Bengal, India
and
Environmental Manager, Consulting Engineering Services, West Bengal, India
e-mail: bipalkjana@gmail.com

S. Biswas
Research Fellow, School of Water Resources Engineering, Jadavpur University, Kolkata-700032, West Bengal, India

M. Majumder
Senior Research Fellow, School of Water Resources Engineering, Jadavpur University, Kolkata-700032, West Bengal, India
and
Geo-information Scientist, Regional Center, National Afforestation and Eco-development Board, Jadavpur University, Kolkata-700032, West Bengal, India

P. Roy
Lecturer, School of Water Resources Engineering, Jadavpur University, Kolkata-700032, West Bengal, India

A. Mazumdar
Coordinator, Regional Center, National Afforestation and Eco-development Board, Jadavpur University, Kolkata-700032, West Bengal, India
and
Director, School of Water Resources Engineering, Jadavpur University, Kolkata-700032, West Bengal, India

accumulation of biomass carbon stock of two young species of *A. lebbek* and *A. integrifolia*. The carbon sequestration rates (mean) as CO_2 from the ambient air as obtained by *A. lebbek* and *A. integrifolia* were 14.86 and 4.22 g/h, respectively. The annual carbon sequestration rates from ambient air were estimated at 11.97 t C/ ha by *A. lebbek* and 3.33 t C/ha by *A. integrifolia*. The percentages of carbon content (except root) in the aboveground biomass of *A. lebbek* and *A. integrifolia* were 47.12 and 43.33, respectively. The total accumulated aboveground biomass carbon stocks in 6 years as estimated for *A. lebbek* and *A. integrifolia* were 6.26 and 7.28 t C/ha, respectively, in these forest stands. Therefore, urban plantation based on better carbon sequestrated species will help to accumulate more biomass carbon stock as well as to offset the increasing CO_2 level in ambient air.

15.1 Introduction

Carbon exists in different natural stocks in the environment. One of the natural stocks is terrestrial system where carbon is sequestrated in rocks, water bodies, green plants and trees, and in the soils of open areas, grasslands, and agricultural land. The role of plants and trees in carbon sequestration in urban area is probably best understood and appears to offer the greatest opportunity as a sink. Carbon is sequestrated in the process of plant growth as carbon is captured in plant cell formation. As the tree biomass experiences growth, the carbon held by the plant also increases carbon stock. Simultaneously, plants grow on the plantation floor and add to this carbon store. Over time, branches, leaves, and other materials fall to the plantation floor and may store carbon until they decompose. Again, soils of the green areas may sequester some of the decomposing plant litter through root–soil interactions. Photosynthesis is a very important vital process by which the green plants synthesize organic matter in the presence of light, carbon dioxide, and water. Photosynthesis is sometimes called as carbon assimilation and is represented by the following traditional equation.

$$6CO_2 + 12H_2O \xrightarrow[\text{GreenPlant}]{\text{Light}} 6O_2 + 6H_2O + \underset{\text{HexoseSugar}}{C_6H_{12}O_6} \tag{15.1}$$
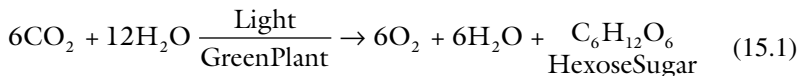
During the process of photosynthesis, the light energy is converted into chemical energy and is stored in the organic matters, which are usually the carbohydrate and along with O_2 forms the end products of photosynthesis.

Work of Veld and Plantinga (2005) reported that the rate of carbon storage increased in young stands, but then declined as the stand ages. An observation from a study on pine species planted on former cropland in the southeastern USA, the rate of carbon storage begins to decline approximately at the age of 20 and is close to zero by the age of 100 (Veld and Plantinga 2005). As the tree biomass experiences growth, the carbon held by the plant also increases carbon stock. The rate of carbon storage increases in

young stands, but then declines as the stand ages. Increasing the atmospheric CO_2 concentration stimulates the photosynthetic rate of trees and can result in increased growth rates and biomass production. Results from free air CO_2 enrichment (FACE) experiments show a 25% increase in growth in twice normal concentrations of CO_2. Growth is therefore almost always higher in air with an elevated concentration of CO_2 (Burley et al. 2004). Lal and Singh (2000) reported that estimated annual carbon uptake increment by Indian forests and plantations has been able to remove about 0.12 Gt of CO_2 from the atmosphere in the year 1995. Ravindranath et al. (1997) reported that the Indian forests based on the forest sector of the year 1986 could sequester around 5 Tg C (1 Tg = Tera gram, 10^{12} g). Haripriya (2003) noted that on the average biomass carbon of the forest ecosystems in India for the year 1994 was 46 Mg C/ha, of which nearly 76% was in aboveground biomass and the rest was in fine and coarse root biomass. The total carbon stock (wood only) for India was 1,085.06 and 1,083.69 Mt in 1984 and 1994, respectively (Manhas et al. 2006). Vast forest areas in India as well as its different provincial states accumulated a large amount of carbon as CO_2 from the atmosphere and play an important role for sequestrating carbon in the regional, national, and world scenarios. Terrestrial (plant and soil) carbon was estimated at 2,000 ± 500 Pg, which represented 25% of global carbon stocks. This review gave a description of a few agroforestry systems practiced in the tropics in relation to their C sequestration potential. The analysis of C stocks from various parts of the world showed that significant quantities of C (1.1–2.2 Pg) could be removed from the atmosphere over the next 50 years if agroforestry systems are implemented on a global scale (FSI 2005).

This study emphasizes the diurnal carbon sequestration rate (CSR) and accumulated aboveground biomass carbon stock of young (6 years age) *Albizzia lebbek* (Sirish) and *Artocarpus integrifolia* (Jackfruit). The sites were located at Indian Botanic Garden in Howrah district for *A. lebbek* and at Banobitan within Kolkata for *A. integrifolia* of the state of West Bengal in India. All the sites are located in the lower Gangetic plain. The study has been carried out by the Regional Centre of National Afforestation & Ecodevelopment Board (NAEB), Ministry of Environment & Forest, Government of India, Jadavpur University in association with the School of Water Resources Engineering, and Jadavpur University in Kolkata. The specific objective of this study is to measure carbon sequestration rate and accumulated aboveground biomass carbon potential of these young plant species.

15.2   The Site and Study Area

Kolkata Metro City is the heart of Kolkata Metropolitan Area (KMA) and Kolkata Municipal Corporation (KMC) is the administrative body of this city. As per the Directorate of Census Operation, West Bengal 2001, the geographical area of Kolkata is 185 km² which is 0.21% of the total area of West Bengal and 5.56% of the total urban area of West Bengal (Directorate of Census, 2001, West Bengal India). Kolkata city with its large infrastructure and dense population is emanating carbon dioxide (a major GHG) from vehicular exhaust, small-scale industries, commercial shops and hotels, residential fuel burning, human respiration, etc. The area of Kolkata Metro city is flat, and it is a part of the lower Bengal delta.

The sites and study areas for measurement of carbon sequestration rate and accumulated aboveground biomass carbon potential of *A. lebbek* (Sirish) and *A. integrifolia* (Jackfruit) are described here. The Indian Botanic Garden, established in 1787, is situated on the west bank of the river Ganga (Hooghly) in Howrah district of West Bengal, India. The location of Indian Botanic Garden is shown in Fig. 15.1. It is located at a distance of 8 km from Howrah railway station and 25 km from Calcutta International Airport (Netaji International Airport). The Indian Botanic Garden covered an area of about 110.52 ha. The garden was divided into 25 sections or divisions. There were 24 lakes in the garden. The garden was the living respiratory of more than 12,000 trees, shrubs, and climbers representing over 1,400 species together with a large number of wild and cultivated herbs. The "Central National Herbarium" is housing more than 2 million herbarium specimens. The "Great Banyan Tree," which is more than 250 years old is one of the main attractions of this garden, and it is mentioned in "Guinness's Book of World Records" (Chowdhery 2001). The selected plant species was *A. lebbek* of 6 years age (Fig. 15.2). It had a height of 5 m. It was
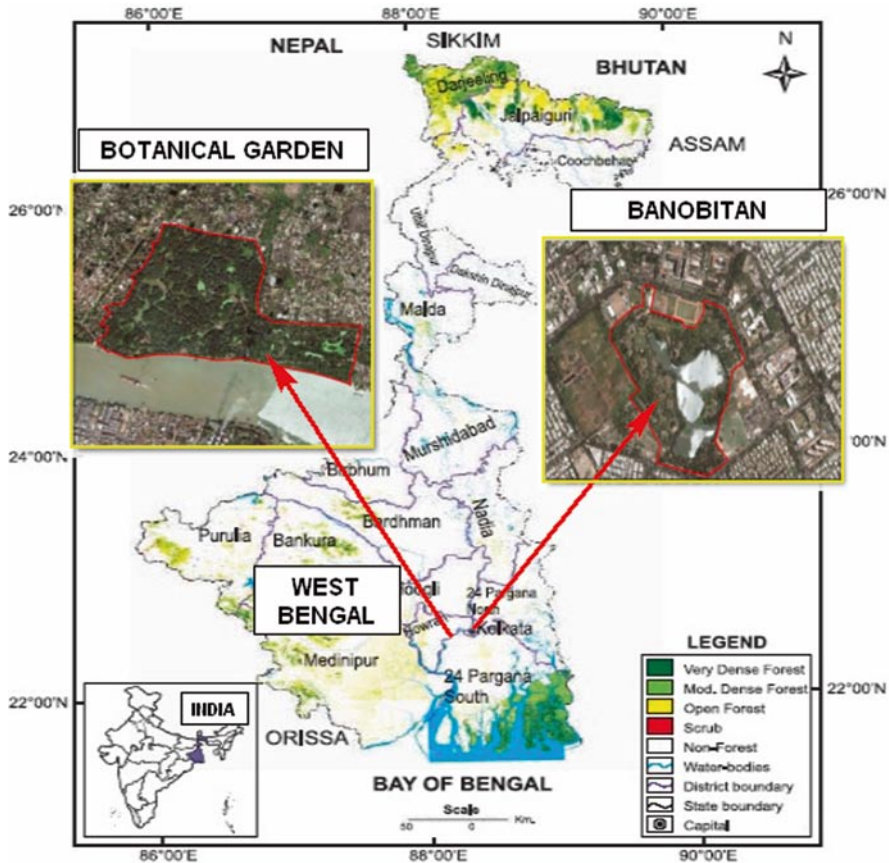
Fig. 15.1 Location of Indian Botanic Garden and Banobitan sites

Fig. 15.2 *Albizzia lebbek* at Botanic Garden and *Artocarpus integrifolia* at Banobitan

situated just in front of the Central National Herbarium (CNH) building. This monitoring site was located at a distance of 500 m from the main gate. The elevation of the working site, as measured by GPS, was Latitude 22°33.42′N and Longitude 88°17.25′E. Altitude of the area was 12 m above MSL. The general climate of the area was seasonal tropical. The climatological data have been collated from Alipur observatory, Indian Meteorological Department, GOI (1991–2005). The mean daily ambient temperature in the area varied from 15°C to 35°C with mean relative humidity ranged from 53% to 86%. The area received an average annual rainfall of 1,823 mm. Texturally the soil of the study area was classified as silty clay.

Banobitan is one of the largest man-made urban forest at Salt Lake in Kolkata Metro City on the east bank of the river Ganga (Hooghly) under the Forest Department of Government of West Bengal. It is also known as Central Park. The location of Banobitan is shown in Fig. 15. 1. It has varieties of plant species among which few were very rare and uncommon. But as it is used for a visiting place in Kolkata, the plant species were not so dense. The garden was very well maintained for the plant species. It has a large lake inside the garden. The selected plant species was Jackfruit, *A. integrifolia* of 6 years of age (Fig. 15. 2). The tree was located at a distance of around 250 m from the main entrance of the forest and 20 m from the lake and situated on left side of the lake. The plant species had a suitable height of 5 m.

15.3   Materials and Methods

15.3.1   *Carbon Dioxide Measurement*

Carbon dioxide (CO_2) has been measured by Automated Vaisala Made Instrument, GMP343 and the data have been collected continuously for 24 h. CO_2 has been measured for: (i) ambient air within and outside the forest areas and (ii) carbon

sequestration rate as CO_2 from ambient air of two young species. Ambient CO_2 monitoring has been carried out for 24 h within and outside the forest areas depending upon the wind direction to measure the CO_2 intake by the forest patch. Carbon sequestration rate has been measured for the particular tree in closed top chamber (CTC) covered with transparent plastic. Like other factors, influence of humidity on carbon sequestration rate of the plant has been ignored to emphasize the carbon sequestration study.

15.3.2   Measurement of Aboveground Biomass of the Tree

The biomass of the tree within a forest includes aboveground biomass, which includes all aboveground living materials (stem, branches, leaves) and belowground or root biomass, which consists of coarse roots and stumps. Biomass of the stem mainly includes the branches. The estimation of the biomass in the stem was performed by knowing the tree height, diameter, and girth size at different heights. These have been measured by Spiegel Relascope and wood volume of the whole tree has been calculated by these data. Weight of the wood biomass has been calculated by multiplying volume of biomass and specific gravity (SG) of the wood, as per the below-mentioned calculation where specific gravity (SG) is the ratio of oven dry weight and green volume of the pieces of wood samples. Leaf biomass has been calculated by the gravimetric method. Total number of leaves present in the tree has been counted from total number of branches and average number of leaves present in a branch. Few of the leaves of the tree were taken and their fresh weight was measured as well as dry weight after properly dried at 70°C for 7 days to a constant weight. From this the biomass of those leaves has been measured or calculated by gravimetric method. The root biomass has not been measured at this moment as the other research works will be conducted on this tree in future.

In the present study, we have estimated the aboveground biomass stock and aboveground biomass carbon of two species by taking volume of biomass and specific gravity (SG) of the tree, as per Rajput et al. (1996) and Negi et al. (2003).

$$\text{Biomass(g)} = \text{volume of biomass(m}^3) \times \text{specific gravity(SG)}$$

where SG is the oven dry weight/green volume and carbon is the biomass × carbon %.

15.3.3   Carbon Content in Accumulated Biomass

The carbon content of different biomass such as stems, branches, and leaves has been measured by taking samples and sent them to Indian Association for Cultivation of Science for estimation of carbon content by CHN Analyzer (ParkinElmer Life and Analytical Sciences, USA). A certain amount of biomass samples have been collected from the particular stems, branches, and leaves and after being properly dried at 70°C for about 7 days to a constant weight, the carbon contents of the samples have been analyzed and estimated as per the above calculation.

15.4 Results and Discussion

15.4.1 Ambient CO_2 Level

Ambient CO_2 has been measured at two locations in Indian Botanic Garden, one at outside the garden near the gate and other within the garden near the tree. Distance between the two locations was 500 m. It is observed that average CO_2 levels in ambient air were 383.82 ppm at outside the garden near Bakultala gate and 359.13 ppm near the *A. lebbek* tree. This is expected that roadside CO_2 level at Bakultala gate was higher than inside garden near the tree. In between the two locations, CO_2 concentration decreased to 24.69 ppm. This reveals that 24.69 ppm CO_2 was sequestered by the plants between two locations.

At Banobitan, ambient CO_2 has been measured at two locations, one at near the *A. integrifolia* tree inside the forest and other near the Banobitan Gate. It is observed that CO_2 level in ambient air were 419.62 ppm at Banobitan Gate and 377.65 ppm near the *A. integrifolia* tree. This is expected that roadside CO_2 level at Banobitan Gate was higher than inside garden near the tree and difference of these two observations was 41.97 ppm. This means that 41.97 ppm CO_2 was sequestered by the plants between the two locations.

15.4.2 Carbon Sequestration Rate (CSR) by A. lebbek and A. integrifolia

Carbon sequestration rate (CSR) as CO_2 is to measure how much carbon can be sequestered by a tree over a certain period (e.g., hour, day, month, or year). In a forest ecosystem, the CSR is closely related to climatic conditions, soil properties, tree species, stand age, and the forest rotation length (Graham et al. 1992; Niu and Duiker 2006).

Carbon dioxide taken up by *A. lebbek* has been measured and the observations are shown graphically in Fig. 15.3. It is to be noted that photosynthesis and respiration occurs simultaneously during day and only respiration occurs during nighttime. Therefore, both CO_2 absorption and CO_2 emission occur during daytime and only CO_2 emission occurs during nighttime. Carbon sequestration rate by the plant has been evaluated by considering the photosynthesis and respiration during day and night time. The respirated CO_2 emission by the plant has been eliminated from the total concentration of CO_2 with respect to time. The volume of closed top chamber (CTC) for the tree has been calculated. The bottom portion of the plastic of CTC was dipped into the soil to avoid any CO_2 contamination with the ambient air. So, soil respiration CO_2 has been eliminated to estimate the actual carbon sequestration rate of the plant. Carbon dioxide taken up by the *A. lebbek* was measured. It is observed that on the starting day at 15:00 hour carbon dioxide sequestration rate was 28.49 g/h. Its rate decreased to the level of 5.16 g/h at 16:00 hour. At 17:00 hour sunlight was absent. Therefore, during 17:00 hour to 7:00 hour on the next day CO_2 level increased due to plant respiration.

Carbon Sequestration of *Albizzia lebbek*
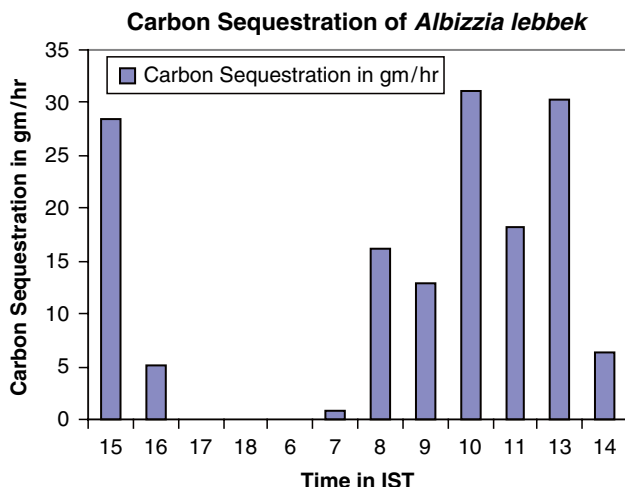
Fig. 15.3 Carbon sequestration rate as CO_2 by *Albizzia lebbek*

In the afternoon, sunlight decreased rapidly. So, that time CO_2 emission through respiration was higher than the CO_2 absorption by the plant. CO_2 concentration has increased by respiration during nighttime in the absence of photosynthesis process. At 7:00 hour, CO_2 sequestration rate reached to 0.89 g/h. At 8:00 hour it reached to 16.25 g/h and at 10:00 hour the rate increased to the maximum at 31.10 g/h. The rate of sequestration at 13:00 hour reached to 30.19 g/h and at 14:00 hour, the rate attained to a level of 6.24 g/h. The rate of CO_2 sequestration sometimes varied may be due to presence of solar light and other factors affecting photosynthesis.

Carbon dioxide taken up by the *A. integrifolia* has been measured during winter season and carbon sequestration rate of *A. integrifolia* is shown graphically in Fig. 15.4. We have started monitoring from 12:00 hour at CO_2 sequestration rate 5.56 g/h. CO_2 sequestration reached to 2.12 g/h at 15:00 hour and 0.61 g/h at 17:00 hour. Between 6:00 hour and 9:00 hour it reached to 7.48 g/h and at 10:00 hour, the rate reached to a maximum of 8.52 g/h with the increase of sunlight.

It could be observed from the result of carbon sequestration rate during winter season that the average CO_2 sequestration rate from the ambient air obtained by *A. lebbek* at Botanical Garden and *A. integrifolia* at Banobitan were 14.86 g/h (equivalent to 4.05 g C/h) and 4.22 g/h (equivalent to 1.15 g C/h) (Jana et al. 2008), respectively. This may be expected a little change of carbon sequestration rate by these species during summer season due to long duration of sunlight. The rate of carbon sequestration depends on the growth characteristics of the tree species, the conditions for growth where the tree is planted, and the density of the tree's wood. This can be observed that carbon sequestration rate of *A. lebbek* from ambient air was higher than *A. integrifolia*. Annual carbon sequestration rate from ambient air estimated for young *species* of 6 years age by considering annual mean duration of effective sunlight for photosynthesis at the rate of 9 h in a day was 1.33×10^{-2} t C
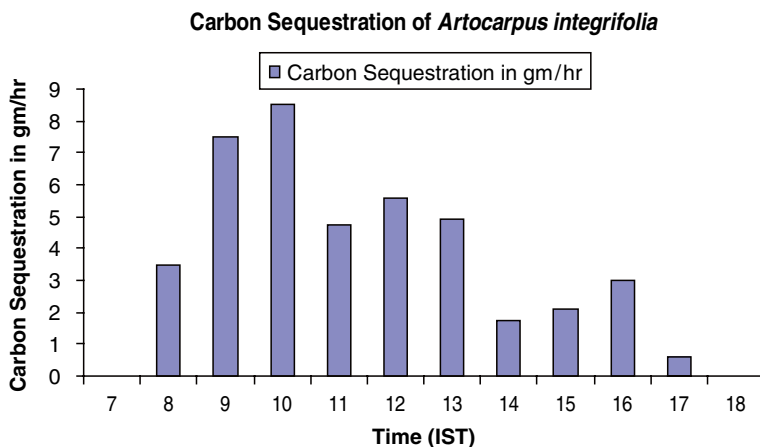
Fig. 15.4 Carbon sequestration rate as CO_2 by *Artocarpus integrifolia*

per tree in this forest stand. As the Botanical Garden and Banobitan have mixed type of plantation, we have considered 81 number (as per consideration of 81 trees in *Shorea robusta* forest in 30 × 30 m quadrate in Paschim Medinipur district in West Bengal) of *A. lebbek* and *A. integrifolia* species present in 30 m × 30 m quadrate. Therefore, annual carbon sequestration rate from ambient air estimated for young *A. lebbek* of 6 years age was 11.97 t C/ha (as per the consideration). This carbon sequestration rate may be expected to increase with the increase of forest stand ages. Similarly, the carbon sequestration rate has been evaluated as per the above consideration for *A. integrifolia* and annual carbon sequestration rate from ambient air estimated for young *species* of 6 years age was 0.37×10^{-2} t C per tree with 3.33 t C/ha for *A. integrifolia* (Jana et al. 2009).

15.4.3 Biomass Carbon Content

The aboveground biomass of the tree such as stems, branches, and leaves (except root) have been collected and dried at laboratory, and the dry biomass of the different sections of the tree are presented in Table 15.1.

The result of biomass analysis through CHN Analyzer is presented in Table 15.2. It is observed that for *A. lebbek*, leaf and stem contained 48.84% and 46.12% carbon and for *A. integrifolia*, leaf contained 41.01% carbon and stem contained 45.65% carbon.

Total carbon stock of a tree has been evaluated by adding all the carbon contents of stems, branches, and leaves of the tree. Carbon content of the tree was established by the works of different Scientists and Researchers, the carbon content in the plant was approximately 50% of the dry matter (World Bank 1998). The carbon concentration of different tree parts was rarely measured directly, but generally assumed to be

Table 15.1 Total aboveground dry biomass of the tree

Study area	Tree	Total weight of dry stem and branch biomass (g)	Total weight of dry leaves biomass (g)	Total dry biomass(g) of the tree (except root)
Botanical Garden	*Albizzia lebbek*	9,309	5,463	14,772
Banobitan	*Artocarpus integrifolia*	7,599	11,286	18,885

Table 15.2 Biomass analysis results

Tree	Parts of the plant	C (%)
Albizzia lebbek	Leaf	48.84
	Stem	46.12
Artocarpus integrifolia	Leaf	41.01
	Stem	45.65

Table 15.3 Carbon content of the aboveground biomass

Tree	Carbon content	Carbon content in individual sample (%)	Total carbon content in the plant species (g)
Albizzia lebbek	Leaf	48.84	2,668.12
	Stem	46.12	4,293.49
Total carbon content in the plant			6,961.61
Artocarpus integrifolia	Leaf	41.01	4,628.38
	Stem	45.65	3,469.31
	Total carbon content in the plant		8,097.69

50% of the dry weight (Losi et al. 2003). Work of Losi et al. (2003) obtained that measured carbon content of dry sample was 47.8% for *A. excelsum* and 48.5% for *D. panamensis*. "Extensive studies in Australia recently of a variety of tree species should above ground dry biomass generally contain 50% carbon. These proportions of carbon in aboveground biomass agreed closely with values of 49% and 47% reported from other parts of the world for *Pinus taeda* (Kinerson et al. 1977) and *Populus* spp. (Deraedt and Ceulemans 1998)" (West 2003). The total carbon content in *A. lebbek* and *A. integrifolia* are presented in Table 15.3.

It is observed from Table 15.3 that the total carbon content of the whole tree (excluding root) of *A. lebbek* and *A. integrifolia* trees were 6,961 and 8,097 g, respectively. This may be concluded that the percentage of total carbon content in the biomass was 47.12 in *A. lebbek* and 43.33 in *A. integrifolia*. Percentage of carbon content of *A. lebbek* was higher than *A. integrifolia*. Total aboveground biomass carbon stock per hectare has been estimated from the aboveground biomass carbon content in 81 *S. robusta* trees (6 years age). Total aboveground biomass carbon stock per hectare has been estimated from the aboveground biomass carbon content of 81 *A. lebbek* trees (6 years age) present in 30 × 30 m quadrate (as per consideration). It is estimated that total aboveground biomass carbon per hectare for *A. lebbek* was 6.26 t C/ha. Likewise, total aboveground biomass carbon per hectare for *A. integrifolia* was 7.28 t C/ha. It may be concluded that total accumulated
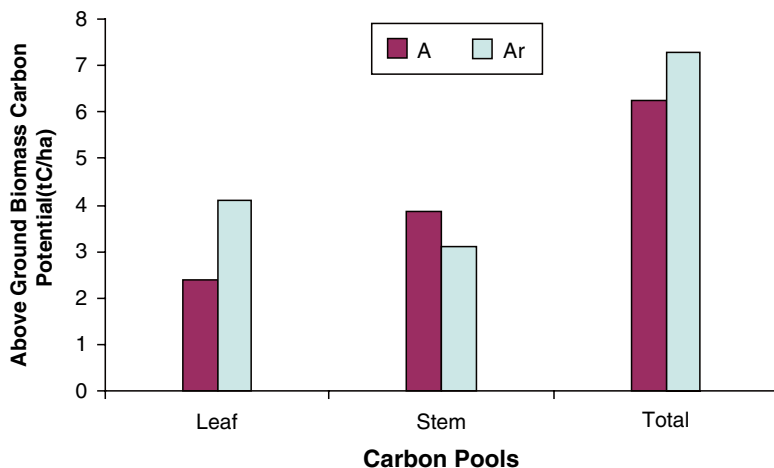
Fig. 15.5 Portioning of aboveground biomass carbon pools of 6 years age *Albizzia lebbek* and *Artocarpus integrifolia. A, A. lebbek; Ar, A. integrifolia*

aboveground biomass carbon stock per hectare in 6 years age of *A. integrifolia* was higher than *A. lebbek* (Jana et al. 2009).

Carbon pool partition of 6 years age *A. lebbek* and *A. integrifolia* is shown in Fig. 15.5. Maximum carbon pools in a forest ecosystem were primarily stored in aboveground tree biomass (Haripriya 2003). It is estimated that annual above ground biomass carbon pools of two young species were observed to yield 1.04 t C/ha/year for *A. lebbek* and 1.21 t C/ha/year for *A. integrifolia.* A short rotation plantation of 20 years age of hybrid poplar (*Populus* spp.) in Minnesota was estimated to yield an average of 1.8–3.1 t C/ha/year (Updegraff et al. 2004) and our estimated annual above ground biomass carbon pools were lower than Updegraff et al. (2004) work. Niu and Duiker (2006) estimated that in 20 years after afforestation a total of about 52 t C/ha could be sequestered in aboveground tree biomass carbon of both conifers and deciduous forests. Our estimated aboveground tree biomass carbon at 20 years age (by linear/proportionate estimation) will be 20.86 t C/ha for *A. lebbek* and 24.2 t C/ha for *A. integrifolia*, which were lower to the Niu and Duiker (2006) estimation. Earlier estimation was made based on linear/proportionate calculation. Normally tree biomass growth increases rapidly upto 20–50 years, not following any linear equation. According to Marland and Marland (1992), it could be expected from our study that tree growth aboveground biomass of *A. lebbek* and *A. integrifolia* will reach to the close value of Niu and Duiker (2006) estimation.

A simplified model proposed by Marland and Marland (1992) was used to simulate aboveground tree biomass carbon growth, in which the biomass carbon accumulates linearly until half of the maximum yield is reached and the growth slows down subsequently to reach the maximum yield asymptotically. With the progress of the forest stand ages, canopy cover and biomass of the trees will experience more rapid growth to a certain age (20–50 years) and the carbon held by these plants will also increase more biomass carbon stock to its optimum level.

At 6 years age, average above ground tree biomass carbon (accumulative biomass carbon) was estimated to 18 t C/ha from Marland and Marland's work, whereas our average aboveground tree biomass carbon (accumulative biomass carbon) for *A. lebbek* and *A. integrifolia* were estimated to 6.26 and 7.28 t C/ha, respectively. It could be concluded that aboveground tree carbon biomass of *A. lebbek* and *A. integrifolia* were lower than the Marland and Marland (1992) estimation. This may be due to different forest types, site qualities, climatic conditions, nonhybrid species, and only 6 years age species (stand age).

15.4   Conclusion

This study illustrates diurnal carbon sequestration rate and accumulated aboveground biomass carbon potential of young *A. lebbek* and *A. integrifolia*. The article concludes that carbon sequestration rate from the ambient air as obtained by *A. lebbek* at Botanical Garden and *A. integrifolia* at Banobitan in lower Gangetic plain were 14.86 g/h with annual carbon sequestration rate 11.97 t C/ha and 4.22 g/h with annual carbon sequestration rate of 3.33 t C/ha respectively. Percentage of carbon content in the aboveground biomass of *A. lebbek* and *A. integrifolia* were 47.12 and 43.33, respectively. Total aboveground biomass carbon stock per hectare for *A. lebbek and A. integrifolia* as estimated were 6.26 and 7.28 t C/ha, respectively. It could be concluded that our estimated results were lower than the previous works done by different scientists, which may be due to consideration of one tree from each species, very young age of the plant, only aboveground biomass carbon considered, chosen similar agroclimatic areas for study, similar soil characteristics, etc. It may be concluded that species identification for plantation in urban area should be made based on the concept of carbon sequestration and accumulated biomass carbon potential to offset the increasing CO_2 level in the ambient air.

References

Burley J, Evans J, Youngquist JA (2004) Mechanical properties of wood. Encycl Forest Sci 1:144–149
Chowdhery HJ (2001) Indian botanic garden, Howrah, Botanical Survey of India, Ministry of Environment and Forests, Government of India

Deraedt W, Ceulemans R (1998) Clonal variability in biomass production and conversion efficiency of poplar during the establishment year of a short rotation coppice plantation. J Biomass Bioenergy 15(4–5):391–398

Directorate of Census (2001) West Bengal, India

FSI (2005) State of forest report 2005. Forest Survey of India, Ministry of Environment & Forests, Dehradun, India

Graham RL, Wright LL, Turhollow AF (1992) The potential for short rotation woody crops to reduce U.S. CO_2 emissions. Climate Change 22:223–238

Haripriya GS (2003) Carbon budget of the Indian forest ecosystem. Climate Change 56:291–319

Indian Meteorological Department (1991–2005) Government of India, Alipur observatory, Meteorological data, 1991–2005

Jana BK, Biswas S, Majumder M, Roy P, Mazumdar A (2008) Carbon sequestration in urban and recreational forest area. *Banabithi*, Aranya Saptaha, Directorate of Forests, Govt. of West Bengal, Kolkata, pp 8–17

Jana BK, Biswas S, Majumder M, Roy P, Mazumdar A (2009) Carbon sequestration rate and aboveground biomass carbon potential of four young species. J Ecol Nat Environ 1(2):15–24

Kinerson RS, Ralston CW, Wells CG (1977) Carbon cycling in a loblolly pine plantation. Oecologia 29:1–10

Lal M, Singh R (2000) Carbon sequestration potential of Indian Forests. Environmental monitoring and assessment, vol 60. Kluwer, The Netherlands, pp 315–327

Losi CJ, Siccama TG, Condit R, Morales JE (2003) Analysis of alternative methods for estimating carbon stock in young tropical plantations. Forest Ecol Manage 184:355–368

Manhas RK, Negi JDS, Kumar R, Chauhan PS (2006) Temporal assessment of growing stock, biomass and carbon stock of Indian Forests. Climate Change 74:191–221

Marland G, Marland S (1992) Should we store carbon in trees? Water Air Soil Pollut 64:181–195

Negi JDS, Manhas RK, Chauhan PS (2003) Carbon allocation in different components of some tree species of India: a new approach for carbon estimation. Curr Sci 85(11):101–104

Niu X, Duiker SW (2006) Carbon sequestration potential by afforestation of marginal agricultural land in the Midwestern U.S. Forest Ecol Manage 223:415–427

PerkinElmer Life and Analytical Sciences, USA. Retrieved from www.perkinelmer.com

Rajput SS, Shukla NK, Gupta VK, Jain JD (1996) Timber mechanics: strength classification and grading of timber. *ICFRE*-Publication-38, New Forest, Dehradun

Ravindranath NH, Somashekhar BS, Gadgil M (1997) Carbon flows in Indian forests. Climate Change 35:297–320

Updegraff K, Baughman MJ, Taff SJ (2004) Environmental benefits of cropland conversion to Hybrid poplar: economic and policy considerations. Biomass Bioenergy 27:411–428

Veld KV, Plantinga A (2005) Carbon sequestration or abatement? The effect of rising carbon prices on the optimal portfolio of greenhouse-gas mitigation strategies. J Environ Econ Manage 50(1):59–81

WB (The World Bank) (1998) Greenhouse gas assessment handbook: a practical guidance document for the assessment of project level greenhouse gas emissions, vol 64. World Bank, USA, 168 pp

West PW (2003) Tree and forest measurement. Springer, New York, p 62

Chapter 16
Conservation of Natural Resource with the Application of Carbon Sequestration and Carbon Economy

Bipal K. Jana, Soumyajit Biswas, Mrinmoy Majumder, Sashi Sonkar, Pankaj Roy, and Asis Mazumdar

Abstract Trees and plants absorb carbon dioxide (CO_2) from the atmosphere and store as biomass carbon in different parts of it. Afforestation is a cost-effective approach to assimilate increased ambient CO_2, which mitigate the predicted effects of global climate change. It is necessary to create public awareness of multiple benefits and environmental services provided by the forests and thereby encourage people's participation in the conservation, protection, and management of forests. Joint Forest Management (JFM)

B.K. Jana (✉)
Senior Research Fellow, School of Water Resources Engineering, Jadavpur University, Kolkata-700032, West Bengal, India
and
Environmental Manager, Consulting Engineering Services, West Bengal, India
e-mail: bipalkjana@gmail.com

S. Biswas
Research Fellow, School of Water Resources Engineering, Jadavpur University, Kolkata-700032, West Bengal, India

M. Majumder
Senior Research Fellow, School of Water Resources Engineering, Jadavpur University, Kolkata-700032, West Bengal, India
and
Geo-information Scientist, Regional Center, National Afforestation and Eco-development Board, Jadavpur University, Kolkata-700032, West Bengal, India

S. Sonkar
Junior Research Fellow, School of Water Resources Engineering, Jadavpur University, Kolkata-700032, West Bengal, India

P. Roy
Lecturer, School of Water Resources Engineering, Jadavpur University, Kolkata-700032, West Bengal, India

A. Mazumdar
Coordinator, Regional Center, National Afforestation and Eco-development Board, Jadavpur University, Kolkata-700032, West Bengal, India
and
Director, School of Water Resources Engineering, Jadavpur University, Kolkata-700032, West Bengal, India

is an approach for sharing of products, responsibilities, control, and decision-making authority over forest land between Forest Departments and local user groups based on a formal agreement. Carbon credit can be generated through carbon sequestration by plantation like reforestation and afforestation project, and this credit can be distributed to the poor people in and around the forest area through different schemes such as employment generation, education, child welfare, small-scale cottage industries, biogas generation, etc. A major part of the earned amount by the carbon credit can be distributed to the forest neighbors who are directly dependent on forest and forest produce for their livelihood. This will give them a fresh look to the forest protection from the forest degradation or illegal felling. Green belt or afforestation is a statutory condition for any development activities where carbon sequestration has not been considered in the concept of green belt or afforestation. This could be recommended to include and select more effective carbon sequestrated plant species in the design of green belt or afforestation for effective mitigation of environmental pollution along with reducing of regional climatic temperature for the sustainable development of any project.

16.1   Climate Change

The policy makers have adopted broad goal for green house gases (GHGs) reductions that reflect commitment to the International Framework Convention on Climate Change that was signed by over 150 nations following Rio de Janeiro 1992 United Nations Conference on Environment and Development (UNCED). The global character of the climate change problem requires an International long-term strategy based on internationally agreed principles, such as sustainable development and the precautionary principles in the context to the "production forestry" (Srivastava and Singh 2007). In the latter, the convention of the Kyoto Protocol in 1997 by the United Nations Framework Convention on Climate Change (UNFCCC) was illustrated about stabilizing green house gas (GHG) concentrations in the atmosphere at a level that would minimize interference with the climate system. Under the protocol in August 2002, India is not required to reduce emission of GHGs, whereas mainly the developed countries were required to reduce emissions by an average of 5.2% below 1990 level by 2012 (C & I India Update 2008). The effect of climate change has already been noted in various evidences, such as:

- Droughts, heavy rainfall, and intense tropical cyclones
- Average Arctic temperatures increased at almost twice the global rate in the past 100 years
- Change of climatic pattern
- Snow cover has declined by some 10% in the mid and high latitudes of the northern hemisphere since the late 1960
- Change of species and communities in the natural ecosystem
- Forests are affected by increased forest diseases and pest infestations, increased forest fires, etc.
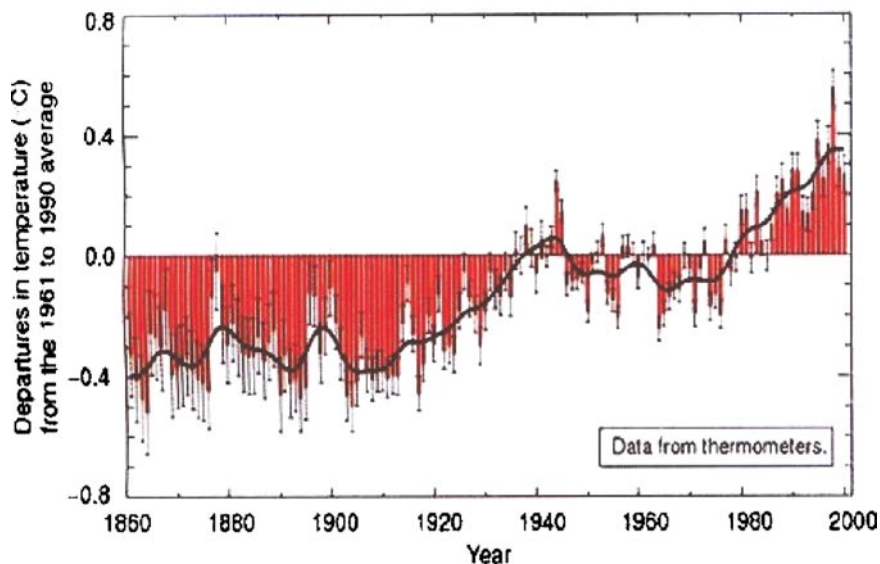
Fig. 16.1 Variations of the Earth's surface temperature over the last 140 years. Earth's surface temperature is shown year by year (*red bars*) and approximately decade by decade (*black line*, a filtered annual curve suppressing fluctuations below near decadal timescales). The annual data with 95% confidence limits (IPCC 2001a)

This is reported that global sea level has risen by 17 cm during twentieth century, due to the melting of snow and ice from mountains and the Polar Regions. Over the course of twenty-first century, more impacts are expected to occur in natural systems (IPCC 2007).Variations of the Earth's surface temperature over last 140 years has been depicted in Fig. 16.1 (IPCC 2001a).

16.2   Contribution of Forests

16.2.1   Introduction

Trees and plants remove carbon dioxide (CO_2) from the atmosphere by photosynthesis and produce carbon as biomass in the form of wood, leaf, bark, root, etc. This process is named as "carbon sequestration." Trees absorb carbon dioxide, the primary gas causing global climate change. Forests are the world's second largest carbon reservoirs after the oceans. Climate change and forests are closely related to each other and forest can minimize the climate change effect. Besides carbon sequestration, the forests also play important role in controlling the atmospheric temperature through evapotranspiration, recharging of ground water, and soil conservation (Srivastava and Singh 2007). This chapter mainly illustrates different aspects of climate change, contribution of forests and its benefit, people's participation in different

modes of forest management, application of carbon reduction through CDM, and approach to the valuation of carbon sequestration. The main objective of this chapter is to evaluate carbon economy through carbon sequestration by plantation for forest neighbors and to introduce more effective carbon-sequestrated plant species in the design of green belt or afforestation plan for any development project.

Green plants have the capacity to absorb carbon dioxide from the atmosphere, hence afforestation has been suggested as a cost-effective approach to mitigate predicted effects of global climate change. Increase in the forest biomass carbon will reduce the build-up atmospheric carbon dioxide (Parks et al. 1992). As a number of forestry options are available in order to stabilize atmospheric deforestation, for example, increasing afforestation and increasing the production of existing forests, forestry sector offers additional strategies to increase carbon sequestration: mainly carbon storage in wood products and the substitution of energy-intensive materials by wood (Srivastava and Singh 2007).

Trees, soil, and forest floor store carbon and is determined by a number of factors including the type of forest, its location, and its age. Forests store large amounts of carbon in trees, understorey vegetation, and soil. The forests contain some 1.2 trillion tons of carbon, just over half the total in all terrestrial vegetation and soils and twice the amount is found floating free in the atmosphere (FAO 2007). Hardwood contains about 48% of carbon in the form of cellulose and wood, and it is estimated that 2.2 t of wood is required to sequester 1 t of carbon (Chaturvedi 1994). On the other hand, while wood is burnt CO_2 is released into the atmosphere. Hence Forests act both as a source and a sink of carbon, depending upon the manner and purpose for which they are raised and managed (Chaturvedi 1994). Matured and climate forests are neither sources nor sinks of atmospheric carbon (Dabas and Bhatia 1996). It is said that forests that experience a net loss of biomass volume through mortality due to disease or fire become net carbon emitters (Kyrklund 1990).

For the expansion of C-sequestration in existing forest, measures involved will be under planting, increased rotation period, shifting to fast-growing tree species, modifying thinning practices, and implanting measures aimed at increasing the C-pool in the organic matter of forest soils. Above all, afforestation of indigenous broad-leaved trees will play an increasing role of silviculture, on the opposite, an extension of nonindigenous tree species would also run counter to biodiversity concerns. Substituting wood products for other materials whose manufacture and usage causes carbon to be emitted are to be taken wherever necessary. Sustainably produced timber, used as a source of energy causes a mitigation of CO_2 emissions as by this means the consumption of fossil fuels is reduced (Bursche et al. 1993).

16.2.2   Forest Benefits and Their Valuation

Valuation of forest goods and services and the inputs used in their production is an integral part of Forest Resource accounting. Valuation can be useful for several purposes such as formulation and appraisal of forest and other natural resources

development projects such as soil conservation, wastelands development, flood control, excursion, wildlife shelter, environmental safeguard for industrial and infrastructural projects, and determining the extent of financial liability of firms and households, who degrade natural resources and pollute the environment. The economic value of a natural resource as asset can be defined as the sum of the discounted present values of the flows of all the services (Myrick 1993). The economic concept of value is based on a premise of neoclassical welfare economics that the purpose of an economic activity is to increase the well-being of the individuals who constitute the society and that each individual is the best judge of what is "good" or "bad" for him or her. The basis for estimating economic value of a resource or an environmental amenity is its probable effect on human welfare (Singh and Mali 2005) (Fig. 16.2).

The economic value of forests can be expressed as below.

$$\text{Total economic value (TEV)} = \text{use value (UV)} + \text{nonuse value (NV)} \qquad (16.1)$$

The use value may be further broken down into direct and indirect use values. The nonuse values comprise option value and existence value.

Forests generate numerous direct and indirect benefits (FAO 1995, as quoted in Verma (2000:7.15)), which are listed below.
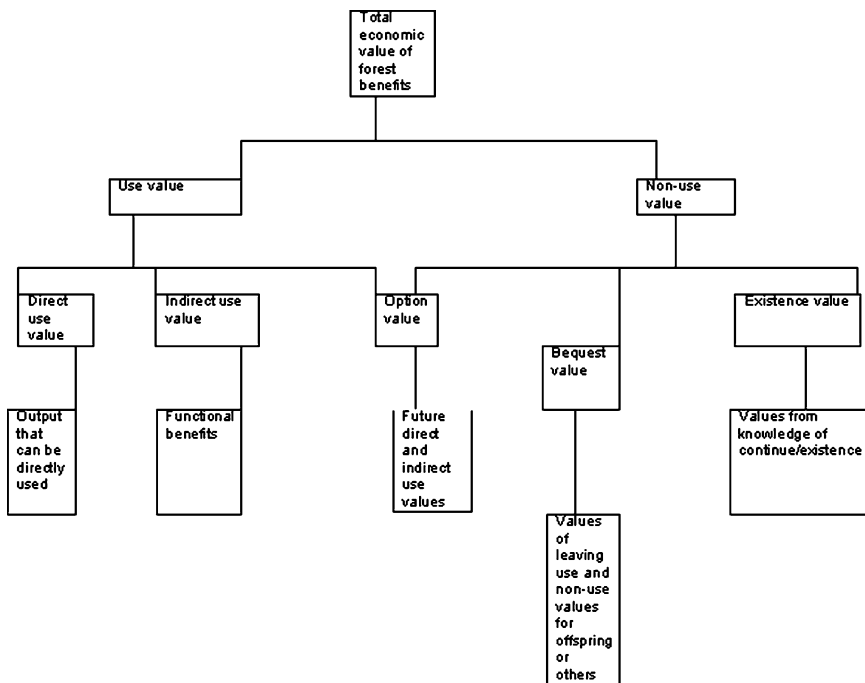
Fig. 16.2 Use and nonuse values of benefits from forests (Munasinghe and Lutz 1993 as quoted in Verma 2000:7.14)

16.2.2.1 Direct Benefits Associated with Consumptive Uses

- Commercial/industrial market goods (fuel, timber, pulpwood, poles, fruits, animals, fodder, medicines, etc.)
- Indigenous nonmarket goods and services (fuel, animals, skin, poles, fruits, nuts, etc.)

16.2.2.2 Nonconsumptive Uses

- Recreation (jungle, cruises, wildlife, photography, trekking, etc.)
- Science/education (forest studies of various kinds)
- Social, cultural, and spiritual values, etc.

16.2.2.3 Indirect Benefits Associated with

- Watershed protection (protection of downstream areas)
- Soil protection/fertility (maintenance of soil fertility, especially important in tropical regions)
- Gas exchange and carbon storage (improvement of air quality, reduction of greenhouse gases)
- Habitat and protection of biodiversity and species (potential drug sources, source of germplasm for future domesticated plants and animals)
- Soil productivity on converted forestland (space and soil productivity for agricultural/ horticultural crops and livestock)

16.2.2.4 Option and Existence Values

- People may value a forest or resource complex purely for its existence and without any intention to directly use the resource in future. This includes intrinsic value of the forest.
- People may value the option to use a forest in the future or merely the option to have it available in the future. Although such values are difficult to measure in economic terms, they should be recognized in valuing the contributions of forests to human welfare.

16.2.2.5 Direct Economic Benefits from Forests

Forest provides following direct economic benefits to the society:

- Energy source
- Employment generation
- Development of cottage and small-scale industries

- Forests as a source of human and animal food
- Raw material for industries
- Revenue to the forest department
- Development of ecotourism
- Carbon credit

16.2.2.6 Indirect Economic Benefits from Forests

Forests confer a number of benefits, which are not directly visible to the human eye and yet they have a great influence in affecting the quality of life. These benefits are as follows:

- Amelioration of climate
- Conservation of moisture
- Conservation of soil
- Flood control
- Beautifying human environment
- Improvement of agroforestry
- Control of environmental pollution like to mitigate noise, air quality pollution, odor, etc.

16.3 Joint Forest Management

A forest management system in which a specific area of a forest is allotted to the local communities where the people share some usufruct rights (they may be tangible or intangible benefits, viz., ecological, economic, and sociocultural aspects) in the forest, but the legal ownership of the forest area and its commodities remains with the forest department (Singh and Mali 2005). Joint Forest Management (JFM) is an approach for sharing of products, responsibilities, control, and decision-making authority over forest land between Forest Departments and local user groups based on a formal agreement. The primary purpose is to give users, a stake in forest benefits and involving users in planning and management of forest conditions and productivity and equal distribution of forest products (Anon 2002; Hill and Shields 1998). From the past 1 decade, JFM has successfully achieved many things and people are actively involving themselves in this approach, which is depicted by the increasing trend in formation of number of Village Forest Committee (VFCs) and area under JFM in India (Bhat et al. 2000). This approach is successful when it is accepted and improves the living conditions of the local people in addition to improving the diversity of species. JFM is the official and popular term in India for partnerships in forest management involving both the state forest departments and local communities. The policies and objectives of JFM are detailed in the Indian Comprehensive National Forest Policy of 1988 and the Joint Forest Management Guidelines of 1990 of the Government of India. Although schemes vary from

state and are known by different names in different Indian languages, usually a village committee known as the Forest Protection Committee/Village Forest Committee (FPC/VFC) and the forest department enter into a JFM agreement. Villagers agree to assist in safeguarding forest resources through protection from fire, grazing, and illegal harvesting in exchange for which they receive Non-Timber Forest Produce (NTFP) and a share of the revenue from the sale of timber products. In order to attract the villagers toward JFM schemes, the government also allocated funds for rural development works as a part of fund allocation for affectation works (Mukhopadhyay et al. 2006).

In view of villagers' dependence on forests for their livelihood, there was constant conflict between villagers and forest department officials. This began to change when the Forest department evolved and introduced the concept of JFM (Khare et al. 2000). JFM originated in West Bengal at the Arabari forest range of erstwhile Midnapore Forest Division in erstwhile Midnapore district (now West Midnapore district), near Midnapore town in 1971. The major hardwood of Arabari is *Shorea robusta*, a commercially profitable forest crop. The experiment was successful and was expanded to other parts of the state in 1987. JFM is still in force at Arabari.

Forests of Doni of Gadag Division were selected to assess the impact of JFM approach on the floristic composition. For the present study, the JMF-managed forests and adjacent natural forests were considered. The Karnataka Forest Department in assistance with external agencies has formed many VFCs in the JFM program in order to manage and protect these forests. The dependency of local people on these forests for fuel wood and grazing of their cattle is enormous, which has led to the degradation of these forests. Hence, the Department has carried out enrichment planting through various JFPM models. In the present study, the growing stock and natural regeneration status have been enumerated in the JFM-managed and adjoining natural forests to know the extent of success (Suryanarayana et al. 2008)

Kumaon is endowed with a rich heritage of flora, fauna, and natural resources. It is predominantly a rural economy, so the rate of removal of biomass by people is increasing day by day. Although the extent and degree of overharvesting of fuel wood and overgrazing are difficult to quantify, they are recognized as major causes of forest degradation (FAO 1997). Hence involvement of people in the management and protection of forest is the only solution for rejuvenation of the forest in the hills. In rural areas of Kumaon hills, it is mainly the women who were responsible for gathering the energy and fodder requirement for their family and animals. Therefore, from the entire house at least one woman visits the forest once in 3 days or sometimes daily. Women also act as helper to men in agriculture activities – harvesting, planting, manuring, etc. Generally, the level of women's participation in planning and implementation of social forestry programs has been inadequate (Nesmith 1991). Socioeconomic backwardness makes them too shy to speak out and restricts their participation in meetings and other such forestry-oriented activities. Forestry has traditionally been among the most "masculine-oriented" rural activities with very little impact of rural women (Brandth et al. 1998).

Labor contribution by women has been emphasized in most of the forestry programs though less attention is given to their priorities. In this way, women's inherent practical knowledge remains unutilized because of their low level of participation. There is a close association of women's development with focused resource development and management. The relationship between trees and rural women forms the basic plank in planning and implementation of afforestation projects and restoration of village institutions for the purpose (Rawat and Bedi 1996). This study focuses on rural women and plantation and thus their perception and participation in the basic need is to educate the women on the beneficial aspect of forestry. With the cooperation of women, we have been able to obtain all the natural resources for the economic betterment of the people living in the area. Thus, a well-conceived JFM program could definitely provide maximum benefits to rural women. Women's lower literacy rate probably leads to lacking of awareness regarding environmental management measures. The participation of women folk in meetings and other forestry activities is severely restricted by various sites and traditions. The women of Kumaon hills respond positively by their active participation in training programs. The proportion of working women ranges from 25.7% to 38.5% which is low in comparison to male section. The fuelwood requirement per family in the selected villages ranges from 12 to 25 kg/day, and fodder requirement per family from 8.3 to 27.4 kg/day, respectively. Village community was found mostly dependent on forest for fuelwood and fodder than other sources. In all the villages the dependency for fuelwood was observed to be confined to forestland. It appears that this dependency may result in the successful accomplishment of the participatory process as only the women folk arrange these requirements from the forests by trekking distances of 1–2 km (Pant and Pandey 2007).

16.4 Carbon Reduction and CDM

According to FAO (2006) 13 million hectares of the world's forests are logged and cleared annually, accounting for 20% of all global greenhouse gas emissions (FAO 2006). This has given rise to evolution of the reduced emissions from deforestation and degradation (REDD) concept, by creating a carbon market mechanism to pay local communities in developing countries for protecting their forests, an alternative income stream to what would be earned by logging or farming the same land. REDD aims to provide inceptives for developing countries to cut emissions by preserving forests or having sustainable forest management practices, all of these in an effort to bring down emissions from this source and to ensure that there are sufficient forests remaining for the uptake of carbon dioxide and for providing variety of useful forest products and ecological services.

India's position is peculiar with a huge population of poor people whose livelihood significantly depends on forest and agriculture. In this context, adaptation becomes critical for a country like India, which has no choice but to develop effective strategies for adapting to probable climate change impacts. The forestry sector, particularly

in tropical situations like India, possibly will face additional difficulties, if not fully prepared to effectively shape its response to global climate change and sustainable mitigation mainly in terms of capacity, infrastructure, and appropriate governance institutions. Planting forests and sustainable forest management can aid in the protection of soil and land against detrimental impacts of flooding. Adaptation strategies that promote sustainable forest management and community-based forest management have the potential to not only protect land and people from some of the harmful effects of rising global temperatures, but also to provide opportunities for greater, more sustainable rural development and poverty alleviation through income generation and employment opportunities.

Options to increase carbon storage in forests include protecting forest lands and reducing the conversion of forest lands to nonforest purpose. Four major strategies are available to mitigate carbon emissions through forestry activities: (i) to increase forested land area through reforestation, (ii) to increase the carbon density of existing forests at both stand and landscape scales, (iii) to expand the use of forest products that sustainably replace fossil fuel CO_2 emissions, and (iv) to reduce emissions from deforestation and degradation. These strategies are covered under clean development mechanism (CDM), which is an arrangement under the Kyoto Protocol allowing industrialized countries with emission reduction commitment to invest through carbon credits in developing countries; reducing emission through deforestation and forest degradation (REDD) in developing countries, substitution of carbon through forestry activities , and some of undefined strategies like restoration. Currently, 13 M ha/year are deforested, almost exclusively in tropical regions, with net emissions of 1.5 Pg C (1 Pg = 1 billion metric ton) per year (FAO 2006).

It is clear that development of successful CDM projects requires substantial effort and sustained local capacity building. The forests, especially tropical forests, harbor the bulk of species, the same as our Indian forests as compared to temperate. Thus, the production forestry to tropic has ample scope to take over mixed-species plantations composed of locally occurring tree species with exotic ones too. In order to capture CO_2 by the productive forest, three categories of forest management practices could play the role: (i) maintaining existing C-pool in the stand, (ii) expanding carbon sequestration in forest biomass and soils, and (iii) producing biofuels and wood products as substitutes for products based on fossil fuels (Srivastava and Singh 2007).

16.5 Carbon Sequestration and Carbon Economy

The most important thing is that the forest sector has to act now and make its impact felt (C & I India Update 2008). A growing crop absorbs carbon dioxide and fixes it in the wood. Adger and Brown (1994) estimated the carbon sequestration value of the Mexican forests to be equivalent of US$300–650/year. Forest is estimated to store carbon – about 20–100 times more per hectare than pastures or croplands. New tree plantation and agroforestry systems have potential to sequester and conserve

upto 10 Gt of carbon annually in the terrestrial biosphere, while at the same time continuing to provide needed goods and services for people. Attempts have been made in several instances recently to quantitatively define carbon sequestration benefits of tree plantations and to evaluate them to provide broad guidelines and indicators of carbon offset projects. The medium cost efficiency across all management practices as determined from establishment costs over a 50-year period is about US$5/t C with an adequate range of US$19 /t C (Chandrasekhran 1996).

Forest neighbors are mostly poor people and belongs to the below poverty line in our country. Their literacy rate is also very poor. For their livelihood they generally used to cut trees/forest wood and sell these to a very low price. A natural forest or social forest can be saved from degradation by improving the livelihood of these forest neighbors and in this regard various management practices have been adopted in our country. Nowadays, carbon credit can be generated through carbon sequestration by plantation like reforestation and afforestation project and this credit can be distributed to the poor people in and around the forest area through different schemes such as employment generation, education, child welfare, small-scale cottage industries, biogas generation, etc. Even in the social forests if more effective carbon-sequestrated plant species are planted, it will generate more carbon credit within a short period, which will promote further reforestation and afforestation programs. By this way, a separate window will open for people's participation in the forest protection as well as forest produce generation.

In our carbon sequestration study (Jana et al. 2009), we have noted that *S. robusta* sequestrated 0.005714 t C, *Albizzia lebbek* sequestrated 0.012559 t C, and *Tectona grandis* sequestrated 0.016099 t C in 6 years. This could be estimated for valuation of carbon sequestration per tree in 6 years; for *S. robusta*, *A. lebbek*, and *T. grandis* are Rs. 3.42, 7.53, and 9.66 by assuming US$12/t C. This valuation must be increased with the increase of age of the respective trees. A major part of the earned amount by the carbon credit can be distributed to the forest neighbors who are directly dependent on forest and forest produce for their livelihood. This will give them a fresh look to the forest protection from the forest degradation or forest hazards. This would also to be mentioned that green belt or afforestation is a statutory condition for any development activities where carbon sequestration has not been considered in the concept of green belt or afforestation purposes. This could be recommended to include and select more effective carbon-sequestrated plant species in the design of green belt or afforestation for effective mitigation of environmental pollution along with reducing regional climatic temperature for the sustainable development of any project.

16.6 Conclusion

Trees absorb carbon dioxide, the primary gas causing global climate change. It is necessary to create public awareness of multiple benefits and environmental services provided by the forests and thereby encourage people's participation in the

conservation, protection, and management of forests. Valuation of forest can be useful for several purposes such as formulation and appraisal of forest and other natural resources development projects such as soil conservation, wastelands development, flood control, excursion, wildlife shelter, environmental safeguard for industrial and infrastructural projects, and determining the extent of financial liability of firms and households, who degrade natural resources and pollute the environment. Development of successful CDM projects requires substantial effort and sustained local capacity building through which a carbon market mechanism can be created to pay local communities (an alternative income) for protecting the forests. Carbon credit can be generated through carbon sequestration by plantation like reforestation and afforestation project and this credit can be distributed to the poor people in and around the forest area through different schemes such as employment generation, education, child welfare, small-scale cottage industries, biogas generation, etc.

In our carbon sequestration study, we have noted that *S. robusta* sequestrated 0.005714 t C, *A. lebbek* sequestrated 0.012559 t C and *T. grandis* sequestrated 0.016099 t C in 6 years. This could be estimated for valuation of carbon sequestration per tree in 6 years for *S. robusta*, *A. lebbek* and *T. grandis* are Rs 3.42, Rs 7.53 and Rs 9.66 by assuming US$ 12/t C. This valuation must be increased with the increase of age of the trees. A major part of the earned amount by the carbon credit can be distributed to the forest neighbors for their livelihood. This may also be recommended to include and select more effective carbon-sequestrated plant species in the design of green belt or afforestation for any development activities for effective mitigation of environmental pollution along with reducing regional climatic temperature for the sustainable development of any project.

References

Adger WN, Brown K (1994) Land use and cause of global warming. Wiley, New York
Anon (2002) Joint forest planning and management in Karnataka. Forest Department, Govt. of Karnataka
Bhat PR, Rao RJ, Murthy IK, Ravindranath NH (2000) JFM and community forestry: ecological and institutional assessment. Oxford/IBH, New Delhi, pp 59–98
Brandth B, Haugen MS, Shortall S, Versated B (1998) Braking into a masculine discourse: women and farm forestry: the empowerment of farm women. Sociologia Ruralis 38:427–442

Burschel P, Kursten E, Larson BC (1993) Die Rolle von Wald and Forestwirtschaft in Kohlenstoffhaushalt Eina Betrachtung fur die Budesrepublik Deutschland Schriftenreihe der Forstwirsenschaftlichen. Faklutat der Universitat Munchen (Hrsg.), Munchen, 135 pp

Chandrasekhran C (1996) Cost, incentives and impediments for implementing sustainable forest management, Paper published in the proceedings of the workshop on financial mechanisms and sources. Project report prepared for MOEF, India

Chaturvedi AN (1994) Sequestration of atmospheric carbon in India's forest. Ambio 23:460–461

C & I India Update (2008) Potential climate change mitigation and adaptation strategies through sustainable forest management. Ind Inst Forest Manage Int Tropical Timber Organ 6(4):3–9

Dabas M, Bhatia S (1996) Carbon sequestration through afforestation: role of industrial plantations. Ambio 25(5):327–330

FAO (1995) Forest resources assessment 1990: Global synthesis. FAO Forestry Paper 124. Rome

FAO (1997) Situation and prospects for forest conservation and development. Food and Agriculture Organization of the UN, Rome, pp 10–34

FAO (2006) Global Forest Resource Assessment 2005. Food and Agriculture Organization of the United Nations, Rome

FAO (2007) Food and Agriculture Organization of the United Nations, Rome

Hill I, Shields D (1998) Incentives for joint forest management in India – analysis methods and case studies. World Bank Technical Paper No. 394

IPCC (2001a) Climate change (2001). The scientific basis. Contribution of Working Group I to the third assessment report of the intergovernmental panel on climate change. Cambridge University Press, Cambridge/New York

IPCC (2007) Fourth assessment report of the intergovernmental panel on climate change, contribution of the Working Group III. Cambridge University Press, Cambridge

Jana BK, Biswas S, Majumder M, Sankar S, Roy P, Mazumdar A (2009) Carbon sequestration in an urban area- Kolkata Metro City, RC:NAEB (MoEF), Govt of India, Jadavpur University, Kolkata, India

Khare A, Mayers J, Morrison E (2000) Joint forest management: policy, practice and prospects: India country study. International Institute for Environment and Development, India, London

Kyrklund B (1990) The potential of forests and forest industry in reducing excess atmospheric CO_2. Unasylva 41:12–14

Mukhopadhyay MK, Adak S, Mazumdar A (2006) Forest regeneration through socioeconomic development: experiments in India. Regional Centre, National Afforestation and Ecodevelopment Board, Kolkata, India

Munasinghe M, Lutz E (1993) Protected area economics and policy: linking conservation and sustainable development. World Bank/IUCN, Washington, DC

Myrick A (1993) Freeman III. The measurement of environmental and resource values: theory and methods. Resources for the future, Washington, DC

Nesmith C (1991) Gender, trees and fuel: social forestry in West Bengal, India. Human Organ 50:337–348

Pant N, Pandey N (2007) Introducing JFM to rural women of Kumaon hills – a case study. Indian Forester 33(12):1690–1694

Parks PJ, Brame SR, Mitchell JE (1992) Opportunities to increase forest area and timber growth on marginal crop and pasture land. In: Sampson RN, Hair D (eds) Forests and global change. American Forestry Association, Washington, DC

Rawat JK, Bedi H (1996) Women and commons towards sustainability in the Haryana Aravallis. Aravallis project, Forest Department, Govt. of Haryana

Singh K, Mali KP (2005) Forest resource valuation and accounting: a critique of the conventional method and a framework for a new system. Indian Institute of Forest Management, Bhopal, pp 15–36

Srivastava RK, Singh B (2007) Carbon sequestration and mitigation through conservation approach. Silviculture Division, Forest Research Institute, Dehradun, India, pp 475–483

Suryanarayana V, Vasantha Reddy KV, Kumar HP, Hareesh TS, Raj VM (2008) Assessment of floristic composition in JFM-managed and adjoining natural forests in Doni area of Gadag division, Karnataka. Indian Forester 134(11):1447–1454

Verma M (2000) Himachal Pradesh forestry sector review annexes, Economic valuation of forests of Himachal Pradesh, International Institute for Environment and Development (IIED) in collaboration with Himachal Pradesh Forest Department. Indian Institute of Forest Management, Bhopal

Chapter 17
Measurement of Diurnal Carbon Sequestration Rate and Aboveground Biomass Carbon Potential of Two Young Species and Soil Respiration in Two Natural Forests in India

Bipal K. Jana, Soumyajit Biswas, Mrinmoy Majumder, Pankaj Roy, and Asis Mazumdar

Abstract Diurnal carbon sequestration rate (CSR) has been measured for young species (6 years age) of *Shorea robusta* at Chadra forest in Paschim Medinipur district and *Tectona grandis* at Chilapata forest in Coochbehar district of West Bengal in India by Automated Vaisala Made Instrument GMP343 and aboveground biomass carbon has been analyzed by CHN analyzer. Soil respiration has also been measured by GMP343. The specific objectives of this article are to measure diurnal carbon sequestration rate

B.K. Jana (✉)
Senior Research Fellow, School of Water Resources Engineering, Jadavpur University, Kolkata-700032, West Bengal, India
and
Environmental Manager, Consulting Engineering Services, West Bengal, India
e-mail: bipalkjana@gmail.com

S. Biswas
Research Fellow, School of Water Resources Engineering, Jadavpur University, Kolkata-700032, West Bengal, India

M. Majumder
Senior Research Fellow, School of Water Resources Engineering, Jadavpur University, Kolkata-700032, West Bengal, India
and
Geo-information Scientist, Regional Center, National Afforestation
and Eco-development Board, Jadavpur University, Kolkata-700032, West Bengal, India

P. Roy
Lecturer, School of Water Resources Engineering, Jadavpur University, Kolkata-700032, West Bengal, India

A. Mazumdar
Coordinator, Regional Center, National Afforestation and Eco-development Board, Jadavpur University, Kolkata-700032, West Bengal, India
and
Director, School of Water Resources Engineering, Jadavpur University, Kolkata-700032, West Bengal, India

and aboveground biomass carbon potential of two young species, and soil respiration in two natural forests. Measurements of soil respiration as conducted in two forests were 0.0050 g/m²/h in Chadra forest and 0.0575 g/m²/h in Chilapata forest. The diurnal carbon sequestration rates (mean) as CO_2 from the ambient air as obtained by *S. robusta* and *T. grandis* were 11.13 and 2.57 g/h in overcast skies. The annual carbon sequestration rates from ambient air were estimated to 8.97 t C/ha by *S. robusta* and 2.07 t C/ha by *T. grandis*. The percentages of carbon content (except root) in the aboveground biomass of *S. robusta* and *T. grandis* were 47.45 and 45.45, respectively. The total aboveground biomass carbon stocks per hectare as estimated for *S. robusta* and *T. grandis* were 5.22 and 7.97 t C/ha, respectively, in these forest stands.

Keywords Aboveground biomass carbon stock • carbon sequestration rate • *Shorea robusta* • soil respiration • *Tectona grandis*

17.1   Introduction

Carbon dioxide (CO_2) is a dominant greenhouse gas. Increased atmospheric CO_2 is attributable mostly to fossil fuel combustion and deforestation worldwide (Hamburg et al. 1997). Trees act as a sink for CO_2 by fixing carbon during photosynthesis and storing excess carbon as biomass. The net long-term CO_2 source/sink dynamics of forests change through time as trees grow, die, and decay. In addition, human influences on forests can further affect CO_2 source/sink dynamics of forests through such factors as fossil fuel emissions and harvesting/utilization of biomass (Nowak and Crane 2002). As the tree biomass experiences growth, the carbon held by the plant also increases carbon stock. The rate of carbon storage increases in young stands, but then declines as the stand ages. An observation from a study on pine species planted on cropland in the southeastern USA, the rate of carbon storage begins to decline at an approximate age of 20 and is close to zero by the age of 100 (Veld and Plantinga 2005). Increasing the atmospheric CO_2 concentration stimulates the photosynthetic rate of trees and can result in increased growth rates and biomass production. Results from free air CO_2 enrichment (FACE) experiments show a 25% increase in growth in twice normal concentrations of CO_2. Growth is therefore almost always higher in air with an elevated concentration of CO_2 (Burley et al. 2004). Scientific evidence suggests that increased atmospheric CO_2 could have positive effect such as improved plant productivity (Schaffer et al. 1997; Pan et al. 1998; Centritto et al. 1999a, b; Idso and Kimball 2001; Keutgen and Chen 2001). Lal and Singh (2000) reported that estimated annual carbon uptake increment by Indian forests and plantations has been able to remove about 0.12 Gt of CO_2 from the atmosphere in the year 1995. Ravindranath et al. (1997) reported the Indian forests based on the forest sector of the year 1986 could sequester around 5 Tg C (1 Tg = Tera gram, 10^{12} g). Haripriya (2003) noted on the average biomass carbon of the forest ecosystems in India for the year 1994 was 46 Mg C/ha, of which nearly 76% was in aboveground biomass and the rest was in fine and coarse root biomass. The total carbon stock (wood only) for India was 1,085.06 and 1,083.69 Mt in 1984 and 1994, respectively. The average carbon stock for the country was 24.94 t C/ha in 1984 and 24.54 t C/ha in 1994. *Shorea robusta* forests stocked 24.07 t C/ha in 1984 and 22.66 t C/ha in 1994, while *Tectona grandis* forests stocked 11.44 t C/ha

in 1984 and 11.25 t C/ha in 1994 (Manhas et al. 2006). In West Bengal, total carbon stocks of *S. robusta* and *T. grandis* were 5.49 Mt in 1984 and 6.19 Mt in 1994, and 0.29 Mt in 1984, and 0.30 Mt in 1994, respectively (Manhas et al. 2006).

The State of Forest Report 2005 (FSI 2005) by the Forest Survey of India (Ministry of Environment & Forests, Dehradun) stated that Forest Resource Assessment (FRA) 2005 of The Food & Agriculture Organization (FAO) of United Nations estimated the total area of the World's forests as 3.952 billion hectare (more or less same as 1948), which was about 30% of the total land area of the world. It is estimated that the world's forests store 283 Giga tones (Gt) of carbon in their biomass alone, and 638 Giga tones (Gt) of carbon in the ecosystem as a whole including dead wood, litter, and soil upto 30 cm depth. As per 2005 Assessment, the total forest cover in India was 677,088 km^2, which constituted 20.60% of the geographic area of the country. The forest cover of West Bengal, based on Satellite data of November–December 2004 was 12,413 km^2, which was 13.99% of the geographic area (FSI 2005). Vast forest areas in India as well as its different provincial states accumulated a large amount of carbon as CO_2 from the atmosphere and play an important role in sequestering carbon in the regional, national, and world scenarios. Terrestrial (plant and soil) carbon was estimated at $2,000 \pm 500$ Pg, which represented 25% of global carbon stocks. This review, gave a description of a few agroforestry systems practiced in the tropics in relation to their C sequestration potential. The analysis of C stocks from various parts of the world showed that significant quantities of C (1.1–2.2 Pg) could be removed from the atmosphere over the next 50 years if agroforestry systems are implemented on a global scale (FSI 2005). Studies carried out by different scientists for different countries in the Earth showed that US forests accumulated 12.1 Pg (Turner et al. 1995), European forests accumulated 7.5 Pg of carbon (Kauppi et al. 1992), Chinese forests stocked 4.63 Pg (Fang et al. 2001), and Japanese forests accumulated 1.39 Pg carbon (Alexandrov et al. 1999). Alexeyev et al. (1995), Isaev et al. (1995), and Krankina et al. (1996) noted that Russian forests accumulated a large amount of carbon, which was 28.04, 35.07, and 42.1 Pg, respectively (Manhas et al. 2006).

Earlier carbon sequestration works were made based on the concept of static biomass carbon with a longer timescale where diurnal carbon sequestration rate (CSR) (minute scale) has not been considered. Earlier works have only considered a concept of linear (proportionate) carbon sequestration as well as biomass, which was practically not feasible in the natural system. As per the knowledge of authors, the determination of diurnal carbon sequestration rate of any plant species is hitherto undone and this work has been attempted for the first time in this field. The specific objectives of this study are to measure diurnal carbon sequestration rate and aboveground biomass carbon content of young (6 years age) *S. robusta* (Sal) and *T. grandis* (Segun), and soil respiration in two natural forests in India. The sites were located at Chadra in Paschim Medinipur district for *S. robusta* and Chilapata forest in Coochbehar district for *T. grandis* in the state of West Bengal in India. The study has been carried out by the Regional Centre of National Afforestation & Ecodevelopment Board (NAEB), Ministry of Environment & Forest, Government of India, Jadavpur University in association with the School of Water Resources Engineering, and Jadavpur University in Kolkata.

17.2 The Site and Study Area

The sites and study areas for measurement of diurnal carbon sequestration rate and aboveground biomass carbon potential of *S. robusta* (Sal) and *T. grandis* (Segun) are described one by one. The study area of *S. robusta* is a tropical dry deciduous forest, located at Chadra in the Paschim Medinipur district of West Bengal and situated at 22°25′N latitude and 87°19′E longitude (District Statistical Handbook 2004). The general climate of the area is seasonal tropical. During summer period the mean daily ambient temperature varied from 12°C to 39°C with mean relative humidity ranged from 46% to 89% at 8:30 hour. During the monsoon period, the area received an average rainfall of 1,490 mm (District Statistical Handbook 2005). The soil of the study area belongs to red lateritic ultisol, which was derived from parent pegmatic rock. Texturally it is classified as loam, sandy loam, or clay loam type (Mallick et al. 2007). The location of Chadra forest is shown in Fig. 17.1. The selected plant species was *S. robusta* of 6 years age (Fig. 17.2). It had a height of 6 m and a diameter of 11.1 cm at breast height. The study considered 30 × 30 m
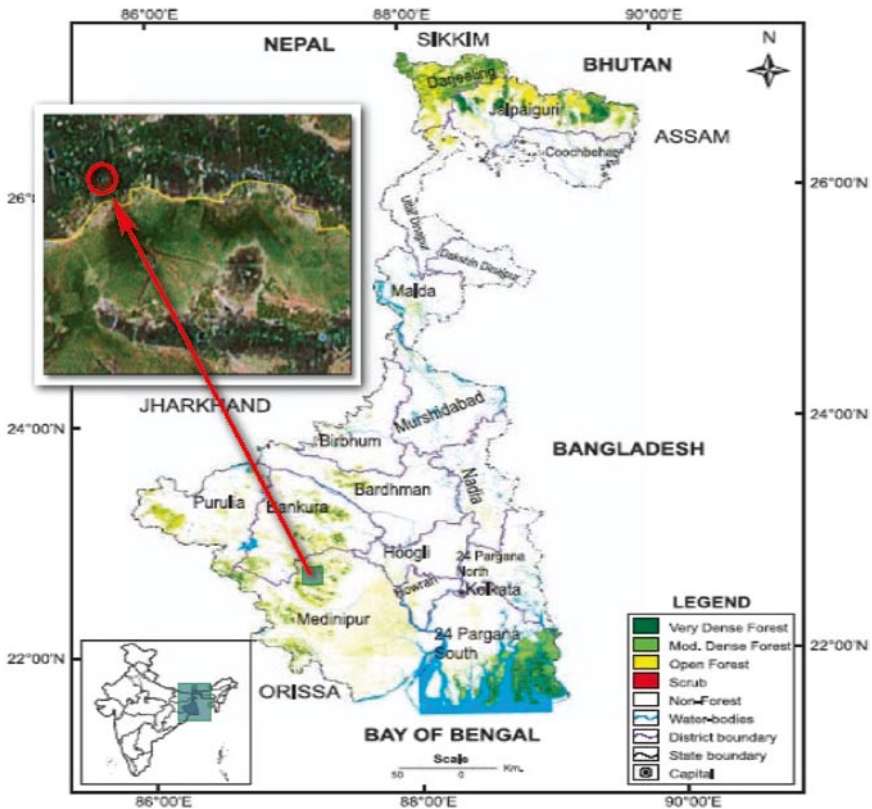
Fig. 17.1 Location of Chadra forest

Fig. 17.2 *Shorea robusta*

quadrate within which 81 *S. robusta* tree species of same age and height were available. Selected *S. robusta* tree was located at 3 km away from the existing road on which vehicular movement on the road was less.

Chilapata Forest in Coochbehar District had an area of 1,975.18 ha. The elevation of the working site, as measured by GPS, was 26°32.85′N latitude and 89°22.99′E longitude. Altitude of the area was 47 m above MSL. The location of Chilapata forest is shown in Fig. 17.3. The forest was surrounded by Malangi and Hasimara Rivers in east and south. The forest had northern dry and mixed deciduous forest. Most of the trees present in the forest were tall and flourished. The forest was mainly composed of Sissoo, Khair, Segun, Chatim, Sal, etc. The selected plant species was *T. grandis* (Segun) of 6 years age (Fig. 17.4).

17.3 Materials and Methods

17.3.1 Carbon Dioxide Measurement

Carbon dioxide (CO_2) has been measured by Automated Vaisala Made Instrument, GMP343 and the data have been collected continuously for 24 h basis. CO_2 has been measured for ambient air within and outside the forest areas and diurnal carbon sequestration rate from ambient air of two young species in closed top chamber (CTC).
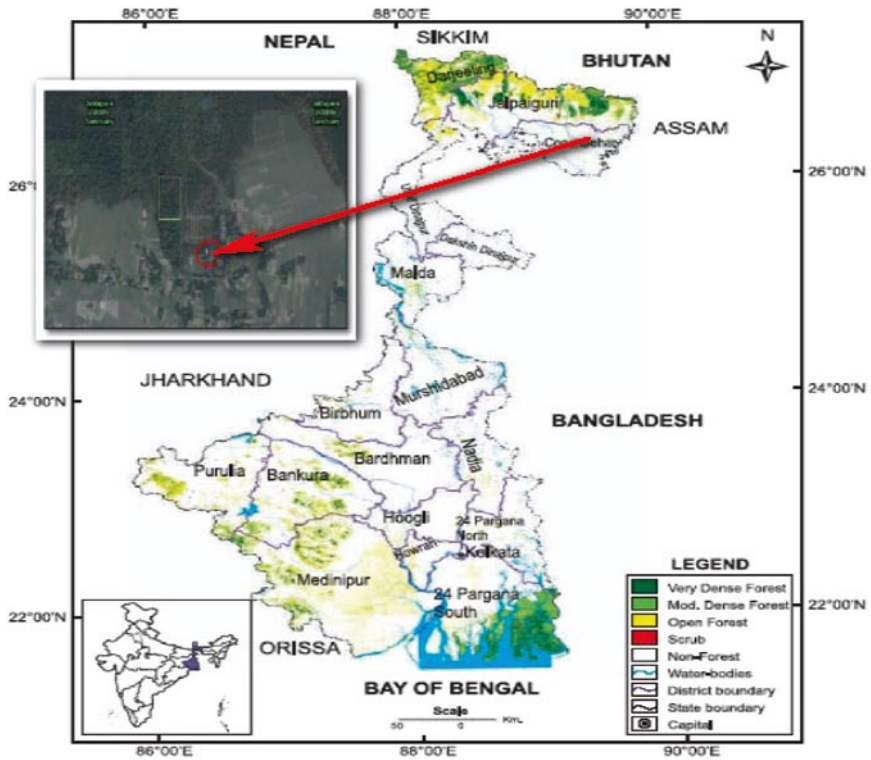
Fig. 17.3 Location of Chilapata forest

Like other factors, influence of humidity on carbon sequestration rate measurement of the plant has been ignored to emphasize the carbon sequestration study.

17.3.2 Measurement of Aboveground Biomass of the Tree

The biomass of the tree within a forest includes aboveground biomass, which includes all aboveground living materials (stem, branches, leaves) and belowground or root biomass, which consist of coarse roots and stumps. Biomass of the stem mainly includes the branches. The estimation of the biomass in the stem was performed by knowing the tree height, diameter, and girth size at different heights, etc. These have been measured by Spiegel Relascope and wood volume of the whole tree has been calculated by these data. Weight of the wood biomass has been calculated by multiplying volume of biomass and specific gravity (SG) of the wood, as per the below mentioned calculation where specific gravity (SG) is the ratio of oven dry weight and green volume of the pieces of wood samples. Leaf biomass has been calculated by the gravimetric method. Total number of leaves present in the tree has been counted from total number of branches and average number of leaves present in a branch. Few of the leaves of the tree were taken and their fresh

Fig. 17.4 *Tectona grandis*

weight was measured as well as dry weight after properly dried at 70°C for 7 days to a constant weight. From this the biomass of those leaves has been measured or calculated by gravimetric method. The root biomass has not been measured at this moment as the other research works will be conducted on this tree in future.

In the present study, we have estimated the aboveground biomass stock and aboveground biomass carbon of two species by taking volume of biomass and specific gravity (SG) of the tree, as per Rajput et al. (1996) and Negi et al. (2003).

$$\text{Biomass (g)} = \text{volume of biomass (m}^3) \times \text{specific gravity (SG)}$$

where SG is the oven dry weight/green volume and carbon = biomass × carbon %.

17.3.3   Carbon Content in Aboveground Biomass

The carbon contents of different biomass such as stems, branches, and leaves have been measured by taking samples and sent them to Indian Association for Cultivation of Science for estimation of carbon content by CHN Analyzer (PerkinElmer 2400 series II CHNS/O Elemental Analyzer). A certain amount of biomass samples have been collected from the particular stems, branches, and

leaves and after being properly dried at 70°C for about 7 days to a constant weight, the carbon content of the samples have been analyzed and carbon content has been estimated as per the above calculation.

17.3.4   Soil Characteristics and Soil Respiration

Physiochemical parameters of the soil samples have been analyzed, which have been collected from two sites, and soil respiration CO_2 emission has been measured by GMP343 continuously for 24 h in a closed chamber.

17.4   Results and Discussion

17.4.1   Ambient CO_2 Level

At Chadra, ambient CO_2 level has been measured at two locations, one at outside forest and other at inside forest near the tree. Distance between the two locations was about 150 m. It could be observed that average CO_2 levels in ambient air were 414.98 ppm at outside the forest and 402.10 ppm near the *S. robusta* tree. In between the two locations CO_2 concentration decreased to 12.88 ppm. This may be concluded that 12.88 ppm CO_2 concentration decreased due to the forest patch between two locations.

Likewise, ambient CO_2 level has been measured at two locations at Chilapata, one at inside the forest and other outside the forest. Distance between the two locations was about 300 m. It is observed that CO_2 levels in ambient air were 379.50 ppm at outside forest and 380.43 ppm inside the forest. It is noticed that the trees were mostly without leaves. Hence, the difference of ambient CO_2 level inside and outside the forest was negligible. It may be expected that in calm and clear sunny day this may have a definite difference of CO_2 level.

17.4.2   Soil Carbon and Soil Respiration

Soil samples from each site were collected from the top surface of the soil and in general, taken at three different depths up to 1 m from the surface and homogenized. About 1 kg of the homogenized soil sample has been taken in an airtight plastic packet for soil quality analysis in our laboratory. We have analyzed physiochemical parameters of soil samples such as soil conductivity, phosphate, soil moisture, pH, available K, water-holding capacity, bulk density, soil texture, soil organic and total carbon, total nitrogen, total sodium, sodium absorption ratio, and total calcium.

It is observed from the physiochemical analysis result of soil sample from Chadra that soils in the area was slightly acidic in nature (pH 5.35); electrical conductivity was 0.022 ms/cm; moisture content was 3.25%; water holding capacity was 0.32 g/kg; and bulk density was 1.48 g/cc. The soil texture was sandy loam (sand – 64.5%, silt – 30.4%, and clay – 5.1%). Total nitrogen and total phosphorus of the soil are 151 and 5.1 mg/kg; total potassium present in the soil was 1,154 mg/kg; total calcium was 544 mg/kg, and sodium absorption ratio of the soil was 3.1. Total carbon and soil organic carbon present in the soil were 15 and 1.4 g/kg, respectively. Carbon to nitrogen ratio (C/N) of the soil was 9.3.

At Chilapata site, soils in the area was slightly acidic in nature (pH 5.33); electrical conductivity was 0.058 ms/cm; moisture content was 22.1%; water-holding capacity was 0.495 kg/kg; and bulk density was 1.36 g/cc. The soil texture was loamy (sand – 35%, silt – 38.7%, and clay – 26.3%). Total nitrogen and total phosphorus of the soil were 1,043 and 424 mg/kg; total potassium present in the soil was 8,067 mg/kg; total calcium level was 9,792 mg/kg, and sodium absorption ratio of the soil was 0.86. Total carbon and soil organic carbon present in the soil were 62.5 and 12.8 g/kg, respectively. Carbon to nitrogen ratio (C/N) of the soil was 12.3.

The implications of soil–plant–atmosphere interaction involve not only the exchanges of water between the components of the system (Fig. 17.5), but also CO_2 fluxes between ecosystems and the atmosphere (Siqueira et al. 2000; Dickinson et al. 2002).

Soil organic matter (SOM) is a complex and varied mixture of organic substances with three main components: plant residues, microorganisms, and biomass and humus (Fig. 17.6). Globally, the soil contains more carbon than the vegetation and atmospheric pools combined. The amount of organic matter in soils
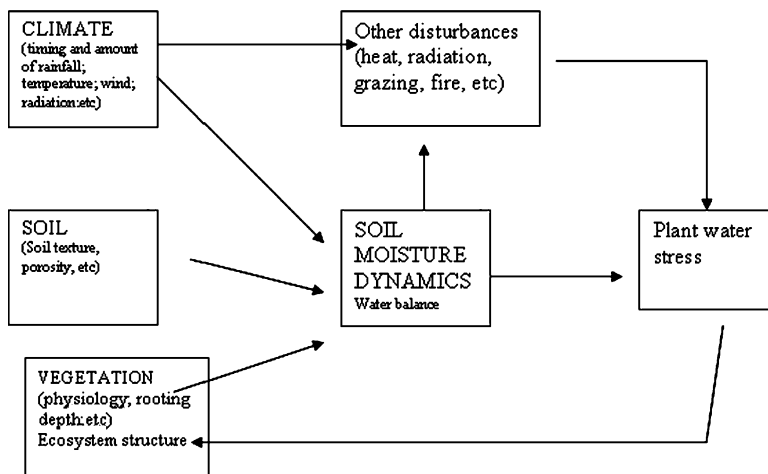
Fig. 17.5 First and main level of description of the climate–soil–vegetation system (Modified by Porporato and Rodriguez-Iturbe 2002, after Rodriguez-Iturbe et al. 2001a))
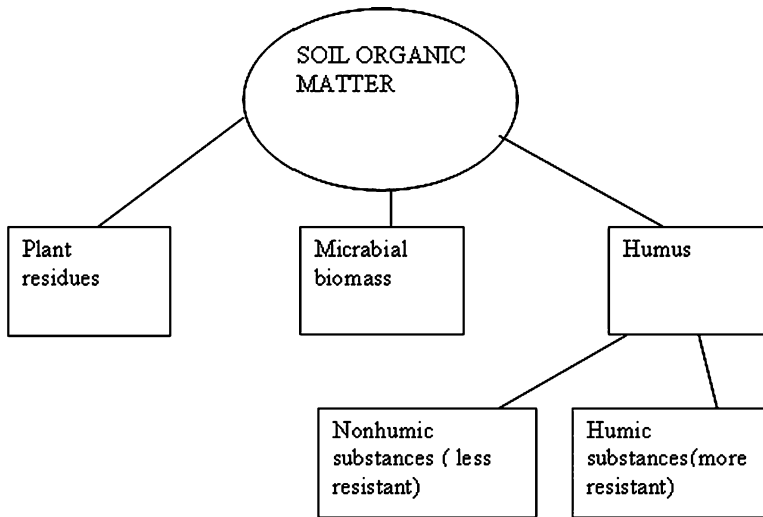
Fig. 17.6 Scheme of the three main components of soil organic matter (SOM) (Redrawn after Brady and Weil 1996). A simplified representation of the soil–plant–atmosphere carbon cycle is depicted in Fig. 17.7

varies widely and usually increases with humidity and to a lesser extent with temperature. Bogs and marshes are very important carbon pools in the terrestrial carbon cycle.

Soil organic matter (SOM) decomposition involves an enzymatic oxidation that produces mineral compounds (e.g., ammonium) and carbon dioxide (CO_2), which is then returned to the atmosphere (soil respiration). While part of the carbon is lost as soil respiration and the simpler compounds are metabolized by soil microbes, the most complex ones are not metabolized, but, along with other compounds polymerized by soil microbes, are combined to form the so-called humic substances, or resistant humus. Other less-resistant substances are also formed (nonhumic substances). Humic substances are very stable and contribute to maintain high organic levels in soils (Fig. 17.7).

When plant residues are added to the soil and the conditions are favorable, the bacterial colonies grow fast, but as soon as the decomposable SOM is reduced, they starve and die easily. The decomposition of dead microbial cells is associated with the release of simple products, such as nitrates and sulfates. Different bacterial colonies exist; each specialized in a given part of the decomposition process. Such bacteria are very sensitive to environmental conditions. Since most of the organic residues are deposited and incorporated at the surface, SOM tends to accumulate in the upper layers of the soils. In general, under similar climatic conditions, total SOM is higher and vertically more uniform in soils under grasslands than under forests; moreover, a relatively high proportion of plant residues in grasslands consists of root matter, which decomposes more slowly and contributes more effectively to soil
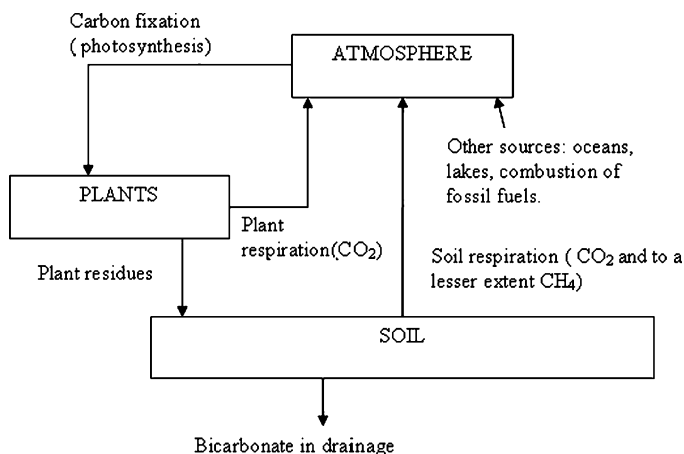
Fig. 17.7 A simplified representation of the soil–plant–atmosphere carbon cycle (After Porporato et al. 2003a)

Table 17.1 Results of CO_2 emission from soil respiration

Sl. no.	Location of project site	Soil CO_2 respiration rate (g/m²/h)
1	Chadra	0.0050
2	Chilapata	0.0575

humus than does forest litter. The mineralization rate depends on the composition of plant residues and in particular, on their C/N ratio. The growth of microbial colonies takes place with fixed proportions of carbon and nitrogen so that their C/N ratio remains practically constant (Rodriguez-Iturbe and Porporato 2006).

Carbon dioxide emissions from soil respiration were measured at two forests continuously for 24 h during winter season. The specified area of the soil was fully covered (airtight) by transparent plastic. We have started monitoring at Chadra forest from 14:10 hour at CO_2 concentration of 463.5 ppm within the closed plastic cover. CO_2 level increased to 1,265.4 ppm at 16:10 hour and at 17:10 hour it reached to 1,461.2 ppm. At 18:10 hour CO_2 concentration increased to maximum level at 1,521.8 ppm. While at 21:01 hour CO_2 level decreased to 1,405.8 ppm and in the morning at 6:10 hour, it decreased to 627.5 ppm. At 13:40 hour CO_2 concentrations decreased to 480.2 ppm. With the increase of sunlight, temperatures within the plastic increased. We have also started monitoring in the afternoon at Chilapata forest from 15:45 hour at CO_2 concentration of 383.8 ppm. CO_2 level increased to 1,296 ppm at 18:45 hour and at 21:45 hour the level reached to 1,546.2 ppm. At 0:45 hour the concentration slightly decreased to 1,538.2 ppm. In the morning at 6:45 hour the level decreased to 1,307.8 ppm and at 11:45 hour, it reached to 1,336.5 ppm.

CO_2 emissions from soil respiration at two forest areas measured during winter season are presented in Table 17.1. The results of CO_2 emission from soil respiration reveal that CO_2 emitted by soil respiration was higher at Chilapata (0.0575 g/m²/h) than that emitted at Chadra (0.0050 g/m²/h).

17.4.3   Carbon Sequestration Rate by S. robusta and T. grandis

Carbon sequestration rate is to measure how much carbon can be sequestered by a tree over a certain period (e.g., hour, day, month, or year). In a forest ecosystem, the CSR is closely related to climatic conditions, soil properties, tree species, stand age, and the forest rotation length (Graham et al. 1992; Niu and Duiker 2006).

Carbon dioxide is captured by the plant during photosynthesis. Carbon dioxide taken up by the Sal tree (*S. robusta*) has been measured for 24 h during winter season and the observations are shown graphically in Fig. 17.8. It is to be noted that photosynthesis and respiration occurs simultaneously during day and only respiration occurs during nighttime. Therefore, both CO_2 absorption and emission occurs during daytime and only CO_2 emission occurs during nighttime. Carbon sequestration rate by the plant has been evaluated by considering the photosynthesis and respiration during day and night. The respirated CO_2 emission by the plant has been eliminated from the total concentration of CO_2 with respect to time. The volume of covered plastic for the tree has been calculated. The bottom portion of the plastic was dipped into the soil to avoid any CO_2 contamination with the ambient air. So, soil respiration CO_2 has been eliminated to estimate the actual carbon sequestration rate as CO_2 of the plant. It is observed that at 7:00 hour carbon dioxide sequestration rate was 0.52 g/h. It increased to a level of 8.13 g/h at 9:00 hour. At 12:00 hour, the rate reached to 24.30 g/h to its maximum. In the afternoon, sunlight decreased rapidly. So, that time CO_2 emission through respiration was higher than the CO_2 absorption by the plant. At 17:00 hour sunlight was absolutely absent and the photosynthesis process turned to an end. Therefore, during 17:00 hour to 7:00 hour CO_2 level increased due to plant respiration. CO_2 concentration was increased by respiration during nighttime in the absence of photosynthesis process. At
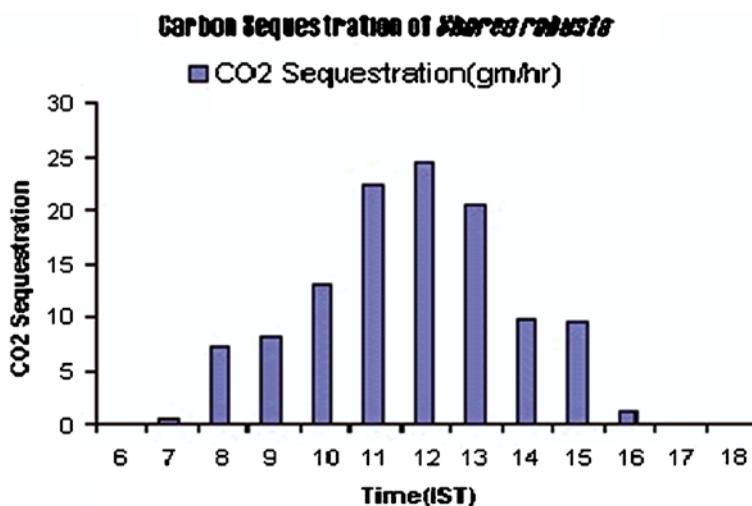
Fig. 17.8 Carbon sequestration rate as CO_2 by *Shorea robusta*
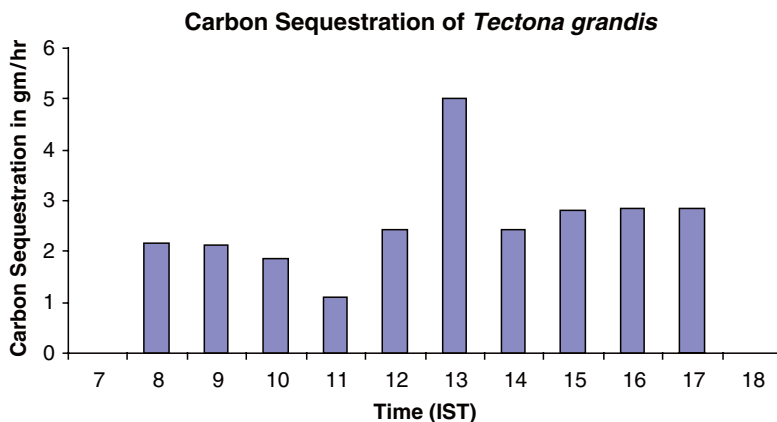
Fig. 17.9 Carbon sequestration rate as CO_2 of *Tectona grandis*

14:00 hour CO_2 sequestration rate reached to 9.82 g/h and at 16:00 hour CO_2 sequestration rate decreased to 1.17 g/h (Jana et al. 2009).

At Chilapata, we have started monitoring from 12:00 hour at CO_2 sequestration rate 2.42 g/h. Maximum CO_2 sequestration observed 5.02 g/h at 13:00 hour. CO_2 sequestration rate decreased to 2.82 g/h at 15:00 hour and 2.86 g/h at 17:00 hour. At 7:00 hour in the next day, no CO_2 sequestration was observed due to overcast skies. At 8:00 hour CO_2 sequestration rate reached to 2.17 g/h and at 10:00 hour the rate decreased to 1.86 g/h. Due to rainfall and bad weather (in overcast skies), CO_2 released by respiration was higher than the CO_2 received by the photosynthesis and hence the CO_2 level increased during daytime (Jana et al. 2009). Carbon sequestration rate of *T. grandis* is shown graphically in Fig. 17.9.

It could be observed from the result of carbon sequestration rate as CO_2 during winter season that the average CO_2 sequestration rate from the ambient air obtained by *S. robusta* at Chadra forest and *T. grandis* at Chilapata forest were 11.13 g/h (equivalent to 3.03 g C/h) and 2.57 g/h (equivalent to 0.70 g C/h). This may be expected a little change of carbon sequestration rate by these species during summer season due to long duration of sunlight. The rate of carbon sequestration depends on the growth characteristics of the tree species, the conditions for growth where the tree is planted, and the density of the tree's wood. This can be observed that carbon sequestration rate as CO_2 of *S. robusta* from ambient air was higher than *T. grandis* . Annual carbon sequestration rate as CO_2 from ambient air estimated for these young *species* of 6 years age by considering annual mean duration of effective sunlight for photosynthesis at the rate of 9 h in a day was 0.99×10^{-2} t C per tree and 8.97 t C/ha in the Chadra forest stand. To compare with the carbon sequestration rate of *S. robusta,* carbon sequestration rate have been evaluated as per the above consideration for *T. grandis* and annual carbon sequestration rate as CO_2 from ambient air estimated for young *species* of 6 years age were 0.23×10^{-2} t C per tree with 2.07 t C/ha for *T. grandis.* The carbon sequestration rate may be

expected to increase with the increase of forest stand ages. It could be noted that carbon sequestration rate of *T. grandis* from ambient air might be increased during the clear sunny days.

17.4.4 Biomass Carbon Content

The aboveground biomass of the tree such as stems, branches, and leaves (except root) have been collected and dried at laboratory, and the dry biomass of the different sections of the tree are presented in Table 17.2.

The result of biomass analysis through CHN Analyzer is presented in Table 17.3. It is observed for *S. robusta* that leaf and stem contained 49.09% and 46.88% carbon, respectively. For *T. grandis*, leaf contained 43.98% carbon and stem contained 46.93% carbon, respectively.

Total carbon stock of a tree has been evaluated by adding all the carbon contents of stems, branches, and leaves of the tree. Carbon content of the tree was established by the works of different scientists and researchers, the carbon content in the plant was approximately 50% of the dry matter (World Bank 1998). The carbon concentration of different tree parts was rarely measured directly, but generally assumed to be 50% of the dry weight (Losi et al. 2003). Work of Losi et al. (2003) obtained that measured carbon content of dry sample was 47.8% for *A. excelsum* and 48.5% for *D. panamensis*. "Extensive studies in Australia recently of a variety of tree species should above ground dry biomass generally contain 50% carbon. These proportions of carbon in aboveground biomass agreed closely with values of 49% and 47% reported from other parts of the world for *Pinus taeda* (Kinerson et al. 1977) and Populus spp. (Deraedt and Ceulemans 1998)" (West 2003). The total carbon contents in *S. robusta* and *T. grandis* are presented in Table 17.4.

Table 17.2 Total aboveground dry biomass of the tree

Study area	Tree	Total weight of dry stem and branch biomass (g)	Total weight of dry leaves biomass (g)	Total dry biomass (g) of the tree (except root)
Chadra forest	*Shorea robusta*	9,035	3,187	12,222
Chilapata forest	*Tectona grandis*	9,690	9,800	19,490

Table 17.3 Biomass analysis results

Tree	Parts of the plant	C (%)
Shorea robusta	Leaf	49.09
	Stem	46.88
Tectona grandis	Leaf	43.98
	Stem	46.93

Table 17.4 Carbon content of the aboveground biomass

Tree	Carbon content in	Carbon content in individual sample (%)	Total carbon content in the plant species (g)
Shorea robusta	Leaf	49.09	1,564.49
	Stem	46.88	4,236.00
Total carbon content in the plant			5,800.49
Tectona grandis	Leaf	43.98	4,310.04
	Stem	46.93	4,547.69
Total carbon content in the plant			8,857.73
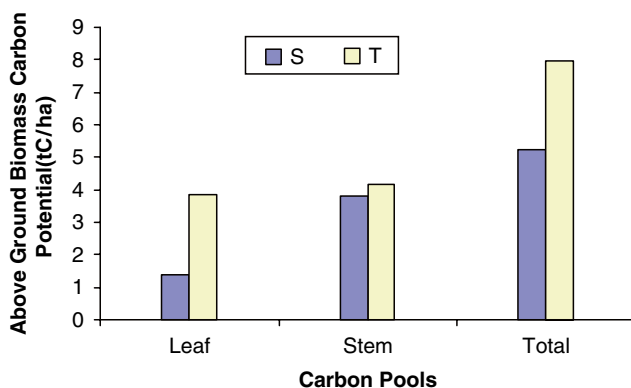
Fig. 17.10 Portioning of above ground biomass carbon pools of 6 years age *Shorea robusta* and *Tectona grandis*. S, *Shorea robusta*; *T, Tectona grandis*

It is observed from Table 17.4 that the total carbon contents of the whole tree (excluding root) of *S. robusta* and *T. grandis* trees were 5,800 g and 8,857 g, respectively. This may be concluded that the percentage of total carbon content in the biomass was 47.45 in *S. robusta* and 45.45 in *T. grandis.* Negi et al. (2003) reported that carbon content in *S. robusta* tree was 46%(Negi et al. 2003), while our analyzed data have shown that leaf and stem contained 49.09% and 46.88% in *S.robusta* tree, which were slightly higher. Total aboveground biomass carbon stock per hectare has been estimated from the aboveground biomass carbon content in 81 *S. robusta* trees (6 years age) within 30 × 30 m quadrate in the study area and total aboveground biomass carbon per hectare as estimated was 5.22 t C/ha. Likewise, total aboveground biomass carbon stock per hectare has been estimated from the aboveground biomass carbon content in 81 *T. grandis* trees (6 years age) present in 30 × 30 m quadrate (as per consideration). It is estimated that total aboveground biomass carbon per hectare for *T. grandis* was 7.97 t C/ha. It may be concluded that total aboveground biomass carbon per hectare of *T. grandis* was higher than *S. robusta* (Jana et al. 2009).

Carbon pool partitions of 6 years age *S. robusta* and *T. grandis* are shown in Fig. 17.10. Maximum carbon pools in a forest ecosystem primarily stored in

aboveground tree biomass (Haripriya 2003). It is estimated that annual above ground biomass carbon pools of two young species were observed to yield 0.87 t C/ha/year for *S. robusta* and 1.33 t C/ha/year for *T. grandis*. A short rotation plantation of 20 years age of hybrid poplar (*Populus* spp.) in Minnesota was estimated to yield an average of 1.8–3.1 t C/ha/year (Updegraff et al. 2004) and our estimated annual above ground biomass carbon pools were lower than Updegraff et al. 2004's work. Niu and Duiker (2006) estimated that in 20 years after afforestation a total of about 52 t C/ha could be sequestered in aboveground tree biomass carbon of both conifers and deciduous forests. Our estimated aboveground tree biomass carbon at 20 years age (by linear/proportionate estimation) will be 17.4 t C/ha[1] for *S. robusta* and 26.6 t C/ha for *T. grandis*, which were lower to the Niu and Duiker (2006)'s estimation. Earlier estimation was made based on linear/ proportionate calculation. Normally, tree biomass growth increases rapidly upto 20–50 years, not following any linear equation. According to Marland and Marland (1992), it could be expected from our study that aboveground tree biomass carbon stock of *S. robusta* and *T. grandis* will reach to the close value of Niu and Duiker (2006)'s estimation.

A simplified model proposed by Marland and Marland (1992) was used to simulate aboveground tree biomass carbon growth, in which the biomass carbon accumulates linearly until half of the maximum yield is reached and the growth slows down subsequently to reach the maximum yield asymptotically. A cumulative growth of aboveground tree biomass over time is illustrated in Fig. 17.11 (Niu and Duiker, 2006). At 6 years age, average aboveground tree biomass carbon (accumulative biomass carbon) was estimated to 18 t C/ha from Marland and Marland's work, whereas our average aboveground tree biomass carbon (accumulative biomass carbon) for *S. robusta* and *T. grandis* were estimated to 5.22 and 7.97 t C/ha, respectively. It could be concluded that aboveground tree carbon biomass of *S. robusta* and *T. grandis* were lower than the Marland and Marland
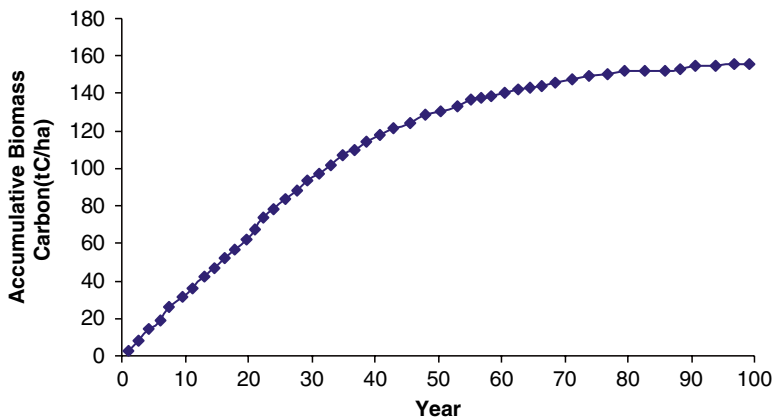
Fig. 17.11 A general tree growth model (Adopted from Marland and Marland 1992)

Table 17.5 Different research works on carbon stock per hectare in India

Year	Components	Carbon stock (t C/ha)	References
1985	AG + BG	31.07	Dadhwal and Nayak (1993)
1986	AG + BG	58.77	Ravindranath et al. (1997)
1988	AG + BG	54.52	Chhabra et al. (2002)
1993	AG + BG	61.06	Chhabra et al. (2002)
1995	AG + BG	31.72	Lal and Singh (2000)
1984	Wood	16.98	Manhas et al. (2006)
1994	Wood	17.12	Manhas et al. (2006)
2008	AG	5.22	Present study on *Shorea robusta* of 6 years age
2008	AG	7.97	Present study on *Tectona grandis* of 6 years age

AG, aboveground; BG, belowground

(1992)'s estimation. This may be due to different forest types, soil qualities, climatic conditions, nonhybrid species, and only 6 years age species (stand age).

Different scientists on their research works found out carbon stock per hectare in India (Table 17.5) and carbon stock per hectare found out by our study has been compared.

Earlier estimates by different scientists were higher than our estimate. The reasons for low carbon stock as estimated by our work may be due to consideration of only aboveground biomass, only one tree from each species was considered for this estimation, very young *S. robusta* and *T. grandis* of 6 years age were considered, and worked in similar agroclimatic areas. Earlier works were estimated mostly based on aboveground and belowground carbon biomass, considering different age groups, different species, and different agroclimatic areas, for which carbon stock per hectare may be in higher side. With the progress of the forest stand ages, canopy cover and biomass of the trees will experience more rapid growth to a certain age (20–50 years) and the carbon held by these plants will also increase more biomass carbon stock to its optimum level (Marland and Marland 1992).

17.5 Conclusion

This study illustrates diurnal carbon sequestration rate and aboveground biomass carbon potential of young *S. robusta and T. grandis,* and emission of soil respiration CO_2 in the areas. Soil respiration results obtained in two forests at Chadra and Chilapata were 0.0050 and 0.0575 $g/m^2/h$, respectively. The article concludes that carbon sequestration rate from the ambient air as obtained by *S. robusta* at Chadra forest and *T. grandis* at Chilapata forest were 11.13 g/h with annual carbon sequestration rate 8.97 t C/ha and 2.57 g/h with annual carbon sequestration rate 2.07 t C/ha in overcast skies. Percentage of carbon content in the aboveground biomass of *S. robusta and T. grandis* were 47.45 and 45.45, respectively. Total aboveground biomass carbon stock per hectare for *S. robusta* and *T. grandis* as

estimated were 5.22 and 7.97 t C/ha, respectively. It could be concluded that our estimated results were lower than the previous works done by different scientists, which may be due to consideration of one tree from each species, very young age of the plant, consideration of only aboveground biomass carbon, similar agroclimatic areas for study, similar soil characteristics, etc.

References

Alexandrov GA, Yamagata Y, Oikawa T (1999) Towards a model for projecting net ecosystem production of the world forests. Eco Model 123:183–191

Alexeyev V, Birdsey R, Stakanov V, Korotkov I (1995) Carbon in vegetation in Russian forests: methods to estimate storage and geographical distribution. Water Air Soil Pollut 82:271–282

Brady NC, Weil RR (1996) The nature and properties of soil, 11th edn. Prentice Hall, Upper Saddle River, NJ

Burley J, Evans J, Youngquist JA (2004) Encycl Forest Sci 1:144–149

Centritto M, Lee HSJ, Jarvis PG (1999a) Interactive effects of elevated $[CO_2]$ and drought on cherry (*Prunus avium*) seedlings, Growth, whole-plant water use efficiency and water loss, whole-plant water use efficiency and water loss. New Phytol 141:129–140

Centritto M, Magnani F, Lee HSJ, Jarvis PG (1999b) Interactive effects of elevated $[CO_2]$ and drought on cherry (*Prunus avium*) seedlings, Photosynthetic capacity and water relations. New Phytol 141:141–153

Chhabra A, Parila S, Dadhwal VK (2002) Growing stock based forest biomass estimate of India. Biomass Bioenergy 22:187–194

Dadhwal VK, Nayak SR (1993) A preliminary estimate of biogeochemical cycle of carbon for India. Sci Cult 59(1/2):9–13

Deraedt W, Ceulemans R (1998) Clonal variability in biomass production and conversion efficiency of poplar during the establishment year of a short rotation coppice plantation. J Biomass Bioenergy 15(4–5):391–398

Dickinson RE, Berry JA, Bonan GB, Collatz GJ, Field CB, Fung IY, Goulden M, Hoffman WA, Jackson RB, Myneni R, Sellers PJ, Shaikh M (2002) Nitrogen control on climate model evapotranspiration. J Climate 15:278–295

District Statistical Handbook (2004) Bureau of Applied Economics & Statistics, Government of West Bengal

District Statistical Handbook (2005) Bureau of Applied Economics & Statistics, Government of West Bengal

Fang JY, Chen AP, Peng CH, Zhao SQ, Ci IJ (2001) Changes in forest biomass carbon storage in China between 1949 and 1998. Science 292:2320–2322

FSI (2005) State of Forest Report, 2005. Forest Survey of India, Ministry of Environment & Forests, Dehradun, India

Graham RL, Wright LL, Turhollow AF (1992) The potential for short rotation woody crops to reduce U.S. CO_2 emissions. Climate Change 22:223–238

Hamburg SP, Harris N, Jaeger J, Karl TR, McFarland M, Mitchell JFB, Oppenheimer M, Santer S, Schneider S, Trenberth KE, Weigley TML (1997) Common questions about climate change. United Nation Environment Programme, World Meteorology Organisation

Haripriya GS (2003) Carbon budget of the Indian forest ecosystem. Climate Change 56:291–319

Idso SB, Kimball BA (2001) CO_2 enrichment of sour orange trees: 13 years and counting. Environ Exp Bot 46:147–153

Rodriguez-Iturbe I, Porporato A (2006) Ecohydrology of water- controlled ecosystems: soil moisture and plant dynamics. Cambridge University Press, New York

Isaev A, Korovin G, Zamolodehikov D, Utkin A, Pryaznikov A (1995) Carbon stock and deposition in phytomass of the Russian forests. Water Air Soil Pollut 82:247–256

Jana BK, Biswas S, Majumder M, Roy P, Mazumdar A (2009) Carbon sequestration rate and aboveground biomass carbon potential of four young species. J Ecol Nat Environ 1(2):15–24

Kauppi PE, Mielikainen K, Kuusela K (1992) Biomass and carbon budget of European forests, 1971 to 1990. Science 256:70–74

Keutgen N, Chen K (2001) Responses of citrus leaf photosynthesis, chlorophyl fluorescence, macronutrient and carbohydrate contents to elevated CO_2. J Plant Physiol 158:1307–1316

Kinerson RS, Ralston CW, Wells CG (1977) Carbon cycling in a loblolly pine plantation. Oecologia 29:1–10

Krankina ON, Harmon ME, Winjum JK (1996) Carbon storage and sequestration in the Russian forest sector. Ambio 25:284–288

Lal M, Singh R (2000) Carbon sequestration potential of Indian forests. Environ Monitor Assess 60:315–327

Losi CJ, Siccama TG, Condit R, Morales JE (2003) Analysis of alternative methods for estimating carbon stock in young tropical plantations. Forest Ecol Manage 184:355–368

Mallick SK, Pati BR, Behera N (2007) A phenological study of some dominant tree species in a tropical dry deciduous forest of Paschim Medinipur District, West Bengal. Ind Forest 133(12):1675–1682

Manhas RK, Negi JDS, Kumar R, Chauhan PS (2006) Temporal assessment of growing stock, biomass and carbon stock of Indian Forests. Climate Change 74:191–221

Marland G, Marland S (1992) Should we store carbon in trees? Water Air Soil Pollut 64:181–195

Negi JDS, Manhas RK, Chauhan PS (2003) Carbon allocation in different components of some tree species of India: a new approach for carbon estimation. Curr Sci 85(11):101–104

Niu X, Duiker SW (2006) Carbon sequestration potential by afforestation of marginal agricultural land in the Midwestern US. Forest Ecol Manage 223:415–427

Nowak DJ, Crane DE (2002) Carbon storage and sequestration by urban trees in the USA. Environ Pollut 116:381–389

Pan Q, Wang Z, Quebedeaux B (1998) Responses of the apple plant to CO_2 enrichment: changes in photosynthesis, sorbitol, other soluble sugars, and starch. Aust J Plant Physiol 25:293–297

PerkinElmer Life and Analytical Sciences, USA. Retrieved from www.perkinelmer.com

Porporato A, Rodriguez-Iturbe I (2002) Ecohydrology – a challenging multidisciplinary research perspective. Hydrol Sci J 47(5):811–822

Porporato A, D' Odorico P, Laio F, Rodriguez-Iturbe I (2003) Hydrologic controls on soil carbon and nitrogen cycles. I. Modelling scheme. Adv Water Res 26(1):45–58

Rajput SS, Shukla NK, Gupta VK, Jain JD (1996) Timber mechanics: strength classification and grading of timber, *ICFRE*-Publication-38, New Forest, Dehradun

Ravindranath NH, Somashekar BS, Gadgil M (1997) Carbon flows in Indian forests. Climate Change 35:297–320

Rodriguez-Iturbe I, Porporato A, Laio F, Ridolfi L (2001) Plants in water controlled ecosystems: active roll in hydrological processes and responses in water stress. I. scope and general outline. Adv Water Resour 24(7):697–705

Schaffer B, Whiley AW, Searle C, Nissen RJ (1997) Leaf gas exchange, dry matter partitioning, and mineral element concentrations in mango as influenced by elevated atmospheric carbon dioxide and root restriction. J Am Soc Hort Sci 122:849–855

Siqueira M, Lai CT, Katul G (2000) Estimating scalar sources, sinks and fluxes in a forest canopy using Lagrangian, Eulerian and hybrid inverse models. J Geophys Res 105(D24)29:475–488

Turner DP, Koerper GJ, Harmon ME, Lee JJ (1995) A carbon budget for forests of the conterminous United States. Ecol Appl 5:421–436

Updegraff K, Baughman MJ, Taff SJ (2004) Environmental benefits of cropland conversion to hybrid poplar: economic and policy considerations. Biomass Bioenergy 27:411–428

Veld KV, Plantinga A (2005) Carbon sequestration or abatement? The effect of rising carbon prices on the optimal portfolio of greenhouse-gas mitigation strategies. J Environ Econ Manage 50(1):59–81

WB (The World Bank) (1998) A practical guidance document for the assessment of project level greenhouse gas emissions. Greenhouse gas assessment handbook, vol 64. World Bank, 168 pp

West PW (2003) Tree and forest measurement. Springer, New York, p 62

Chapter 18
Estimation of Soil Carbon Stock and Soil Respiration Rate of Recreational and Natural Forests in India

Bipal K. Jana, Soumyajit Biswas, Sashi Sonkar, Mrinmoy Majumder, Pankaj Roy, and Asis Mazumdar

Abstract Soil contains good amount of carbon stock. The amount of carbon stock depends on soil texture, climatic parameters, vegetation, land-use pattern, and soil moisture. The study has been conducted at four sites in the recreational and natural forests in India. The main objective of this study is to estimate the soil carbon stock and soil respiration rate of recreational and natural forests in plain land in eastern India. At Banobitan – a recreational forest, soil was slightly alkaline; moisture content

B.K. Jana (✉)
Senior Research Fellow, School of Water Resources Engineering, Jadavpur University, Kolkata-700032, West Bengal, India
and
Environmental Manager, Consulting Engineering Services, West Bengal, India
e-mail: bipalkjana@gmail.com

S. Biswas
Research Fellow, School of Water Resources Engineering, Jadavpur University, Kolkata-700032, West Bengal, India

S. Sonkar
Junior Research Fellow, School of Water Resources Engineering, Jadavpur University, Kolkata-700032, West Bengal, India

M. Majumder
Senior Research Fellow, School of Water Resources Engineering, Jadavpur University, Kolkata-700032, West Bengal, India
and
Geo-information Scientist, Regional Center, National Afforestation and Eco-development Board, Jadavpur University, Kolkata-700032, West Bengal, India

P. Roy
Lecturer, School of Water Resources Engineering, Jadavpur University, Kolkata, Kolkata-700032, West Bengal, India

A. Mazumdar
Coordinator, Regional Center, National Afforestation and Eco-development Board, Jadavpur University, Kolkata-700032, West Bengal, India
and
Director, School School of Water Resources Engineering, Jadavpur University, Kolkata-700032, West Bengal, India

ranged between 7.26% and 9.74%, and soil texture was sandy loam. Total carbon and soil organic carbon (SOC) ranged from 24.2 to 36.5 and 2.8–8.3 g/kg, respectively. At Indian Botanic Garden – a recreational forest, soil was slightly acidic in nature; moisture content varied between 16.2% and 21.7%, and soil texture was clayey loam. Total carbon and soil organic carbon in the soil varied between 58 and 80.1 and 8.3 and 12.6 g/kg, respectively. At Chandra – a natural forest, soil was slightly acidic in nature; moisture content ranged between 3.2% and 11.4%, and soil texture was sandy loam. Total carbon and soil organic carbon ranged from 15 to 23.2 and 1.4–1.5 g/kg, respectively. At Chilapata forest – a natural forest, soil was slightly acidic in nature; moisture content varied between 22.1% and 26.0% and soil texture was loamy. Total carbon and soil organic carbon in the soil varied between 45.7 and 62.5 and 7.4 and 12.8 g/kg, respectively. Estimated mean soil total carbon and mean soil organic carbon stock at Banobitan, Indian Botanic Garden, Chandra, and Chilapata forests were 43.70 and 7.99, 96.32 and 14.57, 27.31 and 2.07, and 75.52 and 13.73 Mg C/ha, respectively. Estimated annual soil respiration rates of Banobitan, Indian Botanic Garden, Chandra, and Chilapata were 2.07, 3.34, 0.61, and 4.18 t C/ha/year, respectively.

18.1   Introduction

Soils contain a good amount of carbon in organic and inorganic or mineral forms. The amount of soil organic carbon (SOC) depends on soil texture, climate, vegetation, and land-use pattern. Soil texture affects SOC. Organic matter can be trapped in the very small spaces between clay particles, making them inaccessible to microorganisms and therefore slowing decomposition. Clay offers chemical protection to organic matter through adsorption onto clay surfaces that indicates more organic matter in clayey soil. Soils under natural forests or grassland tend to have higher SOC content than soils under cropland. The conversion of cropland back to forest or grassland is likely to increase SOC (Eleanor 2008). Lal (2004) estimated that with appropriate use and management, soils have the potential to sequester ~0.9 Pg C/year. This is roughly equal to 13% of the anthropogenic CO_2-C produced annually. Ravindranath et al. (1996, 1997) reported that mean soil carbon rates in top 30 cm for tropical moist deciduous and tropical dry deciduous forests were estimated 57.1 and 58.0 Mg C/ha, respectively. The estimate of average carbon content (in the biomass and forest soil) in Indian forests is 126 Mg C/ha of which 36% (45.8 Mg C/ha) is in biomass and 64% (79.8 Mg C/ha) is in forests soil (Haripriya 2003). SOC is the largest terrestrial carbon pool, which holds a very significant role in global terrestrial ecosystem carbon balance. Eswaran et al. (2000) estimated soil organic carbon stock to 580 Pg in global forest. Based on the average global or regional soil carbon densities, Indian forest soil organic carbon pool is estimated in the range between 5.4 and 6.7 Pg C (Ravindranath et al. (1996, 1997; Dadhwal et al. 1998)). Dadhwal et al. (1998) also estimated forest soil organic carbon pools

of 4.9 and 4.6 Pg C for 1980 and 1990, respectively, using FAO (1993) forest area. Chhabra et al. (2003) estimated that total soil organic carbon pools in top 50 cm and top 1 m soil depth were 4.13 and 6.81 Pg C, respectively.

Kaur et al. (2007) reported that soil respiration, a common measure of soil biological activity, represents the amount of CO_2 evolved from roots, soil microbes, and to a lesser extent by oxidation of root exudates, plant detritus, and humified organic matter (Raich and Schlesinger 1992). Soil contributes about 10% of total CO_2 emissions to atmosphere (the annual efflux of soil CO_2 is about 76.5 Pg C/year – Raich and Potter 1995). Among various factors, soil temperature and moisture are mainly important that influence soil respiration (Howard and Howard 1993; Singh and Gupta 1977; Raich and Tufekcioglu 2000; Vanhala 2002; Frank et al. 2006). Yasuike et al. (2003) and Ikeda et al. (2003) of CRIEPI (Central Research Institute of Electric Power Industry) worked at Kita-Saku site in central Japan and observed that SOC with 34 t C was observed in layer between ground surface and 20 cm depth and annual respiration in Kita-Saku was estimated as 6–7 t C/ha/year. It is also observed that soil respiration highly depends on soil temperature and consequently the value increased during the summer season and decreased during winter. Kelting et al. (1998) reported that total soil respiration is equal to the summation of root respiration, root-free soil respiration, and rhizosphere respiration. Boone et al. (1998) reported that increase in total soil respiration was highly related to root biomass; the pastures with greater root biomass would probably contribute more to soil respiration and such pastures will be more sensitive for CO_2 emissions to change with temperature. If there is an increase in temperature in global climate, predicted by IPCC (2005), then soil CO_2 emissions will most likely increase in pastures with greater root biomass. Ryan and Law (2005) stated that soil respiration is the largest component of ecosystem respiration. Root and associated microrrhizal respiration produce roughly half of soil respiration. In dry conditions, root and microorganism activity is typically low, resulting in low soil CO_2 efflux. Increasing the soil moisture normally increases the bioactivity in the soil. But if there is very high soil moisture, total soil CO_2 efflux is reduced, because of limited diffusion of oxygen and subsequent suppression of CO_2 emissions. Tomonori et al. (2003) reported that annual soil respiration rate in Japan was estimated to be 454–566 g C/m^2/year in an artificial forest. Higher moisture content in the soils is responsible for higher soil respiration rate (Chen et al. 2008). As most of the organic residues are deposited and incorporated at the surface, soil organic matter (SOM) tends to accumulate in the upper layers of the soils. In general, under similar climatic conditions, total SOM is higher and vertically more uniform in soils under grasslands than under forests; moreover, a relatively high proportion of plant residues in grasslands consist of root matter, which decomposes more slowly and contributes more effectively to soil humus than does forest litter (Porporato and Rodriguez-Iturbe 2002).

The study has been conducted at four sites, two at recreational forests and other two at natural forests in India by Regional Centre of National Afforestation & Ecodevelopment Board, MoEF, Government of India in association with School of Water Resources Engineering, Jadavpur University, Kolkata, India. As per the knowledge of authors, the determination of seasonal variation of soil respiration rate in the study area is hitherto undone and this work in the study area has been attempted for the first time. The main objective of this study is to estimate the soil carbon stock and soil respiration rate of recreational and natural forests in eastern India.

18.2   Study Area

The study areas for recreational forests were located at Banobitan within Kolkata and Indian Botanic Garden in Howrah districts in the state of West Bengal in India. The terrain of Kolkata and Howrah are flat and the areas are part of the lower Bengal delta of the river Ganga. Banobitan is one of the largest man-made urban forest at Salt Lake in Kolkata on the eastern bank of the river Ganga (Hooghly) under the Forest Department of Government of West Bengal. It is also known as Central-Park (Fig. 18.1). It has varieties of plant species among which few are very rare and uncommon. The garden was very well maintained for the plant species. It has a large lake inside the garden. The elevation of the working site, as measured by GPS, was 22°35′N latitude and 88°24′E longitude and altitude of the area was 7.5 m above MSL. The Indian Botanic Garden, established in 1787, is situated on the western bank of the river Ganga (Hooghly) in Howrah district of West Bengal, India (Fig. 18.1). It is located at a distance of 8 km from Howrah railway station and 25 km from Calcutta International Airport (Netaji International Airport). The Indian Botanic Garden covered an area of about 110.52 ha (Chowdhery 2001). The Elevation of the working site, as measured by GPS, was 22°33.42′ N latitude and 88°17.25′E longitude. Altitude of the area was 12 m above MSL. The general climate of the area was seasonal tropical.

The study areas for natural forests were located at Chandra forest in West Medinipur district and Chilapata forest in Coochbehar district in the state of West Bengal in India. The study area of Chandra is a tropical dry deciduous forest and situated at 22°25′N latitude and 87°19′E longitude (District Statistical Handbook 2004). The general climate of the area is seasonal tropical. During summer period the mean daily ambient temperature varied from 12°C to 39°C with mean relative humidity ranged from 46% to 89% at 8:30 hours. During the monsoon period, the area received an average rainfall of 1,490 mm (District Statistical Handbook 2005). The soil of the study area belongs to red lateritic ultisol, which was derived from parent pegmatic rock. Texturally, it is classified as loam, sandy loam, or clay loam type (Mallick et al. 2007). The location of Chandra forest is shown in Fig. 18.1. The dominant species in the forest was *Shorea robusta*. Chilapata forest in Coochbehar District had an area of 1,975.18 ha. The elevation of the working site, as measured by GPS, was 26°32.85′N latitude and 89°22.99′E longitude. Altitude of the area was 47 m above MSL. The location of Chilapata forest is shown in Fig. 18.1. The forest was surrounded by Malangi and Hasimara rivers in east and south. The forest had northern dry and mixed deciduous forest. Most of the trees present in the forest were tall and flourished. The forest was mainly composed of Sissoo, Khair, Segun, Chatim, Sal, etc.

18.3   Materials and Methods

Soil samples from each site have been collected from the top surface of the soil and in general, taken at three different depths below 1 m from the surface and homogenized. About 1 kg of the homogenized soil sample has been taken in an airtight plastic packet for soil quality analysis (Fig.18.2). The physiochemical parameters of soil
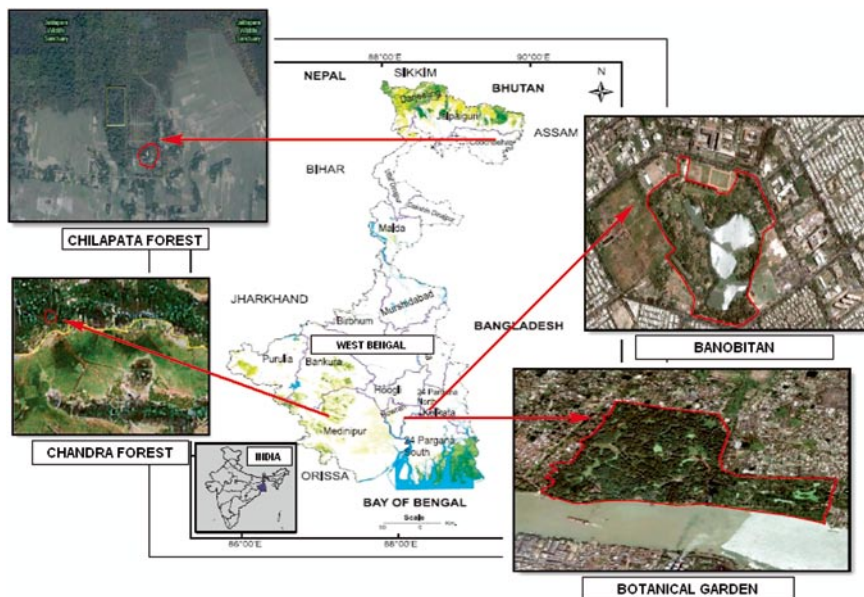
Fig. 18.1 Location of Banobitan, Indian Botanic Garden, Chandra, and Chilapata forests

Fig. 18.2 Soil sample collection at Banobitan

Fig. 18.3 Soil respiration measurement

sample analysis have been analyzed such as pH, soil texture, soil moisture, bulk density, carbon to nitrogen ratio (C/N), soil total carbon, and soil organic carbon.

We have tried to assess the stock of C that is held in a given area of soil, taking into account the depth and the compaction of the soil. Estimates of SOC stock (Eleanor 2008) have generally referred to a given depth of soil (e.g., top 100 cm). The amount of soil organic carbon in a given depth depends on how compacted the soil is, which is measured by determining the soil's bulk density (BD). The SC or SOC stock of a given area of soil with the same soil type can then be expressed as below:

$$\text{SC or SOC stock} = \frac{\text{SC or SOC content of the soil} \times \text{BD} \times \text{area} \times \text{depth}}{10}$$

Soil respiration rate (CO_2 emission) has been measured by Automated Vaisala Made Instrument, GMP343 in a closed chamber of plastic cover (Fig. 18.3). The data of carbon dioxide emission by the soil respiration have been collated. CO_2 was collected in a known volume of plastic cover. CO_2 data have been converted into weight emission, which was liberated from a specific ground area covered with the plastic. Finally, soil carbon dioxide respiration rate ($g/m^2/h$) has been estimated.

18.4 Results and Discussions

The physiochemical parameters of the soil samples have been analyzed as per the standard methods. Soil samples at Banobitan were collected from two locations during December 2007 and May 2008. It is observed from the physiochemical analysis

result of soil samples that soil in the area was slightly alkaline (pH 7.06–8.25); electrical conductivity varied between 0.088 and 0.104 ms/cm; moisture content ranged between 7.26% and 9.74%, and bulk density varied between 1.42 and 1.46 g/cc. The soil texture was sandy loam (sand: 56.3–71.6%, silt: 19.7–36.9%, and clay: 6.8–8.7%). Total carbon and soil organic carbon in the soil ranged from 24.2 to 36.5 and 2.8–8.3 g/kg, respectively. Carbon to nitrogen ratio (C/N) of the soil varied between 10.8 and 11.8.

Soil samples of Botanical Garden have been collected and analyzed during February and October 2008. It is revealed from the analysis result that soil in the area was slightly acidic in nature (pH 5.90–7.01); electrical conductivity varied between 0.107 and 0.097 ms/cm, moisture content varied between 16.2% and 21.7%, and bulk density ranged between 1.37 and 1.42 g/cc. The soil texture was clayey loam (sand – 17.8–43%, silt – 24.9–38.7%, and clay – 18.3–57.2%). Total carbon and soil organic carbon in the soil varied between 58 and 80.1 and 8.3–12.6 g/kg, respectively. Carbon to nitrogen ratio (C/N) of the soil ranged between 10.4 and 11.0 (Jana et al. 2009).

Soil samples of Chandra were collected during December 2007 and September 2008. The physiochemical analysis result of soil samples revealed that soil in the area was slightly acidic in nature (pH 5.35–5.93); electrical conductivity varied between 0.022 and 0.030 ms/cm; moisture content ranged from 3.25% to 11.4%, and bulk density ranged between 1.38 and 1.48 g/cc. The soil texture was sandy loam (sand – 47.4–64.5%, silt – 30.4–45.8%, and clay – 5.1–6.8%). Total carbon and soil organic carbon present in the soil were ranged between 15 and 23.2 and 1.4–1.5 g/kg, respectively. Carbon to nitrogen ratio (C/N) of the soil ranged between 9.3 and 10.6.

Soil samples at Chilapata forest were collected during January, May, and September 2008 and physiochemical parameters were analyzed. It is observed from the analysis result that soils in the area were slightly acidic (pH range 4.60–5.78); electrical conductivity ranged between 0.040 and 0.075 ms/cm; moisture content varied between 22.1% and 26%, and bulk density ranged between 1.34 and 1.38 g/cc. The soil texture was loamy (sand – 35–46.5%, silt – 34.2–39.6%, and clay – 18.2–26.3%). Total carbon and soil organic carbon ranged between 45.7 and 62.5 and 7.4–12.8 g/kg, respectively. Carbon to nitrogen ratio (C/N) of the soil varied between 11 and 12.3.

Among the four sites, maximum total soil carbon was present at Botanical Garden (average 69.05 g/kg) followed by Chilapata (average 55.53 g/kg) and Banobitan (average 30.35 g/kg), and minimum at Chandra (average 19.1 g/kg); while maximum soil organic carbon was obtained at Botanical Garden (average 10.45 g/kg) and minimum obtained at Chandra (average 1.45 g/kg). Carbon to nitrogen ratio of the four sites as analyzed were 11.56 (average) at Chilapata, 11.3 (average) at Banobitan, 10.7 (average) at Botanical Garden, and 9.99 (average) at Chandra forest. The total carbon and soil organic carbon and carbon to nitrogen ratio of different sites are presented in Figs. 18.4 and 18.5, respectively. The mineralization rate depends on the composition of plant residues and, in particular, on their C/N ratio. The growth of microbial colonies takes place with fixed proportions
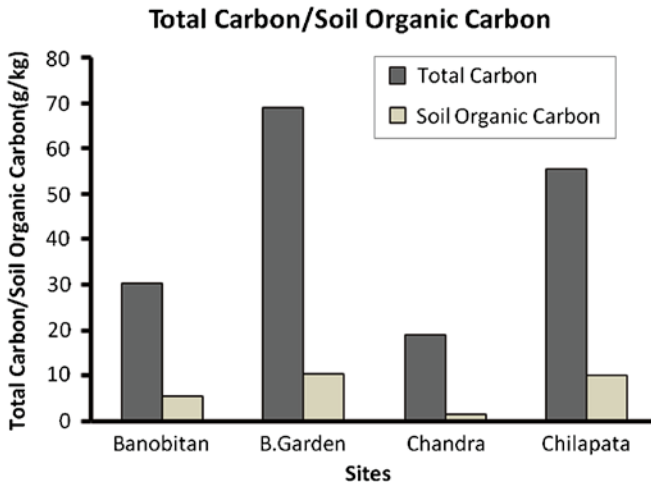
Fig. 18.4 Results of total carbon and soil organic carbon
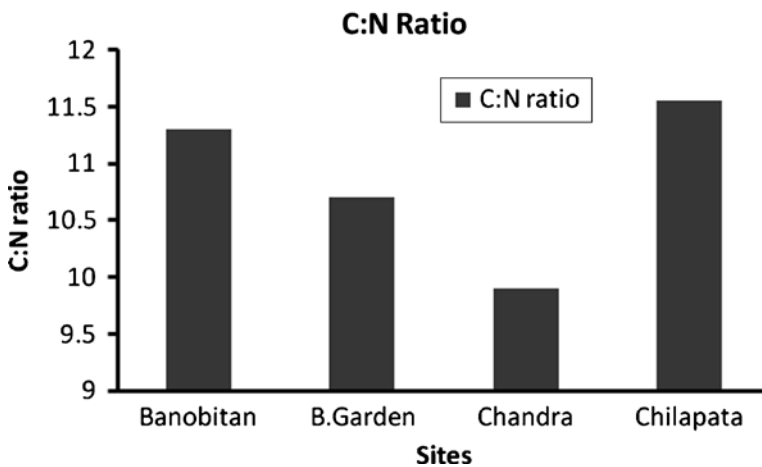
Fig. 18.5 Results of C/N

of carbon and nitrogen so that their C/N ratio remains practically constant (Porporato and Rodriguez-Iturbe 2002).

Mean soil total carbon and soil organic carbon stock have been estimated based on the soil total carbon content and soil organic carbon content, bulk density of the soil, area, and depth of soil collection. Estimated mean soil total carbon and mean soil organic carbon content at Banobitan were 43.70 and 7.99 Mg C/ha (18.28% of total soil carbon), respectively. While at Botanic Garden, mean soil total carbon and

mean soil organic carbon content were 96.32 and 14.57 Mg C/ha (15.13% of soil total carbon). It is evident that soil total carbon content of Botanic Garden was 45.37% higher than Banobitan; while soil organic carbon of Botanic Garden was 54.82% higher than Banobitan soil organic carbon (Jana et al. 2009). Estimated mean soil total carbon and mean soil organic carbon content at Chandra forest were 27.31 and 2.07 Mg C/ha (7.58% of total soil carbon), respectively. While at Chilapata forest, mean soil total carbon and mean soil organic carbon content were 75.52 and 13.73 Mg C/ha (18.18% of soil total carbon). It is evident that soil total carbon content of Chilapata was 36.16% higher than Chandra; while soil organic carbon of Chilapata was 15.07% higher than Chandra soil organic carbon. Ravindranath et al. (1996, 1997) reported that mean soil carbon in top 30 cm for tropical moist deciduous and tropical dry deciduous forests were estimated 57.1 and 58.0 Mg C/ha, respectively. Our estimated mean soil total carbon in top 100 cm at Banobitan and Botanic Garden were estimated 43.70 Mg C/ha, which was close to the estimated value of Ravindranath et al. (1996, 1997) and 96.32 Mg C/ha, which was higher than Ravindranath et al. (1996, 1997)'s estimation. The higher value at Botanic Garden may be due to gradual storing of aboveground biomass and grasses over three centuries old aged garden. It is also observed that soil texture of Botanic Garden was clayey loam and Banobitan was sandy loam. Due to clayey texture at Botanical Garden, it is also noted soil total carbon and soil organic carbon were higher than Banobitan that was also established by different scientists (e.g., Eleanor 2008). Our estimated mean soil total carbon in top 100 cm at Chandra and Chilapata were estimated 27.31 Mg C/ha, which was lower than the estimated value of Ravindranath et al. (1996, 1997) and 75.52 Mg C/ha, which was higher than Ravindranath et al. (1996, 1997)'s estimation. The higher value at Chilapata may be due to more grasses grown on the forest floor than the Chandra forest. It is also observed that soil texture of Chilapata was loamy and Chandra was sandy loam. Due to more clayey texture at Chilapata, it is also noted that soil total carbon and soil organic carbon were higher than Chandra.

Fluxes of CO_2 vary with soil and vegetation type, as well as season, time of day, and weather conditions. The Chamber method is based on monitoring of CO_2 concentration inside a transparent plastic cover on the soil surface. Soil respiration chambers can only be used to measure gas fluxes on the soil surface and not within the soil profile from CO_2 emission. Soil respiration (SR) was measured at Banobitan during December 2007 and May 2008. The soil respiration CO_2 emitted during winter season varied between 0.001 and 0.039 g/m²/h with an average emission of 0.0212 g/m²/h; whereas soil respiration CO_2 during summer ranged from 0.0089 to 0.0671 g/m²/h with an average emission of 0.0261 g/m²/h (Fig. 18.6). It is revealed that CO_2 emission from soil respiration during summer season was higher than during winter season.

Soil respiration CO_2 emission was measured at Botanical Garden during February 2008 and October 2008. The CO_2 emitted from soil respiration within the plastic cover are shown graphically in Fig. 18.7 for winter and monsoon/postmonsoon seasons, respectively. The soil respiration CO_2 emitted during winter season varied between 0.0012 and 0.2099 g/m²/h with an average emission of 0.0512

Soil CO$_2$ Respiration
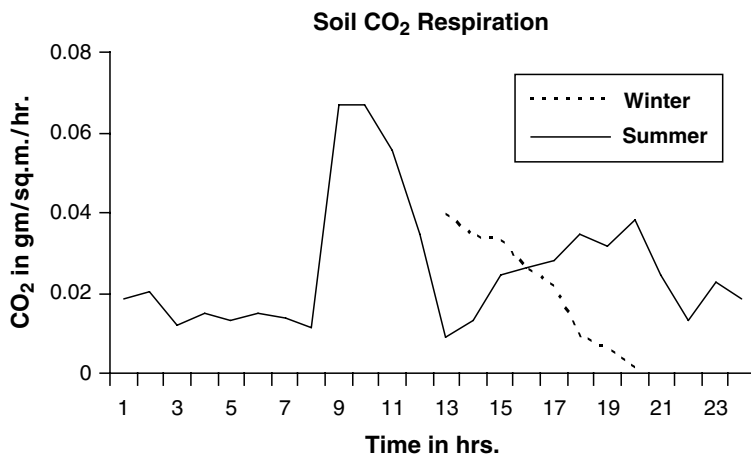
Fig. 18.6 Soil respiration CO$_2$ at Banobitan

Soil CO$_2$ Respiration
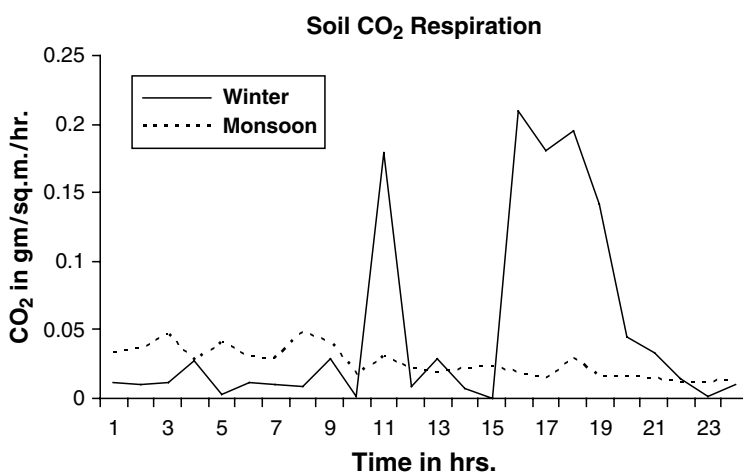
Fig. 18.7 Soil respiration CO$_2$ at botanical garden

g/^{2}m/h; whereas soil respiration CO$_2$ during monsoon/postmonsoon season ranged from 0.0112 to 0.0475 g/m^2/h with an average emission of 0.0253 g/m^2/h. It is revealed that soil respiration CO$_2$ during winter season was higher than the soil respiration CO$_2$ emission during monsoon/postmonsoon season. This may be due to higher moisture content in the soil in monsoon/early postmonsoon season.

Soil respiration was measured at Chandra during December 2007 and September 2008. The CO$_2$ emitted from soil respiration within the plastic cover are shown graphically in Fig. 18.8. The soil respiration CO$_2$ emitted during winter season
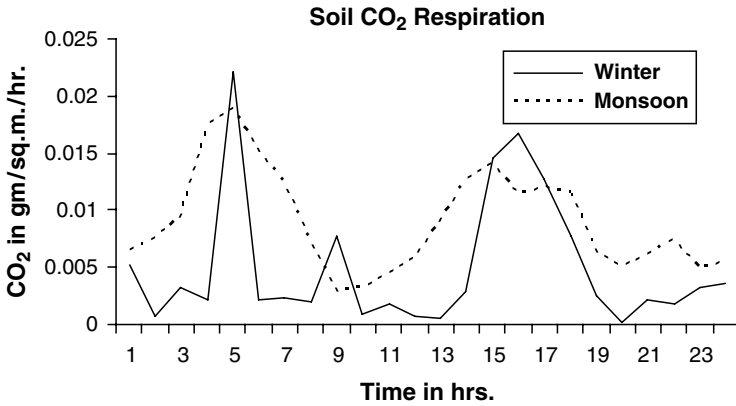
Fig. 18.8 Soil respiration CO_2 at Chandra forest
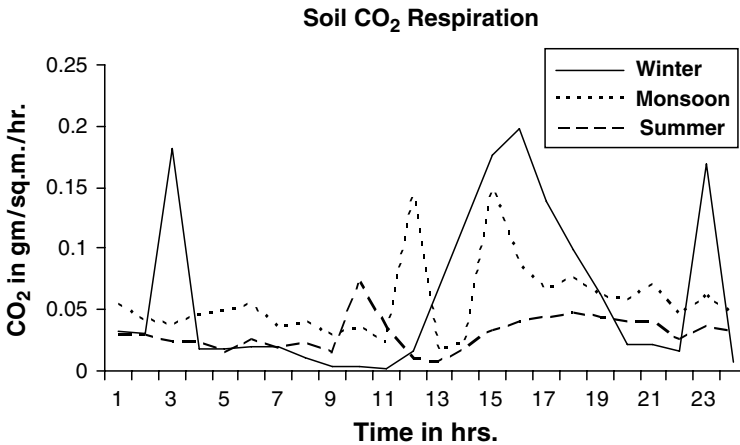
Fig. 18.9 Soil respiration CO_2 at Chilapata forest

varied between 0.0001 and 0.0221 g/m^2/h with an average emission of 0.0050 g/m^2/h; whereas soil respiration CO_2 during monsoon ranged from 0.0028 to 0.0189 g/m^2/h with an average emission of 0.0090 g/m^2/h. It is revealed that soil respiration CO_2 emission during monsoon/postmonsoon season was higher than the soil respiration CO_2 during winter season.

Soil respiration CO_2 emission was measured at Chilapata during January, May, and September 2008. The CO_2 emitted from soil respiration within the plastic cover are shown graphically for winter, summer, and monsoon/postmonsoon seasons in Fig. 18.9. The soil respiration CO_2 emitted during winter season varied between 0.0025 and 0.1765 g/m^2/h with an average emission of 0.0575 g/m^2/h; whereas soil
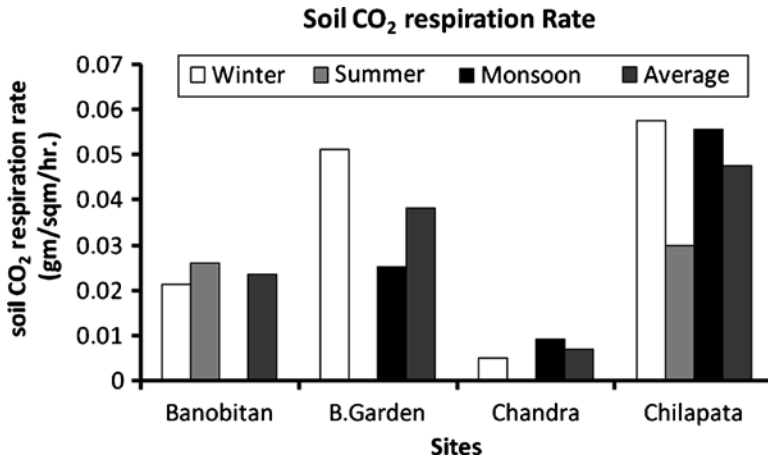
Fig. 18.10 Soil CO_2 respiration rate

respiration CO_2 during summer ranged from 0.0070 to 0.0727 $g/m^2/h$ with an average emission of 0.0299 $g/^2m/h$. The soil respiration CO_2 emitted during monsoon varied between 0.0165 and 0.1486 $g/m^2/h$ with an average emission of 0.0557 $g/m^2/h$. It is revealed that soil respiration CO_2 emission for all the seasons were nearer values, may be due to much closer values of moisture content in the soil samples.

CO_2 emissions from soil respiration for all sites are presented in Fig. 18.10. The results of CO_2 emission from soil respiration reveal that the soil CO_2 respiration rate varied between 0.0212 $g/m^2/h$ during winter season to 0.0261 $g/m^2/h$ during summer season with an average of 0.0236 $g/m^2/h$ at Banobitan; at Botanical Garden the same varied between 0.0253 $g/m^2/h$ during monsoon to 0.0512 $g/m^2/h$ during winter with an average of 0.0382 $g/m^2/h$; at Chandra soil CO_2 respiration rate ranged between 0.0050 $g/m^2/h$ during winter and 0.0090 $g/m^2/h$ in monsoon with an average of 0.0070 $g/m^2/h$ and at Chilapata soil CO_2 respiration rate ranged from 0.0299 $g/m^2/h$ in summer to 0.0575 $g/m^2/h$ in winter with an average of 0.0477 $g/m^2/h$. Maximum CO_2 emitted by soil respiration is observed at Chilapata (average 0.0477 $g/m^2/h$), followed by Botanical Garden (average 0.0382 $g/m^2/h$) and Banobitan (average 0.0236 $g/m^2/h$); and minimum CO_2 emitted by soil respiration is observed at Chandra (average 0.0070 $g/m^2/h$).

Annual emission of CO_2 from soil respiration has been estimated for all the sites. Estimated annual soil respiration rate of Botanical Garden (3.34 t C/ha/year) was higher than Banobitan (2.07 t C/ha/year) Jana et al. (2009). It may be noted that annual soil respiration rate estimated by our work (2.07–3.34 t C/ha/year) is lower than Yasuike et al. (2003) and Ikeda et al. (2003) (annual respiration in Kita-Saku in Japan was 6–7 t C/ha/year) and Tomonori et al. (2003) (annual soil respiration rate in Japan in an artificial forest was 5.10 t C/ha/year). This may be due to different soil texture, climatic condition, forest characteristics, etc. It is also observed

that soil respiration increased during summer season at Banobitan (similar trend observed by Yasuike et al. (2003) and Ikeda et al. (2003) of CRIEPI worked at Kita-Saku site in central Japan) and higher moisture content in the soils at Botanical Garden responsible for higher soil respiration rate than Banobitan (Chen et al. 2008). But if there is very high soil moisture, total soil CO_2 emission by respiration is reduced, because of limited diffusion of O_2 and subsequent suppression of CO_2 emissions (Tang et al. 2003).

Estimated annual soil respiration rate of Chilapata (4.178 t C/ha/year) was higher than Chandra (0.613 t C/ha/year). It may be noted that annual soil respiration rate estimated by our work (0.613–4.178 t C/ha/year) is lower than that estimated by Yasuike et al. (2003), Ikeda et al. (2003) (annual respiration in Kita-Saku in Japan was 6–7 t C/ha/year), and Tomonori et al. (2003) (annual soil respiration rate in Japan in an artificial forest was 5.10 t C/ha/year). It is also observed that soil respiration increased during monsoon/postmonsoon season at Chandra due to higher temperature as well as soil moisture content in the soil (similar trend observed by Yasuike et al. (2003) and Ikeda et al. (2003) of CRIEPI worked at Kita-Saku site in central Japan; Chen et al. 2008). Higher moisture content in the soils at Chilapata forest is responsible for higher soil respiration rate than in the Chandra soil (Chen et al. 2008).

18.5 Conclusion

The study has been conducted at two recreational and two natural forests in eastern India. Soil at Banobitan was slightly alkaline (pH range 7.06–8.25); texture was sandy loam and total carbon and soil organic carbon ranged from 24.2 to 36.5 and 2.8–8.3 g/kg, respectively. Soil at Botanical Garden in the area was slightly acidic in nature (pH range 5.90–7.01); texture was clayey loam and total carbon and soil organic carbon in the soil varied between 58 and 80.1 and 8.3 and 12.6 g/kg, respectively. Soil at Chandra was slightly acidic in nature; texture was sandy loam and total carbon and soil organic carbon ranged from 15 to 23.2 and 1.4–1.5 g/kg, respectively. Soil at Chilapata in the area was slightly acidic in nature; texture was loamy and total carbon and soil organic carbon in the soil varied between 45.7 and 62.5 and 7.4–12.8 g/kg, respectively. Estimated mean soil total carbon and mean soil organic carbon stock at Banobitan and Indian Botanic Garden were 43.70 and 7.99, and 96.32 and 14.57 Mg C/ha. Estimated mean soil total carbon and mean soil organic carbon stock at Chandra and Chilapata forests were 27.31 and 2.07, and 75.52 and 13.73 Mg C/ha, respectively. Estimated annual soil respiration rate of Indian Botanic Garden (3.34 t C/ha/year) was higher than Banobitan (2.07 t C/ha/year). Estimated annual soil respiration rate of Chilapata (4.18 t C/ha/year) was higher than Chandra (0.61 t C/ha/year). There is a need to continue experimental work in different agroclimatic zones over longer period to obtain more outcomes on total carbon, soil organic carbon, and soil respiration rate, which will be of immense importance to the researchers.

References

Boone RD, Nadelhoffer KJ, Canary JD, Kaye JP (1998) Roots exert strong influence on the temperature sensitivity of soil respiration. Nature 396:570–572

Chhabra A, Palria S, Dadhwal VK (2003) Soil organic carbon pool in Indian forests. Forest Ecol Manage 173:187–199

Chen S, Lin G, Huang J, He M (2008) Responses of soil respiration to simulated precipitation pulses in semiarid steppe under different grazing regimes. J Plant Ecol 1(4):237–246

Chowdhery HJ (2001) Indian Botanic Garden, Howrah, Botanical Survey of India, Ministry of Environment and Forests, Government of India

Dadhwal VK, Pandya N, Vora AB (1998) Carbon cycle for Indian forest ecosystem – a preliminary estimate, global change studies, scientific results from ISRO geosphere biosphere programme, India. ISRO, Bangalore, pp 411–429

District Statistical Handbook (2004) Bureau of applied economics and statistics, Government of West Bengal

District Statistical Handbook (2005) Bureau of applied economics and statistics, Government of West Bengal

Eleanor M (2008) Soil organic carbon. In: Cleveland CJ (ed) Encyclopedia of earth. Environmental Information Coalition, National Council for Science and the Environment, Washington, DC. Retrieved June 13, 2009. <http://www.eoearth.org/article/Soil_organic_carbon>

Eswaran HPF, Reich JM, Kimble FH, Beinroth E, Padmanabhan E, Moncharoen P (2000) Global carbon stocks'. In: Lal R, Kimble JM, Eswaran H, Stewart BA (eds) Global climate change pedogenic carbonates. Lewis, Boca Raton, FL, pp 15–25

Frank AB, Liebig MA, Tanaka DL (2006) Management effects on soil CO_2 efflux in northern semiarid grassland and cropland. Soil Till Res 89:78–85

FAO (1993) Forest resources assessment 1990-Tropical countries. United Nations Food and Agriculture Organisation, Rome, p 115

Haripriya GS (2003) Carbon budget of the Indian forest ecosystem. Climate Change 56:291–319

Howard DM, Howard PJA (1993) Relationships between CO_2 evolution, moisture content and temperature for a range of soil types'. Soil Biol Biochem 25:1537–1546

IPCC (Intergovernmental Panel on Climate Change) (2005) Carbon dioxide capture and storage. Cambridge University Press, Cambridge

Ikeda H et al (2003) Migration and fixation of organic carbon in vegetation – forest soil system, Geochimica et Coschimica Acta 67(18S), A167. Retrieved from http://criepi.denken.or.jp/en/e- publication/a2004/04juten16.pdf on 13.06.2009

Jana BK, Biswas S, Sonkar S, Majumder M, Roy P, Mazumdar A (2009) Soil carbon and soil respiration rate of urban forests in lower Gangetic plain. International Journal of Applied Agricultural Research 4(2):103–113

Kelting D, Burger JA, Edward GS (1998) Estimating root respiration, microbial respiration in the rhizosphere, and root-free soil respiration in forest soils. Soil Biol Biochem 30(7): 961–968

Kaur K, Jalota RK, Midmore DJ (2007) Impact of temperature and defoliation (simulated grazing) on soil respiration of pasture grass (*Cenchrus ciliaris* L) in a controlled experiment. J Agric Food Environ Sci 1(1):1–9. Retrieved from http://www.scientificjournals.org/journals2007/articles/1107.pdf on 13.06.2009

Lal R (2004) Soil carbon sequestration to mitigate climate change. Geoderma 123:1

Mallick SK, Pati BR, Behera N (2007) A phenological study of some dominant tree species in a tropical dry deciduous forest of Paschim Medinipur District, West Bengal. Indian Forester 133(12):1675–1682

Porporato A, Rodriguez-Iturbe I (2002) Ecohydrology – a challenging multidisciplinary research perspective. Hydrol Sci J 47(5):811–822

Ravindranath NH, Somasekhar BS, Gadgil M (1996) 1997) Carbon flows in Indian forest. Climate Change 35:297–320

Raich JW, Schlesinger WH (1992) The global carbon dioxide flux in soil respiration and its relationship to vegetation and climate. Tellus 44B:81–99

Raich JW, Potter CS (1995) Global patterns of carbon dioxide emissions from soils. Global Biogeochem Cycle 9:23–36

Raich JW, Tufekcioglu A (2000) Vegetation and soil respiration: correlations and controls. Biogeochemistry 48:71–90

Ryan MG, Law BE (2005) Interpreting, measuring, and modeling soil respiration. Biogeochemistry 73:3–27

Singh JS, Gupta SR (1977) Plant decomposition and soil respiration in terrestrial ecosystems. Botan Rev 43:449–528

Tang J, Baldocchi DD, Qi Y, Xu L (2003) Assessing soil CO_2 efflux using continuous measurements of CO_2 within the soil profile with small solid-state sensors. Agric Forest Meteorol 118:207–220

Tomonori M, Yoshiko K, Makoto T, Satoru T, Tatsuya K, Takumi W (2003) Spatial and temporal variation of soil respiration rate in an artificial forest of Hinoki (*Chamaecyparis obtusa*). J Jpn Soc Revegetat Technol 29(1):153–158

Vanhala P (2002) Seasonal variation in the soil respiration rate in coniferous forest soils. Soil Biol Biochem 34:1375–1379

Yasuike S et al (2003) Development of an evaluation method for spatial distribution of soil–CO_2 efflux in forest sites. CRIEPT report: U03010 (in Japanese). Retrieved from http://criepi.denken.or.jp/en/e-publication/a2004/04juten16.pdf on 13.06.2009

Chapter 19
Estimation of Reservoir Discharge with the Help of Clustered Neurogenetic Algorithm

Mrinmoy Majumder, Rabindra Nath Barman, Pankaj Roy, Bipal K. Jana, and Asis Mazumdar

Abstract This chapter presents a new approach of reservoir out flow prediction using a clustered neurogenetic algorithm. The algorithm combines the learning ability of artificial neural networks with searching capability of the genetic algorithm. The model is tested on the Panchet reservoir in river Damodar using the historical, hydrological, and water supply dataset. The values of the input parameters are classified into six groups based on the magnitude of the input parameters.

M. Majumder (✉)
Senior Research Fellow, School of Water Resources Engineering, Jadavpur University, Kolkata-700032, West Bengal, India
and
Geo-information Scientist, Regional Center, National Afforestation and Eco-development Board, Jadavpur University, Kolkata-700032, West Bengal, India
e-mail: mrinmoy@majumder.info

R.N. Barman
Pertime Research Fellow, School of Water Resources Engineering, Jadavpur University, Kolkata-700032, West Bengal, India
and
Assistant Professor, Department of Production, National Institute of Technology, Agartala, Tripura, India

P. Roy
Lecturer, School of Water Resources Engineering, Jadavpur University, Kolkata-700032, West Bengal, India

B.K. Jana
Senior Research Fellow, School of Water Resources Engineering, Jadavpur University, Kolkata-700032, West Bengal, India
and
Environmental Manager, Consulting Engineering Services, West Bengal, India

A. Mazumdar
Coordinator, Regional Center, National Afforestation and Eco-development Board, Jadavpur University, Kolkata-700032, West Bengal, India
and
Director, School of Water Resources Engineering, Jadavpur University, Kolkata-700032, West Bengal, India

The results showed a highly adaptive and flexible investigating ability of the model in prediction of nonlinear relationships among different variables.

Keywords Classified neurogenetic models • discharge • model performance • multi-reservoirs

19.1 Introduction

The Panchet reservoir of river Damodar, a multi-reservoir network, which is controlled by Damodar Valley Corporation (DVC) was India's first river development project and second large-scale river project of the last century after the Tennessee Valley Authority (TVA) in USA. The British administrator, W.W. Hunter, in his Statistical Account of Bengal described Damodar floods as "rainwater rushing off the hills through innumerable channels into the river bed with such great force and suddenness that the water rose to form a gigantic head wave of great breadth and sometimes rising up to 1.5 m in height." The uncontrolled part of the catchment comprising about 3,200 km^2 from below Maithon and Panchet dams to Durgapur Barrage for about 60 km had faced many high-intensity storms and plays a major role in the agricultural development of the area. The construction of additional dams in the upper reaches (i.e., above Panchet and Mithon) contributes significantly to the runoff. The problem of the distribution of stored water is always pronounced in DVC catchment. When there is enough storage, the supplied water is adequate but in case of adverse conditions, that is, when the storage becomes too high or low, the distribution of the surplus water becomes the main cause of hydrologic devastations (Lahiri-Dutt 2000).

19.1.1 Artificial Neural Networks in Hydrology

In recent years, artificial neural networks (ANNs) have been successfully applied to the modeling and forecasting of time series. ANNs offer a relatively quick and flexible means of modeling and as a result, the application of ANN modeling is widely reported in the hydrological literature. (Zhang and Stanley 1999; Neelakantan and Pundarikanthan 2000; Ray and Klindworth 2000). In the hydrological forecasting context, recent papers have reported that ANNs may offer a promising alternative for rainfall-runoff modeling (Hsu et al. 1995; Fernando and Jayawardena 1998; Tokar and Johnson 1999; Elshorbagy et al. 2000; Liong et al. 2001), stream-flow prediction (Clair and Ehrman 1998; Imrie et al. 2000); reservoir inflow forecasting (Jain et al. 1999; Coulibaly et al. 2000), and in prediction of water quality parameters (Maier and Dandy 1999).

19.1.2 Artificial Neural Networks in Stream-flow Forecasting

Coulibaly et al. (2005) suggested a combined model approach to improve the forecast of reservoir inflow and found that different approaches will work better for different

watersheds, lead times, and types of events. This conclusion was supported by WMO (1992), Singh (1995), Singh and Woolhiser (2002), and others. One day ahead stream-flow forecasting by multiple-layer perceptron (MLP) networks at a daily time step for 47 watersheds was studied by Anctil and Rat (2005). Karaboga et al. (2004) proposed a control method based on fuzzy logic for the real-time operation of spillway gates of a reservoir during any flood of any magnitude up to the probable maximum flood. Ahmed and Sarma (2005) determined the efficiency of neuro-modeling algorithms on generation of synthetic stream flow. Majumder et al. (2007) proposed the pattern for maximum water use for the river Damodar catchments with the help of back-propagation neural networks. The application of neural network on clustered dataset is not very common. Deka and Chandramouli (2005) and Cigizoglu (2005) applied Generalized Regression Neural Networks in prediction of river stream flow and sediment yield Cigizoglu and Alp (2006). Cascade Correlation Algorithm is used by Kisi (2007) to predict discharge of a river. All the above applications of neural network used trial and error process to identify the topology of the neural network and un-clustered dataset to estimate the output.

   The purpose of the present study is the application of neural network and genetic algorithm to find discharge from the Panchet reservoir with the help of clustered data-set of the input parameters. As Panchet is one of the major reservoirs of the entire river Damodar basin, the estimation of the discharge is important due to its direct impact on the irrigational and domestic population. The abnormality as found in the historical records of the Panchet reservoir makes the study more necessary as neural network is popular for its reliability in the prediction of highly complex bivariate dataset.

19.1.3   Description of the River Basin

The Damodar River which lies between the latitudes 23°30′N and 24°19′N and longitudes 85°31′E and 87°21′E, originates from the Palamu Hills of Chota Nagpur at an elevation of about 610 m above mean sea level. It flows in a southeasterly direction, entering the deltaic plains below Raniganj in Burdwan district of West Bengal, India. Near Burdwan the river abruptly changes its course to southerly direction and joins the Hoogli River about 48 km below Kolkata. The slope of the river bed during the first 241 km is about 1.89 m/km. During the next 161 km it is about 0.57 m/km, while the same is about 0.19 m/km in subsequent 145 km. The river is fed by six streams of which the principal tributary, Barakar joins it where river Damodar emerges from the Palamu Hills. The four main multipurpose reservoirs are located at Tilaiya, Konar, Maithon, and Panchet, and a Barrage at Durgapur was commissioned during 1953–1959. Another tributary Khudia, whose catchment is neither intercepted by Maithon nor Panchet reservoirs, joins Damodar near its confluence with Barakar. In the plains river splits into several channels and ultimately joins the rivers Roopnarayan and Hoogli. The total length of the river is about 541 km. The total catchment area of the river is 28,015 km^2 of which 10,985 km^2 lies under Panchet (Konar – 997 km^2. Tenughat – 4,500 km^2 and Panchet 5,488 km^2) and 6,293 km^2 under Maithon (Tilaiya – 984 km^2 and Maithon – 5,309 km^2). Figure 19.1 depicts a schematic diagram of river Damodar and the location of Panchet reservoir.

Fig. 19.1 A schematic diagram of river Damodar

19.1.3.1 Climate of the River Basin

Moderate winters and hot and humid summers characterize the climate of the area. The mean annual rainfall in different catchments of the Damodar valley is 126 cm in Barakar, 127.2 cm in Damodar, and 132.9 cm in lower valley. Eighty-two percent of the mean annual rainfall occurs during the four monsoon months from June to September. The mean daily temperature varies from 40°C to below 20°C in winters. The rainfall in this area during the monsoon season is mainly due to the passage of depressions and low pressure over and near the area and the active monsoon conditions due to accentuation of the seasonal trough.

19.1.3.2 Geomorphology

The upper portion of the catchment consists of rough, hilly regions, where as the lower portion is of the nature of flat deltaic plane.

19.1.3.3 Control Structures

DVC has a network of four dams: Tilaiya and Maithon on river Barakar, Panchet on river Damodar, and Konar on river Konar. Besides, Durgapur barrage and canal network, handed over to Government of West Bengal in 1964, remained a

part of total system of water management. Four multipurpose dams were constructed during the period 1948–1959, namely, Maithon, Panchet, Tilaiya, and Konar reservoir. Among these four reservoirs, first three are used for hydropower generation. Konar is used only for agricultural purpose of the adjacent area. Although the water supplied for hydropower generation is allowed to return back to the reservoir, a small percentage of water get diverted or evaporated. Panchet has a capability of 80 mW of power generation and a part of the supplied water is used for this purpose.

19.2 Data Description

The reservoir inflows, reservoir storage, water supply data, i.e., water used for irrigation, industry, and domestic use in and around Panchet reservoir in the year 1997–1998, and water surplus were considered as inputs and reservoir outflow was considered as output.

The Kurtosis of the datasets are derived as −1.54, 6.01, 0.80,−0.93, 683.95, 8.38, 21.32, and 683.95, respectively, for reservoir water surplus, water supplied for domestic use, water supplied for industrial use, water supplied for hydropower, reservoir water storage, reservoir outflow, Reservoir Inflow, and Reservoir Water Level.

The variation of the output data series is 24.48 where as that of the input data series 1.74, 14.66, 28.01, 906.25, 43.71, 28.36, and 477.90, respectively, for water used in domestic, industrial, hydropower; water storage, inflow, surplus, and water level. Table 19.1 shows the statistical characteristics of the input and output dataset.

19.3 Methodology

19.3.1 Artificial Neural Network

An ANN is a flexible mathematical structure that is capable of identifying complex nonlinear relationships between input and output datasets. The ANN model of a physical system can be considered with n input neurons $(x_1, x_2, ..., x_n)$, h hidden neurons

Table 19.1 Table showing the statistical characteristics of the input and output dataset

	Reservoir water surplus	Water supplied for domestic use	Water supplied for industrial use	Water supplied for hydropower	Reservoir water storage	Reservoir outflow	Reservoir inflow	Reservoir water level
Mean	49.45	1.55	13.59	26.34	270.18	14.74	15.14	142.48
Kurtosis	−1.54	6.01	0.80	−0.93	683.95	8.38	21.32	683.95
Variance	43.71	1.74	14.66	28.01	906.25	24.48	28.36	477.90

$(z_1, z_2, ..., z_n)$, and m output neurons $(y_1, y_2, ..., y_n)$. Let t_j be the bias for neuron z_j and f_k for neuron y_k. Let w_{ij} be the weight of the connection from neuron x_i to z_j and beta is the weight of the connection z_j to y_k. The function that ANN calculates is

$$y_k = g_A \left(\sum z_j b_{jk} + f_k \right) ...(j = 1 - h) \qquad (19.1)$$

In which,

$$z_j = f_A \left(\sum x_i w_{ij} + t_j \right) ...(i = 1 - n) \qquad (19.2)$$

where g_A and f_A are the activation functions (Sudheer 2005).

The development of an artificial neural network, as prescribed by ASCE Task Committee (2000) follows the following basic rules:

1. Information must be processed at many single elements called nodes.
2. Signals are passed between nodes through connection links and each link has an associated weight that represents its connection strength.
3. Each of the nodes applies a nonlinear transformation called activation function to its net input to determine its output signal.

The numbers of neurons contained in the input and output layers are determined by the number of input and output variables of a given system. The size or number of neurons of a hidden layer is an important consideration when solving problems using multilayer feed-forward networks. If there are fewer neurons within a hidden layer, there may not be enough opportunity for the neural network to capture the intricate relationships between indicator parameters and the computed output parameters. Too many hidden layer neurons not only require a large computational time for accurate training, but may also result in overtraining. A neural network is said to be "overtrained" when the network focuses on the characteristics of individual data points rather than just capturing the general patterns present in the entire training set. The network building procedure is divided into three phases which are described next.

19.3.1.1 Selection of Network Topology

Neural networks can be of different types, like feed-forward, radial basis function, time lag delay, etc. The type of network is selected with respect to the knowledge of input and output parameters and their relationship. Once the type of network is selected, selection of network topology is the next concern. Trial and error method is generally used for this purpose, but many studies now prefer the application of genetic algorithm (Ahmed and Sarma 2005). Genetic algorithms are search algorithms based on the mechanics of natural genetic and natural selection. The basic elements of natural genetics – reproduction, crossover, and mutation – are used in the genetic search procedure. A GA can be considered, which consists of the following steps (Yitian and Gu 2003):

1. Select an initial population of strings
2. Evaluate the fitness of each string
3. Select strings from the current population to mate
4. Perform crossover (mating) for the selected strings
5. Perform mutation for selected string elements
6. Repeat steps 2–5 for the required number of generations

Genetic algorithm is a robust method of searching the optimum solution to complex problems like the selection of an optimal network topology where it is difficult or impossible to test for optimality. The basics of GA have already been discussed by many authors like Ahmed and Sarma (2005), Wang (1991), and Wardlaw and Sharif (1999). Hence the details of the basic procedures of GA are not focused in the present literature.

19.3.1.2   Training Phase

To encapsulate the desired input–output relationship, weights are adjusted and applied to the network until the desired error is achieved. This is called as "training the network." There are innumerable "training the network" algorithms, among which, back propagation (ASCE Task Committee 2000) is mostly preferred. Quick Propagation (QP), Bach Back Propagation (BBP), and Common Gradient Descent (CGD), each of them derived from basic back-propagation algorithms, are used as the training algorithm in this present study.

QP is a heuristic modification of the back-propagation algorithm invented by Scott Fahlman. This training algorithm treats the weights as if they were quasi-independent and attempts to use a simple quadratic model to approximate the error surface.

BBP is an advanced variant of back propagation where network weights update takes place once per iteration.

CGD is an advanced method for training multilayer neural networks. It is based on the linear search usage in the line of an optimal network weights' change. The correction of weights is conducted once per iteration.

19.3.1.4   Testing Phase

After training is completed, some portion of the available historical dataset is fed to the trained network and known output is estimated out of them. The estimated values are compared with the target output to compute the MSE. If the value of MSE is less than 1%, the network is said to be sufficiently trained and ready for estimation. The dataset is also used for cross-validation to prevent overtraining during the training phase (Sudheer 2005).

In the present study, the QP, BBP, and CGD algorithms are used to train the model. The best model was selected with the help of the performance validation criteria as explained in the next section.

19.3.2 Evaluation of the Network

The accuracy of results obtained from the network is assessed by comparing its response with the validation set. The commonly used evaluation criteria include mean square error (MSE), correlation coefficient (r), and standard deviation (STDEV) (Bhatt et al. 2007).

$$MSE = \sum \left(T_p - O_p \right) / n \tag{19.3}$$

$$r = \left[\sum \left(\left(T_p - T_m \right) \left(O_p - O_m \right) \right) \Big/ \left(\sum_1^n \left(T_p - T_m \right)^2 \sum_1^n \left(O_p - O_m \right)^2 \right)^{1/2} \right] \tag{19.4}$$

$$STDDEV = \frac{\sum_1^n \left(T_n - \overline{T}_n \right)^2}{n} \tag{19.5}$$

where T_p is the targets value of the pth pattern; o_p is the estimated value of the pth pattern, T_m and o_m are the mean target and estimated groups, respectively, and n is the total number of patterns.

MSE shows the measure of the difference between target (Tp) and estimated (Op) value. r is the degree of correlation between two variables. The STDEV for the actual and predicted series is found out by dividing STDEV of actual series and STDEV of predicted series. A perfect match between observed data and model simulations is obtained when STDDEV approaches 0.0.

19.4 Result and Discussion

19.4.1 Model Development

In the present study three neural models are developed from the historical records of the selected input and output. The model with least MSE, highest r, and minimum STDDEV was selected for the simulation work.

Timescale was one of the major constraints of the estimation problem. In the present study timescale was not ignored but categorized in 12 groups for the month and 30–31 groups for the day scale. The entire datasets of the other inputs are ranked in an ascending way with respect to the magnitude and categorized with the help of the rules explained in the next paragraph. Neural network is a universal classifier (Hassoun 1995). Neural estimate of clustered dataset has always showed more efficiency than the same for the nonclustered dataset. As every neural model follows a binary system of encoding, accuracy of neural models increases if clustered dataset is used.

Unstable dataset is defined as that dataset, which separates maximum or minimum from the others. These datasets help determine the thresholds of the entire dataset. Every peak and every trough, borders the stability of a dataset. And if the categorization of the dataset is done with respect to the stability of parameters, the output is said to be a more accurate representation of a problem (Parasuraman and Elshorbagy 2007). The rules by which the dataset was classified tries to incorporate this theory as explained in the next section:

1. If the rank of the data is lesser than 5, then the data is clustered into group P.
2. If the rank of the data is lesser than 15 but greater than 5, then the data is clustered into group MP.
3. If the rank of the data is lesser than 250 but greater than 15, then the data is clustered into group LP.
4. If the rank of the data is lesser than 500 but greater than 250, then the data is clustered into group LT.
5. If the rank of the data is lesser than 550 but greater than 500, then the data is clustered into group MT.
6. If the rank of the data is greater than 550, then the data is clustered into group T.

The minimum and maximum ranks are found to be 1 and 731, respectively, as there are totally 730 data, which are applied to the neural models to train the same.

Eighty percent of the clustered dataset is used for training, 10% is used for cross-validation, and the rest is earmarked for testing. Table 19.2 shows the average MSE after training and testing the model. The model architecture and connection weight are also shown.

The network topology is selected with the help of genetic and training algorithms, and the optimum result is selected as QP, BBP, and CGD, respectively, for QP, BBP, and CGD models. The average MSE after training with CGD algorithm is found to be 0.02 which is 95.74% and 75% lesser than the QP and BBP networks, respectively. The CGD network is found to be 1% less associated than QP, which has 98% positive association with the target data series. The CGD network has a deviation of 1.12 whereas that of QP and BBP network equals to 1.21 and 0.84 units, respectively, which is 25% more and 8% less deviated than CGD. The connection weight of CGD is 9.09 times heavier than QP, but 200% lighter than BBP. According to the performance validation criteria and the connection weight of the three networks, CGD is selected as the most suitable model out of the three as the MSE of the said network is far less than the other two networks. The CGD model is also lighter than BBP, but not lightest of the three. The said model is also less deviated than QP, but not the least deviated among the three. The coefficient of relationship is found to be highest for the CGD network and also the minimum MSE among the three networks enforced the authors to perform the simulation with the above network.

The estimated output from the CGD model is also compared with the Pseudo Asymptotic Sigmoidal (PAS) Regression method. The governing equation of PAS method is given by Eq. (19.6). Figure 19.2 depicts a comparative diagram of the MSE achieved from CGD and PAS models. The table shows the MSE, r, and

Table 19.2 Summary table showing optimum ANN model's architecture and ANN internal parameters

Network name	QP	BB	CGD
Network topology			
Network type	Feed-forward fully connected network	Feed-forward fully connected network	Feed-forward fully connected network
Number of inputs	9	9	9
Number of hidden layers	1	2	2
Hidden units in the first hidden layer	1	2	1
Hidden units in the second hidden layer	–	5	1
Number of outputs	1	1	1
Connection weight	10	33	11
All the topology was created using genetic algorithms with following parameters			
Population size	40	40	40
Number of generations	60	60	60
Network size penalty	6	6	6
Crossover rate	0.8	0.8	0.8
Mutation rate	0.2	0.2	0.2
Training algorithm and parameters			
Training algorithm	Quick propagation	Batch back propagation	Common gradient decent
Training Iteration	10	10	10
Stop training conditions			
MSE on training subset must be achieved	0.5	0.5	0.5
Maximum allowed number of iterations	1,000,000	1,000,000	1,000,000
Training stop reason	Generalization loss became too high	Error reduction became too low	Generalization loss became too high
Training and testing results			
Average MSE (training)	5.68	0.49	4.07
Average MSE (testing)	63.30	30.02	67.98
Performance validating criteria			
MSE	0.47	0.08	0.02
r	0.98	0.99	0.99
STDEV	0.84	1.21	1.12

STDEV of the CGD and PAS models. According to Table 19.3 MSE of CGD is 4.43 times less than that of PAS. The coefficient of relationship for the CGD network is found to be 93.7% more than that of PAS. PAS is also 4.41 times more deviated than the CGD model.

$$O_p = a + b * \left(1 / \left(1 + \exp^{(-(Tp-c-g/2)/d)}\right)\right) * \left(1 - 1 / \left(1 + \exp^{(-(Tp-c-g/2)/h)}\right)\right) \quad (19.6)$$

where $a = 0.79810259$, $b = 268.39036$, $c = 210.89928$, $d = 10.16617$, $g = 1.757391$, and $h = 24.754849$.
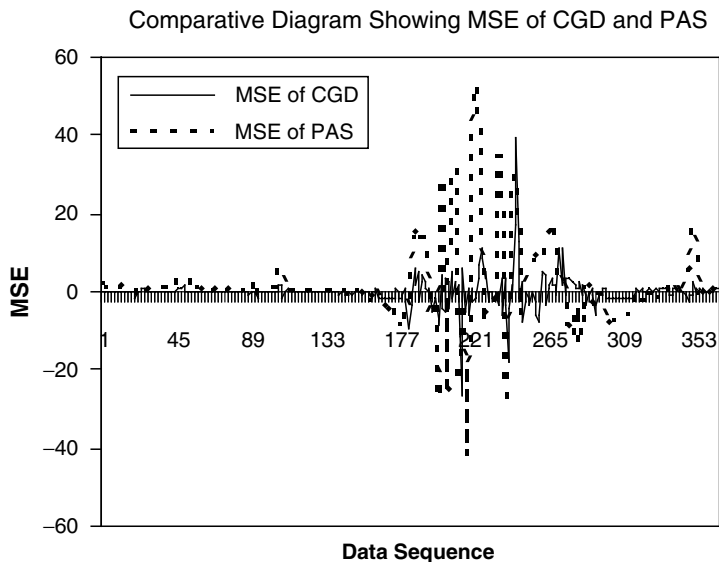
Fig. 19.2 Figure showing comparative diagram of CGD and PAS

Table 19.3 Table showing performance validation criteria of the selected models

Name of the model	MSE	r	STDEV
CGD	0.02	0.99	0.08
PAS	0.08	0.92	3.71

According to the performance validation criteria among PAS and CGD models, CGD is found to be more efficient and reliable than the former. Figure 19.3 depicts a comparative diagram of the actual output and estimated results found from the PAS and CGD models.

According to the results CGD is found to be capable for the estimation of reservoir inflow from the given historical dataset.

19.5   Conclusion

The present study tried to estimate reservoir discharge with the help of clustered neurogenetic algorithm and according to the result the clustered neurogenetic model (CGD) was found to be better than the linear regression model (PAS) with which the CGD model output was compared. The research study had shown the ability of the clustered neurogenetic model in predicting river flow. The model which was termed as CGD was found to be flexible and easy to build, and the transparency of the knowledge gained by the model was also an advantage. The proposed approach

Comparative Diagram of Estimated Reservoir Outflow
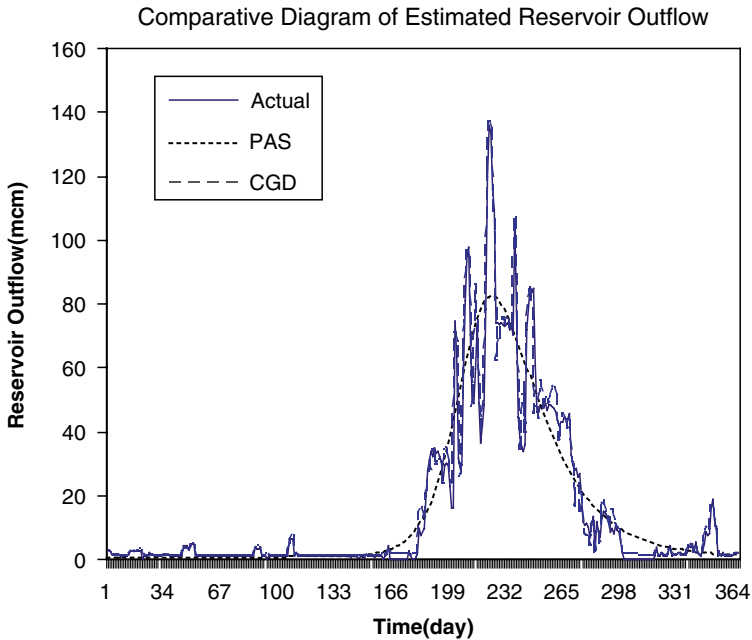
Fig. 19.3 Figure showing a comparative diagram of estimated reservoir outflow found from actual historical records, PAS and CGD models

used the least amount of information in terms of the amount of dataset required, number of parameters essential, and the amount of time needed for the development of the model. The main limitation of this study procedure is that the knowledge contained in the trained networks was difficult to interpret because of the distribution of the connection weights in a complex manner. This preliminary study shows that the CGD approach can also be successful in a wide range of hydrological problems that were unsolved, because of its efficient problem identification approach.

References

Ahmed JA, Sarma AK (2005) Genetic algorithm for optimal operating policy of a multipurpose reservoir. J Water Resour Manage 19:145–161

Anctil F, Rat A (2005) Evaluation of neural network stream flow forecasting on 47 watersheds. J Hydrol Eng 10(1):85–88

ASCE Task Committee (2000) Application of artificial neural networks in hydrology, artificial neural networks in hydrology I: preliminary concepts. J Hydrol Eng 5(2):115–123

Bhatt VK, Bhattacharya P, Tiwari AK (2007) Application of artificial neural network in estimation of rainfall erosivity. Hydrol J 1–2:30–39

Cigizoglu HK (2005) Application of the generalized regression neural networks to intermittent flow forecasting and estimation. ASCE J Hydrol Eng 10(4):336–341

Cigizoglu HK, Alp M (2006) Generalized regression neural network in modelling river sediment yield. Adv Eng Software 37(2):63–68

Clair TA, Ehrman JM (1998) Using neural networks to assess the influence of changing seasonal climates in modifying discharge, dissolved organic carbon, and nitrogen export in eastern Canadian rivers. Water Resour Res 34(3):447–455

Coulibaly P, Anctil F, Bobee B (2000) Daily reservoir inflow forecasting using artificial neural networks with stopped training approach. J Hydrol 230(3–4):244–257

Coulibaly P, Haché M, Fortin V, Bobée B (2005) Improving daily reservoir inflow forecasts with model combination. J Hydrol Eng 10(2):91–99

Deka P, Chandramouli V (2005) Fuzzy neural network model for hydrologic flow routing. J Hydrol Eng 10(4):302–314

Elshorbagy A, Simonovic SP, Panu US (2000) Performance evaluation of artificial neural networks for runoff prediction. J Hydrol Eng 5(4):424–427

Fernando DA, Jayawardena AW (1998) Runoff forecasting using RBF networks with OLS algorithm. J Hydrol Eng 3(3):203–209

Hassoun MH (1995) Fundamentals of artificial neural networks. MIT Press, London, p 1

Hsu K, Gupta HV, Sorooshian S (1995) Artificial neural network modeling of the rainfall-runoff process. Water Resour Res 31(10):251–253

Imrie CE, Durucan S, Korre A (2000) River flow prediction using neural networks: generalization beyond the calibration range. J Hydrol 233(3–4):138–154

Jain SK, Das A, Srivastava DK (1999) Application of ANN for reservoir inflow prediction and operation. J Water Resour Plan Manage 125(5):263–271

Karaboga D, Bagis A, Haktanir T (2004) Fuzzy logic based operation of spillway gates of reservoirs during floods. J Hydrol Eng 9(6):544–549

Kisi Ö (2007) Streamflow forecasting using different artificial neural network algorithms. J Hydrol Eng 12(5):532–539

Lahiri-Dutt K (2000) State and the community in water management case of the Damodar Valley Corporation, India. Report on Resource Management in Asia Pacific Program, The Australian National University

Liong SY, Khu ST, Chan WT (2001) Derivation of Pareto front with genetic algorithm and neural network. J Hydrol Eng 6(1):52–61

Maier HR, Dandy GC (1999) Empirical comparison of various methods for training feed-forward neural networks for salinity forecasting. Water Resour Res 35(8):2591–2596

Majumder M, Roy P, Mazumdar A (2007) Optimization of the water use in the river Damodar In West Bengal In India: an integrated multi-reservoir system with the help of artificial neural network. J Eng Comput Architect 1(2): Article no.1192

Neelakantan TR, Pundarikanthan NV (2000) Neural network based simulation-optimization model for reservoir operation. J Water Resour Plan Manage 126(2):57–64

Parasuraman K, Elshorbagy A (2007) Cluster-based hydrologic prediction using genetic algorithm-trained neural networks. J Hydrol Eng ASCE 12:52–62

Ray C, Klindworth KK (2000) Neural networks for agrichemical vulnerability assessment of rural private wells. J Hydrol Eng 5(2):162–171

Singh VP (1995) Computer models of watershed hydrology. Water Resource Publications, Highlands Ranch, CO

Singh VP, Woolhiser DA (2002) Mathematical modeling of watershed hydrology. J Hydrol Eng 7(4):270–292

Sudheer KP (2005) Knowledge extraction from trained neural network river flow models. J Hydrol Eng 10(4):L264–269

Tokar AS, Johnson PA (1999) Rainfall-runoff modeling using artificial neural networks. J Hydrol Eng 4(3):232–239

Wang QJ (1991) The genetic algorithm and its application to calibrating conceptual rainfall-runoff models. Water Resour Res 27(9):2467–2471

Wardlaw R, Sharif M (1999) Evaluation of genetic algorithms for optimal reservoir system operation. J Water Resour Plan Manage 125(1):25–33

World Metereological Organization (WMO) (1992) Simulated real-time intercomparison of hydrological models. Retrieved from http://www.wmo.int/e-catalog/detail_en.php?PUB_ID=73&SORT =N&q= on 25th June 2008

Yitian L, Gu RR (2003) Modeling flow and sediment transport in a river system using an artificial neural network. J Environ Manage 31(1):122–134

Zhang Q, Stanley SJ (1999) Real-time treatment process control with artificial neural networks. J Environ Eng 125(2):153–160

Chapter 20
Water Availability Analysis and Estimation of Optimal Power Generation for a Fixed Head Multi-Reservoir Hydropower Plant

Biswajit Majumder, Mrinmoy Majumder, Pankaj Roy, and Asis Mazumdar

Abstract Water availability analysis and optimal power generation in a hydropower plant is studied in this chapter. As a case study, the monthly rainfall data in Chuzachen, available annual daily discharges at Rangili and Rangpo intakes, and GPS survey result of catchments area of 99-MW Chuzachen Hydroelectric power project in the East District of Sikkim have been considered. Numerous consideration factors exist when building hydropower plants, each has been measured when discussing this renewable energy source. Availability of water in the project site is one of the most important factors when building a hydropower plant. Thus, it is important to study about the availability of water in the whole year for power generation as well as the optimal power generation period.

B. Majumder
Senior Research Fellow, School of Water Resources Engineering, Jadavpur University, Kolkata-700032, West Bengal, India
e-mail: biswajitmajumder@gmail.com

M. Majumder
Senior Research Fellow, School of Water Resources Engineering, Jadavpur University, Kolkata-700032, West Bengal, India
and
Geo-information Scientist, Regional Center, National Afforestation and Eco-development Board, Jadavpur University, Kolkata-700032, West Bengal, India

P. Roy
Lecturer, School of Water Resources Engineering, Jadavpur University, Kolkata-700032, West Bengal, India

A. Mazumdar
Coordinator, Regional Center, National Afforestation and Eco-development Board, Jadavpur University, Kolkata-700032, West Bengal, India
and
Director, School of Water Resources Engineering, Jadavpur University, Kolkata-700032, West Bengal, India

20.1   Introduction

Electricity is the only form of energy, which is easy to produce, transport, use, and control. So, it is mostly the terminal form of energy for transmission and distribution. Electricity consumption per capita is the index of the living standard of people of a place or country. A hydroelectric power plant uses a renewable source of energy that does not pollute the environment. Hydroelectric power plants are very useful for limiting the emission of green house gasses from power generation plant, as energy becomes the current catchphrase in business, industry, and society, and energy alternatives are becoming increasingly popular.

Numerous consideration factors exist when building hydropower plants; each has been measured when discussing this renewable energy source. Availability of water in the project site is one of the most important factors when building a hydropower plant. In this study, analysis of water availability at the intake of the project site as well as uncertainty analysis (varying the rain fall data) has been done using Map Window GIS and TR-55 models. From the calculation and analysis, optimal power generation region also is obtained. The purpose of this chapter is to calculate the optimal power generation point using Minimum Energy Maximum Power (MEMP) Algorithm.

20.2   Literature Review

Oliveira et al. (2003) emphasized that the optimal active power dispatch is formulated as a network flow optimization model and solved by interior point methods. The primal-dual and predictor-corrector versions of such interior point methods are developed and the resulting matrix structure is explored. This structure leads to very fast iterations since it is possible to reduce the linear system either to the number of buses or to the number of independent loops.

Arce et al. (2002) showed that the optimal dispatch of generating units is of Itaipú, the world's largest hydroelectric plant in operation. Itaipú is a 12.6 GW hydro plant, located on the Paraná River, in South America, composed of 18 identical 700-MW generating units. A dynamic programming model has been developed to optimize the number of generating units in operation at each hour of the day in order to attain the total generation scheduling of the plant in the most economic way.

Keppo (2002) gave a view about an electricity producer's long-term optimality in the case of multi-reservoir hydropower system. The model solves the optimal production process and trading strategy of electricity and weather derivatives by maximizing the utility from production and terminal water reservoir level. The optimal trading strategy hedges the rainfall and electricity price uncertainties.

Birhanu et al. (2007) stated that the Kihansi hydropower plant is located in south central Tanzania, deriving its water from a catchment that has an approximate drainage area of 584 km^2. The availability of high head in a short stretch of the river and the reasonably favorable hydrology with a reliability of flows exceeding 7 cumecs (95% of the time) makes the catchment an ideal source of water for the hydropower plant and the livelihoods of the species in the lower Kihansi gorge.

Kumar et al. (2007) discussed about a large number of river flow diversion type hydropower projects in Himalayan region, which are in different stages of implementation. Assessment of impact of changed flow regime on river bed and river bank ecology and provision of environmental flows have become necessary in the development of hydropower project.

20.3 Study Area

The 99-MW Chuzachen Hydroelectric Power Project, which is about 60 km from Gangtok (Sikkim) and 100 km from Bagdogra Airport (West Bengal) was selected as the study area for the present study. The study area is located in East District of Sikkim having streams like Rangpo and Rangili and situated in the vicinity of Chuzachen Village.

The Chuzachen has a run-off river hydropower project with two interconnected reservoirs with an installed capacity of 99 MW. The Rangpo River is a major tributary of the Teesta River, which is the main river of the state of Sikkim.

The Chuzachen has two intakes, each with a storage reservoir and headrace tunnel, each joining together to a common headrace tunnel, an underground surge shaft, a surface penstock and open air powerhouse with two units and an outdoor switchyard.

20.4 Methodology

The hydrologic data of the dam was collected from the owner.

Time of concentration was calculated with the help of length and slope. Both of these were retrieved by the application of GIS, the retrieval of catchment dimension, estimation of steam flow, water availability, impact of climatic uncertainty and identification of optimal power generation.

Rivers without any gauge stations are called as un-gauged river. Physical survey of un-gauged rivers was known to be complex and time consuming. Catchments of gauged rivers are generally hard to delineate, due to scarcity of proper maps and economic requirements of field-level surveys. But application of GIS can solve this problem and identify river catchments economically with the help of contour maps or some GPS readings along the banks of the river. The study area has only one gauge station, which is situated far away from the study area. Hence, the catchment of the basins around the dams and river flowing beside the dams is un-gauged. So the catchment was delineated with the help of GPS readings and satellite imagery.

GPS readings were taken at the highest points along the river bank (as per eye estimation) and the highest points per ten readings were identified and imported into the MapWindow™ software along with the satellite imagery of the study area. A polygon was drawn by joining these points to get the catchment or total area of influence of the river basins. The distance between the farthest point and outlet along with slope were determined by the following method:

- First, the locations of the dams, junction of the penstocks and power house were identified on Google Earth with the help of GPS data taken from these locations (Figs. 20.1 and 20.2).
- Then, the screen window was captured with the help of some screen capture software and the captured image was imported into the GIS software.
- The coordinate type was changed by going to File > Settings > Project Projection.
- Then, coordinate category was changed to *Geographical Coordinate*, Group was changed to *Asia* as all the locations are in Asia. Name was changed to *Everest (India and Nepal)* as the locations were near Mt. Everest. Projected Projection System (PPS): UTM-WGS-1984 could also be selected but as the measurement of catchment was the objective and as PPS was actually suitable for non-precision works, Geographical Projection System was used.
- A line shape file was created and drawn to connect dams with junction and power house.
- The "Update Measurement Tool" was used to measure the distance between the locations.

Fig. 20.1 Figure showing the satellite (Google Earth™) imagery of Rangpo dam and the points from where data was collected
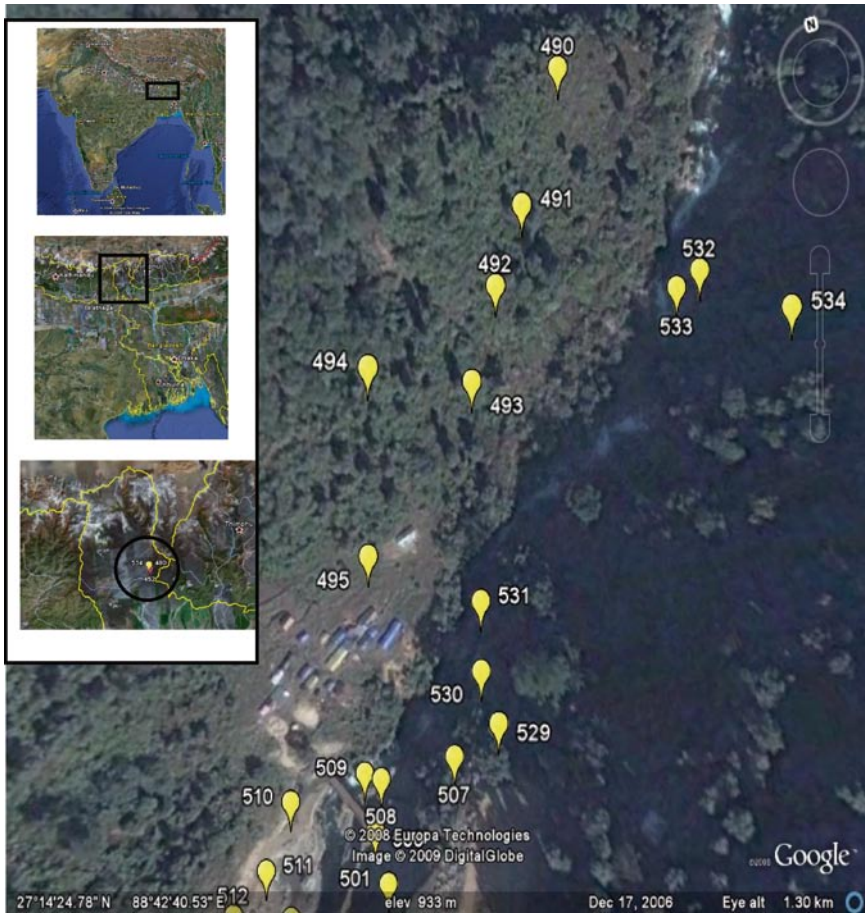
Fig. 20.2 Figure showing the satellite (Google Earth™) imagery of Rangili dam and the points from where data was collected

- The distance between the highest and lowest point, which was nearest to the selected locations were also measured and used in determination of slope.

The detailed description of the procedures of measurement of dimensional properties was given in Chapter 24 and in the book "Digitization Fro Beginners" written by Majumder (2008).

20.4.1 Estimation of Stream Flow

TR-55 model was applied to estimate the discharge of the intake of the hydropower plant. TR-55 model is described in Chapter 6, and the required parameters are

length, slope, area, etc. The model was calibrated with known data and then applied for the estimation of unknown data.

20.4.2   Determination of Water Availability

Water availability for a hydropower plant is actually the discharge, which can be used for generation of hydropower for maximum time of a year.

20.4.3   Generation of Load Duration Curve

A duration curve is a graph representing the percentage of time during which the value of a given parameter (load, flow) is equalled or exceeded. Such a graph can be easily generated using a spreadsheet computer program.

Using available daily steam flow data, a low-duration curve was developed for the site. Data for the curve is generated by (1) ranking the daily flow data from the highest to the lowest and (2) calculating the percentage of days these flows were exceeded (= rank ÷ number of data point).

To develop a load duration curve the estimated discharges were converted into electrical power. The estimated discharges are converted into power using the given formula:

The electrical power, is given by

$$P = 9.81 \times \eta \times Q \times H.K.W \tag{20.1}$$

where Q is the discharge (m^3/s), H is the water head (m), and η is the overall efficiency of the of the turbine alternator set.

20.4.4   Identification of Optimal Power Generation

A graph was drawn based on the discharge and corresponding load generation capacity of the river. The estimated discharge for uncertain rainfall and without river was also included. Optimal load generation point is defined as that point where minimum energy is used to generate maximum power. The plant was rated for 99 MW. In Fig 20.9, points at which 99MW or more was generated identified minimum value of which will give the optimal power generation point.

20.5   Results and Discussion

20.5.1   Data Analysis

The annual average monthly rainfall is shown in Fig. 20.3, and the annual monthly discharges at Rangili and Rangpo intake are shown in Figs. 20.4 and 20.5, respectively. According to Fig. 20.3 maximum rainfall observed in the study area is found to be 1,282.3 mm and average monthly rainfall is equal to 314.26 mm, whereas the minimum rainfall within 9 years at the study area is 0.1 mm. It is worth mentioning that the study area is situated in the Karakoram Range, which is frequented by high wind and snowfall. The dimensional property of the study area is given in Table 20.1.
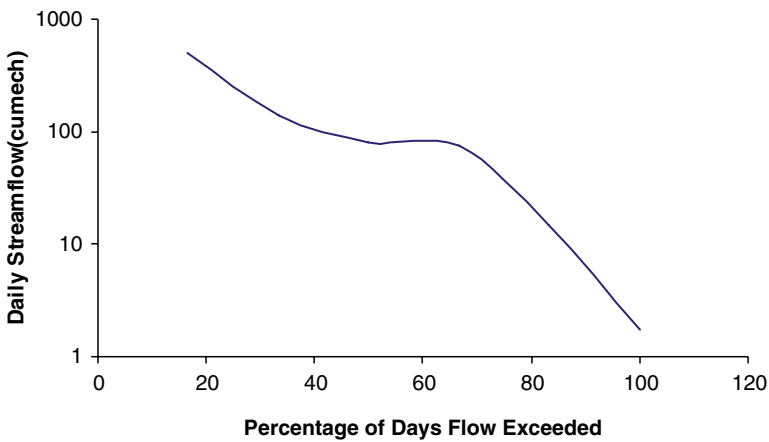
Fig. 20.3 Figure showing flow duration curve drawn from the estimated stream flow data
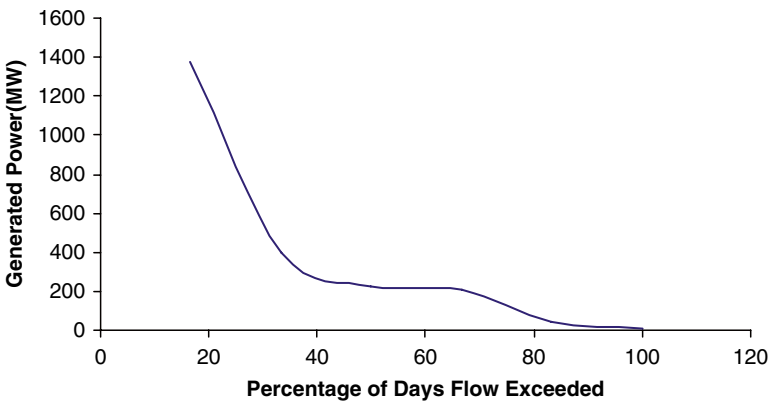
Fig. 20.4 Figure showing load duration curve drawn from the estimated power of the dam
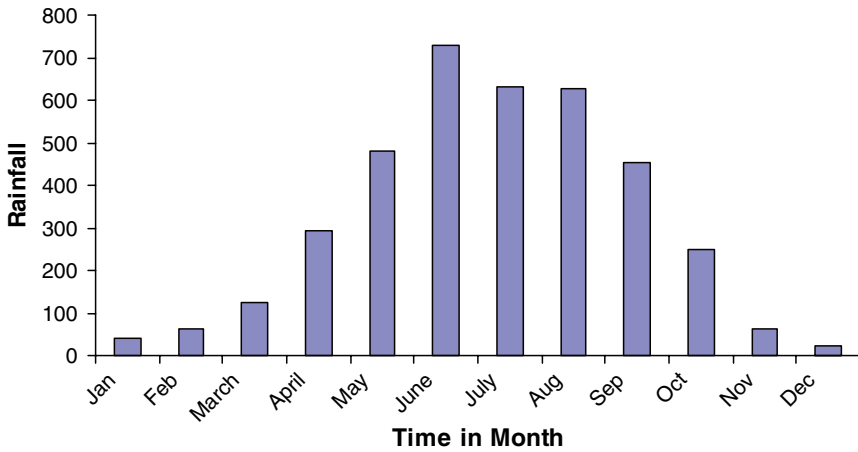
Fig. 20.5 Figure showing observed average monthly rainfall at the study area

Table 20.1 Table showing the main features of the study area

Rain fall	250–300 cm p.a.
Dam Rangpo	
Type	Concrete, gravity
Dam height	48 m
Dam volume	83,000 m³
Dam Rangili	
Type	Concrete, gravity
Dam height	41 m
Dam volume	45,200 m³
Head race tunnel Rangpo	
Length	2,578 m
Initial diameter	3.3 m
Head race tunnel Rangili	
Length	2,258 m
Initial diameter	4 m
Common head race tunnel	
Length	3,225 m
Initial diameter	4.6 m
Surge shaft	
Initial diameter	12 m
Height	103.9 m
Surface penstock	
Length	801.2 m
Diameter	3.3 m
Power house	
Type	Out door
Turbine	Francis, vertical
Generator	2 nos. each 49.5 MW

From the figures it can be observed that the highest discharge at Rangili and Rangpo were found to be equal to 70.23 and 72.09 cumec, respectively in October and August.

20.5.2   Estimated Discharge of the Study Area

The discharge at the 1B to 4B and 1C (Fig. 20.6) was estimated with the help of TR55 model. The results are shown in Table 9.1.

As the model is validated satisfactorily, power possible from the estimated discharge was calculated and shown in Table 20.2. From the table, it could be observed that 211.294 MW of power could be generated in Monsoon. In post-monsoon and pre-monsoon seasons, 4.97 and 221.622 MW power can be generated . Pre-monsoon and monsoon seasons generate more than 99 MW of power. Throughout, for 75% of a year the project could generate more than 99 MW of power. Only in post-monsoon season, the maximum power generated was found to be 40.74 MW, which is less than the rated power of 99 MW. So according to the model estimation, the study area could generate more than the rated amount of power in major part of a year.

20.5.3   Uncertainty Analysis and Identification of Optimal Power Generation Point

Minimum Energy Maximum Power (MEMP) algorithm was run to identify the optimal power generation point. In MEMP, the first step was to apply extreme
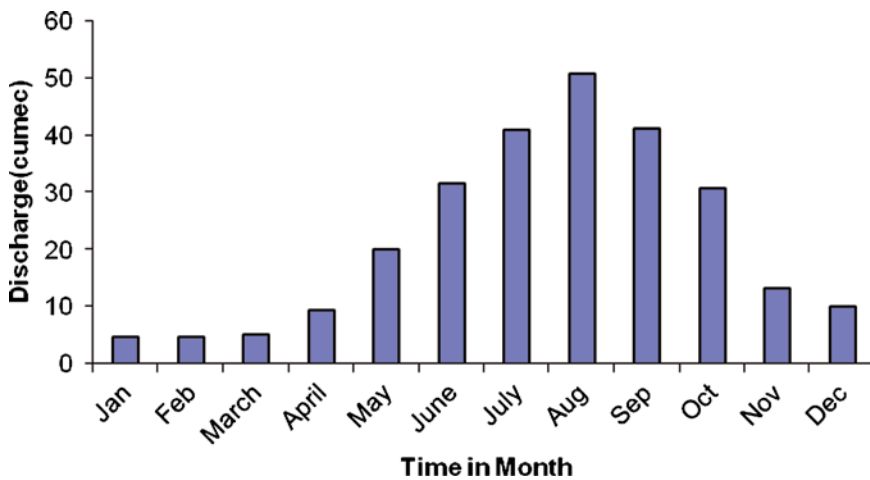
Fig. 20.6   Figure showing observed average monthly discharge at the Rangili dam

Table 20.2 Table showing estimated discharge in post-monsoon, monsoon and pre-monsoon

	Rainfall (mm)	Discharge (cumec)
Post-monsoon		
Maximum	173	14.69
Average	46.815	1.73
Minimum	0.1	733.34
Pre-monsoon		
Maximum	1,281.3	494.37
Average	405.45	79.91
Minimum	77.1	3.25
Monsoon		
Maximum	778.7	141.969
Average	491.95	76.186
Minimum	82.8	3.68
Annual		
Maximum	1,281.3	494.37
Average	314.26	38.93
Minimum	0.1	753.35

rainfall values to the model. The results were noted to understand whether model has the capability to identify uncertainties. The model also estimated the discharge if the adjacent rivers dried out. Now all the dates ware collected, sorted and applied to a curve fit equation named Shifted Power equation (9.1). With the help of the curve fit equation the optimal power generation point was identified, which was found to be equal to 36.23 cumec.

The optimization algorithm considered discharges for uncertain values and more than 99 MW as constraints, which must be avoided. The zone of uncertainty and nonconsideration was identified and separated. Along with these conditions the optimal power generation point was identified.

$$Y = a^{\times (x-c)^b} \tag{20.2}$$

where $a = 2.7213$, $b = 1.00246$, $c = -0.3687$, $x =$ discharge (cumec). $Y =$ Generated Power (MW).

20.6   Conclusion

The optimal power generation point was identified as 36.23 cumec (discharge), the minimum kinetic energy that will be required to give the rated power. The present study tried to estimate the optimal power generation point for a hydropower plant situated in high altitudes of Karakoram Range. Two dam were connected by a penstock and the discharges of both the dams were applied to generate hydropower.

Methods of GIS were applied to get area, length and slope from the dam site to power house and TR55 model was fed this information to estimate the discharge at the dam site and the power house. To identify the optimal power generation point, discharge for extreme rainfall was estimated. The discharge in the power house when the river dried out was also estimated. All the outputs were compared to power and applied to MEMP algorithm to identify the optimal power generation point.

20.6.1 Limitations

- Contouring of the area was based on GPS reading; therefore, accuracy of the GPS decides the accuracy of the work.
- Several parameters were calculated by using the Map Window GIS software. Therefore, the accuracy of the work partially depends on this software.
- The estimated discharges were calculated by using the TR-55 model, but in some cases when the rain fall value was very small, the model gave unexpected values of discharge. For this the uncertainty analysis was done without calculating the discharge, which occurs for very minimum values (Figs. 20.7 and 20.8).
- In this study, snowmelt data were not used.

20.6.2 Future Scope

Limiting the emissions of greenhouse gases from power generation will be minimized by continuing and increased use of hydroelectric power. However, climate change itself may alter rainfall patterns, adversely affecting the financial
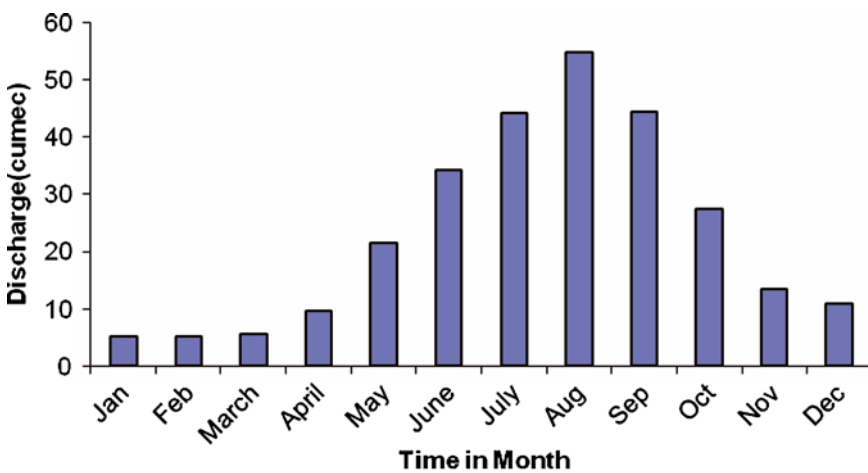
Fig. 20.7 Figure showing observed average monthly discharge at the Rangpo dam
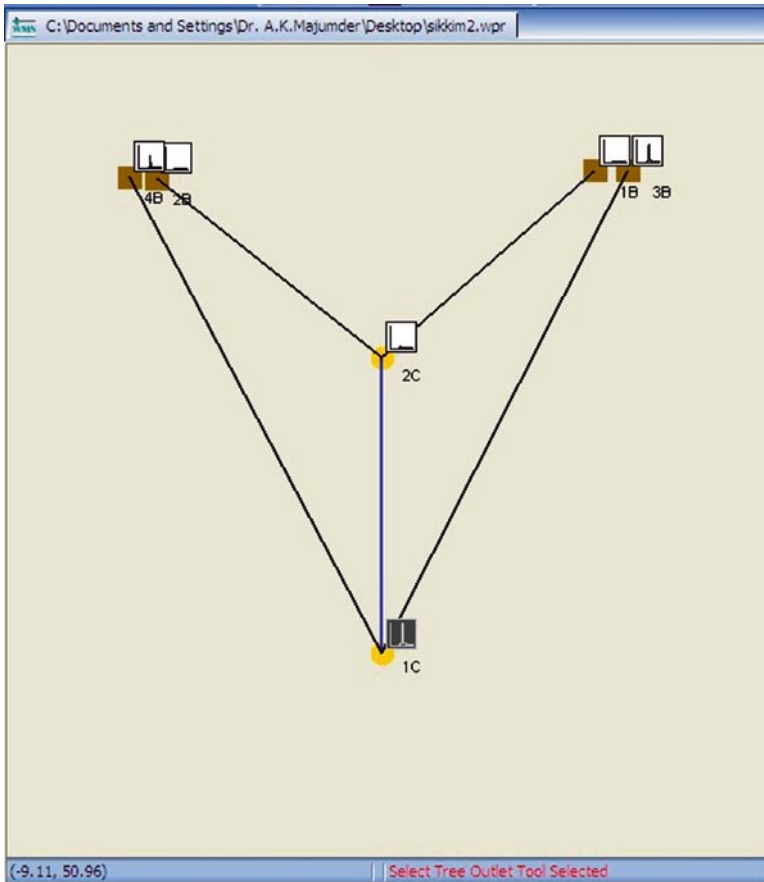
Fig. 20.8 Figure showing the modeling tree of the study area. 4B, Rangili River; 2B, Rangili, inlet sluice gate; 1B, Rangpo River; 3B, Rangpo inlet sluice gate; 2C, Penstock junction; 1C, power house

viability of existing and potential hydro schemes. By developing a methodology for quantifying the potential impact of climate change on the economics of hydropower schemes the reliability of hydropower Plant will be increased. The analysis is extended to examine the potential for changes in project risk. This analysis shows that applied climate change scenarios alter not only the mean financial performance of the scheme, but also the financial risk facing it. This finding has implications for the future provision of hydropower.
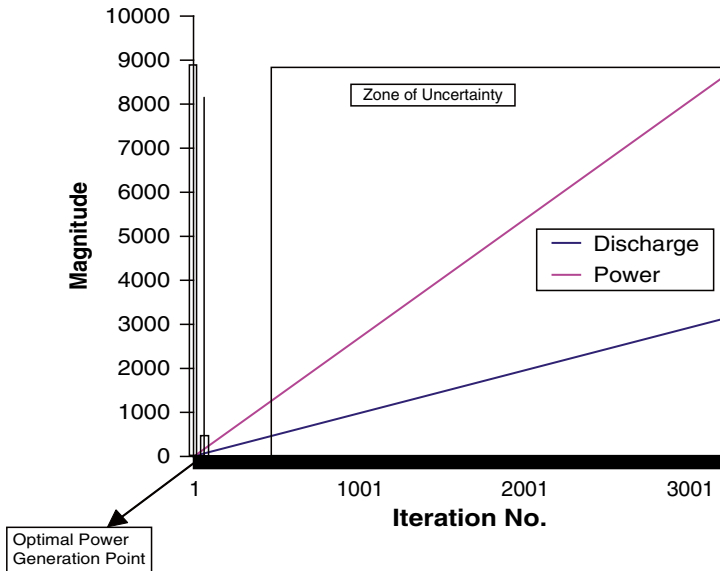
Fig. 20.9 Figure showing the optimal power generation point in the graph showing the discharge and power at different iteration

References

Arce A, Ohishi T, Soares S (2002) Optimal dispatch of generating units of the Itapu hydro plant. IEEE Trans Power Syst 17(1):154–157

Birhanu BZ, Mkhandi S, Mtalo FW, Kachroo RK (2007) Hydrological Study of hydropower and downsteam water release. International conference on Small Hydropower-Hydro, Sri Lanka

Keppo J (2002) Optimality with hydro power system. IEEE Trans Power Syst 17(3):373–413

Kumar P, Chandra CU, Kumar MS (2007) Enviromental flows for hydro power projects – a case study. International conference on small hydropower-hydro Sri Lanka

Majumder M (2008) Digitization for beginners. Lulu Publishers, New York, pp 45–65

Oliveira ARL, Soares S, Nepomuceno L (2003) Optimal active power dispatch combining network flow and interior point approaches. IEEE Trans Power Syst 18(4):1235–1240

Part III
General Overviews

Chapter 21
An Overview of Hydrologic Modeling

Mrinmoy Majumder, Arnab Barua, and Bebapriya Basu

Abstract Hydrologic models are developed for the purpose of imitating the actual relationship between the geo-climato-hydrological variables to estimate the future interactions of the same. Hydrologic models are mainly divided into temporal, spatial, and spatiotemporal hydrologic models based on the type of independent variable (time, space, or both). Further, the models can be divided into single or multievent and lumped or distributed. The hydrologic models are also classified with respect to the tools by which the interrelationship of variables are identified. In the present technical note, an overview of hydrologic models is discussed along with thorough descriptions of the different types of models and their applications in various hydrologic problems are also given.

Keywords Conceptual models • hydrology • Modeling • overview

M. Majumder (✉)
Senior Research Fellow, School of Water Resources Engineering, Jadavpur University, Kolkata-700032, West Bengal, India
and
Geo-information Scientist, Regional Center, National Afforestation and Eco-development Board, Jadavpur University, Kolkata-700032, West Bengal, India
e-mail: mrinmoy@majumder.info

A. Barua
Lecturer, Sylvan Polytechnic College, Bardhaman-713101, West Bengal, India
and
Former PG Student, School of Water Resources Engineering, Jadavpur University, Kolkata-700032, West Bengal, India

D. Basu
Former PG Student, School of Water Resources Engineering, Jadavpur University, Kolkata-700032, West Bengal, India

21.1 Hydrologic Models

The use of models to better understand and to predict the behavior of water in catchments has a long history, and, because models are rarely successful in application outside the catchments for which they were developed, there are many models to be found. The models range from simple "black box" representations of input and output, which are often successful in the prediction of runoff, from rainfall, to more complex representations of some of the spatiotemporal complexity of catchments, which are more capable of fostering a better understanding of the reasons for observed behavior. Catchments themselves are superb simplifiers, converting a spatial complexity of patterns and processes into a relatively simple and well-understood output – the hydrograph. The range of models available reflects the need to predict the outcomes of specific interventions and scenarios for change, the emphasis on prediction, as well as scientific investigation (for the purposes of flood prediction and mitigation or water resource management) and the paucity of data available for large catchments compared with smaller ones.

21.2 Data Statistics and Modeling Watershed Change

Before the 1960s, the availability of hydrologic data was very limited. Short records of stream flow and precipitation were available, but soils data, maps of land cover and use, and data on temporal watershed changes were generally not available. In addition, the availability of computers was limited. These limitations of data and computational firepower restricted the types of hydrologic methods that could be developed for general use. Flood frequency analysis was a staple of hydrologic modelers. It required limited amounts of data and was appropriate for the computational abilities of the era.

Urbanization over the last 40 years, including suburban sprawl, and the resulting increase in flooding necessitated new modeling tools and statistical methods. Watershed change introduced effects into measured hydrologic data that limited the accuracy of the traditional hydrologic computations. For example, frequency analysis assumes a stationary data sequence. The nonstationarity into hydrologic data by watershed change means that T-year (annual) maximum discharge estimates from either predevelopment data or analyses of the nonstationary data would not be accurate estimates of T-year discharges that would occur under the current watershed conditions.

Two statistical advances are required to properly analyze nonstationary data. First, more appropriate statistical tools are necessary to detect the effect of hydrologic change and the characteristics of the change. For example, statistical methods are needed to identify trends, with one class of statistical methods needed for gradual trends and a second class needed for abrupt changes. Second, more sophisticated modeling tools are needed to account for the nonstationarities introduced by watershed change. For example, data measured from an urbanizing watershed would require a model to transform or adjust the data to a common watershed condition before a frequency analysis could be applied to the annual maximum discharge record.

Computers, and advances in software and accessory equipment, have made new, important types of data available that were not generally accessible even a decade ago. For example, maps can be scanned into a computer or taken from a CD-ROM and analyzed to create spatial measures of watershed change. Measured hydrologic data reflect both temporal and spatial changes, and computers make it possible to characterize these change. The greater availability of data enables and requires more accurate models to account for the spatially and temporally induced nonstationarities in the measured hydrologic data.

21.3 Identification of Watershed Change

Watersheds, by nature, are dynamic systems: therefore, they are in a constant state of change. While many changes are not detectable over short periods, major storms can cause extreme changes. While the news media may focus on damage to bridges, buildings, or dams, physical features of the watershed such as channel cross sections may also change drastically during major floods. Thus, natural changes to both the land cover (e.g., afforestation) and the channel (e.g., degradation of the channel bottom) introduce nonstationarities into measured flood records.

In addition to natural watershed changes, the response of a watershed can change drastically due to changes associated with human activities. Changes in agricultural management practices and urban land cover exert significant effects on the responses of watersheds. In-stream changes, such as channelization or the construction of small storage structures, have also had a profound effect on the watershed response to storm rainfall. These changes will also introduce nonstationary effects in measured data.

Changes in hydrologic response due to natural or human-induced causes can change the storage characteristics of the watershed. Agricultural land development often involves both land clearing, which reduces surface roughness and decreases natural storage, and improvements in the hydraulic conveyance of the drainageways. These changes increase the rates of runoff, which decreases the opportunity for infiltration. Thus, peak runoff rates will increase, times to peak will decrease, and volumes of the surface runoff will increase. With less infiltration, baseflow rates will most likely decrease. Increases in flow velocities, which can be major causes of flood damage, accompany the increases in runoff rates, with the higher velocities generally increasing the scour rates of cannel bottoms.

Changes in urban land cover reduce both the natural interception and depression storages and the potential for water to infiltrate, especially where the change involves an increase in impervious surfaces. The hydrologic effects of urban land-use changes are similar to the effects of agricultural changes. The reduction on both surface storage and roughness increases the runoff rates and decreases computed times of concentration. Because of the reduced potential for infiltration, the volume of surface runoff also increases as a watershed becomes urbanized. The construction of storm sewers and curb-and-gutter streets can also decrease the time to peak and increase peak runoff rates.

In-stream modifications may increase or decrease channel storage and roughness. Channelization (straightening and/or lining) of a stream reach reduces the roughness,

which increases flow velocities, and may decrease natural channel storage and/or the flow length (thus increasing channel slope). The net effect is to increase peak runoff rates. Small in-stream detention structures used in urban or rural areas to mitigate the effects of losses to natural storage have the opposite hydrologic effect of channelization. Specifically, the inclusion of in-stream storage decreases peak flow rates of small storms and increases the duration of high-flow conditions. In general, the in-stream detention structure will not significantly change the total volume of runoff but will redistribute the volume over time.

21.4   Time Series Modeling

Time series modeling is the analysis of a temporally distributed sequence of data or the synthesis of a model for prediction in which time is an independent variable. In many cases, time is not actually used to predict the magnitude of a random variable such as peak discharge, but is ordered by time. Time series are analyzed for a number of reasons. One might be to detect a trend due to another random variable. For example, an annual maximum flood series may be analyzed to detect an increasing trend due to urban development over all or part of the period of record. Second, time series may be analyzed to formulate and calibrate a model that would describe the time-dependent characteristics of a hydrologic variable. For example, time series of low-flow discharges might be analyzed in order to develop a model of the annual variation of base flow from agricultural watersheds. Third, time series models may be used to predict future values of a time-dependent variable. A continuous simulation model might be used to estimate total maximum daily loads from watersheds undergoing deforestation.

Methods used to analyze time series can also be used to analyze spatial data of hydrologic systems, such as the variation of soil moisture throughout a watershed or the spatial transport of pollutants in a groundwater aquifer. Instead of having measurements spaced in time, data can be location dependent, possibly at some equal interval along a river or down a hill slope. Just as time-dependent data may be temporally correlated, spatial data may be spatially correlated. The extent of the correlation or independence is an important factor in time-and space-series modeling. While the term time series modeling suggests that the methods apply to time series, most of such modeling techniques can also be applied to space series.

Time and space are not causal variables; they are convenient parameters by which true cause and effect can be brought into proper relationships. For example, evapotranspiration is normally highest in June. This maximum is not caused by the month, but because of the highest insolation in June. The seasonal time of June can be used as a model parameter only because it connects evapotranspiration and insolation.

In its most basic form, time series analysis is a bivariate analysis in which time is used as the independent or predictor variable. For example, the annual variation of air temperature can be modeled by a sinusoidal function in which time determines the point on the sinusoid. However, many methods used in time series analysis differ from the bivariate form of regression in that regression assumes independence

among the individual measurements. In bivariate regression, the order of the x–y data pairs is not important. Conversely, time series analysis recognizes a time dependence and attempts to use dependence to improve either the understanding of the underlying physical processes or the accuracy of prediction. More specifically, time series are analyzed to separate the systematic variation from the nonsystematic variation in order to explain the time-dependence characteristics of the data where some of the variations are time dependent. Regression analysis is usually applied to unordered data, while the order in a time series is an important characteristic that must be considered. Actually, it may not be fair to compare regression with time series analysis because regression is a method of calibrating the coefficients of an explicit function, while time series analysis is much broader and refers to an array of data analysis techniques that handle data in which the independent variable is time (or space). The principle of least squares is often used in time series analysis to calibrate the coefficients of explicit time-dependent models.

A time series consists of two general types of variations: systematic and nonsystematic. For example, an upward-sloping trend due to urbanization or the annual variation of air temperature could be modeled as systematic variation. Both types of variations must be analyzed and characterized in order to formulate a model that can be used to predict or synthesize expected values and future events. The objective of the analysis phase of time series modeling is to decompose the data so that the types of variation that make up the time series can be characterized. The objective of the synthesis phase is to formulate a model that reflects the characteristics of the systematic and nonsystematic variations.

Time series modeling that relies on the analysis of data involves four general phases: detection, analysis, synthesis, and verification. For the detection phase, effort is made to identify systematic components, such as secular trends or periodic effects. In this phase, it is also necessary to decide whether the systematic effects are significant, physically and possibly statistically. In the analysis phase, the systematic components are analyzed to identify their characteristics, including magnitudes, form, and duration over which the effect exists. In the synthesis phase, the information from the analysis phase is used to assemble a model of the time series and evaluate its goodness of fit. In the verification phase, the model is evaluated using independent data, assessed for rationality, and subjected to a complete sensitivity analysis. Poor judgment in any of the four phases will result in a less-than-optimum model.

21.5 Modeling the Spatial Variability

The hydrologically significant properties of catchments are the following:

(a) The topological structure of their drainage network, which determines the lag time for arrival of rainfall to a point in the network and the temporal concentration of the stream flow hydrograph that results.

(b) Their geomorphological and pedological characteristics (and spatial variation), which determine the potential for infiltration and local storage over runoff and

thus contribution to stream flow. The large-scale geomorphology will also control the topology of the drainage network and, in large catchments, this may be the most important control on a catchment's hydrology (Vorosmarty et al. 2000).

(c) Their climatic characteristics (and spatial variation). The spatial distribution of temperature, radiation, and rainfall, which are themselves highly correlated with attitude will determine the spatial distribution of contributions from areas within a catchment.

(d) Their vegetation cover and land-use characteristics and its spatial variation. Chapter 3 on hillslope hydrology indicates the significance of vegetation for the hydrological balance of hillslopes and the partitioning of rainfall into local infiltration and infiltration excess, that is, runoff.

(e) The spatial distribution of their populations. Populations are the source of demand for water and their locations may determine the locations of local extractions and artificial storage of water from the channel network or from locally generated runoff (as in the Aljibes of North Africa and the Mediterranean) and local ground-water sources. The locations of populations will also determine the magnitude of local land-use change with corresponding impacts and the sources of point and nonpoint agricultural, industrial, and domestic pollution to the water courses.

Because of surface and subsurface lateral flows, hydrological catchments are highly connected such that a change in any one part of them can have implications for a number of other parts downstream. Furthermore, the spatial distribution of all of these factors relative to the direction of stream flow is particularly important since it determines the potential for cumulation or diminution of stream flow along the flow path. A series of source areas in line with the flow path will cumulate outflow along the flowline, whereas a mixture of source and sink areas will tend to dominate outflow along the flow path.

21.5.1 Spatially Sensitive Hydrological Models

The types of catchments model available include physically based models, based solidly on an understanding of the physical processes, empirical models based on the patterns observed in data, and conceptual models, which pay little attention to the physics of the processes but, rather, represent the catchment conceptually as, for example, a series of cascading stores for water and the fluxes between them. Models may be deterministic models in which a given set of inputs will always produce the same output, or stochastic models, which represent the variability of processes or events using probability distributions and which thus attempt to handle some of the inherent uncertainties in modeling and data. Models may be lumped at the catchment scale, meaning that data and modeling are aggregated at this scale, they may be lumped at the subcatchment scale (and thus semidistributed at the catchment scale), or they may be fully distributed, that is lumped at the raster grid cell of TIN polygon scale.

Empirical models tend to be lumped, conceptual models tend to be semidistributed, and physically based models tend to be fully distributed. The increase in

computing power and of available spatial data in the form of GIS datasets, especially DEMs, and remotely sensed imagery have vastly increased the potential for distributed modeling. At the catchment scale, to be based on physics, physically based models have to be distributed and so "distributed" and "physically based" often go together in catchment hydrological modeling. Moreover, many large catchments are ungauged and thus cannot provide the calibration data necessary for the development and parameterization of conceptual or empirical models. A driving force for the development of physically based is their application in ungauged catchments, though we will see later that gaps in parameterization data and process knowledge create model uncertainty and thus the requirement for these models to be calibrated against gauging station data.

21.5.2   Distributed Hydrologic Models

Since it was first "blueprinted" by Free and Harlan 1969, distributed physically based modeling has become very widespread, on the assumption that a spatially variable physical system is inherently more realistic than a lumped one. This is likely to be true but must be considered within the context of spatially distributed models being themselves often crude simplifications of any spatial variability that does exist in real catchments. Remote sensing has gone some way toward improving the observability of surface properties at the catchment scale, but subsurface properties are still largely unobservable at any scale other than the point or line transect. Examples of current distributed, physically based models include the SHE model (Systeme Hydrologique European, see Abbott et al. 1986) and the MIKE She and SHETRAN descendants of it (Bathurst et al., 1995; Refsgaard and Storm 1995), the IHDM model (Institute of Hydrology Distributed Model, e.g., Calver and Wood 1995), the CSIRO TOPOG model (e.g., Vertessy et al. 1993), Thales (Grayson et al. 1992), and WEC-C (Croton and Barry 2001), among others, Physically based models should be derived deductively from established physical principles and produce results that are consistent with observations (Beven 2002). In reality, they are often one of these but rarely both.

   SHE was developed jointly by the UK Institute of Hydrology (IH) – the Danish Hydraulic Institute (DHI) and the Societe Grenoblois d' Etudes et d' Applications Hydrauliques (SOGREAH). It was specifically designed to address the impact of human activities on catchment processes. This type of scenario analysis is very difficult to address with empirical or conceptual models, but is the main focus of most physically based models. In SHE a finite difference (grid-based) approach is used in three dimensions with up to 30 horizontal layers. Surface and groundwater flow are two-dimensional while flow in the unsaturated zone is one-dimensional. The model has been widely applied and continuously updated since 1986.

   While remote sensing provides some high quality spatial datasets for properties such as vegetation cover and topography, there are many hydrologically important

properties of catchments, notably those of the soils and the surface that cannot be measured remotely and thus require intensive field campaigns, which still cannot provide the kind of spatial coverage required to justify their distribution in models. For example, most hydrological models are highly sensitive to the (Saturated) hydraulic conductivity of soils (K_{sat}), see Davis et al. (1999) and Chappell et al. (1998) and this is notoriously difficult to measure for volumes greater than a few hundred cubic centimeters, in part because of Baird's (bloody) macrospores of Chapter 3. It is fair to say that there is a significant mismatch in the sophistication of our physically based models and the sophistication of the data collection technologies used to parameterize them. Moreover, as highlighted in Chapter 1, modeling is rather inexpensive compared with fieldwork and is also perhaps more glamorous, more comfortable, and more suited to producing publications – see the discussion by Klemes (1997:48). So, the gap between the models and the data to fill them widens.

It is the imbalance between the model sophistication and the availability of data at appropriate scales (as well as our incomplete understanding and thus mathematization of the processes themselves), that means that even the most sophisticated models rarely perform well in a predictive capacity. Empirical models tend to be better predictors. Thus, a process of parameter calibration is often exercised on physically based distributed models to ensure agreement of predicted versus observed runoff. This process, of course, compromises the physical realism of the model and thus its ability to explain as well as to predict. Since explanation is about why physically based distributed models exist, this compromise is a serious one. If it was not for explanation, then an equally predictive empirical model would always be the best model because of its parsimony. Some authors have argued that calibration can render physically based distributed models closer to over-parameterized conceptual, lumped models (Beven 1989, 1996). Furthermore, physically based, distributed models – even the very widely used ones – have rarely been validated on variables other than the output variables. Very few studies have validated the internal state variables of these models in order to understand whether the models are producing validatable results for the correct physical (internal) reasons. In other words, do the lack of data, lack of detailed process understanding, and over-calibration render physically based models into overly sophisticated conceptual models or do they indeed retain some useful explanatory power? Few researchers still concentrate on validation which is focused specifically on the purpose for which the model is intended, such as suitability for the analysis of the impact of climate or land-use change (Ewen and Parkin 1996). Furthermore, few studies focus on the evaluation of distributed behavior as opposed to catchment-integrated outcomes such as runoff (Grayson et al. 1995): the correct prediction of patterns may be a better measure of explanatory power than is success in the prediction of catchment outflows. In complex models, a number of different parameter sets can give rise to the correct outflow (the problem of equifinality). As a result, and given the uncertainty in most parameterization datasets, understanding whether your calibrated model has produced the right answers for the right physical reasons is rather difficult. Beven

and Binley (1992) and a number of others have used generalized likelihood uncertainty estimator (GLUE) approaches to look at the implications of parameter uncertainty on model outcomes.

It is these problems and others, amply spelled out by Rosso (1994), Beven (1989, 1996) and Refsgard (1997), that are the reasons why physically based distributed models have tended to remain in the research domain and have had relatively little impact on the world of practical hydrology. The problems with building and using distributed, physically based models as per the Free and Harlan (1969) blueprint may be so great that an alternative blueprint is required (Reggiani et al. 2000; Beven 2002). Those problems associated with the application of Darcy's law for matrix flow (see Chapter 3) at a range of scales where it does not apply or, if it does apply, we cannot test that it does, are particularly serious. The alternative blueprint of Beven (2002) emphasized a more observation-based inductive approach over the more theoretical deductive approach of Free and Harlan (1969). See the data-based mechanistic approach outlined by Young et al. in Chapter 22, for example. In this way the observations, and not the theory, determine which models are appropriate (Mulligan).

21.6   Spatiotemporal Hydrologic Models

Spatiotemporal hydrologic models are those models which are both spatially and temporally sensitive. In the development of such models, spatial, temporal, and process complexity must be simplified as described below.

21.6.1   Reduction of Spatial Nonlinearity

So far we have concentrated on understanding the implications of spatial complexity for modeling needs at the catchment scale. We know that lumped models do not represent this complexity and that distributed models do, insofar as they can, but do not insofar as the required data is often not available. Semidistributed (or semi-lumped!) approaches are a compromise between the two end points, but say nothing of the interaction between neighboring patches, which can be important in hydrological studies. Different aspects of the spatial variability of catchments have different magnitudes of impact on the hydrological system and different spatiotemporal scales of interaction with it. Soil and vegetation properties are likely to be more important for small catchments and short periods but their influence will become less as the size of the catchment or length of the period increases, at which point geomorphological and geomorphometric processes become more important. A nested hierarchy of catchment response units might be identified with climate, geomorphology, vegetation, and soils having progressively greater variability and progressively smaller scales of influence (see Mulligan 1996).

21.6.2   Reduction of Temporal Variability

In addition to spatial complexity, catchment models must also handle the temporal complexity of hydrological processes and their interaction with each other, catchments integrate rapid rate processes such as the partitioning of rainfall into runoff and infiltration or the routing of water through channels, with slower rate processes such as the trickle or groundwater recharge and the continuous draw of evapotranspiration. Hydrological models are sensitive to the timestep of simulation; large errors can ensue by aggregating evapotranspiration calculations (from hourly through day/night to daily) and by representing instantaneous rainfall intensities that can reach over 100 mm/h as hourly averages, which are unlikely ever to do so (see Wainwright et al. 1999, for an extended analysis). The temporal and spatial complexity of a catchment model must match the spatiotemporal complexity of the processes, though the availability of data is usually the greater constraint. For simplicity, natural timesteps are always preferable to artificial ones (day and night separated at sunrise and sunset instead of being aggregated into whole day; rainfall-rate-based timesteps reflecting the real passage of rainfall intensities instead of hourly lumps of rainfall).

21.6.3   Simplification of Process Volatility

There are many areas of hydrology where our understanding of processes is basic but still sufficient to develop models. But there are still areas in which the complexity of hydrological processes is so great, or the information so little, that we do not understand the processes well enough to develop reliable models. This complexity of processes is separated from the issues related to spatial and temporal variations and the lack of data available to represent them as outlined above. Some of the areas in which there is still much progress to be made are outlined below:

(a) The hydrology of sparse vegetation. Although techniques for modeling the interception, drainage, and evapotranspiration from forest canopies are now well established, there are still difficulties in understanding the role of canopy properties in determining the partitioning of water between the various fluxes. These difficulties are particularly clear for nonclosed canopies or sparse vegetation where the impact of surface roughness is less well known and the parameterization of evapotranspiration is much more difficult. Furthermore, the separation of vegetation into patches may change evapotranspiration loads in complex ways (Veen et al. 1996). Patchiness is not only important for evapotranspiration, but also affects the generation and propagation of runoff and sediment, especially in arid and semiarid environments (Dunkerly and Brown 1995).

(b) Subsurface quickflow mechanisms. The parameterization of K_{sat} at scales greater than a few hundred cubic centimeters remains a major obstacle to progress in subsurface hydrological modeling, particularly given the importance of macropores in providing a mechanism for subsurface quickflow in many environments

(Elsenbeer and Vertesy 2000; Uchida et al. 2001). Although our understanding of the mechanisms of runoff generation through Hortonian and saturation-excess mechanisms has improved considerably in recent years with the extensive incorporation of partial contributing area concepts into hydrological models, our understanding of subsurface quickflow mechanisms through macroporepipe networks and shallow subsurface quickflow is much less advanced. This lack of progress is partly the result of the difficulty in measuring variations in the physical properties that control these processes at the catchment scale, and partly the result of the relatively recent recognition of subsurface quickflow as hydrologically important.

(c) Hillslope–channel coupling. Modeling catchment is about modeling the hydrology of hillslopes and channels. Many of the processes that determine channelization are still poorly understood and the coupling of hillslopes to channels is an area in which new insights are being made but further research is required to help improve catchment models of streamflow, strom hydrograph, and flooding.

(d) Non-rainfall precipitation. There is still a relative dearth of modeling efforts focused upon the hydrology of non-rainfall inputs such as snow (Bloschl 1999) and occult precipitation (Mulligan 2003) at the catchment scale. These inputs are significant in many catchments, but are more difficult to measure and to model than rainfall.

(e) Tropical lowlands and tropical mountains. The hydrological impacts of land use and cover change in the tropics are much discussed in the literature, but there are very few studies, which apply modeling to better understand these systems (Mulligan 2003) and fewer still combine modeling with intensive field monitoring programs (Chappell et al. 1998). As a result, there is still much confusion about the implications of land-use change in these environments and myths abound (Bruijnzeel 1989; Calder 1999; Mulligan 2003).

(f) Hydrological connectance. A key characteristic of catchment scale studies is the lateral connectance between patches with results from surface and subsurface runoff. The properties of this connectance determine the manner in which patch scale output aggregate to catchment totals. Total catchment runoff is not a simple sum of the constituent patch-level runoff. Recent work by the author using a distributed hydrological model applied in tropical montance environments indicates the importance of hydrological connectance for catchment level outputs and the implications for the study of the hydrological impacts of land-use change. This study is described in more detail on the accompanying website. Look at the implications of progressive deforestation on the catchment scale runoff and the sensitivity of runoff to forest loss. The study concludes that in the initial stages of deforestation (0–75% forest cover lost), the sensitivity of runoff to forest loss is significant but low compared with the situation beyond 75% loss. It is concluded that where patches of forest remain along the surface and subsurface flowlines, these absorb excess water generated on the deforested patches and thus extra runoff does not cumulate downstream. When so much forest is lost that flowlines are more or less deforested along their whole length, runoff generation accumulates down the flowlines and saturated wedges penetrate further

upslope, thus providing a positive feedback for further runoff generation. In this way the sensitivity of catchment scale runoff to the deforestation of patches in this last 25% is very high, each patch contributing greatly to the continuity of deforested flow paths thus to enhanced (flashy) stream flow. Furthermore, the location of the deforestation relative to the geometry of the flow network and the properties of the soil beneath and vegetation above it determine the exact outcome of forest loss. This example only goes to indicate the importance of lateral connectivity in driving the overall response of catchments and in integrating (in a relatively simple way) the complex spatial hydrology of them.

21.7 Some Popular Hydrologic Modeling Systems

21.7.1 Hydrologic Engineering Centre: Hydrologic Modeling System (HEC-HMS)

HEC-HMS considers that all land and water in a watershed can be categorized as follows:

Directly connected impervious surface or pervious surface.

Directly-connected impervious surface in a watershed is that portion of the watershed for which all contributing precipitation runs off, with no infiltration, evaporation, or other volume losses. Precipitation on the pervious surfaces is subject to losses. HEC-HMS includes the following alternative models to account for the cumulative losses:

- The initial and constant-rate loss model
- The deficit and constant-rate model
- The SCS curve number (CN) loss model (composite or gridded)
- The Green and Ampt loss model

With each model, precipitation loss is found for each computation time interval, and is subtracted from the MAP depth for that interval. The remaining depth is referred to as precipitation excess. This depth is considered uniformly distributed over a watershed area, so it represents a volume of runoff.

With a UH model, the excess on pervious portions of the watershed is added to the precipitation on directly connected impervious area, and the sum is used in runoff computations. With the kinematic-wave model, directly connected impervious areas may be modeled separately from pervious areas if two overland flow planes are defined.

Initial and Constant-rate and Deficit and Constant-rate Loss Models.

21.7.1.1 Governing Equation

The underlying concept of the initial and constant-rate loss model is that the maximum potential rate of precipitation loss, fc, is constant throughout an event.

Thus, if *pt* is the MAP depth during a time interval *t* to *t* + Δ*t*, the excess, pe_t, during the interval is given by:

$$pe_t = \begin{cases} p_t - f_c & if\ p_t > f_c \\ 0 & otherwise \end{cases} \tag{21.1}$$

An initial loss, *Ia*, is added to the model to represent interception and depression storage. Interception storage is a consequence of absorption of precipitation by surface cover, including plants in the watershed. Depression storage is a consequence of depressions in the watershed topography; water is stored in these and eventually infiltrates or evaporates. This loss occurs prior to the onset of runoff.

Until the accumulated precipitation on the pervious area exceeds the initial loss volume, no runoff occurs. Thus, the excess is given by

$$pe_t = \begin{cases} 0 & if\ \sum p_i < I_a \\ p_t - f_c & if\ \sum p_i > I_a\ \text{and}\ p_t > f_c \\ 0 & if\ \sum p_i > I_a\ \text{and}\ p_t < f_c \end{cases} \tag{21.2}$$

21.7.2   *Trend Research Manual 55 (TR55)*

21.7.2.1   Governing Equations for TR55

TR-55 specifies units for its equations. The calculation allows here to use other units that may be more convenient. Peak discharge, runoff depth, initial abstraction, unit peak discharge, and pond/swamp factor are computed as follows:

$$Q_P = Q_u A Q F_p \quad Q = \frac{(P - I_a)^2}{P - I_a + s} \quad I_a = 0.2s \quad s = \frac{1000}{CN} - 10$$

$$Q_u = f\left(T_c, \frac{I_a}{P}, \text{Rainfall distribution type}\right)$$

$$F_p = f\left(\%\,\text{Ponds and swamps}\right) \tag{21.3}$$

where *A* is the total watershed area (mi^2), CN is the overall curve number for the watershed, F_p is the pond and swamp adjustment factor, I_a is the initial abstraction (in.), *P* is the precipitation (in.) for 24-h duration storm of return period, *Q* is the depth of runoff over entire watershed (in.), Q_p is the peak discharge (cfs), Q_u is the unit peak discharge (cfs/mi^2-in.), *s* is the potential maximum watershed water retention after runoff begins (in.), and T_c is the time of concentration for the watershed (h).

21.7.2.2 Required Input Parameters and Data

(a) Length of river (ft)
(b) Average overland slope of river (ft/ft)
(c) Volume (ft^3)
(d) Travel time (h) T_t
(e) Time of concentration (h) T_c
(f) Area of basin (m in.)^2
(g) Peak rainfall (in.)
(h) Curve no.

21.7.2.3 Advantages and Limitations

The calculation allows here to use other units that may be more convenient. The TR-55 interface provides a complete graphical interface to the U.S. Soil Conservation Service TR-55 hydrologic analysis model. All modeling parameters and input data are entered through interactive graphics and easy-to-use dialog boxes, enabling the user to easily define the TR-55 hydrologic routing model.

As a simplified "tabular method" for the generation of complete runoff hydrographs, TR-55 is perhaps the most widely used approach to hydrology in the USA. It provides a number of techniques that are useful for modeling small watersheds. TR-55 utilizes the SCS runoff equation to predict the peak rate of runoff as well as the total volume.

The limitations of TR55 model are outlined next.

- Methods based on open and unconfined flow over land and in channels.
- Graphical peak method is limited to a single, homogenous watershed area.
- For multiple homogenous subwatersheds use the tabular hydrograph method.
- Storage-routing curves should not be used if the adjustment for ponding is used.

21.7.3 MODified RATional Hydrologic Model

MODified RATional Hydrologic Model (MODRAT) is a modified rational method computer program developed by the Los Angeles County Department of Public Works (LACDPW) to compute runoff rates under a variety of conditions common to the area of Los Angeles, California. The successor to F0601 and/or MORA, MODRAT contains all the features of the original F0601 as well as updated capabilities for watershed modeling in the Los Angeles area. MODRAT may be used to find flow rates for any watershed with any combination of existing or proposed channels and drains. Further, the watershed may be undeveloped, partially developed, or completely developed. The model will

compute runoff rates for any frequency design storm (storm patterns developed by LACDPW), as well as any other storm, which can be represented by a rainfall mass curve. Given any combination of the above variables, MODRAT will compute a hydrographs for each subarea and mainline or lateral collection point in the watershed.

21.7.3.1   Governing Equation

Flows for the MODRAT have been calculated by the following equations

$$Q = C \times i \times A \tag{21.4}$$

where Q is the flow rate, C is the runoff co-efficient, i is the rainfall intensity, and A is the area of the river basin.

21.7.3.2   Required Input Parameters

  (i) Area of location
 (ii) Soil type
(iii) Time of concentration
(iv) Percentage of impervious area
 (v) Rainfall depth

21.7.3.3   Limitations

• The model relies on many empirical relations to represent physical process.
• It requires a high level of expertise for application.
• There is a limited public domain version and the full package is expensive.

References

Abbott mb, Bathurst JC, Cunge JA, O'Connell PE, Rasmussen J (1986) An introduction to the European Hydrological System – Systeme Hydrologique Europeen, SHE. 2. Structure of a physically-based, distributed modeling system. J Hydrol 87:61–77
Bathurst JC, Wicks JM, O'Connell PE (1995) The SHE/SHFSED basin scale water flow and sediment transport modeling system. In: Singh VP (ed) Computer models of watershed hydrology. Water Resources Publications, Highland Ranch, CO, pp 563–594

Beven K (1989) Change ideas in hydrology-the case of physically based models. J Hydrol 105:157–172

Beven K (1996) A discussion of distributed hydrological modeling. In: Abbott MB, Refsgaard JC (eds) Distributed hydrological modelling. Kluwer, Dordrecht, pp 255–278

Beven K (2002) Towards an alternative blueprint for a physically based digitally simulated hydrologic response modeling system. Hydrol Process 16:189–206

Beven K, Binley A (1992) The furure of distributed models: model calibration and uncertainty prediction. Hydrol Process 6:279–298

Bloschl G (1999) Scaling issues in snow hydrology. Hydrol Process 13:2149–2175

Bruijnzeel LA (1989) (De) forestation and dry season flow in the humid tropies a closer look. J Tropic Forest Sci 1:229–243

Calder I (1999) The Blue revolution: land use and integrated water resources management. Earth Scan, London, 208 pp

Calver A, Wood WL (1995) The Institute of hydrology distributed model. In: Singh VP (ed) Computer models of watershed hydrology. Water Resources Publications, Highland Ranch, CO, pp 595–626

Chappell AA, Franks SW, Larenus J (1998) Multiscale permeability estimation for a tropical catchment. Hydrol Process 12:1507–1523

Croton JT, Barry DA (2001) WEC-C: a distributed, deterministic catchment model theory. Formulation and testing. Environ Model Softw 16:583–599

Davis SH, Vertessy RA, Silberstein RP (1999) The sensitivity of a catchment model to soil hydraulic properties obtained by using different measurement techniques. Hydrol Process 13:677–688

Dunkerly DL, Brown KL (1995) Runoff and runon areas in a patterned chenopod shrubland, arid Western New South Wales, Australia: Characteristic and origin. J Arid Environ 20:41–55

Elsenbeer H, Vertesy RA (2000) Stromflow generation and flowpath characteristics in an Amazonian rainforest catchment. Hydrol Process 14:2367–2381

Ewen J, Parkin G (1996) Validation of catchment models for predicting land use and climate change impacts. 1 Method. J Hydrol 175:583–594

Free RA, Harlan RL (1969) Blueprint for a physically-based, digitally-simulated hydrologic response model. J Hydrol 9:237–258

Grayson RB, Moore LD, McMahon TA (1992) Physically based hydrological modeling, 1 Terrain based modeling for investigative purpose. Water Resour Res 28(10):2639–2658

Grayson RB, Bloschl G, Moore ID (1995) Distributed parameter hydrological modeling using vector elevation data: THALES and TAPES-C. In: Singh VP (ed) Computer models of watershed hydrology. Water Resources Publications, Highland Ranch, CO, pp 669–696

Klemes V (1997) Of carts and horse in hydrological modeling. J Hydrol Eng 1(4):43–49

Mulligan M (1996) Modeling the complexity of landscape response to climate variability in semi-arid environments. In: Anderson MG, Brooks SM (eds) Advances in hillslope processes. Wiley, Chichester, pp 1099–1149

Mulligan M (2003) Modelling the hydrological response of tropical mountainous environments to land cover and land use change. In: Ulli M, Huber H, Bugmann KM, Reasoner MA (eds) global change and mountain regions: a state of knowledge overview. Kluwer, Dordrecht

Refsgaard JC, Storm B (1995) MIKE SHE. In: Singh VP (ed) Computer models watershed hydrology. Water Resources Publications, Highland Ranch, CO, pp 809–846

Refsgard JC (1997) Parameterisation, calibration and validation of distributed hydrological models. J Hydrol 198:69–97

Reggiani P, Sivapalan M, Hassnizadeh SM (2000) Conservation equations governing hillslope responses: exploring the physical basis of water balance. Water Resour Res 36:1845–1863

Rosso R (1994) An introduction to spatially distributed modeling of basin response. In: Rosso R, Peano A, Bechi I, Bemporad GA (eds) Advances in distributed hydrology. Water Resources Publications, Highland Ranch, CO, pp 3–30

Uchida T, Kosugi K, Mizuyama T (2001) Effects of pipeflow on hydrological process and its relation to landslide: a review of pipe-flow studies in forested headwater catchments. Hydrol Process 15:2151–2174

Veen AWL, Klaassen W, Kruijt B, Hutjes RWA (1996) Forest edges and the soil-vegetation-atmosphere interaction at the landscape scale: the state of affairs. Prog Phys Geogr 20:292–310

Vertessy RA, Hatton TJ, O'Shaughnessy PJ, Jayasriya MDA (1993) Predicting water yield from a mountain ash forest using a terrain analysis based catchment model. J Hydrol 150:665–700

Vorosmarty CJ, Fekete BM, Meybeck M, Lammers RB (2000) Geomorphomertric attributes of the global system of river at 30-minute spatial resolution. J Hydrol 237:17–39

Wainwright J, Mulligan M, Thornes JB (1999) Plants and water in drylands. In: Baird AJ, Wilby R (eds) Ecohydrology. Routledge, London, pp 78–126

Chapter 22
A Generalized Overview of Artificial Neural Network and Genetic Algorithm

Mrinmoy Majumder, Pankaj Roy, and Asis Mazumdar

Abstract Artificial Neural Network (ANN) and Genetic Algorithms are now widely used in various scientific problems including hydrology, and the results from the studies recommend more in depth studies in this regard. A neural network generally summed the weighted data of the input variables and with the help of some activation function, output variable is tried to be estimated. The advantages of such networks mainly lie in their ability to learn problems from the observed dataset of the variables. The network structure, number of layers and nodes, activation function varies with variation in problem domains which the model learns from the data with which it was trained. The drawbacks of such models are their disability to predict data for a relation which was not included in the training data which in turn make the model nonflexible. In addition, the required computation energy and model development time are little more than the conceptual hydrologic models. The selection of network structure, training algorithms, and activation functions are determined with the help of trial and error procedures. Variable dataset of different scales also reduces the model performance. The present note tries to give an overview of the different structures, activation functions, learning process of neural network, and the use of genetic algorithm to remove the trial and error methodology of selecting the ideal model structures and configurations Application of the iteration technique is also discussed.

M. Majumder (✉)
Senior Research Fellow, School of Water Resources Engineering, Jadavpur University, Kolkata-700032, West Bengal, India
and
Geo-information Scientist, Regional Center, National Afforestation
and Eco-development Board, Jadavpur University, Kolkata-700032, West Bengal, India
e-mail: mrinmoy@majumder.info

P. Roy
Lecturer, School of Water Resources Engineering, Jadavpur University Kolkata, Kolkata-700032, West Bengal, India

A. Mazumdar
Coordinator, Regional Center, National Afforestation and Eco-development Board, Jadavpur University, Kolkata-700032, West Bengal, India
and
Director, School School of Water Resources Engineering, Jadavpur University, Kolkata-700032, West Bengal, India

Keywords Activation functions • artificial neural network • genetic algorithm • hydrology

22.1   Artificial Neural Network (ANN)

An Artificial Neural Network (ANN) is a flexible mathematical structure that is capable of identifying complex nonlinear relationships between input and output datasets. ANNs offer a relatively quick and flexible means of modeling and as a result, the application of ANN modeling was widely reported in various hydrological literatures (Zhang and Stanley 1999; Neelakantan and Pundarikanthan 2000; Ray and Klindworth 2000). In the hydrological forecasting context, recent papers have reported that ANNs may offer a promising alternative for rainfall-runoff modeling (Hsu et al. 1995; Fernando and Jayawardena 1998; Tokar and Johnson 1999; Elshorbagy et al. 2000; Liong et al. 2001), stream flow prediction (Clair and Ehrman 1998; Imrie et al. 2000), reservoir inflow forecasting (Jain et al. 1999; Coulibaly et al. 2000), and prediction of water quality parameters (Maier and Dandy 1999). All the papers reported a high degree of satisfaction with the neural network estimations.

Artificial neural networks are viable computational models for a wide variety of problems. These include pattern classifications; speech synthesis and recognition; adaptive interfaces between humans and complex physical systems; function approximation; image compression; associative memory, clustering, forecasting, and prediction; combinatorial, associative memory, clustering, forecasting, and prediction; combinatorial optimization; nonlinear system modeling; and control. These networks are "neural" in the sense that they may have been inspired by neuroscience, but not necessarily because they are faithful models of biologic neural or cognitive phenomena. In fact, the majority of the networks covered in this book are more closely related to traditional mathematical and/or statistical models such as non-parametric pattern classifiers, clustering algorithms, nonlinear filters, and statistical regression models than they are to neurobiologic models.

22.2   Mathematical Representation of Artificial Neural Network

An ANN is a flexible mathematical structure that is capable of identifying complex nonlinear relationships between input and output datasets. The ANN model of a physical system can be considered with n input neurons ($x_1, x_2, ..., x_n$), h hidden neurons ($z_1, z_2, ..., z_n$), and m output neurons ($y_1, y_2, ..., y_n$). Let tj be the bias for neuron z_j and f_k for neuron y_k. Let w_{ij} be the weight of the connection from neuron x_i to z_j and beta is the weight of the connection z_j to y_k. The function that ANN calculates is:

$$y_k = g_A \left(\sum z_j b_{jk} + f_k \right)....(j = 1 - h) \tag{22.1}$$

In which,

$$Z_j = f_A \left(\sum x_i w_{ij} + t_j \right)....(i = 1 - n) \tag{22.2}$$

where g_A and f_A are the activation functions (Sudheer 2005).

The development of an artificial neural network, as prescribed by ASCE Task Committee on Application of Artificial Neural Networks in Hydrology (2000) follows the following basic rules:

1. Information must be processed at many single elements called nodes.
2. Signals are passed between nodes through connection links and each link has an associated weight that represents its connection strength.
3. Each of the nodes applies a nonlinear transformation called as activation function to its net input to determine its output signal.

The number of neurons contained in the input and output layers are determined by the number of input and output variables of a given system. The size or number of neurons of a hidden layer is an important consideration when solving problems using multilayer feed-forward networks. If there are fewer neurons within a hidden layer, there may not be enough opportunity for the neural network to capture the intricate relationships between indicator parameters and the computed output parameters. Too many hidden layer neurons not only require a large computational time for accurate training, but may also result in overtraining. A neural network is said to be "over-trained" when the network focuses on the characteristics of individual data points rather than just capturing the general patterns present in the entire training set. The network building procedure is divided into three phases which are described next in a broad way (Figs. 22.1 and 22.2).
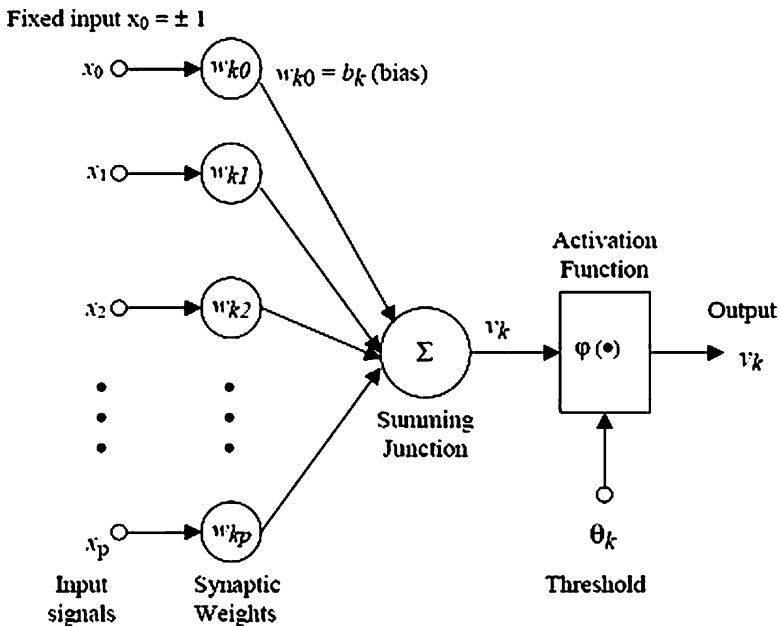
Fig. 22.1 Figure showing a schematic diagram of artificial neural network
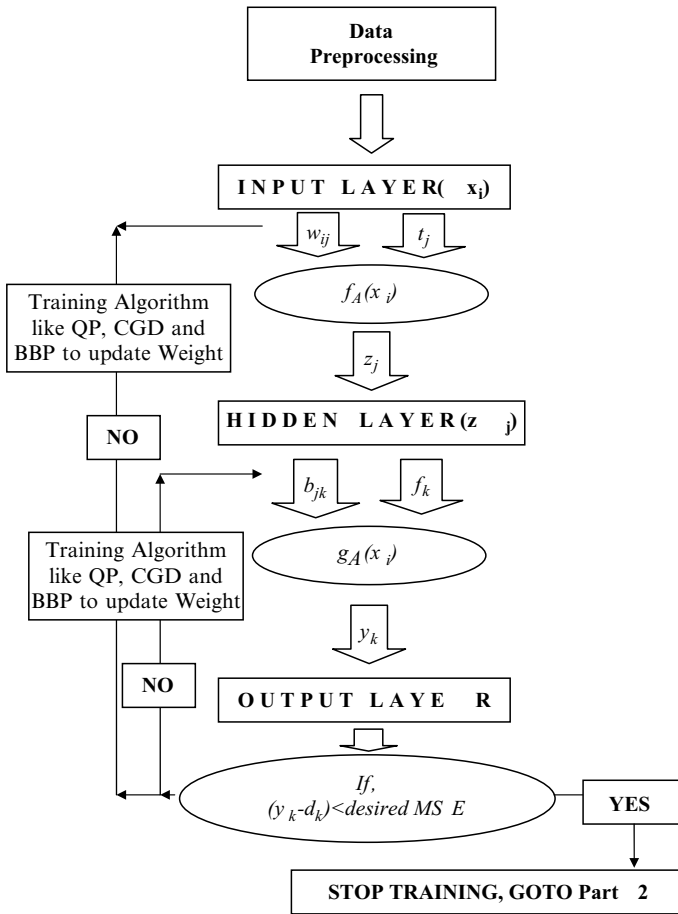
Fig. 22.2 Figure showing the basic methodology of model development by ANN

22.3 Network Building Procedure

22.3.1 Selection of Network Topology

Neural networks can be of different types, like feed forward, radial basis function, time lag delay, etc. The type of the network is selected with respect to the knowledge of input and output parameters and their relationship. Once the type of network is selected, selection of network topology is the next concern. Trial and error method is generally used for this purpose but many studies now prefer the application of genetic algorithm (Ahmed and Sarma 2005). Genetic algorithms are search algorithms based on the mechanics of natural genetic and natural selection. The basic elements of natural genetics – reproduction, crossover, and

mutation – are used in the genetic search procedure. A GA can be considered to consist of the following steps (Burn and Yulianti 2001):

1. Select an initial population of strings.
2. Evaluate the fitness of each string.
3. Select strings from the current population to mate.
4. Perform crossover (mating) for the selected strings.
5. Perform mutation for selected string elements.
6. Repeat steps 2–5 for the required number of generations.

Genetic algorithm is a robust method of searching the optimum solution to complex problems like the selection of an optimal network topology where it is difficult or impossible to test for optimality. The basics of GA have already been discussed by many authors like Ahmed and Sarma (2005), Wang (1991), Wardlaw and Sharif (1999). Hence the details of the basic procedures of GA are not focused in the present literature.

22.3.2   Training Phase

To encapsulate the desired input–output relationship, weights are adjusted and applied to the network until the desired error is achieved. This is called as "training the network." There is innumerable number of "training the network" algorithms which were discussed in more detail in Section 22.3.7.

22.3.3   Testing Phase

After training is completed, some portion of the available historical dataset is fed to the trained network and known output is estimated out of them. The estimated values are compared with the target output to compute the MSE. If the value of MSE is less than 1%, the network is said to be sufficiently trained and ready for estimation. The dataset is also used for cross-validation to prevent over-training during the training phase (Sudheer 2005).

22.4   Structure of Neural Network

22.4.1   Feed-Forward Connections

If data from neurons of a lower layer are propagated forward to neurons of an upper layer via feedforward connections, the structure is called as feedforward connection.

22.4.2 Feedback Connections

Feedback networks bring data from neurons of an upper layer back to neurons of a lower layer.

22.4.3 Lateral Connections

One typical example of a lateral network is the winners-takes-all circuit, which serves the important role of selecting the winner. In the feature map example, by allowing neurons to interact via the lateral network, a certain topological ordering relationship can be preserved. Another example is the lateral orthogonalization network which forces the network to extract orthogonal components.

22.4.4 Time-Delayed Connections

Delay elements may be incorporated into the connections to yield temporal dynamics models. They are more suitable for temporal pattern recognitions.

22.5 Classification of Neural Networks

Broadly, neural networks can be classified into the following classes:

22.5.1 Feedforward Neural Network

The feedforward neural network was the first and arguably simplest type of artificial neural network devised. In this network, the information moves in only one direction, forward, from the input nodes, through the hidden nodes (if any) and to the output nodes. There are no cycles or loops in the network.

22.5.2 Radial Basis Function (RBF) Network

Radial Basis Functions are powerful techniques for interpolation in multidimensional space. A RBF is a function which has built into a distance criterion with respect to a center. Radial basis functions have been applied in the area of neural networks where they may be used as a replacement for the sigmoidal hidden layer transfer characteristic in Multi-Layer Perceptrons. RBF networks have two layers

of processing: In the first, input is mapped onto each RBF in the "hidden" layer. The RBF chosen is usually a Gaussian. In regression problems the output layer is then a linear combination of hidden layer values representing mean predicted output. The interpretation of this output layer value is the same as a regression model in statistics. In classification problems, the output layer is typically a sigmoid function of a linear combination of hidden layer values, representing a posterior probability. Performance in both cases is often improved by shrinkage techniques, known as ridge regression in classical statistics and known to correspond to a prior belief in small parameter values (and therefore smooth output functions) in a Bayesian framework.

RBF networks have the advantage of not suffering from local minima in the same way as Multi-Layer Perceptrons. This is because the only parameters that are adjusted in the learning process are the linear mapping from hidden layer to output layer. Linearity ensures that the error surface is quadratic and therefore has a single easily found minimum. In regression problems this can be found in one matrix operation. In classification problems the fixed nonlinearity introduced by the sigmoid output function is most efficiently dealt with using iteratively reweighted least squares.

RBF networks have the disadvantage of requiring good coverage of the input space by radial basis functions. RBF centers are determined with reference to the distribution of the input data, but without reference to the prediction task. As a result, representational resources may be wasted on areas of the input space that are irrelevant to the learning task. A common solution is to associate each data point with its own center, although this can make the linear system to be solved in the final layer rather large, and requires shrinkage techniques to avoid overfitting.

Associating each input datum with an RBF leads naturally to kernel methods such as Support Vector Machines and Gaussian Processes (the RBF is the kernel function). All three approaches use a nonlinear kernel function to project the input data into a space where the learning problem can be solved using a linear model. Like Gaussian Processes, and unlike SVMs, RBF networks are typically trained in a Maximum Likelihood framework by maximizing the probability (minimizing the error) of the data under the model. SVMs take a different approach to avoiding overfitting by maximizing instead a margin. RBF networks are outperformed in most classification applications by SVMs. In regression applications they can be competitive when the dimensionality of the input space is relatively small.

22.5.3 Kohonen Self-organizing Network

The self-organizing map (SOM) invented by Teuvo Kohonen performs a form of unsupervised learning. A set of artificial neurons learn to map points in an input space to coordinates in an output space. The input space can have different dimensions and topology from the output space and the SOM will attempt to preserve these.

22.5.4   Recurrent Network (RN)

Contrary to feedforward networks (Section 3.2.1), recurrent neural networks (RNs) are models with bidirectional data flow. While a feedforward network propagates data linearly from input to output, RNs also propagate data from later processing stages to earlier stages.

22.5.4.1   Simple Recurrent Network

A simple recurrent network (SRN) is a variation on the Multi-Layer Perceptron, sometimes called an "Elman network" due to its invention by Jeff Elman. A three-layer network is used, with the addition of a set of "context units" in the input layer. There are connections from the middle (hidden) layer to these context units fixed with a weight of one. At each time step, the input is propagated in a standard feed-forward fashion, and then a learning rule (usually back-propagation) is applied. The fixed back connections result in the context units always maintaining a copy of the previous values of the hidden units (since they propagate over the connections before the learning rule is applied). Thus the network can maintain a sort of state, allowing it to perform such tasks as sequence-prediction that is beyond the power of a standard Multi-Layer Perceptron.

22.5.4.2   Hopfield Network

The Hopfield network is a recurrent neural network in which all connections are symmetric. Invented by John Hopfield in 1982, this network guarantees that its dynamics will converge. If the connections are trained using Hebbian learning then the Hopfield network can perform as robust content-addressable (or associative) memory, resistant to connection alteration.

22.5.4.3   Echo State Network

The echo state network (ESN) is a recurrent neural network with a sparsely connected random hidden layer. The weights of output neurons are the only part of the network that can change and be learned. ESN are good to (re) produce temporal patterns.

22.5.4.4   Long Short-Term Memory Network

The Long short-term memory is an artificial neural net structure that unlike traditional RNNs doesn't have the problem of vanishing gradients. It can therefore use long delays and can handle signals that have a mix of low and high frequency components.

22.5.5   Stochastic Neural Networks

A stochastic neural network differs from a typical neural network because it introduces random variations into the network. In a probabilistic view of neural networks, such random variations can be viewed as a form of statistical sampling, such as Monte Carlo sampling.

22.5.5.1   Boltzmann Machine

The Boltzmann machine can be thought of as a noisy Hopfield network. Invented by Hinton and Sejnowski (1986), the Boltzmann machine is important because it is one of the first neural networks to demonstrate learning of latent variables (hidden units). Boltzmann machine learning was at first slow to simulate, but the contrastive divergence algorithm of Geoff Hinton (ca. 2000) allows models such as Boltzmann machines and products of experts to be trained much faster.

22.5.6   Modular Neural Networks

Biological studies have shown that the human brain functions not as a single massive network, but as a collection of small networks. This realization gave birth to the concept of modular neural networks, in which several small networks cooperate or compete to solve problems.

22.5.6.1   Committee of Machines

A committee of machines (CoM) is a collection of different neural networks that together "vote" on a given example. This generally gives a much better result compared to other neural network models. Because neural networks suffer from local minima, starting with the same architecture and training but using different initial random weights often gives vastly different networks. A CoM tends to stabilize the result.

22.5.6.2   Associative Neural Network (ASNN)

The ASNN is an extension of the committee of machines that goes beyond a simple/weighted average of different models. ASNN represents a combination of an ensemble of feedforward neural networks and the k-nearest neighbor technique (kNN). It uses the correlation between ensemble responses as a measure of distance amid the analyzed cases for the kNN. This corrects the bias of the neural network ensemble. An associative neural network has a memory that can coincide with the

training set. If new data become available, the network instantly improves its predictive ability and provides data approximation (self-learn the data) without a need to retrain the ensemble. Another important feature of ASNN is the possibility to interpret neural network results by analysis of correlations between data cases in the space of models.

Besides the above classes of neural network, following are some new network structure which has shown recommendable improvement from the older neural networks.

22.6 Activation Functions

Each node of a neural network transforms the input signals of the node into output node with the help of activation or base or net function. The activation function acts as a squashing function, such that the output of a neuron in a neural network is between certain values (usually 0 and 1, or –1 and 1). In general, there are six types of activation functions which are described in the following section.

22.6.1 Threshold Function (Step or Ramp)

The Threshold Function takes on a value of 0 if the summed input is less than a certain threshold value (v), and becomes equal to 1 if the summed input is greater than or equal to the threshold value.

22.6.2 Piecewise-Linear Function

The Piecewise-Linear function is a transfer function which can take the values of 0 or 1 or between that, depending on the amplification factor in a certain region of a linear operation.

22.6.3 Sigmoid Function

Many natural processes and complex system learning curves display a history-dependent progression from small beginnings that accelerates and approaches a climax over time. For lack of complex descriptions, a sigmoid function is often used. A sigmoid curve is produced by a mathematical function having an "S" shape. Often, sigmoid function refers to the special case of the logistic function defined by the formula:

$$P(t) = \frac{1}{1 + e^{-t}} \tag{22.3}$$

22.6.4   Linear Basis Function

Linear-Basis function (LBF) is a hyperplane-type function. This is a first-order basis function. The net value is a linear combination of the inputs.

22.6.5   Radial Basis Function

A radial basis function (RBF) is a real-value function whose value depends only on the distance from the origin, so that,

$$\varphi(\mathbf{x}) = \varphi(\|\mathbf{x}\|) \tag{22.4}$$

or alternatively on the distance from some other point c, called a center, so that

$$\varphi(\mathbf{x}, \mathbf{c}) = \varphi(\|\mathbf{x} - \mathbf{c}\|) \tag{22.5}$$

22.6.6   Gaussian Function

In probability theory and statistics, the normal distribution or Gaussian distribution is a continuous probability distribution that describes data that clusters around a mean or average. The basic equation of Gaussian function is defined as,

$$f(x) = ae^{-\frac{(x-b)^2}{2c^2}} \tag{22.6}$$

for some real constants $a > 0$, b, $c > 0$, and $e \approx 2.718281828$

The graph of a Gaussian is a characteristic symmetric "bell curve" shape that quickly falls off towards plus/minus infinity. The parameter a is the height of the curve's peak, b is the position of the center of the peak, and c controls the width of the "bell" (Fig. 22.3).

22.7   Learning Rules

As described in Section 22.3.2 a neural network has to be configured such that the application of a set of inputs produces (either "direct" or via a relaxation process) the desired set of outputs. Various methods to set the strengths of the connections exist. One way is to set the weights explicitly, using a priori knowledge. Another way is to "train" the neural network by feeding it teaching patterns and letting it change its weights according to some learning rule.

We can categorize the learning situations in three distinct sorts. These are:
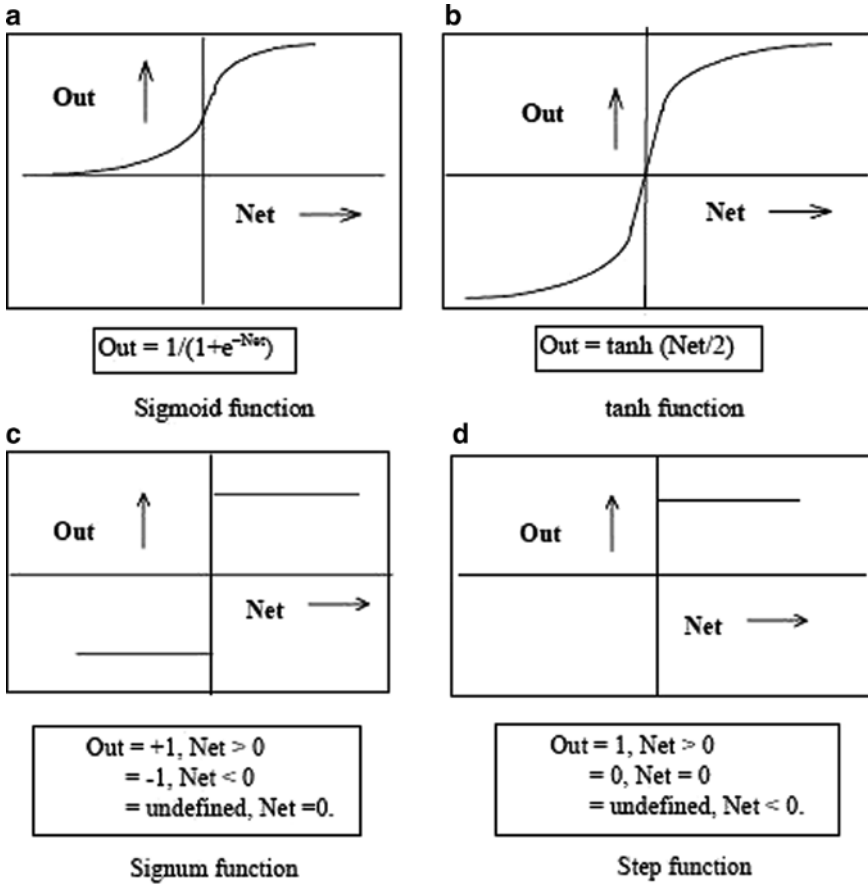
Fig. 22.3 Figure showing common non-linear functions used for synaptic inhibition

22.7.1 Supervised Learning

Supervised learning (Fig. 22.4) or Associative learning in which the network is trained by providing it with input and matching output patterns. These input–output pairs can be provided by an external teacher, or by the system which contains the neural network (self-supervised).

22.7.2 Unsupervised Learning

Unsupervised learning or Self-organization in which an (output) unit is trained to respond to clusters of pattern within the input. In this paradigm the system is supposed to discover statistically salient features of the input population. Unlike the supervised
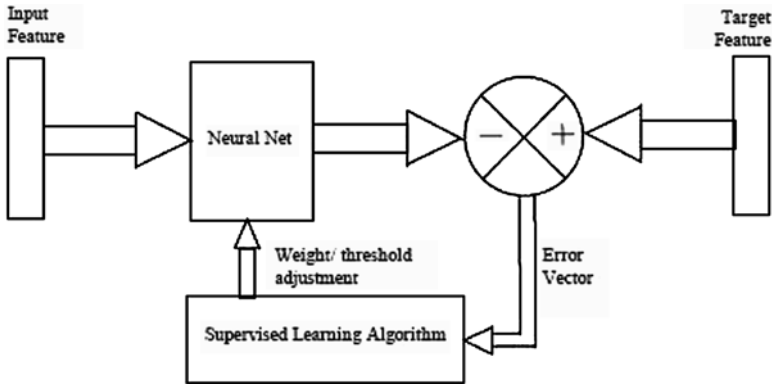
Fig. 22.4 Figure showing a schematic diagram of supervised learning algorithm

learning paradigm, there is no a priori set of categories into which the patterns are to be classified; rather the system must develop its own representation of the input stimuli.

22.7.3   Reinforcement Learning

Reinforcement Learning may be considered as an intermediate form of the above two types of learning. Here the learning machine does some action on the environment and gets a feedback from the environment. The learning system grades its action good (rewarding) or bad (punishable) based on the environmental response and accordingly adjusts its parameters. Generally, parameter adjustment is continued until an equilibrium state occurs, following which there will be no more changes in its parameters. The self-organizing neural learning may be categorized under this type of learning.

22.8   Training Algorithms

Training a neural network model essentially means selecting one model from the set of allowed models (or, in a Bayesian framework, determining a distribution over the set of allowed models) that minimizes the cost criterion. There are numerous algorithms available for training neural network models; most of them can be viewed as a straightforward application of optimization theory and statistical estimation.

22.8.1   Single or Multilayer Perceptron Learning Algorithm

The network adapts with change in weight by an amount proportional to the difference between the desired output and the actual output.

As an equation:

$$\Delta Wi = \eta * (D - Y).Ii \qquad (22.7)$$

where η is the learning rate, D is the desired output, and Y is the actual output.

Minsky and Papert (1969) showed that the above procedure converges correctly if the training examples are linearly separable. However, if η is too big, the system may end up in oscillation. In practice, η is set to 0.1 and is reduced as a function of the loop counter variable. Both can learn arbitrary mappings or classifications.

22.8.2 Back Propagation Learning Algorithm

Back propagation (BP) (Scott 1988) is a learning algorithm which follows the supervised learning rules and is an implementation of the Delta rule. It requires a teacher that knows, or can calculate, the desired output for any given input.

BP is a better training algorithm for multilayer neural networks than algorithms which follows Delta or Hebian rule. BP defines rules of propagating the network error back from network output to network input units and adjusting network weights along with this back propagation. The iterations require lower memory resources than most learning algorithms and usually get acceptable results, although it can be too slow to reach the error minimum and sometimes does not find the best solution.

The assumptions for BPA is a follows:

1. All outputs will be computed using sigmoid function of the inner product of the corresponding weight and input vectors.
2. All outputs at stage n are connected to all the inputs at stage n + 1.
3. The errors are propagated backwards by apportioning them to each unit according to the amount of this error the unit is responsible for.

Let,
$\vec{x}_j$ = input vector for unit j (x_{ji} = ith input to the jth unit)
$\vec{w}_j$ = weight vector for unit j (w_{ji} = weight on x_{ji})
$z_j = \vec{w}_j \cdot \vec{x}_j$, the weighted sum of inputs for unit j,
o_j = output of unit j where,
$o_j = \sigma(z_j)$
t_j = target for unit j
Downstream (j) = set of units whose immediate inputs include the output of j
Outputs = set of output units in the final layer

Since the weights are updated after each training example, the training set can be simplified somewhat by imagining that the training set consists of exactly one example and so the error can simply be denoted by E.

The objective of the algorithm will be to calculate $\dfrac{\partial E}{\partial w_{ji}}$ for each input weight

w_{ji} for each output unit j since z_j is a function of w_{ji} regardless of where in the network unit j is located,

$$\frac{\partial E}{\partial w_{ji}} = \frac{\partial E}{\partial z_j} \cdot \frac{\partial z_j}{\partial w_{ji}}$$

$$\cdot = \frac{\partial E}{\partial z_j} x_{ji} \tag{22.8}$$

Furthermore, $\dfrac{\partial E}{\partial z_j}$ is the same regardless of input weight of unit j that was being improved or updated. So this quantity is denoted by δ_j.

In case of, $j \in Outputs$. It is known, that,

$$E = \frac{1}{2} \sum_{k \in Outputs} (t_k - \sigma(z_k))^2 \tag{22.9}$$

Since the outputs of all the units $k \neq j$ are independent of w_{ji}, the effect of summation was dropped and contribution to E was only considered by j.

$$\delta_j = \frac{\partial E}{\partial z_j} = \frac{\partial}{\partial z_j} \frac{1}{2}(t_j - o_j)^2$$

$$= -(t_j - o_j)\frac{\partial o_j}{\partial z_j}$$

$$= -(t_j - o_j)\frac{\partial}{\partial z_j}\sigma(z_j)$$

$$= (t_j - o_j)(1 - \sigma(z_j))\sigma(z_j)$$

$$= (t_j - o_j)(1 - o_j)o_j$$

Thus

$$\Delta w_{ji} = -\eta \frac{\partial E}{\partial w_i j} = \eta \delta_j x_{ji} \tag{22.10}$$

In the case, when j is a hidden unit. Like before, the following two important observations is made,

1. For each unit k downstream from j, z_k is a function of z_j
2. The contribution to error by all units $l \neq j$ in the same layer as j is independent of w_{ji}

w_{ji} influences just z_j now which influences o_j which again influences

$$z_k \forall k \in Downstream(j)$$

each of which influence E. So,

$$\frac{\partial E}{\partial w_{ji}} = \sum_{k \in Downstream(j)} \frac{\partial E}{\partial z_k} \cdot \frac{\partial z_k}{\partial o_j} \cdot \frac{\partial o_j}{\partial z_j} \cdot \frac{\partial z_j}{\partial w_{ji}} \qquad (22.11)$$

$$= \sum_{k \in Downstream(j)} \frac{\partial E}{\partial z_k} \cdot \frac{\partial z_k}{\partial o_j} \cdot \frac{\partial o_j}{\partial z_j} \cdot x_{ji}$$

Again note that all the terms except x_{ji} in the above product are the same regardless of which input weight of unit j we are updated. Like before, this is denoted by common quantity δj. Also,

$$\frac{\partial E}{\partial z_k} = \delta_k \quad \frac{\partial z_k}{\partial o_j} = w_{kj},$$

and

$$\frac{\partial o_j}{\partial z_j} = o_j(1 - o_j).$$

Substituting,

$$\delta_j = \sum_{k \in Downstream(j)} \frac{\partial E}{\partial z_k} \cdot \frac{\partial z_k}{\partial o_j} \cdot \frac{\partial o_j}{\partial z_j}$$

$$= \sum_{k \in Downstream(j)} \delta_k w_{kj} o_j(1 - o_j)$$

Thus,

$$\delta_k = o_j(1 - o_j) \sum_{k \in Downstream(j)} \delta_k w_{kj} \qquad (22.12)$$

Application of the algorithm is useful for feedforward networks. Quick Propagation (QP), Incremental Batch Back Propagation (IBB), and Batch Back Propagation (BBP) are some of the training algorithms that were developed based on Back Propagation algorithm.

BBP is an advanced variant of Back Propagation where network weights update takes place once per iteration whereas Quick Propagation is a heuristic modification of the back propagation algorithm invented by Fahlam (1988). Where weights are treated as quasi-independent and attempts to use a simple quadratic model to approximate the error surface. In spite the fact that the algorithm hasn't theoretical foundation, it is proved to be much faster than standard back-propagation for many problems. Although sometimes the quick propagation algorithm may be instable and inclined to be stuck in a local minima, the accuracy of QP depends on QP coefficient which is an additional training parameter controls the magnitude of increment size of the weights.

IBB is a variation of the BP where the network weights are updated after presenting each case from the training subset, rather than once per iteration. IBBP is

originally an invented variant of back propagation which is sometimes referred to as Standard Back Propagation. The algorithm is most suitable for problems which have large datasets.

22.8.3   Gradient Descent Learning Algorithm

Most of the algorithms used in training artificial neural networks are employing some form of gradient descent. This is done by simply taking the derivative of the cost function with respect to the network parameters and then changing those parameters in a gradient-related direction. Gradient descent is a first-order optimization algorithm. To find a local minimum of a function using gradient descent, one takes steps proportional to the negative of the gradient (or the approximate gradient) of the function at the current point. If instead one takes steps proportional to the gradient, one approaches a local maximum of that function; the procedure is then known as gradient ascent. Gradient descent is also known as the steepest descent, or the method of steepest descent. When known as the latter, gradient descent should not be confused with the method of steepest descent for approximating integrals.

The first unthresholded perceptron is considered where the output o is given by

$$o(\vec{x}) = \vec{w} \cdot \vec{x} \tag{22.13}$$

The training error E is expressed as a function of $\vec{w}$ as follows,

$$E(\vec{w}) = \frac{1}{2 \cdot} \sum_{d \in D} (t_d - o_d)^2 \tag{22.14}$$

where t_d and o_d are the target and output values for training example x_d.

The gradient of this surface, $\nabla E \rightarrow \perp$, then specifies a vector in whose direction the greatest increase in E can be obtained.

Again, the greatest decrease can be observed if the direction is changed to opposite. The following update rule is therefore used to train the net using gradient descent.

$$\vec{w} \leftarrow \vec{w} - \eta \nabla E(\vec{w}) \tag{22.15}$$

where again, η is a positive constant called the learning rate. If η is sufficiently small, the system will not overstep a minimum and can be guaranteed to settle into one (albeit a local one).

The above can also be written as,

$$w_i \leftarrow w_i + \Delta w_i \tag{22.16}$$

where,

$$\Delta w_i = -\eta \frac{\partial E}{\partial w_i}$$

$\dfrac{\partial E}{\partial w_i}$ is easy to calculate. Since,

$$E = \frac{1}{2}\sum_{d \in D}\left(t_d - \vec{w}\cdot\vec{x}\right)^2 \quad \frac{\partial E}{\partial w_i} = \sum_{d \in D}\left(t_d - \vec{w}\cdot\vec{x}\right)\left(-x_{id}\right)$$

$$\text{So,}\,\Delta w_i = \eta\sum_{d \in D}\left(t_d - o_d\right)x_{id}$$

(22.17)

Conjugate Gradient Descent (CGD) is an example of a training algorithm based on the GDR. CGD is an advanced method for training multilayer neural networks. It is based on the linear search usage in the line of an optimal network weights' change. The correction of weights is conducted once per iteration. In most cases, this method works faster than Back Propagation and provides more precise forecasting results.

22.9 Genetic Algorithm

First pioneered by John Holland in the 1960s, Genetic Algorithms (GA) has been widely studied, experimented and applied in many fields in engineering worlds. Not only does GAs provide alternative methods to solving problem, it consistently outperforms other traditional methods in most of the problems link.

22.9.1 Concept of GA

A genetic algorithm (GA) is a search technique used in computing to find exact or approximate solutions to optimization and search problems. Genetic algorithms are categorized as global search heuristics which are a particular class of evolutionary algorithms (EA) that use techniques inspired by evolutionary biology such as inheritance, mutation, selection, and crossover (also called recombination).

Genetic algorithms are implemented in a computer simulation in which a population of abstract representations (called chromosomes or the genotype of the genome) of candidate solutions (called individuals, creatures, or phenotypes) to an optimization problem evolves toward better solutions. Traditionally, solutions are represented in binary as strings of 0s and 1s, but other encodings are also possible.

The evolution usually starts from a population of randomly generated individuals and happens in generations. In each generation, the fitness of every individual in the population is evaluated, multiple individuals are stochastically selected from the current population (based on their fitness), and modified (recombined and possibly randomly mutated) to form a new population. The new population is then used in the next iteration of the algorithm. Commonly, the algorithm terminates when

either a maximum number of generations has been produced, or a satisfactory fitness level has been reached for the population. If the algorithm has terminated due to a maximum number of generations, a satisfactory solution may or may not have been reached.

22.9.2   Procedures to Solve Problems with GA

A typical genetic algorithm requires:

1. A genetic representation of the solution domain.
2. A fitness function to evaluate the solution domain.

A standard representation of the solution is as an array of bits. Arrays of other types and structures can be used in essentially the same way. The main property that makes these genetic representations convenient is that their parts are easily aligned due to their fixed size, which facilitates simple crossover operations. Variable length representations may also be used, but crossover implementation is more complex in this case. Tree-like representations are explored in genetic programming and graph-form representations are explored in evolutionary programming.

The fitness function is defined over the genetic representation and measures the quality of the represented solution. The fitness function is always problem dependent. Once the genetic representation and the fitness function were defined, GA proceeds to initialize a population of solutions randomly, then improve it through repetitive application of mutation, crossover, inversion, and selection operators.

22.9.3   Outline of the Basic Genetic Algorithm

1. [Start] Generate random population of n chromosomes (suitable solutions for the problem).
2. [Fitness] Evaluate the fitness f(x) of each chromosome x in the population.
3. [New population] Create a new population by repeating following steps until the new population is complete.
    3.1. [Selection] Select two parent chromosomes from a population according to their fitness (the better fitness, the bigger chance to be selected).
    3.2. [Crossover] With a crossover probability cross over the parents to form a new offspring (children). If no crossover was performed, offspring is an exact copy of parents.
    3.3. [Mutation] With a mutation probability mutate new offspring at each locus (position in chromosome).
    3.4.   [Accepting] Place new offspring in a new population.
4. [Replace] Use new generated population for a further run of algorithm.

5. [Test] If the end condition is satisfied, stop, and return the best solution in current population.
6. [Loop] Go to step 2.

22.9.4   Limitations of GA

As a general rule of thumb genetic algorithms might be useful in problem domains that have a complex fitness landscape as recombination is designed to move the population away from local optima that a traditional hill climbing algorithm might get stuck in.

22.10   Application of ANN and GA in Hydrology

22.10.1   Application of ANN in Hydrologic Problems

The research in artificial intelligence has increased dramatically during the 1990s. The Artificial Neural Network (ANN) was originally developed to mimic basic biological neural systems – the human brain. In general, ANN is composed of a number of interconnected simple processing elements called neurons or nodes with attractive attribute of information processing characteristics such as nonlinearity, parallelism, noise tolerance, and learning and generalization capability. Contrary to the traditional model-based methods, ANNs are data-driven, self-adaptive methods in which there are few a priori assumptions about the models for problems in the study. Examples may include Eslami and Mohammadi (2002); Jain and Prasad Indurthy (2003); Kisi (2004); Lapedes and Farber (1987); Majumder et al. (2007); Wang et al. (2006); Wei and Hsu (2007); Xu and Li (2001); and Yitian and Gu (2003).

Neural networks learn from examples and capture subtle functional relationships among the data even if the underlying relationships are unknown or difficult to be described. Thus, ANNs are well suited for problems whose solutions require knowledge that is difficult to specify, but for which there are enough data or observations. In this sense, they can be treated as multivariate nonlinear nonparametric statistical methods. Absence of adequate data and ignorance of the embedded concept can induce large errors in estimations. Such models are not recommended for prediction of something that is not included in the available dataset.

22.10.2   Application of GA in Hydrologic Problems

GA is widely applied in different problem-solving techniques. Hydrological science, in recent years, has also adopted GA for solving various types of dependency and optimization problems. Parasuraman and Elshorbagy (2007) had selected

GA-trained cluster-based neural network models as a better performer than traditional cluster-based neural network models. Sanderson (2009) tried to establish the capability of GA in determination of variable dependency from largescale dataset. The study output approves the use of GA for such problems. Confesor and Whittaker (2007) applied Multi Objective Evolutionary Algorithm and a set of Pareto optimal data or objective oriented prioritized dataset for automatic calibration of Soil and Water Assessment Tool (SWAT) model. The auto-calibrated SWAT was found to be better optimized than manually calibrated SWAT. GA algorithms were also used in optimization of multi-reservoirs (Kim and Heo 2006; Tospornsampan et al. 2005; Reddy and Kumar 2006), hydropower reservoirs (Cheng et al. 2007), leakage control of water distribution systems (Araujo et al. 2006), hydraulic characteristic determination of production wells (Jha et al. 2004), multiobjective water system design (Jourdan et al. 2005), operation of artificial groundwater recharge (Eusuff and Lansey 2004), reservoir dispatching (Jian-Xia et al. 2005), and auto-calibration of different models like HSPF (Castanedo et al. 2006), Nash (Dong 2008), etc.

References

Ahmed JA, Sarma AK (2005) Genetic algorithm for optimal operating policy of a multipurpose reservoir. J Water Resour Manage 19:145–161

Araujo L, Ramos H, Coelho S (2006) Pressure control for leakage minimisation in water distribution systems management. Water Resour Manage 20(1):133–149

ASCE Task Committee on Application of Artificial Neural Networks in Hydrology (2000) Artificial neural networks in hydrology I: preliminary concepts. J Hydrol Eng 5(2):115–123

Burn DH, Yulianti JS (2001) Waste-load allocation using genetic algorithms. J Water Resour Plan Manage ASCE 127(2):121–129

Castanedo F, Patricio M, Molina J (2006) Evolutionary computation technique applied to HSPF model calibration of a Spanish watershed. pp 216–223

Cheng C-T, Wang W-C, Xu D-M, Chau K (2007) Optimizing hydropower reservoir operation using hybrid genetic algorithm and chaos. Water Resour Manage. URL http://dx.doi.org/10.1007/s11269-007-9200-1

Clair TA, Ehrman JM (1998) Using neural networks to assess the influence of changing seasonal climates in modifying discharge, dissolved organic carbon, and nitrogen export in eastern Canadian rivers. Water Resour Res 34(3):447–455

Confesor RB, Whittaker GW (2007) Automatic calibration of hydrologic models with multi-objective evolutionary algorithm and Pareto optimization. J Am Water Resour Assoc 43(4):981–989

Coulibaly P, Anctil F, Bobee B (2000) Daily reservoir inflow forecasting using artificial neural networks with stopped training approach. J Hydrol 230(3–4):244–257

Dong S-H (2008) Genetic algorithm based parameter estimation of Nash model. Water Resour Manage 22(4):525–533

Elshorbagy A, Simonovic SP, Panu US (2000) Performance evaluation of artificial neural networks for runoff prediction. J Hydrol Eng 5(4):424–427

Eslami HR, Mohammadi K (2002) Application of ANN for reservoir inflow forecasting using snowmelt equivalent in the Karaj river watershed. Lowland Technol Int 4(2):17–26

Eusuff MM, Lansey KE (2004) Optimal operation of artificial groundwater recharge systems considering water quality transformations. Water Resour Manage 18(4):379–405

Fahlam SE (1988) An empirical study of learning speed in back-propagation networks. Technical Report cwU-CS-88-w, June

Fernando DA, Jayawardena AW (1998) Runoff forecasting using RBF networks with OLS algorithm. J Hydrol Eng 3(3):203–209

Hinton GE, Sejnowski TJ (1986) Learning and relearning in Boltzmann machines. In Rumelhart, D. E. and McClelland, J. L., editors, Parallel Distributed Processing: Explorations in the Microstructure of Cognition. Volume 1: Foundations, MIT Press, Cambridge, MA

Hsu K, Gupta HV, Sorooshian S (1995) Artificial neural network modeling of the rainfall-runoff process. Water Resour Res 31(10):2517–2253

Imrie CE, Durucan S, Korre A (2000) River flow prediction using neural networks: generalization beyond the calibration range. J Hydrol 233(3–4):138–154

Jain A, Prasad Indurthy SKV (2003) Comparative analysis of event-based rainfall-runoff modeling techniques – deterministic, statistical, and artificial neural networks. J Hydrol Eng 8:93–98

Jain SK, Das A, Srivastava DK (1999) Application of ANN for reservoir inflow prediction and operation. J Water Resour Plan Manage 125(5):263–271

Jha MK, Nanda G, Samuel MP (2004) Determining hydraulic characteristics of production wells using genetic algorithm. Water Resour Manage 18(4):353–377

Jian-Xia C, Qiang H, Yi-Min W (2005) Genetic algorithms for optimal reservoir dispatching. Water Resour Manage 19(4):321–331

Jourdan L, Corne D, Savic D, Walters G (2005) Preliminary investigation of the 'learnable evolution model' for faster/better multiobjective water systems design, Springer Verlag, Berlin pp 841–855

Kisi O (2004) Multilayer perceptrons with Levenberg–Marquardt training algorithm for suspended sediment concentration prediction and estimation. Hydrol Sci J 49(6):1025–1040

Kim T, Heo JH (2006) Application of multi-objective genetic algorithms to multireservoir system optimization in the Han River basin. KSCE J Civil Eng 10(5):371–380

Lapedes A, Farber R (1987) Nonlinear signal processing using neural networks: prediction, and system modelling, LA-VR-87-2662, Los Alamos

Liong SY, Khu ST, Chan WT (2001) Derivation of Pareto front with genetic algorithm and neural network. J Hydrol Eng 6(1):52–61

Majumder M, Roy P, Mazumdar A (2007) Optimization of the water use in the river Damodar in West Bengal in India: an integrated multi-reservoir system with the help of artificial neural network. J Eng Comput Architect 1(2):1192

Maier HR, Dandy GC (1999) Empirical comparison of various methods for training feed-forward neural networks for salinity forecasting. Water Resour Res 35(8):2591–2596

Minsky M, Papert S (1969) Perceptrons. MIT Press, Cambridge.

Neelakantan TR, Pundarikanthan NV (2000) Neural network based simulation-optimization model for reservoir operation. J Water Resour Plan Manage 126(2):57–64

Parasuraman K, Elshorbagy A (2007) Cluster-based hydrologic prediction using genetic algorithm-trained neural networks. J Hydrol Eng 12(ASCE):52–62

Ray C, Klindworth KK (2000) Neural networks for agrichemical vulnerability assessment of rural private wells. J Hydrol Eng 5(2):162–171

Reddy M, Kumar D (2006) Optimal reservoir operation using multi-objective evolutionary algorithm. Water Resour Manage 20(6):861–878

Sanderson L (2009) Using genetic algorithms to explore the effects of changes in hydrologic variables and suspended sediment on fish biodiversity, Sandusky river, Ohio. Geol Soc Am Abst Program 41(4):13

Scott F (1988) An empirical study of learning speed in back-propagation networks, CMU technical report, CMU-CS-162, Sep. 1988

Sudheer KP (2005) Knowledge extraction from trained neural network river flow models. J Hydrol Eng 10(4):264–269

Tokar AS, Johnson PA (1999) Rainfall-runoff modeling using artificial neural networks. J Hydrol Eng 4(3):232–239

Tospornsampan J, Kita I, Ishii M, Kitamura Y (2005) Optimization of a multiple reservoir system operation using a combination of genetic algorithm and discrete differential dynamic programming: a case study in Mae Klong system, Thailand. Paddy Water Environ 3(1):29–38

Wang QJ (1991) The genetic algorithm and its application to calibrating conceptual rainfall-runoff models. Water Resour Res 27(9):2467–2471

Wardlaw R, Sharif M (1999) Evaluation of genetic algorithms for optimal reservoir system operation. J Water Resour Plan Manage 125(1):25–33

Wang AP, Liao HY, Kou CH, Huang CY (2006) Artificial neural networks on reservoir inflows forecasting during typhoon season – a case in Taiwan. WSEAS Trans Math 5(4):416–422

Wei CC, Hsu NS (2007) Development of a real-time optimization model for flood control of a multipurpose reservoir. J Chinese Inst Civil Hydraulic Eng 19(3):355–365

Xu ZX, Li JY (2001) Short-term inflow forecasting using an artificial neural network model. Wiley, New York

Yitian L, Gu RR (2003) Modeling flow and sediment transport in a river system using an artificial neural network. J Environ Manage 31(1):122–134

Zhang Q, Stanley SJ (1999) Real-time treatment process control with artificial neural networks. J Environ Eng 125(2):153–160

Chapter 23
Introduction to Climate Change and Climate Models

Mrinmoy Majumder

Abstract Climate change is defined as the change in the weather pattern of a region. The models which are employed to predict climate change of the future are collectively called as climate models. The present note describes the formation, structures, and working principles of global as well as regional climate models. The note also describes the climate change scenarios that are presently created.

Keywords Climate • climate models • global warming • IPCC

23.1 Climate Change and Climate Models

Global warming is defined as a natural- or human-induced increase in the average global temperature of the atmosphere near the earth's surface. The earth as a planet is a complex combination of many elements which constitute the solid earth, atmosphere, biosphere, cryo-sphere, and the hydrosphere. These components interact with each other in a non-linear manner involving the feedbacks of energy, mass, and momentum. The energy is derived from the sun in the form of shortwave solar radiation which penetrates the earth's surface with little loss of energy in transit. In the process, the heated earth emits thermal or long wave radiation outward which mostly gets absorbed by the atmospheric constituent. Water vapor and several other gases including carbon dioxide, methane, and CFCs warm the earth's atmosphere because they absorb and remit radiations. They trap some of the heat energy radiations from the earth's atmospheric system. The trapping or warming is somewhat analogous to a greenhouse, which also traps heat; thus the process has

M. Majumder (✉)
Senior Research Fellow, School of Water Resources Engineering, Jadavpur University, Kolkata-700032, West Bengal, India
and
Geo-information Scientist, Regional Center, National Afforestation
and Eco-development Board, Jadavpur University, Kolkata-700032, West Bengal, India
e-mail: mrinmoy@majumder.info

been called the greenhouse effect. The excessive increase in the concentration of green house gases makes the atmosphere warmer which in turn induces the climate to change.

23.2   Impact of Global Warming

The effect of global warming is now predominant in many parts of the world. Twelve warmest years have occurred in 1900s among which ten have occurred between 1987 and 1998. The energy availability which was increased due to increase in temperature had created a ripple effect throughout the Earth system with local, regional, and global positive feedbacks feeding on each other to amplify and accelerate warming (Stewart and Vemuri 2006). Abnormality in climatic pattern, induced by the accelerated warming, had started to effect catchment specific hydrologic cycles. In the last 10 years, floods have caused more damage than in the previous 30 years. Higher temperatures lead to a high rate of evaporation and very dry conditions in some areas of the world. Severe weather events are now more common. The number and strength of hurricanes, tornadoes, and other events had increased over the last 15–20 years. As per IPCC (2007), global climate change is expected to affect the performance of water resource systems according to current indicators and findings.

23.3   Special Report on Emissions Scenarios

The Special Report on Emissions Scenarios (SRES) was a report prepared by the Intergovernmental Panel on Climate Change (IPCC) for the Third Assessment Report (TAR) in 2001, on future emission scenarios to be used for driving global circulation models to develop climate change scenarios. It was used to replace the IS92 scenarios used for the IPCC Second Assessment Report of 1995. The SRES Scenarios were also used for the Fourth Assessment Report (AR4) in 2007.

23.3.1   Purpose

Because projections of climate change depend heavily upon future human activity, climate models are run against scenarios. There are 40 different scenarios, each making different assumptions for future greenhouse gas pollution, land-use, and other driving forces. Assumptions about future technological development as well as the future economic development are thus made for each scenario. Most include an increase in the consumption of fossil fuels; some versions of B1 have lower levels of consumption by 2100 than in 1990. Overall, the world GDP will increase with a factor between 5 and 25 in the emission scenario. It is questionable whether this form of assumptions will hold as several limits to growth appears to be upon the world. Peak Oil is for instance not discussed in the emission scenarios.

These emission scenarios are organized into families, which contain scenarios that are similar to each other in some respects. IPCC assessment report projections for the future are often made in the context of a specific scenario family.

23.3.2 Scenario Families

Scenario families contain individual scenarios with common themes. The six families of scenarios discussed in the IPCC's Third Assessment Report (TAR) and Fourth Assessment Report (AR4) are A1FI, A1B, A1T, A2, B1, and B2.

Scenario descriptions are based on those in AR4, which are identical to those in TAR.

23.3.2.1 A1 Scenario

The A1 scenarios are of a more integrated world. The A1 family of scenarios is characterized by

- Rapid economic growth
- A global population that reaches 9 billion in 2050 and then gradually declines
- The quick spread of new and efficient technologies
- A convergent world-income and way of life converge between regions
- Extensive social and cultural interactions worldwide

  There are subsets to the A1 family based on their technological emphasis:
  A1FI – an emphasis on fossil fuels
  A1B – a balanced emphasis on all energy sources
  A1T – emphasis on non-fossil energy sources

23.3.2.2 A2 Scenario

The A2 scenarios are of a more divided world. The A2 family of scenarios is characterized by
- A world of independently operating, self-reliant nations
- Continuously increasing population
- Regionally oriented economic development
- Slower and more fragmented technological changes and improvements to per capita income

23.3.2.3 B1 Scenario

The B1 scenarios are of a world more integrated, and more ecologically friendly. The B1 scenarios are characterized by
- Rapid economic growth as in A1, but with rapid changes towards a service and information economy

- Population rising to 9 billion in 2050 and then declining as in A1
- Reductions in material intensity and the introduction of clean and resource efficient technologies
- An emphasis on global solutions to economic, social, and environmental stability

21.3.2.4   B2 Scenario

The B2 scenarios are of a world more divided, but more ecological friendly. The B2 scenarios are characterized by
- Continuously increasing population, but at a slower rate than in A2
- Emphasis on local rather than global solutions to economic, social and environmental stability
- Intermediate levels of economic development
- Less rapid and more fragmented technological change than in A1 and B1

23.3.3   SRES Scenarios and Climate Change Initiatives

While some scenarios assume a more environment friendly world than others, none include any climate-specific initiatives, such as the Kyoto Protocol.

Total cumulative SRES carbon emissions from all sources through 2100 range from approximately 770 GtC to 2,540 GtC. According to the IPCC Second Assessment Report (SAR), "any eventual stabilized concentration is governed more by the accumulated anthropogenic CO_2 emissions from now until the time of stabilization than by the way emissions change over the period."

Total anthropogenic methane (CH_4) and nitrous oxide (N_2O) emissions span a wide range by the end of the twenty-first century. Emissions of these gases in a number of scenarios begin to decline by 2050. The range of emissions is wider than in the IS92 scenarios due to the multimodel approach, which leads to a better treatment of uncertainties and to a wide range of driving forces. These totals include emissions from land use, energy systems, industry, and waste management.

Methane and nitrous oxide emissions from land use are limited in A1 and B1 families by slower population growth followed by a decline, and increased agricultural productivity. After the initial increases, emissions related to land use peak and decline. In the B2 family, emissions continue to grow, albeit very slowly. In the A2 family, both high population growth and less rapid increases in agricultural productivity result in a continuous rapid growth in those emissions related to land use.

The range of emissions of Hydro Fluro Carbons (HFC) in the SRES scenario is generally lower than in earlier IPCC scenarios. Because of new insights about the availability of alternatives to HFCs as replacements for substances controlled by the Montreal Protocol, initially HFC emissions are generally lower than in previous IPCC scenarios. In the A2 and B2 scenario families HFC emissions increase rapidly in the second half of the this century, while in the A2 and B2 scenario families the growth of emissions is significantly slowed down or reversed in that period.

Sulfur emissions in the SRES scenarios are generally below the IS92 range, because of structural changes in the energy system as well as concerns about local and regional air pollution. These reflect sulfur control legislation in Europe, North America, Japan, and (more recently) other parts of Asia and other developing regions. The timing and impact of these changes and controls vary across scenarios and regions.

23.4   Climate Models

Climate models use quantitative methods to simulate the interactions of the atmosphere, oceans, land surface, and ice. They are used for a variety of purposes from study of the dynamics of the climate system to projections of future climate.

All climate models take account of incoming energy as short wave electromagnetic radiation (which in this context means visible and ultraviolet, not to be confused with shortwave) to the earth as well as outgoing energy as long wave (infrared) electromagnetic radiation from the earth. Any imbalance results in a change in the average temperature of the earth.

The most talked-about models of recent years have been those relating temperature to emissions of carbon dioxide. These models project an upward trend in the surface temperature record, as well as a more rapid increase in temperature at higher altitudes.

Models can range from relatively simple to quite complex.

A simple radiant heat transfer model that treats the earth as a single point and averages outgoing energy this can be expanded vertically (radiative-convective models), or horizontally.

Finally, (coupled) atmosphere–ocean–sea ice global climate models discretize and solve the full equations for mass and energy transfer and radiant exchange.

This is not a full list; for example "box models" can be written to treat flows across and within ocean basins. Furthermore, other types of modeling can be inter-linked, such as land use, allowing researchers to predict the interaction between climate and ecosystems.

Climatic models are broadly divided into Global Climate Models and Regional Climate Models. The uncertainty in the climatic pattern had made the estimation of future climate more complex.

23.4.1   Global Climate Models

The Global Climate Models (GCM) were widely used to estimate future climatic parameters but the complexity of the present climatic pattern had forced many modifications.

HadCM2 AOGCM model was developed by Met Office Hadley in 1994 and its successor, HadCM3 AOGCM (Atmosphere-Ocean General Circulation Models), was published in 1998. AOGCM coupled with an atmospheric chemistry model which can predict the changes in concentration of other atmospheric constituents in response to climate change and to the changing emissions of various gases was later
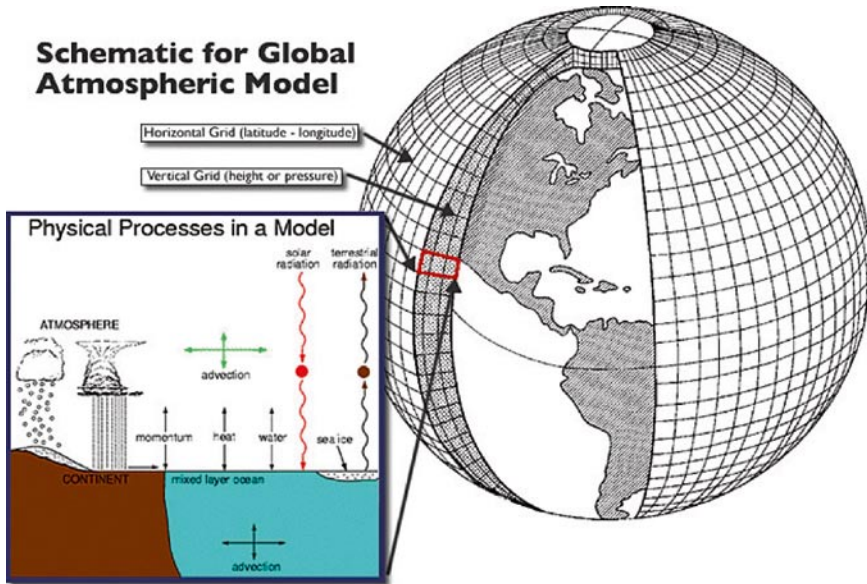
Fig. 23.1 Figure showing a schematic diagram of global atmospheric model

built on 1999. In HadCM3, thermohaline circulation, ventilation, vertical mixing of chemical constituents along with decadal variability in the ocean was included.

Local climate change is influenced greatly by local features such as mountains, which are not well represented in global models (GCMs) because of their coarse resolution, and models of higher resolution could not practically be used for global simulation for long periods of time due to spatial variance of the considered parameters. These problems were tried to be mitigated with the help of regional climate models (RCM). The RCM had higher resolution (typically 50 km), were constructed for limited areas and allowed to run for shorter periods (20 years or so). The Met Office Hadley Centre had run RCMs for three regions, Europe, the Indian subcontinent and southern Africa and had developed an RCM to run on PCs for any region as part of a regional climate modeling system called PRECIS (Fig. 23.1).

23.4.1.1   Structure of Global Climatic Models

Three-dimensional (more properly four-dimensional) GCMs discretize the equations for fluid motion and integrate these forward in time. They also contain parametrizations for processes – such as convection – that occur on scales too small to be resolved directly. More sophisticated models may include representations of the carbon and other cycles.

A simple general circulation model (SGCM), a minimal GCM, consists of a dynamical core that relates material properties such as temperature to dynamical

properties such as pressure and velocity. Examples are codes that solve the primitive equations, given energy input into the model, and energy dissipation in the form of scale-dependent friction, so that atmospheric waves with the highest wavenumbers are the ones most strongly attenuated. Such models may be used to study atmospheric processes within a simplified framework but are not suitable for future climate projections.

Atmospheric GCMs (AGCMs) model the atmosphere (and typically contain a land-surface model as well) and impose sea surface temperatures (SSTs). A large amount of information including model documentation is available from AMIP (Atmospheric Model Intercomparison Project 2009) they may include atmospheric chemistry.

A GCM contains a number of prognostic equations that are stepped forward in time (typically winds, temperature, moisture, and surface pressure) together with a number of diagnostic equations that are evaluated from the simultaneous values of the variables. As an example, pressure at any height can be diagnosed by applying the hydrostatic equation to the predicted surface pressure and the predicted values of temperature between the surface and the height of interest. The pressure diagnosed in this way then is used to compute the pressure gradient force in the time-dependent equation for the winds.

Oceanic GCMs (OGCMs) model the ocean (with fluxes from the atmosphere imposed) and may or may not contain a sea ice model. For example, the standard resolution of HadOM3 is 1.25° in latitude and longitude, with 20 vertical levels, leading to approximately 1,500,000 variables.

Coupled atmosphere-ocean GCMs (AOGCMs) (e.g., HadCM3, GFDL CM2.X) combine the two models. They thus have the advantage of removing the need to specify fluxes across the interface of the ocean surface. These models are the basis for sophisticated model predictions of future climate, such as are discussed by the IPCC.

AOGCMs represent the pinnacle of complexity in climate models and internalize as many processes as possible. They are the only tools that could provide detailed regional predictions of future climate change. However, they are still under development. The simpler models are generally susceptible to simple analysis and their results are generally easy to understand. AOGCMs, by contrast, are often nearly as hard to analyze as the real climate system.

23.4.1.2 Model Grids

The fluid equations for AGCMs are discretized using either the finite difference method or the spectral method. For finite differences, a regular grid (i.e., with constant grid spacing) in latitude and longitude is most common. However, variable resolution grids can be used. The "LMDz" model can be arranged to give high resolution over any given section of the planet. HadGEM1 (and other ocean models) use an ocean grid with higher resolution in the tropics to help resolve processes believed to be important for ENSO. Spectral models generally use a Gaussian grid, because

of the mathematics of transformation between spectral and grid-point space. Typical AGCM resolutions are between 1° and 5° in latitude or longitude: the Hadley Centre model HadAM3, for example, uses 2.5° in latitude and 3.75° in longitude, giving a grid of 73 by 96 points; and has 19 levels in the vertical. This results in approximately 500,000 "basic" variables, since each grid point has four variables (u, v, T, Q), though a full count would give more (clouds; soil levels). HadGEM1 uses a grid of 1.25° in latitude and 1.875° in longitude.

For a standard finite difference model, the gridlines converge towards the poles. This would lead to computational instabilities (see CFL condition) and so the model variables must be filtered along lines of latitude close to the poles. Ocean models suffer from this problem too, unless a rotated grid is used in which the North Pole is shifted onto a nearby landmass. Spectral models do not suffer from this problem. There are experiments using geodesic grids (UniSci 2001) and icosahedral grids, which (being more uniform) do not have pole-problems.

23.4.1.3   Different Types of GCMs Based on Model Structure

One-Dimensional Models

One-Dimensional Radiative-Convective Atmospheric Models

These models are globally averaged horizontally but contain many layers within the atmosphere. They treat processes related to the transfer of solar and infrared radiation within the atmosphere in considerable detail, and are particularly useful for computing the changes in net radiation – one of the possible drivers of climatic change – associated with changes in the composition of the atmosphere (e.g., Lal and Ramanathan 1984; Ko et al. 1993). The change in atmosphere water vapor amount as climate changes must be prescribed (based on observations), but the impact on radiation associated with a given change in water vapor can be accurately computed. The increase in water vapor in the atmosphere is thought to be the single most important feedback that amplifies an initial radiative perturbation, and radiative-convective models provide one means for assessing this feedback through a combination of observations and well-established physical processes.

One-Dimensional Upwelling-Diffusion Ocean Models

In this type of model, which was first applied to questions of climatic change by Hoffert and Hseih (1980), the atmosphere is treated as a single well-mixed box that exchanges heat with the underlying ocean and land surface. The absorption of solar radiation by the atmosphere and surface depends on the specified surface reflectivity and the atmosphere transmissivity and reflectivity. The emission of infrared radiation to space is a linearly increasing function of atmospheric temperature in this model; this increase serves to "dampen" temperature changes and thus limits the final temperature response for a given radiative perturbation through an appropriate

choice of the constant of proportionality in the parameterization of infrared radiation to space. The model can be forced to have any desired climate responsiveness to a given radiative perturbation. This process is in turn useful if one is trying to replicate the behavior of more complex models in a computationally efficient way for the purpose of scenario analysis and testing the interactions between different model components. The ocean is treated as a one-dimensional column that represents a horizontal average over the real ocean, excluding the limited regions where deep water forms and sinks to the ocean bottom, which are treated separately.

One-Dimensional Energy Balance Models

In these models, the only dimension that is represented is the variation with latitude: the atmosphere is averaged vertically and in the east west direction, and often combined with the surface to form a single layer. The multiple processes of meridional (north-south) heat transport by the atmosphere and oceans are usually represented as diffusion, while infrared emission to space is represented in the same way as in the upwelling diffusion model. These models have provided a number of useful insights concerning the interaction of horizontal heat transport feedbacks and high-latitude feedbacks involving ice and snow (e.g., Held and Suarez 1974).

Two-Dimensional Atmosphere and Ocean Models

Several different two-dimensional (latitude-height or latitude-depth) models of the atmosphere and oceans have been development (e.g., Peng et al. 1982, for the atmosphere: Wright and Stocker 1991, for the ocean). The two-dimensional models permit a more physically based computation of horizontal heat transport than in one-dimensional energy balance models.

Three-Dimensional Atmosphere and Ocean General Circulation Models

The most complex atmosphere and ocean models are the three-dimensional atmosphere general circulation models (AGCMs) and ocean general circulation models (OGCMs), both of which are extensively reviewed in Gates et al. (1996) and in various chapters of Trenberth (1992). These models divide the atmosphere or ocean into a horizontal grid with a typical resolution of 2–40 longitude in the latest models and typically 10–20 years in the vertical. They directly simulate winds, ocean currents, and many other features and processes of the atmosphere and oceans. Figure 23.1 provides a schematic illustration of the major processes that occur within a single horizontal grid cell of an AGCM. Both AGCMs and OGCMs have been used extensively in a stand-along mode, with prescribed ocean-surface temperature in the case of AGCMs and with prescribed surface temperatures and

salinities, or the corresponding heat and freshwater fluxes, in the case of OGCMs. Only when the two models are coupled together do we have what can be considered to be a climate model, in which all the temperatures are freely determined. Coupled AOGCMs automatically compute the feedback processes associated with water vapor, clouds, seasonal snow and ice, as well as the uptake of heat by the oceans when driven by a prescribed, anthropogenic increase of atmospheric CO_2. The uptake to heat by the oceans delays and distorts the surface temperature response but contributes to sea-level through expansion of ocean water as it warms. AOGCMs compute radiative transfer through the atmosphere (explicitly modeling clouds, water vapor, and other atmosphere components), snow and sea-ice, surface fluxes, transport of heat and water by the atmosphere and ocean, and storage of heat in the ocean. Because of computational constraints, the majority of these processes are parameterized to some extent (see Dickinson et al. 1996, concerning processes in atmosphere and oceanic GCMs). More detailed representations are not practical, or have not been developed, for use in a global model. Some parameterizations inevitably include constants which have been tuned to observations of the current climate (1991), the intensity of the thermohaline overturning is determined by the model itself, while in others (e.g., de wolde et al. 1995), it is prescribed, as in the one-dimensional upwelling-diffusion model. The one-dimensional energy balance atmosphere–surface climate model has also been coupled to a two-dimensional ocean model (Harvey 1992; Bintanja 1995; de wolde et al. 1995.

23.4.1.4 Different Types of GCMs Based on Model Parameters

Models of Carbon Parameter

The upwelling-diffusion model that was described above can be used as the oceanic part of the carbon cycle, as in the work of Hoffert et al. (1981). The global mean atmosphere–ocean exchange of CO_2, the vertical mixing of total dissolved carbon by themohaline overturning and diffusion, and the sinking of particulate material produced by biological activity can all be represented in this model. A two-dimensional ocean model has been used as the oceanic component of the global carbon cycle (Stocker et al. 1994). Finally, OGCMs can be used as the oceanic component of the global carbon cycle, in which the model-computed ocean currents and other mixing processes, are used, in combination with simple representations of biological processes and air–sea exchange (e.g., Bacastow and Maier-Reimer 1990; Najjar et al. 1992). CO_2 uptake calculations using 3-D models have so far been published only for stand-alone OGCMs, in which the circulation filed and surface temperature have been fixed. In a coupled simulation, changes in both of these variables in response to increasing greenhouse gas concentrations would alter the subsequent uptake of CO_2 to some extent.

The terrestrial biosphere can be represented by a series of interconnected boxes, where the boxes represent components such as leafy material, woody material, roots, detritus, and one or more pools of soil carbon. Each box can be globally

aggregated such that, for example, the detrital box represents all the surface detritus in the world. The commonly used, globally aggregated box models are quantitatively compared globally aggregated terrestrial biosphere model, where numbers inside boxes represent the steady state amounts of carbon (Gt) prior to human disturbances, and the numbers between boxes represent the annual rates of carbon transfer (Gt a-1). In globally aggregated box models, it is not possible to separate responses in different latitude zones (e.g., net release of carbon through temperature effects at high latitudes, net uptake of carbon in the tropics due to CO_2 fertilization). Since regional responses vary nonlinearly with temperature and atmospheric CO_2 concentration, extrapolation into the future using globally aggregated models undoubtedly introduces errors. An alternative is to separate box models for major regions, as in van Minnen et al. (1996), rather than lumping everything together.

The role of the terrestrial biosphere in global climatic change has also been simulated using relatively simple models of vegetation on a global grid with resolution as fine as 0.50 latitude × 0.50 longitude. These models have been used to evaluate the impact on net ecosystem productivity of higher atmospheric CO_2 (which tends to stimulate photosynthesis and improve the efficiency of water use by plants) and higher temperatures (which can increase or decrease photosynthesis and increase decay processes). These models distinguish, as a minimum, standing biomass from soil organic matter. The more sophisticated varieties track the flows of both carbon and nitrogen (taken to be the limiting nutrient), and include feedbacks between nitrogen and the rates of both photosynthesis and decay of soil carbon (e.g., Rastetter et al. 1992; Melillo et al. 1993).

Grid-point models of the terrestrial biosphere have been used to assess the effect on the net biosphere–atmosphere CO_2 flux of hypothetical (or GCM-generated) changes in temperature and/or atmospheric CO_2 concentration, but generally without allowing for shifts in the ecosystem type at a given grid point as climate changes. More advanced ecosystem models are being developed and tested that link biome models (which predict changing ecosystem types) and ecophysiological models (which predict carbon fluxes) (e.g., Plochl and Cramer, 1995). Different biomes vary in the proportion of "plant functional types," examples of which are tropical evergreen forest, cool-temperate evergreen trees, and cool grasses. An alternative to simulating the location of specific ecosystems is to predict the proportions of different plant functional types at each grid cell based on the carbon balance for each functional type, as determined from an ecophysiological model (Foley et al. 1996). This effectively allows for the simulation of both rapid biophysical processes and the long-term adjustment of ecosystems to changing climate and atmospheric CO_2 concentration. Simulations with these and earlier models demonstrate the potential importance of feedbacks involving the nutrient cycle and indicate the potential magnitude of climate-induced terrestrial biosphere–atmosphere CO_2 fluxes. However, individual models still differ considerably in their responses (VEMAP Members 1995). As with models of the oceanic part of the carbon cycle, such simulations have yet to be carried out interactively with coupled AOGCMs. These models also have not yet been combined with ocean carbon uptake OGCMs.

Rather detailed models of the marine biosphere, involving a number of species and interactions, have also been developed and applied to specific sites or regions (e.g., Gregg and Walsh 1992; Sarmiento et al. 1993; Antoine and Morel 1995; Oschlies and Garcon 1999; Oschlies et al. 2000).

Models of Atmospheric Chemistry and Aerosols

Atmospheric chemistry is central to the distribution and amount of ozone in the atmosphere. The dominant chemical reactions and sensitivities are significantly different for the stratosphere and troposphere. These processes can be adequately modeled only with three-dimensional atmospheric models (in the case of the troposphere) or with two-dimensional (latitude-height) models (in the case of the stratosphere). Atmospheric chemistry is also critical to the removal of CH_4 from the atmosphere and, to a lesser extent, all other greenhouse gases except H_2O and CO_2 in the case of CH_4, a change in its concentration affects its own removal rate and, hence, subsequent concentration changes. An accurate simulation of changes in the removal rate of CH_4 requires specification of the concurrent concentrations of other reactive species, in particular NO_x (nitrogen oxides), CO *carbon monoxide), and the VOCs (volatile organic compounds); and use of a model with latitudinal and vertical resolution. However, simple globally averaged models of chemistry–climate interactions have been developed. These models treat the global CH_4-CO-OH cycle in a manner which takes into account the effects of the heterogeneity of the chemical and transport processes, and provide estimates of future global or hemispheric mean changes in the chemistry of the earth's atmosphere. Some of the models also simulate halocarbon concentrations and the resulting atmospheric chorine concentration as well as radiative effects due to halocarbons (Prather et al. 1992). An even simpler approach, adopted by Osborn and Wigley (1994), is to treat the atmosphere as a single well-mixed box but to account for the effects of atmospheric chemistry by making the CH_4 lifetime depend on CH_4 concentration in a way that roughly mimics the behavior of the above-mentioned globally averaged models or of models with explicit spatial reevaluation. Atmospheric O_3 and CH_4 chemistry has not yet been incorporated in AGCMs used for climate simulation purposes, although two-dimensional interactive chemistry–climate models have been built (Wang et al. 1998).

Atmospheric chemistry is also central to the distribution and radiative properties of small suspended particles in the atmosphere referred to as aerosols, although chemistry is only part of what is required in order to simulate the effects of aerosols on climate. The primary aerosols that are affected by atmospheric chemistry are sulfate aerosols (produced from the emission of SO_2 and other S-containing gases), nitrate aerosols (produces from emission of nitrogen oxides), and organic carbon aerosols (produces from the emission of a variety of organic compounds from plants and gasoline). The key processes that need to be represented are the source emissions of aerosols or aerosol precursors; atmospheric transport, mixing, and chemical and physical transformation; and removal processes (primarily deposition in rainwater and direct dry deposition onto the earth's surface). Since part of the

effect of aerosols on climate arises because they serve as cloud condensation nuclei, it is also important to be able to represent the relationship between changes in the aerosol mass input to the atmosphere and, ultimately, the radiative properties of clouds. Establishing the link between aerosol emissions and could properties, however, involves several poorly understood steps and is highly uncertain.

Geographically distributed sulfur–aerosol emissions have been used as the input to AGCMs and, in combination with representations of aerosol chemical and physical processes, have been used to compute the geographical distributions of sulfur–aerosol mass using only natural emission sources and using natural + anthropic emission sources (e.g., Langner and Rodhe 1991; Chin et al. 1996; Pham et al., 1996). Given the differences in the GCM-simulated aerosol distributions assumptions concerning the aerosol optical properties, other studies have estimated the possible range of direct (cloud-free) effects on radiative forcing (e.g., Haywood et al. 1997). With yet further assumptions concerning how clouds respond to sulfur aerosols, a range of indirect (cloud-induced) effects can also be computed (e.g., Boucher and Lohmann 1995; Jones and Slingo 1996; Kogan et al. 1996; Lohmann and Feichter 1997). The results of these and other calculations are extensively reviewed in Harvey (2000a: Chapter 7).

Models of Ice Sheets

High-resolution (20 × 20 km horizontal grid), two- and three-dimensional models of the polar ice sheets have been developed and used to assess the impact on global mean sea level of various idealized scenarios for temperature and precipitation changes over the ice sheets (e.g., Huybrechts and Oerlemans 1990; Huybrechts et al. 1991). AGCM output has also recently been used to drive a three-dimensional model of the East Antarctic ice sheet (Verbitsky and Saltzman 1995), but has not yet been used to assess the possible contribution of changes in mountain glaciers to future sea-level rise. Output from high-resolution ice-sheet models can be used to develop simple relationships in which the contribution of ice-sheet changes to future sea level is scaled with changes in global mean temperature.

23.4.2 Regional Climate Models

A key limitation of GCMs is the fairly coarse horizontal resolution. The climate *prediction*.net atmospheric resolution is 3.75° × 2.5°. For the practical planning of water resources, flood defences, etc., countries require information on a much more local scale than GCMs are able to provide. There are three possible solutions to this problem:

- Run the full GCM at a finer resolution. As the model would then take much longer to complete a simulation, either a very powerful computer (such as the Earth Simulator in Japan) or a much shorter simulation period (e.g., 5 years) is required.

- Use statistical techniques to "downscale" the coarse, GCM results to local. These techniques assume that the relationship between large-scale climate variables (e.g., grid box rainfall and pressure) and the actual rainfall measured at one particular rain gauge will always be the same. So, if that relationship is known for current climate, the GCM projections of future climate can be used to predict how the rainfall measured at that rain gauge will change in the future.
- Embed a Regional Climate Model (RCM) in the GCM. RCMs are a more dynamically consistent way than statistical downscaling to produce a regional forecast.

RCMs work by increasing the resolution of the GCM in a small, limited area of interest. An RCM might cover an area the size of western Europe, or southern Africa – typically 5,000 × 5,000 km. The full GCM determines the very large-scale effects of changing greenhouse gas concentrations, volcanic eruptions, etc. on global climate. The climate (temperature, wind, etc.) calculated by the GCM is used as input at the edges of the RCM. The models are typically coupled together (information is only passed from the GCM to the RCM) once every 24 modeled hours. RCMs can resolve the local impacts given small-scale information about orography (land height), land use, etc., giving weather and climate information at resolutions as fine as 50 or 25 km (Fig. 23.2) Climate Prediction (2009).

In regions where the land surface is flat for thousands of kilometers, and there is no ocean anywhere near, the coarse resolution of a GCM may be enough to accurately simulate weather changes. However, most land areas have mountains, coastlines, changing vegetation characteristics, etc. on much smaller scales, and RCMs can represent the effects of these on the weather much better than GCMs (Figs. 23.3–23.5).
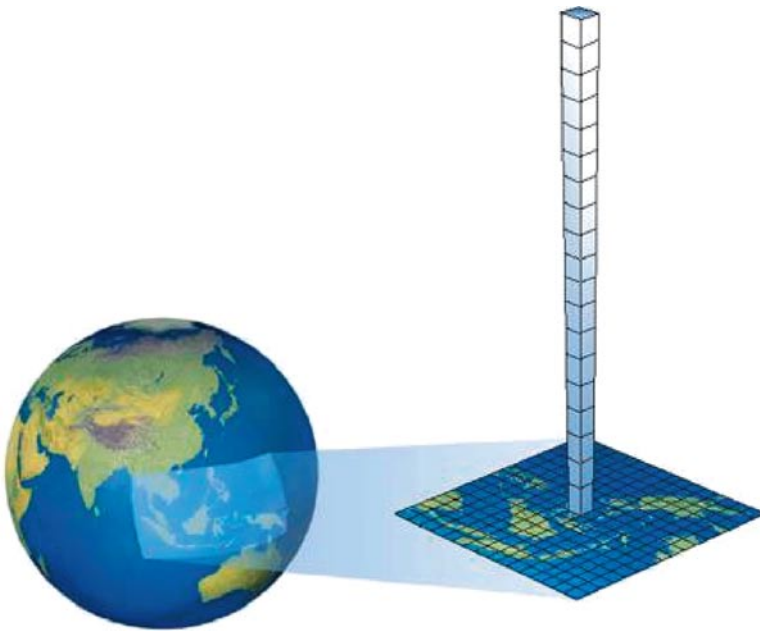
Fig. 23.2 Figure showing model domain of GCMs and RCMs
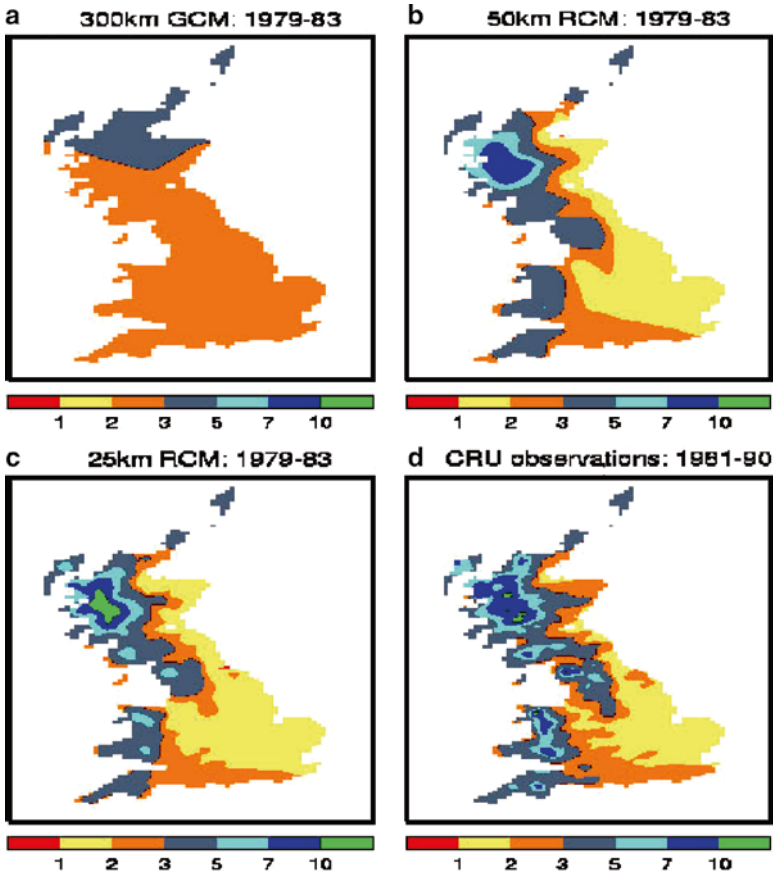
Fig. 23.3 Winter precipitation over Britain as predicted by (**a**) a GCM with resolution 300 km, (**b**) a regional model with 50 km resolution and (**c**) a regional model with 25 km resolution compared to (**d**) actual observations
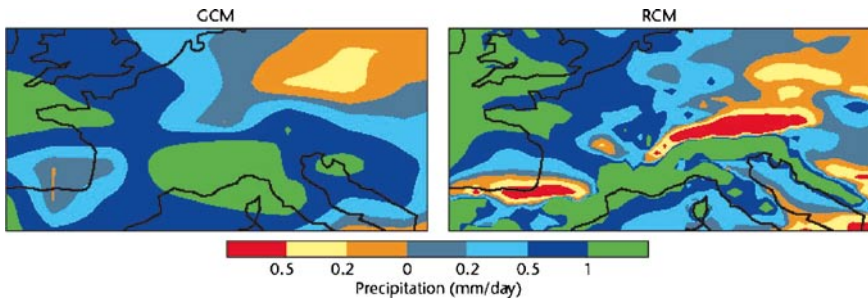
Fig. 23.4 Predicted changes in winter precipitation over central/southern Europe between the present day and 2080. The areas of red, where precipitation has fallen by more than 0.5 mm/day, indicate large reductions over the Alps and Pyrenees predicted by the RCM (*right*), but not the large scale GCM (*left*)
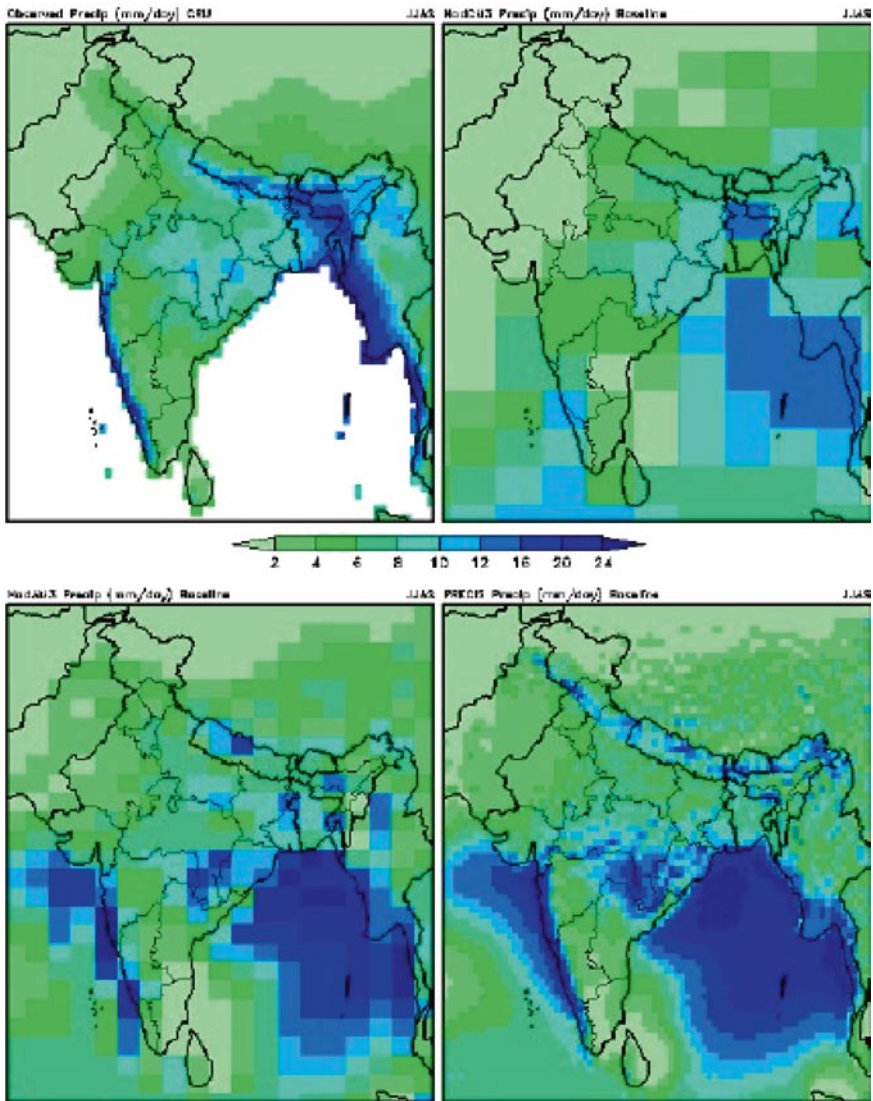
Fig. 23.5 Prediction of seasonal precipitation over India as predicted by PRECIS model with 50 km resolution (Krishnakumar 2009)

The weather in one part of the world is not independent of the weather elsewhere in the world. For example, the El Nino Southern Oscillation, focused in the South Pacific, has effects which can be detected over most of the planet.

23.4.3   Examples of Climate Models

23.4.3.1   Reading Intermediate General Circulation Model (IGCM)

The Reading Intermediate General Circulation Model (IGCM), is a simplified or "intermediate" Global climate model, which is developed by members of the Department of Meteorology at the University of Reading, and by members of the Stratospheric Dynamics and Chemistry Group of the Department of Atmospheric and Oceanic Sciences at McGill University

The IGCM is a fast GCM based on the primitive-equations baroclinic model of Hoskins and Simmons, which has been converted to run on workstations. Several versions have been developed with representations of the physics.

- IGCM1: Portable version of the original spectral dry baroclinic model formulated in sigma-levels, with an option for Newtonian relaxation and Rayleigh friction, no surface.
- IGCM2: Includes simplified moist parameterizations, a cheap "radiation scheme" (i.e., constant tropospheric cooling), a bulk formulation scheme for the boundary layer, fixed surface temperatures and humidity, a uniform vertical diffusion, and can advect tracers.
- IGCM3x: Intermediate climate model which includes more sophisticated moist/clouds parameterizations, a radiation scheme with various gas absorbers, and a more realistic surface with an orography and land, sea surface schemes.

The adiabatic version, IGCM1, is freely available. Access to IGCM2 and IGCM3 is restricted to members of the Department of Meteorology at the University of Reading and collaborating researchers.

23.4.3.2   Hadley Centre Coupled Model, Version 3 (HadCM3)

HadCM3 (abbreviation for Hadley Centre Coupled Model, version 3) is a coupled atmosphere–ocean general circulation model (AOGCM) developed at the Hadley Centre in the United Kingdom (Gordon et al. 2000, Pope et al. 2000, and Collins et al. 2001). It was one of the major models used in the IPCC Third Assessment Report in 2001.

Unlike earlier AOGCMs at the Hadley Centre and elsewhere (including its predecessor HadCM2), HadCM3 does not need flux adjustment (additional "artificial" heat and freshwater fluxes at the ocean surface) to produce a good simulation. The higher ocean resolution of HadCM3 is a major factor in this; other factors include a good match between the atmospheric and oceanic components; and an improved ocean mixing scheme (Gent and McWilliams). HadCM3 has been run for over 1,000 years, showing little drift in its surface climate.

HadCM3 is composed of two components: the atmospheric model HadAM3 and the ocean model (which includes a sea ice model). Simulations often use a 360-day calendar, where each month is 30 days.

23.4.3.3 Hadley Centre Atmospheric Model, Version 3 (HadAM3)

HadAM3 is a grid point model and has a horizontal resolution of $2.5° \times 3.75°$ in latitude × longitude. This gives 96×73 grid points on the scalar (pressure, temperature, and moisture) grid; the vector (wind velocity) grid is offset by 1/2 a grid box (this gives a resolution of approximately 300 km, roughly equal to T42 in a spectral model. There are 19 levels in the vertical).

The timestep is 30 min (with three sub-timesteps per timestep in the dynamics). Near the poles, fields are Fourier-filtered to prevent instabilities due to the CFL criterion.

This is the model behind PRECIS (Providing Regional Climates for Impacts Studies)

23.4.3.4 Hadley Centre Global Environmental Model, Version 1 (HadGEM1)

HadGEM1 is a coupled climate model developed at the Met Office's Hadley Centre. It represents a significant advance on its predecessor, HadCM3, in terms of its science and provides an enhanced capability for carrying out new climate experiments. HadGEM1 also provides a foundation for further modeling advances across a range of applications, particularly involving enhanced resolution and full Earth System modeling.

Evaluation of the atmospheric performance of HadGAM/GEM1,

23.4.3.5 Geophysical Fluid Dynamics Laboratory Coupled Model, Version 2.X (GFDL CM2.X)

GFDL CM2.X is a coupled atmosphere–ocean general circulation model (AOGCM) developed at the NOAA Geophysical Fluid Dynamics Laboratory in the United States. It is one of the leading climate models used in the Fourth Assessment Report of the IPCC, along with models developed at the Max Planck Institute for Climate Research, the Hadley Centre and the National Center for Atmospheric Research. The solutions of these GFDL CM2 models are described in a series of papers published in the Journal of Climate in 2006.

23.4.3.6 EdGCM

EdGCM is a global climate model (GCM) that has been ported for use on desktop computers and integrated with a relational database, a graphical user interface, and

scientific visualization utilities, all of which are aimed at helping improve the quality of teaching and learning of climatology. EdGCM is developed at Columbia University by scientists and programmers in the Center for Climate Systems Research. The Global Climate Model at the core of EdGCM was developed at NASA's Goddard Institute for Space Studies and is referred to in climate modeling literature as the GISS Model II. It is currently in use by researchers to study climates of the past, present, and future. EdGCM permits teachers and students to conduct in-depth investigations of current climate science topics, in near real-time, just as they are being studied by climate scientists.

23.4.3.7 Providing REgional Climates for Impacts Studies (PRECIS)

PRECIS (pronounced as in the French précis – "PRAY-sea") is based on the Hadley Centre's regional climate modeling system. It has been ported to run on a PC (under Linux) with a simple user interface, so that experiments can easily be set up over any region.

PRECIS was developed in order to help generate high-resolution climate change information for as many regions of the world as possible. The intention is to make PRECIS freely available to groups of developing countries in order that they may develop climate change scenarios at national centers of excellence, simultaneously building capacity, and drawing on local climatological expertise. These scenarios can be used in impact, vulnerability and adaptation studies, and to aid in the preparation of National Communications, as required under Articles 4.1 and 4.8 of the United Nations Framework Convention on Climate Change (UNFCCC).

23.4.3.8 Fifth-Generation NCAR/Penn State Mesoscale Model (MM5)

The MM5 is a regional mesoscale model used for creating weather forecasts and climate projections. It is maintained by Penn State University and the National Center for Atmospheric Research.

Mesoscale meteorology is the study of weather systems smaller than synoptic scale systems but larger than microscale and storm-scale cumulus systems. Horizontal dimensions generally range from around 5 km to several hundred kilometers. Examples of mesoscale weather systems are sea breezes, squall lines, and mesoscale convective complexes.

Vertical velocity often equals or exceeds horizontal velocities in mesoscale meteorological systems due to nonhydrostatic processes such as buoyant acceleration of a rising thermal or acceleration through a narrow mountain pass.

As in synoptic frontal analysis, literature about mesoscale analysis uses cold, warm, and occluded fronts on the mesoscale to help describe phenomena. On weather maps mesoscale fronts are depicted as smaller and with twice as many bumps or spikes as the synoptic variety. In the United States, opposition to the use

of the mesoscale versions of fronts on weather analyses, has led to the use of an overarching symbol (a trough symbol) with a label of outflow boundary as the frontal notation (Roth 2006).

23.5 Use of Connected Climatic and Hydrologic Models

A dynamic downscaling method, referred as pseudo-warming, was used by Fujihara et al. (2008), to connect the output of raw general circulation models (GCMs) into river basin hydrologic models which was applied to explore the potential impact of climate change on hydrology and water resources of the Seyhan River Basin in Turkey. The results showed that the decreased precipitation as formulated by the climate model would result in a considerably decreased inflow and time of peak. Hotchkiss et al. (2000) predicted the changes in global river flow under the IPCC SRES A1B and A2 scenarios found from HadGEM1-TRIP model and concludes that there will be significant change in the seasonality of river flow, such as earlier peaks in spring runoff, large increases in monthly maximum flow, and decreases in monthly minimum flow. Cliimatologic databases (SICLIM and CLICOM) built by the Servicio Meteorológico Nacional (SMN) of Mexico (Mendoza et al. 2008) was fed to a hydrologic model to predict the annual volume of superficial available water. A climate variability indicator (the El Niño-Southern Oscillation, ENSO) was applied by Muluye and Coulibaly (2007) to predict seasonal reservoir inflows. Global climate models (GCM), CGCM2, CSIROMk2, and HadCM3 was applied by Merritt et al. (2006) to estimate future water availability of Okanagan Basin in England. Each of the research work advocates decrease in quantity of water as the common effect of climate change.

References

Antoine D, Morel A (1995) Modeling the seasonal course of the upper ocean pCO_2 (i): development of a one-dimensional model. Tellus 47B:103–121

Atmospheric Model Intercomparison Project (2009). Retrieved from http://www-pcmdi.llnl.gov/projects/amip/index.php

Bacastow R, Maier-Reimer E (1990) Ocean-circulation model of the carbon cycle. Climate Dyn 4:95–125

Bintanja R (1995) The Antarctic ice sheet and climate. Ph.D. thesis, Utrecht University, Utrecht

Boucher O, Lohmann U (1995) The sulfate-CCN-cloud albedo effect: a sensitivity study with two general circulation models. Tellus 47B:281–300

Chin M, Jacob DJ, Gardner GD, Foreman-Fowler MS, Spiro PA (1996) A global three-dimensional model of tropospheric sulfate. J Geophys Res 101:18667–18690

Climate Prediction (2009) Regional Climate Models. Retrieved from http://www.climateprediction.net/content/regional-climate-models on 28 July 2009

Collins M, Tett SFB, Cooper C (2001) The internal climate variability of HadCM3, a version of the Hadley Centre coupled model without flux adjustments. Climate Dyn 17:61–81. doi:10.1007/s003820000094

De Wolde JR, Bintanja R, Oerlemans J (1995) On thermal expansion over the last one hundred years. J Climate 8:2881–2891

Dickinson RE, Meleshko V, Randall D, Sarachik E, Silva-Dias P, Slingo A (1996) Climate processes. In: Houghton JT, Filho LGF, Callander BA, Harris N, Kattenberg A, Kattenberg A, Maskell K (eds) Climate change 1995: the science of climate change. Cambridge University Press, Cambridge, pp 193–227

Foley JA, Prentice C, Ramankutty N, Levis S, Pollard D, Sitch S, Haxeltine A (1996) An intergrated biosphere model of land surface processes, terrestrial carbon balance, and vegetation dynamics. Global Biogeochem Cycle 10:603–628

Fujihara Y, Tanaka K, Watanabe T, Nagano T, Kojiri T (2008) Assessing the impacts of climate change on the water resources of the Seyhan River Basin in Turkey. J Hydrol 353(1–2):33–48

Gordon C, Cooper C, Senior CA, Banks H, Gregory JM, Johns TC, Mitchell JFB, Wood RA (2000) The simulation of SST, sea ice extents and ocean heat transports in a version of the Hadley Centre coupled model without flux adjustments ([dead link]). Climate Dyn 16:147–168. doi:10.1007/s003820050010. http://www.met-office.gov.uk/research/hadleycentre/models/gordon00/index.html

Gregg WW, Walsh JJ (1992) Simulation of the 1979 spring bloom in the mid-Atlantic bight: a coupled physical/biological model. J Geophys Res 97:5723–5743

Harvey LD (1992) A two-dimensional ocean model for long-tern climate simulations: stability and coupling to atmospheric and sea ice models. J Geophys Res 97:9435–9453

Harvey LDD (2000) Global Warming: The Hard Science. Prentice Hall, Harlow

Haywood JM, Roberts DI, Slingo A, Edwards JM, Shine KP (1997) General circulation model calculations of the direct radiative forcing by anthropogenic sulfate and fossil-fuel soot aerosol. J Climate 10:1562–1577

Held 1M, Suarez MJ (1974) Simple albedo feedback models of the icecaps. Tellus 26:613–630

Hotchkiss RH, Jorgensen SF, Stone MC, Fontaine TA (2000) Regulated river modeling for climate change impact assessment: the Missouri river. J Am Water Resour Assoc 36(2):375–386

Hoffert MI, Callegari AJ, Hseih CT (1980) The role of deep sea heat storage in the secular response to climatic forcing. J Geophys Res 85:6667–6679

Hoffert HI, Callegari AJ, Hseih CT (1981) A box-diffusion carbon cycle model with upwelling, polar bottom water formation and a marine biosphere. In: Bolin B (ed) Carbon cycle modeling, SCOPE 16. Wiley, New York, pp 287–305

Huybrechts P, Oerlemans J (1990) Response of the Antarctic ice sheet to future greenhouse warming. Climate Dyn 5:93–102

Huybrechts P, Letreguilly A, Rech N (1991) The Greenland ice sheet and greenhouse warming. Palaeogeogr Palaeoclimatol Palaeoecol 89:399–412

IPCC (2007) Climate change 2007: the physical sciences basis, retrieved on http://ipcc-wg1.ucar.edu/wg1/wg1-report.html. on 30th April, 2009

Jones A, Slingo A (1996) Predicting cloud-droplet effective radius and indirect sulphate aerosol forcing using a general circulation model. Q J Roy Meteorol Soc 122:1573–1595

Ko MKW, Size ND, Wang WC, Shia G, Goldman A, Muecary FJ, Murcaray DG, Rinsland CP (1993) Atmospheric sulfur hexafluoride: sources, sinks, and greenhouse warming. J Geophys Res 98:10499–10507

Kogan ZN, Kogan YL, Lilly DK (1996) Evaluation of sulfate aerosol's indirect effect in marine stratocumulus clouds using observation-derived cloud climatology. Geophys Res Lett 23:1937–1940

Krishnakumar K (2009) Climate change scenario. Proceeding of NATCOM 2 Workshop, organized by Indian Institute of Tropical Meteorology, Pune

Lal M, Ramanathan V (1984) The effects of moist convection and water-vapor rediative processes on climate sensitivity. J Atmos Sci 41:2238–2249

Langner J, Rodhe H (1991) A global dimensional model of the tropospheric sulfur cycle. J Atmos Chem 13:225–263

Lohmann U, Feichter J (1997) Impact of sulfate aerosols on albedo and lifetime of clouds: a sensitivity study with the ECHAM4 GCM. J Geophys Res 102:13685–13700

Melillo JM, McGuire AD, Kicklighter DW, Moore B III, Vorosmarty CJ, Schloss AL (1993) Global climate change and terrestrial net primary production. Nature 363:234–240

Merritt WS, Alila Y, Barton M, Taylor B, Cohen S (2006) Hydrologic response to scenarios of climate change in sub watersheds of the Okanagan basin, British. J Hydrol 326:79–108

Mendoza VM, Villanueva EE, Garduño R, Nava Y, Santisteban G, Mendoza AS, Oda B, Adem J (2008) Thermo-hydrological modelling of the climate change effect on water availability in two hydrologic regions of Mexico. Royal Meteorol Soc 29(8):1131–1153

Muluye GY, Coulibaly P (2007) Seasonal reservoir inflow forecasting with low-frequency climatic indices: a comparison of data-driven methods. Hydrol Sci J 52(3):508–522

Najjar RG, Sarmiento JL, Toggweiler JR (1992) Downward transport and fate of organic matter in the ocean: simulations with a general circulation model. Global Biogeochem Cycle 6:45–76

Osborn TJ, Wigley TML (1994) A simple model for estimating methane concentrations and lifetime variations. Climate Dyn 9:181–193

Oschlies A, Garcon V (1999) An eddy-permitting coupled physical-biological model of the North Atlantic, 1, sensitivity to physics and numerics. Global Biogeochem Cycle 13:135–160

Oschlies A, Koeve W, Garcon V (2000) An eddypermitting coupled physical model of the North Atlantic 2. Ecosystem dynamics and comparison with satellite and JGOFS local studies data. Global Biogeochem Cycle 14:499–523

Peng L, Chou M-D, Arking A (1982) Climate studies with a multi-layer energy balance model. Part I: model description and sensitivity to the solar constant. J Atmos Sci 39:2639–2656

Pham M, Muller J-F, Brasseur GP, Granier C, Megie G (1996) A 3D model study of the global sulphur cycle: contributions of anthropogenic and biogenic sources. Atmos Environ 30:1815–1822

Plochl M, Cramer W (1995) Coupling global models of vegetation structure and ecosystem processes. Tellus 47B:240–250

Pope VD, Gallani ML, Rowntree PR, Stratton RA (2000) The impact of new physical parameterizations in the Hadley centre climate model – HadAM3" ([dead link]). Climate Dyn 16:123–146. doi:10.1007/s003820050009. http://www.met-office.gov.uk/research/hadleycentre/models/pope00/index.html

Prather M, Ibrahim AM, Sasaki T, Stordal F (1992) Future chlorine-bromine loading and ozone depletion in United Nations Environment Programme Staff (eds) Scientific Assessment of Ozone Depletion: 1991. World Meteorological Organization, Geneva

Rastetter EB, McKane RB, Shaver GR, Melillo JM (1992) Changes in C storage by terrestrial ecosystems: how C-N interactions restrict responses to CO_2 and temperature. Water Air Soil Pollut 64:327–344

Roth D (2006) Hydrometeorological prediction center. Unified Surface Analysis Manual. Retrieved on 2006-10-24

Sarmiento JL, Slater RD, Fasham MJR, Ducklow HW, Toggweiler JR, Evans GT (1993) A seasonal three-dimensional ecosystem model of nitrogen cycling in the North Atlantic euphotic zone. Global Biogeochem Cycle 7:417–450

Stewart P, Le CF, Vemuri SR (2006) (Anticipated) Climate change impacts on Australia. Int J Ecol Dev 4(W06)

Stocker TF, Broecker WS, Wright DG (1994) Carbon uptake experiment with a zonally averaged global ocean circulation model. Tellus 46B:103–122

Trenberth KE (ed) (1992) Climate system modeling. Cambridge University Press, Cambridge

UniSci (2001) Climate model will be first to use a geodesic grid. Retrieved from http://www.unisci.com/stories/20013/0924011.htm on 30 July 2009

Van Minnen JG, Goldewijk KK, Leemans R (1996) The importance of feedback processes and vegetation transition in the terrestrial carbon cycle. J Biogeogr 22:805–814

Members VEMAP (1995) Vegetation ecosystem modeling and analysis project: comparing bioge-
ography and biogeochemistry models in a continental-scale study of terrestrial ecosystem
responses to climate change and CO_2 doubling. Global Biogeochem Cycle 9:407–437

Verbitsky M, Saltzman B (1995) Behaviour of the Esat Antractic ice sheet as deduced from a
coupled GCM/Ice-sheet models. Geophys Res Lett 22:2913–2916

Wang C, Prinn RG, Sokolov A (1998) A global interactive chemistry and climate model: formulation
and testing. J Geophys Res 103:3399–3417

Wright DG, Stocker TK (1991) A zonally averaged ocean model for the themohaline circulation, I.
Model development and flow dynamics. J Phys Oceanogr 21:1713–1724

Chapter 24
A Brief Introduction to Remote Sensing and GIS

Mrinmoy Majumder

Abstract Remote sensing is the operation of sensing remote pictures of the Earth. Geographical information system (GIS) is a system through which geographical informations can be retrieved. Hydrologic science now uses both the techniques in various methodologies to reduce the amount of field work and problems regarding data scarcity. From catchment delineation to identification of hydrologically similar units, GIS and remote sensing are used very frequently and with greater accuracy. The present note gives a simple, introductory overview of both the techniques along with their application methodology for water science, especially in river hydrology.

24.1 The Concept of Remote Sensing

Remote sensing can be defined as the study of something without making actual contact with the object of study. According to Short Sr. (2009): "Remote Sensing in the most generally accepted meaning refers to instrument-based techniques employed in the acquisition and measurement of spatially organized data/information on some property(ies) (spectral; spatial; physical) of an array of target points (pixels) within the sensed scene that correspond to features, objects, and materials, doing this by applying one or more recording devices not in physical, intimate contact with the item(s) under surveillance (thus at a finite distance from the observed target, in which the spatial arrangement is preserved); techniques involve amassing knowledge pertinent to the sensed scene (target) by utilizing electromagnetic

M. Majumder (✉)
Senior Research Fellow, School of Water Resources Engineering, Jadavpur University, Kolkata-700032, West Bengal, India
and
Geo-information Scientist, Regional Center, National Afforestation
and Eco-development Board, Jadavpur University, Kolkata-700032, West Bengal, India
e-mail: mrinmoy@majumder.info

radiation (EMR), force fields, or acoustic energy sensed by recording cameras, radiometers and scanners, lasers, radiofrequency receivers, radar systems, sonar, thermal devices, sound detectors, seismographs, magnetometers, gravimeters, scintillometers, and other instruments."

24.1.1 Electromagnetic Spectrum: Transmittance, Absorptance, and Reflectance

Any beam of photons from some source passing through medium 1 (usually air) that impinges upon an object or target (medium 2) will experience one or more reactions such as transmittance, absorptance, and reflectance.

The primary source of energy that illuminates natural targets is the Sun. Solar irradiation (also called insolation) arrives at the Earth at wavelengths, which are determined by the photospheric temperature of the sun (peaking near 5,600°C). The main wavelength interval is between 200 and 3,400 nm (0.2 and 3.4 μm), with the maximum power input close to 480 nm (0.48 μm), which is in the visible green region. As solar rays arrive at the Earth, the atmosphere absorbs or backscatters a fraction of them and transmits the remainder

The solar energy strikes the land and ocean surface (and objects thereon), and atmospheric targets, such as air, moisture, and clouds, and the incoming radiation (irradiance) partitions into three modes of energy-interaction response:

1. Transmittance – Some fraction (up to 100%) of the radiation penetrates into certain surface materials such as water and if the material is transparent and thin in one dimension, normally passes through, generally with some diminution.
2. Absorptance – Some radiation is absorbed through electron or molecular reactions within the medium; a portion of this energy is then reemitted, usually at longer wavelengths, and some of it remains and heats the target.
3. Reflectance – Some radiation (commonly 100%) reflects (moves away from the target) at specific angles and/or scatters away from the target at various angles, depending on the surface roughness and the angle of incidence of the rays.

The above three parameters are dimension-less numbers (between 0 and 1), but are commonly expressed as percentages.

A fourth situation, when the emitted radiation results from internal atomic/molecular excitation, usually related to the heat state of a body, is a thermal process. When a remote sensing instrument has a line-of-sight with an object that is reflecting solar energy, then the instrument collects that reflected energy and records the observation.

24.2 Concept of Geographical Information System

A wide divergence of view exists with regard to what constitutes a geographical information system (GIS), but the most accepted definition of GIS states that: "GIS is a decision support system comprising of computer hardware, software, geo-

graphic data, and personnel designed to efficiently capture, store, manipulate, analyze and display all forms of spatial and non-spatial (attribute) data for better management of geographical area."

24.2.1   Components of Geographical Information System

GIS have three important components:

- Computer hardware
- Sets of application software modules
- A proper organizational context

24.2.2   Computer Hardware

The general hardware components of a geographical information system are – the main computer system or the central processing unit (CPU) and the peripherals namely, the terminal – keyboard and visual display unit (VDU), digitizer/scanner, disk drive, tape drive, plotter, printer, etc.

24.2.3   Software Modules

The software package for a GIS consists of five basic technical modules:

- Data input, editing and verification
- Data storage and database management
- Data analysis, modeling, and cartographic manipulation
- Data output and presentation
- User interface/interaction

24.2.3.1   Data Input, Editing and Verification

Data for input are acquired in a variety of formats including graphic, descriptive (nonspatial information or attribute), and digital imagery (satellite data). All these data require manual or automated preprocessing such as, format conversion, error detection and editing, and edge matching and registration, prior to encoding. Data input covers all aspects of data transformation.

24.2.3.2   Data Storage and Database Management

Data storage and database management is concerned with the way the data are structured and organized, both with respect to the way they should be handled in the computer and, as prescribed by the users. Data management allows a database

to be used through a combination of hardware and software facilities and operations. It is designed to provide the following:

- Effective data storage, retrieval, and updating facilities
- Multiuser environment
- Data independence, security, and integrity

24.2.3.3 Data Analysis, Modeling, and Cartographic Manipulation

One of the most important characteristics of GIS is the capability for data analysis and spatial modeling. Conventional GIS analysis and manipulation capabilities include map overlaying, reclassification procedures, proximity analysis, buffering and corridoring techniques, network analysis, and other cartographic modeling tools, computed as a function of independent values associated with that location on two or more existing maps.

24.2.3.4 Data Output and Presentation

Data output and presentation concern the way the data have to be displayed and the results of the analyses reported to the users. The data may be presented in a variety of ways, such as maps, tables, and figures (graphs and charts). But most users of GIS seem to favor the output that is similar to a conventional map.

24.2.4 Spatial Data Models and Structures

Unlike many other kinds of data handle routinely by modern information systems, geographical data are complicated by the fact that they must include information about position, possible topological connections, and attributes of the objects recorded. All geographical data can be reduced to three basic topological concepts: the point, the line, and the area. Every geographical phenomenon can in principle be represented by a point, line, or area plus a label saying what is it.

24.3 Sensors and Satellites

24.3.1 Sensors

A sensor is a device comprising of optical component or system and a detector with electronic circuitry. All sensors employed on earth observation platforms use electromagnetic radiation (EMR) to observe the terrain features. The entire electromagnetic spectrum (EMS) is divided into different wavelength regions, which are broadly known by different names, viz., cosmic rays, rays, x-rays, ultraviolet, visible, near infrared (NIR), short-wave infrared (SWIR), middle infrared (MIR), thermal infrared (TIR), microwave (MW), etc.

The detecting media (sensors) commonly used for earth resources monitoring may be broadly divided into: (1) The Photographic Camera, (2) The Vidicon Television Camera, (3) The Optical Scanner, (4) The Microwave Radiometer, and (5) The Microwave Rader 2.0. The two broadest classes of sensors are passive, where energy comes from an external source and active, where energy generated from within the sensor system is beamed outward, and the fraction returned is measured. The following section will give an overview of available sensors.

24.3.1.1   Example of Sensors

Photographic Camera

The detecting medium used in the photographic camera is a film similar to that used in the normal photography. The only difference in remote sensing photography is in imaging the objects in specific spectral bands of interest. However, there are certain drawbacks with the photographic remote sensing. Firstly, the film sensitivities are limited only to a particular wavelength region and secondly, in retrieving the exposed films from long-term unmanned space platforms. But the photographic camera is undoubtedly an operationally attractive sensor for short-term manned space platforms. Photographic quality is invariably taken as a standard by which the performance of other imaging systems is judged.

Vidicon Television Camera

The television type camera generally favored for orbital remote sensing is based on the return beam vidicon (RBV) tube. It employs a lens and a shutter similar to those of a photographic camera to form an image at the focal plane of the system. Instead of being formed on a film the image forms on an electrically charged photosensitive tube causing changes in the electrical charge of the tube. A beam of electrons from an electron gun smartly scans the tube in a raster pattern of parallel lines similar to that of television screen. The electron beam, which returns from the tube to detector, changes in intensity proportional to the electrical charge of the image on the tube. This can be digitized and recorded on-board or transmitted to ground receiving stations where it is recorded on a magnetic tape. After the image is scanned and transmitted, the tube is electronically erased and is ready to receive the next image. The recorded images are played back onto film to produce black and white images.

Television systems have been used successfully in many space projects, namely, TIROS, NIMBUS, SALYUT, MARINER, APOLLO, BHASKARA, and LANDSATS 1–3.

Optical Scanner

Instead of recording the whole scene by one single instantaneous exposure as is the case with the photographic camera and with the vidicon system, it is possible to

record sequentially the area elements of the scene as narrow shivers and to produce a complete image from these area elements. If the area elements are made very small and if this sampling process is performed in space as well as in time in a very regular manner, it is called scanning. An orbiting infrared radiometer whose photo-electric detector receives focused EMR through a telescope system from a small area element width (ground resolution element) and which scans optically in the Y direction will produce a video signal representing a rectangular image matrix. A multispectral scanner (MSS) may, therefore, be regarded as selective scanning radiometer. A few such optical scanners are described with reference to satellites such as LANDSAT, SPOT, and IRS NOAA.

Optical Mechanical Scanners

Multispectral Scanner Subsystems (MSS): All the five LANDSATs carried MSS and TM sensors operating in this mode. MSS has a cross-track scanning system with a rotating mirror that scans the earth over a 11.56°. Field of view to give a swath 185 km wide normal to the orbit path from an altitude of 918 km is shown in Fig. 1.4 in the case of LANDSAT 1–3. While the LANDSATs 4 and 5 were placed at an altitude of 705 km with a scan angle 14.9° to sweep the same 185 km swath. The ground resolution cell (pixel) 79 × 79 m remains the same in all the LANDSATs.

The emery reflected from each such ground resolution cell after passing through a set of lenses and fillers is sensed by the detectors, which convert that energy into electrical signals for recording and transmission as image data to a ground receiving station where the data are recorded on magnetic tapes. In MSS, the image data are acquired only during east-bound mirror sweep as continuous strip of scan lines along the orbit path. Such a data strip is divided into image scenes, each scene covering a 185 by 185 km area on the ground during the playback of the data tape at the ground station. Successive scan lines are offset (skewed) to the west to compensate for the Earth's rotation. Orbit of LANDSATs 1–3 provided complete earth coverage in 18 days, whereas orbit of LANDSATs 4 and 5 provides in 16 days.

Thematic Mapper

Thematic mapper (TM) is also a cross-track scanner similar to MSS with a bidirectional oscillating scan mirror and arrays of detectors. But TM is an improvement over MSS in the following respects.

Push Broom Scanners

The "push broom" or linear array scanner is technologically one step ahead of the optical mechanical scanner of the MSS or TM type. While the across-track data collection is effected mechanically by a rotating or oscillating mirror in MSS and

TM in case of push broom scanner, there is an array of detectors (for each band) "viewing" the entire swath simultaneously. Thus, there is no moving part in the sensor of the latter, which improves its reliability emanated from the much larger integration time.

24.3.1.2   Satellites

Satellites are those robots, which carry sensors. Examples of some popular satellites carrying some popular sensors are given below.

SPOT-HRV

Push broom type of scanner is first used on SPOT and then on IRS. SPOT employs High Resolution Visible (HRV) imaging system. The HRV system operates in either multispectral mode or a high-resolution panchromatic mode. The 6,000 CCD (charge coupled detector) array of the high-resolution mode have a 10 by 10 m ground resolution cell and record a single panchromatic image in the 0.51–0.73 μm spectral band. The multispectral mode of HRV employs three arrays of 300 CCDs with a ground resolution cell of 20 by 20 m. The multispectral mode records green, red, and reflected IR images. In either mode, the HRV ground swath is 60 km wide. Spot employs two HRV systems that may be operated in the nadir position to acquire parallel strips of imagery with a total of 117 km (including 3 km side lap).

   An innovation in SPOT is the off-nadir viewing capability. The mirror is tilt up to 27° on either side (in 45 steps each of 0.6°) to obtain image strips at distances up to 475 km away from the nadir. Because of greater viewing distance at the extreme angles, the ground resolution cells are larger and the coverage is up to 80 km wide (in place of nominal 60 km). Off-nadir viewing provides considerable flexibility in scheduling times of image acquisition. Without this capability an orbit path would be revisited at 26 days intervals.

   SPOT's capability to image the same from several orbits during a 26-day cycle is illustrated. Localities at the equator can be imaged seven times during a cycle whereas those at latitude 45° can be imaged 11 times. Repeated off-nadir viewing of ground swath produces overlapping image pairs that are suitable for stereoviewing. The base to height ratio is determined by the distance between the two satellite positions divided by the altitude (832 km). At 24° tilt to both East and West, the base to height ratio becomes 1. For a strong relief perception the base to height ratio should be around 0.25.

IRS-LISS

The Indian remote sensing (IRS) satellite IRS-1A & 1B employs two different Linear Imaging Self-Scanning Sensors (LISS) cameras each with 2,048 detectors arranged in the form of linear arrays, which are based on the push broom scanning concept.

LISS-I is single low-resolution camera giving a swath width of 148 km and a spatial resolution of 72.5 m. LISS-II has two cameras aligned in parallel to give the same swath width but at an improved spatial resolution of 36.25 m. Four similar spectral bands have been chosen for both the cameras in the wavelength range 0.45–0.86 μm. At present there is a battery of satellites under IRS series, viz., IRS-1B, -1C, P2, and P3 with much improved spatial resolution (up to 5.8 m in IRS-IC Pan – World's finest civilian resolution till date) and spectral resolution (up to 10 nm width with 13 channels in IRS-P3 MOS-B sensor).

INSAT-VHRR

Very High Resolution Radiometer (VHRR): A two channel VHRR is employed on INSAT-I for meteorological earth observations. It operates in the visible (0.55–0.75 μm) and infrared (10.5–12.5 μm) wavelength region with a spatial resolution of 2.75×2.75 km and 11×11 km, respectively. The VHRR on the proposed INSAT-II will have an improved spatial resolution of 2 km in visible and 8 km in infrared ranges. Insat satellite takes about 23 min to scan a 20° by 20° by 20° coverage of the Earth.

NOAA-AVHRR

Advanced Very High Resolution Radiometer (A VHRR): The A VHRR flown on NOAA satellites has five spectral channels on visible and four on infrared, with a capability to acquire data in the morning and afternoon of a day at each location. There are many such scanners employed on various satellites (NIMBUS, GOES, METEOSAT, etc.) with similar spectral bandwidths and varying swath widths.

Microwave Radiometers

The microwave radiometer operating in millimeter and centimeter wavelength bands is a passive radiometer, which intercepts the earth's electromagnetic waves by means of large aperture directional antenna. The various frequencies used in microwave remote sensing are listed in addition to the frequency band designation and corresponding wavelengths ranges.

The advantage of microwave radiometry over the infrared and other radiometry is the fact that the microwave windows remain largely 'clear' even in the presence of clouds.

Microwave Radar

Radar systems provide their own 'illumination' and record the radar returns from the ground and are active systems. The high degree of control over the illumination and the fact that is based on a single frequency as compared with frequency bands used

by passive systems makes radar a potentially more accurate system for surfacial target recognition. The type of imaging radar generally considered for 'earth observation work' is the side looking (SL) radar. There are two types of radars: real aperture and synthetic aperture. The relatively coarse resolution of a real, short antenna can be considerably improved by synthesizing longer antenna to create a synthetic Aperture Radar (SAR). This is accomplished by storing over a time period, both the outgoing and returning radar wave field in their space–time frame.

Microwave reflectance is determined by the complex dielectric constant and surface roughness of the target. For a target which is a poor conductor (i.e., partially translucent for microwaves) this constant is low, which means that reflection does occur at various depths below the surface. However, the penetration depth depends also on the wavelengths.

Shuttle Imaging Radar

Shuttle Imaging Radar (SIR) flown on the US space shuttle missions, for example, was employed to exploit the capability of radar signals in penetrating surface materials.

LANDSAT Satellite

On July 23, 1972, the first Earth Resources Technology Satellite, now called as LANDSAT, was launched. The satellite's prime remote sensing devise are the vidicon TV-type cameras operating in three separate visible wavelength bands, and an optical multispectral scanning system providing four wavelength bands of information in the visible and near infrared portion of the spectrum. The satellite operates in a polar orbit about 912 km above the Earth and circles the Earth every 103 min completing 14 orbits a day with repetitive coverage of 18 days. LANDSAT 4/5 fly on their nominal orbital altitude of 705 km and both equatorial crossing time and cycle repetitive coverage are maintained at 9.45 h and 16 days, respectively. LANDSAT-MSS was carried by all the five LANDSAT satellites and it has a cross-track scanning system by LANDSAT-TM, which is also a cross-track scanner similar to MSS with a bidirectional oscillating scan mirror and arrays of detectors. Some of the improvements of LANDSAT-TM over LANDSAT-MSS are having seven spectral bands and extended spectral range in the visible and reflected IR region, improved detector sensitivity and radiometric resolution, and also presence of Thermal IR band with 120 m resolution.

24.3.1.3 Indian Remote Sensing (IRS) Satellites

The advantages of satellite remote sensing has so far been harnessed for survey and mapping and it is now being explored for monitoring natural resources on

real-time basis. The unique capability of remote sensing technology is mainly due to a wide range of information available from electromagnetic spectrum, synoptic view, frequent repetitively, multispectral mode of data coupled with real-time data acquisition and dissemination. In view of these added advantages, the technology becomes an inevitable tool in the sustainable development and utilization of our natural resources.

The remote sensing program was initiated in India in the year 1970 when aerial surveys were conducted using a Hasselblad camera to obtain infrared imagery to study coconut wilt disease in Kerala. Indian space scientists took advantage of 'LANDSAT' system, which was made available by the USA, and developed ground stations and analysis capabilities to make full use of data from these satellites. Before venturing on our own operational remote sensing satellite system, like Indian Remote Sensing satellite (IRS), ISRO embarked on two experimental remote sensing mission's, viz., Aryabhata and Bhaskara.

Aryabhata was the first experimental satellite that was successfully launched in April 1975 in an approximately 600 km orbit above the Earth, with the help of Soviet intercosmos rocket. The orbit was inclined at about –50° to the polar axis. It provided the opportunity to set up ground-based receiving, transmitting, and tracking systems. This satellite functioned for 6 years providing confidence in indigenous design and fabrication of space-worthy satellites, and also to evolve the methodology of conducting a series of complex operations.

Bhaskara-I satellite was launched with Soviet assistance on June 7, 1979, mainly as an earth observation experiment to collect, process, analyze, and disseminate data on hydrology, forestry, and geology using two television cameras. Its life was for 1 year.

Bhaskara-II was launched on November 20, 1981 with Soviet assistance. It was a non-sun synchronous satellite; the data over a particular region was not acquired at the same local time in repeated orbits, thus resulting in a wide variation in the solar illumination angle. This introduces radiometric variations which may pose difficulties in the analysis and utilization of multiitem portal data. At the end of 2 years this satellite had completed 11,000 orbits around the earth.

Bhaskara-III TV payload system consists of two TV cameras, one operating in the 0.54–0.66 μm band and the other in 0.75–0.85 μm band. Each picture frame covers an area of 340 × 340 km with a ground resolution of 1 km and a typical overlap of 10% between successive picture frames. Although the Bhaskara TV payload capabilities were very coarse compared to the remote sensing satellites available at that time, Bhaskara program gave tremendous experience in organizing space-based remote sensing system.

Remote sensing satellite IRS-1A was launched on March 17, 1988 from Baikanur consmodrome in then USSR. This 975-kg satellite circles the globe at an altitude of 904 k in a polar sun-synchronous orbit, crosses the equator at 10:25 hour local time and returns to its original orbital trace every 22 days enabling repetitive collection of data over the same area at the same local time. Where it passes over India, the satellite images about 148-km wide strip of the country in the so-called push-broom mode. As the orbital period of IRS-1A is 103 min the satellite

completes 14 orbits in a day. The satellite path over India shifts day 1.17° of longitude to the west every day for the satellite to cover the entire Indian subcontinent. After conducting a series of application projects, the best spectral bands to discriminate different classes were found as similar to the first four spectral bands of Thematic Mapper. Various combinations of the below-mentioned bands (which were adopted in LISS-I and LISS-II cameras of IRS) provide information for specific themes.

Band 1 – (0.45–0.52 µm): A strong relationship exists between spectral reflectance in this regions and plant pigment. Comparatively higher penetration in water. This band is useful for mapping suspended sediments/water quality and various studies related to coastal region.

Band 2 – (0.52–0.59 µm): It is useful for vegetation discrimination and allows for study of senescence rate of leaves. Also sensitive to iron oxides.

Band 3 – (0.62–0.68 µm): It is centered around the chlorophyll absorption band of vegetation, and useful for identification of plant species.

Band 4 – (0.77–0.86 µm): Shows high reflectance for healthy vegetation and is useful for green biomass estimation, crop vigor studies, etc. Water absorption in this region clearly demarcates land and water boundary.

LISS

LISS-I Camera has spatial resolution of 72.5 m having a swath of 14.48 km. The two cameras of LISS-II, LISS-IIA, and LISS-IIB, with spatial resolution of 36.25 m and a swath of 74.24 km provide a combined swath of 145.45 km allowing a 3-km overlap. The IRS-IB was launched on August 29, 1991 to give back up to IRS-1A. It carried identical payloads as that of IRS-IA, IRS-1A, and IRS-1B, and together provide us a revisit to the same area every 11 days.

IRS-1C-D

The second-generation Remote Sensing Satellites are IRS-1C and IRS-1D; IRS-1C has been successfully launched on December 7, 1995 and put into polar sun-synchronous orbit at an altitude of 817 km. The most important improvements are that it can have a revisit capability of 5 days, a high-resolution panchromatic camera system giving around resolution of 5.8 m. Apart from improving the spatial and temporal resolution, off-nadir viewing helps a revisit frequency of 5 days, which can provide stereoimages. A payload steering mechanism supports and rotates the PAN camera to a predetermined angle in the pitch-yaw plane with the maximum scan range being ±26. This corresponds to an off-nadir coverage of ±398 km on the ground.

The wide Field Sensor (WIFS), with a ground swath of 770 km and resolution of 188 m, enables the dynamic monitoring of natural resources and observed the same region once in every 5 days. It has red and infrared bands, which are useful in generating vegetation indices.

IRS-P2

With the successful launch of PSLV-D3 on March 21, 1996 from Sriharikota Range (SHAR), AP, IRS-P2, a 922-kg remote sensing satellite was put in to a 817-km polar sun-synchronous orbit with equatorial crossing at 10:30 hours. This satellite has similar LISS-II cameras as that of IRS-1A and 1B, orbits at 817 km, with a revisit capability of once in 24th day, providing a ground resolution of 33–37 m in four spectral bands.

IRS-P2 has two remote sensing payloads and a payload for x-ray astronomy. The WIFS payload is similar to that of IRS-IC but with an additional short wave infra-red (SWIR) band. This band is sensitive to moisture content in vegetation, provides data for crop condition assessment, and has applications like snow and cloud cover differentiation, snow-melt runoff studies, flood damage assessment, and geology.

The IRS-P3 remote sensing payload is a Modular Opto electronic Scanner (MOS) of the German space agency, DLR. MOS has 18 spectral bands. Data from this are primarily used in ocean-related studies, chlorophyll mapping for biomass estimation, coastal water discrimination, sediment transport, and ocean dynamics. The capability of different satellites, viz., BHASKARA, LANDSAT, SPOT, and IRS are given in Tables 1 and 2 and scanning techniques used for LANDSAT and SPOT and revisit/stereo capability of SPOT are also shown in Figs. 1–6 for reference.

24.4   Interpretation of Remotely Sense Data

Data interpretation aspects of remote sensing can involve analysis of pictorial (image) and/or numerical data. Visual interpretation of pictorial image data has long been the workhorse of remote sensing. Visual techniques make use of the excellent ability of the human mind to qualitatively evaluate spatial patterns in a scene. Visual interpretation techniques have certain disadvantages, however, in that they may require extensive training and are labor intensive. In addition, spectral characteristics are not always fully evaluated in visual interpretation efforts. In applications where spectral patterns are highly informative, it is, therefore, preferable to analyze numerical, rather than pictorial image data. In this case, the image is described by a matrix of numerical brightness (radiometric) values covering the scene. The values may be analyzed by quantitative procedures employing a computer.

The use of computer-assisted analysis techniques permits the spectral patterns in remote sensing data to be thoroughly examined. It also permits the data analysis process to be largely automated, providing cost advantage over visual interpretation techniques in some cases. However, just as humans are limited in their ability to interpret spectral patterns, computers are limited in their ability to evaluate spatial patterns. Therefore, visual and numerical techniques are complimentary in nature and consideration must be given to the approach that best fits a particular application.

24.4.1   Soil

The soil curve shows considerably less peak and valley variations in reflectance. That is, the factors that influence soil reflectance act over leas spectral bands. Some of the factors affecting soil reflectance are moisture content, soil texture (proportion of sand, silt, and clay), surface roughness, the presence of iron oxide, and organic matter content. These factors are complex, variable, and interrelated. For example, presence of moisture in soil will decrease its reflectance. Soil moisture content is strongly related to the soil texture: coarse sandy soils are usually well drained resulting in low moisture content and have relatively high reflectance; poorly drained fine-textured soils will generally have lower reflectance. Two other factors that reduce soil reflectance are surface roughness and the content of organic matter. The presence of iron oxide in a soil will also significantly decrease reflectance at least in the lower part of visible wavelength.

24.4.2   Water

Considering the spectral reflectance of water, probably the most distinctive characteristic is the energy absorption at reflected infrared (also known as near-infrared) wavelengths. In short, water absorbs energy in these wave lengths. Locating and delineating water bodies with remote sensing data is done most easily due to its reflected infrared absorption property. However, various conditions of water bodies manifest themselves primarily in visible wavelengths. The energy–matter interactions at these wavelengths are very complex and depend on a number of interrelated factors. For example, the reflectance from a water body can stem from an interaction with the water's surface (specular reflection), with material suspended in the waters or with the bottom of the water body. Clean water absorbs relatively less energy having wavelength less than about 0.6 μm. However, as the turbidity changes (because of the presence of organic and inorganic materials) transmittance – therefore reflectance – changes dramatically. For example, water containing large quantities of suspended sediments resulting from soil erosion normally has much higher visible reflectance than other 'clean' water in the same geographical area.

24.4.3   Vegetation

Spectral reflectance curve for healthy green vegetation almost always manifest the 'peak and valley' configuration. The valleys in the visible portion of the spectrum are dictated by the pigments in plant leaves. Chlorophyll, for example, strongly absorbs energy in the wave length bands centered at about 0.45 and 0.65 μm. Hence, our eyes perceive healthy vegetation as green in color because of the very

high absorption of blue and red energy by plant leaves and the very high reflection of green energy. As we go from the visible to the reflected infrared portion of the spectrum beyond 0.7 μm the reflectance of healthy vegetation increases dramatically. In the range from about 0.7 to 1.3 μm, a plant leaf reflects about 50% of the energy incident on it. Plant reflectance in 0.7–1.3 μm range results primarily from the internal structure that is highly variable between plant species. Reflectance measurement in this range often permits us to discriminate between species, even if they look the same in visible wave lengths. Beyond 1.3 μm, energy incident upon vegetation is essentially absorbed or reflected, with little to no transmittance of energy. Dips in reflectance occur at 1.4, 1.9, and 2.7 μm because water in the leaf absorbs strongly at these wave lengths.

24.5   Global Positioning Satellites

An extraordinary geographic locating technology available to everyone – including the "man in the street" – is the Global Positioning System (GPS) operated by the US Department of Defense. US government policy has made this satellite system available for civilian use – hence GPS has become almost routine in daily use by anyone. This system utilizes 24 (21 active; three as spares) small satellites each transmitting radio signals at the same two frequencies (L1 = 1,575.4 MHz; L2 = 1,227.6 MHz). Each satellite follows a circular orbit inclined to 55° to the equator at an altitude of 20,200 km. This constellation of satellites is placed, four each, within six orbital planes spaced 60° apart.

Location is established by pseudoranging, which determines distance to each satellite (which transmits its own unique identification as a pseudo-random-noise [PRN] code) by analyzing the radio signals that travel at the speed of light. The signal contains modulated time-tagged data bits that permit transmission (hence travel) times to be determined as the difference between time of origin and time of arrival. To establish ground location a variant of the classical triangulation method used in surveying is applied, as indicated by this diagram.

If signals from just three satellites are received, the location solution involves two possible points – one correct, and the other false. To resolve this positional dilemma, a signal from a fourth satellite provides a solution that is unique. The position of each satellite must be closely fixed at any moment by knowing its ephemeris (orbital parameters that determine where a satellite is relative to some ground reference), which can be calculated from signals sent to a network of control stations. There must also be high precision atomic clocks (two each of cesium and rubidium) on the satellite and a corresponding clock in any ground receiver whose location is desired. Electronics and computer processing at the receiver facilitate calculation of Coordinated Universal Time (UTC) (effectively, Greenwich Mean Time), which can then be adjusted to GPS Time, so that time differences between corresponding signals from the several satellites can be determined with high exactitude.

24.6   Aerial Photography

Aerial photographs have been a main source of information about what is at the Earth's surface almost since the beginning of aviation more than 100 years ago. Until space imagery, aerial photos were the principal means by which maps are made of features and spatial relationships on the surface. Cartography, the technology of mapping, depends largely on aerial/satellite photos/images to produce maps in two dimensions or three (see next section). Aerial photos are obtained using mapping cameras that are usually mounted in the nose or underbelly of an aircraft that then flies in discrete patterns or swathes across the area to be surveyed.

An aerial photo is just a black and white (b & w) or color "picture" of an area on the Earth's surface (plus clouds), either on print or in a transparency, obtained by a film or digital camera located above that surface. This camera shoots the picture from a free-flying platform (airplane, helicopter, kite, or balloon) some preplanned distance above the surface. Two types depend on the angle of view relative to the surface. The first, oblique photography snaps images from a low to high angle relative to vertical. Among the most obvious features in a photograph are tones and tonal variations (as grays or colors) and patterns made by these. These, in turn, depend on the physical nature and distribution of the elements that make up a picture. These "basic elements" can aid in identifying objects on aerial photographs.

24.6.1   Tone (Closely Related to Hue or Color)

Tone refers to the relative brightness or color of elements on a photograph. It is, perhaps, the most basic of the interpretive elements because without tonal differences none of the other elements could be discerned.

24.6.2   Size

The size of objects must be considered in the context of the scale of a photograph. The scale will help you determine if an object is a stock pond or Lake Minnetonka.

24.6.3   Shape

The shape refers to the general outline of objects. Regular geometric shapes are usually indicators of human presence and use. Some objects can be identified

almost solely on the basis of their shapes: for example, the Pentagon Building (American) football fields, cloverleaf highway interchanges

24.6.4 Texture

The impression of "smoothness" or "roughness" of image features is caused by the frequency of change of tone in photographs. It is produced by a set of features too small to identify individually. Grass, cement, and water generally appear "smooth," while a forest canopy may appear "rough."

24.6.5 Pattern (Spatial Arrangement)

The patterns formed by objects in a photo can be diagnostic. Consider the difference between (1) the random pattern formed by an unmanaged area of trees and (2) the evenly spaced rows formed by an orchard.

24.6.6 Shadow

Shadows aid interpreters in determining the height of objects in aerial photographs. However, they also obscure objects lying within them.

24.6.7 Site

The site refers to topographic or geographic location. This characteristic of photographs is especially important in identifying vegetation types and landforms. For example, large circular depressions in the ground are readily identified as sinkholes in central Florida, where the bedrock consists of limestone. This identification would make little sense, however, if the site were underlain by granite.

24.6.8 Association

Some objects are always found in association with other objects. The context of an object can provide insight into what it is. For instance, a nuclear power plant is not (generally) going to be found in the midst of single-family housing.

24.7   Application of Remote Sensing and GIS in Hydrology

24.7.1   Catchment Delineation

Water balance of wetlands within lowland floodplains is strongly influenced by the temporally variable spatial extent of the interactions between groundwater and surface water. A robust algorithm will be introduced, which makes it possible to delineate the interaction zone between the lowland river and the floodplain. This interaction zone is specified as the "Direct Catchment" which is defined by the part of the connected floodplain in which wetland water balance is mainly affected by the surface water dynamics of the adjacent river. The delineation algorithm is based on transfer functions, which were assessed by local simulation results of the integrated water balance and nutrient dynamics model IWAN. The transfer functions are further determined by mean annual groundwater depths and by simulated groundwater dynamics. They are controlled by simulation results of the maximal transversal extent of surface water influence on groundwater stages. The regionalization of the developed delineation algorithm leads to the specification of the maximal extent of groundwater – surface water – interaction processes along the river. By application of this approach to the Havel River basin, located within lowlands of Northeaster Germany, it was possible to specify a 998.1 km^2 part of the floodplain, which is directly connected with the surface waters and thus called the "Direct Catchment" of the Havel River. The IWAN model was applied to simulate the water balance of the floodplain. The simulation results prove the tight interaction between river and floodplain. It is shown that the spatially and temporally variable influences of the connected floodplain on the river discharge were only important during low discharge in summer (Lu et al. 1989).

A GIS map showing the approximate groundwater flow routes within the karst aquifer in the vicinity of Bowling Green, Kentucky was prepared based upon dye tracing, cave mapping, cave locating by microgravity and electrical resistively, and water table measurements. The research was performed by the faculty, professional staff and students of the Center for Cave and Karst Studies from 1976 to the present and was directed by Nicholas Crawford. The numerous dye traces are shown as red lines with arrows on the map. Water table elevation contours are shown as blue lines. They were estimated from measurements taken at water wells and storm water drainage wells that are only cased to bedrock and then extend as open holes below the water table, cave streams, springs, and perennial surface streams. The approximate groundwater basin catchment boundaries, based upon dye traces and water table elevations, are shown as dashed green lines. The map identifies the approximate groundwater flow routes to springs and the approximate groundwater basin catchment areas for (1) Lost River Rise, (2) Graham Springs, (3) Hobson Grove Springs, (4) Double Springs, (5) Mt. Ayr Blue Hole and Bluff Springs, and (6) Harris Spring. Included on the map are dye traces and water table contours northeast of Barren River. This compilation of karst groundwater data into one map was prepared to assist the

City of Bowling Green in meeting the US Environmental Protection Agency Phase II Storm Water Management Plan requirements and to assist Bowling Green with emergency response to any future spills of hazardous liquids (Dong and Wanchang 2006).

24.7.2 Distributive Modeling

Watersheds may be modeled by a lumped model using basin average input data and producing total basin stream flow. Such a model may produce reasonable result but because of the distributed nature of hydrological properties like soil type, slope, and land use, the model cannot be expected to accurately represent the watershed conditions. For connection of topography, the computer-based methodology known as Geographic Information System (GIS) is quite good to cover the link between the topographic land use and other information related to geographical location. It is applied to a hydrologic system to assess the impact due to land-use change. Remote sensing technique, because of its capability of synoptic viewing and repetitive coverage, provides useful information on land-use dynamics. With the development of GIS, the hydrological catchment models have been more physically based and distributed considering spatial heterogeneity. The purpose of this study is to develop a spatially distributed hydrological model using remote sensing and GIS, which can be used to assess the runoff changes due to land-use changes.

The SCS-CN method is the most popular method for computing of surface runoff for rainfall event. This approach involves the use of simple empirical formula and readily available tables and curves. It is the only method, which can incorporate the land use for computation of runoff from rainfall. It provides a rapid means for estimating runoff change due to land-use change. The method continues to be most satisfactory when used for different types of hydrologic problems that were designed to solve evaluating the effects of land-use changes. The GIS and SCS-CN method were combined to the model rainfall–runoff relations and the watershed parameters were estimated while computation of other parameters required significant user interaction. Purwanto and Donker proposed semidistributed hydrologic modeling using SCS-CN method and assessed the effect of land-use change for hypothetical cases of reforestation and deforestation conditions. When hypothetical case of 5% reforestation or deforestation conditions are considered, the peak flow was reduced by 14% for reforestation and increased by 12% for deforestation case for hydrologic soil group C when compared to normal land use. Kite and Kouwen developed a lumped hydrologic model for computing rainfall–runoff and snowmelt processes separately from different land cover classes. They found that using a semidistributed model results in better goodness of fit than the lumped basin approach. Schumann developed a conceptual semidistributed hydrological model using GIS for a limited consideration of spatial heterogeneity described by area distribution function of the hydrological characteristics and successfully applied for estimation of model parameters (Shrestha 1985).

Urbanization has evolved to become one of the main driving forces of anthropogenic-related environmental change. Urbanization modifies many natural processes, starting from the local level (runoff, pollution loading, erosion, etc.) and to the global (surface albedo, climate). In this chapter we describe an integrated GIS-based model for complex analysis of regional environmental changes driven by land-use change in the Upper Wabash River basin. Varied spatial scales of model components produced additional challenges. The model was designed to eventually become the core of a decision support system with the goal to assist in making informed decisions on urban development (Ajami et al. 2006).

24.7.3   Identification of Hydrological Representative Unit (HRU)

The fundamental objective of hydrological modeling is to gain an understanding of the hydrological system in order to provide reliable information for managing water resources. Hydrological models have become more physically based and applied in spatially distributed input to reflect heterogeneous and complex basin structures and the various interactive processes controlling basin response. In the case of distributed modeling, there are several ways of representation of catchment based on land use, flow configuration, etc., such as square grids, nonrectangular grids, or by subcatchments. In all these representations, there exists variability of the hydrologic behavior within each unit. With the introduction of hydrologic response unit (HRU), it is possible to expect similar hydrologic behavior in each unit, which can be modeled easily. An attempt has been made in this study to delineate HRUs in a basin, which has high spatial heterogeneity. Using basin characteristics such as physiography, land use, soil, elevation, and slope in a Geographic Information System, HRUs are delineated in Nagwan basin in India. The hydrologic behavior of these HRUs is also discussed based on basin characteristics, which can be used in a physically based or conceptual hydrologic model to simulate runoff (Ajami et al. 2004).

The responses of ADAPT, a daily water table management simulation model, to variations in the principal input parameters, which define hydrologic response units on a watershed were evaluated. The study was conducted on a small agricultural watershed in Ohio. The results suggest that useful estimates of monthly flows could be obtained by using NRCS soils information, land use, and tillage information estimated from LANDSAT-TM data, a 30-m digital elevation model, and readily available information on the prevailing farming systems. Water quality and quantity responses were sensitive to combinations of the slope, soil type, land use, tillage, crop rotations, and drainage practice, and should be taken into account in defining the hydrologic response units. The sediment load predictions were sensitive to the field size. Approximations of when planting occurred did not affect the flow and sediment predictions, but had an impact on nitrate and pesticide predictions (Guo et al. 1995).

References

Ajami NK, Gupta H, Wagener T, Sorooshian S (2006) Calibration of a semi-distributed hydrologic model for streamflow estimation along a river system. J Hydrol 329(1–2):174–185

Ajami NK, Gupta H, Wagener T, Sorooshian S (2004) Calibration of a semi-distributed hydrologic model for streamflow estimation along a river system. Retrieved from http://www.sciencedirect.com/science/journal/00221694 on May 20, 2009.

Dong Z, Wanchang Z (2006) Distributed hydrological modeling study with the dynamic water yielding mechanism and RS/GIS techniques. Retrieved from http://adsabs.harvard.edu/cgi-bin/nph-abs.html on May 20, 2009

Guo S, Wang J, Yang J (1995) A large scale and semi-distributed hydrological model and its application in the Ganjiang river basin. College of Water Resources and Hydropower, Wuhan University, Wuhan, 430072, China

Lu M, Koike T, Hayakawa N (1989) A distributed hydrological modeling system linking GIS and hydrological models. Retrieved from http://lmj.nagaokaut.ac.jp/~lu/publ/96HGIS/node1.html on May 20, 2009

Shrestha MN (1985) Spatially distributed hydrological modelling considering land-use changes using remote sensing and GIS. Retrieved from http://www.gisdevelopment.net/application/nrm/overview/ma03041abs.htm on May 20, 2009

Short NM (2009) Remote Sensing Tutorial, NASA. Retrieved from http://rst.gsfc.nasa.gov/Intro/Part2_1.html on June 2009

Chapter 25
An Introduction and Current Trends of Damodar and Rupnarayan River Network

Mrinmoy Majumder, Pankaj Roy, and Asis Mazumdar

Abstract Rivers are the important primary resource of landed community for their primary sustenance. Losses of navigability, gradient fall within a short distance, deltaic formations in lower reaches, anthropogenic actions or manipulations such as construction of embankments and guard walls, silt depositions or encroachment of river beds, monsoon induced changes, etc., can cause a river to die. As per the current status of West Bengal (Eastern part of India) and Jharkhand rivers, the effect of the creation of reservoirs, industrial extractions, and climate change can be observed easily. Damodar and Rupnarayan river systems are two major river networks of eastern India which are one of the major sources of water for irrigation, agriculture, and industrial purposes of the people living in the river banks. The present note tries to give an overview of the current trends, geomorphological characteristics, and economical resources of the two rivers which can give an idea of the impact of vulnerabilities on the natural water resources of the two catchments.

Keywords Current trends • Jharkhand • rivers • West Bengal

M. Majumder (✉)
Senior Research Fellow, School of Water Resources Engineering, Jadavpur University, Kolkata-700032, West Bengal, India
and
Geo-information Scientist, Regional Center, National Afforestation
and Eco-development Board, Jadavpur University, Kolkata-700032, West Bengal, India
e-mail: mrinmoy@majumder.info

P. Roy
Lecturer, School of Water Resources Engineering, Jadavpur University, Kolkata-700032, West Bengal, India

A. Mazumdar
Coordinator, Regional Center, National Afforestation and Eco-development Board, Jadavpur University, Kolkata-700032, West Bengal, India
and
Director, School of Water Resources Engineering, Jadavpur University, Kolkata-700032, West Bengal, India

The river network of river Damodar flows through Jharkhand and West Bengal, two states of Eastern India whereas Rupnarayan river, with its tributaries and distributaries, flows mainly through West Bengal's south-west region. Both the rivers had their confluence points with river Hooghly which is the downstream of river Bhagirathi, a tributary of river Ganga.

West Bengal is situated within the Himalayas in the north to the Bay of Bengal in the south. The state has a total area of 88,752 km² (34,267 square miles). The Darjeeling Himalayan hill region in the northern extreme of the state belongs to the eastern Himalayas. The narrow Terai region separates this region from the plains, which in turn transitions into the Ganges delta toward the south. The Rarh region intervenes between the Ganges delta in the east and the western plateau and high lands. A small coastal region is on the extreme south, while the Sundarban mangrove forests form a remarkable geographical landmark at the Ganges delta.

The Ganges is the main river, which divides in West Bengal. One branch enters Bangladesh as the Padma or Pôdda, while the other flows through West Bengal as the Bhagirathi river and Hooghly river. The Teesta, Torsa, Jaldhaka, and Mahananda rivers are in the northern hilly region. The western plateau region has rivers such as the Damodar, Ajay, and Kangsabati. The Ganges delta and the Sundarbans area have numerous rivers and creeks.

West Bengal's climate varies from tropical savannah in the southern portions to humid subtropical in the north. The main seasons are summer, rainy season, a short autumn, and winter. While the summer in the delta region is noted for excessive humidity, the western highlands experience a dry summer like northern India, with the highest day temperature ranging from 38°C (100°F) to 45°C (113°F). At nights, a cool southerly breeze carries moisture from the Bay of Bengal.

The state of West Bengal is primarily inhabited by rural population. The rural economy largely depends on agriculture. It is recorded that nearly 50% of the working people are directly connected with agriculture. Of these, nearly 27% represent large, medium, or small farmer communities while the rest act as agricultural farm laborers. Of the 8,684,000 hectares of total area, nearly 67% are cultivable. The intensification of cropping in the agricultural sector in West Bengal has placed the state above others during the last decade. The cropping intensity in 1994–1995 stood at 163. Although the agricultural productivity of the state is higher than any other states of India, due to urbanization, the net-cropable land area has decreased rapidly in most of the districts of the state (Ghosh 1998).

The river network of Rupnarayan, such as Dwarakeshwar, Gandheswari, Silai, etc., lies entirely on the state of West Bengal. The river networks of river Damodar enters West Bengal through Kulti and meets with river Rupnarayan at Gadiara. The upsream of the Damodar river is entirely situated in the state of Jharkhand.

Most of the Jharkhand state lies on the Chota Nagpur Plateau, which is the source of the Koel, Damodar, Brahmani, Kharkai, and Subarnarekha rivers, whose upper watersheds lie within Jharkhand. Major part of the state is still covered by forest. Forest preserves support populations of tigers and Asian Elephants. Soil content of the state mainly consists of soil formed from disintegration of rocks and stones, and soil composition is further divided into:

1. Red soil, found mostly in the Damodar valley, and Rajmahal area
2. Micacious soil (containing particles of mica), found in Koderma, Jhumeritilaiya, Barkagaon, and areas around the Mandar hill
3. Sandy soil, generally found in Hazaribagh and Dhanbad
4. Black soil, found in Rajmahal area
5. Laterite soil, found in western part of Ranchi, Palamu, and parts of Santhal Parganas and Singhbhum

Jharkhand Rivers are divided into two parts: rivers flowing from the southern part of the Chotanagpur plateau and the rivers flowing from the Chotanagpur plateau towards the north. It goes without mention that the river Ganges is one of the most important rivers of Jharkhand: the other rivers in Jharkhand flow as tributaries to the river Ganga. Some of the rivers at Jharkhand that join the Ganges from the north are Gandak, Ghaghra, Burhi Gandak, Mahananda, Kosi, etc: whereas the rivers that join Ganga from the southern part of the territory are Sakri, Punpun, Karmansa, Phalgu, Kiul, etc. Besides, the river Damodar, known as the 'Dev' river in Jharkhand, is one of the longest rivers at Jharkhand.

Jharkhand is a mineral-rich state. Table 25.1 shows the minerals found and their corresponding rank of production According to the production ranks of the minerals, main income from minerals come from coal, followed by iron-ore and sandstone though the difference between income from coal and iron is over 88% (State Jharkhand 2003)

Jharkhand has a population of 26.93 million, consisting of 13.88 million males and 13.08 million females. The sex ratio is 941 females to 1,000 males. The population consists of 28% tribals, 12% Scheduled Castes, and 60% others. The population density of the state is 274 persons per km^2 of land. However, it varies from as low as

Table 25.1 Table showing the productivity rank of minerals found in the state of Jharkhand

Name of minerals	Productivity rank of minerals
Coal	1
Iron-ore	2
Stone	3
Bauxite	4
Lime stone	5
Brick	6
Dolomite	7
Sand of stowing	8
China clay	9
Copper ore	10
Uranium	11
Quartz/felspar	12
Graphite	13
Pyroxanite	14
Fire clay	15

148 per km² in Gumla district to as high as 1,167 per km² in Dhanbad district. Around 10% of the population is Bengali speaking and 70% speak various dialects of Hindi.

Jharkhand's gross state domestic product for 2004 is estimated at US$14 billion at current prices. The state has a concentration of some of the country's highly industrialized cities such as Jamshedpur, Ranchi, Bokaro Steel City, and Dhanbad. The urbanization ratio of the state is stated to be 42.25% and the per capita annual income is US$ 1,490.

The main sources of irrigation in the state of Jharkhand are through canals (17.53%), ponds (19.07%), groundwater wells (29.38%), and tube wells (8.25%). The district-wise percentage of irrigated land is depicted in Table 25.2. According to the table, Palamu and Dhanbad have the maximum (24.25%) and minimum (2.08%) amount of irrigated land respectively (State Jharkhand 2003).

The river networks of Damodar, comprising river Bokaro and Damodar, is the main source of water which is supplied for irrigation, industry, and domestic purposes. The river had caused 16 major floods in its basin during 1823–1943 though after construction of reservoirs the voracity of flood had reduced but the number of floods had been increased. The river is also plagued by problems of erosion, sedimentation, and pollution. The entire catchment of Damodar River is controlled and managed by the Damodar Valley Corporation. The Rupnarayan river on the other hand was created from the joint flow of river Dwarekeshwar and river Gandheswari. The rivers flows through Purulia, Bankura and Hooghly districts and meet with river Hooghly in a place called as Gadiara. All the tributaries of Rupnarayan flows in a south-easterly direction and regularly causes flood-related problems in the downstream districts. The river was also responsible for agricultural output of the region. A short introduction along with the status of industry and agriculture of both Damodar and Rupnarayan river networks is explained in the next section. Figure 25.1 depicts the location of the two river networks, and Fig. 25.2 shows the exact flowpath of the tributaries and distributaries of the same rivers along with the position of the reservoirs and barrages. Figure 25.3a explains the network diagram and Fig. 25.3b shows the sketch diagram of the two river basins.

Table 25.2 Table showing the percentage of irrigated land found in different districts of Jharkhand

Districts	Percentage of irrigated land
Godda	14.21
Dumka	9.47
Sahebganj (Pakur)	3.86
Deoghar	14.22
Dhanbad (Bokaro)	2.08
Hazaribagh (Chatra)	10.51
Giridih	6.99
Palamu (Garhwa)	24.25
Ranchi	6.12
Lohardagga	8.87
Gumla	2.45
E. Singhbhum	5
W. Singhbhum	4

Fig. 25.1 Figure showing the location of the networks of river Damodar and Rupnarayan. (Note: The flag icons show the sampling points considered. The image was downloaded from Google Earth™.)

25.1   An Introduction to Damodar River Network

The British administrator, W.W. Hunter, in his Statistical Account of Bengal (1876) described Damodar floods; "rainwater rushing off the hills through innumerable channels into the river bed with such great force and suddenness that the water rose to form a gigantic head wave of great breadth and sometimes rising up to 1.5 m in height. These waves and accompanying flash floods were locally known as *harka ban*. These floods washed away weeds and water hyacinths, cleaned up the drainage congestion in the lower channels and helped maintain the Calcutta port." The deltaic stretch with an unusual concentration of agrarian population and settlements, land and water being the two primary resources for farmers, give evidence to the rural prosperity these floods led to. Floods in the Damodar have been represented as an aberrant and uncivil behavior of the river, making "river training" "river control," "taming" and "harnessing" of it very problematic and often critical.

25.1.1   Damodar Valley Corporation

The difficultness to manage river Damodar enforced the built up of Damodar Valley Corporation which came into being on July 7, 1948 as a joint endeavor between the
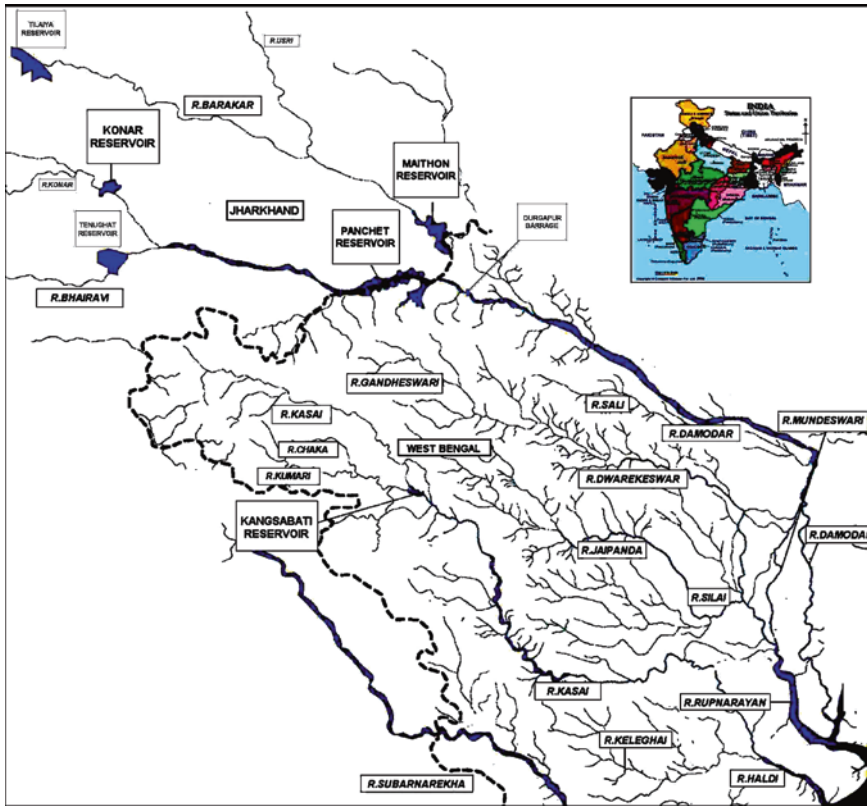
Fig. 25.2 Figure showing the entire network of river Damodar and Rupnarayan

Government of India and state government of Bengal and Bihar (now Jharkand) to build a dam across the Damodar valley. It was in fact the first multipurpose river valley project that the Government of India enforced after independence. Then Prime Minister of India Jawaharlal Nehru, chief minister of West Bengal Dr. B.C. Roy and Chief Minister of Bihar Sri Krishna Sinha, took special interest for the expansion and development of this plan. Covering the total area of 24, 235 km², the corporation has so far constructed four dams, a barrage for irrigation and a canal of 2,495 km. Apart from this, DVC has three hydelpower stations, five thermal power stations, and one gas turbine station with the total generating capacity of 2,761.5 mw.

The project Damodar Valley Corporation was defined by the following objectives:

- Flood control and irrigation
- Generation of electricity
- Transmission and distribution of electricity
- Water resource management
- Eco-conservation and afforestation
- Promotion of public health
- Industrial and economic development
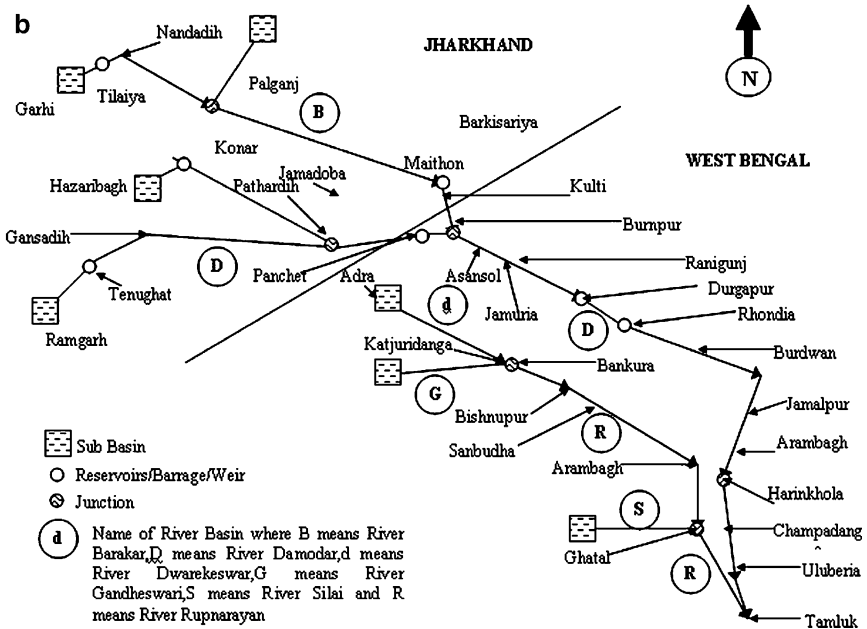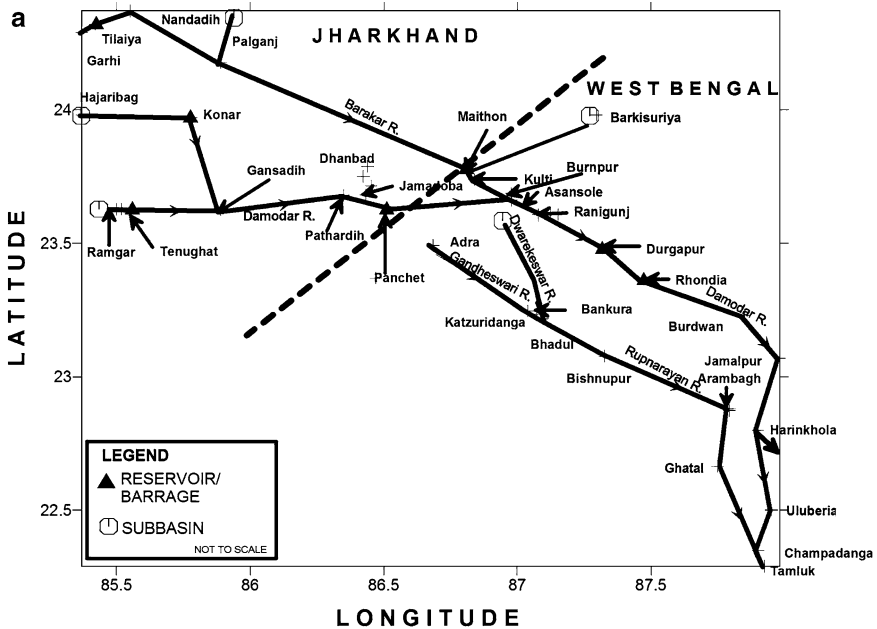
Fig. 25.3 (**a**) Figure showing the network diagram of the two river basins and their tributaries and distributaries. (**b**) Figure showing the sketch diagram of the river networks of Damodar and Rupnarayan

25.1.2 Catchment Description

The Damodar river basin (DRB) is a sub-basin and part of the Ganges river spread over an area of about 23,370.98 km^2 in the states of Jharkhand and West Bengal. The geographical boundary of the basin lies between 22″15′ and 24″30′N latitude and 84°30′ and 88°15′E longitude

The basin is bounded by Giridih and Santhal Pargana districts in the north; Hazaribagh and Palamau districts in the west; Ranchi, Purulia and Bankura districts in the south; and Hooghly and Howrah districts in the east and southeast. The basin extends over six districts of Jharkhand viz., Palamau, Hazaribagh, Giridih, Dhanbad, Santhal Pargana, and Ranchi and five districts of West Bengal, viz., Purulia, Bankura, Burdwan, Hooghly, and Howrah. The basin represents about 8.1% and 10.4% of the total population of undivided Bihar and West Bengal, respectively. The three fourth of the basin area representing the upper catchment falls in Jharkhand, while the low-lying flood plains entirely lies in West Bengal.

The dams in the valley have a capacity to check the peak floods of 650,000–250,000 ft^3/s. DVC has created many irrigation potential of 3,640 km^2. Damodar River was earlier known as the river of Sorrows as it used to flood vast areas of Bardhaman, Hooghly, Howrah, and Medinipur districts. Even today the floods sometimes distress the lower Damodar Valley but the chaos it brought about in earlier years is huge. However, after building the dams this flood factor has become a matter of history. The Chota Nagpur Plateau receives an average annual rainfall of around 1,400 mm, almost all of it in the monsoon months between June and August. Huge volume of water flows down the Damodar and during the monsoons its tributaries used to flow ferociously in the upper courses of the valley but in the lower valley it used to spill over its banks and flood extensive areas.

The floods were almost an annual ritual in this region but in some years the harm was probably more and so many of the great floods of the Damodar are available in documentation – 1770, 1855, 1866, 1873–1874, 1875–1876, 1884–1885, 1891–1892, 1897, 1900, 1907, 1913, 1927, 1930, 1935, and 1943. In four of these flooded years (1770, 1855, 1913, and 1943) majority regions of Bardhaman town was flooded. In 1789 a contract was signed between Maharaja Kirti Chand of Burdwan and the East India Company. In this contract the Maharaja was asked to pay an extra amount of Rs. 1, 93,721 for the construction and maintenance of embankment to prevent floods. However, these ran into dispute and in 1866 and 1873 the Bengal Embankment Act was passed, transferring the powers to build and maintain embankment to the government.

The first dam was built across the Barakar river, which is a tributary of the Damodar river at Tilaiya in 1953. The second dam was built across the Konar river, another tributary of the Damodar River at Konar in 1955. Two dams across the rivers Barakar and Damodar were built at Maithon in 1957 and Panchet in 1959. Both the dams are some 8 km upstream of the convergence point of the rivers. These four major dams are owned by DVC. Durgapur barrage was build downstream of the four dams in 1955, across the Damodar river at Durgapur in 1955, with head

regulators for canals on either side for feeding an widespread system of canals and distributaries. In 1978, the Government of Bihar, which was the formation of the state of Jharkhand formerly, constructed the Tenughat dam across the Damodar river outside the control of DVC. This program proposes to construct a dam across the Barakar river at Belpahari in Jharkhand state.

25.1.3   Geomorphological Features

The Damodar river basin has four prominent physiographic zones like extensive plateaus and hills, rolling uplands developed over Archaean rock, rolling plains with sharply raised terraces and low-lying alluvial plains with riverine aggregates and marshes. The basin has various types of lithology, slope, soil, and vegetation. The region is also richly endowed with varied mineral resources. Consequently, the region supports several economic activities related to mining and mine-based industries (311 coalmines, 182 non-coal mines, 78 urban centers, and 82 industrial centers) (Singh and Tiwary 2007).

The geology of the basin is spelt out by different types of rocks ranging from Archaean to recent age with economic deposits like coal and mica. The Upper and middle basin is covered by Archaean deposits but the lower basin is characterized by alluvium soil. The Gondwana and Vindhyan deposits, covering considerable areas are in the middle part of the basin. At most places, the crystalline and Gondwana areas are criss-crossed by post-Gondwana intrusions and are punctuated by multidirectional faults and lineaments (Singh and Tiwary 2007). The lineaments are mainly responsible for the many confined and unconfined aquifers that exist in the Damodar River basin but most of the upstream aquifers are useful only in monsoon due to the brittled and porous rocks of the basin. The downstream of the river, which falls in the state of West Bengal, shows the characteristics of two physiographic zones, namely, the Rarh Upland (Bardhaman districts) and the Riverine Delta (Hooghly districts).

The Rarh Upland is characterized by undulating landform which is subjected to extensive soil erosion. During heavy rains such zones experience sheet wash, but hardly any inundation. Although the soil is friable and porous, runoff is dominant over percolation. Hence groundwater endowment is poor. Nevertheless, the percolated water escape as non-perennial springs where the streams have cut deep channels.

The Riverine Delta zone shows processes of alluviation which had pushed away the sea front from a shallow off-shore zone. Acute meander loops with oxbow lakes occur profusely and conspicuously on the outward margins of all these deltas, suggesting decreased gradients of the delta forming streams. All these deltas have now merged with their respective neighbors to form a near-continuous physiographic zone. Nevertheless, the composition of the soils of the different deltas still mark their distinctive origins (Ghosh 1998).

Six subtypes of soils have been identified under the main alluvium in and around the different parts of Damodar basin where open Sal forests thrive on the

laterite zones and dense Sal forest can be found on the red and yellow loams of the upper valley.

The geology of Damodar river indicates heavy metal concentrations at various zones of the river. At two sites in Damodar river near mining areas, the coarser particles show similar or even higher heavy metal concentrations than the finer ones.

Figure 25.6 showed the spatial variation of Loss coefficient (Chapter 2) which represented the intensity of watershed degradation. Higher values of Loss coefficient will imply healthy watershed, that is, watershed has a high storage capacity but lower values of the coefficient will represent the degraded condition of the watershed where storage capacity would be low, that is, the watershed cannot retain water. The later type of watersheds will have lower availability of water than the former. According to Fig. 25.6, healthy watershed is observed in the downstream and upstream of river Damodar but the status changes in the midstream of river Damodar (near Kulti, Asansol, Burnpur, etc. regions which has a high concentration of coal mines) and upstream of river Barakar.

25.1.4 Hydrologic and Meterologic Characteristic

The hydrologic and Meterologic characteristic of Damodar basins were shown in Table 3. The table depicts the values of peak average monthly rainfall (P), basin runoff (Q), Ground Water Balance (GWB), Time of Concentration (T_c), Loss Coefficient (L_c), Water Availability, Water Stress, Virtual Water, Green Water, Weighted Average Water Quality (WAWQ), Industrial Pollution (IP) factor, Organic Pollution (OP) factor and Population (p) of the river Damodar according to observed data records found from Goswami et al. (ground water table) (2000) and samples collected from various locations of the river (WAWQ, IP and OP). The spaial variation of runoff, rainfall and loss coefficient was depicted by the Figs. 25.4–25.6.

The Water Availability was calculated as per the UNFCC recommended water budget equation which states that,

Water Availability is equal to,

$$= \left(\frac{p - (Q + E + G + T)}{p} \right) \tag{25.1}$$

$$= \left(\frac{p - (Q + \text{ET} + L_\text{C} + T)}{p} \right) \tag{25.2}$$

Evaporation (*E*) and Transpiration (*T*) could collectively represent as Evapo-Transpiration (ET) and Infiltration could be replaced by Basin Loss coefficient (Chapter 2). All parameters are represented as volume and unit of Water Availability is cubic meter per capita per year. The Water Availability data was fed to UNFCC recommended conditions for Water Stress to find the stressful regions
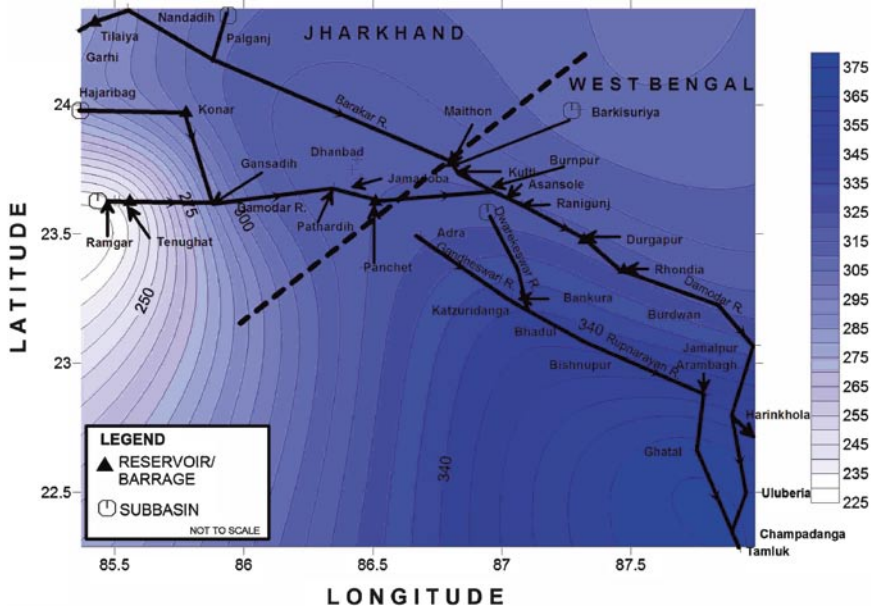
Fig. 25.4 Figure showing the spatial variation of rainfall in mm within the Damodar and Rupnarayan river networks
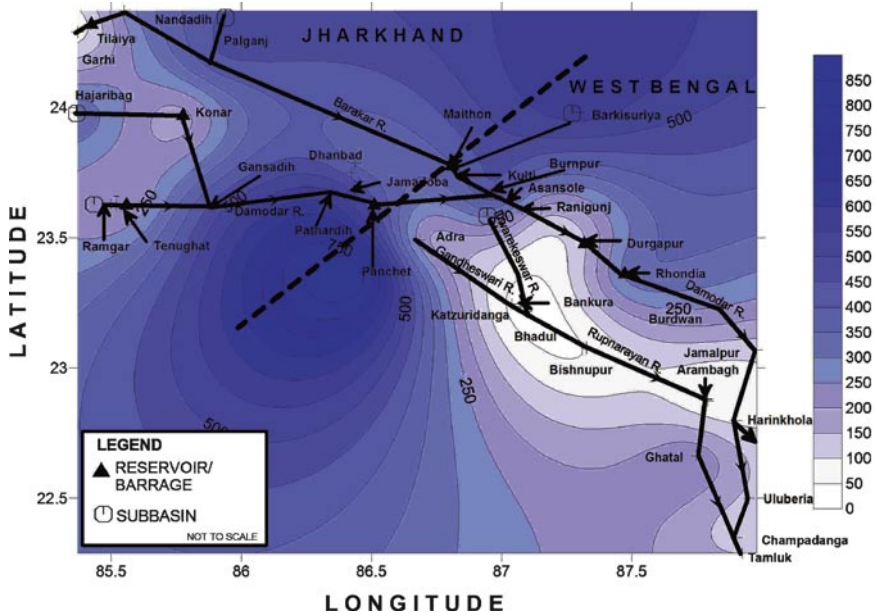
Fig. 25.5 Figure showing the spatial variation of runoff in cumecs within the Damodar and Rupnarayan river networks

Table 25.3 Table Showing Hydrologic and Meterologic Characteristic of River Damodar and Average Water Quality, Industrial Pollution, Organic Pollution and Population of each Considered

Location	Latitude	Longitude	Rainfall	Basin Runoff	PET	GWB	Tc(hr)
Garhi	24.29	85.37	321.99	7.06	8.36	41.67	1.194
Tilaiya	24.32	85.42	190.60	37.10	8.36	44.67	21.660
Nandadih	24.37	85.55	334.40	336.79	8.36	472	34.477
Palganj	24.18	85.89	302.99	508.38	8.36	472	30.001
Barkisuriya	23.98	87.30	303.07	610.50	8.31	189	21.660
Maithon	23.78	86.82	318.41	411.90	8.31	190	8.441
Ramgarh	23.63	85.50	335.72	327.67	8.54	28	9.082
Tenughat	23.63	85.52	55.84	5.53	8.54	22	9.082
Hazaribagh	23.98	85.37	321.99	432.88	8.45	606.16	51.159
Konar	23.97	85.78	315.97	65.39	8.45	607	8.523
Phusro	23.63	85.52	332.73	346.00	8.45	31	10.674
Gansadih	23.62	85.89	332.73	498.07	8.29	177.51	9.425
Bhowrah	23.68	86.35	318.41	610.49	8.29	177.51	3.451
Dhanbad	23.79	86.44	318.41	311.87	8.29	177.51	5.519
Jharia	23.75	86.42	318.41	406.62	8.29	177.51	0.876
Jamadoba	23.71	86.45	318.41	468.83	8.29	177.51	0.464
Pathardih	23.68	86.43	318.41	509.65	8.29	177.51	0.588
Panchet	23.37	86.47	318.41	1021.13	8.29	177.51	1.902
Kulti	23.74	86.84	319.53	344.64	7.85	1556	0.601
Burnpur	23.66	86.98	319.53	695.15	7.85	1556	2.432
Asansol	23.69	86.98	319.53	400.15	7.85	1556	2.746
Jamuria	23.61	87.08	319.53	238.17	7.85	1556	2.238
Ranigunj	23.61	87.12	319.53	143.75	7.85	1556	1.078
Kajora	23.61	87.15	319.53	92.41	7.85	1556	1.731
Durgapur	23.48	87.32	319.53	81.73	7.85	1835	7.096
Rhondia	23.36	87.47	319.53	433.70	7.85	1820	4.514
Burdwan	23.23	87.85	319.53	265.13	7.85	1835	5.196
Arambagh	22.88	87.79	354.05	106.45	7.25	690	3.479
Jamalpur	23.07	87.98	319.53	105.90	7.85	690	5.621
Harinkhola	22.80	87.90	354.05	73.86	7.25	690	2.355
Champadanga	22.35	87.90	354.05	46.04	7.25	687	5.526
Uluberia	22.50	87.95	374.46	133.55	6.83	689	1.910
Adra	23.49	86.69	321.98	10.54	8.29	123	1.046
Katjuridanga	23.25	87.04	342.23	17.25	8.08	123	0.282
Bankura	23.23	87.07	342.23	14.88	8.08	123	0.162
Sanbudha	23.23	87.10	342.23	7.16	8.08	123	0.487
Bhadul	23.22	87.10	342.23	10.21	8.08	123	0.433
Bishnupur	23.08	87.33	342.23	16.46	8.08	1035	0.240
Arambagh	22.88	87.79	354.05	14.29	7.25	690	0.060
Salepur	22.87	87.79	354.05	7.61	7.25	123	0.014
Ghatal	22.67	87.75	382.19	322.87	7.35	123	1.388
Tamluk	22.29	87.92	382.19	208.81	7.35	120.6	0.139
Maximum within the two basins			382.19	1021.13	8.54	1835.00	51.16
Minimum within the two basins			55.84	5.53	6.83	22.00	0.01
Maximum for Damodar Basin			374.46	1021.13	8.54	1835.00	51.16
Minimum for Damodar Basin			55.84	5.53	6.83	22.00	0.46
Maximum for Rupnarayan Basin			382.19	322.87	8.29	1035.00	1.39
Minimum for Rupnarayan Basin			321.98	7.16	7.25	120.60	0.01
Maximum for Jharkhand			335.72	1021.13	8.54	607.00	51.16
Minimum for Jharkhand			55.84	5.53	8.29	22.00	0.46
Maximum for West Bengal			382.19	695.15	8.29	1835.00	7.10
Minimum for West Bengal			319.53	7.16	6.83	120.60	0.01

Note: Water stress was represented by 3 classes where class "1" regions has no water stress, scarcity and facing severe stress for water.

Rupnarayan along with the existing Water Availability, Stress, Virtual Water, Green Water, Weighted Gauged and Ungauged Sampling Regions

Loss Coefficient	Water Availability	Stress	Virtual Water	Green Water	Water Quality	Industrial Pollution	Organic Pollution	Population
0.670	4728.52	1	2.01	208.94	116.46	0.18	0.59	6363
0.650	236.16	3	1.09	94.91	126.46	0.17	0.60	69444
0.770	613.11	3	2.66	230.63	136.46	0.16	0.61	65000
0.734	185.75	3	1.49	129.13	146.46	0.15	0.59	120121
0.780	-127.81	3	-0.73	-76.04	156.46	0.14	0.57	85678
0.807	386.27	3	0.51	52.92	166.46	0.13	0.55	19,728
0.863	32.37	3	3.88	16.51	102.00	0.81	0.83	73455
0.790	56.24	3	9.00	38.27	106.78	0.76	0.80	97991
0.780	330.49	3	68.70	292.09	93.78	0.86	0.78	127,269
0.840	14038.62	1	497.66	509.48	80.78	1.07	0.75	5226
0.770	9.60	3	5.44	5.57	90.78	1.02	1.03	83,463
0.860	1482.06	2	2.27	2.33	100.78	0.97	1.00	226
0.827	-239.87	3	-72.00	-73.71	110.78	0.92	0.98	44,253
0.640	76.21	3	24.80	105.46	120.78	0.87	0.95	199,258
0.720	85.38	3	47.48	48.61	0.18	0.82	1.02	81,979
0.761	47.79	3	11.02	11.28	0.18	0.82	1.02	33,981
0.790	-48.13	3	-12.90	-13.21	-23.36	0.80	1.06	39,527
0.587	-5518.35	3	-312.68	-320.10	132.90	0.50	0.82	8,353
0.667	453.67	3	778.58	609.22	119.92	0.09	0.84	290,057
0.670	244.03	3	599.40	469.02	122.00	0.12	0.76	415141
0.690	118.79	3	750.20	587.01	120.00	0.46	0.75	1,067,369
0.692	1087.55	2	833.01	651.81	125.00	0.44	0.67	129,456
0.710	1212.03	2	881.27	689.57	132.00	0.43	0.65	122,891
0.680	6146.40	1	907.52	710.11	134.00	0.45	0.67	24955
0.870	361.89	3	1055.61	1445.47	160.76	0.55	0.55	492,996
0.860	2542.56	1	868.01	1188.59	160.76	0.55	0.55	57,700
0.845	490.01	3	961.85	1505.24	175.31	0.38	0.38	331,759
0.650	1432.10	2	475.60	744.28	175.40	0.40	0.40	56129
0.910	60.61	3	457.93	716.63	174.76	0.40	0.42	1276853
0.816	573776.99	1	492.25	770.35	174.76	0.40	0.42	145
0.850	69724.46	1	504.94	790.21	174.76	0.40	0.42	1224
0.860	394.64	3	471.88	738.46	149.76	0.76	0.67	202095
0.679	1671.34	2	279.22	277.00	160.00	0.43	0.56	22030
0.720	1487.22	2	288.22	285.94	164.00	0.28	0.50	25556
0.870	298.28	3	417.15	287.48	166.52	0.27	0.57	128111
0.720	17318.07	1	424.43	292.49	166.52	0.27	0.57	2245
0.780	45324.02	1	421.56	290.51	166.52	0.27	0.57	852
0.810	12043.71	1	1275.85	879.25	164.39	0.08	0.57	9704
0.840	1573.96	2	522.71	715.75	158.68	0.11	0.60	56129
0.740	191988.05	1	199.67	323.54	152.38	0.15	0.65	208
0.700	293.05	3	39.05	122.48	149.44	0.22	0.71	51586
0.78	540.40	3	63.98	200.64	124.48	0.86	0.84	45,826
0.91	573776.99		1275.85	1505.24	175.40	1.07	1.06	1276853.00
0.59	-5518.35		-312.68	-320.10	-23.36	0.08	0.38	145.00
0.91	573776.99		1055.61	1505.24	175.40	1.07	1.06	1276853.00
0.59	-5518.35		-312.68	-320.10	-23.36	0.09	0.38	145.00
0.87	191988.05		1275.85	879.25	166.52	0.86	0.84	128111.00
0.68	293.05		39.05	122.48	124.48	0.08	0.50	208.00
0.86	14038.62		497.66	509.48	166.46	1.07	1.06	199258.00
0.59	-5518.35		-312.68	-320.10	-23.36	0.13	0.55	226.00
0.91	573776.99		1275.85	1505.24	175.40	0.86	0.84	1276853.00
0.65	60.61		39.05	122.48	119.92	0.08	0.38	145.00

class "2" regions has medium scarcity of water and class "3" regions were totally under water
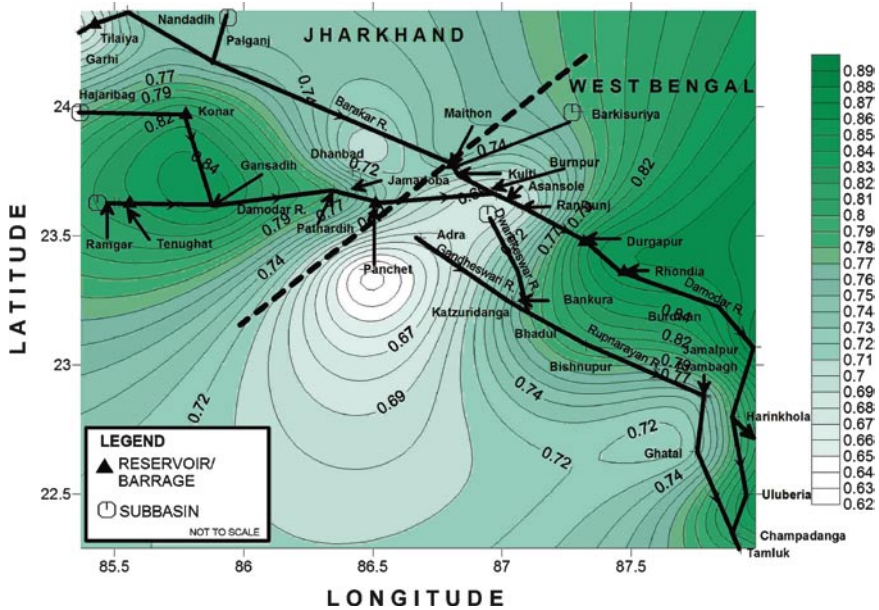
Fig. 25.6 Figure showing the spatial variation of loss coefficients within the Damodar and Rupnarayan river networks

within the two basins. Water stress was represented by three classes where class "1" regions has no water stress, class "2" regions has medium scarcity of water, and class "3" regions were totally under water scarcity and facing severe stress for water.

Amount of virtual water and green water was calculated with the help of water use data found from the DVC and RRI, converting it to percentage use of water for industry and agriculture and ultimately into amount of water used as virtual and green water in the considered two river basins. The unit of both Virtual and Green water is cubic meters.

The Weighted Average Water Quality (WWAQ) was calculated by averaging the water quality parameters giving maximum weightage to parameters which mainly influences the overall quality of water and minimum weightage to parameters with minor influence on water quality of a river basin. As the average was normalized, it has no unit and the quality of water is proportional to value of WWAQ.

Some parameters of water quality get increased due to presence of industries or human population. Parameters like TDS, Turbidity will show an increasing trend if adjacent basin has a largescale presence of industry whereas Total coliform and fecal colliform along with BOD will get increased if there is a concentration of human population along the river channel. Another weighted average was calculated giving maximum weightage to those parameters which generally get increased due to industry and minimum weightage was given to those parameters which are invariant to industrial activities. The average was normalized and given a name of Industrial Pollution Index or IP. Similarly a weighted average was calculated and

normalized for parameters which get influenced by presence of human population and given a name of Organic Pollution Index or OP. Both IP and OP is proportional to pollution of the river basin, that is, higher values of IP and OP implies higher amount of pollution and vice-versa.

According to climatic zones, the Damodar basin falls within dry and subhumid climatic zones. The upstream region, which is located in the state of Jharkhand falls within the dry climatic region and the downstream, situated in Bardhaman and Hooghly districts falls within the subhumid regions of climatic zones. The first region, dry climatic zone, is characterized by high temperature, low humidity, and occasional, but high rainfall. A 10°C and above temperature, rainfall below 1,500 mm, and 60–70% humidity characterized the subhumid climatic zone. Occasional droughts are also observed in the later climatic zone though the lower downstream, near the confluence point of Hooghly, also observe frequent floods that's why many scientists suggested classifying the east Bardhaman and Hooghly district in a separate climatic zone known as sub-humid-east.

According to Fig. 25.4, high values of rainfall can be observed in the downstream of river Damodar but rainfall of 250–300 mm is experienced in the upstream of the same river along with river Barakar. Though, Barakar has more average maximum rainfall than the upstream of river Damodar.

According to Fig. 25.5., the upstream of river Damodar generates higher runoff than the downstream of the same river. If Fig. 25.5 is compared with Fig. 25.6, the relationship between runoff and loss coefficient can be interpreted as inversely proportional as where the former is more in upstream later is less and when former is less in downstream, later is relatively less than the loss coefficients of upstream.

25.1.5   Industrial and Agricultural Status

The Damodar Valley has large reserves of coal and mica, and the area is a highly developed as an industrial belt. The Ruhr of India is referred to as the Damodar Valley by many because of its similarities with the Ruhr mining-industrial area of Germany. The dams on the Damodar river have a number of hydroelectric power plants. Of late, the Damodar has become one of the most contaminated rivers of India, with chemicals, mine effluents, and poisonous wastes flowing into the river. The mines and industries are located in the valley. Efforts are being made to reduce the level of pollution in the river.

Three integrated steel plants like the Bokaro, Burnpur and Durgapur, moreover the Steel Authority of India Limited (SAIL) and other factories are situated in the valley. Damodar Valley contains a variety of mineral deposits, including very large deposits of coal and refractory materials. The largest (almost the only) reserves of coking coal in the country are found in the Jharia coalfields in the valley.

The valley also generates 60% of India's average grade coal. Coal India Limited operates in the valley in a big way. Several dams have been built in the valley, for the generation of hydroelectric power. The valley is called "the Ruhr of India" and

Damodar Valley Corporation is popularly known as DVC, which came into being on July 7, 1948 by an Act of the Constituent Assembly of India (Act No. XIV of 1948) as the first versatile river valley project of independent India. The project is designed on the basis of the Tennessee Valley Authority of the USA.

25.1.6 Water Pollution

The Damodar is the most polluted river in the country today due to the coal-based industries that dot the Damodar valley along with country's major iron and steel plants; thermal power plants. Zinc, glass, and cement plants. The pollution was caused by mine overburden, fly ash, oil, toxic metals, and coal dust. The people living in the basin were slowly being poisoned because the Damodar and its tributaries were the only source of drinking water for most people living in the area (Rain Water Harvesting 2008). Also, the uncontrolled use of Damodar water for sanitation are causing increase of colliform bacterias in the river.

25.2 An Introduction to Rupnarayan River Network

25.2.1 Catchment Description

The Rupnarayan and its tributaries lie within the latitude of 23.49N and 22.29N and longitudes of 86.69E and 87.92E. The Rupnarayan river is a river in eastern India. It begins as the Dhaleswari (Dhalkisor) in the Chhota Nagpur plateau foothills northeast of the town of Purulia. It then follows a tortuous southeasterly course past the town of Bankura, where it is known as the Dwarakeswar river. Near the town of Ghatal, the Silai joins it, where it takes the name Rupnarayan. Finally, it joins the Hoogli river. The Rupnarayan river is famous for the Hilsa fish that breed in it and are used widely in Bengali cuisine. It is also distinguished for the West Bengal Power Development Corporation Limited (WBPDCL) thermal power plant at Kolaghat.

The Rupnarayan river Networks are bordered by Hooghly district in the East, Purulia and Bankura in the West, and East and West Midnapore districts in the South and Bardhaman district in the North.

25.2.2 Geomorphological Features

The physiographic zones through which Rupnarayan and its tributaries has flowed includes the Puruliya High plains, the Rarh Upland, and the Riverine Delta. The characteristics of such physiographic zones are described next.

25.2.2.1   The Puruliya High Plain

"Excluding the Ayodhya plateau, the rest of the District of Puruliya can be described as high plain sloping eastward. It is an eastern extension of the Deccan Shield. Eastward extension of this shield below the younger lithofacies has been traced over considerable distance in the east. The so-buried extensions of the shield are found in increasingly deeper layers eastward. It seems as if the Deccan shield has bent downwards in the east. Similar physiographic formations are found in the western margins of the Districts of Bankura and Medinipur as also in western Birbhum District.

The Puruliya High Plain is composed of ancient metamorphic rocks like gneiss, schists, and many varieties of phyllites. Bands of differentially metamorphosed rocks are arranged regionally with east–west orientation nearly parallel to the Dalma orogenic belt located at the southern margin of the zone. These are also parallel to the Gondwana rift valley located on the northern margin of the zone. Higher order metamorphics, because of their chemical instability under modern conditions, have been decomposed faster. Similarly, the lower order metamorphics, because of their poor strength, have been eroded faster. Both of these support the river valleys. The valley crests are generally formed of middle order metamorphics, like quartzite and gneiss, which in many places support tors. The topography is undulating in nature where the valley crests extend as spurs, becoming narrower while losing heights as the river valleys widen concurrently eastward. Many residual hillocks are found scattered on this high plain, some of which are formed of intrusives. There are evidences of ancient volcanism in this part of the world, manifested in the shapes of dykes, batholiths (e.g., Kuilapal granites) and volcanic cones (e.g., Mama Bhagney Pahar north of Adra). No traps like the Rajmahal basalt are found.

The rocks are highly fractured and jointed. Along these joints and fractures are found some amount of ground water. Otherwise, surface runoff is the major source of consumable water. The major part of this zone was once under forests, which got largely reduced in tune with expansion of area under cultivation with commensurate population growth. In the recent decades, the valley crests are getting planted with trees. The otherwise exposed surfaces are subjected to gully erosion. The soil is oxidized, very porous, and friable.

25.2.2.2   The Rarh Upland

To the east of the Puruliya High Plain extends the Rarh Upland formed of ferralitic soils. The origin of this physiographic zone has already been explained. The original materials composed of a wide variety of rocks were deposited in the Miocene period through repeated marine transgressions. The pebble beds of Dhalbhum and Durgapur are the evidences in this regard.

After the fluvial-marine deposits were laid and the sea finally moved away, fluctuating groundwater table coupled with rain and dry weather conditions have

led to the formation of lateritic patches in many parts of this zone. However, once brought under the plough, these lose their lateritic properties and tend to support limonitic soils because of accentuation of the leaching processes.

The Rarh Upland is undulating in character subjected to extensive soil erosion. During heavy rains are experienced sheet wash, but hardly any inundation. Although the soil is friable and porous, runoff is dominant over percolation. Hence groundwater endowment is poor. Nevertheless, the percolated water escape as non-perennial springs where the streams have cut deep channels.

The ferralitic formations extend like spurs of increasingly narrower width eastward. The major streams passing through this zone contain many river terraces and, thereby, reveal the mobile nature of the basement complex.

This zone was once thickly forested. It still contains a large share of the forest lands of West Bengal. Like in all other places, expansion of area under agriculture is proceeding up the valleys. In many places, agricultural fields now occupy the valley crests.

25.2.2.3 The Riverine Delta

Towards the earlier sea-face of the Rarh Upland extend a distinct physiographic zone formed of many deltas. In the north-east, covering the eastern part of the District of Murshidabad, is located the largest delta formed by the Ganges river. This delta extends southward up to the border zone of the Districts of Nadia and North 24-Parganas. To the south-west of the Ganges delta, primarily in the eastern Bardhaman District and northern Hughli District, had formed another large delta with the materials carried by the Ajoy and the Damodar rivers. Further to the south-west, the Kansabati river had formed its delta primarily in the District of Medinipur. Further south, also within Medinipur District, a delta was built by the Subarnarekha River.

Below all these deltas, extensions of the ferralitic formations, similar to those of the Rarh Upland, can be traced. This suggests down warp of the basement complex, making room for these rivers to overlay truly alluvial deposits. The deltaic formations do not show any sign of fertilization. The processes of alluviation pushed away the sea front from a shallow off-shore zone. Acute meander loops with oxbow lakes occur profusely and conspicuously on the outward margins of all these deltas, suggesting decreased gradients of the delta forming streams. All these deltas have now merged with their respective neighbors to form a near continuous physiographic zone. Nevertheless, the composition of the soils of the different deltas still marks their distinctive origins.

As the deltas merged, some tracts between them escaped alluviation. These are now found to contain some of the flood prone zones of this physiographic division. Khanakul and Ghatal of respectively the Hughli and Medinipur Districts is one such region between the Damodar and Kansabati deltas. But more conspicuous example of unfilled parts is given by the wetlands of eastern Birbhum and western Murshidabad Districts. Hijal Bil and Langalhata Bil are the more well-known examples of such wetlands. These bils remained cut-off from the Ganges delta because of the formation

of alluvial levee along the right bank of the Bhagirathi river. It obstructed passage of water brought by the streams of the Mayurakshi system towards the east. Along the western margin of this levee now flows the Babla river as escape channel of water into the Ajoy river. The streams of the Mayurakshi system are now engaged in filling up these wetlands from the west.

Except the smaller deltas of the Mayurakshi and also the larger delta of the Damodar, the riverine deltaic zone is now moribund under all considerations. The processes of fresh alluviation have practically ceased to operate. The distributaries of the Ganges have now been cut-off from supplies from the mother river. The Kangsabati is no longer a vigorous stream to produce alluviation. The Subarnarekha has moved away from its original delta towards south west. The smaller deltas of the Mayurakshi system are still advancing against the aforementioned wetlands. The Damodar delta, on the other hand, is experiencing changes in the river course and consequent flooding and alluviation.

The entire area is extensively cultivated. Apart from surface water, the agricultural fields use the richly endowed groundwater of this physiographic zone. The Ganges and the Damodar deltas have richer endowments of groundwater than the deltas of either the Kansabati or the Subarnarekha. The Ganges delta has the thickest section of alluvium and acts as a passage for subterranian flow of water of the entire Ganges valley of north India. Below the Damodar delta extends the Gondwana rift valley to guide the sub-terrainian flow of the entire catchment area. The deltas of the Kansabati and the Subarnarekha, on the other hand, is formed of alluvium of shallow depth overlying the ferralitic formations" (Ghosh 1998).

25.2.3 Hydrologic and Meterologic Characteristic

The hydrologic and Meterologic characteristic of Rupnarayan basins were shown in Table 3. The spaial variation of runoff, rainfall and loss coefficient was depicted by Figs. 25.4–25.6. The maximum and minimum values of rainfall, ET, and other variables within the Rupnarayan basins were also given in Table 3.

According to climatic zones, the entire basins of Rupnarayan fall within the subhumid west. According to the Fig. 4, heavy and regular rainfall is observed in the Rupnarayan basin though in the banks of Dwarekeshwar river, the climate is dry and occasional rainfall is received even during the monsoon season.

25.2.4 Industrial and Agricultural Status

In Bankura and Purulia, due to the presence of fireclay, pottery industry makes the livelihood of the people living in these districts. Haldia is a center of industrial activity with its chemical and oil factories situated on the banks of river Hooghly near the confluence point of the Rupnarayan and Damodar with Hooghly. Midnapur

district is also popular for its textile and paper and in Ghatal, the controlling center of East Midnapore and the junction point of river Silai and Rupnarayan is famous for its tin and bronje industries. Arambagh, the head office of the Hooghly districts, is famous for its poultries and paper industries. Besides these, rubber industry is found in some pockets of the catchment.

Most of the people living in the banks of Rupnarayan basin depend upon agriculture. Kharif and Rabi, both types of crops are cultivated here along with Bittle tree cultivation. The East and West Midnapore are famous for their Bittle Industries.

References

Ghosh AK (1998) State of environment report. Retrieved from http://wbenvironment.nic.in/html/StatuaOfEnvironment/status12.htm on 1 August 2009

Goswami AB, Mazumdar A, Bose B (2000) Status of water resources in West Bengal, report published by school of water resources, Jadavpur University

Hunter WW (1876) A statistical account of bengal, Retrieved from http://www.archive.org/details/astatisticalacc20huntgoog on 22nd June, 2009

Rain Water Harvesting Members (2008) Pollution of river Damodar. Retrieved from http://www.rainwaterharvesting.org/Crisis/Damodar.htm on 1 August, 2009

State Jharkhand (2003) Retrieved from http://jharkhand.nic.in/mineral_collection.htm on 1 August, 2009

Singh PKGS, Tiwary BK (2007) Critical evaluation of geo-environmental scenario of Damodar river basin, India, First international conference on MSECCMI, New Delhi, India

Impact of Climate Change on Natural Resource Management

Edited by B.K. Jana and M. Majumder

Page ix, lines 7/8 the correct name is Prof. Dr. Pradip Narayan Ghosh
Page ix, lines 8/9 the correct name is Prof. Dr. Manoj Mitra

Pages xiii and 375: the correct name of the third author is Debapriya Basu

On pages iv, 3, 19, 45, 71, 93, 111,131, 143, 161, 183, 203, 227, 247 267, 281, 295, 309, 329, 345, 359, 375, 393, 417, 441, 461 and 481 the correct affiliations of Bipal K. Jana and/or Mrinmoy Majumder are:

B.K. Jana
Former Research Scientist (Per Time)
School of Water Resources Engineering
Jadavpur University
Kolkata-700032, West Bengal
India

M. Majumder
Former Senior Research Fellow
School of Water Resources Engineering
Jadavpur University
Kolkata-700032, West Bengal
India

The publishers apologize for the inconvenience caused.

Index